OCT in Central Nervous System Diseases

The Eye as a Window to the Brain

Andrzej Grzybowski
Piero Barboni *Editors*

Springer

OCT in Central Nervous System Diseases

Andrzej Grzybowski • Piero Barboni
Editors

OCT in Central Nervous System Diseases

The Eye as a Window to the Brain

Springer

Editors
Andrzej Grzybowski
Professor of Ophthalmology
Head of Ophthalmology Department
Poznan City Hospital
Poznan
Poland

Chair of Department of Ophthalmology
University of Warmia and Mazury
Olsztyn
Poland

Piero Barboni
Studio Oculistico d'Azeglio
Bologna
Italy

ISBN 978-3-319-24083-1 ISBN 978-3-319-24085-5 (eBook)
DOI 10.1007/978-3-319-24085-5

Library of Congress Control Number: 2015956209

Springer Cham Heidelberg New York Dordrecht London

Printed on acid-free paper

Springer International Publishing AG Switzerland is part of Springer Science+Business Media (www.springer.com)

Contents

Chapter 1
Introduction: Retina Imaging – Past and Present

Andrzej Grzybowski and Piero Barboni

Abstract The retina raised the interest of scientists since the 4th century BC, when the Greek anatomist Herophilos, known as the Father of Anatomy, described it for the first time. It was not until the 18th century that scientists started to visualize the retina in the living animal and, later on, in the human eye. The histology of the retina was investigated in the 19th century and by the end of the 20th it was believed that its histological and functional characteristics were largely known. However new and somehow surprising information continues to be collected also in current days. One example is the discovery of Melanopsin-Containing Retinal Ganglion Cells (RCGs), which represent a novel class of photoreceptors. Optical coherence tomography (OCT) has been one of the most significant innovations in ophthalmology and has enabled us to improve our knowledge about specific cells and structures of the retina, such as the RCGs and the retinal nerve fiber layer (RNFL). Since the retina and optic nerve originate from the diencephalon, OCT measurements of both RCGs and RNFL have been shown to be sensitive parameters to investigate different diseases of the central nervous system.

The retina is a mysterious structure. The first use of the term comes, as to our present knowledge, from Herophilos (335–280 or 255 BC), Greek anatomist, who was of founders Greek school in Alexandria. He used two different words, arachnoeides and amfiblesteroides, for retina. For many years, both meanings were related to casting net, and retiform, a word which the modern "retina" is derived. However, as it was nicely shown recently, there might be another explanation of

A. Grzybowski, MD, PhD, MBA (✉)
Professor of Ophthalmology, Head of Ophthalmology Department, Poznan City Hospital, Poznan, Poland

Chair of Department of Ophthalmology, University of Warmia and Mazury, Olsztyn, Poland
e-mail: ae.grzybowski@gmail.com

P. Barboni
University of Bologna, Bologna, Italy

A. Grzybowski, P. Barboni (eds.), *OCT in Central Nervous System Diseases: The Eye as a Window to the Brain*, DOI 10.1007/978-3-319-24085-5_1

these original terms [1]. Amfiblesteroides meant at that time also anything that is thrown around and encircling walls. For many years it was believed, however, that the lens, not retina is the reception organ of the eye responsible for vision and there was even no agreement as to whether the eye emanated light (extramission theory) or received it (intromission theory) [2, 3]. Leonardo da Vinci (1452–1519) and Johannes Kepler (1571–1630) questioned the role of the lens in light reception. Felix Plater (1536–1614), attributed that role to the retina, what was further experimentally supported by Christopher Scheiner (1575–1650) who, by removing part of the sclera and choroids, was able to notice the reversed picture projected onto the bottom of the eye [3–6].

For the next two centuries, it was disputable weather retina or choroid was a precise structure responsible for vision reception [7]. This was finally settled by Herman von Helmholtz (1821–1894), who also constructed and popularized the first ophthalmoscope in 1851 [8]. This revolutionized the development of retinology.

The first visualization of the eye fundus of the living animal, however, was conducted by Jean Mery (1654–1718) in 1704 (Fig. 1.1). By plunging the head of a cat in water, Mery was able to observe the retinal vessels, the optic nerve head and the choroid [9]. This was later confirmed by Adolf Kussmaul in 1845 [10], Johann Nepomuk Czermak in 1851 [11] and Adolf Ernst Coccius in 1852, who introduced a water-box named ‘orthoscope”, to neutralize the corneal curvature [12, 13]. It was, however, Johannes Purkinje (1787–1869) in 1823 who described the basics of ophthalmoscopy based on his observations living animal and human eye [14]. One of the pioneers in the use of ophthalmoscopy for the diagnosis of central nervous system disorders was Xavier Galezowski (1832–1907), who published one of early textbooks on this subject and coined a term of cerebroscopy for this examination [15] (Fig. 1.2).

The microscopical structure of the retina was described in the 19th century, and by the end of the 20th century it was believed that its histological and functional characteristics was largely recognized. Then, the discovery of intrinsically photosensitive ganglion cells, a novel class of retinal photoreceptors, which express melanopsin, are sensitive to short-wavelength blue light and project throughout the brain, have presented a completely unknown area of retina-brain possible interactions [16, 17]. It is quite clear today that other cellular components of the retina, namely amacrine cells, bipolar cells and microglial cells, although somehow neglected in the past, play important functions both in physiology and pathology of the retina. For example, it was recently proposed that microglia might accelerate damage wrought by retinitis pigmentosa and that they might provide a target for entirely new therapeutic strategies [18].

One of the major developments in recent years in retinal imaging was the introduction of optical coherence tomography (OCT). OCT was firstly reported by Huang et al. in 1991 [19]. In vivo studies were first reported in 1993 [20, 21], and in 1995 imaging of the normal retina [22] and macular pathology [23] was presented. OCT delivers high-resolution cross-sectional or 3-dimensional images of the retinal and choroid structures, which are generated by an optical beam scanned across the

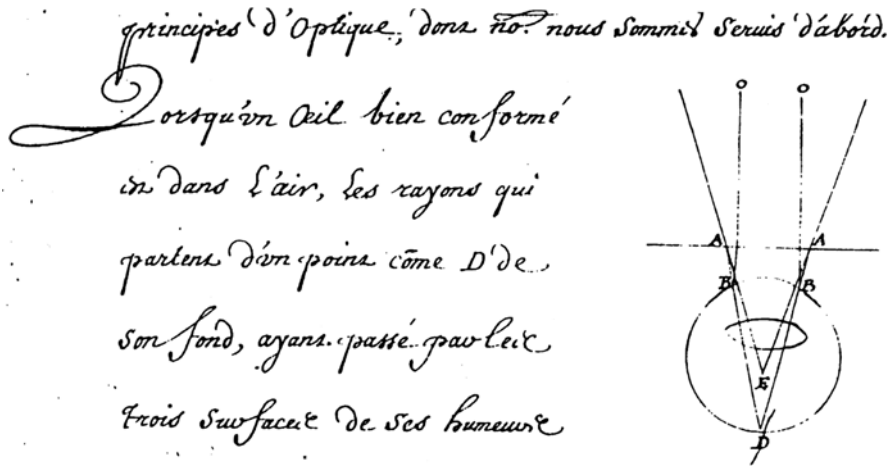

Fig. 1.1 Extract from the Proceedings of the Royal Academy of Sciences for the year 1709 — Session of 20th March 1709. By this diagram, La Hire explains the visualization of the fundus of the submerged cat by the fact that the surface of the water having abolished the corneal dioptric power, the rays coming out of the eye would no longer be parallel, but would diverge and that would make the eye fundus visible to the observer (Source: Heitz [9])

retina (and choroid). OCT testing is quick, easy and noninvasive, and pupil dilation is typically not required. Moreover, OCT yields quantitative anatomical data and is related with low variation for repeated measurements, low intra-individual and inter-individual variation and low variability across different centers using the same device.

Retinal ganglion cells axons are nonmyelinated within the retina, thus retinal nerve fiber layer (RNFL) is an optimal structure to visualize the process of neuro-degeneration, neuro-protection and neuro-repair [24]. Moreover, OCT enables evaluation of retinal ganglion cells (RGC). For example, it was reported in patients with MS a dropout of RGC in 79 % of eyes and inner nuclear layer atrophy (including amacrine cells and bipolar cells) in 40 % of eyes [25]. It was also argued that OCT might reveal RNFL abnormalities in many patients with no clinical symptoms [26].

Retina and optic nerve originates from diencephalon, thus are a part of central nervous system (CNS). RGC present the typical morphology of CNS neurons. Optic nerve, like all fiber tracts in CNS, is covered with myelin and is unsheathed in all three meningeal layers. Insult to the optic nerve, similar to CNS, lead to retrograde and anterograde degeneration of damaged axons [27]. Because of these many similarities, it has not been very surprising that many CNS diseases can be also detected on the retina level. They include multiple sclerosis, Alzheimer disease, Parkinson disease, and many others. Moreover, it was shown that there are some common degenerative mechanisms between Alzheimer disease and eye diseases, like glaucoma and age-related macular degeneration [28]. Thus, the aim of this book is to present and review all aspects of OCT retina studies in CNS diseases.

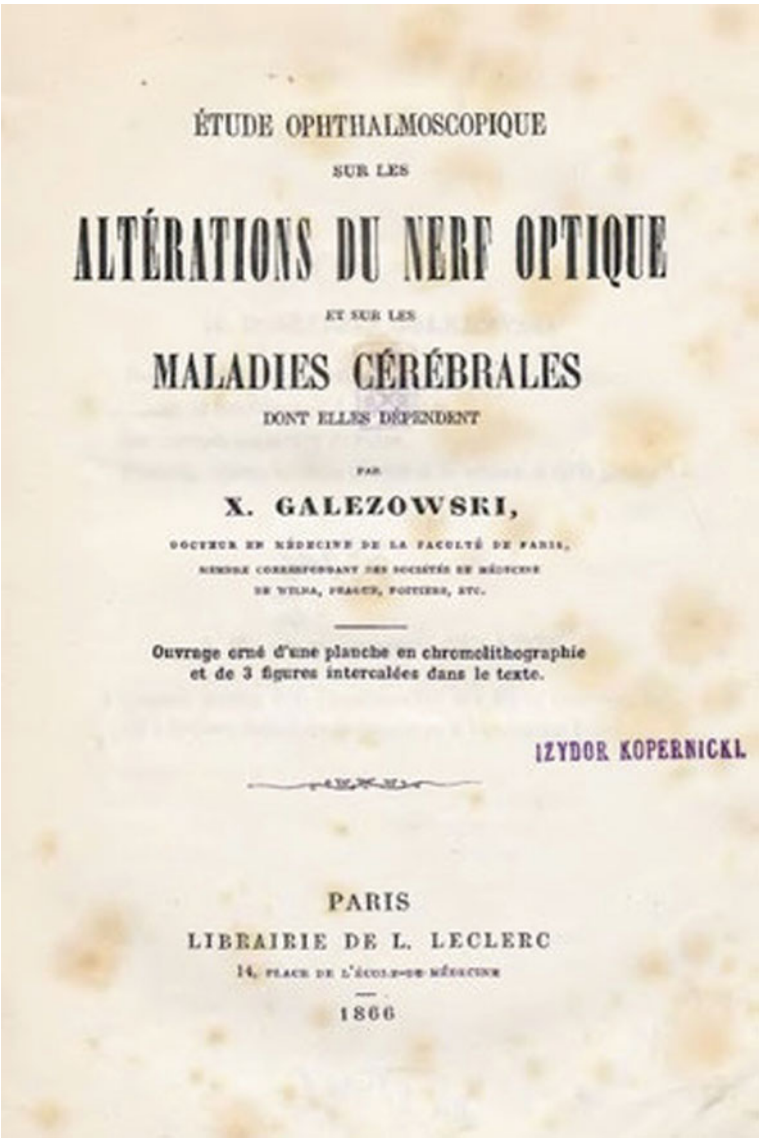
ÉTUDE OPHTHALMOSCOPIQUE

SUR LES

ALTÉRATIONS DU NERF OPTIQUE

ET SUR LES

MALADIES CÉRÉBRALES

DONT ELLES DÉPENDENT

PAR

X. GALEZOWSKI,

DOCTEUR EN MÉDECINE DE LA FACULTÉ DE PARIS,

MEMBRE CORRESPONDANT DES SOCIÉTÉS DE MÉDECINE

DE WILNA, PRAGUE, POITIERS, ETC.

Ouvrage orné d'une planche en chromolithographie
et de 3 figures intercalées dans le texte.

PARIS

LIBRAIRIE DE L. LECLERC

14, PLACE DE L'ÉCOLE-DE-MÉDECINE

1866

Fig. 1.2 Cover page of the book "Etude ophtalmoscopique sur les altérations du nerf optique et les maladies cérébrales dont elles dépenden " (By Xavery Gałęzowski, Paris, 1866)

References

1. de Jong PT. From where does "rete" in retina originate? Graefes Arch Clin Exp Ophthalmol. 2014;252:1525–7.

2. Magnus H. Ophthalmology of the ancients. Translated by Waugh RL. Vol 2. Wayenborgh, Oostende; 1999. p. 461–9.
3. Duke-Elder S, Wybar KC. The history of ophthalmic optics. In: Duke-Elder S, editor. System of ophthalmology, vol. 5. London: Henry Kimpton; 1970. p. 3–23.
4. Mark H. Johanees Kepler on the eye and vision. Am J Ophthalmol. 1971;72:869–78.
5. Daxecker F. Further studies by Christoph Scheiner concerning the optics of the eye. Doc Ophthalmol. 1994;86:153–61.
6. Daxecker F. Christoph Scheiner's eye studies. Doc Ophthalmol. 1992;81:27–35.
7. Grzybowski A, Aydin P. Edme mariotte (1620–1684): pioneer of neurophysiology. Surv Ophthalmol. 2007;52:443–51.
8. Helmholtz H.L.F. v., Beschreibung eines Augenspiegels zur Untersuchung der Netzhaut im lebenden Auge, Forstner, Berlin 1851.
9. Heitz RF. Earliest visualizations of the living eye's fundus by immersion in water. Archiwum Historii I Filozofii Medycyny. 2012;75:11–5.
10. Kussmaul A. Die Farben-Erscheinungen im Grunde des menschlichen Auges. Heidelberg: Groos; 1845.
11. Czermak JN. Ueber eine neue Methode zur genaueren Untersuchung des gesunden und kranken Auges [in:] Vjschr prakt Heilk. 1851;8:154–65.
12. Coccius AE. Ueber die Ernährungsweise der Hornhaut und die Serum führenden Gefässe im menschlichen Körper. Leipzig: Muller; 1852.
13. Coccius AE. Ueber die Anwendung des Augen-Spiegels nebst Angabe eines neuen Instruments. Leipzig: Muller; 1853.
14. Reese PD. The neglect of Purkinje's technique of ophthalmoscopy prior to Helmholtz's invention of the ophthalmoscope. Ophthalmology. 1986;93:1457–60.
15. Gałęzowski X. Etude ophtalmoscopique sur les altérations du nerf optique et les maladies cérébrales dont elles dépendent. Paris: Librairie de L. Leclerc; 1866.
16. Lucas RJ, Freedman MS, Munoz M, Garcia-Fernandez JM, Foster RG. Regulation of the mammalian pineal by non-rod, non-cone, ocular photoreceptors. Science. 1999;284:505–7.
17. Schmidt TM, Chen SK, Hattar S. Intrinsically photosensitive retinal ganglion cells: many subtypes, diverse functions. Trends Neurosci. 2011;34:572–80.
18. Zhao L, Zabel MK, Wang X, et al. Microglial phagocytosis of living photoreceptors contributes to inherited retinal Degeneration. EMBO Mol Med. 2015. doi:10.15252/emmm.201505298.
19. Huang D, Swanson EZ, Lin CP, et al. Optical coherence tomography. Science. 1991;254: 1178–81.
20. Swanson EA, Izatt JA, Hee MR, et al. In vivo retinal imaging by optical coherence tomography. Opt Lett. 1993;18:1864–6.
21. Fercher AF, Hitzenberger CK, Drexler W, et al. In vivo optical coherence tomography. Am J Ophthalmol. 1993;116:113–4.
22. Hee MR, Puliafito CA, Wong C, et al. Optical coherence tomography of the human retina. Arch Ophthalmol. 1995;113:325–32.
23. Puliafito CA, Hee MR, Lin CP, et al. Imaging of macular diseases with optical coherence tomography. Ophthalmology. 1995;102:217–29.
24. Galetta KM, Calabresi PA, Frohman EM, Balcer LJ. Optical coherence tomography (OCT): imaging the visual. Pathway as a model for neurodegeneration. Neurotherapeutics. 2011;8: 117–32.
25. Green A, McQuaid S, Hauser SL, Allen IV, Lyness R. Ocular pathology in multiple sclerosis: retinal atrophy and inflammation irrespective of disease duration. Brain. 2010;133:1591–601.
26. Cettomai D, Hiremath G, Ratchford J, et al. Associations between retinal nerve fiber layer abnormalities and optic nerve examination. Neurology. 2010;75:1318–25.
27. London A, Benhar I, Schwartz M. The retina as a window to the brain-from eye research to CNS disorders. Nat Rev Neurol. 2013;9:44–53.
28. Sivak JM. The aging eye: common degenerative mechanisms between the Alzheimer's brain and retinal disease. Invest Ophthalmol Vis Sci. 2013;54:871–80.

Chapter 2
OCT Technique – Past, Present and Future

Tigran Kostanyan, Gadi Wollstein, and Joel S. Schuman

Abstract Optical coherence tomography (OCT) has become the cornerstone technology in clinical and research imaging in the past two decades. OCT performs in vivo, real-time, noncontact scanning and provides cross-sectional and volumetric images with a resolution approaching that of histology. The technology is used in various medical disciplines, but it is still most profoundly used in the field of ophthalmology where it was initially applied. OCT is continuously evolving with newly developed applications.

This chapter will describe the basic principles of OCT techniques, its history, current status, and major ophthalmic applications and research that will determine the future of the technology.

Keywords Time domain (TD-) OCT • Spectral domain (SD-) OCT • Swept source (SS-) OCT • Polarization sensitive (PS-) OCT • Adaptive optics (AO) • OCT blood flow

Abbreviations

OCT	Optical coherence tomography
RNFL	Retinal nerve fiber layer
TD	Time-domain

T. Kostanyan, MD
Department of Ophthalmology, University of Pittsburgh School of Medicine, UPMC Eye Center, Eye and Ear Institute, Ophthalmology and Visual Science Research Center, Pittsburgh, PA 15213, USA

G. Wollstein, MD • J.S. Schuman, MD (✉)
Department of Ophthalmology, University of Pittsburgh School of Medicine, UPMC Eye Center, Eye and Ear Institute, Ophthalmology and Visual Science Research Center, Pittsburgh, PA 15213, USA

Department of Bioengineering, Swanson School of Engineering, University of Pittsburgh, Pittsburgh, PA 15213, USA
e-mail: schumanjs@upmc.edu

A. Grzybowski, P. Barboni (eds.), *OCT in Central Nervous System Diseases: The Eye as a Window to the Brain*, DOI 10.1007/978-3-319-24085-5_2

SD	Spectral domain
FD	Fourier domain
SS	Swept source
AO	Adaptive optics
PS	Polarization sensitive
2D	Two-dimensional
3D	Three-dimensional
CCD	Charge-coupled device
ONH	Optic nerve head
ILM	Internal limiting membrane
IS	Inner segment
OS	Outer segment
RPE	Retinal pigment epithelium
LC	Lamina cribrosa
RGC	Retinal ganglion cell
IPL	Inner plexiform layer
GCC	Ganglion cell complex
EDI	Enhanced depth imaging

2.1 Introduction

Optical coherence tomography (OCT) is a diagnostic imaging technology that has gained a leading position in research and clinical practice due to its ability to obtain noncontact, in vivo, high-resolution, micron-scale images of tissue structures. OCT makes *in situ* imaging of tissue microstructure possible with a resolution approaching that of light microscopy histology without the need for tissue excision and processing, referred to as *optical biopsy* [1].

The technology uses the principle of low-coherence interferometry, which was originally applied to ophthalmology for in vivo measurements of the axial length of the eye [2]. OCT has been used to visualize various types of biological tissue [1, 3–9], but it is most profoundly used in ophthalmology due to the almost perfect optical accessibility of the eye.

At the time of introduction, the technology was used to acquire in vivo cross-sectional images of the anterior segment [10], as well as retinal pathologies such as macular edema, epiretinal membranes, macular holes, macular detachment, and idiopathic central serous chorioretinopathy [11]. Optic disc and retinal nerve fiber layer (RNFL) measurements were obtained with OCT shortly afterward [12–14].

OCT has evolved significantly, with improvements in both imaging method and image analysis. The evolution of OCT began with the time domain (TD) technique, followed by spectral domain (SD) and later newer iterations with faster scanning aquisition speeds [15–17] and higher axial resolution [18, 19].

This chapter will describe the basic principles of OCT techniques, its history, current status, and major ophthalmic applications and research that will determine the future of the technology.

2.2 Basic Principles

OCT provides cross-sectional and volumetric images of areas of interest by acquiring either the echo time delay or frequency information of back-reflected light. Differences in the optical properties of biological tissues allow the recognition of layered structures. The speed of light makes it impossible to analyze the acquired information directly, since it would be in the order of femtoseconds, thus OCT systems use the optical technique known as *interferometry*. Low-coherence interferometry enables analysis of this information and the creation of a depth-resolved reflectivity profile (A-scan) of the scanned tissue by matching the light profiles from the scanning and reference arms.

Utilization of light provides OCT technology the ability to obtain images in a non-contact fashion and to achieve resolutions of 1–15 μm, which is one to two orders of magnitude finer than other conventional clinical imaging technologies such as ultrasound, computerized tomography, or magnetic resonance. Light is highly absorbed or scattered in most biological tissues, and therefore the use of this technology is limited only to locations that are optically accessible or that can be imaged using devices such as endoscopes or catheters.

OCT technique can be classified into two major groups: TD and Fourier (or frequency) domain (FD). FD can be further classified into spectral-domain (SD) and swept-source (SS) techniques. In TD-OCT, a broad-bandwidth laser or a low-coherence superluminescent diode light source projects light that is then divided into two arms by a partially reflecting mirror (beam splitter). In the first arm light is projected toward the sampling location, while in the second arm light is projected toward a moving reference mirror at a known position. The backscattered light from both sites travel back to a detector and recombine to form an interference pattern, which is sensed by the interferometer. The interference is only observed when both the sample and the reference arm light beams travel the same distance [12]. Changing the position of the reference mirror allows the machine to sequentially acquire information from different depths in the tissue sample. A cross-sectional image, also known as a B-scan, is generated by performing fast, subsequent axial scans (A-scans) at different transverse positions. Each axial scan represents the echo time delay of back-reflected light from the tissue and gives a profile of the tissue's dimensions along the optical beam. The scanning speed of TD-OCT technology is limited to 400 axial scans/sec, due to the maximal oscillating speed of the reference mirror [20].

SD-OCT is similar in principle, but the data acquisition varies slightly, yet fundamentally, from TD-OCT. The main difference of this iteration is the use of light frequency information instead of time delay data to determine the spatial location of reflected light. SD technology utilizes the Fourier transformation of the reflected light frequencies to encode distances within tissue microstructure [21]. Instead of a moving reference mirror, the mirror is stationary and the interference signal is split into its frequency components using a diffraction grating. The signal is simultaneously detected by a charge-coupled device (CCD). The CCD has an array of photodetectors that are each sensitive to a range of specific frequencies [22, 23].

SD technology allows the acquisition of information from all points along each A-scan simultaneously, substantially increasing scan speed to the range of ~25,000–

75,000 axial scans/sec in the commercially available systems [24, 25] and up to 20.8 million axial scans/sec in research devices [16]. The substantial increase in scanning speed allows for the acquisition of three-dimensional (3D) data sets, which is done by combining rapidly acquired subsequent cross-sectional scans. The wide bandwidth of the light source also enables a substantial enhancement in axial resolution up to 1 μm [26, 27] and an improved signal-to-noise ratio [28].

SS-OCT is a form of Fourier domain technology that uses a single tunable laser that sweeps through different frequencies to rapidly cover the entire broad spectrum. The reflectance of the light from the scanned area is captured by a photodetector, which is much faster than the CCD camera used in SD-OCT technology [17, 29]. This allows the SS technology to further enhance the scanning speed up to 400,000 axial scans/sec. Another important advantage of this iteration of OCT technology is the absence of the depth dependent signal drop-off observed with SD-OCT technology [30]. Most SS-OCT devices operate with light sources centered at around 1030 μm (compared with 840 μm in the commercially available TD- and SD-OCT), which reduces the axial resolution to approximately 8 μm but allows for better penetration of the tissue. The combination of improved tissue penetration and reduced signal attenuation allow detailed scanning of structures such as the choroid and the lamina cribrosa inside the optic nerve head. The major characteristics of these three different OCT techniques are presented in Table 2.1.

The key technological parameters that are typically used to characterize OCT technology are the wavelength of the light source, axial or longitudinal resolution,

Table 2.1 Comparison of TD-, SD-, and SS-OCT technologies

Technology	Light source	Ophthalmic device commercially available	Primary advantages	Primary disadvantages
TD-OCT	Relatively narrow band width	Yes	Intensity information acquired in time domain; no complex conjugate image	Moving reference mirror required, limiting acquisition rate
SD-OCT	Broadband width	Yes	No moving reference mirror required; higher resolution than TD-OCT; high scanning speed and axial resolution can be attained	Noticeable signal drop-off with depth
SS-OCT	Narrow band, swept through broad range	Yes	No moving reference mirror required; very high scanning speeds can be attained; minimal signal drop-off with depth	Most ophthalmic systems are operating at longer wave lengths ($\lambda = 1–1.3$ μm) with lower axial resolution than SD-OCT but with improved penetration into structures

lateral or transverse resolution, scanning speed, and imaging depth. The wavelength is inversely related to the axial resolution of the acquired images, with longer wavelength providing lower resolution compared with shorter wavelength.

Axial resolution determines the smallest distance along the axial direction where two adjacent points are discernable, and it is related to the bandwidth or the coherence-length of the source. In posterior segment eye imaging, the light should travel through transparent media, which mostly contains water that absorbs infrared radiation. This limits the technology to the use of light sources of only certain wavelength. Current commercial OCT devices achieve axial resolutions up to 4 μm, and research systems achieve up to ~ 1–2 μm [19].

Transverse resolution is independent of the coherence properties of the light source, and is determined by the spot size, which is limited by the optics of the scanned system. As such, the transverse resolution of OCT among the different generations is within a range of 15–20 μm. Improving the transverse resolution requires the correction of the optical aberrations of the eyes using technologies such as adaptive optics.

Scanning speed is dictated by mechanical constrains such as the maximal oscillating rate of the reference arm (TD-OCT) and the sensitivity of the detector to the back-reflected light. As scanning speed increases, the time the detector remains in the same location is shorter, thus reducing the light that can be detected in each location. Since the power of the projected light is limited in order to be within safety limits, faster scans require a more sensitive detector that can function with a lower level of light.

The imaging depth in TD technology is given by the reference arm's range of movement, while in SD technology it is related to the center wavelength. Longer wavelengths provide increased imaging depth [31, 32], but the use of longer wavelengths for imaging depth improvement is limited by the increased optical absorption of water [33].

2.3 The Past

OCT technology was first described by Huang and colleagues in 1991 [34]. The authors scanned human retinas and atherosclerotic plaques ex vivo with a prototype device using infrared light at a ~ 800-nm wavelength. The axial resolution of cross-sectional images of the retina, optic nerve, and coronary artery wall was 15 μm, which allowed the visualization of some retinal layers, optic nerve head structures, and the composition of the coronary artery. In vivo retinal scanning was conducted using a prototype device based on a slit-lamp biomicroscope that was modified to provide a view of the fundus while scanning with OCT. The development of scan patterns that enabled the acquisition of reproducible measurements [35] led to the use of the technology in clinical practice.

The first commercially available OCT, called OCT 1000, was marketed in 1996 by Zeiss (Dublin, CA). The technology went through two iterations, resulting in OCT 2000 in the year 2000 and then OCT three (Stratus OCT), which became commercially available in 2002. The Stratus OCT had an axial resolution of ~10 μm, a

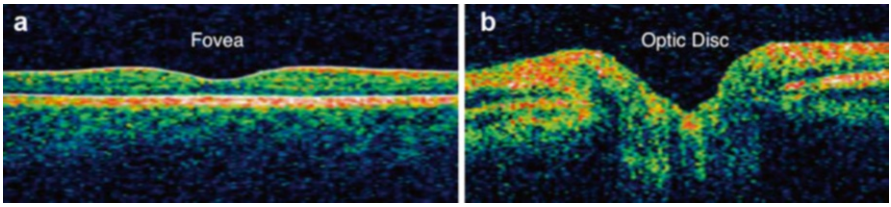

Fig. 2.1 OCT image of a healthy fovea (**a**) and optic disc (**b**). Images were obtained using TD technology and have an axial resolution of ~10 μm

transverse resolution of 20 μm, and a scan speed of 400 axial scans/sec [1, 12]. The typical cross-sectional scan was composed of 128–512 axial scans, comprising an image area of 4–6 mm.

Due to its ability to obtain quantitative and reproducible measurements of the macula [36, 37], retinal nerve fiber layer thickness [35, 38], and optic nerve head [39, 40], TD-OCT technology became the gold standard in-vivo clinical imaging device for posterior segment pathologies in a relatively short period of time. Figure 2.1 shows an example of a cross-sectional scan of the macula and the ONH of a healthy eye obtained with TD technology (Stratus OCT).

The most routine scan patterns used with TD-OCT were a scan comprises of six equally spaced radial scans through the macula (6 mm diameter) and optic nerve (4 mm) and a circular scan with a diameter of 3.4 mm centered on the optic nerve head (ONH). Using automated segmentation, the macular thickness (internal limiting membrane (ILM) to the photoreceptor inner segment-outer segment (IS–OS) junction) can be quantified from the macular scan pattern, and the retinal nerve fiber layer (RNFL) thickness measurements can be quantified from the circumpapillary scan. Cup area, disc area, cup diameter, disc diameter, and rim area are provided after the software detects the ONH margin, allowing quantification of the ONH.

Several improvements in OCT hardware have been introduced since the first commercial TD-OCT system became available. Better axial resolution [26, 27] and increased scanning speed [22, 41] are the two main advancements that were incorporated into the commercial systems. Ultra-high resolution OCT retinal imaging that used specially designed broadband light sources was introduced in 2001 [42]. This OCT device had an axial resolution of ~3 μm, which was markedly better than the 10 μm axial resolution provided by the commercial devices at that time [42, 43]. Further improvements in OCT technology lead to the introduction of SD-OCT (discussed in detail in the next section) which had a faster scanning speed and better resolution than TD-OCT. This can be easily appreciated by comparing Figs. 2.1 and 2.2, in which the same healthy eye was scanned with TD- and SD-OCT, respectively.

In addition to acquiring tissue structural information, OCT has been incorporated into multimodal imaging systems that provide further insight into the functional characteristics of tissue [44–50].

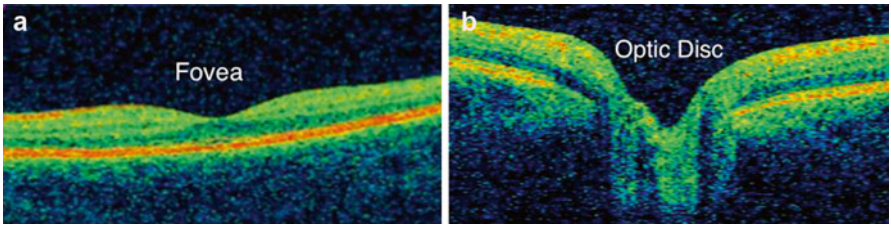

Fig. 2.2 OCT image of a healthy fovea (**a**) and optic disc (**b**). Images were obtained using SD technology and have an axial resolution of ~5 μm

2.4 The Present

OCT has become a key ophthalmic diagnostic imaging tool due to its ability to provide reliable and reproducible information about tissue microstructure. The majority of current commercial OCT systems use SD technology for posterior eye imaging and can visualize the cross-sectional structure of the retina and optic disc [1, 51]. OCT is used extensively in the diagnosis and management of a wide range of ocular pathologies including glaucoma, age-related macular degeneration, macular edema, macular holes, diabetic retinopathy, alterations in the vitreoretinal interface, papill-edema, and others. OCT systems possess different built-in scanning protocols for obtaining data on macular, peripapillary, and optic disc structures. In addition to providing a cross-sectional and volumetric dataset of the scanned area, individual layers and structures of the retina and optic disc are measured by automatic image processing. In many devices, these measurements are compared to normative data acquired from the population, with some devices also factoring in ethnicity. The comparison with normative data simplifies the recognition of abnormal locations. The ability of OCT to provide reproducible, quantitative information makes it useful in tracking small changes in tissue structure along the course of disease.

Some scan patterns used in SD-OCT are similar to those described above for TD-OCT, but a dramatic increase in scanning speed substantially extended the abilities of SD-OCT. SD-OCT is able to acquire a larger number of axial scans or transverse pixels per image, as well as a larger number of cross-sectional images for a given scan time, which results in improved image quality and retinal coverage. The faster scanning speed reduces eye motion artifacts, due to the shorter acquisition time, and improves the accuracy of the acquired images. The faster scanning speed also enables the acquisition of a 3D volumetric dataset in a time comparable to that of the scanning protocols of previous generations OCT. A 3D dataset allows a thorough sampling of the scanned region, advanced post-processing, and improved registration of consecutive scans. One of the common uses of the advanced processing is the OCT en face image generated by integrating each individual axial-scan [52]. The en face image is similar to the conventional retinal fundus view and can be used for subjective assessment of image quality, comparison with clinical findings, and to assist with correcting eye motion that may have occurred during the scan. The en

face view can be used to further focus on slab within the region of interest, allowing detailed visualization of structures such as the fine intra-retinal vascular network.

Evaluation of the ONH using SD-OCT can provide important diagnostic information in multiple ocular and central nervous system pathologies. Figure 2.3 shows an OCT cross-sectional image of a healthy optic disc (a) and a 3D volumetric scan (b).

ONH imaging is performed using different scan patterns among the various commercially available SD-OCT devices. This includes 3D cube scans, radial scans, circular scans, and a combination of radial and concentric scans. The 3D volumetric cube is obtained by the raster scanning of a square area centered on the ONH. The radial scan is composed from various numbers of cross-sections at equal angular orientation all centered on the ONH. Circular scans are centered at the ONH, similar to the scan pattern performed with TD-OCT. A scan that is a combination of a radial and concentric scan is beneficial because it features dense sampling adjacent to the intersection of the radial scans while the circular scanning at the periphery fill in the gaps between the radial scans that are further out from the intersection. All of the devices can automatically detect the optic disc boundaries from each acquired image as the location at which the photoreceptor layer, retinal pigment epithelium (RPE), and choriocapillaries terminate.

One of the most useful measurements provided by OCT is the circumpapillary RNFL thickness, which quantifies the retinal ganglion cell's axons from the entire retina on their way toward the ONH. This measurement can be extracted from a circle centered on the ONH with a diameter of 3.4 mm, similar to the method used in TD-OCT. The limitation of this approach is that the sampling of the tissue is performed only along the circle, and therefore any misplacement of the circle during repetitive scanning will result in increased measurement variability.[53] Another option is to extract the RNFL thickness from the 3D cube scanning pattern. This

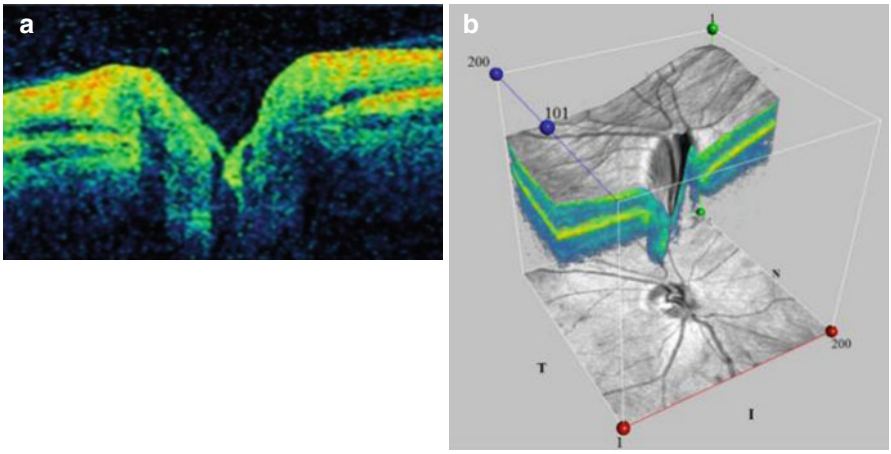

Fig. 2.3 Cross-sectional (**a**) and volumetric (**b**) SD-OCT imaging of the optic nerve head of a healthy eye

method can ensure that the tissue sampling location is consistent through multiple scans, as the repositioning of the circle is possible if needed.

SD-OCT devices provide average RNFL thickness measurements, thicknesses in four quadrants (temporal, superior, nasal and inferior) and sectoral thicknesses at each of the 12 clock-hours or in 16 equal sectors. The RNFL thickness profile in the peripapillary region follows the ISNT rule, with thickest RNFL seen in the inferior quadrant, followed by superior, nasal and temporal quadrants.

Several devices also report the RNFL thickness as a color-coded thickness map of the entire peripapillary region. This map provides additive information to the circumpapillary RNFL thickness, as it can highlight small, localized thinning or defects outside the circumpapillary sampling location.

Figure 2.4 shows Cirrus HD-OCT ONH scan printout that provides the RNFL thickness map (a) and cross-section (c). The deviation map (b) compares the RNFL measurements at each superpixel with an age-matched normative database, and locations thinner than the lower 95 % of the normal range are highlighted. At the

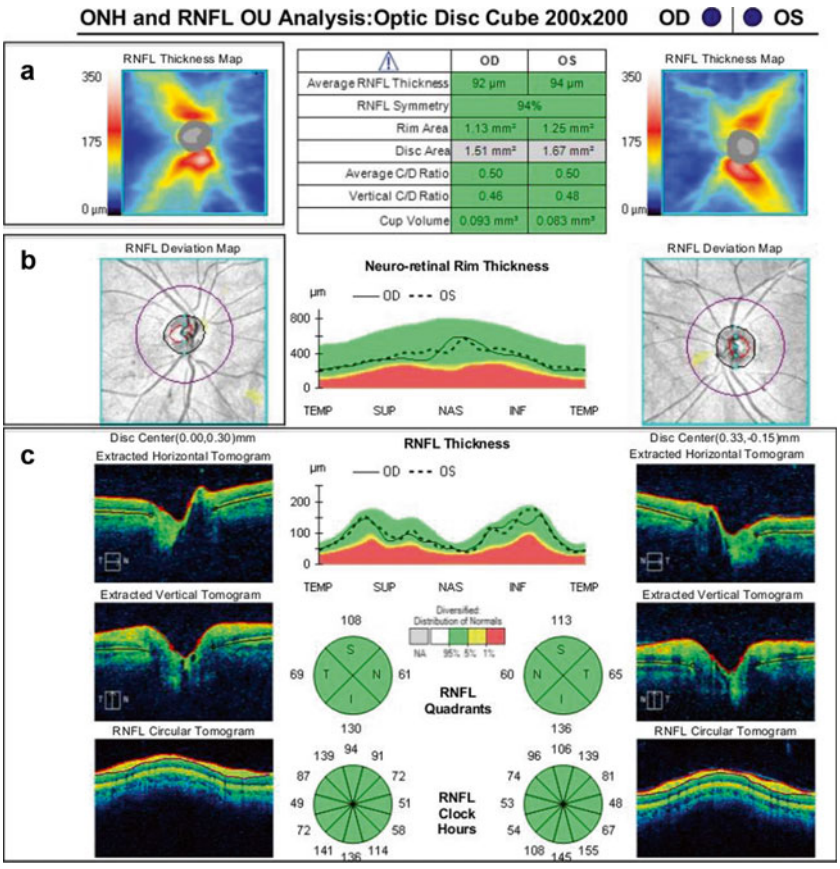

Fig. 2.4 Cirrus HD-OCT ONH scan printout with RNFL thickness map (**a**), deviation map (**b**) and cross section (**c**)

center panel quantitative parameters are provided for ONH structures, along with RNFL thickness. The background coloring reflects the comparison with the normative results, with green representing the normal range, yellow representing <5 % of the normal population, and red representing and <1 %.

Figure 2.5 demonstrates the circumpapillary RNFL scans obtained with the Spectralis OCT (a). Spectralis measure RNFL thickness by assessing a total of 2,325 data points along the sampling circle, and the built-in software constructs the final cross-section by averaging 16 consecutive B-scans. The averaging of multiple scans reduces the background noise and improves signal quality. The actual thickness values and color-coded comparison results are presented as global average thickness, thickness in four quadrants, and thickness in six sectors (b).

The RTVue Premier peripapillary scan acquire 13 circular scans with diameters of 1.3–4.9 mm centered on the ONH. The comparison with the normative database is performed in 16 sectors and presented as the deviation map that surrounds the RNFL thickness map in Fig. 2.6a.

The improvements introduced in SD-OCT had a substantial impact on macular imaging. Thorough sampling of the macula, the improved visualization of the retina and choroid, and the ability to automatically segment the various layers of the retina substantially impacted clinical management. The scan patterns that are often used to image the macula include the 3D cube, line and cross-line, raster, mesh, and radial scan patterns. The principle of the volumetric cube scan is similar to the 3D ONH scan patterns described above.

Figure 2.7 shows a macular 3D scan obtained with Cirrus HD-OCT (a) and Spectralis OCT (b) from two different healthy subjects. These types of scans are

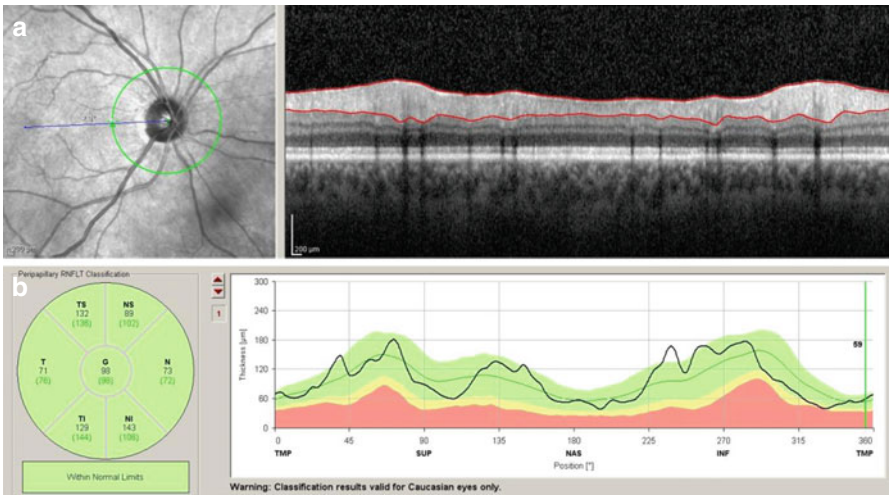

Fig. 2.5 Spectralis OCT RNFL Analysis with circumpapillary RNFL cross section (**a**), thickness profile and sectoral measurements (**b**)

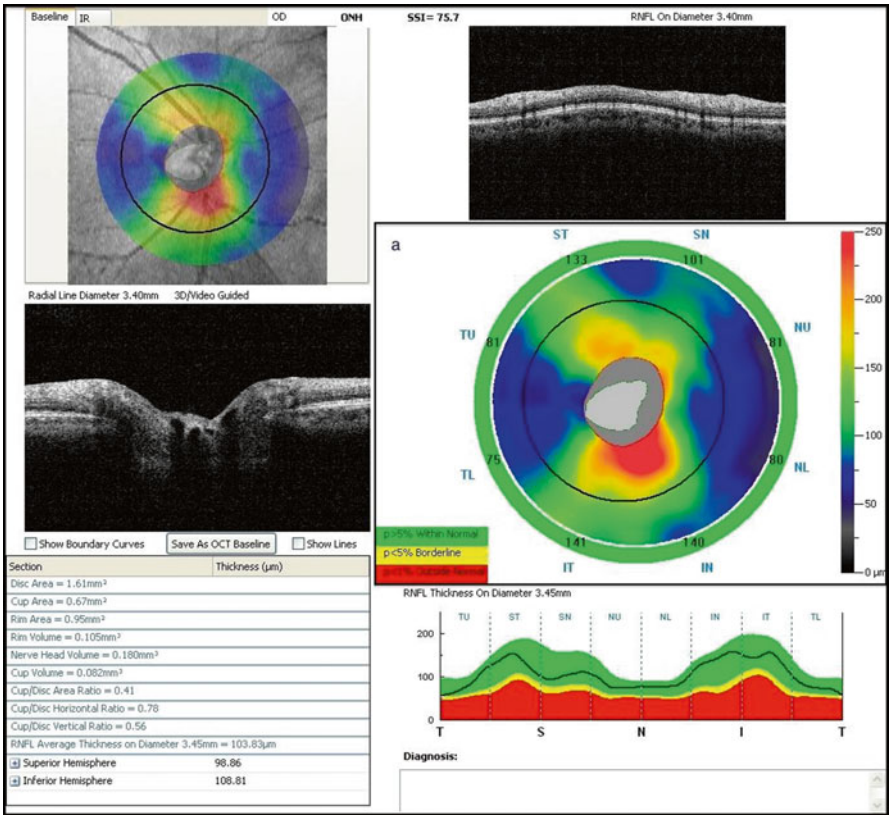

Fig. 2.6 ONH and peripapillary RNFL thickness protocol of RTVue premier

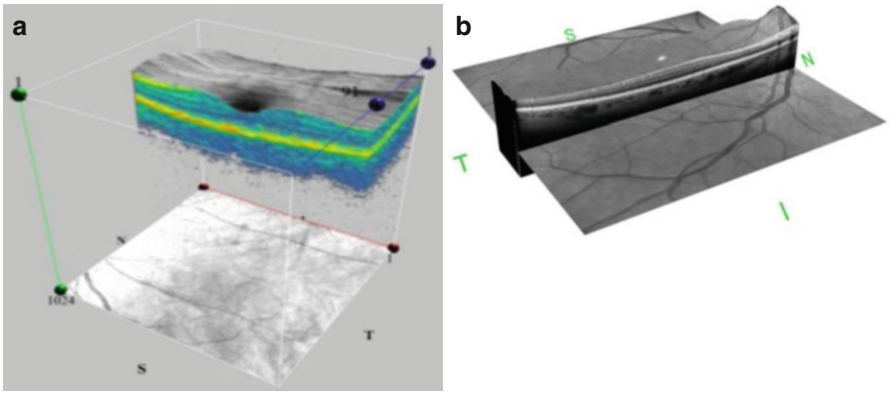

Fig. 2.7 3D-OCT images of healthy maculas obtained with Cirrus HD-OCT (**a**) and spectralis OCT (**b**)

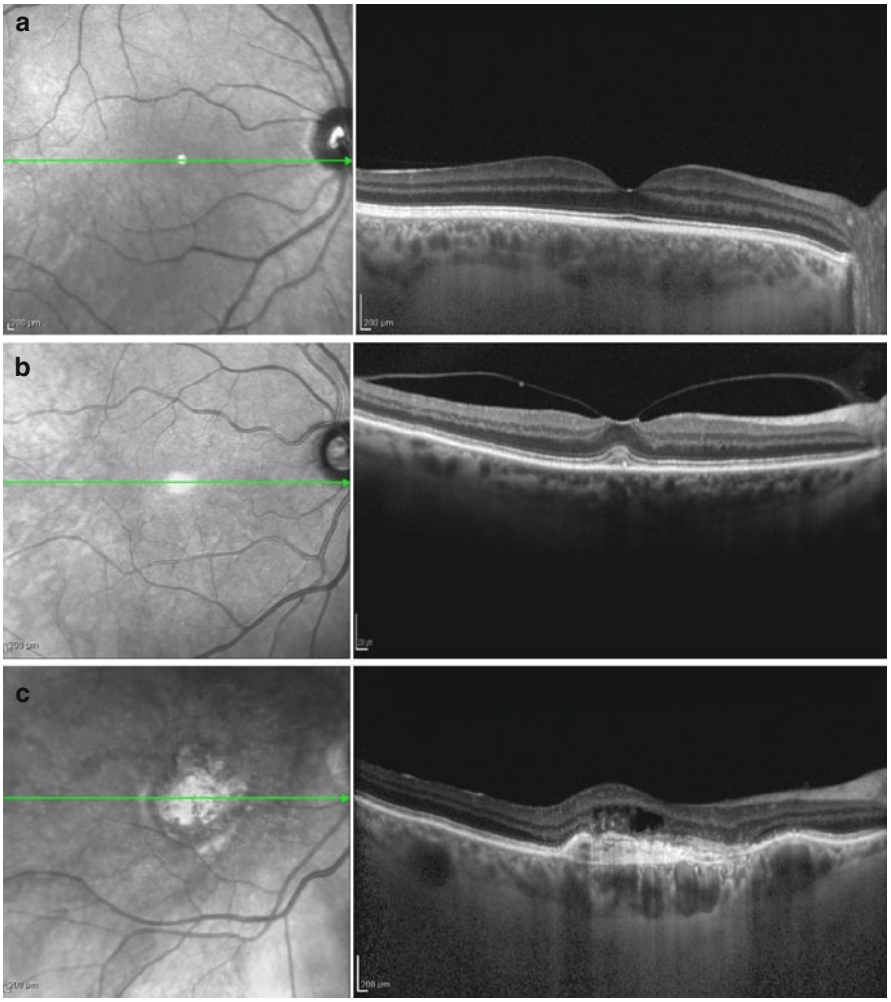

Fig. 2.8 Line scans of the macular region obtained with spectralis OCT from a healthy eye (**a**), and eyes with vitreomacular traction (**b**) and wet age-related macular degeneration (**c**)

often helpful in the estimation of the volume and extent of pathologies in the macula, such as macular edema or macular holes.

Line scans are typically composed from the averaging of multiple scans at the same location, as explained above. This is typically performed along a single location (Fig. 2.8) or along several parallel lines (Fig. 2.9). Line scans are clinically useful for obtaining retinal images with highest level of detail.

Some SD-OCT systems are capable of acquiring scans in horizontal and vertical orientations to provide a mesh scan pattern. The logic behind this scan pattern is that even at a fast scanning rate there is a relatively long temporal gap between adjacent points that are perpendicular to the scan orientation. For example, in a horizontal

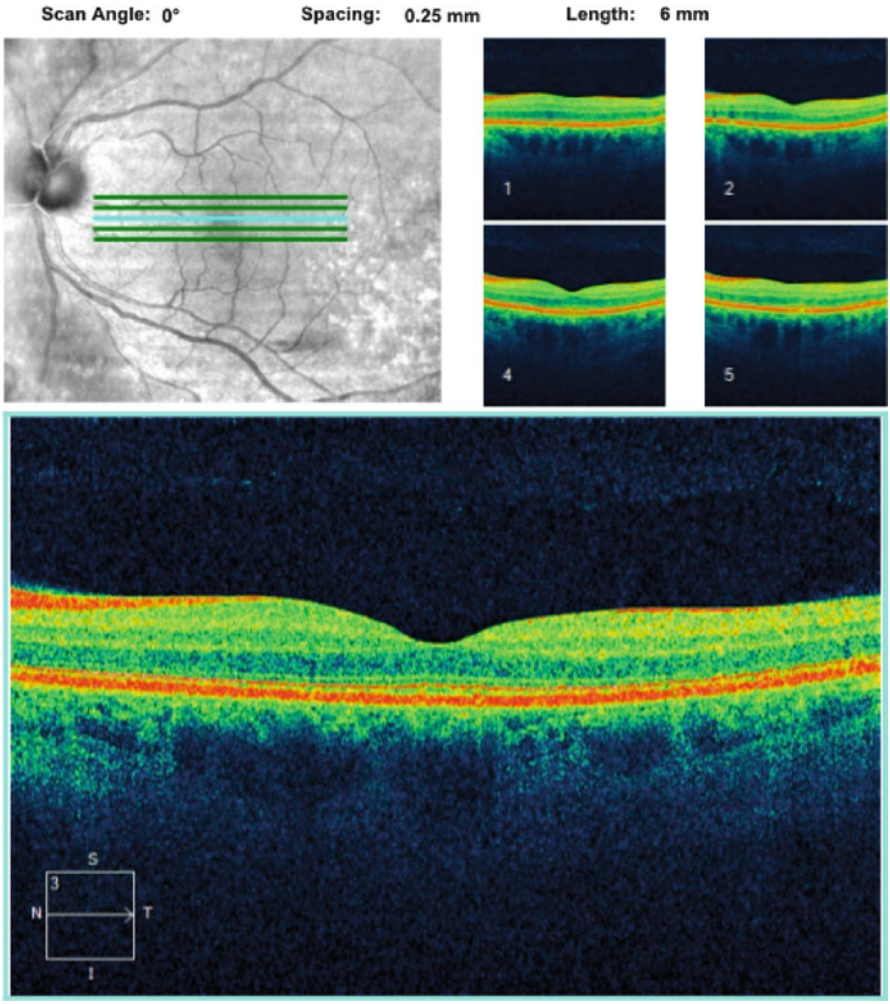

Fig. 2.9 Macular five line raster scanning pattern obtained with cirrus HD-OCT

raster scan, the time gap between adjacent points in the horizontal direction is much shorter than the gap between adjacent points vertically. This can lead to image distortion along the slow axis of the scan. Registering the horizontal and vertical scans together can reduce the distortion in the slow axis and improve scan quality. Figure 2.10 shows a mesh scanning pattern (b) of the macula centered on the fovea with correspondent cross-sectional image (a) obtained with RTVue Premier. The pattern consists of an inner, dense grid and outer grid, visible as white grid lines.

Radial scan protocols acquire multiple evenly spaced linear scans which all intersect at the fovea. This pattern provides information from the entire macular region, with dense coverage near the fovea where the lines intersect and sparse coverage at the macula periphery. Figure 2.11 demonstrates a radial scanning pattern of

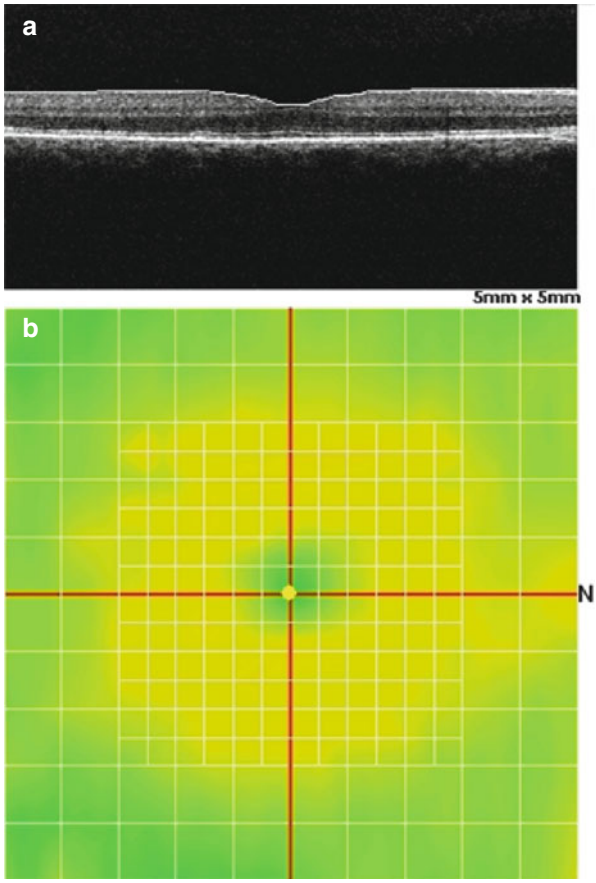

Fig. 2.10 Macular mesh scanning pattern (**a**) obtained with RTVue Premier and (**b**) with corresponding cross-sectional image

the macula from two different healthy subjects using different commercial SD-OCT systems.

The high resolution of SD-OCT allows the acquisition of reproducible segmentation and the analysis of individual macular layers that are of particular diagnostic interest [54, 55]. It has been suggested that three innermost retinal layers: the nerve fiber layer, the retinal ganglion cell (RGC) layer, and the inner plexiform layer (IPL) are directly prone to glaucomatous damage [56]. Cirrus HD-OCT extracts the information from an ellipse (vertical radius of 2 mm, horizontal radius of 2.4 mm) centered on the fovea and provides a combined measurement that includes RGC layer and IPL. The macula protocol of RTVue Premier provides the ganglion cell complex (GCC) that includes the macular NFL, RGC layer, and IPL. The data is captured from a 7 mm^2 area centered 1 mm temporal to the fovea (Figs. 2.12 and 2.13).

Enhanced depth imaging (EDI) is a scanning protocol that allows the acquisition of images from deeper ocular tissues. This method switches the point of maximal focus in the interference signal so that it is centered on deeper tissues. The advantages of this method have been shown in the visualization of the choroid [57], optic nerve head [58], and deeper structures within the optic nerve such as the LC [59].

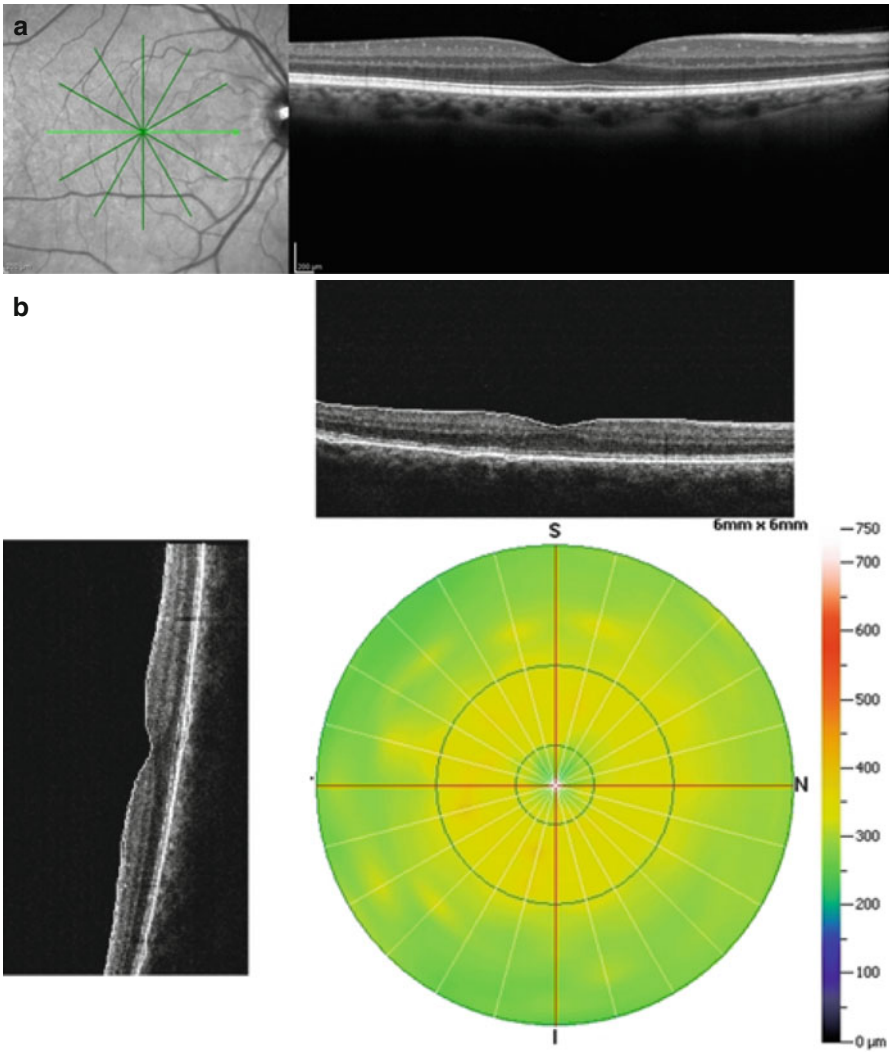

Fig. 2.11 Macular radial scanning pattern obtained with spectralis OCT (**a**) and RTVue premier (**b**)

Because OCT provides highly reproducible micron scale measurements, small structural changes occurring over time due to disease deterioration can be detected. Several commercial SD-OCT devices include a progression analysis tool. Automatic progression algorithms utilize trend-based analysis methods, primarily linear regression analysis, for computing the rate of change in structural parameters over time. The computed rate is compared to a no change slope to determine if the rate is statistically significant. This rate of change is also used to predict future progression beyond the most recent visit. This prediction can be useful when discussing disease forecast with a patient or to assess the effect of treatment modification. Several

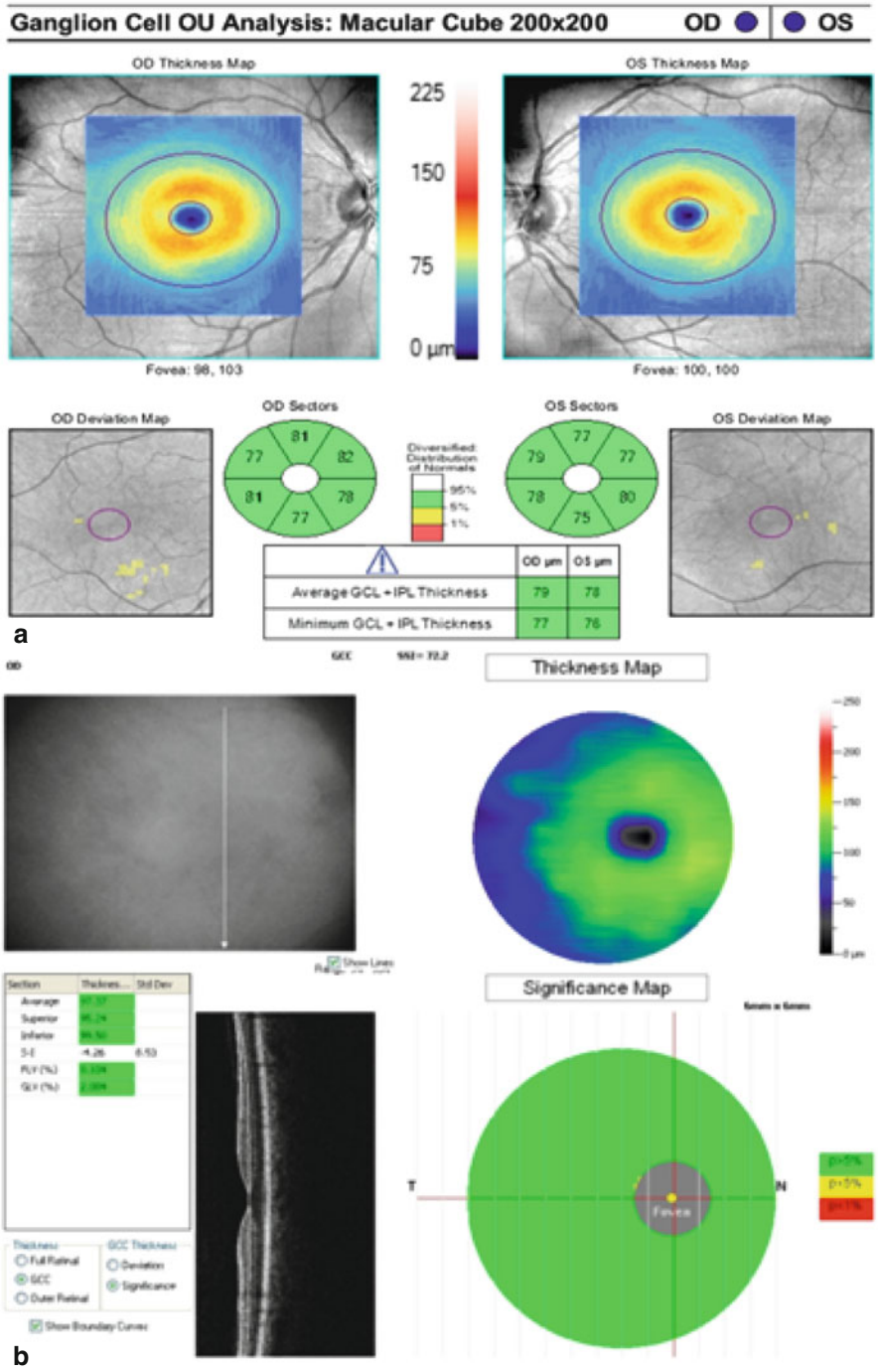

Fig. 2.12 Cirrus HD-OCT ganglion cell analysis (**a**) and RTVue premier GCC analysis (**b**)

commercial devices also provide event-based analysis, where a series of follow up measurements are compared with baseline measurements and progression is defined when measurements exceed a predetermined threshold for change from baseline.

2.5 The Future

As OCT technology keeps rapidly evolving, at the time of this writing several innovative OCT technologies are being tested. The following sections will provide a brief description of some of the most promising developments.

2.6 Swept Source OCT

As previously discussed, SS-OCT is a form of Fourier domain technology that obtains time-encoded spectral information by sweeping a narrow-bandwidth laser through a broad optical spectrum. This method uses a narrow-bandwidth light source and photodetector, in contrast to SD-OCT, which applies a broad bandwidth light source and detects the interference spectra with a CCD camera and spectrometer. The use of a photodetector allows SS-OCT to achieve higher scanning speeds and better sensitivity with imaging depth (Fig. 2.14) [17, 29, 60]. While SD-OCT suffers from signal attenuation along the axial path, SS-OCT is less prone to this effect, maintaining good imaging quality throughout the axial path. In addition, many SS-OCT systems use a light source centered at a ~1050 nm wavelength, allowing for better tissue penetration than SD-OCT, which typically uses a light source centered at ~840 nm. This enables visualization of structures such as the choroid (Fig. 2.15) [61, 62] and lamina cribrosa (LC) (Fig. 2.16) [63, 64] along with structures at the anterior segment of the eye [65]. Increased scanning speed results in a shorter scanning time and the reduction of image distortions caused by motion artifacts, which results in improved scan quality and better visualization of fine structures [15, 66]. These properties can improve visualization of retinal sub-RPE pathologies such as central serous chorioretinopathy, AMD, choroidal tumors, and retinitis pigmentosa [67].

The only commercially available anterior segment SS-OCT device (CASIA SS-1000, Tomey, Nagoya, Japan), at the time of this writing, provides automatic measurements of anterior chamber structures [68]. Examination of the LC and posterior sclera might improve the understanding of the mechanical aspects of glaucoma pathogenesis [69, 70].

The fast scanning speed of the SS-OCT allows the acquisition of widefield scans covering large areas of the fundus [71]. Another investigative development is a scanning method that allow the acquisition of data from the entire eyeball, from the cornea to the retina [72]. The clinical utility of all these features is still under investigation.

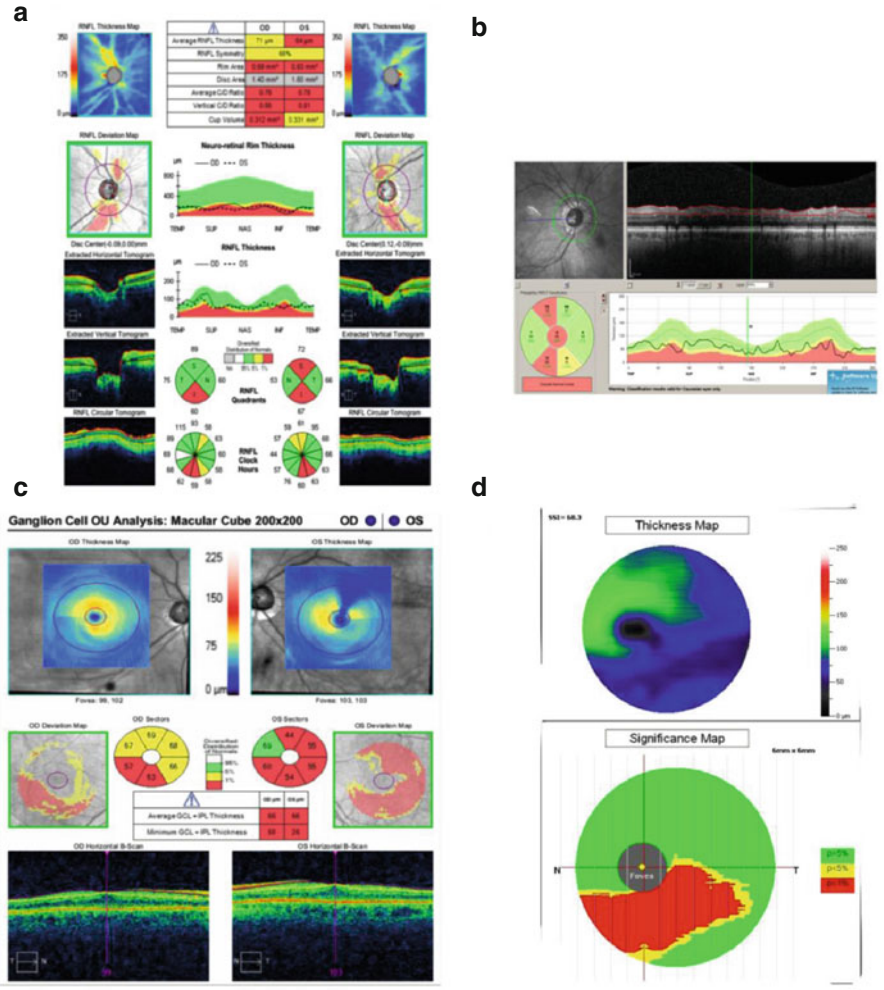

Fig. 2.13 Automated analysis for the detection of glaucomatous retinal and optic nerve damage provided by cirrus HD-OCT in the ONH region (**a**) and macula (**c**), spectralis OCT of the ONH (**b**), and RTVue premier of the macula (**d**)

2.7 Adaptive Optics

Adaptive optics (AO) is an optical method designed to dynamically adjust monochromatic aberrations in optical systems. AO was initially used in astronomy for correcting distortions of light passing through the atmosphere. The first in vivo examination of the retina with an AO fundus camera using a Hartmann-Shack wavefront sensor and a deformable mirror was introduced in 1997 [73]. A few years

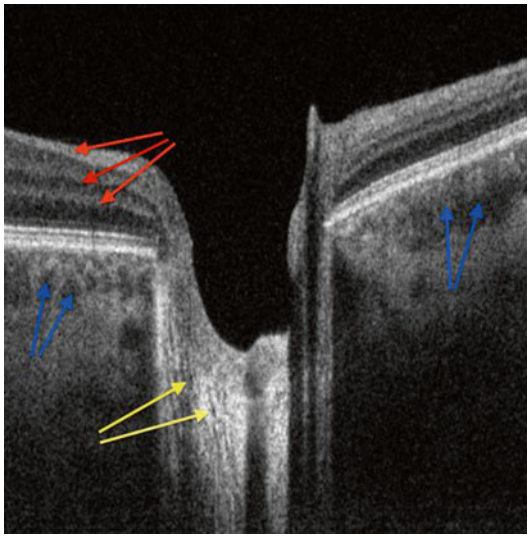

Fig. 2.14 Swept-source OCT cross section. The same scan can capture retinal layers (*red arrows*), nerve fiber fascicles passing through lamina cribrosa (*yellow arrows*), and choroidal vessels (*blue arrows*) because this technology is less prone to signal drop-off in comparison with other OCT iterations

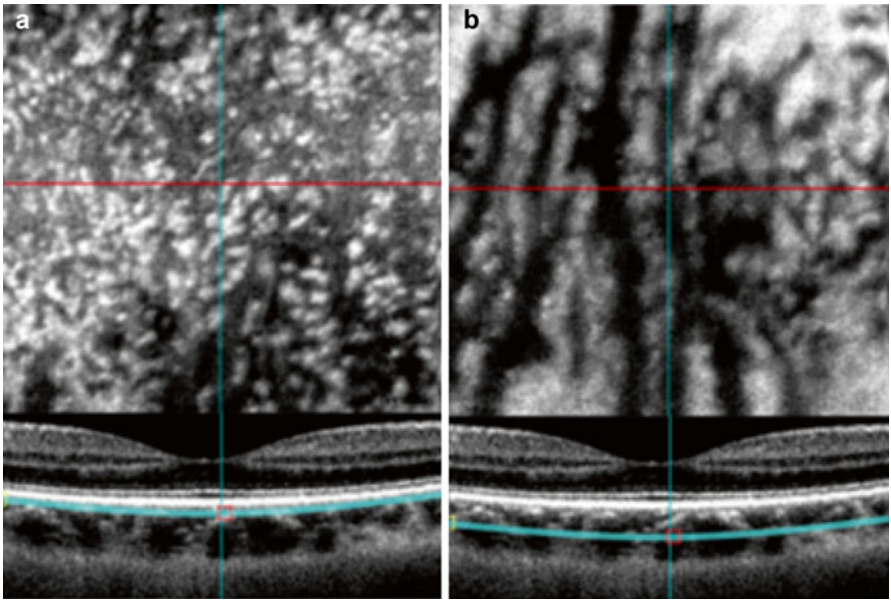

Fig. 2.15 Swept-source OCT macular cross-section. The upper panel of the figure demonstrates en-face image of choriocapillaries (**a**) and choroid (**b**) with correspondent cross-sectional scans at the bottom panel. The thick turquoise line in the cross-section images marks the plane where the en-face is acquired

later, AO was combined with scanning laser ophthalmoscope [74] and OCT systems [75, 76]. The transverse resolution of all conventional OCT systems is limited to the range of 20 μm due to the optical aberrations of the light beam when passing through

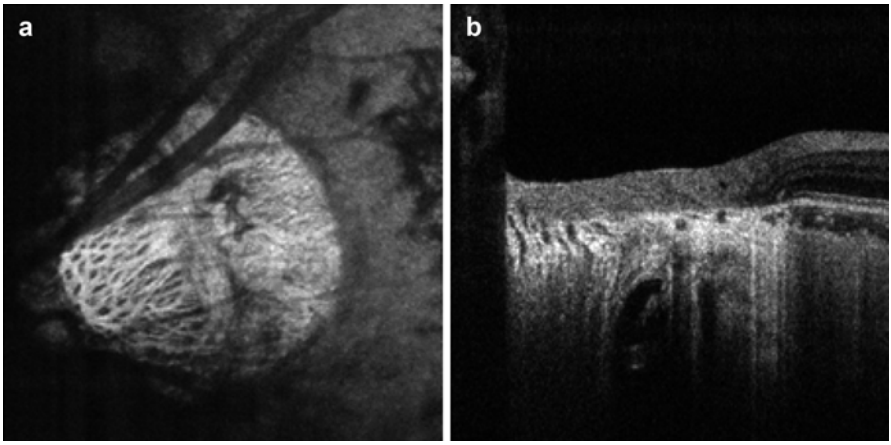

Fig. 2.16 Swept-source OCT lamina cribrosa en-face and cross-section. En-face image (**a**) of lamina cribrosa demonstrating the intricate structure of the hyperreflective beams (*white*) and hyporeflective pores (*black*) with corresponding cross-sectional scan (**b**)

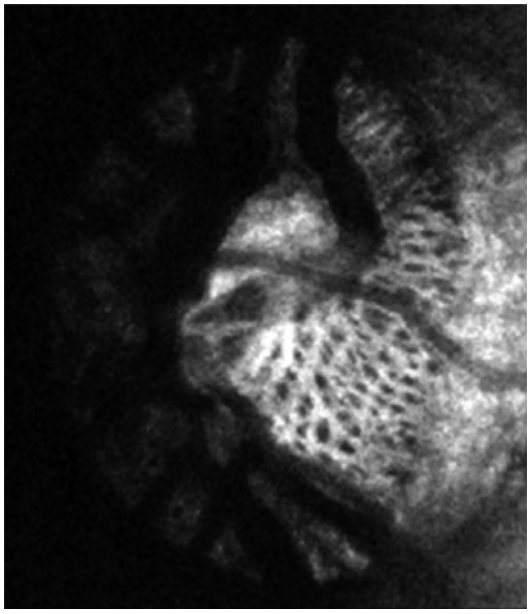

Fig. 2.17 Adaptive optic SD-OCT en-face lamina cribrosa image demonstrating the highly detailed visualization of this complex structure

various media in the eye. AO measures and corrects the optical aberrations, reduces the projected spot size, and improves the transverse resolution to the range of 5–10 μm [75]. This resolution allows the acquisition of highly detailed images, enabling the visualization of fine details such as the retinal microvasculature, photoreceptor mosaic [77], LC (Fig. 2.17), and microstructures within the RNFL [18, 78] and ganglion cell layer. The ability to acquire highly detailed in vivo images of

these structures allow further insight into ocular anatomy in health and disease, providing the opportunity to expand the understanding of pathologic processes in the eye.

The major limitation of the AO technique is the small field of view, which is restricted to approximately 1° to 3°. The use of an eye-tracking system to acquire a series of neighboring scans to cover a larger volume might resolve this limitation, though the longer scanning time might prohibit large scale clinical use [79]. Similarly, the focusing depth of the AO technique is also limited, and therefore acquiring high quality images of structures such as the choroid and retina in the same image is difficult to obtain. It may be possible to address this limitation by varying the focal plane while scanning in depth [80, 81].

2.8 Polarization Sensitive OCT

Polarization sensitive OCT (PS-OCT) uses the polarization state of polarized light for the assessment of tissue function [44]. Different ocular structures and tissues alter the polarization state of light in different ways, such as through birefringence (sclera, RNFL), polarization-preservation (photoreceptors), and depolarization (RPE) (Fig. 2.18). PS-OCT estimates these light state alterations by simultaneously measuring intensity, retardation, and optic axis information, thus providing both tissue structural and functional information. The technology was initially incorporated

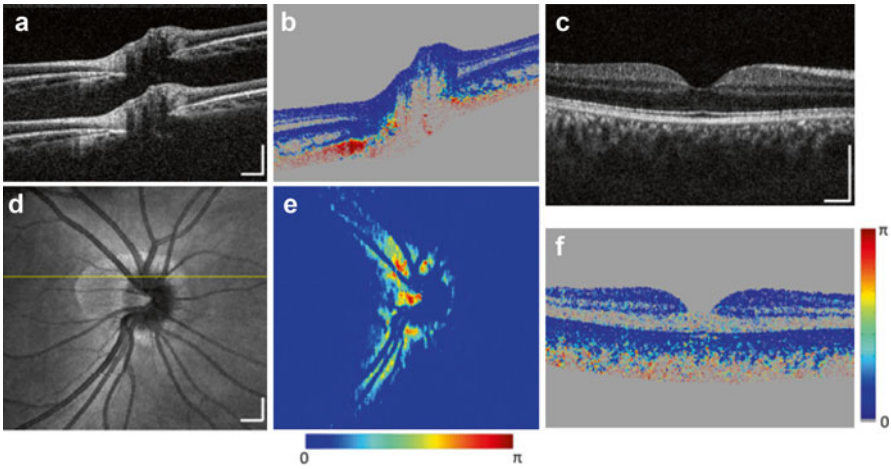

Fig. 2.18 PS-OCT optic nerve head and retinal imaging in healthy subjects. (**a**) A cross-sectional intensity image with two depth-encoded copies of the optic nerve head region. (**b**) Corresponding PS-OCT image shows high retardance in the RNFL and sclera. (**c**) OCT fundus image. (**d**) Corresponding PS-OCT map shows high retardance around the optic nerve head region. (**e**) A cross-sectional intensity image at the fovea region. (**f**) Corresponding PS-OCT image shows low retardance in the retinal layers. Scale bar: 500 μm

into TD-OCT system, with subsequent introduction into all known OCT iterations such as SD-OCT [49], SS-OCT [50], and AO-OCT [82]. Recent studies demonstrated that functional alteration in ocular tissues might precede the occurrence of structural alteration, and thus evaluation of the functional properties of the RNFL [83], sclera [84], and RPE [85, 86] using PS-OCT technology could be an attractive candidate for improving the detection of ocular pathologies such as glaucoma and age-related macular degeneration.

2.9 OCT Blood Flow and Angiography

Other methods of estimating the functional characteristics of tissue using OCT are Doppler OCT and OCT angiography [87].

Doppler OCT (Fig. 2.19) uses the information from the shift of light's optical frequency when it scatters from moving red blood cells. Two approaches have been taken to measure absolute blood flow: (1) post processing techniques to determine directionality of the vessels and than extract the moving signal from the blood and (2) multiple illumination beams to unambiguously determine Doppler angle by comparing the flow measurements from different directions. Using these techniques, a reduced retinal blood flow has been detected in glaucomatous eyes that corresponded with locations of visual field damage [88, 89]. Investigators are also actively investigating the use of Doppler OCT to measure neurovascular coupling [90], which is thought to be disturbed in subjects with diabetes as well as glaucoma.

OCT angiography (Fig. 2.20), aims to contrast moving blood vessels against static tissue. The general concept behind this method is that regions that are moving (i.e., regions with blood flow) when the same region is scanned repeatedly, will be different from scan to scan (decorrelated). This decorrelation is then used to create a depth resolved map of the vasculature of the eye. Different algorithms are used by the various manufacturer to perform OCT angiography, including intensity based

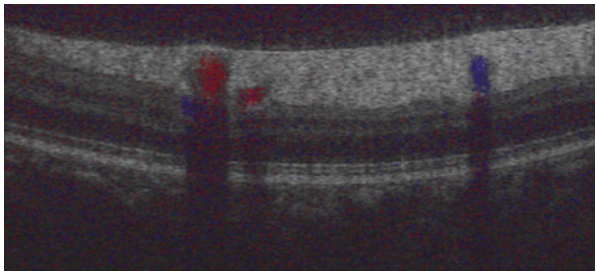

Fig. 2.19 Doppler OCT retina cross-section. The red and blue regions mark locations where blood flows toward or away from the scanning path

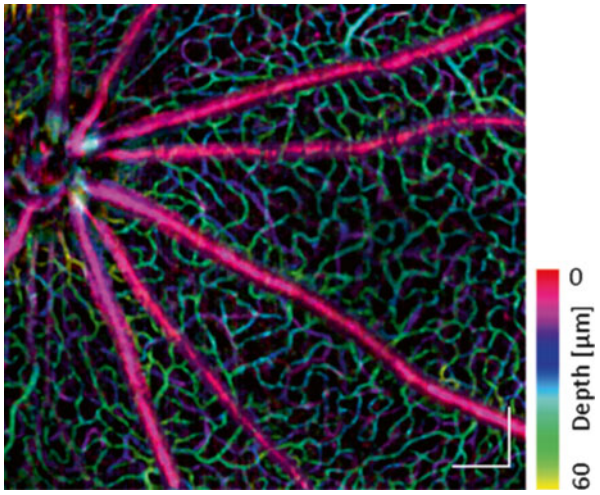

Fig. 2.20 OCT angiography of the peripapillary region in rat. Retinal vessels are color coded with depth showing large vessels on the retinal surface and fine vascular network in the inner retina (Image courtesy of W Liu and H Zhang, Functional Optical Imaging Laboratory, Department of Biomedical Engineering, Northwestern University, Evanston, IL. Scale bar: 200 µm)

and phase based algorithms. OCT angiography has benefited from the increase in OCT imaging speed, which permit imaging of flow in small capillaries as well as wide field OCT angiography [91]. The modality is most promising for assessment of various retinal pathologies involving alterations in the vasculature such as diabetic retinopathy and macular degeneration, where retinal and choroid vasculature can be evaluated with capillary level resolution [91, 92].

It should be noted that while OCT can provide high quality Doppler and angiography information, the technology is not capable of capturing leakage or blood pooling.

2.10 Phase Sensitive OCT

The Phase Sensitive OCT technique is able to provide in vivo information on micron scale movements or vibrations within the tissue [93]. The technology analyzes the phase information of the back-reflected light beam, which is typically ignored in conventional OCT systems. OCT phase imaging has been demonstrated with SD [94] and SS [95] technologies. Phase sensitive OCT offers the advantage of simultaneously assessing both the structural and functional information of the scanned tissue.

In conclusion, OCT has an important clinical role in the diagnosis of disease and the tracking of changes overtime, leading to better insight into the pathophysiology of diseases. The constant improvement in this technology ensures that clinicians will have an indispensible diagnostic tool in their armamentum.

References

1. Fujimoto JG, Brezinski ME, Tearney GJ, Boppart SA, Bouma B, Hee MR, et al. Optical biopsy and imaging using optical coherence tomography. Nat Med. 1995;1(9):970–2.
2. Fercher AF, Mengedoht K, Werner W. Eye-length measurement by interferometry with partially coherent light. Opt Lett. 1988;13(3):186–8.
3. Brezinski ME, Tearney GJ, Bouma BE, Izatt JA, Hee MR, Swanson EA, et al. Optical coherence tomography for optical biopsy. Properties and demonstration of vascular pathology. Circulation. 1996;93(6):1206–13.
4. Cobb MJ, Chen Y, Underwood RA, Usui ML, Olerud J, Li X. Noninvasive assessment of cutaneous wound healing using ultrahigh-resolution optical coherence tomography. J Biomed Opt. 2006;11(6):064002.
5. Hsiung P-L, Phatak DR, Chen Y, Aguirre AD, Fujimoto JG, Connolly JL. Benign and malignant lesions in the human breast depicted with ultrahigh resolution and three-dimensional optical coherence tomography. Radiology. 2007;244(3):865–74.
6. Chen Y, Andrews PM, Aguirre AD, Schmitt JM, Fujimoto JG. High-resolution three-dimensional optical coherence tomography imaging of kidney microanatomy ex vivo. J Biomed Opt. 2007;12(3):034008.
7. Gambichler T, Regeniter P, Bechara FG, Orlikov A, Vasa R, Moussa G, et al. Characterization of benign and malignant melanocytic skin lesions using optical coherence tomography in vivo. J Am Acad Dermatol. 2007;57(4):629–37.
8. Vincent KL, Vargas G, Wei J, Bourne N, Motamedi M. Monitoring vaginal epithelial thickness changes noninvasively in sheep using optical coherence tomography. Am J Obstet Gynecol. 2013;208(4):282.e1–7.
9. Boone M, Draye JP, Verween G, Pirnay J-P, Verbeken G, De Vos D, et al. Real-time three-dimensional imaging of epidermal splitting and removal by high-definition optical coherence tomography. Exp Dermatol. 2014;23(10):725–30.
10. Izatt JA, Hee MR, Swanson EA, Lin CP, Huang D, Schuman JS, et al. Micrometer-scale resolution imaging of the anterior eye in vivo with optical coherence tomography. Arch Ophthalmol. 1994;112(12):1584–9.
11. Puliafito CA, Hee MR, Lin CP, Reichel E, Schuman JS, Duker JS, et al. Imaging of macular diseases with optical coherence tomography. Ophthalmology. 1995;102(2):217–29.
12. Hee MR, Izatt JA, Swanson EA, Huang D, Schuman JS, Lin CP, et al. Optical coherence tomography of the human retina. Arch Ophthalmol. 1995;113(3):325–32.
13. Schuman JS, Hee MR, Arya AV, Pedut-Kloizman T, Puliafito CA, Fujimoto JG, et al. Optical coherence tomography: a new tool for glaucoma diagnosis. Curr Opin Ophthalmol. 1995;6(2):89–95.
14. Schuman JS, Hee MR, Puliafito CA, Wong C, Pedut-Kloizman T, Lin CP, et al. Quantification of nerve fiber layer thickness in normal and glaucomatous eyes using optical coherence tomography. Arch Ophthalmol. 1995;113(5):586–96.
15. Potsaid B, Gorczynska I, Srinivasan VJ, Chen Y, Jiang J, Cable A, et al. Ultrahigh speed spectral / Fourier domain OCT ophthalmic imaging at 70,000 to 312,500 axial scans per second. Opt Express. 2008;16(19):15149–69.
16. Wieser W, Biedermann BR, Klein T, Eigenwillig CM, Huber R. Multi-megahertz OCT: high quality 3D imaging at 20 million a-scans and 4.5 GVoxels per second. Opt Express. 2010;18(14):14685–704.
17. Potsaid B, Baumann B, Huang D, Barry S, Cable AE, Schuman JS, et al. Ultrahigh speed 1050 nm swept source/Fourier domain OCT retinal and anterior segment imaging at 100,000 to 400,000 axial scans per second. Opt Express. 2010;18(19):20029–48.
18. Kocaoglu OP, Cense B, Jonnal RS, Wang Q, Lee S, Gao W, et al. Imaging retinal nerve fiber bundles using optical coherence tomography with adaptive optics. Vision Res. 2011;51(16):1835–44.

19. Kuroda H, Baba M, Suzuki M, Yoneya S. A high speed three-dimensional spectral domain optical coherence tomography with <2 μm axial resolution using wide bandwidth femtosecond mode-locked laser. Appl Phys Lett. 2013;102(25):251102.
20. Fercher AF, Hitzenberger CK, Drexler W, Kamp G, Sattmann H. In vivo optical coherence tomography. Am J Ophthalmol. 1993;116(1):113–4.
21. Fercher AF, Hitzenberger CK, Kamp G, El-Zaiat SY. Measurement of intraocular distances by backscattering spectral interferometry. Opt Commun. 1995;117(1–2):43–8.
22. Wojtkowski M, Leitgeb R, Kowalczyk A, Bajraszewski T, Fercher AF. In vivo human retinal imaging by Fourier domain optical coherence tomography. J Biomed Opt. 2002;7(3):457–63.
23. Fujimoto JG. Optical coherence tomography for ultrahigh resolution in vivo imaging. Nat Biotechnol. 2003;21(11):1361–7.
24. Kim JS, Ishikawa H, Sung KR, Xu J, Wollstein G, Bilonick RA, et al. Retinal nerve fibre layer thickness measurement reproducibility improved with spectral domain optical coherence tomography. Br J Ophthalmol. 2009;93(8):1057–63.
25. Ahlers C, Schmidt-Erfurth U. Three-dimensional high resolution OCT imaging of macular pathology. Opt Express. 2009;17(5):4037–45.
26. Drexler W, Morgner U, Kärtner FX, Pitris C, Boppart SA, Li XD, et al. In vivo ultrahigh-resolution optical coherence tomography. Opt Lett. 1999;24(17):1221–3.
27. Lim H, Jiang Y, Wang Y, Huang Y-C, Chen Z, Wise FW. Ultrahigh-resolution optical coherence tomography with a fiber laser source at 1 microm. Opt Lett. 2005;30(10):1171–3.
28. Leitgeb R, Hitzenberger CK, Fercher AF. Performance of fourier domain vs. time domain optical coherence tomography. Opt Express. 2003;11(8):889–94.
29. Huber R, Adler DC, Fujimoto JG. Buffered Fourier domain mode locking: unidirectional swept laser sources for optical coherence tomography imaging at 370,000 lines/s. Opt Lett. 2006;31(20):2975–7.
30. Yaqoob Z, Wu J, Yang C. Spectral domain optical coherence tomography: a better OCT imaging strategy. Biotechniques. 2005;39(6 Suppl):S6–13.
31. Unterhuber A, Povazay B, Hermann B, Sattmann H, Chavez-Pirson A, Drexler W. In vivo retinal optical coherence tomography at 1040 nm – enhanced penetration into the choroid. Opt Express. 2005;13(9):3252–8.
32. Yasuno Y, Hong Y, Makita S, Yamanari M, Akiba M, Miura M, et al. In vivo high-contrast imaging of deep posterior eye by 1-um swept source optical coherence tomography andscattering optical coherence angiography. Opt Express. 2007;15(10):6121–39.
33. Hale GM, Querry MR. Optical constants of water in the 200-nm to 200-?m wavelength region. Appl Opt. 1973;12(3):555–63.
34. Huang D, Swanson EA, Lin CP, Schuman JS, Stinson WG, Chang W, et al. Optical coherence tomography. Science. 1991;254(5035):1178–81.
35. Schuman JS, Pedut-Kloizman T, Hertzmark E, Hee MR, Wilkins JR, Coker JG, et al. Reproducibility of nerve fiber layer thickness measurements using optical coherence tomography. Ophthalmology. 1996;103(11):1889–98.
36. Otani T, Kishi S, Maruyama Y. Patterns of diabetic macular edema with optical coherence tomography. Am J Ophthalmol. 1999;127(6):688–93.
37. Sánchez-Tocino H, Alvarez-Vidal A, Maldonado MJ, Moreno-Montañés J, García-Layana A. Retinal thickness study with optical coherence tomography in patients with diabetes. Invest Ophthalmol Vis Sci. 2002;43(5):1588–94.
38. Medeiros FA, Zangwill LM, Bowd C, Weinreb RN. Comparison of the GDx VCC scanning laser polarimeter, HRT II confocal scanning laser ophthalmoscope, and stratus OCT optical coherence tomograph for the detection of glaucoma. Arch Ophthalmol. 2004;122(6):827–37.
39. Paunescu LA, Schuman JS, Price LL, Stark PC, Beaton S, Ishikawa H, et al. Reproducibility of nerve fiber thickness, macular thickness, and optic nerve head measurements using StratusOCT. Invest Ophthalmol Vis Sci. 2004;45(6):1716–24.
40. Kamppeter BA, Schubert KV, Budde WM, Degenring RF, Jonas JB. Optical coherence tomography of the optic nerve head: interindividual reproducibility. J Glaucoma. 2006;15(3):248–54.

41. Nassif N, Cense B, Park BH, Yun SH, Chen TC, Bouma BE, et al. In vivo human retinal imaging by ultrahigh-speed spectral domain optical coherence tomography. Opt Lett. 2004;29(5):480–2.
42. Drexler W, Morgner U, Ghanta RK, Kärtner FX, Schuman JS, Fujimoto JG. Ultrahigh-resolution ophthalmic optical coherence tomography. Nat Med. 2001;7(4):502–7.
43. Ko TH, Fujimoto JG, Duker JS, Paunescu LA, Drexler W, Baumal CR, et al. Comparison of ultrahigh- and standard-resolution optical coherence tomography for imaging macular hole pathology and repair. Ophthalmology. 2004;111(11):2033–43.
44. De Boer JF, Milner TE, van Gemert MJC, Nelson JS. Two-dimensional birefringence imaging in biological tissue by polarization-sensitive optical coherence tomography. Opt Lett. 1997;22(12):934–6.
45. Izatt JA, Kulkarni MD, Yazdanfar S, Barton JK, Welch AJ. In vivo bidirectional color Doppler flow imaging of picoliter blood volumes using optical coherence tomography. Opt Lett. 1997;22(18):1439–41.
46. Bizheva K, Pflug R, Hermann B, Povazay B, Sattmann H, Qiu P, et al. Optophysiology: depth-resolved probing of retinal physiology with functional ultrahigh-resolution optical coherence tomography. Proc Natl Acad Sci U S A. 2006;103(13):5066–71.
47. Srinivasan VJ, Wojtkowski M, Fujimoto JG, Duker JS. In vivo measurement of retinal physiology with high-speed ultrahigh-resolution optical coherence tomography. Opt Lett. 2006;31(15):2308–10.
48. Kagemann L, Wollstein G, Wojtkowski M, Ishikawa H, Townsend KA, Gabriele ML, et al. Spectral oximetry assessed with high-speed ultra-high-resolution optical coherence tomography. J Biomed Opt. 2007;12(4):041212.
49. Gotzinger E, Pircher M, Baumann B, Ahlers C, Geitzenauer W, Schmidt-Erfurth U, et al. Three-dimensional polarization sensitive OCT imaging and interactive display of the human retina. Opt Express. 2009;17(5):4151–65.
50. Yamanari M, Makita S, Lim Y, Yasuno Y. Full-range polarization-sensitive swept-source optical coherence tomography by simultaneous transversal and spectral modulation. Opt Express. 2010;18(13):13964–80.
51. Cheong W-F, Prahl SA, Welch AJ. A review of the optical properties of biological tissues. IEEE J Quan Elec. 1990;26(12):2166–85.
52. Wojtkowski M, Srinivasan V, Fujimoto JG, Ko T, Schuman JS, Kowalczyk A, et al. Three-dimensional retinal imaging with high-speed ultrahigh-resolution optical coherence tomography. Ophthalmology. 2005;112(10):1734–46.
53. Leung CK-S, Cheung CY-L, Weinreb RN, Qiu Q, Liu S, Li H, et al. Retinal nerve fiber layer imaging with spectral-domain optical coherence tomography: a variability and diagnostic performance study. Ophthalmology. 2009;116(7):1257–63, 1263.e1–2.
54. Tan O, Li G, Lu AT-H, Varma R, Huang D. Advanced imaging for glaucoma study group. Mapping of macular substructures with optical coherence tomography for glaucoma diagnosis. Ophthalmology. 2008;115(6):949–56.
55. Asrani S, Rosdahl JA, Allingham RR. Novel software strategy for glaucoma diagnosis: asymmetry analysis of retinal thickness. Arch Ophthalmol. 2011;129(9):1205–11.
56. Tan O, Chopra V, Lu AT-H, Schuman JS, Ishikawa H, Wollstein G, et al. Detection of macular ganglion cell loss in glaucoma by Fourier-domain optical coherence tomography. Ophthalmology. 2009;116(12):2305–14.e1–2.
57. Margolis R, Spaide RF. A pilot study of enhanced depth imaging optical coherence tomography of the choroid in normal eyes. Am J Ophthalmol. 2009;147(5):811–5.
58. Silverman AL, Tatham AJ, Medeiros FA, Weinreb RN. Assessment of optic nerve head drusen using enhanced depth imaging and swept source optical coherence tomography. J Neuroophthalmol. 2014;34(2):198–205.
59. Park H-YL, Shin H-Y, Park CK. Imaging the posterior segment of the eye using swept-source optical coherence tomography in myopic glaucoma eyes: comparison with enhanced-depth imaging. Am J Ophthalmol. 2014;157(3):550–7.
60. Liu B, Brezinski ME. Theoretical and practical considerations on detection performance of time domain, Fourier domain, and swept source optical coherence tomography. J Biomed Opt. 2007;12(4):044007.

61. Hirata M, Tsujikawa A, Matsumoto A, Hangai M, Ooto S, Yamashiro K, et al. Macular choroidal thickness and volume in normal subjects measured by swept-source optical coherence tomography. Invest Ophthalmol Vis Sci. 2011;52(8):4971–8.
62. Adhi M, Liu JJ, Qavi AH, Grulkowski I, Lu CD, Mohler KJ, et al. Choroidal analysis in healthy eyes using swept-source optical coherence tomography compared to spectral domain optical coherence tomography. Am J Ophthalmol. 2014;157(6):1272–81.e1.
63. Takayama K, Hangai M, Kimura Y, Morooka S, Nukada M, Akagi T, et al. Three-dimensional imaging of lamina cribrosa defects in glaucoma using swept-source optical coherence tomography. Invest Ophthalmol Vis Sci. 2013;54(7):4798–807.
64. Wang B, Nevins JE, Nadler Z, Wollstein G, Ishikawa H, Bilonick RA, et al. Reproducibility of in-vivo OCT measured three-dimensional human lamina cribrosa microarchitecture. PLoS One. 2014;9(4):e95526.
65. Mak H, Xu G, Leung CK-S. Imaging the iris with swept-source optical coherence tomography: relationship between iris volume and primary angle closure. Ophthalmology. 2013;120(12):2517–24.
66. Srinivasan VJ, Adler DC, Chen Y, Gorczynska I, Huber R, Duker JS, et al. Ultrahigh-speed optical coherence tomography for three-dimensional and en face imaging of the retina and optic nerve head. Invest Ophthalmol Vis Sci. 2008;49(11):5103–10.
67. Keane PA, Ruiz-Garcia H, Sadda SR. Clinical applications of long-wavelength (1,000-nm) optical coherence tomography. Ophthalmic Surg Lasers Imaging. 2011;42(Suppl):S67–74.
68. Mishima K, Tomidokoro A, Suramethakul P, Mataki N, Kurita N, Mayama C, et al. Iridotrabecular contact observed using anterior segment three-dimensional OCT in eyes with a shallow peripheral anterior chamber. Invest Ophthalmol Vis Sci. 2013;54(7):4628–35.
69. Wang B, Nevins JE, Nadler Z, Wollstein G, Ishikawa H, Bilonick RA, et al. In vivo lamina cribrosa micro-architecture in healthy and glaucomatous eyes as assessed by optical coherence tomography. Invest Ophthalmol Vis Sci. 2013;54(13):8270–4.
70. Lopilly Park H-Y, Lee NY, Choi JA, Park CK. Measurement of scleral thickness using swept-source optical coherence tomography in patients with open-angle glaucoma and myopia. Am J Ophthalmol. 2014;157(4):876–84.
71. Považay B, Hermann B, Hofer B, Kajić V, Simpson E, Bridgford T, et al. Wide-field optical coherence tomography of the choroid in vivo. Invest Ophthalmol Vis Sci. 2009;50(4):1856–63.
72. Grulkowski I, Liu JJ, Potsaid B, Jayaraman V, Lu CD, Jiang J, et al. Retinal, anterior segment and full eye imaging using ultrahigh speed swept source OCTwith vertical-cavity surface emitting lasers. Biomed Opt Express. 2012;3(11):2733–51.
73. Liang J, Williams DR, Miller DT. Supernormal vision and high-resolution retinal imaging through adaptive optics. J Opt Soc Am A. 1997;14(11):2884–92.
74. Roorda A, Romero-Borja F, Donnelly WI, Queener H, Hebert T, Campbell M. Adaptive optics scanning laser ophthalmoscopy. Opt Express. 2002;10(9):405–12.
75. Hermann B, Fernández EJ, Unterhuber A, Sattmann H, Fercher AF, Drexler W, et al. Adaptive-optics ultrahigh-resolution optical coherencetomography. Opt Lett. 2004;29(18):2142–4.
76. Zawadzki RJ, Jones SM, Olivier SS, Zhao M, Bower BA, Izatt JA, et al. Adaptive-optics optical coherence tomography for high-resolution and high-speed 3D retinal in vivo imaging. Opt Express. 2005;13(21):8532–46.
77. Kocaoglu OP, Lee S, Jonnal RS, Wang Q, Herde AE, Derby JC, et al. Imaging cone photoreceptors in three dimensions and in time using ultrahigh resolution optical coherence tomography with adaptive optics. Biomed Opt Express. 2011;2(4):748–63.
78. Takayama K, Ooto S, Hangai M, Ueda-Arakawa N, Yoshida S, Akagi T, et al. High-resolution imaging of retinal nerve fiber bundles in glaucoma using adaptive optics scanning laser ophthalmoscopy. Am J Ophthalmol. 2013;155(5):870–81.
79. Burns SA, Tumbar R, Elsner AE, Ferguson D, Hammer DX. Large-field-of-view, modular, stabilized, adaptive-optics-based scanning laser ophthalmoscope. J Opt Soc Am A Opt Image Sci Vis. 2007;24(5):1313–26.
80. Fernández EJ, Povazay B, Hermann B, Unterhuber A, Sattmann H, Prieto PM, et al. Three-dimensional adaptive optics ultrahigh-resolution optical coherence tomography using a liquid crystal spatial light modulator. Vision Res. 2005;45(28):3432–44.

81. Zawadzki RJ, Choi SS, Fuller AR, Evans JW, Hamann B, Werner JS. Cellular resolution volumetric in vivo retinal imaging with adaptive optics-optical coherence tomography. Opt Express. 2009;17(5):4084–94.
82. Cense B, Gao W, Brown JM, Jones SM, Jonnal RS, Mujat M, et al. Retinal imaging with polarization-sensitive optical coherence tomography and adaptive optics. Opt Express. 2009;17(24):21634–51.
83. Liu S, Wang B, Yin B, Milner TE, Markey MK, McKinnon SJ, et al. Retinal nerve fiber layer reflectance for early glaucoma diagnosis. J Glaucoma. 2014;23(1):e45–52.
84. Baumann B, Rauscher S, Glösmann M, Götzinger E, Pircher M, Fialova S, et al. Peripapillary rat sclera investigated in vivo with polarization sensitive optical coherence tomography. Invest Ophthalmol Vis Sci. 2014;55(11):7686–96.
85. Michels S, Pircher M, Geitzenauer W, Simader C, Götzinger E, Findl O, et al. Value of polarisation-sensitive optical coherence tomography in diseases affecting the retinal pigment epithelium. Br J Ophthalmol. 2008;92(2):204–9.
86. Ahlers C, Götzinger E, Pircher M, Golbaz I, Prager F, Schütze C, et al. Imaging of the retinal pigment epithelium in age-related macular degeneration using polarization-sensitive optical coherence tomography. Invest Ophthalmol Vis Sci. 2010;51(4):2149–57.
87. Leitgeb RA, Werkmeister RM, Blatter C, Schmetterer L. Doppler optical coherence tomography. Prog Retin Eye Res. 2014;41:26–43.
88. Jia Y, Wei E, Wang X, et al. Optical coherence tomography angiography of optic disc perfusion in glaucoma. Ophthalmology. 2014;121(7):1322–32.
89. Sehi M, Goharian I, Konduru R, et al. Retinal blood flow in glaucomatous eyes with single-hemifield damage. Ophthalmology. 2014;121(3):750–8.
90. Wang Y, Fawzi AA, Tan O, Zhang X, Huang D. Flicker-induced changes in retinal blood flow assessed by Doppler optical coherence tomography. Biomed Opt Express. 2011;2(7):1852.
91. Blatter C, Klein T, Grajciar B, et al. Ultrahigh-speed non-invasive widefield angiography. J Biomed Opt. 2012;17(7):0705051–3.
92. Cheung CY-L, Lamoureux E, Ikram MK, et al. Retinal vascular geometry in Asian persons with diabetes and retinopathy. J Diabetes Sci Technol. 2012;6(3):595–605.
93. Choma MA, Ellerbee AK, Yang C, Creazzo TL, Izatt JA. Spectral-domain phase microscopy. Opt Lett. 2005;30(10):1162–4.
94. Joo C, Akkin T, Cense B, Park BH, de Boer JF. Spectral-domain optical coherence phase microscopy for quantitative phase-contrast imaging. Opt Lett. 2005;30(16):2131–3.
95. Sarunic MV, Weinberg S, Izatt JA. Full-field swept-source phase microscopy. Opt Lett. 2006;31(10):1462–4.

Chapter 3
Optical Coherence Tomography and Optic Nerve Edema

Kendra A. Klein and Thomas R. Hedges III

Abstract Optical coherence tomography (OCT) continues to advance our understanding of the various diseases characterized by optic disc edema. In acute papilledema, OCT has demonstrated subretinal fluid extending from the optic disc to the subfoveal region, assisting in our understanding of the pathophysiology of vision loss in these cases. In evolving cases of optic disc edema, OCT of the RNFL can thus be an objective measurement of nerve swelling. By analyzing the ganglion cell complex, OCT can now help detect early axonal damage in optic nerve disease, even when the RNFL is edematous, and may be helpful in predicting visual outcomes. Finally, OCT has also proven to be a reliable tool in assisting clinicians in differentiating between cases of frank papilledema and pseudopapilledema, such that occurs in optic nerve head drusen, vitreopapillary traction, Bergmeister papilla, and myelinated nerve fiber layer.

Keywords Papilledema • Pseudopapilledema • Increased intracranial pressure • Optic nerve sheath meningioma • Optic disc edema • Vitreopapillary traction • Bergmeister papilla • Myelinated nerve fiber layer • Nonarteritic optic neuropathy (NAION) • Optic disc drusen • Retinal nerve fiber layer (RNFL) • Ganglion cell complex (GCC) layer • Lebers herediary optic neuropathy (LHON)

OCT and optic nerve edema

1. Papilledema
2. Optic disc edema secondary to ischemia
3. Optic disc edema secondary to toxic/hereditary/nutritional optic neuropathies
4. Pseudopapilledema
    - Vitreopapillary traction
    - Optic nerve head drusen
    - Bergmeister's papilla and myelinated nerve fiber layer

K.A. Klein, MD (✉) • T.R. Hedges III, MD
Ophthalmology, New England Eye Center at Tufts Medical Center, Boston, MA, USA
e-mail: kendra.klein@gmail.com

A. Grzybowski, P. Barboni (eds.), *OCT in Central Nervous System Diseases: The Eye as a Window to the Brain*, DOI 10.1007/978-3-319-24085-5_3

3.1 Papilledema

Information given to us by optical coherence tomography (OCT) has advanced our understanding of the pathophysiology of papilledema and pseudopapilledema. In 1860, von Graefe described engorgement and distention of the retinal veins as an early manifestation of papilledema, suggesting that increased intracranial pressure lead to increased intracranial venous pressure and eventual venous stasis [1]. Subsequent investigators described dilatation of the optic nerve sheath in cases of papilledema, suggesting that increased pressure within the sheath could obstruct the central retinal vein [2, 3].

In 1963, in a study of rhesus monkeys, Hedges showed that with acute and subacute increases in intracranial pressure, there was always an associated rise in ophthalmic vein pressure. He proposed that impairment of orbital venous outflow at the level of the cavernous sinus, arterial pressure elevation, and a local hemodynamic effect within the orbit all contribute to the elevation if orbital venous pressure [4]. In 1977, in an experimental model of rhesus monkeys, Tso and Hayreh demonstrated that unlike swelling in the central nervous system, which is characterized by fluid accumulation in glial cells and extracellular space, the primary pathologic change in papilledema is severe swelling of axons with disruption of mitochondria and neurotubules [5]. The Tso and Hayreh study also demonstrated that the edematous axons displaced the peripapillary retinal laterally, with extension of tracer into the subretinal space surrounding the optic nerve head. This idea of a direct communication between the swollen optic disc and the submacular space was first put forth by Samuel's histopathologic study in 1938, suggesting that the intermediary tissue of Kuhnt can be disrupted from optic nerve swelling with subsequent escape of peripapillary fluid [6]. Visual acuity loss, when it is seen in papilledema, is typically in conjunction with these macular changes [7].

Visual acuity loss is infrequent in papilledema. More commonly, chronic papilledema leads to degeneration of optic nerve fibers with resultant peripheral visual field defects [7]. In 1980, Morris and Sanders described visual acuity loss from papilledema due to macular changes, including retinal hemorrhages, macular exudates, and choroidal folds. They suggested that cerebrospinal fluid pressure in the optic nerve sheath produces hemodynamic and mechanical effects causing compensatory dilatation of the retinal papillary and peripapillary plexus and distention of the optic nerve sheath, indenting the posterior globe causing choroidal and pigment epithelial wrinkling in the macula [8].

Shortly after, Corbett et al. showed that peripapillary fluid in the context of papilledema could lead to enlargement of the blind spot, hyperopia, and refractive scotoma [9]. In patients with papilledema retinal pigment epithelial changes, as seen in cases of chronic macular edema, have also been observed [10]. Even choroidal neovascular membranes have been described in patients with papilledema [11–19].

In 2001, Hoye et al. evaluated 55 patients with papilledema from increased intracranial pressure using OCT of the optic nerve and retinal nerve fiber layer (RNFL). Nineteen of the patients also had OCT of the macula during times of acute, subacute, or recurrent papilledema. OCT demonstrated subretinal fluid in association with decreased visual acuity in a subset of patients. In some cases this fluid was localized to the subfoveal region, and in others the fluid appeared to be continuous from the optic disc to the subfoveal region, suggesting fluid leakage from the optic nerve head. In these cases, fluorescein angiography failed to demonstrate leakage from the retinal or choroidal vasculature. In cases in which the visual acuity was not substantially affected, there was thickening of the maculopapillary retina on OCT, suggesting intraretinal edema, without clear separation of the retina and underlying choroid. They further noted an improvement in visual acuity after resolution of subretinal edema [7].

A common clinical problem is the inability to differentiate mild papilledema from pseudopapilledema. Although following these patients with repeat exams would eventually yield an answer, such action is subjective and could delay diagnosis.

In a study of patients under 20 years of age, peripapillary RNFL thickness on OCT has been found to be a reliable tool in assisting in the differentiation between frank papilledema and pseudopapilledema. The mean RNFL thickness in eyes with papilledema was 218 % (340 microns versus 156 microns) above the eyes with pseudopapilledema [20]. However, patients with moderate to severe papilledema can be readily distinguished from pseudopapilledema on clinical examination. Differentiating cases of *mild* papilledema from congenital crowding without optic disc drusen is much more challenging. In 2005, OCT showed that both congenital crowding and mild papilledema mean RNFL thickness was significantly increased in comparison to normal control patients. Although the patients with mild papilledema had higher RNFL values than those with congenital crowding, the difference was not statistically significant, and it was concluded that distinction between these similar appearing entities could not be made by OCT RNFL analysis alone. However, this finding suggests pseudopapilledema and papilledema share a similar pathogenesis, in which axonal swelling is the result of delayed axoplasmic transport [21].

Fard et al. studied 42 eyes with mild papilledema, 37 eyes with pseudopapilledema from congenitally crowded discs, and 34 normal eyes with SD-OCT. Patients with optic disc drusen, moderate to severe papilledema, atrophic papilledema, and previous retinal disease were excluded. As previously found, eyes with both papilledema and pseudopapilledema had statistically significant increased RNFL thickness in comparison to normal subjects. They found that the difference between the average outer peripapillary total retinal volume in the papilledema and pseudopapilledema groups was statistically significant. However, the difference between the outer ring peripapillary total retinal volume in pseudopapilledema and normal eyes was not. They concluded that outer peripapillary total retinal ring volumes might be useful in helping to differentiate between papilledema and pseudopapilledema [22].

OCT can be a helpful tool in evaluating the optic nerve head in cases of optic nerve sheath meningioma (Fig. 3.1). Sibony et al. used OCT to examine the biomechanical changes of the optic nerve head in patients with presumed optic nerve sheath meningiomas (pONSM) and compare the shape of the peripapillary retinal pigment epithelium-Bruch's membrane layer (ppRPE) with normal subjects. In patients with pONSM, the ppRPE surrounding the neural canal opening was found to be indented, creating an inverted-U shaped deformation towards the vitreous. This varied significantly from normal subjects, in which the ppRPE bordering the neural canal opening was V-shaped, pointing away from the vitreous. This deformation of the ppRPE was correlated with both the size of the tumor and the proximity of the tumor to the globe and was indistinguishable from the shape of the ppRPE-layer in patients with intracranial hypertension and papilledema previously reported by the authors. Interestingly these changes were not seen in disc edema from NAION or optic neuritis [23].

Fig. 3.1 Optic nerve sheath meningioma. A 53-year-old woman was referred for painless, gaze-induced, "dimming out" of vision in her right eye. On examination, visual acuities were 20/20 in both eyes, there was no afferent papillary defect, and color vision was preserved. Fundoscopy revealed optic disc edema in the right eye (**a**). Humphrey visual field 24–2 examination demonstrated temporal depression and an enlarged blind spot in the right eye and was full in the left eye. OCT demonstrated diffuse thickening of the RNFL in the right eye (**b**). OCT through the nerve and macula demonstrated swelling of the optic nerve and deformation of the peripapillary RPE toward the vitreous (**c**). Ganglion cell analysis was normal in both eyes. Given the concern for a compressive optic neuropathy, MRI of the orbits with and without contrast with fat saturation was performed and revealed abnormal enhancement of the right optic nerve sheath, consistent with optic nerve sheath meningioma (**d**)

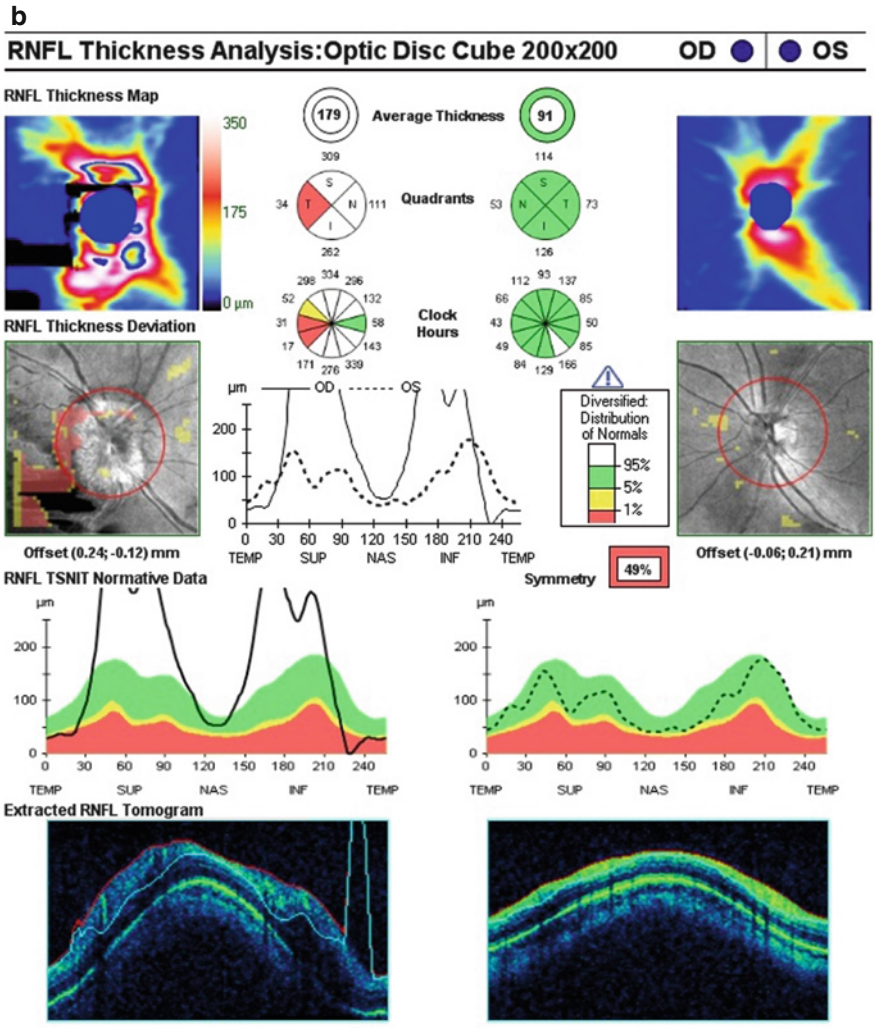

Fig. 3.1 (continued)

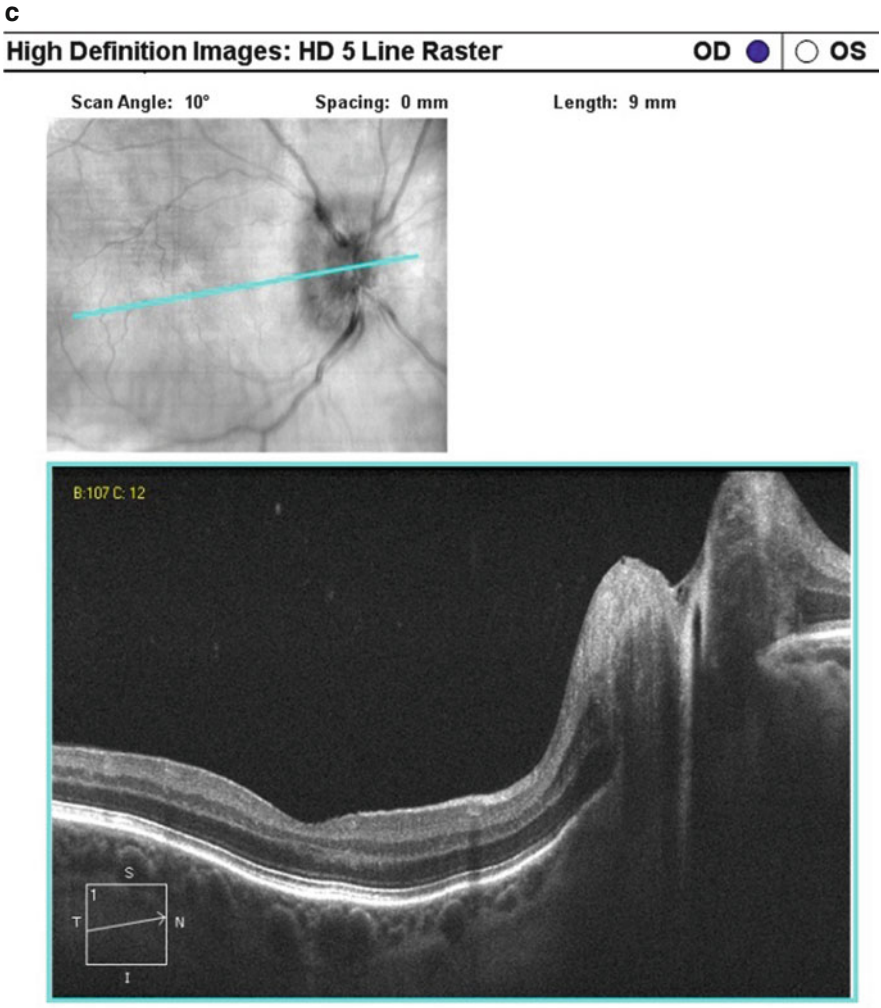

Fig. 3.1 (continued)

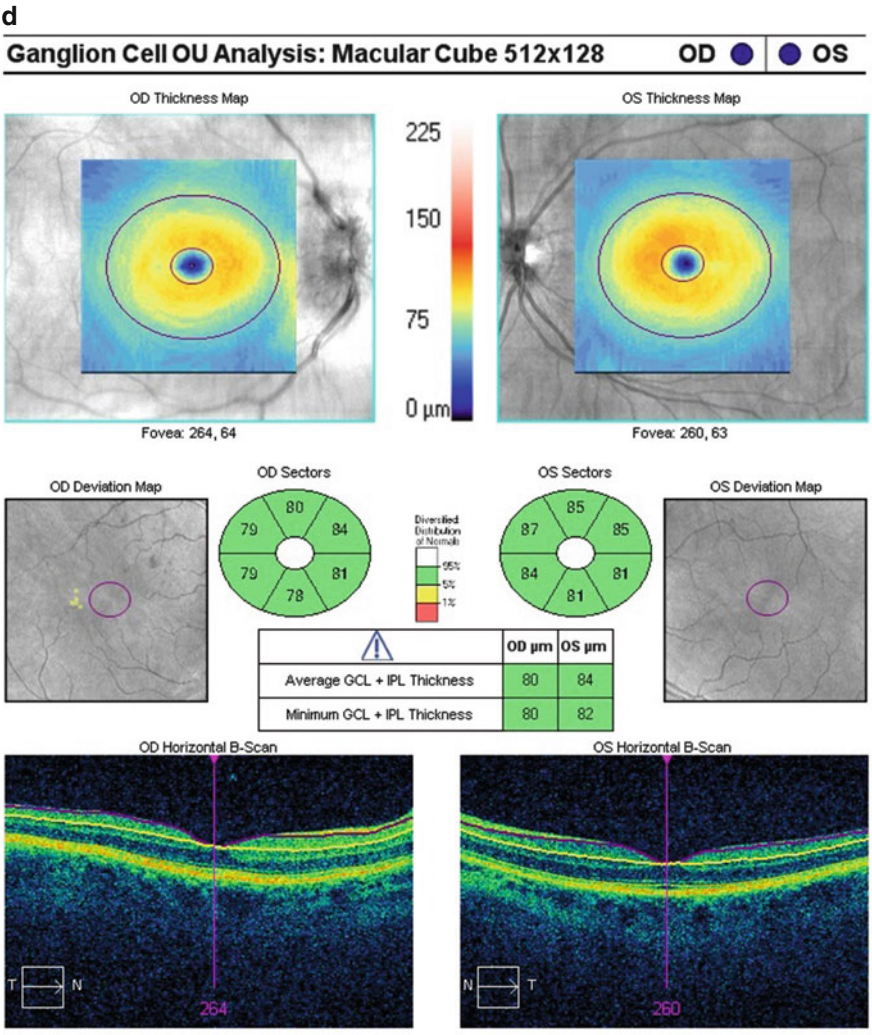

Fig. 3.1 (continued)

OCT has also been valuable in demonstrating the natural history of optic disc edema from a variety of causes, by measuring the RNFL thickness. OCT can objectively quantify the amount of RNFL swelling, and thus axonal swelling, which is the main pathological event in optic nerve edema; conversely confocal scanning laser ophthalmoscope can not due to disruption of mitochondria and neurotubules in the swelling axons [5, 24]. OCT can thus be an objective tool in following the clinical course of optic disc edema. After the period of acute edema, during which the RNFL is diffusely thickened, OCT can be used to monitor resolution of axonal swelling and thinning of the RNFL. Long term, RNFL thinning on OCT can be used to monitor for evolution towards optic atrophy [24].

Monteiro and Afonso found using frequency domain optical coherence tomography in patients with pseudotumor cerebri and clinically resolved papilledema and stable visual fields for at least 6 months, that macular and RNFL thickness measurements were significantly reduced when compared with normal eyes, and that the degree of RNFL and retinal axonal loss correlated with visual field loss. This study highlights that OCT can be used as an objective tool in guiding management, and may estimate axonal loss following chronic papilledema [25].

The retinal nerve fiber layer is composed of the unmyelinated axons that originate from ganglion cell bodies in the macula [26]. Since the retinal nerve fibers originate from retinal ganglion cells, the degeneration of the RNFL may lead to decreased average macular thickness reductions, at least in part secondary to ganglion cell death from retrograde axonal degeneration [27].

Papchenko et al. demonstrated a robust association between visual field sensitivity using automated perimetry and structural changes in OCT macular thickness in patients with NAION, suggesting macular thickness could be a surrogate for determining the extent of neuronal damage in nonglaucomatous optic neuropathy. Further, there was a topographical correlation between regions of macular thinning with corresponding visual field loss [28].

Average thickness measurements represent multiple layers of the macula, including diverse cell types with diverse functions. However, recent advancements segmentation algorithms have made it possible to measure discrete retinal layers. SD-OCT can now analyze individual retinal layers such as the ganglion cell complex (GCC) layer in the macula, and can detect early axonal damage acutely, even when the peripapillary RNFL is edematous (Fig. 3.2). This is useful because initial optic disc edema as evidenced by RNFL thickness on OCT has limited prognostic value; it is not correlated with final thickness, visual acuity, or visual field mean deviation. Quantification of the retinal ganglion cell layer in the macula, therefore, may provide a more specific assessment of a discrete retinal neuronal population. Analysis of the ganglion cell complex (GCC) in the macula has therefore become an important tool in assessing various optic neuropathies [29].

Bianchi et al. showed that measurements of GCC thickness correlated better with visual field mean deviation decrease than RNFL measurements. They concluded that mean GCC thickness measurements give a more reliable estimate and an objective estimate of early retrograde optic nerve damage even in cases without papilledema of visual loss [30].

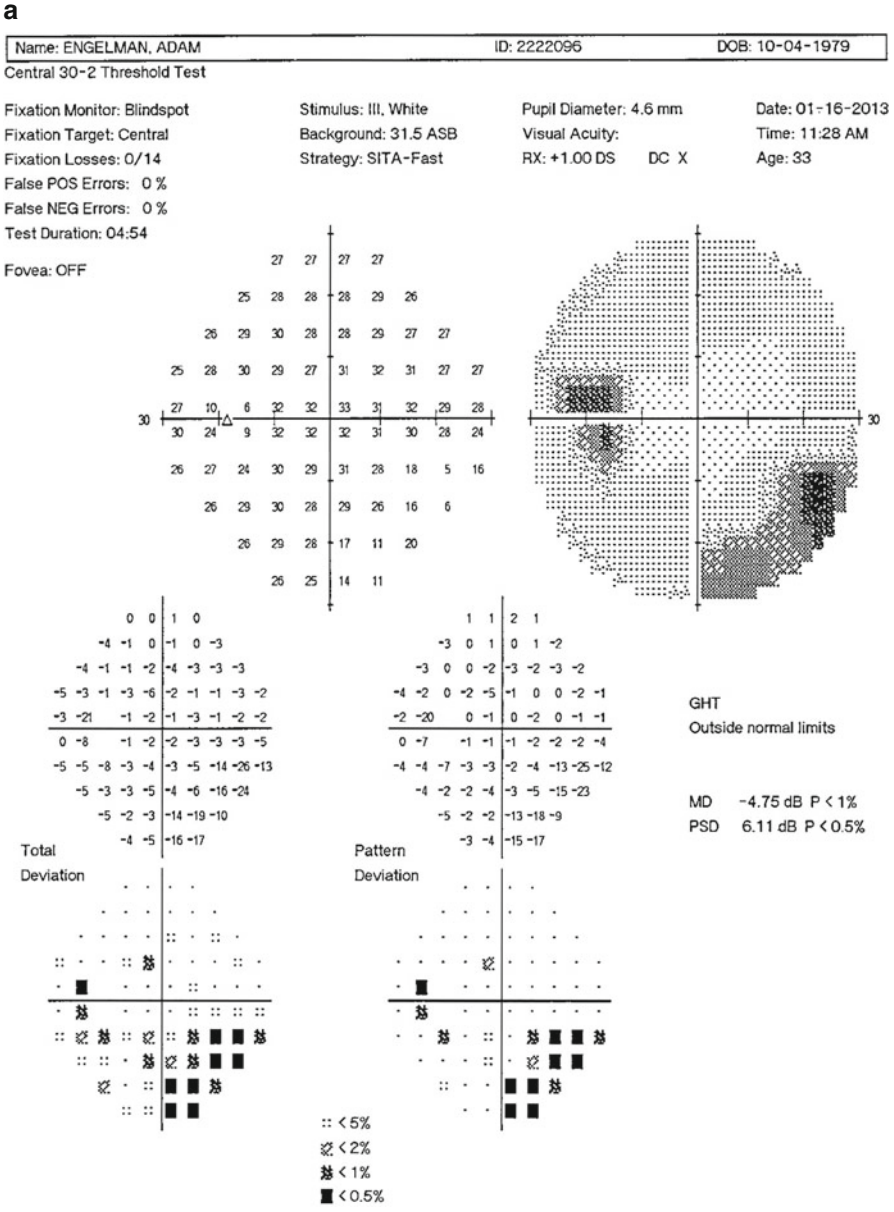

Fig. 3.2 Papilledema. A 33-year-old man with idiopathic intracranial hypertension treated with daily acetazolamide and optic nerve sheath fenestration in both eyes 5 years prior presented with blurred vision in both eyes and headache. There was moderate papilledema on fundoscopy and visual field examination revealed inferior arcuate scotomata in the right (**b**), and left (**a**) eyes. OCT demonstrated diffuse thickening on the RNFL bilaterally (**c**). Ganglion cell analysis revealed segmental thinning, despite the papilledema (**d**). The opening pressure was elevated on lumbar puncture, and he underwent left transverse sinus stenting. Post stenting, his visual field examination remained largely unchanged in the right (**e**) and left (**f**) eyes. Although the optic disc swelling significantly improved (**g**), segmental ganglion cell loss remained apparent in (**h**)

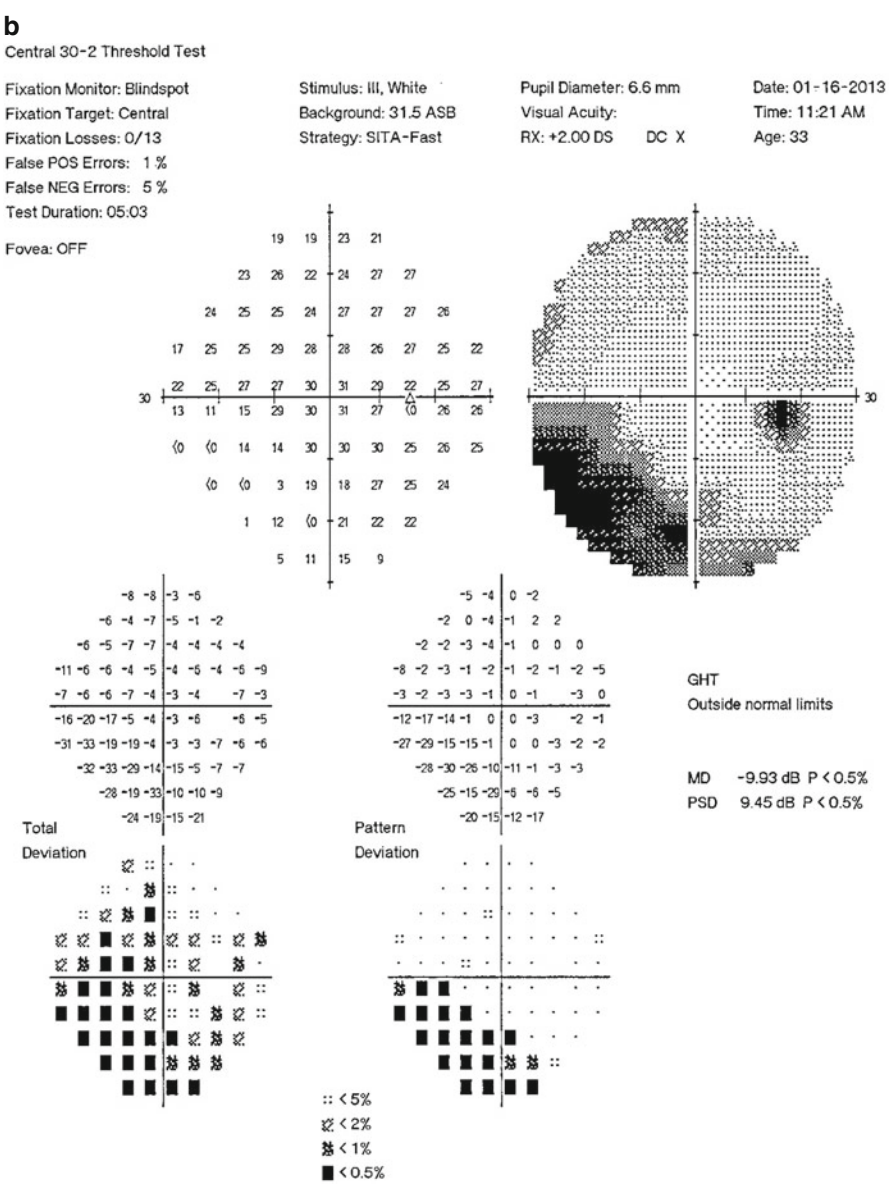

Fig. 3.2 (continued)

c

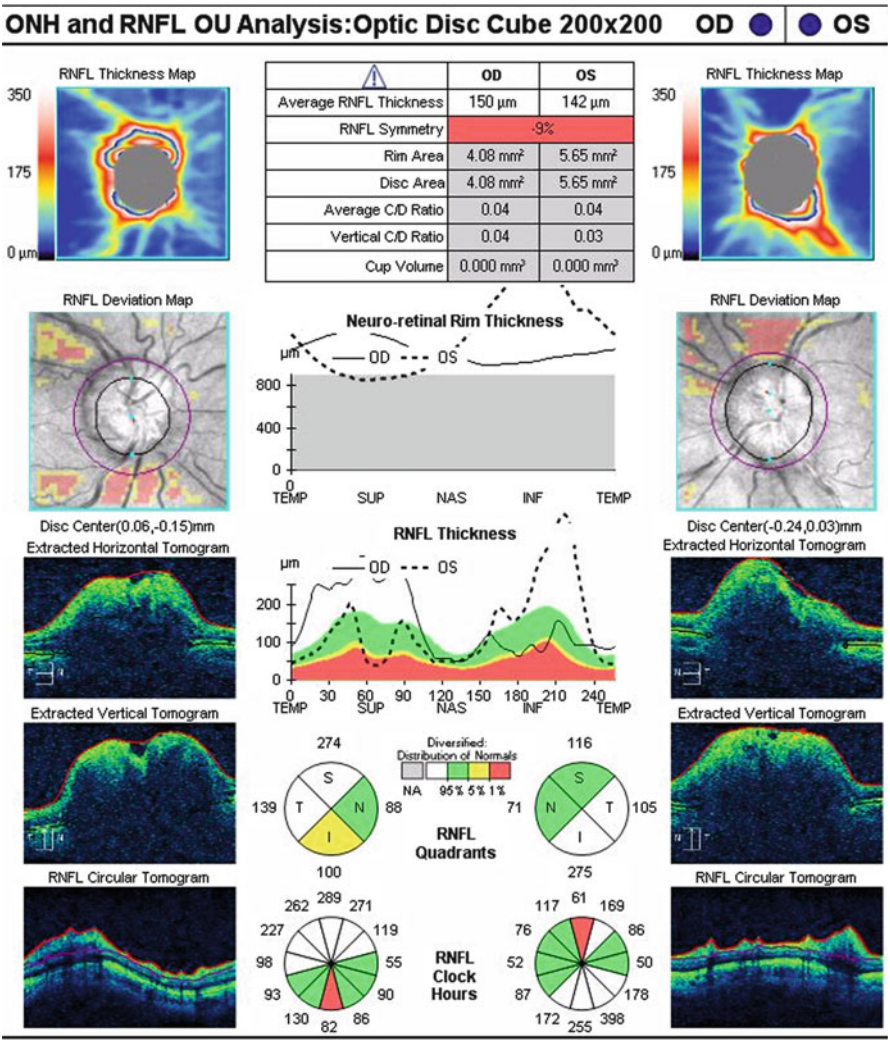

Fig. 3.2 (continued)

d

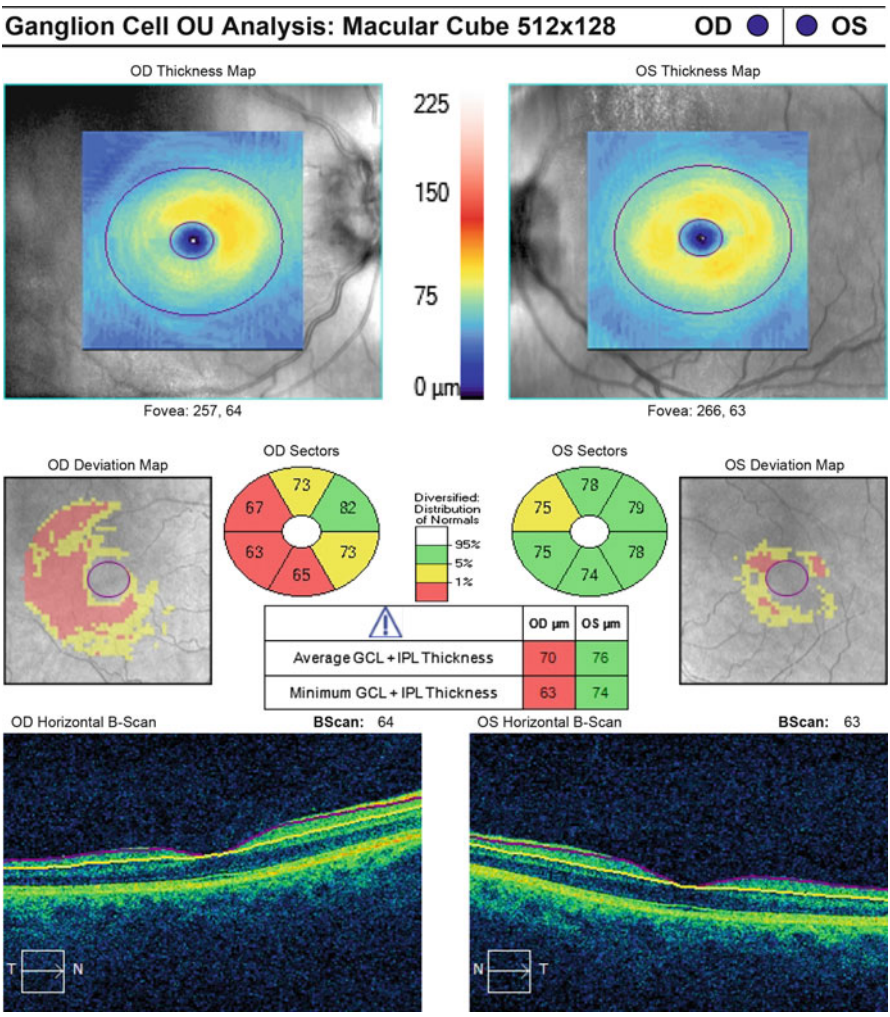

Fig. 3.2 (continued)

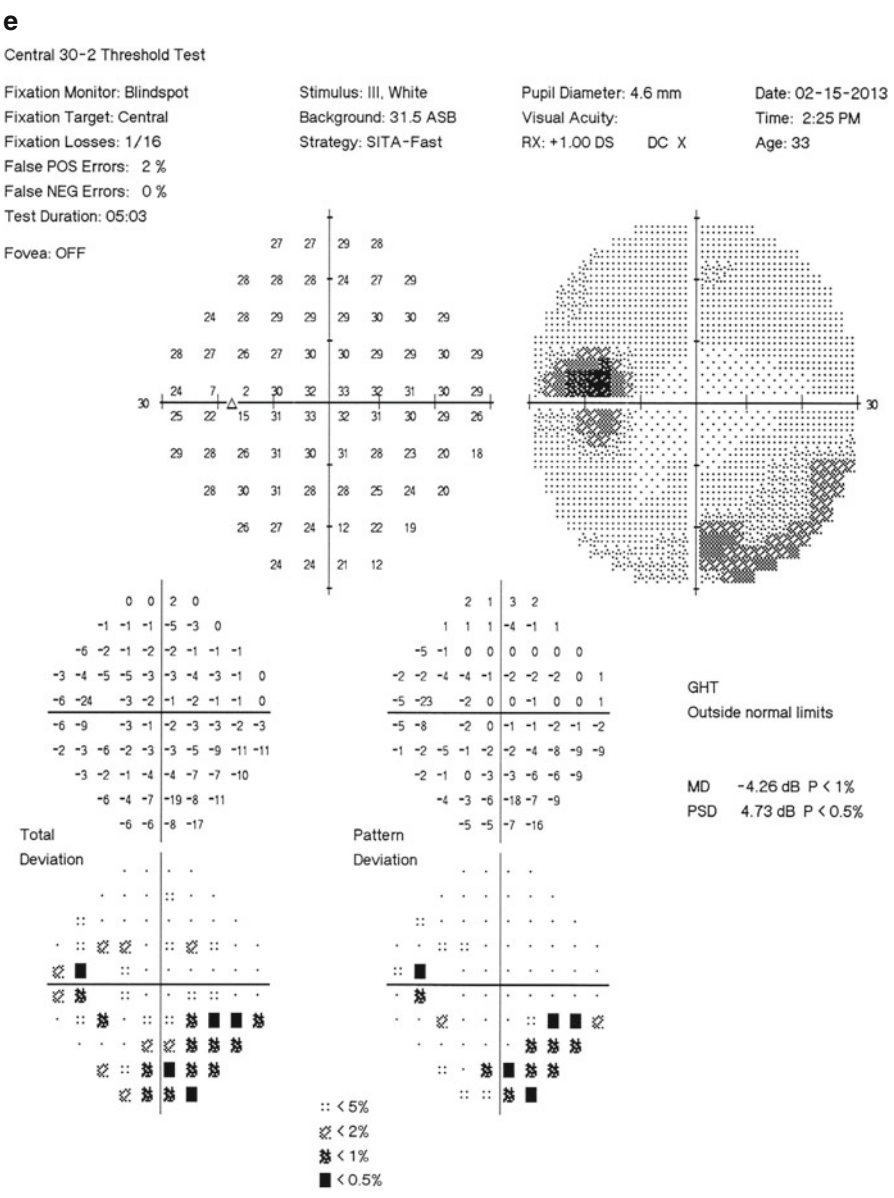

Fig. 3.2 (continued)

f

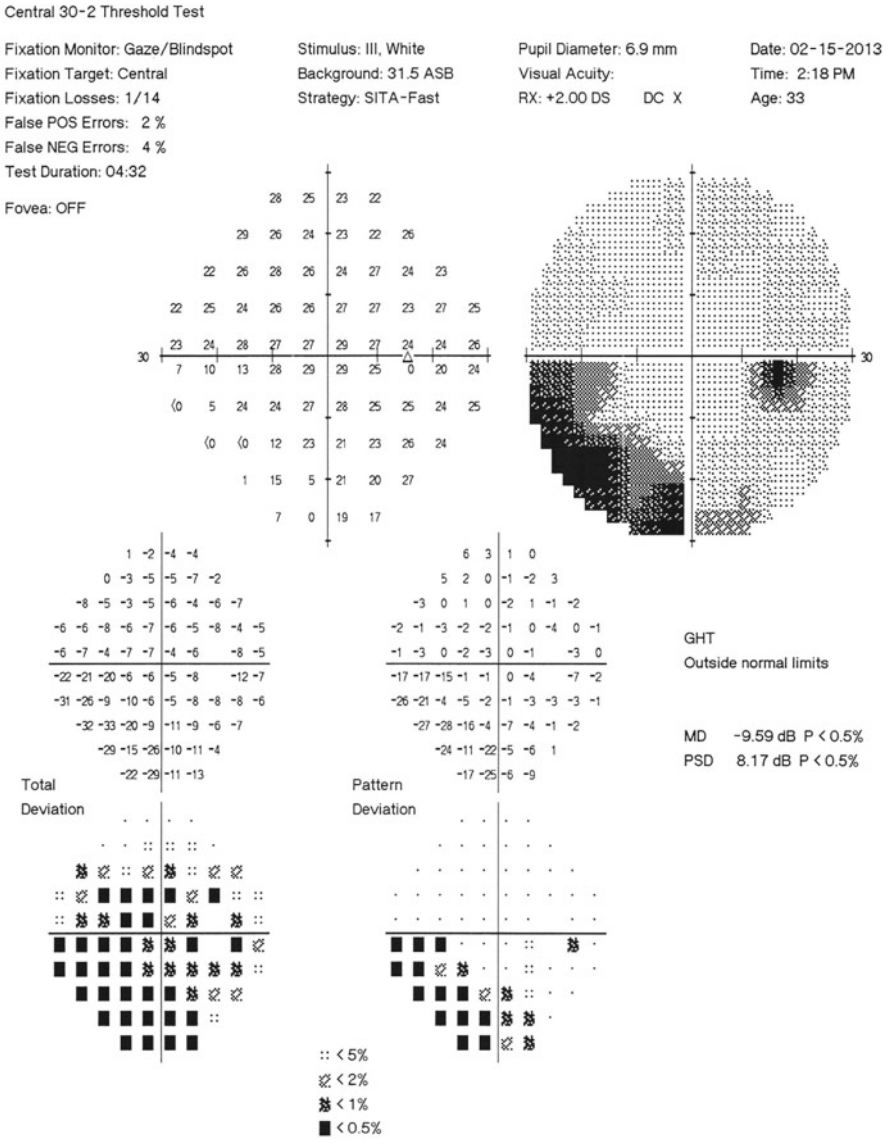

Fig. 3.2 (continued)

g

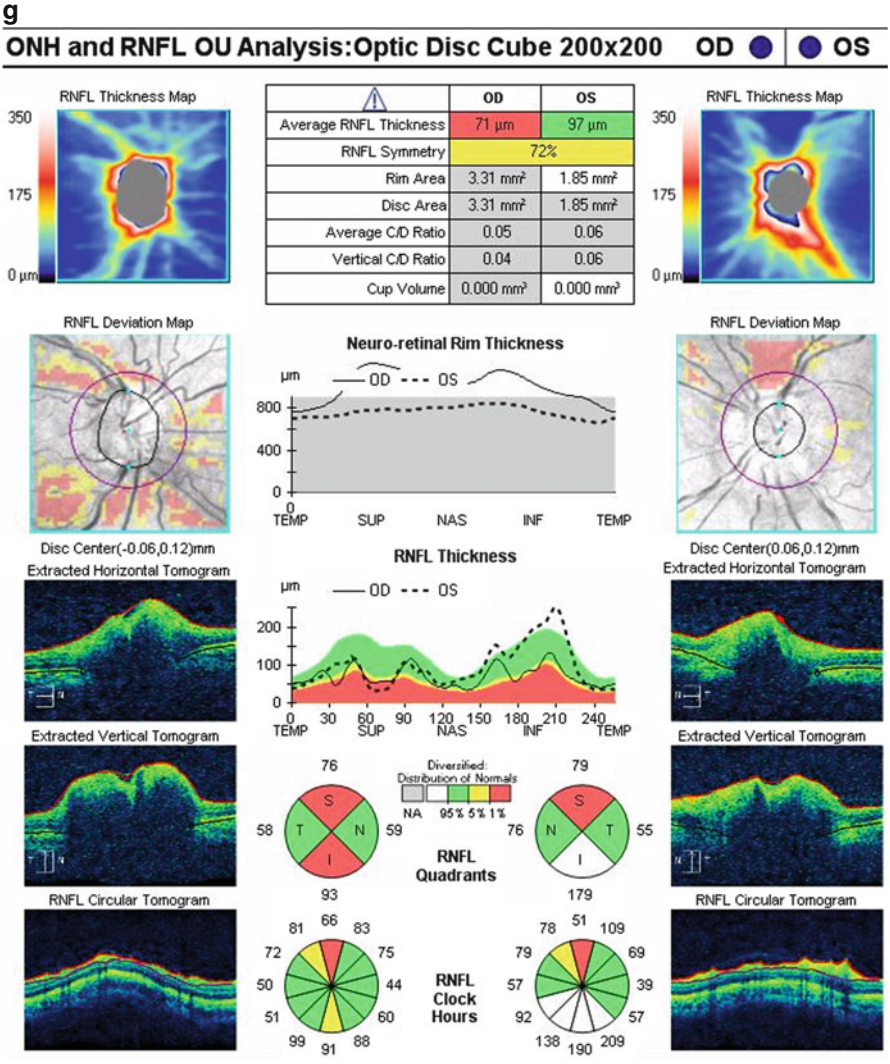

Fig. 3.2 (continued)

h

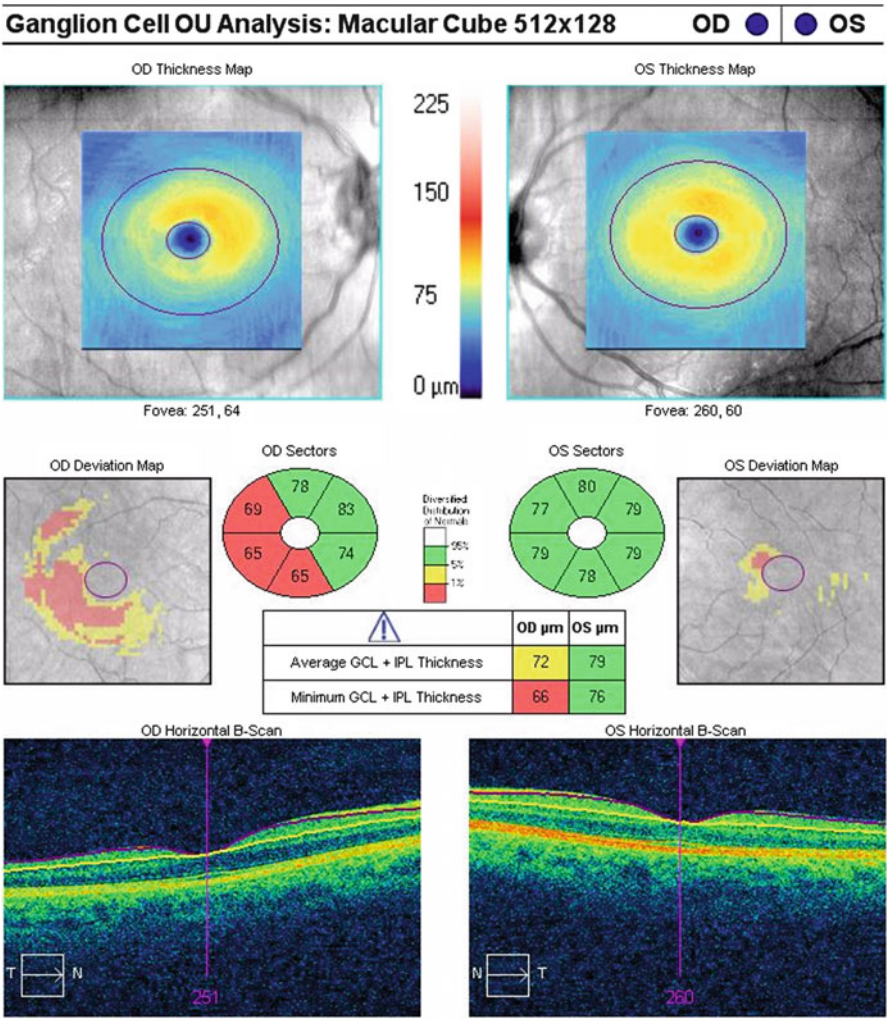

Fig. 3.2 (continued)

Using Fourier-domain OCT, Aggarwal et al. showed high correlation of the macular GCC thickness with visual field losses in both magnitude and location in patients with NAION, with hemispheric GCC loss correlating with altitudinal visual field loss [29]. Larrea et al. showed a significant correlation between GCC averages at the onset of NAION and visual field losses in both acute and chronic stages, suggesting that GCC thickness in the acute stage may be a determining factor to predict final visual field defects, with good correlation between location of damage in the GCC in the macular region and location of the scotoma [31].

Syc et al. demonstrated that GCC analysis can be used to evaluate neuronal injury acutely in eyes with optic neuritis from multiple sclerosis or neuromyelitis optica, when inflammation may lead to swelling of the optic disc and peripapillary RNFL, masking the early stages of axonal thinning and confounding accurate quantification of RNFL thickness. Such acute swelling precludes an accurate baseline measure of RNFL thickness to use as a point of reference for longitudinal assessment of axonal degeneration. Interestingly, there was absence of detectable swelling within the ganglion cell complex during the acute phase of optic neuritis, with subsequent thinning over time. Further, ganglion cell layer thickness was lower in optic neuritis patients when compared with healthy controls, and correlated with visual function [32].

3.2 Optic Disc Edema Secondary to Ischemia

Anterior ischemic optic neuropathy (AION) is characterized by abrupt visual loss with associated optic disc edema [33]. It is believed to be secondary to disrupted blood flow in a disc with retinal nerve fiber crowding and minimal to no physiologic cup. Although typically occurring unilaterally, optic disc edema secondary to AION can be confused with papilledema resulting from increased intracranial pressure. Both conditions have been associated with axonal swelling axoplasmic flow stasis in the optic nerve head, and can appear similar on ophthalmoscopy with disc swelling, obscured disc margins, and peripapillary hemorrhages [34].

AION occurs acutely, and is followed by a period of axonal swelling and subsequent thinning. After atrophy of the retinal ganglion cells has occurred, the optic neuropathy remains relatively stable [24].

At presentation, OCT can detect RNFL edema in AION. In the acute phase, the RNFL of the involved eye is significantly thicker than the fellow eye, and can be nearly doubled [35, 36]. The mean RNFL from superior, inferior, temporal, and nasal quadrants have been shown to all be significantly higher than the corresponding normal values [6]. This corresponds to histopathologic studies [37–39].

Over time, the optic disc edema decreases, and the RNFL undergoes thinning, corresponding to progressive optic atrophy and pallor. OCT can follow this evolution of initial thickening and progressive thinning of the RNFL as a proxy for estimating optic disc damage. By 2 months after the AION event, the RNFL thickness is similar to the fellow eye, marking resolution of optic disc edema. By 3–4 months,

RNFL thickness is decreased nearly 40 % in comparison to the fellow eye. By 12 months, the retinal nerve fiber loss is typically stabilized, with only a 6 % further reduction in RNFL thickness [35, 36]. Resolution of optic disc edema from the onset of visual acuity loss may be longer in patients with diabetes and maybe shorter in patients with worse initial visual field and visual acuity loss. Resolution of edema may be quicker in patients with more severe vision loss because the greater destruction of axons results in fewer axons to swell and cause edema [40].

Bellusci et al. used OCT to detect different patterns of RNFL damage in 16 eyes with NAION, classified by visual field loss. They found that eyes with NAION and VF loss limited to the inferior hemifield had RNFL atrophy limited to the superior half of the optic nerve head. Patients with diffuse VF loss had diffuse RNFL atrophy involving all quadrants around the disc. Patients with central or centrocecal scotoma had RNFL atrophy limited to the superior and temporal sectors [41]. Alasil et al. found similar correlation between the peripapillary nerve fiber layer thinning on OCT and severity and location of visual field defects. They also showed that the division between affected and nonaffected hemispheres is more complicated than the altitudinal defects seen on visual field testing, illustrated by the greatest relative loss of RNFL to be in the superior quadrant and superotemporal octant, correlating with visual field loss greatest inferonasally [42].

OCT demonstrates that some patients with optic disc edema secondary to non-arteritic optic neuropathy (NAION) develop subretinal fluid, similar to that which occurs in papilledema [7, 43]. Hedges et al. found 8 out of 76 patients studied with NAION had subfoveal fluid, when examined within 4 weeks of developing acute vision loss. Additional patients had peripapillary subretinal fluid and peripapillary subretinal fluid extending toward but not involving the fovea. OCT findings in the patients with subfoveal fluid included peripapillary subretinal hyporeflectivity next to the elevated optic nerve head with retinal nerve fiber thickening and hyporeflectivity under the fovea. Decreased visual acuity corresponded to degree of macular thickening. Similar to the subretinal fluid reported in some patients with papilledema, half of the patients had subretinal fluid that appeared to extend from the optic disc to the fovea. The other half of the patients had subretinal fluid in the peripapillary region and a separate area of subfoveal fluid. Reduction in OCT RNFL thickness and resolution of subretinal fluid corresponded to improvement in visual acuity [43].

In non-glaucomatous optic neuropathies, like NAION, greater damage occurs in the papillomacular fibers, with resultant loss of central acuity. Therefore, although the site of damage occurs at the optic nerve head, axons have cell bodies in the macula and contribute to macular thickness [44].

Papchenko et al. studied the macular thickness in addition to the retinal nerve fiber layer thickness in patients with NAION, and found a stronger correlation between macular thickness and Humphrey visual field sensitivity than RNFL parameters, suggesting that macular thickness may be a surrogate marker for determining the extent of nerve injury in NAION. They found that in patients with inferior visual field defects, the total macula thickness and temporal thickness were thinner when compared to control eyes [28]. Similarly, Fernandez-Beunaga et al. found that nasal macular thickness correlated with visual acuity in ischemic optic neuropathy [44].

Ganglion cell thickness has been shown in both the acute and chronic stages to correlate with visual field parameters and may predict final visual field defects in NAION. Further, location of ganglion cell damage in the macular region correlates with location of visual field scotoma. Thus, ganglion cell thickness as measured by OCT may detect axonal damage in acute NAION, when the RNFL is still grossly edematous (Fig. 3.3) [28, 29, 31].

a

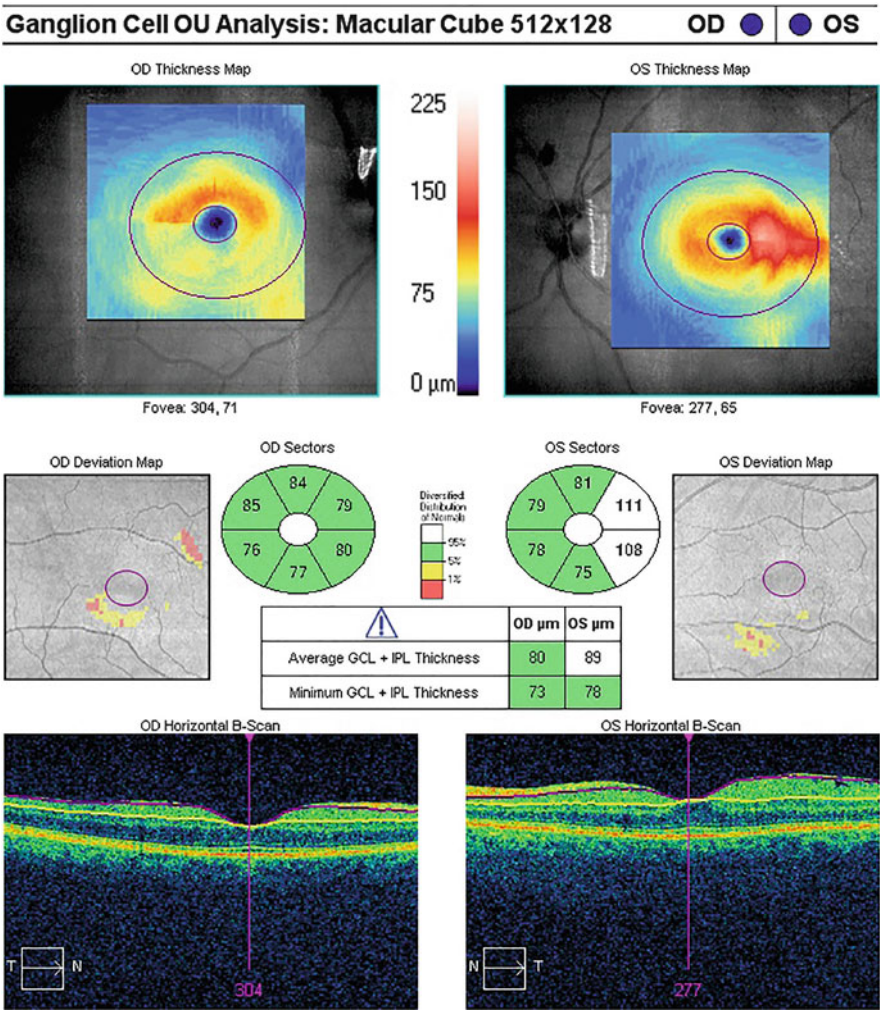

Fig. 3.3 Optic disc edema secondary to NAION. A 78-year-old man with hypertension awoke with a dark shadow in his right eye upon awakening. He had a superior hemifield defect in his right eye on HVF 30–2 testing. Fundoscopy and OCT RNFL analysis revealed diffuse swelling of the optic nerve in the right eye (**a**). Despite the edema on RNFL analysis, there was thinning inferiorly in the right eye on ganglion cell analysis, suggesting neuronal loss (**b**)

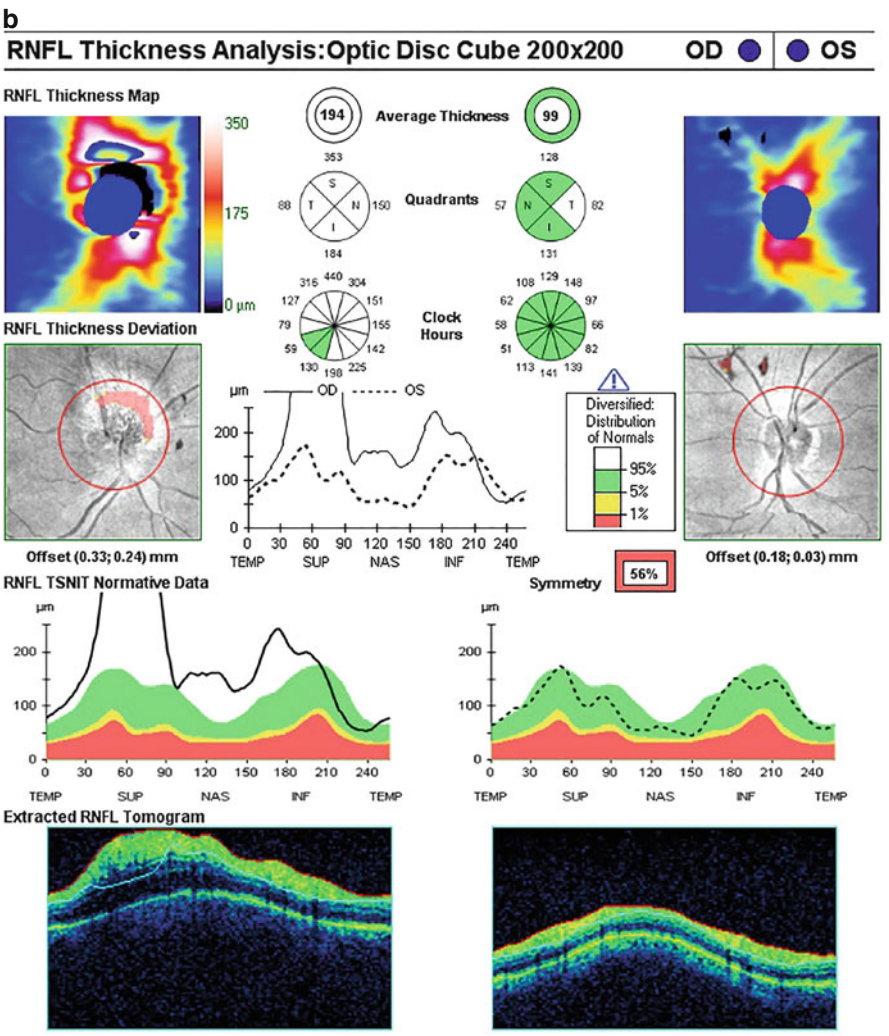

Fig. 3.3 (continued)

3.3 Optic Disc Edema Secondary to Toxic/Hereditary/ Nutritional Optic Neuropathies

High definition optical coherence tomography (OCT) has shed some light on the events occurring at the optic nerve head in LHON, including a more clear depiction of axonal swelling, which precedes and is present at the time of visual loss. Furthermore, OCT clearly shows and can measure atrophy of the nerve fiber layer (RNFL) following the acute event, which in most cases, is confined to the papillomacular bundle [45–47]. We have noted in the early phase, when visual acuity begins to decline, the GCC remains relatively normal, while the RNFL becomes swollen and frequently is associated with peripapillary telangiectasias. Within days, as vision further declines, the GCC starts to appear thinner. The RNFL thickening resolves or becomes thin only until the chronic phase in most patients. In some cases, average RNFL thickness remains relatively normal despite GCC loss, creating a mismatch between RNFL and GCC thickness measurements. In cases where RNFL loss is mild, the papillomacular bundle is affected. The degrees of GCC thinning or RNFL loss does not correlate with final visual acuity or visual fields even if there is visual recovery.

3.4 Pseudopapilledema

3.4.1 Pseudopapilledema: Vitreopapillary Traction

OCT has been useful in distinguishing other causes of pseudopapilledema, such as vitreopapillary traction (Fig. 3.4), optic nerve head drusen (Fig. 3.5), myelinated nerve fiber layer, and Bergmeister papillae (Fig. 3.6).

Posterior vitreous detachment is a dynamic process characterized by the liquefaction and separation of the posterior vitreous cortex from the inner limiting membrane of the retina. Proliferative disorders, such as the development of premacular membranes, and tractional disorders, such as macular hole formation can result from faulty separation at this interface. If the vitreous partially or anomalously separates from the internal limiting membrane, it can lead to persistent adhesion and even traction on posterior pole structures [48].

Vitreomacular traction syndrome, a result of a partially or anomalously separated vitreous face, is a well-known clinical entity that has been well described in the literature. In 1954, Schepens used the term pseudopapilledema when he demonstrated the histopathology of partially detached vitreous at the optic nerve head, usually in the context of co-existing retinal disease [49], such as proliferative diabetic retinopathy [50], central retinal vein occlusion [51], and non-arteritic ischemic optic neuropathy [52]. Using slit lamp biomicroscopy and ultrasonography, Katz and Hoyt observed peripapillary and intrapapillary hemorrhage in eight young patients with mildly dysplastic discs and persistent vitreopapillary traction, postulating that transmitted forces traumatized disc

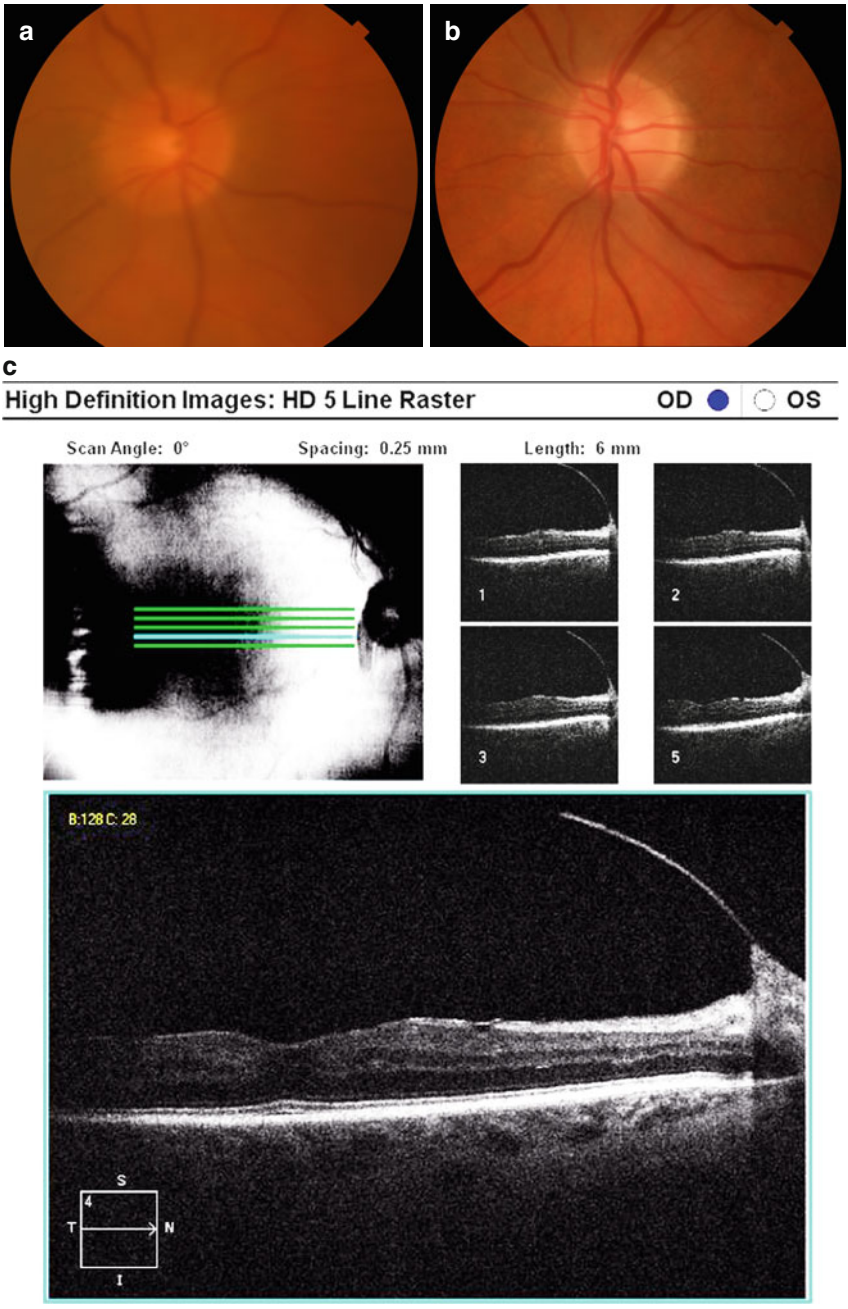

Fig. 3.4 Vitreopapillary traction. A 79-year-old man was referred for declining vision in both eyes. The view to the optic disc in the right eye was hazy secondary to cataract, and the optic disc margins appeared somewhat indistinct (**a**). The left eye had clear media and no obvious disc edema (**b**). OCT revealed vitreopapillary traction in the right (**c**) and the left (**d**) eyes. The RNFL showed no true optic disc swelling in either eye (**e**)

d

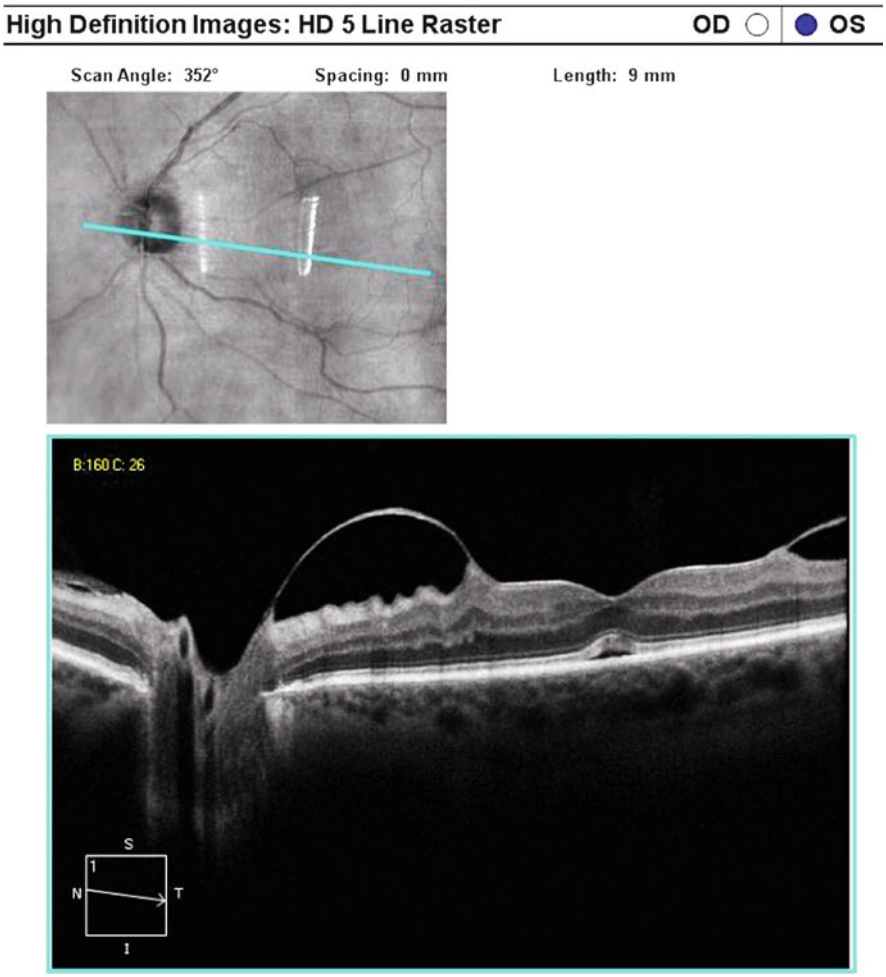

Fig. 3.4 (continued)

e

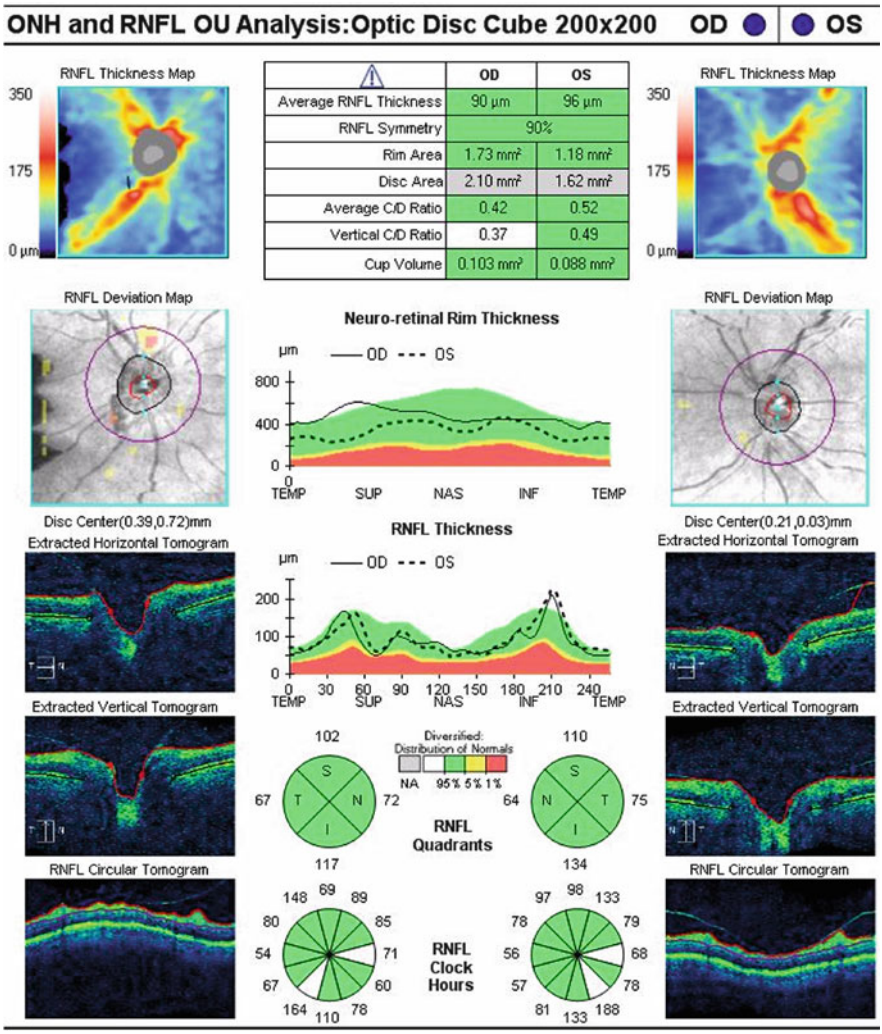

Fig. 3.4 (continued)

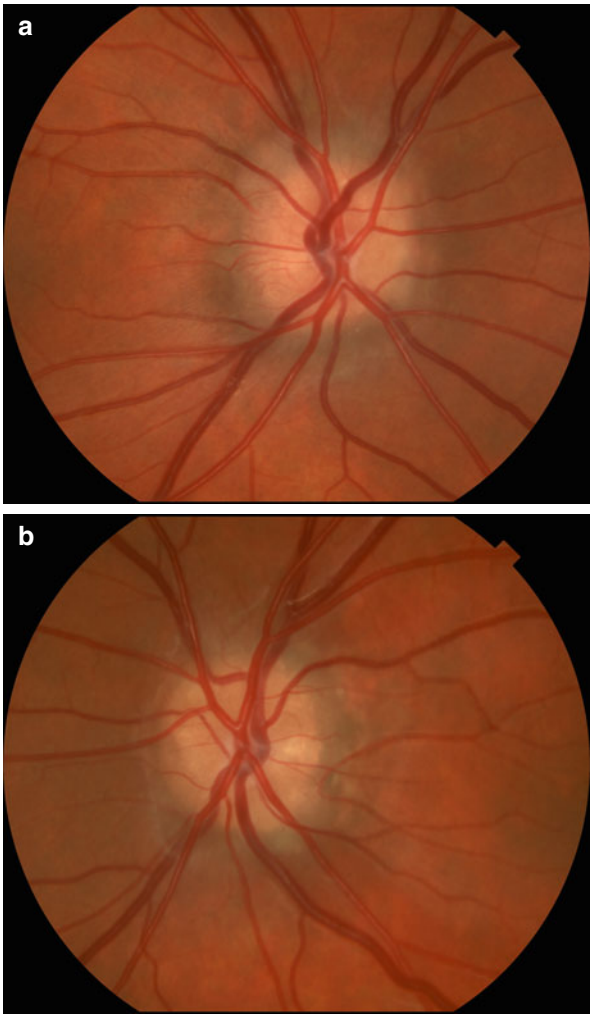

Fig. 3.5 Optic disc drusen. An 18-year-old man was referred for bilateral visual field defects noted on routine examination. On examination, visual acuities were 20/20 in both eyes, there was no afferent papillary defect, and color vision was preserved. The optic discs appeared crowded, with indistinct margins in the right (**a**) and left (**b**) eyes. OCT of the optic discs revealed an elevated optic nerve head with an irregular internal optic nerve contour in the right (**c**) and left (**d**) eyes. Despite the crowded appearance, OCT RNFL analysis revealed thinning superiorly and inferiorly in both eyes (**e**). Fundus auto-fluorescence revealed numerous round lesions with increased auto-fluorescence on the optic nerve head in both eyes, consistent with optic nerve head drusen. He remained stable at follow-up 1 year later

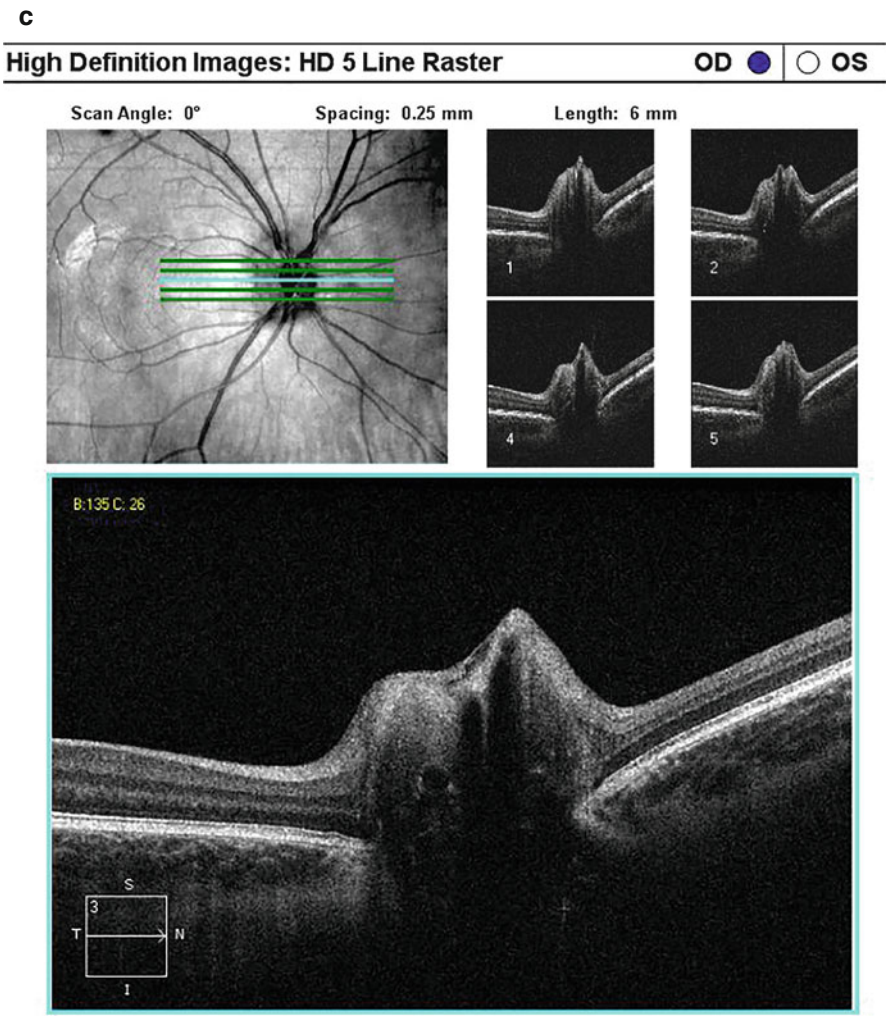

Fig. 3.5 (continued)

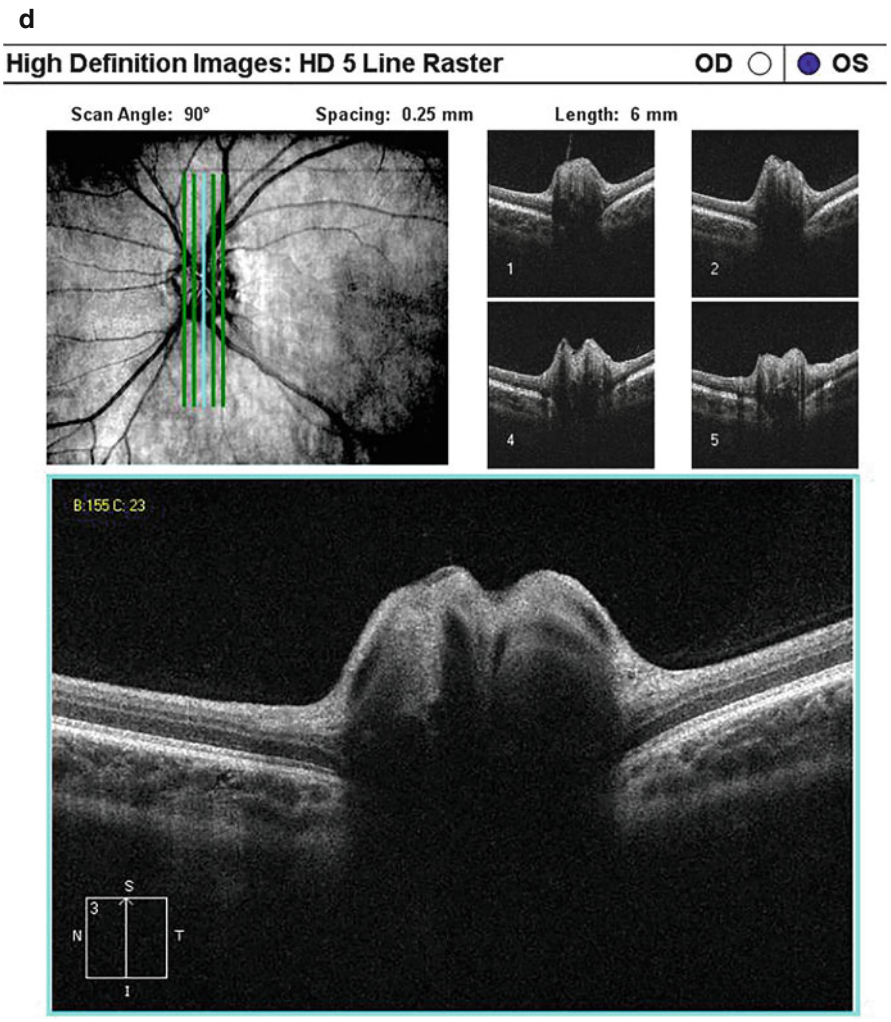

Fig. 3.5 (continued)

e

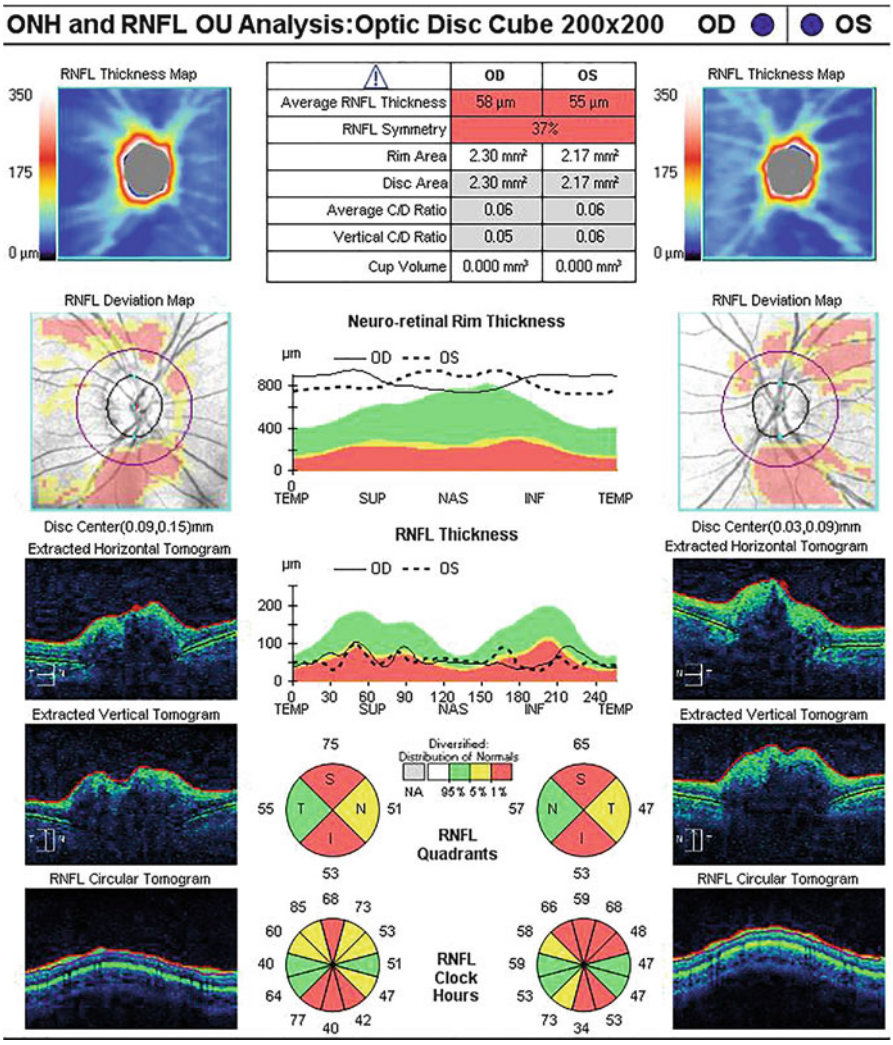

Fig. 3.5 (continued)

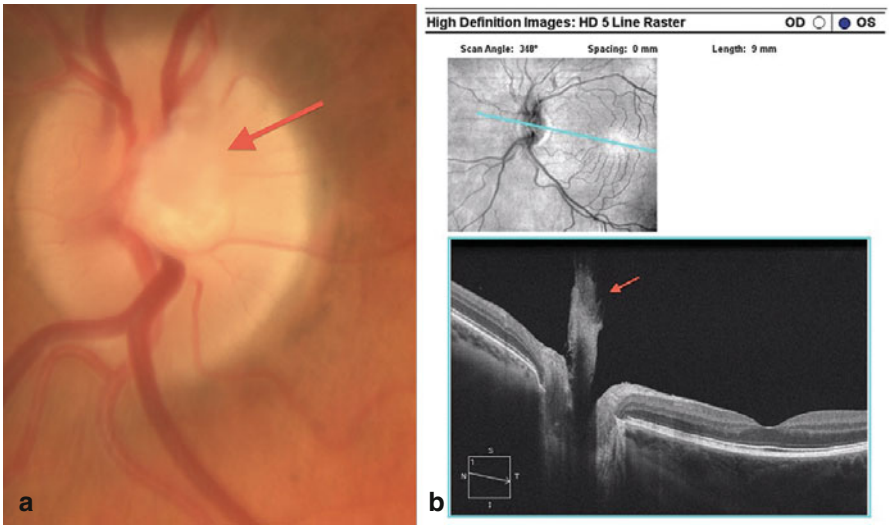

Fig. 3.6 Bergmeister papilla. A 43-year-old woman was referred for pain in her left eye. Incidentally, a small tuft of tissue was visualized at the optic disc (**a**) and appeared to be continuous with the optic disc on OCT (**b**), consistent with Bergmeister papillae

vessels [53]. In addition, Wisotsky et al. demonstrated in two patients that vitreopapillary traction could cause highly elevated optic discs with blurring of the margins [54].

In 2006, Hedges et al. demonstrated by OCT that persistent vitreopapillary traction could occur as an isolated phenomenon, in the absence of proliferative fibrocellular membranes or vascular insult [55]. Tractional forces from vitreous adhesion on the optic nerve alone were sufficient in causing optic disc elevation, obscured disc margins, and peripapillary hemorrhage in these patients [55]. Vitreopapillary traction has even been shown to cause focal disc leakage on fluorescein angiography [56]. When occurring bilaterally, vitreopapillary traction can be confused with papilledema, potentially leading to costly and invasive diagnostic procedures and even unnecessary treatment [56].

3.4.2 Pseudopapilledema: Optic Nerve Head Drusen

ONHD are calcified hyaline deposits and have been associated with small, crowded optic discs [57]. Histopathologically, they are associated with elevation of the optic nerve head, compression of optic nerve fibers, disc hemorrhages, and juxtapapillary retinal scarring [58]. Several predisposing factors for the development of ONHD have been proposed, including a small scleral canal, altered axoplasmic transport, and abnormal vasculature [59].

When ONHD are superficially located on the nerve, they can be recognized as refractile deposits. When they are buried within the optic nerve head, however, they can be much more difficult to identify by ophthalmoscopy alone. Further, they can elevate the optic nerve head and obscure the margins of the optic disc. It is estimated that in approximately 2/3–4/5 of cases, ONHD occurs bilaterally [59]. In these cases, ONHD can simulate papilledema. This pseudopapilledema secondary to ONHD is typically benign, whereas true papilledema requires emergent work-up for a potentially life-threatening condition. Thus, differentiating true optic disc edema caused by papilledema or other optic neuropathies is crucial for the ophthalmologist.

Various methodologies have been used to study buried ONHD, including fundus autofluoresence, B-scan ultrasonography, computerized tomography, and fluorescein angiography [60]. Currently, B-scan ultrasonography is commonly used in the clinical evaluation of ONHD. Although useful, B-scan ultrasonography necessitates a skilled ultrasonographer and interpreter, and is not always available. OCT is a widely available and can give information regarding the size, structure, and location of ONHD within the optic disc.

Thinning of the RNFL OCT is often associated with optic atrophy, and thickening of the RNFL OCT is often associated with optic disc edema [21]. However, both ONHD and optic disc edema can present with either RNFL thinning or RNFL thickening on OCT [61]. Therefore, the presence or absence of RNFL thinning or thickening alone does not help the clinician distinguish between ONHD and optic disc edema [62].

Savini et al. examined nine patients with optic disc edema due to various causes. In addition to noting a significant increase in the mean RNFL thickness in all optic nerve quadrants in patients with optic disc edema, they described a triangular-shaped hyporeflective subretinal space above the retinal pigment epithelium, possibly representing subretinal fluid, with the widest part of the triangle abutting the optic nerve head and the tapered apex pointing away. They hypothesized that swelling induced by the optic disc edema could produce an upward traction producing a subretinal space with the hydrostatic forces overcoming osmotic forces [24].

Expanding on this idea of subretinal hyporeflective space, Johnson et al., used OCT images to examine the qualitative and quantitative differences between ONHD and optic disc edema. They found that patients with ONHD tended to have an elevated optic nerve head with a “lumpy bumpy” internal optic nerve contour, a rapid and abrupt decline in subretinal hyporeflective space with a normal thickness at the 2.0 mm radius, and normal or mildly increased RNFL thickness with the nasal RNFL being less than 86 microns. Patients with optic disc edema, on the other hand, had an elevated optic nerve head with a smooth internal contour, a recumbent “lazy V” pattern of the subretinal hyporeflective space with an increased thickness at the 2.0 mm radius, and an increased RNFL thickness with a nasal RNFL greater than 86 microns. They found a nasal RNFL thickness greater than 86 microns has 80 % specificity and a subretinal hyporeflective space thickness greater than 169 microns at 2.0 mm radius has 90 % specificity in differentiating between optic disc edema and ONHD [60].

Using SD-OCT, Lee et al. found ONHD to be focal, hyperreflective subretinal masses with distinct margins. They found the RNFL to be deformed with high reflectance and the ONHD to be beneath the outer nuclear layer and on the retinal pigment epithelium. They proposed that the increased thickness and deposition of axonal transport materials in the RNFL in optic disc edema could increase peripapillary RNFL reflectance and induce shadowing of the underlying retinal layers, mimicking subretinal fluid space rather than representing it. Like Johnson et al., they found RNFL thickness in the nasal section to be a good differential marker for optic disc edema from ONHD, with a thinner cut-off value of 78 microns [63].

Enhanced depth imaging OCT (EDI-OCT), a technique developed to give superior imaging quality of the deeper structures of the retina and optic nerve head, has also shown useful in detecting ONHD. Merchant et al., in an analysis of 34 patients with clinically visible or suspected ONHD based on ophthalmoscopy or optic disc stereophotography, EDI OCT had a significantly higher ONHD detection rate than B-scan ultrasound [64].

3.4.3 Pseudopapilledema: Bergmeister's Papilla and Myelinated Nerve Fiber Layer

OCT can help characterize other conditions causing pseudopapilledema. In cases of myelinated retinal nerve fiber layer, OCT can show significant hyper-reflectivity and increased thickness of the RNFL in the area of the myelinated fibers [65, 66]. The recent use of wide field three-dimensional swept source OCT (SS-OCT), which utilizes better sensitivity with imaging depth and longer imaging range, has enabled enhanced imaging of vitreous and vitreo-retinal interface. SS-OCT can offer superior resolution of vitreo-retinal entities, such as Bergmeister's papillae that may simulate papilledema [67].

References

1. Von Graefe A. Ueber Komplikation von Sehnervenentzundung mit Gehirnkrankheiten. Arch F Ophth. 1860;7:58–71.
2. Paton L, Holmes G. The pathology of papilledema. Brain. 1911;33:289–432.
3. Fry WE. The pathology of papilledema. Am J Ophth. 1931;14:874–83.
4. Hedges TR. A correlative study of orbital vascular and intracranial pressure in the Rhesus monkey. Trans Am Ophthalmol Soc. 1963;61:589–637.
5. Tso MO, Hayreh SS. Optic disc edema in raised intracranial pressure III: a pathologic study of experimental papilledema. Arch Ophthalmol. 1977;95:1448–57.
6. Samuels B. Histopathology of papilledema. Am J Ophthalmol. 1938;21:1242–8.
7. Hoye III VJ, Berrocal AM, Hedges III TR, Amaro-Quireza ML. Optic coherence tomography demonstrates subretinal macular edema from papilledema. Arch Ophthalmol. 2001; 119:1287–9.
8. Morris AT, Sanders MD. Macular changes resulting from papilloedema. Br J Ophthalmol. 1980;64:211–6.

9. Corbett JJ, Jacobson DM, Mauer RC, Thompson HS. Enlargement of the blind spot caused by papilledema. Am J Ophthalmol. 1988;105:261–5.
10. Gittinger Jr JW, Asdourian GK. Macular abnormalities in papilledema from pseudotumor cerebri. Ophthal. 1989;96:192–4.
11. Jamerson SC, Arunagiri G, Ellis BD, Leys MJ. Intravitreal bevacizumab for the treatment of choroidal neovascularization secondary to pseudotumor cerebri. Int Ophthalmol. 2009;29:183–5.
12. Jamison RR. Subretinal neovascularization and papilledema associated with pseudotumor cerebri. Am J Ophthalmol. 1978;85:78–81.
13. Mas AM, Villegas VM, Garcia JM, Acevedo S, Serrrano L. Intravitreal bevacizumab for peripapillary subretinal neovascular membrane associated to papilledema: a case report. P R Health Sci J. 2012;31:148–50.
14. Lee IJ, Maccheron LJ, Kwan AS. Intravitreal bevacizumab in the treatment of peripapillary choroidal neovascular membrane secondary to idiopathic intracranial hypertension. J Neuroophthalmol. 2013;33:155–7.
15. Morse PH, Leveille AS, Antel JP, Burch JV. Bilateral juxtapapillary subretinal neovascularization associated with pseudotumor cerebri. Am J Ophthalmol. 1981;91:312–7.
16. Caballero-Presencia A, Diaz-Guia E, Martinex-Perez M, Lopez-Lopez J. Neo-vascularisation sous-retinienne jiuxtapapillaire bilaterale dans un cas de pseudotumor cerebri. J Fr Ophtalmol. 1986;9:105–10.
17. Sathornsumetee B, Webb A, Hill DL, Newman NJ, Biousse V. Subretinal hemorrhage from a peripapillary choroidal neovascular membrane in papilledema caused by idiopathic intracranial hypertension. J Neuroophthalmol. 2006;26:197–9.
18. Kaeser PF, Borruat FX. Peripapillary neovascular membrane: a rare cause of acute vision loss in pediatric idiopathic intracranial hypertension. J AAPOS. 2011;15:83–6.
19. Troost BT, Sufit RL, Grand MG. Sudden monocular visual loss in pseudotumor cerebri. Arch Neurol. 1979;36:440–2.
20. Martinez MR, Ophir A. Optical coherence tomography as an adjunctive tool for diagnosing papilledema in young patients. J Pediatr Ophthalmol Strabismus. 2011;48:174–81.
21. Karam EZ, Hedges TR. Optical coherence tomography of the retinal nerve fibre layer in mild papilloedema and pseudopapilloedema. Br J Ophthalmol. 2005;89:294–8.
22. Fard MA, Fakhree S, Abdi P, Hassanpoor N, Subramanian PS. Quantification of peripapillary total retinal volume in pseudopapilledema and mild papilledema using spectral-domain optical coherence tomography. Am J Ophthalmol. 2014;158:136–43.
23. Sibony P, Straachovsky M, Honkanen R, Kupersmith MJ. Optical coherence tomography shape analysis of the peripapillary retinal pigment epithlium layer in presumed optic nerve sheath meningiomas. J Neuroophthalmol. 2014;34:130–6.
24. Savini G, Bellusci C, Carbonelli M, Zanini M, Carelli V, Sadun AA, Barboni P. Detection and quantification of retinal nerve fiber layer thickness in optic disc edema using stratus OCT. Arch Ophthalmol. 2006;124:1111–7.
25. Monteiro ML, Afonso CL. Macular thickness measurements with frequency domain-OCT for quantification of axonal loss in chronic papilledema from pseudotumor cerebri syndrome. Eye (Lond). 2014;28:390–8.
26. Perry VH, Lund RD. Evidence that the lamina cribrosa prevents intraretinal myelination of retinal ganglion cell axons. J Neurocytol. 1990;19:265–72.
27. Burkholder BM, Osborne B, Loguidice MJ, Bisker E, Frohman TC, Conger A, Ratchford JN, Warner C, Markowitz CE, Jacobs DA, Galetta SL, Cutter GR, Maguire MG, Calabresi PA, Balcer LJ, Frohman EM. Macular volume determined by optical coherence tomography as a measure of neuronal loss in multiple sclerosis. Arch Neurol. 2009;66:1366–72.
28. Papchenko T, Grainger BT, Savino PJ, Gamble GD, Danesh-Meyer HV. Macular thickness predictive of visual field sensitivity in ischaemic optic neuropathy. Acta Ophthalmol. 2012;90:e463–9.
29. Aggarwal D, Tan O, Huang D, Sadun AA. Patterns of ganglion cell complex and nerve fiber layer loss in nonarteritic ischemic optic neuropathy by Fourier-domain optical coherence tomography. Invest Ophthalmol Vis Sci. 2012;53:4539–45.

30. Bianchi MS, Ciasca P, Curone M, Cammarata G, Melzi L, Criscuoli A, Bussone G, D'Amico D. Quantitative analysis of optic nerve damage in idiopathic intracranial hypertension (IIH) at diagnosis. Neurol Sci. 2013;34 Suppl 1:S143–5.
31. Larrea BA, Iztueta MG, Indart LM, Alday NM. Early axonal damage detection by ganglion cell complex analysis with optical coherence tomography in nonarteritic anterior ischaemic optic neuropathy. Graefes Arch Clin Exp Ophthalmol. 2014;252:1839–46.
32. Syc SB, Saidha S, Newsome SD, Ratchford JN, Levy M, Ford E, Crainiceanu CM, Durbin MK, Oakley JD, Meyer SA, Frohman EM, Calabresi PA. Optical coherence tomography segmentation reveals ganglion cell layer pathology after optic neuritis. Brain. 2012;135:521–33.
33. Hayreh SS. Anterior ischemic optic neuropathy. Arch Neurol. 1981;38:675–8.
34. Hayreh SS. Fluids in the anterior part of the optic nerve in health and disease. Surv Ophthalmol. 1978;23:1–25.
35. Contreras I, Noval S, Rebolleda G, Munoz-Negrete FJ. Follow-up of nonarteritic anterior ischemic optic neuropathy with optical coherence tomography. Ophthalmology. 2007;114:2338–44.
36. Contreras I, Rebolleda G, Noval S, Munoz-Negrete FJ. Optic disc evaluation by optical coherence tomography in nonarteritic anterior ischemic optic neuropathy. Invest Ophthalmol Vis Sci. 2007;48:4087–92.
37. Quigley HA, Miller NR, Green WR. The pattern of optic nerve fiber loss in anterior ischemic optic neuropathy. Am J Ophthalmol. 1985;100:769–76.
38. Traustason OI, Feldon SE, Leemaster JE, Weiner JM. Anterior ischemic optic neuropathy: classification of field defects by Octopus automated static perimetry. Graefes Arch Clin Exp Ophthalmol. 1988;226:206–12.
39. Hayreh SS, Zimmerman MB. Visual field abnormalities in nonarteritic anterior ischemic optic neuropathy: their pattern and prevalence at initial examination. Arch Ophthalmol. 2005;23: 1554–62.
40. Hayreh SS, Zimmerman MB. Optic disc edema in non-arteritic anterior ischemic optic neuropathy. Graefes Arch Clin Exp Ophthalmol. 2007;245:1107–21.
41. Bellusci C, Savini G, Carbonelli M, Carelli V, Sadun AA, Barboni P. Retinal nerve fiber layer thickness in nonarteritic ischemic optic neuropathy: OCT characterization of the acute and resolving phases. Graefes Arch Clin Exp Ophthalmol. 2008;246:641–7.
42. Alasil T, Tan O, Lu ATH, Huang D, Sadun AA. Correlation of fourier domain optical coherence tomography retinal nerve fiber layer maps with visual fields in nonarteritic ischemic optic neuropathy. Ophthalmic Surg Lasers Imaging. 2008;39:S71–9.
43. Hedges III TR, Vuong LN, Gonzalez-Garcia AO, Mendoza-Santiesteban CE, Amaro-Quierza ML. Subretinal fluid from anterior ischemic optic neuropathy demonstrated by optical coherence tomography. Arch Ophthalmol. 2008;126:812–5.
44. Fernandez-Buenaga R, Rebolleda G, Munoz-Negrete FJ, Contreras I, Casas-Llera P. Macular thickness. Ophthalmology. 2009;116:1587.
45. Barboni P, Savini G, Valentino ML, et al. Retinal nerve fiber layer evaluation by optical coherence tomography in Leber's hereditary optic neuropathy. Ophthalmology. 2005;112:120–6.
46. Zhang Y, Huang H, Wei S, et al. Characterization of macular thickness changes in Leber's hereditary optic neuropathy by optical coherence tomography. BMC Ophthalmol. 2014; 14:105.
47. Savini G, Barboni P, Valentino ML, et al. Retinal nerve fiber layer evaluation by optical coherence tomography in unaffected carriers with Leber's hereditary optic neuropathy mutations. Ophthalmology. 2005;112:127–31.
48. Sebag J. Anatomy and pathology of the vitreo-retinal interface. Eye. 1992;6(6):541–52.
49. Schepens CL. Clinical aspects of pathologic changes in the vitreous body. Am J Ophthalmol. 1954;38:8–21.
50. Kroll P, Weigrand W, Schmidt J. Vitreopapillary traction in proliferative diabetic vitreoretinopathy. Br J Ophthalmol. 1999;83:261–4.
51. Rumelt S, Karatas M, Pikkel J, Majlin M, Ophir A. Optic disc traction syndrome associated with central retinal vein occlusion. Arch Ophthalmol. 2003;121:1093–7.

52. Modarres M, Sanjari MS, Falavarjani KG. Vitrectomy and release of presumed epipapillary vitreous traction for treatment of nonarteritic anterior ischemic optic neuropathy associated with partial posterior vitreous detachment. Ophthalmology. 2007;114(2):340–4.
53. Katz B, Hoyt WF. Intrapapillary and peripapillary hemorrhage in young patients with incomplete posterior vitreous detachment: signs of vitreopapillary traction. Ophthalmology. 1995;102:349–54.
54. Wisotsky BJ, Magat-Gordon CB, Puklin JE. Vitreopapillary traction as a cause of elevated optic nerve head. Am J Ophthalmol. 1998;126:137–9.
55. Hedges TR, Flattem NL, Bagga A. Vitreopapillary traction confirmed by optical coherence tomography. Arch Ophthalmol. 2006;124(2):349–54.
56. Houle E, Miller NR. Bilateral vitreopapillary traction demonstrated by optical coherence tomography mistaken for papilledema. Case Rep Ophthalmol Med. 2012;2012:682659.
57. Lam BL, Morais Jr CG, Pasol J. Drusen of the optic disc. Curr Neurol Neurosci Rep. 2008;8: 404–8.
58. Friedman AH, Gartner S, Modi SS. Drusen of the optic disc: a retrospective study in cadaver eyes. Br J Ophthal. 1975;59:413–21.
59. Auw-Haedrich C, Staubach F, Witschel H. Major review: optic disk drusen. Surv Ophthalmol. 2002;47:515–32.
60. Johnson LN, Diehl ML, Hamm CW, Sommerville DN, Petroski GF. Differentiating optic disc edema from optic nerve head drusen on optical coherence tomography. Arch Ophthalmol. 2009;127:45–9.
61. Katz BJ, Pomeranz HD. Visual field defects and retinal nerve fiber layer defects in eyes with buried optic nerve drusen. Am J Ophthalmol. 2006;141:248–53.
62. Roh S, Noecker RJ, Schuman JS, Hedges III TR, Weiter JJ, Mattox C. Effect of optic nerve head drusen on nerve fiber layer thickness. Ophthalmol. 1998;105:878–85.
63. Lee KM, Woo SJ, Hwang JM. Differentiation of optic nerve head drusen and optic disc edema with spectral domain optical coherence tomography. Ophthalmology. 2011;118:971–7.
64. Merchant KY, Su D, Park SC, Qayum S, Banik R, Liebmann JM, Ritch R. Enhanced depth imaging optical coherence tomography of optic nerve head drusen. Ophthalmology. 2013;120:1409–14.
65. Salvatore S, Iannetti L, Fragiotta S, Vingolo EM. Optical coherence tomography and myelinated retinal nerve fibers: anatomical description and comparison between time-domain and spectral domain OCT. Minerva Oftalmol. 2011;53:31–8.
66. Nourinia R, Behdad B, Montahaei T. Optical coherence tomography findings in a patient with myelinated retinal nerve fiber layer. J Ophthalmic Vis Res. 2013;8:280–1.
67. Liu JJ, Witkin AJ, Adhi M, Grulkowski I, Kraus MF, Dhalla AH, Lu CD, Hornegger J, Duker JS, Fukimoto JG. Enhanced vitreous imaging in healthy eyes using swept source optical coherence tomography. PLoS One. 2014;9(7):e102950.

Chapter 4
OCT and Compressive Optic Neuropathy

Mário Luiz Ribeiro Monteiro

Abstract Optical coherence tomography (OCT) has provided new and important resources for quantification of retinal neural loss in many different optic nerve diseases including compressive optic neuropathies. As in other optic neuropathies OCT can be useful for diagnosis and follow-up of both optic nerve and chiasmal compressive diseases. Axonal loss can be assessed both through peripapillary retinal nerve fiber layer measurements as well as using macular thickness measurements, particularly when segmented analysis of different retinal layers are analyzed. By analyzing the amount of axonal loss OCT can also be of help in estimating the possibility of visual improvement in such conditions. In this chapter we discuss the main use of OCT in compressive optic neuropathies including primary optic nerve tumors, extrinsic optic nerve compression by tumors or other orbital lesions and the important group of diseases causing chiasmal compression.

Keywords Optic neuropathy • Optic nerve compression • Optic nerve tumor • Chiasmal syndrome • Pituitary tumors • Band atrophy • Optical coherence tomography • Retinal nerve fiber layer • Macular thickness measurements

4.1 Introduction

Compressive optic neuropathies are among the most important diseases of the anterior visual pathway and can lead to severe visual handicap particularly when an early diagnosis is not obtained. It encompass a wide array of conditions including optic nerve glioma and meningioma, extrinsic optic nerve compression by orbital tumor, enlarged muscles in Graves' orbitopathy, sinus expansive disease or intracranial tumors affecting the optic nerve and chiasm such as occurs in pituitary

M.L.R. Monteiro, MD, PhD
Division of Ophthalmology, Department of Ophthalmology and Otolaryngology,
University of São Paulo Medical School, Av. Angélica 1757 conj. 61,
São Paulo, SP, 01227-200, Brazil
e-mail: mlrmonteiro@terra.com.br

A. Grzybowski, P. Barboni (eds.), *OCT in Central Nervous System Diseases: The Eye as a Window to the Brain*, DOI 10.1007/978-3-319-24085-5_4

adenomas, craniopharyngiomas, aneurysms, meningioma, glioma, germ cell tumors and metastases [1].

The diagnosis of compressive optic neuropathy usually relies on the history of progressive visual loss and on imaging studies, particularly modern magnetic resonance imaging (MRI) and computed tomography (CT) scanning devices. On ophthalmic examination patients with tumors compressing the anterior visual pathway usually present with visual acuity (VA) and visual field (VF) loss in one or both eyes. Visual loss may occur rapidly in fast growing or hemorrhagic tumors but most of the times visual loss (either central or in the peripheral field) is slow. Optic disc pallor is also commonly found in longstanding diseases while proptosis may be present when optic nerve compression occurs at the orbit.

Traditionally evaluation of the visual pathway in such cases is restricted to VA, color vision and VF assessment as well as fundus observation of structural abnormalities in the optic nerve head such as optic disc pallor or edema and peripapillary retinal nerve fiber layer (RNFL) loss. However, recent technological development has greatly modified our ability to evaluate structural fundoscopic abnormalities in anterior visual pathway diseases with the introduction of new equipment for estimating retinal and optic nerve structures including scanning laser polarimetry, confocal laser scanning and particularly optical coherence tomography (OCT) [2–5]. Among those technologies, OCT evolved to become the most useful instrument for structural evaluation of the fundus. The instrument was introduced as a means of detecting retinal abnormalities but quickly progressed to include measurements that estimate axonal loss in diseases such as glaucoma and hereditary, demyelinating or compressive lesions of the anterior optic pathways [6].

Earlier generations of OCT used time-domain (TD-OCT) technology that provided an axial resolution of approximately 8–10 μm of tissue [7]. Newer generation spectral domain OCT (SD-OCT) in the modern era allows for scanning rates of up to 52,000 A-scans per second to achieve a resolution of 5–7 μm [8]. The current technologies allow for OCT to be of help in the diagnosis and follow-up of compressive optic neuropathies both by quantifying peripapillary RNFL and also by measuring retinal thickness in the macular area for estimating RNFL and ganglion cell loss [9, 10].

Compressive lesions of the anterior visual pathways may go unnoticed by examiners until a significant amount of retinal axonal loss has occurred and clinically detected optic atrophy is present [11]. In such conditions, OCT-measured RNFL and macular thickness measurements may be reduced indicating retinal neuronal loss. By quantifying RNFL and retinal ganglion cells the technology can therefore be very useful for an early diagnosis.

Reduced OCT-measured RNFL may help detecting an optic neuropathy occurring from intrinsic or extrinsic optic nerve tumors. When visual loss is subtle, with mild decrease in visual acuity, VF and color vision, the finding of RNFL thinning provides more objective evidence that there is an optic neuropathy. Since compressive optic neuropathies usually have an insidious presentation such finding can be extremely important to raise suspicion and pursue with further investigation [12].

In patients with compressive optic neuropathies OCT may not only be of help in the diagnosis but also be useful for estimating the chances of visual improvement after treatment. Ideally such conditions should be detected before retinal axonal loss

is present based on history, ophthalmic examination and neuroimaging studies. In such cases, the finding of normal or only mildly reduced OCT measurements in a patient with significant visual loss from compressive optic neuropathy indicates that visual recovery is possible at least to a large extent. Finally detailed analysis with modern SD-OCT analysis can be of help when judging treatment efficacy, particularly when complete removal of lesions is not possible. Efficacy of treatment can be estimated with OCT by repeating retinal and optic nerve measurements over time [6].

While not all conditions have been studied using OCT, the technology should probably provide important data in all compressive optic neuropathies. Irrespective of the etiology the most frequent utility of OCT is to assess optic neuropathy through quantification of peripapillary RNFL thickness measurements. More recently macular thickness measurements, particularly segmented measurements of retinal ganglion cell layer (GCL) in the macula, have been introduced in practice and are available in most modern SD-OCT equipments [10, 13]. In the following paragraphs we discuss briefly the most important compressive lesions of the anterior visual pathway, particularly those that have been subject to previous OCT studies.

4.2 Optic Nerve Tumors

Tumors of the optic nerve represent approximately 4–10 % of all orbital tumors [14–16]. Although uncommon lesions such as hemangiopericytomas and medulloepitheliomas are occasionally reported, the great majority are either optic nerve gliomas or optic nerve meningiomas. Gliomas usually occur in children while most optic nerve meningiomas are tumors affecting middle-aged persons with progressive visual loss, proptosis, disc edema and optociliary veins on fundus examination [14, 16].

Meningiomas of the anterior visual pathway are important compressive lesions of the optic nerve that usually occur in middle aged patients leading to progressive VA and VF loss, optic atrophy or optic disc edema and abnormalities on imaging studies such as MRI and CT scan. The tumors can originate from the sheaths of the optic nerve or from the meninges near the nerves [1].

Optic nerve sheath meningiomas (ONSM) are tumors that originate from the meninges of the optic nerve. The tumors are slow growing but generally lead to gradual visual deterioration. Patients with ONSM and progressive but recent visual loss or those with long-standing loss but still visual function can be treated with conformational fractioned radiation therapy [17, 18]. By contrast, surgical resection of ONSM leads to significant or complete visual loss and should be restricted to patients with severe irreversible visual loss for correction of disfiguring proptosis or preventing intracranial extension.

OCT can be important in the diagnosis of ONSM and in estimating the chances of visual recovery. When visual loss occurs in a patient with little or no retinal neuronal loss visual improvement may be expected (Fig. 4.1). On the other hand, when significant RNFL and macular GCL is present indicating established axonal loss, successful treatment should be aimed at preventing further visual loss and absence of visual improvement is not an indication of treatment failure (Fig. 4.2).

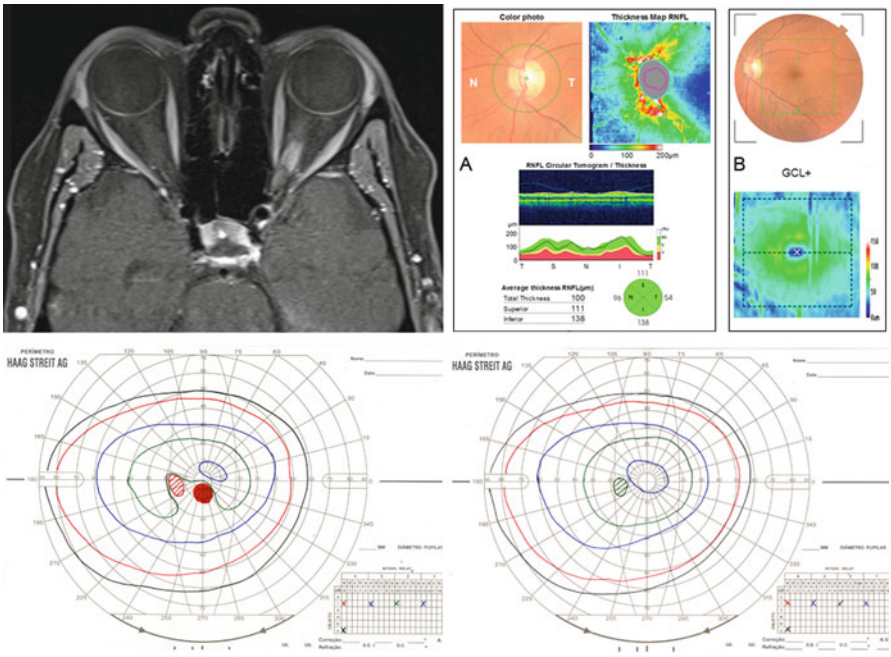

Fig. 4.1 A 51-year-old woman with progressive visual loss in the left eye for 1 year was found to have an optic nerve sheath meningioma (*upper left*). Optical coherence tomography (Topcon 3D-OCT 2000™) revealed normal peripapillary retinal nerve fiber layer (*upper right*, *A*). Segmented macular thickness measurements indicated normal macular ganglion cell layer (*upper right*, *B*). The patient presented with an inferior paracentral scotoma and constricted field (*lower left*) and showed significant improvement after conformational radiation therapy (*lower right*)

While ONSM are usually treated with radiotherapy, patients with tumors from the skull base meninges but compressing the optic pathway are usually treated with surgery. Visual outcome after decompressive surgery however is variable; while a significant number of patients experience improvement or stability of vision, 20–30 % deteriorate [19]. Although several risk factors for poor visual outcomes are known including prolonged duration of symptoms, the presence of disc pallor and incomplete tumor resection, estimating the potential for visual recovery may be difficult based on the clinical exam and imaging finding alone. Loo et al. [20] performed a study to determine the prognostic value of pretreatment OCT measurement of the peripapillary RNFL in final visual outcomes of patients with anterior visual pathway meningioma and optic neuropathy. The authors evaluated the outcome of 14 eyes of 12 patients treated in which pretreatment and post-treatment OCT along with clinical examination were performed. After treatment, the group with normal RNFL experienced significant improvement in the VA, color vision, and VF compared with the group with reduced peripapillary RNFL. The findings in this study is a further indication that patients with compressive optic neuropathy due to anterior pathway meningioma are more likely to improve post-treatment if they have a normal pretreatment RNFL.

Optic nerve gliomas are the most common tumors of the optic nerve but represent only 1 % of all intracranial tumors [21]. While malignant gliomas may occur in

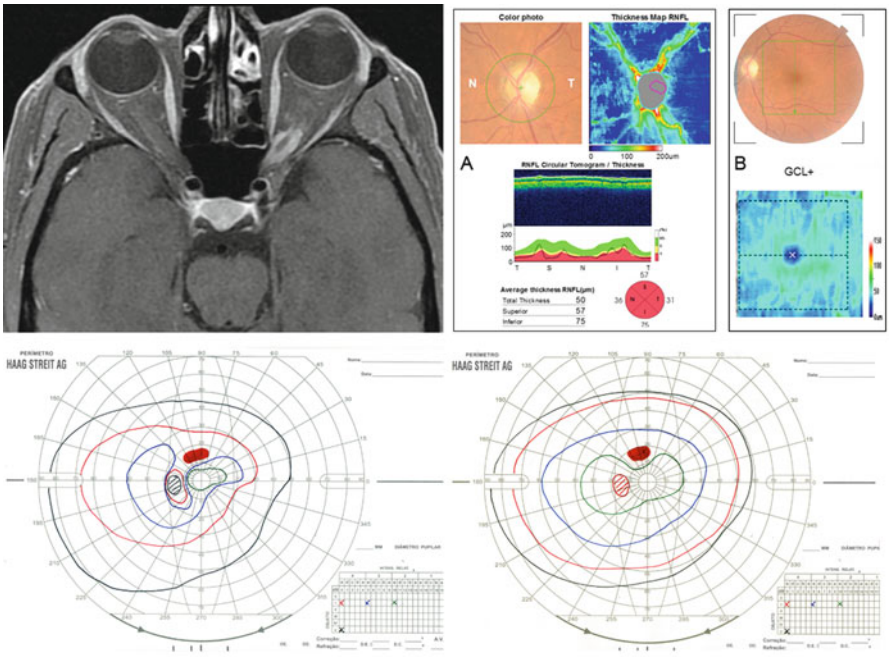

Fig. 4.2 A 49-year-old woman with a 7-year history of visual loss in the left eye from an optic nerve sheath meningioma (*upper left*). Optical coherence tomography (Topcon 3D-OCT 2000™) revealed severely reduced peripapillary retinal nerve fiber layer (*upper right*, *A*). Segmented macular thickness measurements indicated markedly reduced macular ganglion cell layer (*upper right*, *B*). The patient presented with a severe constriction, enlarged blind spot and superior paracentral scotoma (*lower left*). There was only mild visual improvement after conformational radiation therapy (*lower right*)

the adult, the large majority of gliomas are benign juvenile pilocytic astrocytomas that present primarily among children in the first decade of life. The natural history of childhood optic nerve gliomas is almost always benign and most patients retain stable visual function without treatment. A conservative management is usually recommended to patients with unilateral optic nerve gliomas, particularly those with neurofibromatosis type 1 (NF-1) [22]. On the other hand in uncommon cases of more aggressive tumors, particularly those near of affecting the optic chiasm chemotherapy can be use to help stabilize the lesion [23].

Both in patients optic pathway gliomas (OPG) followed with conservatively without treatment as well as in those submitted to chemotheraphy, assessment of visual function along with imaging studies is the main parameters used to evaluate disease progression on follow-up examinations. However, monitoring young children with OPGs for visual deterioration can be difficult owing to age-related noncompliance. OCT measures of peripapillary RNFL and macular thickness can be of significant help in monitoring the integrity of the visual pathway and has been proposed as a surrogate marker of vision in previous studies evaluating OCT findings in patients with OPG.

Chang et al. [24] evaluated, using the Stratus OCT, both macular and RNFL thickness measurements in patients with NF-1 with or without optic gliomas and controls. The authors found that NF-1 subjects with OPG had average RNFL thickness and

macular volume significantly reduced compared to those without gliomas. The study suggests that OCT can be used to detect RNFL thinning secondary to NF-1 related OPGs and that it may be a useful adjunct to routine clinical ophthalmologic evaluation in children with NF-1.

Avery et al. [25] prospectively evaluated 62 patients with NF-1 and optic nerve gliomas submitted to neuro-ophthalmic examination including TD-OCT of the optic nerve head. Eighty-nine eyes of patients with OPG were included and 41 classified as having abnormal VA or VF loss. Reduced RNFL thickness was associated significantly reduced VA and contrast sensitivity. The study indicated that reduced OCT-measured RNFL is a sensitive technology to detect visual loss in OPG.

Parrozzoni et al. [26] compared visual function and SD-OCT measured RNFL thickness for the screening of OPG in 57 pediatric patients affected by NF-1. Visual function assessment, RNFL analysis, and optic disc evaluation results correlated with the presence of OPGs, but only RNFL analysis reached statistically significant sensitivity and positive predictive value. The authors concluded that RNFL analysis assessment using SD-OCT is superior to visual function assessment and optic disc evaluation as a clinical screening tool for OPGs. Macular thickness measurements were not investigated.

Fard et al. [27] studied 38 eyes of 23 children with OPG and evaluated the relationship between SD-OCT findings and clinical/radiological changes at diagnosis and on a 24-month follow-up evaluation. Mean changes in average RNFL and macular thickness measurements were significantly higher in patients that had clinical/radiological progression of the gliomas compared to those that did not progressed. OCT measurements were significantly different in patients with tumor progression compared to those that did not progress indicating that OCT measurements may be helpful in monitoring OPG.

More recently, Gu et al. [28] evaluated the macular GC-inner plexiform layer (GC-IPL) thickness in children with or without visual loss from OPG using SD-OCT. Decreased GC-IPL thickness was able to discriminate between children with and without vision loss from their OPG. The authors concluded that GC-IPL thickness could be used as a surrogate marker of vision in children with OPGs.

While the above-mentioned studies have indicated the value of OCT in monitoring visual function in OPG, an important limitation for obtaining OCT measurements in this condition is that gliomas usually occur in young patients, when the technique is also limited by patient cooperation. However, more recently Avery et al. [29] used a hand-held OCT to obtain optic nerve and retinal thickness measurements during sedation in 33 young children with OPGs. The authors concluded that for young children who do not cooperate with vision testing, hand-held OCT measures may be a surrogate marker of vision.

4.3 Dysthyroid Optic Neuropathy

Graves' orbitopathy (GO) is an autoimmune inflammatory process affecting the orbital and periorbital tissues, mainly the extraocular muscles but also the retrobulbar fat. GO occurs before, during or after the onset of hyperthyroidism and, less frequently, in

euthyroid or hypothyroid patients [30]. The enlargement of the extraocular muscles is responsible for most of the debilitating manifestations of the disease, including proptosis, diplopia, congestive signs and dysthyroid optic neuropathy (DON) [30, 31].

DON is a serious complication of GO occurring in 3.4 % of patients [32], almost always as a result of optic nerve compression at the orbital apex by enlarged extraocular muscles. The diagnosis of DON rests mainly on clinical findings, such as decreased VA, abnormal VF, altered color and brightness perception, abnormal visual evoked potentials, afferent pupillary defects and edema or atrophy of the optic nerve head [33]. Nevertheless, DON is often subclinical and in many cases difficult to diagnose due to confounding signs and symptoms, especially significant orbital congestion or decreased corneal transparency due to exposure keratopathy. Establishing a diagnosis may also be difficult because many tests of optic nerve dysfunction, such as VA, color and brightness perception and VF, especially when performed with standard automated perimetry, require full cooperation of an alert and motivated patient and will not infrequently render false positive results, particularly in patients with congestive GO.

Because the prognosis of DON improves significantly with early diagnosis and treatment, much effort has been put into designing objective tests capable of identifying patients at high risk for developing DON. Therefore imaging studies, particularly CT scanning of the orbit are often used to investigate the possibility of DON [34]. Several studies have tested the ability of CT parameters (linear, area and volume measurements of the orbital muscles) to raise suspicion and facilitate the diagnosis of DON [34, 35]. More recently OCT measurements have been introduced in the management of GO.

In patients with GO, OCT can be of help in the diagnosis and in follow-up of DON. Because DON can present with optic disc edema, OCT can help its detection and measurement to monitor treatment efficacy. While no previous studies have specifically evaluated the use of OCT for monitoring optic disc edema in GO, many studies have documented the ability of the equipment for that purpose in patients with papilledema [36, 37]. Presumably the same rationale applies for measuring optic disc edema in patients with DON. On the other hand, many patients with DON present without optic disc edema, either with atrophy or with normal optic disc appearance. As in any other compressive optic neuropathy, OCT thickness measurements can help quantifying axonal loss in patients with DON both help establishing the diagnosis as well as to estimate the chances of reversing visual loss (Fig. 4.3).

Very few studies, however, have critically evaluated OCT in GO and in special those with DON. Forte et al. [38] evaluated the RNFL in patients with GO and ocular hypertension using OCT. The authors found that RNFL loss on OCT was found in 9 of the 30 patients evaluated. However, apparently the patients did not have well-defined DON and the authors concluded that RNFL loss was important to detect the presence of optic neuropathy but could not differentiate whether the causative effect was DON or the elevated intraocular pressures.

One study evaluated patients with DON using OCT but as a secondary measurements when investigating the value o multifocal visual evoked potentials (mfVEP). Pérez-Rico et al. evaluated 65 eyes of 34 consecutive patients with GO using mfVEP, SAP and OCT (Stratus TD-OCT). The authors found mfVEP abnormalities

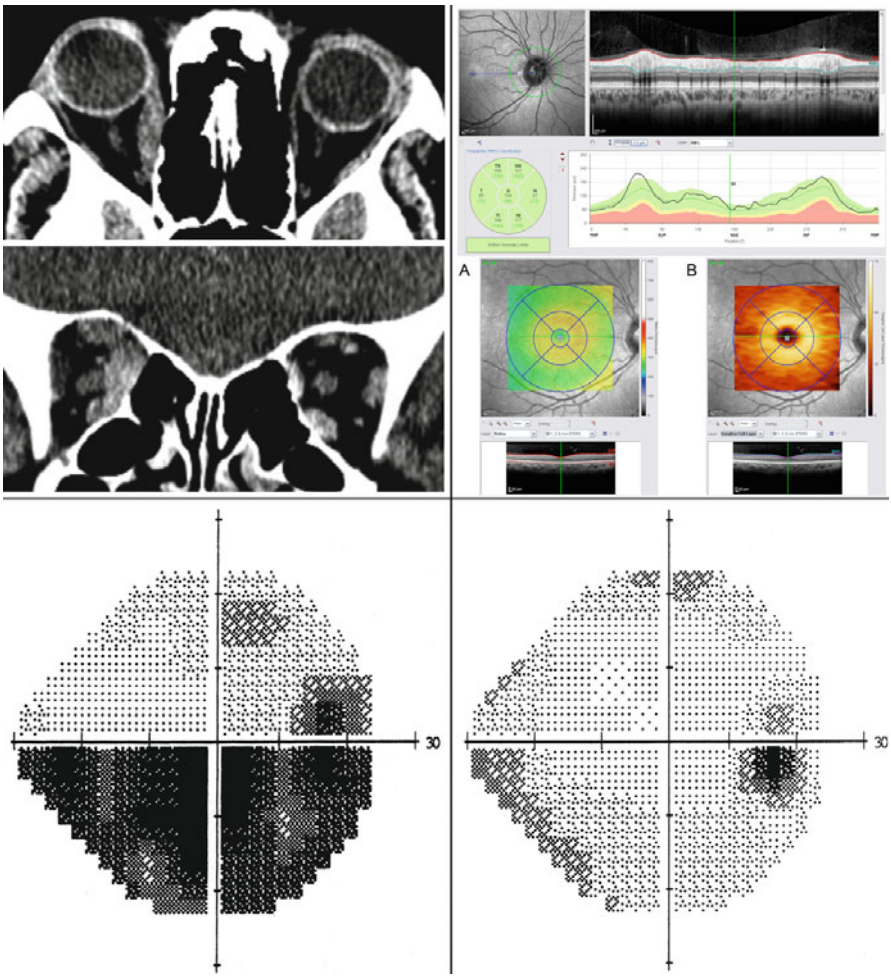

Fig. 4.3 A 50-year-old woman with Graves' orbitopathy presented with double vision, proptosis for 3 months and a 2-week history of visual loss in the right eye (OD). Computerized tomography scan showed enlarged medial and inferior rectus muscles and crowding at the orbital apex (*upper left*). Visual acuity was 20/200 and there was inferior altitudinal field loss (*lower left*). Optical coherence tomography (OCT) scan (HRA Spectralis™, Heildelberg Engeneering) showed normal peripapillary retinal nerve fiber layer (*upper right*). Macular thickness measurements showed normal full-thickness (*A*) and normal macular ganglion cell layer (*B*). There was marked improvement of both visual acuity and visual field after orbital decompressive surgery (*lower right*) in accordance with the normal retinal neural integrity as assessed by OCT

in 27 % of eyes and diffuse VF defects in 20 % indicating that a significant number of eyes had DON. OCT-measured RNFL did not differ from normal and no correlation was found between mfVEP, VF and OCT data. While the study might indicate a poor sensitivity to detect abnormalities on OCT it may also be interpreted as indicating reversibility of visual function abnormalities in the patients.

It is widely known that visual loss in DON can be reversible when properly treated, provided there is no significant permanent optic nerve damage. The finding of normal RNFL in a patient with significant visual loss would therefore be a strong indicator for further treatment to obtain visual recovery (Fig. 4.3). However, further, prospective studies are necessary to better define the use of OCT in patients with GO.

4.4 Other Compressive Optic Nerve Diseases

Optic nerve compression can also be due to a number of orbital and adnexal conditions including extrinsic tumors of the orbit, osseous diseases leading to optic nerve compression at the canal, sinusal process invading the orbit, metastases and lymphomatous that can lead to optic nerve dysfunction. Very few of these conditions have been evaluated systematically using OCT but the instrument can certainly be an important additional data in a number of them both in the diagnosis by characterizing the presence of an optic neuropathy as well as estimating the chances of visual recovery after treatment (Fig. 4.4).

4.5 Compressive Chiasmal Diseases

Compressive lesions at the optic chiasmal region are among the most important lesions of the anterior visual pathway and can be caused by a number of lesions including pituitary adenoma, craniopharyngioma, meningioma, and aneurism. The lesions produce loss of VA, color vision and particularly VF defects. However, because visual symptoms are usually vague early on the course of the disease, the diagnosis may be retarded until later stages when permanent damage of the visual pathway has already occurred.

Chiasmal lesions can lead to a wide variety of visual and axonal damage to the visual pathway fibers, ranging from mild VF defect and focal peripapillary RNFL and macular GCL loss to severe and diffuse visual loss and optic nerve atrophy and retinal GCL loss. In most cases, however, typical bitemporal VF defect occur and a specific pattern of axonal loss develops. In patients with mid-chiasmal lesions, temporal hemianopia and preserved nasal field, the crossed nerve fibers are lost with preservation of the uncrossed nerve fibers, which originate in the temporal hemiretina and penetrate the optic nerve through the superior and inferior arcuate fiber bundles. Thus, RNFL loss occurs predominantly on the nasal and temporal side of the optic disc, a pattern identified on ophthalmoscopy as band atrophy (BA) of the optic nerve [39], and the retina shows a clear distinction in axonal loss when the temporal hemiretina is compared with the affected nasal hemiretina (Fig. 4.5).

Chiasmal lesions were the first compressive anterior visual pathway diseases to be evaluated using OCT. Approximately a decade ago, we and other authors have

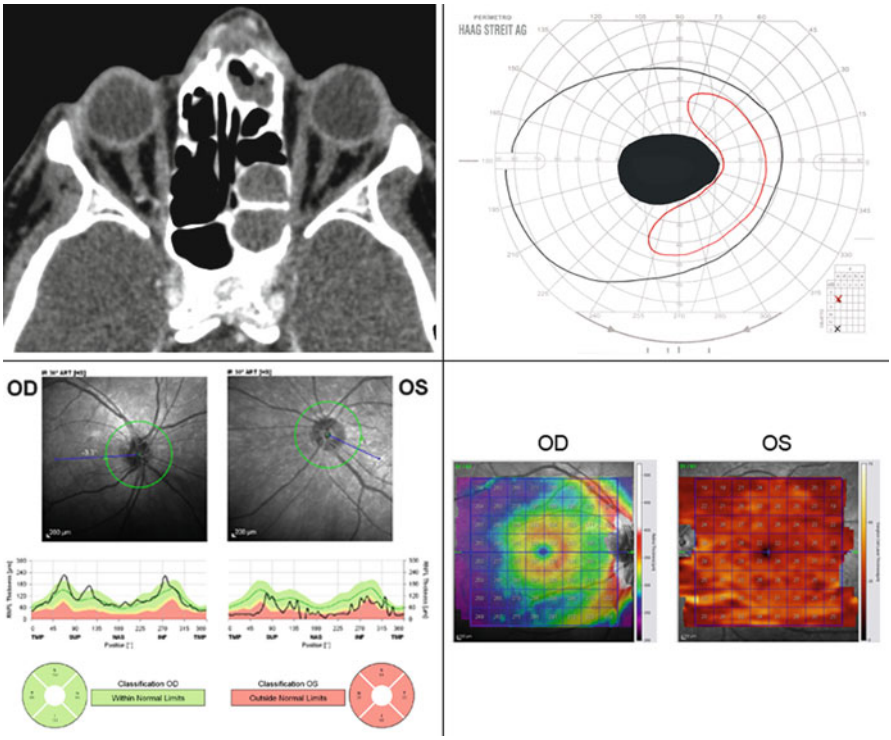

Fig. 4.4 A 52-year-old man had severe visual loss in the left eye (OS) due to a spheno-ethmoidal mucocele compressing the optic nerve at the optic canal and the orbital apex (*upper left*). Visual field showed a dense central scotoma (*upper right*) and visual acuity was reduced to finger counting. Optical coherence tomography (OCT) scan (HRA Spectralis™, Heildelberg Engeneering) showed severely reduced peripapillary retinal nerve fiber layer in OS and was normal in the right eye (OD) (*lower left*). Segmented macular scans showed normal macular ganglion cell layer in OD and severely reduced in OS (*lower right*). There was no significant improvement of vision after surgery in accordance with the severe retinal neural loss observed on OCT

demonstrated that retinal thickness measurements could detect neural loss in patients with chiasmal compression and that such measurements were able to identify the pattern of axonal loss found in this condition, based peripapillary RNFL thickness measurements using early generation OCT devices (Fig. 4.6) [4, 40–42].

Subsequently we have demonstrated that full-thickness macular thickness measurements were also able to detect axonal loss in chiasmal compression and correlated well both with peripapillary RNFL and with VF defects [9, 43, 44]. Discrimination ability and the relationship between OCT thickness measurements and VF loss were similar with both sets of measurements although macular thickness measurements allowed a better correlation when quadrantic measurements of the macula were obtained [9]. Because the RNFL of different quadrants and different hemifields enter the optic disc in a way that the fibers from different quadrants

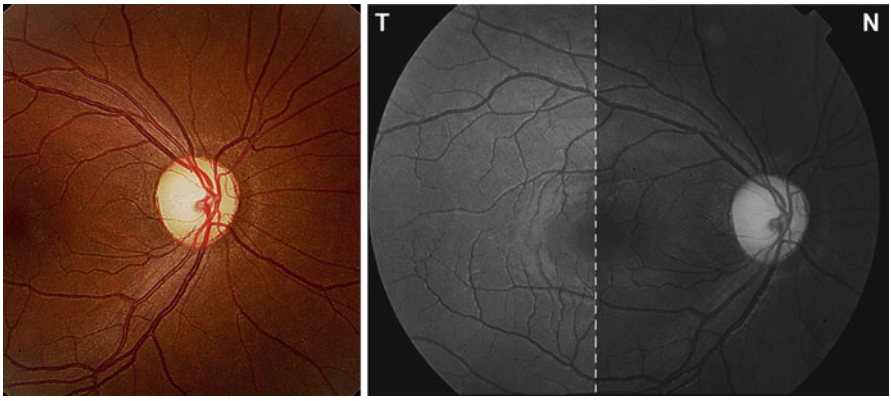

Fig. 4.5 Optic nerve (*left*) and fundus photograph (*right*) of a patient complete temporal hemianopia with normal nasal hemifield, band atrophy of the optic nerve and a pattern of retinal nerve fiber layer loss in the temporal and nasal portions of the optic nerve with relative preservation of the superior and inferior arcuate fibers (left) and the demarcation between the retinal area with preserved ganglions cells (temporal) and the ares with atrophic ganglion cells (nasal). *T* temporal, *N* nasal (Modified from Cunha et al. [57])

superimpose one with the other, specific correlation of RNFL with VF is somewhat cumbersome at the optic disc. With the exception of the nasal area of the disc all other sectors receive retinal nerve fibers from both the nasal and the temporal hemiretina. The result is a lack of specificity between VF loss and optic disc sectors in patients with lesions of the optic chiasm [9, 10]. For example, when a VF defect affecting the superotemporal quadrant is present, it results in RNFL loss in the nasal, temporal and inferior regions of the optic disc. Since the inferior region of the optic disc also receives nerve fibers from the unaffected nasal VF, there is presumably a lack of specificity in the structure-function relationship.

On the other hand, with macular thickness measurements a superotemporal VF defect may be related to reduced macular thickness below and nasally to the fovea, with a direct correspondence to the quadrantic VF defect. The advantage of macular thickness measurements is even greater in patients with temporal hemianopia, affecting both the superior and the inferior temporal quadrants. Based on the distribution of the RNFL on the optic disc [45], such patients may be expected to have RNFL loss in every quadrant of the optic disc, with a resultant lack of specificity in the structure-function relationship, while macular thickness reduction would be observed almost exclusively nasally to the fovea, probably with a much higher specificity. In previous studies we have demonstrated a closest structure-function relationships observed between macular thickness measurements and VF abnormalities compared to the relationship between RNFL thickness measurements and VF defects [9]. The relationship between OCT-measured macular thickness parameters and VF defects were even greater when segmented macular thickness measurements were used and separate analysis of the retina GCL is possible (Fig. 4.7) [10, 13, 46].

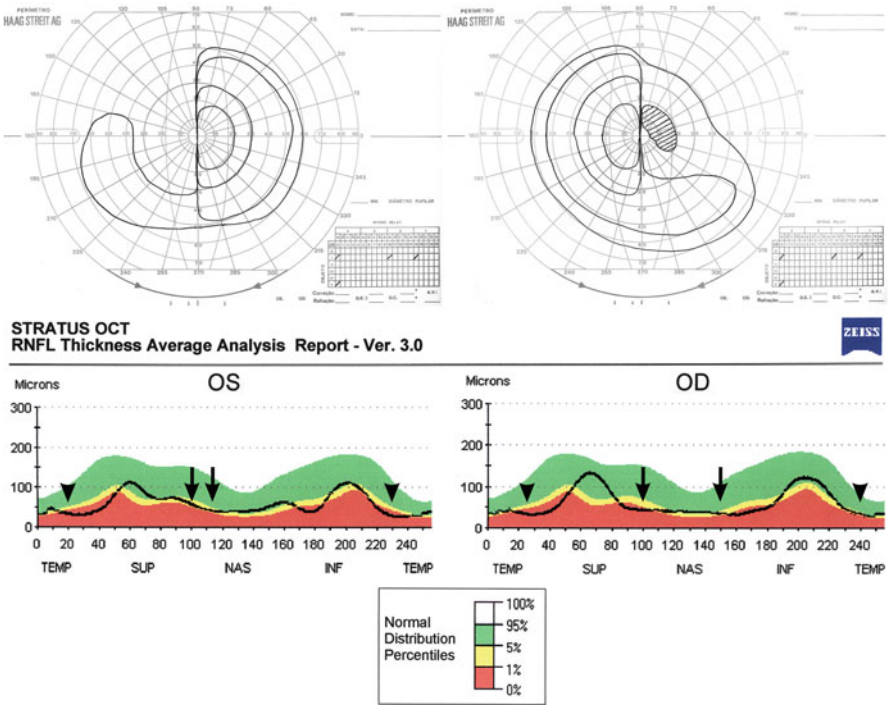

Fig. 4.6 *Above*, Goldmann visual fields showing bitemporal severe loss in a patient with pituitary adenoma. *Below*, Stratus™ (Carl Zeiss, Meditec), time-domain Optical coherence tomography showing diffuse retinal nerve fiber layer loss in both eyes mostly in the nasal (*arrows*) and temporal (*arrowheads*) aspects of the optic nerve (From Leal et al. [58])

Previous studies have evaluated the relationship between OCT findings and VF or electrophysiological testing. In one study, we have also shown that OCT measurements correlated well both with VF and pattern electroretinogram in patients with chiasmal compression [47]. Moon et al. [48] showed an important correlation between reduced RNFL thickness and decreased b wave on photopic negative response, both associated with worse VF outcome. Therefore OCT can also be associated with other electrophysiological methods as prognostic indicator in the preoperative assessment of chiasmal compression.

While in most patients with chiasmal compression treatment is usually necessary, estimating the prognosis for visual recovery is particularly important in patients with recurrent tumors where the need for further surgery is in question. Although it is expected that visual improvement may occur after optic pathway decompression, in many cases such recovery is variable and many times unpredictable [49–52]. While other predictive values such as duration of symptoms, age, size of tumor, the severity of VA and VF loss as the presence or absence of optic disc pallor have been used to estimate visual recovery, the results are far from ideal [50–53]. However, the grading of optic disc pallor is difficult and subjective [53].

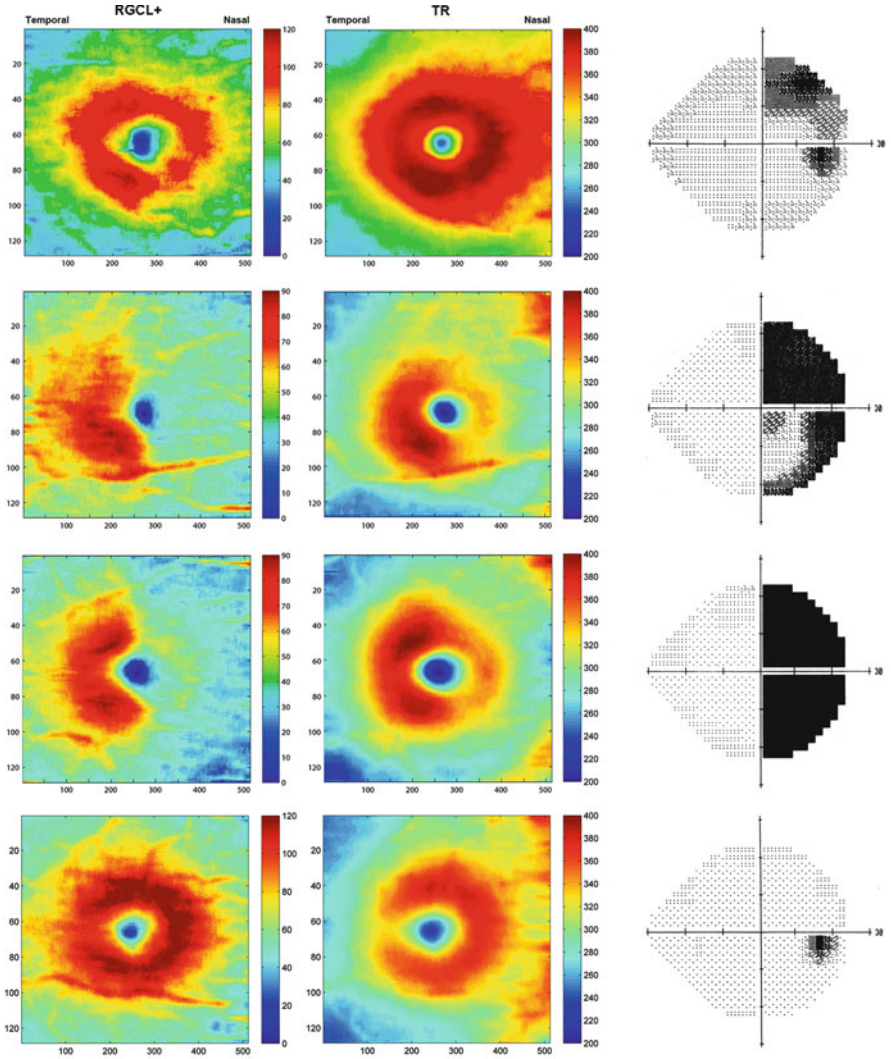

Fig. 4.7 Pseudo-color thickness map generated from cube scan based on the thickness of the macular layers obtained using spectral-domain optical coherence tomography (Topcon 3D-OCT 1000™). First, second and third lines = eyes with band atrophy of the optic nerve and different degrees of visual field loss. Fourth line = a normal control. *RGCL+* retinal ganglion cell layer associated with the inner plexiform layer, *TR* total retinal thickness. Notice that thickness reduction in the nasal hemiretinas is more evident in the RGCL+ when compared to TR (Modified from Monteiro et al. [10])

Therefore the use of OCT to quantify axonal loss through peripapillary RNFL thickness measurements and through measurements of retinal neural elements at the macula arouse as one of the most important predictor of visual recovery (Figs. 4.8 and 4.9).

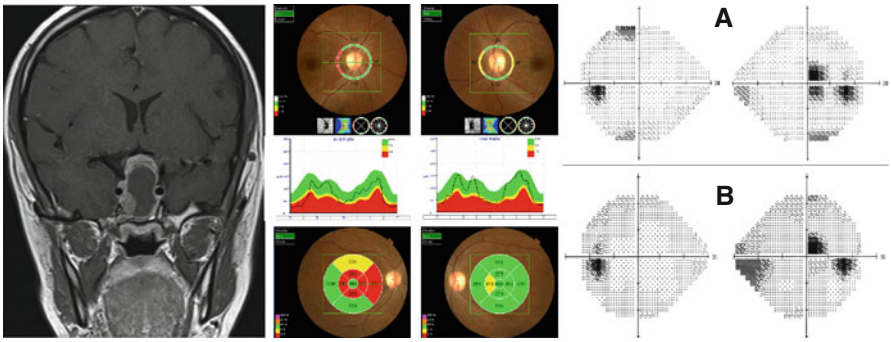

Fig. 4.8 A 32-year-old woman with a large pituitary adenoma with chiasmal compression (*left*). *Middle*: optical coherence tomography (OCT) scan (Topcon 3D-OCT 1000™) revealed reduced peripapillary retinal nerve fiber layer in the temporal portion of the right eye (in *red*) and in the nasal and temporal portions of the left eye (in *yellow*). Full-thickness macular measurements showed thinning mostly of the nasal macula (in *red* or *yellow*) indicating retinal axonal loss. *Right*: visual fields showing bilateral defect pre-operatively (*A*) and no significant improvement after surgery (*B*) in accordance with the finding of permanent retinal axonal loss on OCT

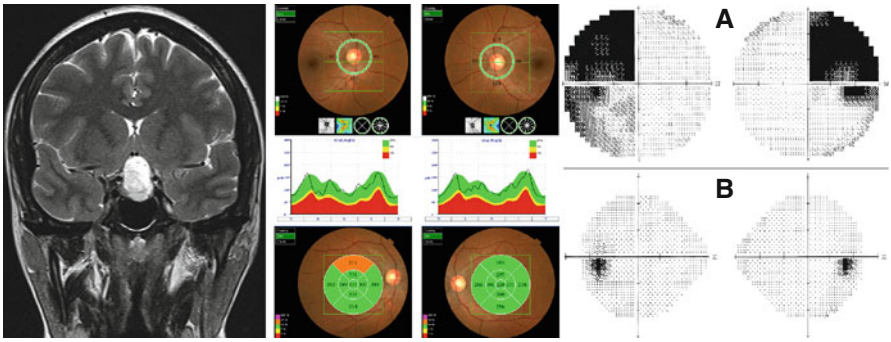

Fig. 4.9 A 24-year-old pregnant woman developed a large pituitary adenoma with chiasmal compression (*left*). *Middle*: optical coherence tomography (Topcon 3D-OCT 1000™) revealed normal peripapillary retinal nerve fiber layer in both eyes. Full-thickness macular measurements showed normal measurements indicating retinal axonal normality. *Right*: visual fields showing bitemporal quadrantic defect pre-operatively (*A*) and normal visual field after surgery (*B*) in accordance with normal OCT findings

A few studies have evaluated prospectively the ability of OCT in predicting visual improvement in chiasmal compression. Such studies have shown a significant correlation between the depth and thickness of the RNFL measured by OCT and the possibility of improvement in patients that undergo surgery for tumors involving the chiamal region [12, 54]. Danesh-Meyer et al. [12] evaluated OCT's ability to predict visual recovery from optic nerve and chiasmal compression due to parachiasmal lesions. Forty patients with various etiologies were evaluated with Stratus-OCT (time-domain, Carl Zeiss-Meditec, Inc) and VF both pre- and post-surgical decompression. Patients with thin RNFL, defined preoperatively as below 97.5 % of normal values did not demonstrate significant improvement in visual acuity and VF

mean deviation in the post-operative period while those with normal RNFL thickness had significant improvement in visual acuity. The authors found that there was an increased likelihood of postoperative improvement with thicker preoperative RNFL until approximately 85 um.

Jacob et al. [54] evaluated 37 eyes of 19 consecutive patients suffering from pituitary adenomas compressing the anterior visual pathways. Seventeen patients underwent trans-sphenoidal surgery and 2 received dopamine agonists. VF and OCT were performed before treatment and in the 2 weeks and 3 months after treatment. The study showed that the odds of complete recovery after 3 months from the initial VF defect was multiplied by 1.29 for each increase in 1 μm of mean RNFL. The authors concluded that RNFL thinning measured by OCT leads to a decreased chance of recovery of an initial VF defect 3 months after treatment.

Ohkubo et al. [55] evaluated the relationship between macular GCL and VF parameters in chiasmal compression and the potential for GCL parameters in order to predict the short-term post- surgical VF. Examining the macular GCL was useful for evaluating structural damage in patients with chiasmal compression. Preoperative GCL parameters, especially focal loss of GCL, may be useful in predicting visual function following surgical decompression of chiasmal compression.

On the other hand, it is important to consider that axonal loss may appear later in the course of the disease, even after optic pathway decompression has occurred. Moon et al. [56] evaluated 19 patients undergoing chiasmal decompression before and 1 and 3 months after surgery. Visual recovery was significantly correlated with the changes in retinal GCL and RNFL thickness measurements. However, prolonged retrograde degeneration progressed for some period, even after surgical decompression and visual recovery occurred.

4.6 Conclusions

While much more work is still necessary to better understand the precise relationship between OCT and VA, VF and other modalities of visual function evaluation, a number of previous studies as well as clinical observation clearly indicate the importance of using OCT in diagnosis, treatment as well as follow-up of compressive optic neuropathies. As both technology and interpretation of data advances we expect the use of OCT will certainly increase in the management of this important group of optic nerve diseases.

References

1. Chan JW. Compressive and infiltrative optic neuropathies. In: Chan JW, editor. Optic nerve disorders diagnosis and management. New York: Springer; 2007. p. 88–129.
2. Monteiro ML, Medeiros FA, Ostroscki MR. Quantitative analysis of axonal loss in band atrophy of the optic nerve using scanning laser polarimetry. Br J Ophthalmol. 2003;87(1):32–7.
3. Sergott RC, Balcer LJ. The latest on optical coherence tomography. J Neuroophthalmol. 2014;34(Suppl):S1–2.

4. Monteiro ML, Leal BC, Rosa AA, Bronstein MD. Optical coherence tomography analysis of axonal loss in band atrophy of the optic nerve. Br J Ophthalmol. 2004;88(7):896–9.
5. Mendoza-Santiesteban CE, Lopez-Felipe D, Fernandez-Cherkasova L, Hernandez-Echavarria O, Hernandez-Silva Y, Gonzalez-Garcia A. Microperimetry in the study of neuro-ophthalmic diseases. Semin Ophthalmol. 2010;25(4):136–43.
6. Subei AM, Eggenberger ER. Optical coherence tomography: another useful tool in a neuro-ophthalmologist's armamentarium. Curr Opin Ophthalmol. 2009;20(6):462–6.
7. Sull AC, Vuong LN, Price LL, Srinivasan VJ, Gorczynska I, Fujimoto JG, et al. Comparison of spectral/Fourier domain optical coherence tomography instruments for assessment of normal macular thickness. Retina. 2010;30(2):235–45.
8. Adhi M, Duker JS. Optical coherence tomography--current and future applications. Curr Opin Ophthalmol. 2013;24(3):213–21.
9. Monteiro ML, Costa-Cunha LV, Cunha LP, Malta RF. Correlation between macular and retinal nerve fibre layer Fourier-domain OCT measurements and visual field loss in chiasmal compression. Eye (Lond). 2010;24(8):1382–90.
10. Monteiro ML, Hokazono K, Fernandes DB, Costa-Cunha LV, Sousa RM, Raza AS, et al. Evaluation of inner retinal layers in eyes with temporal hemianopic visual loss from chiasmal compression using optical coherence tomography. Invest Ophthalmol Vis Sci. 2014;55(5):3328–36.
11. Pasol J. Neuro-ophthalmic disease and optical coherence tomography: glaucoma look-alikes. Curr Opin Ophthalmol. 2011;22(2):124–32.
12. Danesh-Meyer HV, Papchenko T, Savino PJ, Law A, Evans J, Gamble GD. In vivo retinal nerve fiber layer thickness measured by optical coherence tomography predicts visual recovery after surgery for parachiasmal tumors. Invest Ophthalmol Vis Sci. 2008;49(5):1879–85.
13. Kardon RH. Role of the macular optical coherence tomography scan in neuro-ophthalmology. J Neuroophthalmol. 2011;31(4):353–61.
14. Dutton JJ. Optic nerve sheath meningiomas. Surv Ophthalmol. 1992;37(3):167–83.
15. Spencer WH. Primary neoplasms of the optic nerve and its sheaths: clinical features and current concepts of pathogenetic mechanisms. Trans Am Ophthalmol Soc. 1972;70:490–528.
16. Dutton JJ. Optic nerve gliomas and meningiomas. Neurol Clin. 1991;9(1):163–77.
17. Saeed P, Blank L, Selva D, Wolbers JG, Nowak PJ, Geskus RB, et al. Primary radiotherapy in progressive optic nerve sheath meningiomas: a long-term follow-up study. Br J Ophthalmol. 2010;94(5):564–8.
18. Solda F, Wharram B, De Ieso PB, Bonner J, Ashley S, Brada M. Long-term efficacy of fractionated radiotherapy for benign meningiomas. Radiother Oncol. 2013;109(2):330–4.
19. Rosenberg LF, Miller NR. Visual results after microsurgical removal of meningiomas involving the anterior visual system. Arch Ophthalmol. 1984;102(7):1019–23.
20. Loo JL, Tian J, Miller NR, Subramanian PS. Use of optical coherence tomography in predicting post-treatment visual outcome in anterior visual pathway meningiomas. Br J Ophthalmol. 2013;97(11):1455–8.
21. Dutton JJ. Gliomas of the anterior visual pathway. Surv Ophthalmol. 1994;38(5):427–52.
22. Miller NR. Primary tumours of the optic nerve and its sheath. Eye (Lond). 2004;18(11):1026–37.
23. Kelly JP, Leary S, Khanna P, Weiss AH. Longitudinal measures of visual function, tumor volume, and prediction of visual outcomes after treatment of optic pathway gliomas. Ophthalmology. 2012;119(6):1231–7.
24. Chang L, El-Dairi MA, Frempong TA, Burner EL, Bhatti MT, Young TL, et al. Optical coherence tomography in the evaluation of neurofibromatosis type-1 subjects with optic pathway gliomas. J AAPOS. 2010;14(6):511–7.
25. Avery RA, Liu GT, Fisher MJ, Quinn GE, Belasco JB, Phillips PC, et al. Retinal nerve fiber layer thickness in children with optic pathway gliomas. Am J Ophthalmol. 2011;151(3):542–9. e2.
26. Parrozzani R, Clementi M, Kotsafti O, Miglionico G, Trevisson E, Orlando G, et al. Optical coherence tomography in the diagnosis of optic pathway gliomas. Invest Ophthalmol Vis Sci. 2013;54(13):8112–8.

27. Fard MA, Fakhree S, Eshraghi B. Correlation of optical coherence tomography parameters with clinical and radiological progression in patients with symptomatic optic pathway gliomas. Graefes Arch Clin Exp Ophthalmol. 2013;251(10):2429–36.
28. Gu S, Glaug N, Cnaan A, Packer RJ, Avery RA. Ganglion cell layer-inner plexiform layer thickness and vision loss in young children with optic pathway gliomas. Invest Ophthalmol Vis Sci. 2014;55(3):1402–8.
29. Avery RA, Hwang EI, Ishikawa H, Acosta MT, Hutcheson KA, Santos D, et al. Handheld optical coherence tomography during sedation in young children with optic pathway gliomas. JAMA Ophthalmol. 2014;132(3):265–71.
30. McKeag D, Lane C, Lazarus JH, Baldeschi L, Boboridis K, Dickinson AJ, et al. Clinical features of dysthyroid optic neuropathy: a European Group on Graves' Orbitopathy (EUGOGO) survey. Br J Ophthalmol. 2007;91(4):455–8.
31. Hallin ES, Feldon SE, Luttrell J. Graves' ophthalmopathy: III. Effect of transantral orbital decompression on optic neuropathy. Br J Ophthalmol. 1988;72(9):683–7.
32. Ben Simon GJ, Syed HM, Douglas R, Schwartz R, Goldberg RA, McCann JD. Clinical manifestations and treatment outcome of optic neuropathy in thyroid-related orbitopathy. Ophthalmic Surg Lasers Imaging. 2006;37(4):284–90.
33. Neigel JM, Rootman J, Belkin RI, Nugent RA, Drance SM, Beattie CW, et al. Dysthyroid optic neuropathy. The crowded orbital apex syndrome. Ophthalmology. 1988;95(11):1515–21.
34. Goncalves AC, Gebrim EM, Monteiro ML. Imaging studies for diagnosing Graves' orbitopathy and dysthyroid optic neuropathy. Clinics (Sao Paulo). 2012;67(11):1327–34.
35. Goncalves AC, Silva LN, Gebrim EM, Monteiro ML. Quantification of orbital apex crowding for screening of dysthyroid optic neuropathy using multidetector CT. AJNR Am J Neuroradiol. 2012;33(8):1602–7.
36. Wang JK, Kardon RH, Kupersmith MJ, Garvin MK. Automated quantification of volumetric optic disc swelling in papilledema using spectral-domain optical coherence tomography. Invest Ophthalmol Vis Sci. 2012;53(7):4069–75.
37. Kupersmith MJ, Sibony P, Mandel G, Durbin M, Kardon RH. Optical coherence tomography of the swollen optic nerve head: deformation of the peripapillary retinal pigment epithelium layer in papilledema. Invest Ophthalmol Vis Sci. 2011;52(9):6558–64.
38. Forte R, Bonavolonta P, Vassallo P. Evaluation of retinal nerve fiber layer with optic nerve tracking optical coherence tomography in thyroid-associated orbitopathy. Ophthalmologica. 2010;224(2):116–21.
39. Unsold R, Hoyt WF. Band atrophy of the optic nerve. The histology of temporal hemianopsia. Arch Ophthalmol. 1980;98(9):1637–8.
40. Kanamori A, Nakamura M, Matsui N, Nagai A, Nakanishi Y, Kusuhara S, et al. Optical coherence tomography detects characteristic retinal nerve fiber layer thickness corresponding to band atrophy of the optic discs. Ophthalmology. 2004;111(12):2278–83.
41. Danesh-Meyer HV, Carroll SC, Foroozan R, Savino PJ, Fan J, Jiang Y, et al. Relationship between retinal nerve fiber layer and visual field sensitivity as measured by optical coherence tomography in chiasmal compression. Invest Ophthalmol Vis Sci. 2006;47(11):4827–35.
42. Monteiro ML, Leal BC, Moura FC, Vessani RM, Medeiros FA. Comparison of retinal nerve fibre layer measurements using optical coherence tomography versions 1 and 3 in eyes with band atrophy of the optic nerve and normal controls. Eye (Lond). 2007;21(1):16–22.
43. Moura FC, Medeiros FA, Monteiro ML. Evaluation of macular thickness measurements for detection of band atrophy of the optic nerve using optical coherence tomography. Ophthalmology. 2007;114(1):175–81.
44. Costa-Cunha LV, Cunha LP, Malta RF, Monteiro ML. Comparison of Fourier-domain and time-domain optical coherence tomography in the detection of band atrophy of the optic nerve. Am J Ophthalmol. 2009;147(1):56–63.e2.
45. Garway-Heath DF, Poinoosawmy D, Fitzke FW, Hitchings RA. Mapping the visual field to the optic disc in normal tension glaucoma eyes. Ophthalmology. 2000;107(10):1809–15.

46. Shin HY, Park HY, Choi JA, Park CK. Macular ganglion cell-inner plexiform layer thinning in patients with visual field defect that respects the vertical meridian. Graefes Arch Clin Exp Ophthalmol. 2014;252(9):1501–7.
47. Monteiro ML, Cunha LP, Costa-Cunha LV, Maia Jr OO, Oyamada MK. Relationship between optical coherence tomography, pattern electroretinogram and automated perimetry in eyes with temporal hemianopia from chiasmal compression. Invest Ophthalmol Vis Sci. 2009;50(8):3535–41.
48. Moon CH, Hwang SC, Kim BT, Ohn YH, Park TK. Visual prognostic value of optical coherence tomography and photopic negative response in chiasmal compression. Invest Ophthalmol Vis Sci. 2011;52(11):8527–33.
49. Kerrison JB, Lynn MJ, Baer CA, Newman SA, Biousse V, Newman NJ. Stages of improvement in visual fields after pituitary tumor resection. Am J Ophthalmol. 2000;130(6):813–20.
50. Findlay G, McFadzean RM, Teasdale G. Recovery of vision following treatment of pituitary tumours; application of a new system of assessment to patients treated by transsphenoidal operation. Acta Neurochir (Wien). 1983;68(3–4):175–86.
51. Gnanalingham KK, Bhattacharjee S, Pennington R, Ng J, Mendoza N. The time course of visual field recovery following transphenoidal surgery for pituitary adenomas: predictive factors for a good outcome. J Neurol Neurosurg Psychiatry. 2005;76(3):415–9.
52. Monteiro ML, Zambon BK, Cunha LP. Predictive factors for the development of visual loss in patients with pituitary macroadenomas and for visual recovery after optic pathway decompression. Can J Ophthalmol. 2010;45(4):404–8.
53. Cohen AR, Cooper PR, Kupersmith MJ, Flamm ES, Ransohoff J. Visual recovery after transsphenoidal removal of pituitary adenomas. Neurosurgery. 1985;17(3):446–52.
54. Jacob M, Raverot G, Jouanneau E, Borson-Chazot F, Perrin G, Rabilloud M, et al. Predicting visual outcome after treatment of pituitary adenomas with optical coherence tomography. Am J Ophthalmol. 2009;147(1):64–70.e2.
55. Ohkubo S, Higashide T, Takeda H, Murotani E, Hayashi Y, Sugiyama K. Relationship between macular ganglion cell complex parameters and visual field parameters after tumor resection in chiasmal compression. Jpn J Ophthalmol. 2012;56(1):68–75.
56. Moon CH, Hwang SC, Ohn YH, Park TK. The time course of visual field recovery and changes of retinal ganglion cells after optic chiasmal decompression. Invest Ophthalmol Vis Sci. 2011;52(11):7966–73.
57. Cunha LP, Oyamada MK, Monteiro ML. Pattern electroretinograms for the detection of neural loss in patients with permanent temporal visual field defect from chiasmal compression. Doc Ophthalmol. 2008;117:223–32.
58. Leal BC, Moura FC, Monteiro MLR. Retinal nerve fiber layer loss documented by Stratus OCT in patients with pituitary adenoma: case report. Arq Bras Oftalmol. 2006;69:251–4.

Chapter 5
Optical Coherence Tomography (OCT) and Multiple Sclerosis (MS)

Rachel C. Nolan, Kannan Narayana, Laura J. Balcer, and Steven L. Galetta

Abstract Acute optic neuritis (ON) is a common manifestation of multiple sclerosis (MS). ON is the first clinical demyelinating event in MS for about 20 % of patients. In the Optic Neuritis Treatment Trial (ONTT), the overall cumulative probability of developing clinically-definite MS, defined as a second clinical event, was 50 % by 15 years after the onset of acute ON. Furthermore, those patients with a positive brain MRI consistent with demyelination had a far greater risk of developing of MS compared to those with a normal baseline MRI (72 % vs. 25 %). The subsequent development of MRI-based diagnostic criteria for MS has led to a paradigm shift in our clinical approach to patients with ON as a first clinical demyelinating event. In those patients with MRI scans consistent with demyelination, platform MS therapies have become standard treatment for patients with clinically isolated syndromes (CIS), including ON. Our ability to diagnose MS with a single MRI scan has allowed us to more expeditiously establish the diagnosis of MS while advances in OCT (optical coherence tomography) has provided us an opportunity to better

R.C. Nolan, BA • K. Narayana, MD
Department of Neurology, New York University School of Medicine,
240 East 38th Street, 20th Floor, New York, NY 10016, USA
e-mail: rachel.nolan@nyumc.org; kannan.narayana@nyumc.org

L.J. Balcer, MD, MSCE
Department of Neurology, New York University School of Medicine,
240 East 38th Street, 20th Floor, New York, NY 10016, USA

Department of Population Health, New York University School of Medicine,
New York, NY USA

Department of Ophthalmology, New York University School of Medicine,
New York, NY USA
e-mail: laura.balcer@nyumc.org

S.L. Galetta, MD (✉)
Department of Neurology, New York University School of Medicine,
240 East 38th Street, 20th Floor, New York, NY 10016, USA

Department of Ophthalmology, New York University School of Medicine,
New York, NY USA
e-mail: steven.galetta@nyumc.org

A. Grzybowski, P. Barboni (eds.), *OCT in Central Nervous System Diseases: The Eye as a Window to the Brain*, DOI 10.1007/978-3-319-24085-5_5

resolve the visual dysfunction that occurs in this disorder. OCT permits the correlation of structural aspects of anterior visual pathway axonal and neuronal loss with visual function in ON. It is now known that patients with MS have thinning of the retinal nerve fiber layer (RNFL, axons) and ganglion cell/inner plexiform layer (GCL+IPL, neurons) even in the absence of a history of acute ON. Such patients have clinically meaningful worsening of vision and quality of life (QOL). Furthermore, OCT is useful in patients with MS for distinguishing macular disease from ON, and for monitoring patients for macular edema associated with use of fingolimod. In this chapter, we summarize the data and current concepts for use of OCT in the evaluation and monitoring of patients with MS. Importantly, we will highlight how OCT has expanded our thinking about the pathogenesis of visual pathway dysfunction, and how RNFL and GCL+IPL thickness may serve as structural markers for monitoring disease in our patients.

Keywords Optic neuritis (ON) • MS-associated optic neuritis (MSON) • Optical coherence tomography (OCT) • Retinal nerve fiber layer (RNFL) • Total macular volume (TMV) • Ganglion cell/inner plexiform layer (GCL+IPL) • Microcystic macular edema (MMO)

5.1 Background

The Optic Neuritis Treatment Trial (ONTT) [1–5] was a landmark study in the field of neuro-ophthalmology. This study provided a large-scale systematic view into the course and clinical characteristics of acute demyelinating optic neuritis (ON). ON may be the first clinical demyelinating event in up to 20 % of patients with multiple sclerosis (MS) [6] and the overall cumulative probability of developing clinically-definite MS, defined as a second clinical event, was 50 % by 15 years after the onset of acute ON [7]. Presence of magnetic resonance imaging (MRI)-detected brain lesions and oligoclonal bands [7, 8] were found to be associated with an increased risk of developing clinically definite MS (CDMS), defined by a second clinical demyelinating event. Patients with one or more MRI lesions at baseline had a 56 % risk of CDMS at 10 years and a 72 % risk at 15 years [7, 9]. While visual recovery from ON as a first demyelinating event and in the setting of established MS is said to be good [5, 10], studies of vision in MS have shown that patients will have continued deficits that are not well captured by high-contrast visual acuity (VA) alone. Visual symptoms in MS may result from a variety of pathological processes, including inflammation, demyelination, and axonal degeneration in the afferent visual pathways [11, 12]. Subclinical optic neuropathy and involvement of the optic chiasm or post-chiasmal regions of the visual pathway have been reported [13–15].

Significant progress has been made in understanding the additional ways to assess qualitative and quantitative visual function in patients with MS. Tests of low-contrast vision, particularly low-contrast letter acuity (LCLA), have emerged as methods that demonstrate the greatest capacity to capture visual impairment in patients with MS

[16–19]. Vision-specific quality of life (QOL), measured by 25-Item National Eye Institute Visual Functioning Questionnaire (NEI-VFQ-25) and the 10-Item Neuro-Ophthalmic Supplement has been shown to be reduced among patients with worse visual function by low-contrast letter acuity and with structural changes of RNFL and GCL+IPL thinning by OCT [20–22]. These measurements from an ongoing collaborative study [23] of visual structure, function and QOL in MS are presented in Table 5.1.

5.2 Optical Coherence Tomography (OCT) in MS

Optical coherence tomography (OCT) is a non-invasive technique that is close to a tissue level *in vivo* optical biopsy of the retina. During the past decade, OCT has become increasingly recognized as a highly sensitive method for imaging the retina and optic disc. Imaging of the RNFL, both in the peripapillary region (pRNFL) and in the macula (mRNFL), represents a unique opportunity in the central nervous system to image axons without myelin sheaths (retinal ganglion cell axons are not myelinated until they traverse behind the lamina cribosa). Measures of ganglion cell layer/inner plexiform layer (GCL+IPL) thickness and total macular volume (TMV) also may be used to monitor neuronal integrity in the anterior visual pathway.

5.3 OCT in Patients with MS and ON

As OCT imaging has advanced to provide retinal detail that is nearly histologic in its level of detail, autopsy studies have likewise have shown that up to 94–99 % of MS patients have detectable optic nerve lesions [24, 25]. The earliest application of OCT technology to the study of ON in patients with MS was reported by Parisi et al. in 1999 [26], utilizing a first-generation OCT technology. In those patients with MS-associated ON (MSON), pRNFL thickness was reduced by an average of 46 % in eyes with an ON history, compared to disease-free control eyes. Even fellow eyes had RNFL thickness reductions of 28 %. In 2005, Trip et al. [27] reported further findings using time-domain (TD-) OCT. This study revealed a 33 % reduction in pRNFL thickness in eyes with a history of ON and incomplete recovery. There was a 27 % reduction in the affected eyes compared to the unaffected fellow eyes ($P < 0.001$). Eyes with a history of ON had macular volume reductions of 11 %. These first reports of OCT were thus able to show both axonal loss and retinal ganglion cell loss.

In 2010, Petzold et al. [28] performed a meta-analysis of available published reports on OCT in patients with MS and found pRNFL thinning by an average of 20.38 μm (95 % CI 17.91–22.86, $n = 2063$, $p < 0.0001$) in MS eyes with a history of acute ON, and by an average of 7.08 μm (5.52–8.65, $n = 3154$, $p < 0.0001$) in MS eyes without an ON history compared to disease-free controls. Peripapillary RNFL thickness also was found to correlate with visual and neurological functioning.

In 2006, Costello et al. [29] reported that the majority of patients (approximately 75 %) with acute ON, 94 % of whom had a clinically isolated syndrome, will sustain

Table 5.1 Mean reference values from recent investigations of vision, QOL, and OCT in MS

	Disease-free controls	All MS	MS, No History of ON	MS, History of ON
High-contrast visual acuity (VA), ETDRS, number of letters correct	59 ± 6 (n = 52 eyes)	53 ± 10 (n = 559 eyes)	55 ± 7 (n = 301 eyes)	52 ± 12 (n = 252 eyes)
Binocular testing	62 ± 4 (n = 26 pts)	58 ± 7 (n = 273 pts)	59 ± 6 (n = 147 pts)	57 ± 8 (n = 123 pts)
Low-contrast letter acuity (2.5 %), number of letters correct	35 ± 6 (n = 52 eyes)	25 ± 12 (n = 550 eyes)	27 ± 11 (n = 296 eyes)	23 ± 13 (n = 248 eyes)
Binocular testing	44 ± 4 (n = 26 pts)	34 ± 11 (n = 273 pts)	36 ± 9 (n = 147 pts)	32 ± 112 (n = 123 pts)
Low-contrast letter acuity (1.25 %), number of letters correct	21 ± 9 (n = 52 eyes)	13 ± 11 (n = 550 eyes)	15 ± 11 (n = 296 eyes)	11 ± 11 (n = 248 eyes)
Binocular testing	32 ± 5 (n = 26 pts)	23 ± 11 (n = 271 pts)	25 ± 11 (n = 146 pts)	21 ± 12 (n = 122 pts)
NEI-VFQ-25 composite score, best score = 100	98 ± 2 (n = 27 pts)	85 ± 15 (n = 264 pts)	88 ± 14 (n = 142 pts)	82 ± 15 (n = 119 pts)
10-Item Neuro-Ophthalmic Supplement to the NEI-VFQ-25, best score = 100	97 ± 5 (n = 28 pts)	78 ± 18 (n = 256 pts)	83 ± 16 (n = 137 pts)	73 ± 18 (n = 117 pts)
Time-domain (TD) OCT				
Peripapillary RNFL thickness, μm	104.5 ± 10.7 (n = 219 eyes)	92.5 ± 16.7 (n = 1,058 eyes)	95.6 ± 14.5 (n = 730 eyes)	85.7 ± 19.0 (n = 328 eyes)
Total macular volume, mm^3	6.84 ± 0.36 (n = 219 eyes)	6.54 ± 0.51 (n = 1,058 eyes)	6.63 ± 0.48 (n = 730 eyes)	6.36 ± 0.53 (n = 328 eyes)
Spectral-domain (SD) OCT				
Peripapillary RNFL thickness, μm	93.0 ± 9.0 (n = 48 eyes)	83.1 ± 12.9 (n = 529 eyes)	86.4 ± 10.9 (n = 287 eyes)	79.1 ± 14.1 (n = 236 eyes)
Ganglion cell + inner plexiform layer (GCL+IPL), μm	88.9 ± 6.9 (n = 61 eyes)	84.1 ± 8.4 (n = 239 eyes)	87.0 ± 6.6 (n = 150 eyes)	79.7 ± 9.2 (n = 87 eyes)
Macular Thickness, μm	10.1 ± 0.4 (n = 50 eyes)	9.8 ± 0.6 (n = 509 eyes)	9.9 ± 0.5 (n = 282 eyes)	9.7 ± 0.6 (n = 221 eyes)

Abbreviations: *MS* multiple sclerosis, *ETDRS* Early Treatment Diabetic Retinopathy Study, *QOL* quality of life *NEI-VFQ-25* 25-Item National Eye Institute Visual Functioning Questionnaire, *TD* time-domain (OCT-3 platform), *SD* spectral-domain (Cirrus platform), *OCT* optical coherence tomography, *RNFL* retinal nerve fiber layer

10–40 μm thinning of the pRNFL within a period of 3–6 months following the acute event. Importantly, pRNFL thinning to the level of 75–80 μm in that study was found to be a "threshold level" below which there were more severe decrements in visual function, as measured by automated perimetry mean deviation. To provide perspective on these measurements, normal pRNFL thickness by TD OCT is approximately 105 μm, with an estimated physiological loss due to aging of only about 0.017 % per year from age 18 years onward (approximately 10–20 μm loss over 60 years) [30].

Pro et al. [31] demonstrated mild, relative thickening of the pRNFL in eight patients with clinical retrobulbar optic neuritis (no visible optic disc swelling on ophthalmoscopy). Even though these OCT findings were subtle, and were within the range of the normal (100.7 μm in affected eye versus 92.9 μm in unaffected eye), the authors pointed out that these represented true change, as the unaffected eye remained stable over follow up. There was subsequent RNFL thinning in these affected eyes below the expected value for disease-free control eyes (approximately 105 μm) despite visual improvement [31]. The RNFL thinning was seen as early as 2–4 months following the acute ON. OCT was thus able to identify very mild, and in some cases clinically undetectable, optic disc edema in eyes with acute ON. These findings represent one way in which OCT has helped to refine the clinical profile of acute ON and of visual pathway structure in MS even in the absence of ON (see Case Study 5.1).

5.4 OCT Changes in the Subacute Phase and Recovery from ON

The time course of RNFL axonal loss following acute ON may be important for determining the "window of opportunity" for potential intervention with therapies that could protect and repair the nervous system. Reductions in pRNFL thickness in affected eyes, usually by 10–40 μm, are maximal after acute ON within 3–6 months. This pattern of rapid RNFL thinning suggests that significant axonal degeneration follows immediately after the primary demyelinating event [29, 32]. There is stabilization of RNFL thickness within 7–12 months from the beginning of the disease [32]. However, we now recognize that thinning of the GCL-IPL layer begins within weeks of the onset of acute ON and may precede the thinning of the RNFL, thus narrowing the window of therapeutic window of neuro-repair [33].

Henderson et al. [32] performed comprehensive qualitative and quantitative visual assessments in a study of 23 patients with acute clinically isolated unilateral ON. The mean time to 90 % of maximum loss from baseline in pRNFL thickness for affected eyes was 2.38 months. Ninety-nine percent of the degree of pRNFL loss occurred by an average of 4.75 months. The time of first detectable pRNFL thinning compared to the baseline fellow eye value was 1.64 months (95 % CI, 0.96–2.32; $p<0.05$). Eyes with poor recovery had a significantly greater decline of RNFL from baseline to 3 months ($p=0.002$). Macular volumes also declined significantly at the time of last follow-up.

5.5 OCT in MS Subtypes

Costello et al. [34] demonstrated that patterns of OCT RNFL thinning may be able to distinguish MS disease subtypes. For ON eyes among the different MS subtypes, differences among groups were noted in the overall and temporal RNFL regions. Patients with CIS had the highest overall RNFL thickness values (mean 87.8 μm), while patients with secondary progressive MS (SPMS) had the greatest degree of thinning compared to control reference values (mean RNFL thickness 70.8 μm). For MS non-ON eyes, RNFL thickness was reduced in patients with primary progressive MS (PPMS, average 94.3 μm $p=0.04$), relapsing remitting MS (RRMS, average 99.6 μm, $p=0.02$), and SPMS (average 84.7 μm, $p<0.0001$) relative to eyes of patients with CIS (average RNFL thickness 105.7 μm). RNFL thickness may thus represent an important structural marker of disease progression.

In a study by Pulicken et al. [35], progressive MS patients showed more marked decreases in RNFL and macular volume than relapsing-remitting MS. However, even patients with "benign MS" may have pRNFL axonal loss that is as marked as that of typical RRMS and have reduced vision and QOL. While overall neurologic impairment may be mild in such cases, visual dysfunction may account for a substantial degree of disability in benign MS [36].

5.6 RNFL Thickness in Asymptomatic Fellow Eyes in ON

Thinning of RNFL has been observed not only in the eyes with a history of ON, but also in the asymptomatic fellow eyes of MS patients, as well as in MS patients without a clinical history of ON. The average pRNFL thickness was found to be between 91.08 and 109.3 μm in the fellow eye in patients with MSON [27, 31, 35, 37–49].

In MS patients with no history suggestive of ON, the average RNFL thickness was between 93.9 and 110.9 μm [35, 49–52]. These findings emphasize the common occurrence of subclinical anterior visual pathway axonal loss in patients with MS even in eyes without history of ON.

5.7 RNFL Thinning and Visual Loss

One of the most important findings that has resulted from the use of OCT MS studies is the association of RNFL thinning to visual loss, as measured by low-contrast letter acuity [23]. In 2006, Fisher et al. [40] conducted a cross-sectional study that compared RNFL thickness among MS eyes with a history of ON (MS ON eyes), MS eyes without a history of ON (MS non-ON eyes), and disease-free control eyes. These investigators found that RNFL thickness was reduced significantly among MS eyes as a group overall (92 μm) vs. controls (105 μm , $p<0.001$, generalized estimating equation models, accounting for age and within-patient, inter-eye

correlations) and particularly reduced in MS ON eyes (85 mm, $p<0.001$). Furthermore, lower visual function scores were associated with reduced average overall RNFL thickness in MS eyes; for every 1-line decrease in low-contrast letter acuity or contrast sensitivity score, the mean RNFL thickness decreased by 4 μm. These findings supported the validity of low-contrast visual assessment and suggested a potential role for OCT in trials that may examine neuroprotective and other disease-modifying therapies. Several other investigations have demonstrated correlations between RNFL thinning and visual loss [53–55] (see Case Study 5.2). Costello et al. [56] found that RNFL thickness after an episode of isolated ON cannot be used to predict the risk of MS.

5.8 Relation of RNFL Thickness to Visual Evoked Potential (VEP) and MRI Findings

Several recent studies have highlighted the structure function-correlations provided by neuroimaging (MRI) and electrophysiological testing (visual evoked potentials) [57–60].

In a retrospective study, visual evoked potential (VEP) latency was found to be sensitive for detecting demyelination [61], while RNFL thickness reflects more structural aspects of optic nerve damage following acute ON. As might be expected, OCT RNFL thickness correlated well with VEP amplitude, but not with the latency [43]. In another study, retinal ganglion cell (RGC) axonal loss was associated with retinal dysfunction in eyes of MS patients without a history of ON and evidence of postchiasmal involvement of the visual pathway [62]. In a study that compared 112 partners of patients with MS to a control group of 93 volunteers, abnormal VEP latency in 5 of the partners and one clinically definite case of MS was found. Studies of OCT among partners of people with MS may provide further context for this finding [63].

In terms of brain MRI studies, RNFL thickness has been shown to reflect the volumes of brain white and gray matter as well as the normalized volumes of whole brain and white matter [53, 64]. The correlations between RNFL thickness and MRI measurements of brain atrophy were more significant in the subset of patients with no clinical history of ON than in those who had an ON history in either eye. Studies also suggest that RNFL thickness measurements could be considered a marker for brain atrophy in MS [40]. The relation of RNFL thicknesses and brain parenchymal fraction (BPF), measured using high-resolution MRI was also recently shown to reflect the likely global nature of axonal and neuronal loss in MS [49]. A correlation between RNFL thickness, volume of T1 and T2 lesions, gray matter atrophy, MTR and diffusion tensor imaging measures (DTI) measurements in MS patients with or without a history of ON was also reported [39]. These MRI parameters also correlated with low-contrast letter acuity measurements, consistent with prior studies suggesting that both posterior and anterior visual pathway disease contribute to visual function in MS [65]. Interestingly, in MS patients with optic radiation lesions, a correlation was found between the volume of the lesion and RNFL thickness ($p<0.001$) [66].

5.9 Role for OCT in Monitoring MS Therapy Adverse Events and Efficacy

Fingolimod, an oral sphingosine-1-phosphate receptor modulator approved for treatment of MS, has been shown in clinical trials to cause macular edema in 0.3–1.2 % of patients, with uveitis and other ocular pathology elevating this risk [67] (see Case Study 5.3). Patients present with blurred vision, decreased visual acuity or eye pain. Macular edema resolves in most cases when fingolimod treatment is discontinued [67, 68]. OCT studies of patients on fingolimod have shown elevations in macular volume consistent with diffuse macular edema; some of these patients were symptomatic, presenting with metamorphopsia and blurred vision [69]. Ophthalmologic evaluations, including OCT scans of the macula, are recommended before initiating treatment. Follow-up at 3–4-month intervals is also recommended.

Though not common, cases of retinopathy associated with interferon-beta 1a treatment in MS have been reported [70–73]. This retinopathy was characterized by clinical/OCT findings of retinal hemorrhages or cotton wool spots at the posterior fundus and improved with discontinuation of medication.

In a prospective study of 94 MS patients and 50 healthy subjects followed over 3 years, the authors evaluated whether treatment with interferon 1a, interferon 1b or glatiramer acetate was associated with reduced degrees of RNFL thinning. Progressive RNFL thinning was detected in both the treated and untreated groups, but untreated patients had lower mean RNFL thicknesses. Otherwise, no differences in the treatment groups were noted [74].

Another study showed that the peripapillary RNFL, ganglion cell layer thicknesses, and macular volumes measured by OCT were all reduced among patients with or without disease modifying therapy when compared with controls. The abnormal findings were more prominent for MS eyes with an ON history [75].

5.10 Microcystic Inner Nuclear Layer Abnormalities

Microcystic changes in the inner nuclear layer (MMO, microcystic macular oedema) are characterized by retinal microcysts in the inner nuclear layer and are easily identified perifoveally on macular spectral-domain OCT. These findings are typically not identifiable by direct ophthalmoscopy, and may be associated with reductions in VA. In many cases, a perifoveal hyporeflective crescent shape can be seen on confocal infrared laser fundus imaging directly correlating with the area of microcysts observed on OCT (see Case Study 5.4). It has been hypothesized that inner nuclear layer microcysts associated with various forms of optic neuropathy could be either a sign of inflammation [76, 77], autoantibodies against AQP4 and KIR4.1, microglial activation, blood–retina barrier breakdown or retrograde or anterograde transsynaptic degeneration changes secondary to neurodegeneration [78, 79]. Microcystic changes in the inner nuclear layers in eyes of patients with MS were first described

by Gelfand et al. [76]. These findings were seen in association with increased disease severity (4.7 % of patients), with higher prevalence in patients with a history of ON [76]. Further evaluation of microcystic macular oedema (MMO) found that patients with neuromyelitis optica (NMO), who are known to have a high incidence of ON, had a higher prevalence of MMO (20–26 %) [80, 81]. Microcystic inner nuclear layer abnormalities are not specific to MS and ON and have been found associated with other optic neuropathies, including hereditary optic neuropathy [82–92].

5.11 Segmentation and Newer trends

Segmentation of the macular retinal layers is now possible for use in the clinical and research setting. Thinning of the ganglion cell layer has been demonstrated to be greatest among patients with decrements in vision-specific QOL and among those with the highest degrees of visual loss [93].

In a study by Gabilondo et al., retinal changes by OCT in ON were evaluated using the latest segmentation techniques. Changes in ganglion cell layer thickness within the first month were predictive of visual impairment by 6 months [33]. These studies, and others, have confirmed an important role for neuronal loss as measured by ganglion cell layer thickness in determining visual disability in MS.

OCT angiography is a newer technique that demonstrates the optic nerve blood flow, which may be reflective of the metabolic demand. This is hypothesized to be a sensitive measure of axonal loss. Wang and colleagues showed that eyes of patients with MS and ON had lower flow indices as compared to controls and MS eyes without an ON history. In addition, the flow index was abnormal in a greater proportion of eyes with a history of ON than was the peripapillary RNFL [94]. One caution in interpreting these findings might be the very high threshold (thickness below 5th percentile) for categorizing an RNFL thickness measurement as abnormal.

5.12 Conclusions

OCT has provided a basis for correlating structural aspects of anterior visual pathway axonal and neuronal loss with visual function in ON as well as in MS. It is now known that patients with MS have thinning of the retinal nerve fiber layer (RNFL, axons) and ganglion cell/inner plexiform layer (GCL+IPL, neurons) even in the absence of a history of acute ON. Such patients have clinically meaningful worsening of vision and quality of life (QOL). Furthermore, OCT is useful in patients with MS for distinguishing macular disease from ON, and for monitoring patients for macular edema associated with use of fingolimod. OCT is a powerful tool that may be used to assess neuro-repair and neuroprotective mechanisms in both acute and chronic optic nerve injury.

5.13 Figures/Representative Cases

Case 1: MS patient with unilateral ON – cross sectional
Case 2: Bilateral RNFL thinning – MS patient with no optic neuritis
Case 3: Fingolimod related macular edema
Case 4: Microcystic Inner Nuclear Layer Abnormalities

Case 5.1: MS Patient with Unilateral ON – Cross Sectional
55-year old man with history of MS and right ON in his 20s. At time of imaging, 35 years after onset of visual loss, his visual acuities were 20/30 OD and 20/20 OS. Patient could not correctly read color plates with the right eye, but read all with the left eye. He had a small right relative afferent pupillary defect. Both optic discs appeared mildly pale bilaterally, OD greater than OS. His neuro-ophthalmological exam revealed mild disc atrophy in OD. OCT showed decreased RNFL in OD measuring 76 μm (93 μm in OS) and reduced GCL and TMV in OD.

RNFL Thickness (*left*)**, GCL Thickness** (*Top Right*)**, Macular Volume** (*Bottom Right*)

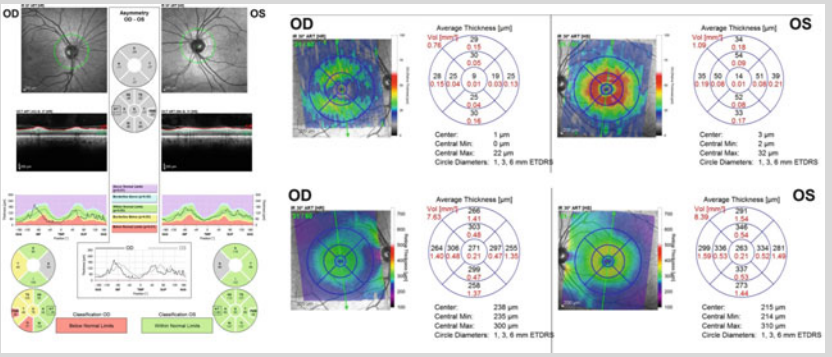

Case 5.2: Bilateral RNFL Thinning – MS Patient with No Optic Neuritis
49-year old female with history of RRMS and disease duration of 13 years and no history of optic neuritis. She had an Expanded Disability Severity Scale (EDSS) of 4.5 and was treated with Tysabri. The picture shows a global symmetric RNFL loss in the absence of acute ON.

Peripapillary RNFL Thinning in MS patient with no history of optic neuritis

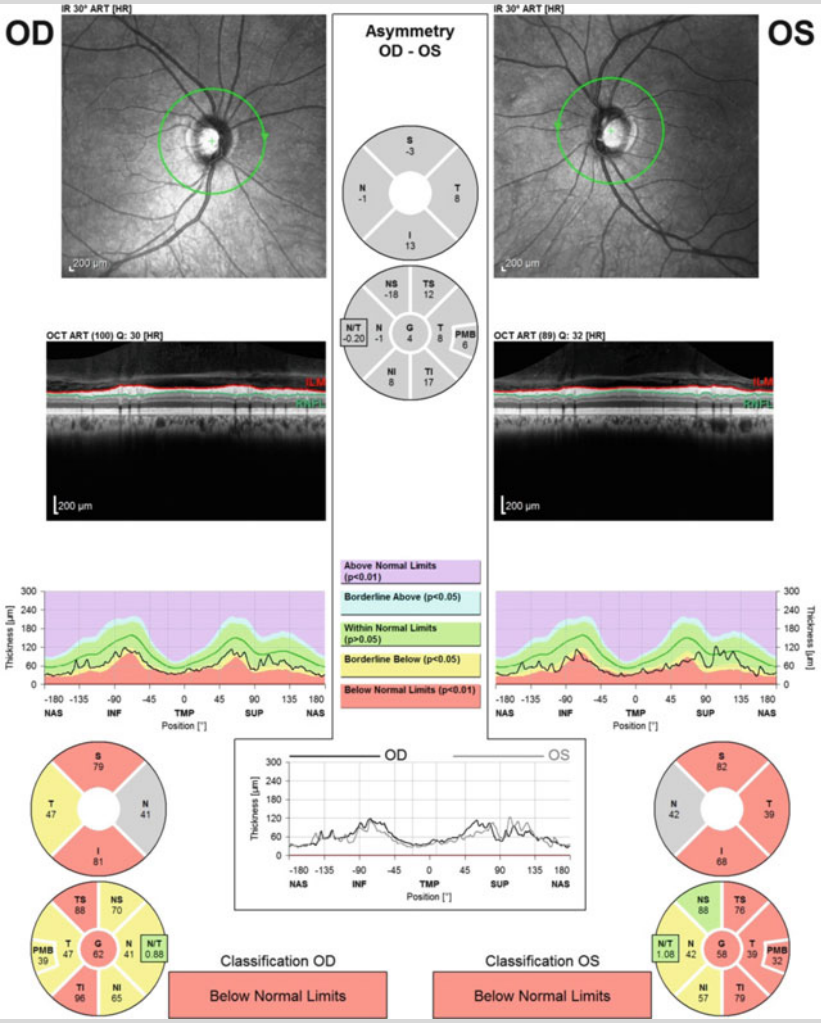

Case 5.3: Fingolimod Related Macular Edema

51-year old female w/history of MS and retinitis pigmentosa. One month post-fingolimod initiation, new cystoid macular edema was seen in macula. This resolved after immediate discontinuation of medication, however there was additional macular volume loss beyond the initial increase.

Line Scan through fovea (*top*). Macular volume increases of 0.19 mm^3 after 1 month of treatment initiation (*bottom left*). Macular volume decreases after stopping treatment of 0.34 mm^3 (−0.15 mm^3 from baseline) (*bottom right*) (Courtesy by Sam Arnow and Ari Green, University of California, San Francisco)

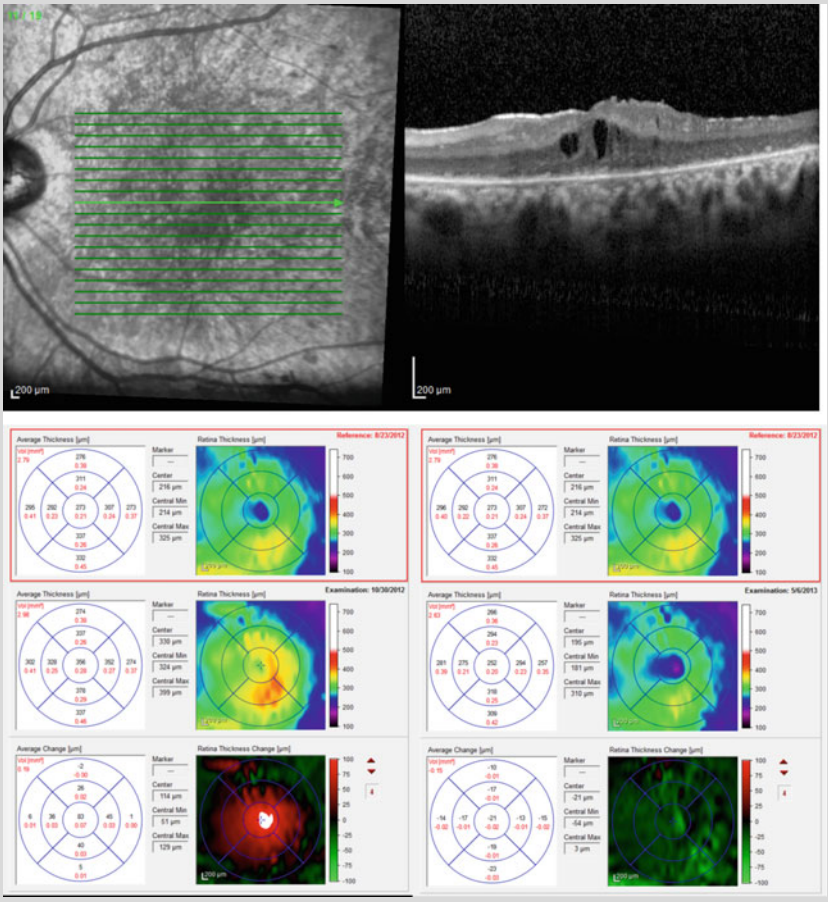

Case 5.4: Microcystic Inner Nuclear Layer Abnormalities
23-year old female with RRMS, previous history of ON OS and evident microcysts stable over 2.5 years.

(a) Baseline macular SD-OCT of left eye with prior history of ON. Microcystic inner nuclear layer abnormalities (*white arrow*) are found perifoveally. Hyporeflectant crescent shape perifoveally on infrared image (*red arrow*) corresponds to areas of microcysts on OCT. (b) Follow-up macular SD-OCT scan referenced to original scan. Microcysts are dynamic but relatively stable since baseline. (c) IR images of fundus. (d) Red-Free image of fundus. (e) Autofluorescence image of fundus (Courtesy by Sam Arnow and Ari Green, University of California, San Francisco

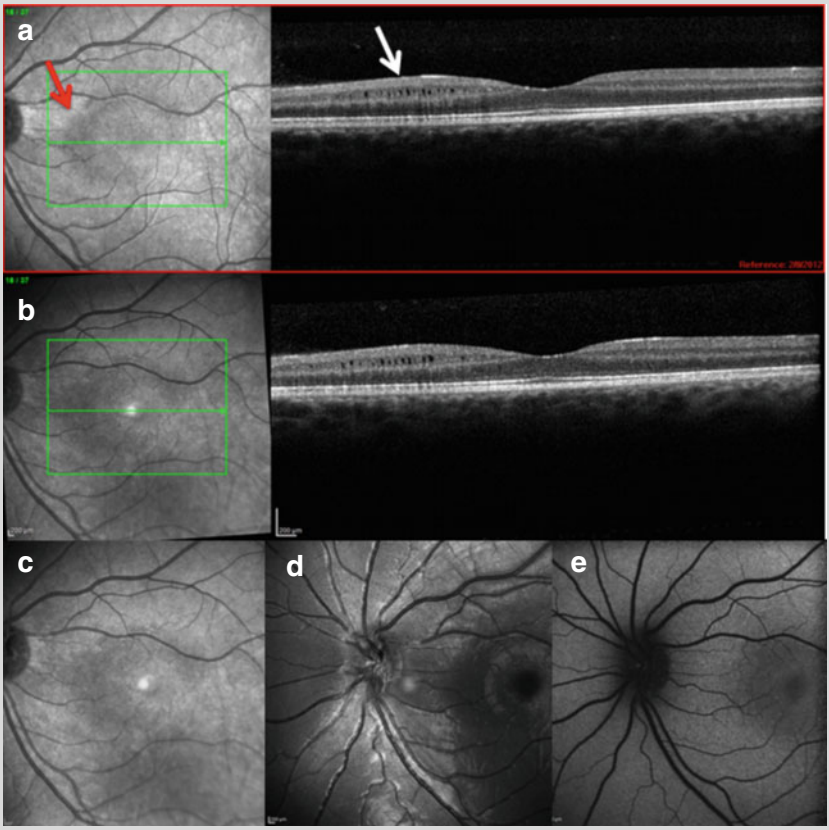

References

1. Beck RW. The optic neuritis treatment trial. Arch Ophthalmol. 1988;106(8):1051–3.
2. The clinical profile of optic neuritis. Experience of the Optic Neuritis Treatment Trial. Optic Neuritis Study Group. Arch Ophthalmol. 1991;109(12):1673–8.
3. Beck RW, Cleary PA, Anderson Jr MM, Keltner JL, Shults WT, Kaufman DI, et al. A randomized, controlled trial of corticosteroids in the treatment of acute optic neuritis. The Optic Neuritis Study Group. N Engl J Med. 1992;326(9):581–8.
4. Beck RW, Kupersmith MJ, Cleary PA, Katz B. Fellow eye abnormalities in acute unilateral optic neuritis. Experience of the optic neuritis treatment trial. Ophthalmology. 1993;100(5):691–7; discussion 7–8.
5. Cleary PA, Beck RW, Bourque LB, Backlund JC, Miskala PH. Visual symptoms after optic neuritis. Results from the Optic Neuritis Treatment Trial. J Neuroophthalmol. 1997;17(1):18–23; quiz 4–8.
6. Sorensen TL, Frederiksen JL, Bronnum-Hansen H, Petersen HC. Optic neuritis as onset manifestation of multiple sclerosis: a nationwide, long-term survey. Neurology. 1999;53(3):473–8.
7. Optic Neuritis Study Group. Multiple sclerosis risk after optic neuritis: final optic neuritis treatment trial follow-up. Arch Neurol. 2008;65(6):727–32.
8. Soderstrom M, Ya-Ping J, Hillert J, Link H. Optic neuritis: prognosis for multiple sclerosis from MRI, CSF, and HLA findings. Neurology. 1998;50(3):708–14.
9. Beck RW, Trobe JD, Moke PS, Gal RL, Xing D, Bhatti MT, et al. High- and low-risk profiles for the development of multiple sclerosis within 10 years after optic neuritis: experience of the optic neuritis treatment trial. Arch Ophthalmol. 2003;121(7):944–9.
10. Beck RW, Gal RL, Bhatti MT, Brodsky MC, Buckley EG, Chrousos GA, et al. Visual function more than 10 years after optic neuritis: experience of the optic neuritis treatment trial. Am J Ophthalmol. 2004;137(1):77–83.
11. Evangelou N, Konz D, Esiri MM, Smith S, Palace J, Matthews PM. Size-selective neuronal changes in the anterior optic pathways suggest a differential susceptibility to injury in multiple sclerosis. Brain J Neurol. 2001;124(Pt 9):1813–20.
12. DeLuca GC, Williams K, Evangelou N, Ebers GC, Esiri MM. The contribution of demyelination to axonal loss in multiple sclerosis. Brain. 2006;129(Pt 6):1507–16.
13. Sisto D, Trojano M, Vetrugno M, Trabucco T, Iliceto G, Sborgia C. Subclinical visual involvement in multiple sclerosis: a study by MRI, VEPs, frequency-doubling perimetry, standard perimetry, and contrast sensitivity. Invest Ophthalmol Vis Sci. 2005;46(4):1264–8.
14. Lycke J, Tollesson PO, Frisen L. Asymptomatic visual loss in multiple sclerosis. J Neurol. 2001;248(12):1079–86.
15. Engell T, Trojaborg W, Raun NE. Subclinical optic neuropathy in multiple sclerosis. A neuro-ophthalmological investigation by means of visually evoked response, Farnworth-Munsell 100 Hue test and Ishihara test and their diagnostic value. Acta Ophthalmol. 1987;65(6):735–40.
16. Trobe JD, Beck RW, Moke PS, Cleary PA. Contrast sensitivity and other vision tests in the optic neuritis treatment trial. Am J Ophthalmol. 1996;121(5):547–53.
17. Balcer LJ, Baier ML, Cohen JA, Kooijmans MF, Sandrock AW, Nano-Schiavi ML, et al. Contrast letter acuity as a visual component for the Multiple Sclerosis Functional Composite. Neurology. 2003;61(10):1367–73.
18. Baier ML, Cutter GR, Rudick RA, Miller D, Cohen JA, Weinstock-Guttman B, et al. Low-contrast letter acuity testing captures visual dysfunction in patients with multiple sclerosis. Neurology. 2005;64(6):992–5.
19. Balcer LJ, Baier ML, Pelak VS, Fox RJ, Shuwairi S, Galetta SL, et al. New low-contrast vision charts: reliability and test characteristics in patients with multiple sclerosis. Mult Scler. 2000;6(3):163–71.
20. Ma SL, Shea JA, Galetta SL, Jacobs DA, Markowitz CE, Maguire MG, et al. Self-reported visual dysfunction in multiple sclerosis: new data from the VFQ-25 and development of an MS-specific vision questionnaire. Am J Ophthalmol. 2002;133(5):686–92.

21. Raphael BA, Galetta KM, Jacobs DA, Markowitz CE, Liu GT, Nano-Schiavi ML, et al. Validation and test characteristics of a 10-item neuro-ophthalmic supplement to the NEI-VFQ-25. Am J Ophthalmol. 2006;142(6):1026–35.
22. Mowry EM, Loguidice MJ, Daniels AB, Jacobs DA, Markowitz CE, Galetta SL, et al. Vision related quality of life in multiple sclerosis: correlation with new measures of low and high contrast letter acuity. J Neurol Neurosurg Psychiatry. 2009;80(7):767–72.
23. Sakai RE, Feller DJ, Galetta KM, Galetta SL, Balcer LJ. Vision in multiple sclerosis: the story, structure-function correlations, and models for neuroprotection. J Neuroophthalmol. 2011;31(4):362–73.
24. Ikuta F, Zimmerman HM. Distribution of plaques in seventy autopsy cases of multiple sclerosis in the United States. Neurology. 1976;26(6 PT 2):26–8.
25. Toussaint D, Perier O, Verstappen A, Bervoets S. Clinicopathological study of the visual pathways, eyes, and cerebral hemispheres in 32 cases of disseminated sclerosis. J Clin Neuroophthalmol. 1983;3(3):211–20.
26. Parisi V, Manni G, Spadaro M, Colacino G, Restuccia R, Marchi S, et al. Correlation between morphological and functional retinal impairment in multiple sclerosis patients. Invest Ophthalmol Vis Sci. 1999;40(11):2520–7.
27. Trip SA, Schlottmann PG, Jones SJ, Altmann DR, Garway-Heath DF, Thompson AJ, et al. Retinal nerve fiber layer axonal loss and visual dysfunction in optic neuritis. Ann Neurol. 2005;58(3):383–91.
28. Petzold A, de Boer JF, Schippling S, Vermersch P, Kardon R, Green A, et al. Optical coherence tomography in multiple sclerosis: a systematic review and meta-analysis. Lancet Neurol. 2010;9(9):921–32.
29. Costello F, Coupland S, Hodge W, Lorello GR, Koroluk J, Pan YI, et al. Quantifying axonal loss after optic neuritis with optical coherence tomography. Ann Neurol. 2006;59(6):963–9.
30. Kanamori A, Escano MF, Eno A, Nakamura M, Maeda H, Seya R, et al. Evaluation of the effect of aging on retinal nerve fiber layer thickness measured by optical coherence tomography. Ophthalmologica. 2003;217(4):273–8.
31. Pro MJ, Pons ME, Liebmann JM, Ritch R, Zafar S, Lefton D, et al. Imaging of the optic disc and retinal nerve fiber layer in acute optic neuritis. J Neurol Sci. 2006;250(1–2):114–9.
32. Henderson AP, Altmann DR, Trip AS, Kallis C, Jones SJ, Schlottmann PG, et al. A serial study of retinal changes following optic neuritis with sample size estimates for acute neuroprotection trials. Brain. 2010;133(9):2592–602.
33. Gabilondo I, Martínez-Lapiscina EH, Fraga-Pumar E, Ortiz-Perez S, Torres-Torres R, et al. Dynamics of retinal injury after acute optic neuritis. Ann Neurol. 2015;77(3):517–28.
34. Costello F, Hodge W, Pan YI, Eggenberger E, Freedman MS. Using retinal architecture to help characterize multiple sclerosis patients. Can J Ophthalmol. 2010;45(5):520–6.
35. Pulicken M, Gordon-Lipkin E, Balcer LJ, Frohman E, Cutter G, Calabresi PA. Optical coherence tomography and disease subtype in multiple sclerosis. Neurology. 2007;69(22):2085–92.
36. Galetta KM, Graves J, Talman LS, Lile DJ, Frohman EM, Calabresi PA, et al. Visual pathway axonal loss in benign multiple sclerosis: a longitudinal study. J Neuroophthalmol. 2012;32(2):116–23.
37. Cheng H, Laron M, Schiffman JS, Tang RA, Frishman LJ. The relationship between visual field and retinal nerve fiber layer measurements in patients with multiple sclerosis. Invest Ophthalmol Vis Sci. 2007;48(12):5798–805.
38. Costello F, Hodge W, Pan YI, Freedman M, DeMeulemeester C. Differences in retinal nerve fiber layer atrophy between multiple sclerosis subtypes. J Neurol Sci. 2009;281:74–9.
39. Frohman EM, Dwyer MG, Frohman T, Cox JL, Salter A, Greenberg BM, et al. Relationship of optic nerve and brain conventional and non-conventional MRI measures and retinal nerve fiber layer thickness, as assessed by OCT and GDx: a pilot study. J Neurol Sci. 2009;282(1–2):96–105.
40. Fisher JB, Jacobs DA, Markowitz CE, Galetta SL, Volpe NJ, Nano-Schiavi ML, et al. Relation of visual function to retinal nerve fiber layer thickness in multiple sclerosis. Ophthalmology. 2006;113(2):324–32.

41. Grazioli E, Zivadinov R, Weinstock-Guttman B, Lincoff N, Baier M, Wong JR, et al. Retinal nerve fiber layer thickness is associated with brain MRI outcomes in multiple sclerosis. J Neurol Sci. 2008;268:12–7.
42. Henderson AP, Trip SA, Schlottmann PG, Altmann DR, Garway-Heath DF, Plant GT, et al. An investigation of the retinal nerve fibre layer in progressive multiple sclerosis using optical coherence tomography. Brain. 2008;131(Pt 1):277–87.
43. Klistorner A, Arvind H, Nguyen T, Garrick R, Paine M, Graham S, et al. Axonal loss and myelin in early ON loss in postacute optic neuritis. Ann Neurol. 2008;64(3):325–31.
44. Merle H, Olindo S, Donnio A, Beral L, Richer R, Smadja D, et al. Retinal nerve fiber layer thickness and spatial and temporal contrast sensitivity in multiple sclerosis. Eur J Ophthalmol. 2010;20(1):158–66.
45. Pueyo V, Martin J, Fernandez J, Almarcegui C, Ara J, Egea C, et al. Axonal loss in the retinal nerve fiber layer in patients with multiple sclerosis. Mult Scler. 2008;14(5):609–14.
46. Ratchford JN, Quigg ME, Conger A, Frohman T, Frohman E, Balcer LJ, et al. Optical coherence tomography helps differentiate neuromyelitis optica and MS optic neuropathies. Neurology. 2009;73(4):302–8.
47. Spain RI, Maltenfort M, Sergott RC, Leist TP. Thickness of retinal nerve fiber layer correlates with disease duration in parallel with corticospinal tract dysfunction in untreated multiple sclerosis. J Rehabil Res Dev. 2009;46(5):633–42.
48. Zaveri MS, Conger A, Salter A, Frohman TC, Galetta SL, Markowitz CE, et al. Retinal imaging by laser polarimetry and optical coherence tomography evidence of axonal degeneration in multiple sclerosis. Arch Neurol. 2008;65(7):924–8.
49. Toledo J, Sepulcre J, Salinas-Alaman A, Garcia-Layana A, Murie-Fernandez M, Bejarano B, et al. Retinal nerve fiber layer atrophy is associated with physical and cognitive disability in multiple sclerosis. Mult Scler. 2008;14(7):906–12.
50. Gundogan FC, Demirkaya S, Sobaci G. Is optical coherence tomography really a new biomarker candidate in multiple sclerosis?--A structural and functional evaluation. Invest Ophthalmol Vis Sci. 2007;48(12):5773–81.
51. Jeanjean L, Castelnovo G, Carlander B, Villain M, Mura F, Dupeyron G, et al. Retinal atrophy using optical coherence tomography (OCT) in 15 patients with multiple sclerosis and comparison with healthy subjects. Rev Neurol. 2008;164(11):927–34.
52. Pueyo V, Ara JR, Almarcegui C, Martin J, Guerri N, Garcia E, et al. Sub-clinical atrophy of the retinal nerve fibre layer in multiple sclerosis. Acta Ophthalmol. 2010;88(7):748–52.
53. Sepulcre J, Murie-Fernandez M, Salinas-Alaman A, Garcia-Layana A, Bejarano B, Villoslada P. Diagnostic accuracy of retinal abnormalities in predicting disease activity in MS. Neurology. 2007;68(18):1488–94.
54. Galetta KM, Calabresi PA, Frohman EM, Balcer LJ. Optical coherence tomography (OCT): imaging the visual pathway as a model for neurodegeneration. Neurotherapeutics. 2011;8(1):117–32.
55. Bock M, Brandt AU, Kuchenbecker J, Dorr J, Pfueller CF, Weinges-Evers N, et al. Impairment of contrast visual acuity as a functional correlate of retinal nerve fibre layer thinning and total macular volume reduction in multiple sclerosis. Br J Ophthalmol. 2012;96(1):62–7.
56. Costello F, Hodge W, Pan YI, Metz L, Kardon RH. Retinal nerve fiber layer and future risk of multiple sclerosis. Can J Neurol Sci. 2008;35(4):482–7.
57. Horwitz H, Degn M, Modvig S, Larsson HB, Wanscher B, Frederiksen JL. CSF abnormalities can be predicted by VEP and MRI pathology in the examination of optic neuritis. J Neurol. 2012;259(12):2616–20.
58. Kantorová E, Ziak P, Kurča E, Koyšová M, Hladká M, Zeleňák K, Michalik J. Visual evoked potential and magnetic resonance imaging are more effective markers of multiple sclerosis progression than laser polarimetry with variable corneal compensation. Front Hum Neurosci. 2014;8:10.
59. Ellidag HY, Eren E, Erdogan N, Ture S, Yilmaz N. Comparison of neurophysiological and MRI findings of patients with multiple sclerosis using oligoclonal band technique. Ann Neurosci. 2013;20(4):149–54.
60. Chirapapaisan N. Diagnostic value of visual evoked potentials for clinical diagnosis of multiple sclerosis. Doc Ophthalmol. 2015;130(1):25–30.

61. Naismith RT, Tutlam NT, Xu J, Shepherd JB, Klawiter EC, Song SK, et al. Optical coherence tomography is less sensitive than visual evoked potentials in optic neuritis. Neurology. 2009;73(1):46–52.
62. Sriram P, Wang C, Yiannikas C, Garrick R, Barnett M, Parratt J, et al. Relationship between optical coherence tomography and electrophysiology of the visual pathway in non-optic neuritis eyes of multiple sclerosis patients. PLoS One. 2014;9(8):e102546.
63. Hawkes CH, Chawda S, Derakshani S, Muhammed N, Visentin E, Boniface D. MRI and visual-evoked potentials in partners of multiple sclerosis patients. Acta Neurol Scand. 2012;125(6):424–30.
64. Siger M, Dziegielewski K, Jasek L, Bieniek M, Nicpan A, Nawrocki J, et al. Optical coherence tomography in multiple sclerosis: thickness of the retinal nerve fiber layer as a potential measure of axonal loss and brain atrophy. J Neurol. 2008;255(10):1555–60.
65. Wu GF, Schwartz ED, Lei T, Souza A, Mishra S, Jacobs DA, et al. Relation of vision to global and regional brain MRI in multiple sclerosis. Neurology. 2007;69(23):2128–35.
66. Sinnecker T, Oberwahrenbrock T, Metz I, Zimmermann H, Pfueller CF, Harms L, et al. Optic radiation damage in multiple sclerosis is associated with visual dysfunction and retinal thinning--an ultrahigh-field MR pilot study. Eur Radiol. 2015;25(1):122–31.
67. Zarbin MA, Jampol LM, Jager RD, Reder AT, Francis G, Collins W, et al. Ophthalmic evaluations in clinical studies of fingolimod (FTY720) in multiple sclerosis. Ophthalmology. 2013;120(7):1432–9.
68. Turaka K, Bryan JS. Does fingolimod in multiple sclerosis patients cause macular edema? J Neurol. 2012;259(2):386–8.
69. Nolan R, Gelfand JM, Green AJ. Fingolimod treatment in multiple sclerosis leads to increased macular volume. Neurology. 2013;80(2):139–44.
70. Ohira M, Ito D, Shimizu T, Shibata M, Ohde H, Suzuki N. Retinopathy: an overlooked adverse effect of interferon-beta treatment of multiple sclerosis. Keio J Med. 2009;58(1):54–6.
71. Bakri SJ, Swanson JW. Asymptomatic peripheral retinal hemorrhages as a manifestation of interferon Beta 1a retinopathy. Semin Ophthalmol. 2015;30(1):56–7.
72. Sallansonnet-Froment M, Roux X, de Greslan T, Bounolleau P, Taillia H, Ricard D, et al. Interferon-beta retinopathy. Rev Neurol. 2009;165(11):971–4.
73. Martinez de Aragon JS, Pulido JS, Haupert CL, Blodi CF, Nielsen JS, Jampol LM. Interferon-beta-associated retinopathy. Retin Cases Brief Rep. 2009;3(1):24–6.
74. Herrero R, Garcia-Martin E, Almarcegui C, Ara JR, Rodriguez-Mena D, Martin J, et al. Progressive degeneration of the retinal nerve fiber layer in patients with multiple sclerosis. Invest Ophthalmol Vis Sci. 2012;53(13):8344–9.
75. Tugcu B, Soysal A, Kılıc M, Yuksel B, Kale N, Yıgıt U, et al. Assessment of structural and functional visual outcomes in relapsing remitting multiple sclerosis with visual evoked potentials and optical coherence tomography. J Neurol Sci. 2013;335(1–2):182–5.
76. Gelfand JM, Nolan R, Schwartz DM, Graves J, Green AJ. Microcystic macular oedema in multiple sclerosis is associated with disease severity. Brain. 2012;135(Pt 6):1786–93.
77. Petzold A. Microcystic macular oedema in MS: T2 lesion or black hole? Lancet Neurol. 2012;11(11):933–4.
78. Abegg M, Dysli M, Wolf S, Kowal J, Dufour P, Zinkernagel M. Microcystic macular edema: retrograde maculopathy caused by optic neuropathy. Ophthalmology. 2014;121(1):142–9.
79. Sotirchos ES, Saidha S, Byraiah G, Mealy MA, Ibrahim MA, Sepah YJ, et al. In vivo identification of morphologic retinal abnormalities in neuromyelitis optica. Neurology. 2013;80(15):1406–14.
80. Gelfand JM, Cree BA, Nolan R, Arnow S, Green AJ. Microcystic inner nuclear layer abnormalities and neuromyelitis optica. JAMA Neurol. 2013;70(5):629–33.
81. Saidha S, Sotirchos ES, Ibrahim MA, Crainiceanu CM, Gelfand JM, Sepah YJ, et al. Microcystic macular oedema, thickness of the inner nuclear layer of the retina, and disease characteristics in multiple sclerosis: a retrospective study. Lancet Neurol. 2012;11(11):963–72.
82. Balk LJ, Killestein J, Polman CH, Uitdehaag BM, Petzold A. Microcystic macular oedema confirmed, but not specific for multiple sclerosis. Brain. 2012;135(Pt 12):e226; author reply e7.

83. Kisimbi J, Shalchi Z, Mahroo OA, Mhina C, Sanyiwa AJ, Mabey D, et al. Macular spectral domain optical coherence tomography findings in Tanzanian endemic optic neuropathy. Brain. 2013;136(Pt 11):3418–26.
84. Shalchi Z, Mahroo OA, Shunmugam M, Mohamed M, Sullivan PM, Williamson TH. Spectral domain optical coherence tomography findings in long-term silicone oil-related visual loss. Retina. 2015;35(3):555–63.
85. Wolff B, Azar G, Vasseur V, Sahel JA, Vignal C, Mauget-Faysse M. Microcystic changes in the retinal internal nuclear layer associated with optic atrophy: a prospective study. J Ophthalmol. 2014;2014:395189.
86. Tawse KL, Hedges 3rd TR, Gobuty M, Mendoza-Santiesteban C. Optical coherence tomography shows retinal abnormalities associated with optic nerve disease. Br J Ophthalmol. 2014;98 Suppl 2:ii30–3.
87. Burggraaff MC, Trieu J, de Vries-Knoppert WA, Balk L, Petzold A. The clinical spectrum of microcystic macular edema. Invest Ophthalmol Vis Sci. 2014;55(2):952–61.
88. Kaufhold F, Zimmermann H, Schneider E, Ruprecht K, Paul F, Oberwahrenbrock T, et al. Optic neuritis is associated with inner nuclear layer thickening and microcystic macular edema independently of multiple sclerosis. PLoS One. 2013;8(8):e71145.
89. Bhargava P, Calabresi PA. The expanding spectrum of aetiologies causing retinal microcystic macular change. Brain. 2013;136(Pt 11):3212–4; author reply.
90. Gills Jr JP, Wadsworth JAC. Retrograde transsynaptic degeneration of the inner nuclear layer of the retina. Invest Ophthalmol Vis Sci. 1967;6(4):437–48.
91. Wen JC, Freedman SF, El-Dairi MA, Asrani S. Microcystic macular changes in primary open-angle glaucoma. J Glaucoma. 2014. doi: 10.1097/IJG.0000000000000129. [Epub ahead of print]
92. Barboni P, Carelli V, Savini G, Carbonelli M, La Morgia C, Sadun AA. Microcystic macular degeneration from optic neuropathy: not inflammatory, not trans-synaptic degeneration. Brain. 2013;136(Pt 7):e239; author reply.
93. Walter SD, Ishikawa H, Galetta KM, Sakai RE, Feller DJ, Henderson SB, et al. Ganglion cell loss in relation to visual disability in multiple sclerosis. Ophthalmology. 2012;119(6):1250–7.
94. Wang X, Jia Y, Spain R, Potsaid B, Liu JJ, Baumann B, et al. Optical coherence tomography angiography of optic nerve head and parafovea in multiple sclerosis. Br J Ophthalmol. 2014;98(10):1368–73.

Chapter 6
OCT and Parkinson's Disease

Shahnaz Miri, Sofya Glazman, and Ivan Bodis-Wollner

Abstract Research in Parkinson's disease (PD) using Optical coherence tomography (OCT) is rapidly expanding. These studies aim to better understand the pathobiology of PD and define an accessible biomarker for early diagnosis, monitoring disease severity and progression. Peripapillary retinal nerve fiber layer (pRNFL) and macular scans in many, but not in all studies, demonstrated significant retinal thinning in PD patients and its correlation with disease severity. There is a critical need to define the best region of interest in OCT scans for PD patients. In this chapter, we describe the detailed method of OCT application and evaluation of the retinal thickness in PD. Establishing a unified method of retinal thickness analysis by OCT would be a major advance for further research studies and clinical application of OCT.

Keywords Parkinson's disease • Optical coherence tomography • OCT • The retina • Foveal thinning • Disease severity • Retinal biomarker • Inner retinal layer • Peripapillary nerve fiber layer • Dopaminergic amacrine cells • Ganglion cell complex

6.1 Introduction: Retinopathy in Parkinson's Disease

Parkinson's disease (PD) is the second most common movement disorder after essential tremor, characterized by neurodegeneration of the dopaminergic cells in the basal ganglia. Although PD presents with motor symptoms including resting tremor, bradykinesia, rigidity and postural instability, non-motor symptoms are also

S. Miri, MD
Department of Medicine, Medstar Union Memorial Hospital,
201 E. University Parkway, Baltimore, MD 21218, USA
e-mail: shahnaz.miri@medstar.net

S. Glazman, MD • I. Bodis-Wollner, MD, DSc (✉)
Department of Neurology, SUNY Downstate Medical Center,
450 Clarkson Avenue, MSC 1213, Brooklyn, NY 11203, USA
e-mail: sofya.glazman@downstate.edu; ivan.bodis-wollner@downstate.edu

A. Grzybowski, P. Barboni (eds.), *OCT in Central Nervous System Diseases: The Eye as a Window to the Brain*, DOI 10.1007/978-3-319-24085-5_6

prevalent, including mood disorders, sleep disturbances, orthostatic hypotension, loss of smell, cognitive decline and visual impairment.

Retinal involvement and ganglion cell receptive field re-organization in Parkinson disease were described decades ago [1, 2]. Since then many studies put forward functional evidence that foveal vision is impaired in PD. Foveal visual deficits are manifested by decreased contrast sensitivity [3–6] and color vision abnormalities [4, 6–8]. Flash and pattern electroretinography demonstrated a decline in retinal bioelectrical activity [9–14]. The results of psychophysical and electrophysiological functional studies of pharmacological interventions in the dopaminergic system imply that impaired retinal processing in PD is caused by dopaminergic deficiency [10, 15–18]. In recent years, optical coherence tomography (OCT) provided direct in-vivo visualization of retinal structure and retinopathy in PD [19, 20]. Peripapillary nerve fiber layer [19] and the inner retina [21] are thinned and the shape of the foveal pit is altered in PD [22]. Recent histopathological studies confirmed the involvement of the retina in PD by describing the presence of alpha-synuclein deposition in the inner retina [23, 24].

The retina is a multilayered structure, with three layers of nerve cell bodies and two layers of synapses (Fig. 6.1a). The outer nuclear layer (ONL) contains cell bodies of cones and rods photoreceptors; the inner nuclear layer (INL) includes cell bodies of bipolar, horizontal, and dopaminergic amacrine cells (Fig. 6.1b); and the ganglion cell layer (GCL) contains ganglion cells and displaced amacrine cells [25]. The fovea is a highly specialized area of the retina, located at temporal side of the optic disc. This area contains the highest concentration of the cone photoreceptors, responsible for best visual acuity. As cone density diminishes with distance from the center of the fovea, other retinal neurons successively emerge at the slope and at the edge of the foveal pit. The interaction between receptors and their organization into a receptive field structure is responsible for high contrast sensitivity [26]. The foveal region is the thickest part of the retina, mainly due to increased density of photore-

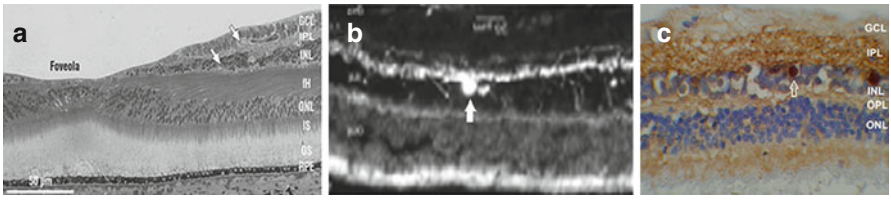

Fig. 6.1 (**a**) Histology of the foveal pit and retinal layers (After Provis and Hendrickson [27]). The interrupted line represents the end of the foveal avascular zone. (**b**) Thyrosine-Hydroxylase staining of the retina demonstrating immunoreactivity in the inner plexiform layer. The *arrow* shows a dopaminergic amacrine cell on the border of the innerplexiform and inner nuclear layers (After Witkovsky [28]). (**c**) Postmortem slide of the PD retina with Alpha-Synuclein immunoreactivity (dark brown staining) in the inner retina: GCL, IPL and the margin of INL reveal immunorectivity with AS staining. The *arrow* shows a neuron with dense glubular AS aggregation. *GCL* ganglion cell layer, *IPL* inner plexiform layer, *INL* inner plexiform layer, *fH* fiber layer of Henle, *OPL* outer plexiform layer, *ONL* outer nuclear layer, *IS* inner segment of the photoreceptors, *OS* outer segment of the photoreceptors, *RPE* retinal pigment epithelium

ceptors (cones) and ganglion cells compared to the peripheral retina. There are abundant synaptic interactions in the central retina leading to a thick inner plexiform layer (IPL) [25]. The Retinal Nerve Fiber Layer (RNFL) functions as the retinal output emanating from retinal ganglion cells. The nerve fibers are the axons of retinal ganglion cells and form the optic nerve behind the globe toward the lateral geniculate body and then onto the visual cortex. Further visual processing takes place in visual cortical areas [26].

The cellular pathology in PD, as shown by intracellular alpha-synuclein aggregates are in postmortem PD retina [23] at the border of INL in a typical position of dopaminergic amacrine cells, and in the IPL and GCL (Fig. 6.1c).

OCT quantifies in-vivo microscopic retinal structure for differentiating PD and to predict disease severity. In this chapter, we discuss the application of OCT in PD for diagnosis, disease monitoring and possible therapeutic efficacy evaluations.

6.2 Optical Coherence Tomography Equipment and Data Acquisition

OCT was developed in 1991, and first applied to in vivo retinal imaging in 1993 [29, 30]. OCT is a rapid, non-invasive method which provides high resolution cross-sectional and three-dimensional images of the retina. OCT has been applied to evaluate neurodegenerative disease of the retina, such as glaucoma and in CNS neurodegenerative diseases including multiple sclerosis (MS), Alzheimer's disease (AD), and Parkinson disease (PD) which have all shown to affect differently the retina [20, 31–33].

Original OCT technology used time domain OCT (TD-OCT) in which retinal thickness data were obtained through successive "slices" through the retina. TD-OCT takes time. Third-generation TD-OCT, Stratus OCT (Carl Zeiss Meditec AG, Jena, Germany), has been widely used with scanning rate of 400 axial scans per second and 10 μm axial resolution [34]. The more recent introduction of Fourier domain or spectral domain OCT (SD-OCT) provides retinal imaging with faster scan rate and higher resolution, compared to older generation TD-OCT. SD-OCT uses spectral interference and Fourier transform to extract the frequency spectrum of a signal. Fourier domain OCT can measure all light echoes with different delay time simultaneously which increase speed and sensitivity of detection [35]. SD-OCT provides at least 18,000 axial measurements per seconds with 5 μm axial resolution [36]. SD-OCT systems have a higher sensitivity, even in low light levels, with high speed detection [37].

Here we concentrate on different commercially available SD-OCT with wide distribution in the Western hemisphere and in major Asian countries. They have somewhat different data analysis algorithms and different sampling rate. These are presented in detail in Table 6.1. The macular area sampled is sampled at somewhat different for each device [38, 39].

The recently developed high-penetration OCT (HP-OCT) with a long wavelength (1050 nm, versus 840 nm in SD-OCT) provides deeper visualization of

Table 6.1 Comparison of commercial OCT devices

Device	Manufacturer	Axial image resolution (μm)	Scanning speed
Cirrus OCT	Carl Zeiss Meditec	5	27,000 axial scans/s
RTVue-100	Optovue	5	26,000 axial scans/s
3D OCT-1000	Topcon	6	18,000 axial scans/s
Spectralis HRA+OCT	Heidelberg Engineering	3.8	40,000 axial scans/s
Spectral OCT/SLO	Ophthalmic technologies	8	27,000 axial scans/s

HRA Heidelberg retinal angiography, *SLO* scanning laser ophthalmoscope

microstructures beneath the retinal pigmented epithelium. HP-OCT (Topcon, Tokyo, Japan) has a scanning rate of 100,000 per second [40]. To our knowledge HP-OCT has not been applied in neurological diseases.

Different sampling rate and retinal segmentation algorithms lead to difference between macular thickness values obtained by different OCT equipment [41]. Matlach et al. [42], have demonstrated a high degree of repeatability for both Cirrus and RTvue-100 in measurements of peripapillary RNFL and inner retinal layer (IRL) thickness among idiopathic and atypical PD. Despite a high correlation between measurements of the two OCT devices and a high consistency in the measurements of the two devices, RTVue reported thicker macular RNFL-GCL-IPL and pRNFL thickness [42].

6.3 OCT Data Analysis

To visualize the three-dimensional retinal structure, cross-sectional OCT images in the 3D data set can be rendered volumetrically by the OCT software. The number of horizontal and vertical pixels obtained by OCT is different according to company's scan protocols. The produced image is obtained over an area of 5×5 or 6×6 mm with 1 mm depth [35].

OCT image analysis is based on outlining the retinal layers and measuring the distances between the layers. Image analysis starts with correct detection of the Internal Limiting Membrane (ILM) [43]. Commercially available OCT devices use different layer segmentation algorithm based on quantification of the optical properties of the retinal layers [44]. "Segmentation" refers to the establishment of the demarcation of different histological layers. Device dependent algorithm difference affect retinal thickness measures [45]. Accordingly, different sensitivities are reported for different OCT devices when the results are compared in the same subjects. One of the critical variables is the estimation of the borders of different layers. However, the histological borders between layers is not a straight line. Hence thickness measurements idealized to a straight line approximation of the edges of different layers can suffer various inaccuracies.

As mentioned, three-dimensional rendering of OCT images is acquired based on consecutive 2D OCT slices. Reconstructing methods are recently developed to quantify raw voxel data from 2-D OCT slices and visualize them as 3D retinal images. These 3D rendering methods provide a more reliable segmentation and evaluation of volumetric images [22, 46].

Raw volumetric data obtained from OCT can be imported into MATLAB software environment in order to analyze and reconstruct the data. This method, by not relying on straight line approximation in the segmentation method, minimizes analysis errors. Based on finely sampled volumetric data of perifoveolar raw thickness data, a mathematical equation for the foveal pit was developed [47]. This method does describes the shape of the fovea by "segmenting" at every 0.25 mm (RT-Vue) or 0.3 mm (Cirrus).

6.4 Methods of OCT Data Evaluation

Commercially available OCT devices have different scan protocols to evaluate areas in the retina (Fig. 6.2a, b). The optic nerve head (ONH) protocol is used to obtain peripapillary Retinal Nerve Fiber Layer (pRNFL) measurements. This protocol generates an RNFL thickness map measured along a circle of 3.45 mm in diameter centered on the ONH. The overall average thickness is separated into the superior hemisphere, inferior hemisphere, and temporal, superior, nasal, and inferior quadrants.

Macular scans provide images of the macula with 5–6 mm in diameter, centered at the foveola. Different companies have their own software and protocol with a normative database for statistical comparison of data [48]. This scan protocol was developed to automatically measure macular thickness averages for each of the 9 map sectors as defined by the Early Treatment Diabetic Retinopathy Study (ETDRS). The inner and outer rings were segmented into 4 quadrants, with radii of 1.5 mm and 3 mm, respectively [49].

The retinal regions of interest for neurodegenerative disease are not clearly defined and no specific scan protocol is developed for them. In PD, there are findings of thickness changes in both pRNFL scans and macular area [20]. Decreased pRNFL thickness, macula volume, and foveal thickness are well established by Schneider et al. [50] in 1-methyl-4-phenyl-1,2,3,6-tetrahydropyridine (MPTP)-treated cynomolgus monkeys. Here, we review in detail the OCT studies in human PD studies based on the type of scan and region of interest separately.

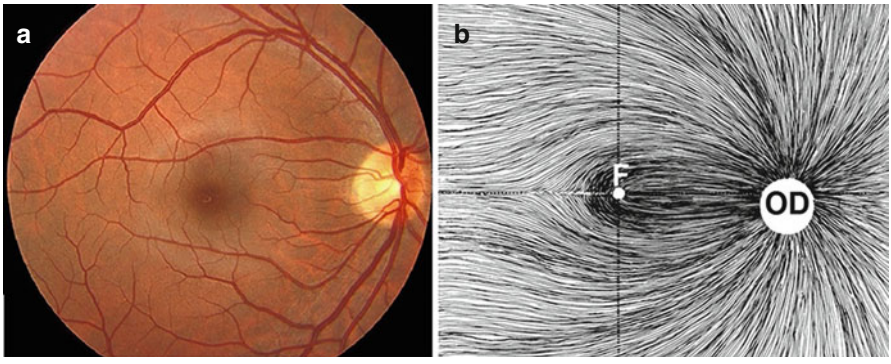

Fig. 6.2 (**a**) Fundoscopic image of the retina which shows the peripapillary and the macular region, capillaries, the optic disc. (**b**) Schematic image of the optic disc and the fovea which illustrates retinal nerve fiber layer (After Bodis-Wollner et al. [20]). *OD* optic disc, *F* fovea

6.5 Macular Volume in PD

The rationale for sampling the macular area in PD is based on the localization of dopaminergic neurons and the nature of visual deficits in PD. There is dopaminergic deficiency in the PD retina [10, 15–18, 51]. Dopaminergic neurons in the retina are located at the border of inner nuclear layer and IPL and dopaminergic fibers are present in IPL [28]. Spatial geometry of the dopaminergic amacrine neurons is described in the foveal avascular zone (FAZ) (Fig. 6.3a–c) [52]. The FAZ is the central area of the fovea without any inner retinal vascular supply. The neural retina within the FAZ receives its nutritional supplementation through diffusion from choroidal vascular supply [53].

In most OCT programs, macular volume is measured as a total volume in a 6.00 mm macular map. The algorithm developed by Hu et al. [44], quantifies total macular thickness in a macular cube scan pattern of 496 × 1024 × 37 voxels. They reported the thickness of the IPL as 31 μm while full retinal thickness was reported as 279 μm from NFL to RPE. Thus the IPL an average, contributes less than 12 % to average thickness of the macular area (Fig. 6.4a, b). However, at the very center

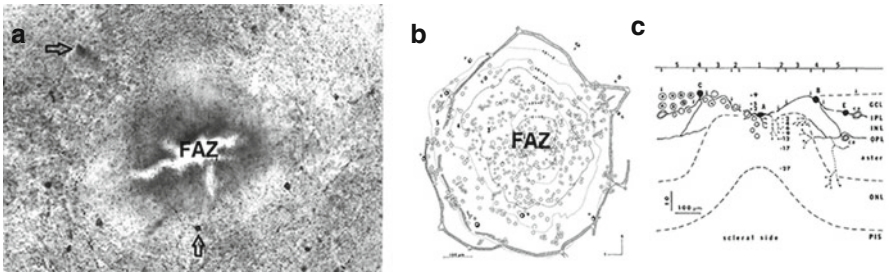

Fig. 6.3 (**a**) Tyrosine-Hydroxylase staining of dopaminergic neurons (*arrows*) in the human foveal avascular zone. Immunoreactivity is observed within the FAZ area, limited to the margin of the FAZ; (After Savy et al. [52]). (**b**) Schematic view of spatial geometry of dopaminergic (DA) neurons in the FAZ within capillary borders. (**c**) The vertical profile view of the retina, showing the distribution of the DA neurons in the FAZ (After Savy et al. [52])

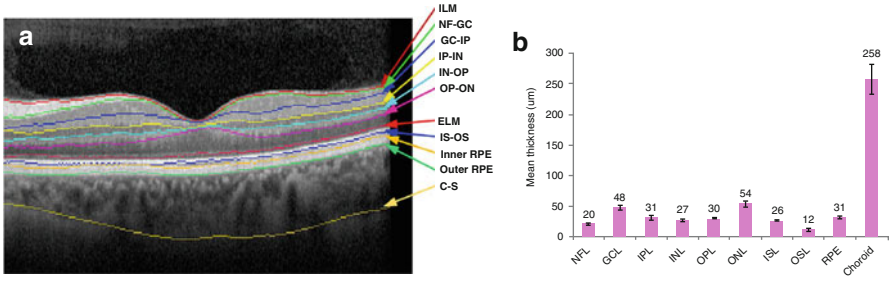

Fig. 6.4 (**a**) Layer segmentation of the retinal SD-OCT volume scans by the automated graph search algorithm to sequentially segment 11 retinal surfaces. (**b**) Average thickness of each individual retinal layer in total macular volume in healthy eyes (After Hu et al. [44])

of the foveal pit, there is no contribution to the macular volume (or thickness) by the INL, IPL and GCL.

A thinned and remodeled foveal pit in PD (Fig. 6.5) is consistent with this unequal contribution of the inner retina (Fig. 6.6) [22]. The difference between PD and healthy controls (HC) becomes evident in an annular zone between 0.5 and 2 mm from the foveola. Retinal thickness in the radial zone of 0.75–1.5 mm yields the optimal area for discriminating a PD retina from HC subjects [54].

Several studies compared total macular volume in PD and HC. Given only 11.1 % contribution of IPL to the total macular volume, finding a significant difference in total macular volume in PD compared to healthy controls may be an unrewarding task. Altintaş et al. [55] reported a significant total macular volume reduction in 17 PD compared to 11 HC (6.82 ± 0.32 mm^3 vs. 7.09 ± 0.23 mm^3).

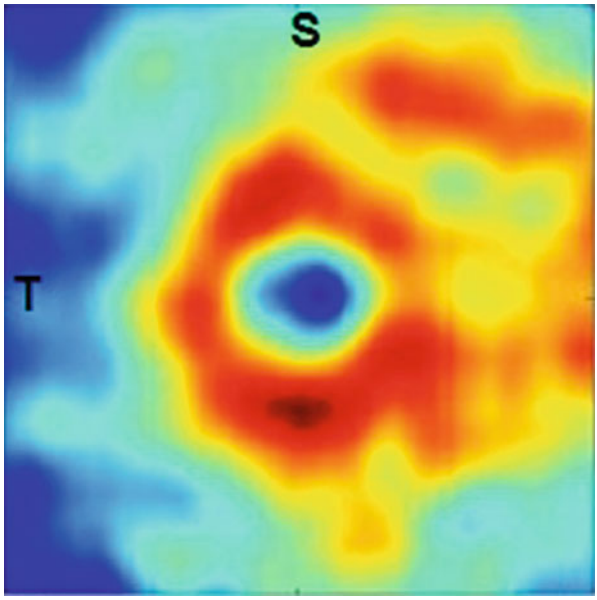

Fig. 6.5 Perifoveolar thickness attenuation in PD patients. This figure demonstrates mean foveal thickness difference between healthy controls and subjects. The reddish ring which is around 1–1.5 mm radial distance from the foveola, illustrates the zone of the largest difference of retinal thickness of PD and HC. Note: the course and distribution of the density of the NFL superior and inferior of the macula. This density contains the axons of the foveal ganglion cells. *S* superior, *T* temporal (After Spund et al. [22])

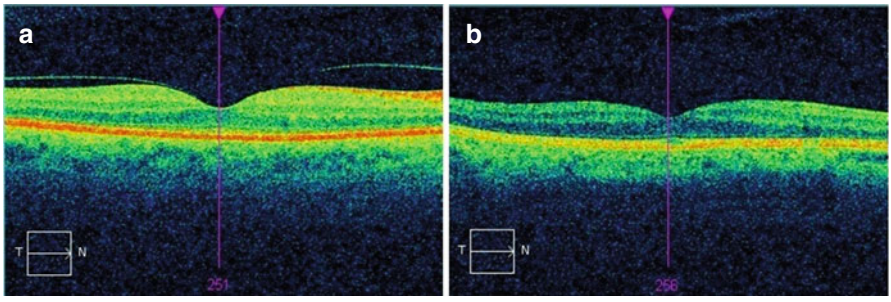

Fig. 6.6 OCT macular scan in a healthy control (**a**) and a PD patient (**b**). Notice the foveal thinning in the PD patient. Notice the thinning of the inner retina at the fovea and the flattening of the foveal pit in PD patient

However, in the study by Archibald et al. [56] no difference was observed in total macular volume between PD and HC (6.47 ± 0.4 vs. 6.54 ± 0.4 mm^3 in right eyes; and 6.61 ± 0.5 vs. 6.47 ± 0.4 mm^3 in the left eyes). Cubo et al. [14] also did not find any difference in total macular volume in PD vs. HC (6.8 ± 0.3 vs. 7.0 ± 0.3 mm^3).

6.6 Macular Thickness in PD

Altinaş et al. [55] reported the first macular study in PD patients which implied a decreased superior segment thickness of the IRL and temporal, nasal, and inferior segment of the outer retinal layer (ORL). Hajee et al. [21] reported a thinned inner foveal retina in PD. A number of studies [22, 57–63] reported thinning in macular scan of PD patients, mainly in temporal, inferior and superior quadrants.

Automated segmentation software recently has been developed to evaluate the specific layers involvement in PD compared to HC and other Parkinsonian syndromes [64]. However, the results of these studies [62, 64–66] are difficult to compare due to application of different algorithms and using different devices.

Out of 16 macular studies in PD (Table 6.2), 13 studies have listed thinning of the retina [21, 22, 54, 55, 57–63, 65, 66]. Aaker et al. [46], Archibald et al. [56] and Cubo et al. [14] did not find thinning. Furthermore, Roth et al. [65] who used a new segmentation algorithm, reported a thinning in ONL/PRL (photoreceptor layer) but not in other layers. Previous studies also using segmentation methods reported thinning of RNFL, GCL, IPL, outer plexiform layer (OPL) [66] and INL [58, 62].

Thinning of the entire parafovea (or inner macular ring) which contains an annular area with about 1.5 mm radius has been reported by five studies [22, 54, 59, 60, 63]. However, other studies have shown thinning only in specific quadrants, mainly in superior, temporal and inferior segments of the macula [21, 55, 58, 62].

Lee et al. [62] segmented macular data obtained from PD and HC, using the caliper tool within the Spectral OCT/SLO at the fovea center, temporally 1, 2, and 3 mm and nasally 1 mm from the fovea center. They compared the 6 retinal layer including RNFL, IPL+ GCL, INL, OPL, ONL+PIS (photoreceptor inner segments), and the photoreceptor outer segments and retinal pigment epithelium (POS+RPE). Using this method, they observed thinning in the outer superior zone of the macula and INL layer at temporally 1 mm from the fovea center in PD patients [62].

Roth et al. [65] have applied an automated segmentation software for macular scan analysis in three dimensions. This method yields the thicknesses of the following macular layers: ganglion cell layer/inner plexiform layer (GCIP), inner nuclear layer/outer plexiform layer (INL/OPL), and outer nuclear layer including inner and outer photoreceptor segments (ONL/PRL). They reported significant ONL/PRL thinning in PD versus HC. However, no difference in total macular volume, or the other retinal layer thicknesses was observed between PD and HC. Impaired function of blue cones that receive their input from dopaminergic cells was previously described in PD [65]. This impaired synaptic input from DA neurons to photoreceptors may hypothetically lead to transsynaptic degeneration of ONL neurons in the PD retina and results in ONL thinning [65].

Satue et al. [63] reported a significant decrease in RNFL and macular thickness in 153 PD compared to 242 healthy controls (Cirrus, Zeiss; Spectralis, Heidelberg).

Schneider et al. [64] performed a semiautomatic, retinal single-layer analysis with calculation of the average thickness of retinal layers to compare foveal scans of 65 PD, 16 progressive supranuclear palsy (PSP), and 12 multiple system atrophy (MSA) patients as well as 41 matched controls. There was no difference in thickness

Table 6.2 Investigations of macular thickness in PD compared to healthy controls

Reference	Sample size (eyes)	Equipment	Main results of the comparison in PD
Altinaş et al. (2008) [55]	17 (34) PD, 11 (22) HC	3000 unit Zeiss	↓sup IRL; ↓temp, nasal, inf ORL; No difference in fovea
Hajee et al. (2009) [21]	24 (45) PD, 17 (31) HC	Optovue	↓IRL in sup and inf quads; No change in ORL
Aaker et al. (2010) [46]	9 (18) PD, 9 (16) HC	Spectralis	No difference in IRL thickness; Compared to published normal values, ↓ORL sup; ↑ORL nasal; ↑IRL inf quad
Cubo et al. (2010) [57]	9 (18) PD, 9 (18) HC	OCT3 Zeiss	↓fovea; thinner fovea in the contralateral to the more affected side
Archibald et al. (2011) [56]	34 (63) PD, 19 (33) HC	Stratus	No difference in foveal thickness and macular volume
Albrecht et al. (2012) [58]	40 (80) PD, 35 (70) HC	Spectralis	↓INL especially in temp quad; No difference in other layers
Shrier et al. (2012) [54]	23 (26) PD, 18 (36) HC	Optovue	↓macular volume at 0.5–0.75 mm from the foveola; IOA in IRL
Adam et al. (2013) [59]	14 (28) PD, 14 (28) HC	Optovue	↓IRL at radial distances (1–1.75 mm) form the foveola, especially sup quadrant
Spund et al. (2013) [22]	30 (50) PD, 27 (50) HC	Optovue	↓IRL at 1–2 mm distance from the foveola
Garcia-Martin et al. (2014) [60]	46 (46) PD, 33 (33) HC	Cirrus/ Spectralis	↓fovea, IRL all quad; ↓inf ORL (Cirrus); ↓sup, nasal ORL (Spectralis)
Satue et al. (2013) [61]	100 PD, 100 HC	Cirrus/ Spectralis	↓mean macular, fovea, ORL inf quad
Lee et al. (2014) [62]	56 PD, 30 HC	OPKO/OTI Spectral	↓temparafoveal INL, no difference in other layers; ↓supouter segment of the total macular thickness
Roth et al. (2014) [65]	68 PD (114), 32 (63) HC	Cirrus	↓ONL/PRL No difference in GCL+IPL, GCL+IPL+mRNLF, INL/OPL; No difference in macular volume
Garcia-Martin et al. (2014) [66]	129 (PD), 129 (HC)	Spectralis	↓in RNFL, GCL, IPL, OPL; ↑in INL

(continued)

Table 6.2 (continued)

Reference	Sample size (eyes)	Equipment	Main results of the comparison in PD
Satue et al. (2014) [63]	153 PD and 242 HC	Cirrus	↓fovea, ↓full thickness nasal and inf quads of outer macular ring
		Spectralis	↓in full macular thickness in all quads, no foveal thickness difference
Cubo et al. (2014) [14]	30 PD, 30 HC		No difference in full-thickness macular measures

Equipments: Carl Zeiss company: Cirrus, Stratus; Heidelberg company: Spectralis; Optovue, RTvue
IRL inner retinal layer, *ORL* outer retinal layer thickness, *sup* superior quadrant, *inf* inferior quadrant, *temp* temporal quadrant, *INL* inner nuclear layer, ↓ significant decrease in thickness, *IOA* interocular asymmetry

of any retinal layer between PD and HC. Thickening of the outer nuclear layer in PSP and the outer plexiform layer in MSA was highly specific for these disease entities and allowed differentiating PSP from MSA with high sensitivity and specificity.

Ding et al. [47] developed a mathematical equation of the foveal pit, based on finely sampled volumetric data of perifoveolar thickness to describe the foveal pit in PD and healthy eyes. Using this model, based on the RT-Vue 100 of the parameters foveal model had an over 70 % discriminating power of PD.

6.7 Peripapillary Retinal Nerve Fiber Layer Scan in PD

Another region of interest in the PD retina is peripapillary retinal nerve fiber layer (pRNFL) (Table 6.3). The first OCT study in PD by Inzelberg et al. [19] reported thinned average RNFL, specifically in inferior and temporal quadrants. Most of further studies have shown findings consistent with Inzelberg et al. [19]. However, Aaker et al. [46], Archibald et al. [56], Tsironi et al. [67], Albrecht et al. [58], and Roth et al. [65] did not find difference between PD and HC.

In a meta-analysis by Yu et al. [68] for 13 case-control studies of pRNFL measurements in PD, a significant pRNFL thinning was reported in all quadrants in PD patients compared to controls.

6.8 OCT and Disease Severity in PD

Retinal thinning was reported to relate to disease severity and functional disabilities in PD patients. Altintaş et al. [55] first reported an inverse correlation between foveal thickness and the unified Parkinson's Disease rating scale (UPDRS) total and motor scores. A non-significant inverse correlation between total macular volume and P100 latency measured by pattern visual evoked potential was reported in PD [55].

Table 6.3 Investigations of retinal nerve fiber layer in PD compared to healthy controls

Reference	Sample size (eyes)	Equipment	Results of comparison in PD
Inzelberg et al. (2004) [19]	10 (10) PD, 10 (10) HC	Not mentioned (NM)	↓mean RNFL thickness, ↓inf, temp quad
Altinaş et al. (2008) [55]	17 (34) PD, 11 (22) HC	Stratus	↓mean RNFL thickness, ↓sup, nasal quad
Moschos et al. (2011) [69]	16 (32) PD, 20 (40) HC	Stratus	No mean RNFL thickness difference, ↓inf, temp quad
Aaker et al. (2010) [46]	9 (18) PD, 16 (19) HC	Spectralis	No RNFL thickness difference
Archibald et al. (2011) [56]	51 (66) PD, 25 (35) HC	Stratus	No RNFL thickness difference
Tsironi et al. (2012) [67]	24 (24) PD, 24(24) HC	Stratus	No RNFL thickness difference
Albrecht et al. (2012) [58]	40 (80) PD, 35 (70) HC	Spectralis	No RNFL thickness difference
Garcia-Martin et al. (2012) [70]	75 (75) PD, 75 (75) HC	Cirrus/Spectralis	↓RNFL thickness all quads, Spectralis more sensitive device than Cirrus
Rohani et al. (2013) [71]	27 (54) PD, 27 (50) HC	TOPCON, 3D-OCT Mark II	↓RNFL thickness all quads, ↓inf, nasal quad more in akinetic rigid
Kirbas et al. (2013) [72]	42 (84) PD, 40 (80) HC	Cirrus	↓mean RNFL thickness, ↓temp quad
Garcia-Martin et al. (2014) [60]	46 (46) PD, 33 (33) HC	Cirrus/Spectralis	↓mean RNFL thickness, ↓sup, temp, inf quad
La Morgia et al. (2013) [73]	43 (86) PD, 86 (86) HC	Stratus	No mean RNFL thickness difference, ↓temp quad, contralateral to d-side
Satue et al. (2013) [61]	100 PD, 100 HC	Cirrus/Spectralis	↓mean RNFL thickness, ↓inf-temp, sup-temp quad
Moreno-Ramos et al. (2013) [74]	10 PD, 10 HC	NM	PD with dementia had ↓RNFL thickness compared to HC
Sen et al. (2014) [75]	18 PD, 11 HC	RTvue	↓mean RNFL thickness, and ↓inf, sup-temp, inf-temp segments
Roth et al. (2014) [65]	68 PD (111), 32 (62) HC	Cirrus	No difference in RNFL thickness
Jimenez et al. (2014) [76]	52 (102) PD, 50 (97) HC	Stratus	↓average RNFL thickness and ↓RNFL thickness in all quads
Garcia-Martin et al. (2014) [66]	129 (PD), 129 (HC)	Spectralis	↓mean RNFL thickness, and ↓RNFL in nasal-inferior, temp-inf, tem-sup
Satue et al. (2014) [63]	153 PD, 242 HC	Cirrus	↓average RNFL thickness, and ↓RNFL thickness in sup, inf, and temp quads
		Spectralis	↓average RNFL thickness, and ↓RNFL thickness in sup, inf, sup-nasal, inf-nasal, inf-temp, sup-temp

Equipments: Carl Zeiss company: Cirrus, Stratus; Heidelberg company: Spectralis; Optovue, RTvue

HC healthy controls, *quad* quadrant, *sup* superior, *inf* inferior, *temp* temporal, ↓ significant decrease in thickness, *d-side* tremor dominant side of the body, *NM* not mentioned in the abstract

Lee et al. [62] compared retinal layers' thickness among three subgroup of PD and observed the thinnest macular RNFL thickness in the subgroup with hallucinations without dementia. There were no significant correlations between retinal thicknesses and duration or severity of PD and medication dosages.

Satue et al. [63] reported a significant decrease in RNFL and macular thickness in PD. Hoehn and Yahr (H&Y) scores were significantly and inversely correlated with all macular thickness parameters [63].

Garcia-Martin et al. [60] reported that visual functional parameters, as well as structural retinal parameters were affected in PD patients. Both pRNFL and macular thickness were negatively correlated with the H&Y scores, and positively correlated with the Schwab and England Activities of Daily Living Scale (SE-ADL). Foveal thickness predicted PD severity and quality of life, and amplitude of the Pattern ERG N95 component predicted a lower SE-ADL score [60].

In another study by Garcia-Martin et al. [66], macular RNFL, GCL, and IPL were significantly thinner in PD patients with disease duration longer than 10 years compared to those with shorter disease duration. This study reported that thickness inversely correlated with longer disease duration.

Jimenez et al. [76] found that average pRNFL thickness, and inferior and nasal quadrants of pRNFL thinning were correlated with higher UPDRS score and its motor and activity of daily living (ADL) sub scores. They [76] further developed equations based on the pRNFL thickness and PD duration which predicted UPDRS motor and ADL sub scores, as shown in Table 6.4.

6.9 ERG and OCT

When OCT, VEP, and PERG data were compared, only the P50 and N95 amplitudes of the PERG were smaller in the PD group compared to controls [14]. Age, PD duration, levodopa dose, NMSQ, and SPES/SCOPA scores were not significantly correlated with OCT, VEP, and PERG, except for age with P50 latency ($r=-0.36$, $p=0.007$), and SPES/SCOPA with nasal temporal external ring thickness. The area under the curve of OCT, VEP, and PERG receiver operative characteristic curves were less than 0.50, and did not discriminate between PD subjects and controls [14].

Table 6.4 Equations for predicting UPDRS and ADL scores, based on retinal thickness and PD duration

UPDRS motor score	24 + 8.2 * log PD duration20.3 * RNFL thickness
UPDRS ADL score	32.3 + 4.7 * log PD duration 20.3 * RNFL thickness
Total UPDRS score	81.6 + 29.6 * log PD duration20.6 * RFNL thickness

After Jimenez et al. [76]

However, by stratifying patients by disease stage showed a significantly decreased thickness of the temporal retina and a decreased PERG P50 latency, PERG P50 amplitude and PERG N95 amplitude in H&Y stage 2 patients compared to stage 1.

6.10 PD Treatment Effect on the Retina

Yavas et al. [77] studied the effects of levodopa and dopamine agonists on retinal nerve fiber layer using scanning laser ophthalmoscope. Forty-four patients with PD (receiving levodopa or dopamine agonist monotherapy) and 21 normal subjects were included in the study. The optic nerve head imaging was performed using Heidelberg Retina Tomograph. RNFL was significantly decreased in PD patients compared with control group. They also found that rim volume of optic nerve head and RNFL were significantly greater in the group treated with levodopa while it was the thinnest in the group receiving dopamine agonists. Therefore, they suggested that levodopa compared to dopamine agonists had a protective effect on the RNFL in PD.

Sen et al. [75] described the effects of levodopa on the PD retina using OCT. In their cross-sectional study, they included 35 patients with PD (17 with levodopa monotherapy, 18 untreated) and 11 healthy control. According to the findings, the average RNFL thickness of PD patients was significantly lower than controls'. In addition, retinal thickness of PD patients who underwent dopaminergic treatment was compared with the untreated group. According to this study, although the disease in patients with treated PD was more severe than in the untreated group, no significant difference in the thickness of retina was found between the two groups. Therefore, the authors also proposed a protective effect of L-dopa on the retina in patients with PD.

Shrier et al. [78] suggested the possible effect of Deep Brain Stimulation (DBS) on the retina in Parkinson disease. They reported in a PD patient, a 31 μm thickness increase in the inferior quadrant of the retina, 1 year after DBS. The patient had no change in medication before and after DBS, suggesting that the increase in retinal thickness was not attributable to pharmacotherapy. Specifying the mechanism of the possible effect of DBS on the retina warrants further studies.

6.11 Conclusion

Most but not all studies of both macular and pRNFL scans demonstrate thinning in PD. Some studies report correlation between disease severity and retinal thinning. It is crucial to consider the region of interest of the retina scanned and the algorithm used to quantify thinning. OCT is a promising device to be applied in clinical setting as a biomarker for PD diagnosis, disease monitoring, and evaluating treatment response.

References

1. Bodis-Wollner I, Yahr MD. Measurements of visual evoked potentials in Parkinson's disease. Brain. 1978;101:661–71.
2. Bodis-Wollner I, Marx MS, Mitra S, Bobak P, Mylin L, Yahr M. Visual dysfunction in Parkinson's disease loss in spatiotemporal contrast sensitivity. Brain. 1987;110:1675–98.
3. Bulens C, Meerwaldt JD, Van der Wildt GJ, Keemink CJ. Contrast sensitivity in Parkinson's disease. Neurology. 1986;36:1121–5.
4. Price MJ, Feldman RG, Adelberg D, Kayne H. Abnormalities in color vision and contrast sensitivity in Parkinson's disease. Neurology. 1992;42:887–90.
5. Rodnitzky RL. Visual dysfunction in Parkinson's disease. Clin Neurosci. 1998;5:102–6.
6. Pieri V, Diederich NJ, Raman R, Goetz CG. Decreased color discrimination and contrast sensitivity in Parkinson's disease. J Neurol Sci. 2000;172:7–11.
7. Haug BA, Kolle RU, Trenkwalder C, Oertel WH, Paulus W. Predominant affection of the blue cone pathway in Parkinson's disease. Brain. 1995;118:771–8.
8. Büttner T, Kuhn W, Müller T, Patzold T, Heidbrink K, Przuntek H. Distorted color discrimination in 'de novo' parkinsonian patients. Neurology. 1995;45:386–7.
9. Gottlob I, Schneider E, Heider W, Skrandies W. Alteration of visual evoked potentials and electroretinograms in Parkinson's disease. Electroencephalogr Clin Neurophysiol. 1987;66:349–57.
10. Ikeda H, Head GM, Ellis CJ. Electrophysiological signs of retinal dopamine deficiency in recently diagnosed Parkinson's disease and a follow up study. Vision Res. 1994;34:2629–38.
11. Tagliati M, Bodis-Wollner I, Yahr MD. The pattern electroretinogram in Parkinson's disease reveals lack of retinal spatial tuning. Electroencephalogr Clin Neurophysiol. 1996; 100:1–11.
12. Sartucci F, Orlandi G, Lucetti C, Bonuccelli U, Murri L, Orsini C, Porciatti V. Changes in pattern electroretinograms to equiluminant red-green and blue-yellow gratings in patients with early Parkinson's disease. J Clin Neurophysiol. 2003;20:375–81.
13. Nowacka B, Lubiński W, Karczewicz D. Ophthalmological and electrophysiological features of Parkinson's disease. Klin Oczna. 2010;112:247–52.
14. Cubo E, López Peña MJ, Diez-Feijo Varela E, Pérez Gil O, Garcia Gutierrez P, Araus González E, et al. Lack of association of morphologic and functional retinal changes with motor and non-motor symptoms severity in Parkinson's disease. J Neural Transm. 2014;121:139–45.
15. Nguyen-Legros J. Functional neuroarchitecture of the retina: hypothesis on the dysfunction of retinal dopaminergic circuitry in Parkinson's disease. Surg Radiol Anat. 1988;10:137–44.
16. Bodis-Wollner I. Visual deficits related to dopamine deficiency in experimental animals and Parkinson's disease patients. Trends Neurosci. 1990;13:296–302.
17. Harnois C, Di Paolo T. Decreased dopamine in the retinas of patients with Parkinson's disease. Invest Ophthalmol Vis Sci. 1990;31:2473–5.
18. Büttner T, Kuhn W, Patzold T, Przuntek H. L-Dopa improves colour vision in Parkinson's disease. J Neural Transm Park Dis Dement Sect. 1994;7:13–9.
19. Inzelberg R, Ramirez JA, Nisipeanu P, Ophir A. Retinal nerve fiber layer thinning in Parkinson disease. Vision Res. 2004;44:2793–7.
20. Bodis-Wollner I, Miri S, Glazman S. Venturing into the no-man's land of the retina in Parkinson's disease. Mov Disord. 2014;29:15–22.
21. Hajee ME, March WF, Lazzaro DR, Wolintz AH, Shrier EM, Glazman S, Bodis-Wollner I. Inner retinal layer thinning in Parkinson disease. Arch Ophthalmol. 2009;127:737–41.
22. Spund B, Ding Y, Liu T, Selesnick I, Glazman S, Shrier EM, Bodis-Wollner I. Remodeling of the fovea in Parkinson disease. J Neural Transm. 2013;120:745–53.
23. Bodis-Wollner I, Kozlowski PB, Glazman S, Miri S. Alpha-synuclein in the inner retina in Parkinson's disease. Ann Neurol. 2014;75(6):964–6.
24. Beach TG, Carew J, Serrano G, Adler CH, Shill HA, Sue LI, et al. Phosphorylated α-synuclein-immunoreactive retinal neuronal elements in Parkinson's disease subjects. Neurosci Lett. 2014;571:34–8.

25. Kolb H. Simple anatomy of the retina. In: Kolb H, Nelson R, Fernandez E, Jones B, editors. Webvision. The organization of the retina and visual system. University of Utah; 2012. PMID: 21413391
26. Bodis-Wollner I. Foveal vision is impaired in Parkinson's disease. Parkinsonism Relat Disord. 2013;19:1–14.
27. Provis JM, Hendrickson AE. The foveal avascular region of developing human retina. Arch Ophthalmol. 2008;126:507–11.
28. Witkovsky P. Dopamine and retinal function. Doc Ophthalmol. 2004;108:17–39.
29. Huang D, Swanson EA, Lin CP, Schuman JS, Stinson WG, Chang W, et al. Optical coherence tomography. Science. 1991;254:1178–81.
30. Swanson EA, Izatt JA, Lin CP, Fujimoto JG, Schuman JS, Hee MR, et al. In vivo retinal imaging by optical coherence tomography. Opt Lett. 1993;18:1864–6.
31. Parisi V, Manni G, Spadaro M, Colacino G, Restuccia R, Marchi S, et al. Correlation between morphological and functional retinal impairment in multiple sclerosis patients. Invest Ophthalmol Vis Sci. 1999;40:2520–7.
32. Parisi V, Restuccia R, Fattapposta F, Mina C, Bucci MG, Pierelli F. Morphological and functional retinal impairment in Alzheimer's disease patients. Clin Neurophysiol. 2001;112:1860–7.
33. Frohman EM, Fujimoto JG, Frohman TC, Calabresi PA, Cutter G, Balcer LJ. Optical coherence tomography: a window into the mechanisms of multiple sclerosis. Nat Clin Pract Neurol. 2008;4:664–75.
34. Lange AP, Sadjadi R, Saeedi J, Lindley J, Costello F, Traboulsee AL. Time-domain and spectral-domain optical coherence tomography of retinal nerve fiber layer in MS patients and healthy controls. J Ophthalmol. 2012;2012:564627.
35. Wojtkowski M, Srinivasan V, Fujimoto JG, Ko T, Schuman JS, Kowalczyk A, Duker JS. Three-dimensional retinal imaging with high-speed ultrahigh-resolution optical coherence tomography. Ophthalmology. 2005;112:1734–46.
36. Leung CK, Cheung CY, Weinreb RN, Lee G, Lin D, Pang CP, Lam DS. Comparison of macular thickness measurements between time domain and spectral domain optical coherence tomography. Invest Ophthalmol Vis Sci. 2008;49:4893–7.
37. Leitgeb R, Hitzenberger C, Fercher A. Performance of fourier domain vs. time domain optical coherence tomography. Opt Express. 2003;11:889–94.
38. Sull AC, Vuong LN, Price LL, Srinivasan VJ, Gorczynska I, Fujimoto JG, et al. Comparison of spectral/Fourier domain optical coherence tomography instruments for assessment of normal macular thickness. Retina. 2010;30:235.
39. Reznicek L, Dabov S, Kayat B, Liegl R, Kampik A, Ulbig M, Kernt M. Scanning laser 'en face' retinal imaging of epiretinal membranes. Saudi J Ophthalmol. 2014;28:134–8.
40. Sayanagi K, Gomi F, Ikuno Y, Akiba M, Nishida K. Comparison of spectral-domain and high-penetration OCT for observing morphologic changes in age-related macular degeneration and polypoidal choroidal vasculopathy. Graefes Arch Clin Exp Ophthalmol. 2014;252:3–9.
41. Wolf-Schnurrbusch UE, Ceklic L, Brinkmann CK, Iliev ME, Frey M, Rothenbuehler SP, et al. Macular thickness measurements in healthy eyes using six different optical coherence tomography instruments. Invest Ophthalmol Vis Sci. 2009;50:3432–7.
42. Matlach J, Wagner M, Malzahn U, Göbel W. Repeatability of peripapillary retinal nerve fiber layer and inner retinal thickness among two spectral domain optical coherence tomography devices. Invest Ophthalmol Vis Sci. 2014;55:6536–46.
43. Wieclawek W, Pietka E. Retina analysis in optical coherence tomography images. Inf Technol Biomed. 2014;3:247–58.
44. Hu Z, Wu X, Hariri A, Sadda SR. Multiple layer segmentation and analysis in three-dimensional spectral-domain optical coherence tomography volume scans. J Biomed Opt. 2013;18:76006.
45. Terasaki H, Shirasawa M, Yamashita T, Yamashita T, Yamakiri K, Sonoda S, Sakamoto T. Comparison of foveal microstructure imaging with different spectral domain optical coherence tomography machines. Ophthalmology. 2012;119:2319–27.
46. Aaker GD, Myung JS, Ehrlich JR, Mohammed M, Henchcliffe C, Kiss S. Detection of retinal changes in Parkinson's disease with spectral-domain optical coherence tomography. Clin Ophthalmol 2010;4:1427–32.

47. Ding Y, Spund B, Glazman S, Shrier EM, Miri S, Selesnick I, Bodis-Wollner I. Application of an OCT data-based mathematical model of the foveal pit in Parkinson disease. J Neural Transm. 2014;121:1367–76.
48. Garas A, Vargha P, Hollo G. Diagnostic accuracy of nerve fibre layer, macular thickness and optic disc measurements made with the RTVue-100 optical coherence tomograph to detect glaucoma. Eye (Lond). 2010;25:57–65.
49. Chan A, Duker JS, Ko TH, Fujimoto JG, Schuman JS. Normal macular thickness measurements in healthy eyes using Stratus optical coherence tomography. Arch Ophthalmol. 2006;124:193–8.
50. Schneider JS, Ault ME, Anderson DW. Retinal pathology detected by optical coherence tomography in an animal model of Parkinson's disease. Mov Disord. 2014;29:1547–51.
51. Djamgoz MBA, Hankins MW, Hirano J, Archer SN. Neurobiology of retinal dopamine in relation to degenerative states of the tissue. Vision Res. 1997;37:3509–29.
52. Savy C, Simon A, Nguyen-Legros J. Spatial geometry of the dopamine innervation in the avascular area of the human fovea. Vis Neurosci. 1991;7:487–98.
53. Wang RK, An L, Francis P, Wilson DJ. Depth-resolved imaging of capillary networks in retina and choroid using ultrahigh sensitive optical microangiography. Opt Lett. 2010;35:1467–9.
54. Shrier EM, Adam CR, Spund B, Glazman S, Bodis-Wollner I. Interocular asymmetry of foveal thickness in Parkinson disease. J Ophthalmol. 2012;2012:728457.
55. Altintaş Ö, Işeri P, Özkan B, Çağlar Y. Correlation between retinal morphological and functional findings and clinical severity in Parkinson's disease. Doc Ophthalmol. 2008;116:137–46.
56. Archibald NK, Clarke MP, Mosimann UP, Burn DJ. Retinal thickness in Parkinson's disease. Parkinsonism Relat Disord. 2011;17:431–6.
57. Cubo E, Tedejo RP, Rodriguez Mendez V, Lopez Pena MJ, Trejo Gabriel Y, Galan JM. Retinal thickness in Parkinson's disease and essential tremor. Mov Disord. 2010;25:2461–2.
58. Albrecht P, Muller AK, Sudmeyer M, et al. Optical coherence tomography in parkinsonian syndromes [serial online]. PLoS One. 2012;7:e34891.
59. Adam C, Shrier E, Bodis-Wollner I, Ding Y, Glazman S. Correlation of inner retinal thickness evaluated by spectral-domain optical coherence tomography and contrast sensitivity in Parkinson disease. J Neuroophthalmol. 2013;33:137–42.
60. Garcia-Martin E, Rodriguez-Mena D, Satue M, Almarcegui C, Dolz I, Alarcia R, et al. Electrophysiology and optical coherence tomography to evaluate Parkinson disease severity. Invest Ophthalmol Vis Sci. 2014;55:696–705.
61. Satue M, Garcia-Martin E, Fuertes I, et al. Use of Fourier-domain OCT to detect retinal nerve fiber layer degeneration in Parkinson's disease patients. Eye (Lond). 2013;27:507–14.
62. Lee JY, Kim JM, Ahn J, Kim HJ, Jeon BS, Kim TW. Retinal nerve fiber layer thickness and visual hallucinations in Parkinson's Disease. Mov Disord. 2014;29:61–7.
63. Satue M, Seral M, Otin S, Alarcia R, Herrero R, Bambo MP, et al. Retinal thinning and correlation with functional disability in patients with Parkinson's disease. Br J Ophthalmol. 2014;98:350–5.
64. Schneider M, Müller HP, Lauda F, Tumani H, Ludolph AC, Kassubek J, Pinkhardt EH. Retinal single-layer analysis in Parkinsonian syndromes: an optical coherence tomography study. J Neural Transm. 2014;121:41–7.
65. Roth NM, Saidha S, Zimmermann H, Brandt AU, Isensee J, Benkhellouf-Rutkowska A, et al. Photoreceptor layer thinning in idiopathic Parkinson's disease. Mov Disord. 2014;29:1163–70.
66. Garcia-Martin E, Larrosa JM, Polo V, Satue M, Marques ML, Alarcia R, et al. Distribution of retinal layer atrophy in patients with Parkinson disease and association with disease severity and duration. Am J Ophthalmol. 2014;157:470–8.
67. Tsironi EE, Dastiridou A, Katsanos A, et al. Perimetric and retinal nerve fiber layer findings in patients with Parkinson's disease. BMC Ophthalmol. 2012;12:54.
68. Yu JG, Feng YF, Xiang Y, Huang JH, Savini G, Parisi V, et al. Retinal nerve fiber layer thickness changes in Parkinson disease: a meta-analysis. PLoS One. 2014;9:e85718.

69. Moschos MM, Tagaris G, Markopoulos I, Margetis I, Tsapakis S, Kanakis M, Koutsandrea C. Morphologic changes and functional retinal impairment in patients with Parkinson disease without visual loss. Eur J Ophtalmol. 2011;21:24–29.
70. Garcia-Martin E, Satue M, Fuertes I, et al. Ability and reproducibility of Fourier-domain optical coherence tomography to detect retinal nerve fiber layer atrophy in Parkinson's disease. Ophthalmology. 2012;119:2161–7.
71. Rohani M, Langroodi AS, Ghourchian S, Falavarjani KG, Soudi R, Shahidi G. Retinal nerve changes in patients with tremor dominant and akinetic rigid Parkinson's disease. Neurol Sci. 2013;34:689–93.
72. Kirbas S, Turkyilmaz K, Tufekci A, Durmus M. Retinal nerve fiber layer thickness in Parkinson disease. J Neuroophthalmol. 2013;33:62–5.
73. La Morgia C, Barboni P, Rizzo G, et al. Loss of temporal retinal nerve fibers in Parkinson disease: a mitochondrial pattern? Eur J Neurol. 2013;20:198–201.
74. Moreno-Ramos T, Benito-Leon J, Villarejo A, Bermejo-Pareja F. Retinal nerve fiber layer thinning in dementia associated with Parkinson's disease, dementia with Lewy bodies, and Alzheimer's disease. J Alzheimers Dis. 2013;34:659–64.
75. Sen A, Tugcu B, Coskun C, Ekinci C, Nacaroglu SA. Effects of levodopa on retina in Parkinson disease. Eur J Ophthalmol. 2014;24:114–9.
76. Jiménez B, Ascaso FJ, Cristóbal JA, López del Val J. Development of a prediction formula of Parkinson disease severity by optical coherence tomography. Mov Disord. 2014;29:68–74.
77. Yavas GF, Yilmaz O, Küsbeci T, Oztürk F. The effect of levodopa and dopamine agonists on optic nerve head in Parkinson disease. Eur J Ophthalmol. 2007;17:812–6.
78. Shrier EM, Miri S, Glazman S, Bodis-Wollner I. Longitudinal retinal thickness changes in Parkinson's disease before and after deep brain stimulation: case report based on macular optical coherence tomography. Mov Disord. 2014;29 Suppl 1:1229.

Chapter 7
Optical Coherence Tomography in Alzheimer's Disease

Gianluca Coppola, Vincenzo Parisi, Gianluca Manni, Francesco Pierelli, and Alfredo A. Sadun

Abstract Alzheimer's disease (AD) is a neurodegenerative disorder, which is likely to start as mild cognitive impairment (MCI) several years before its full-blown clinical manifestation. In the last two decades, optical coherence tomography (OCT) has been used to observe a significant loss in peripapillary retinal nerve fiber layer (RNFL) and in macular thickness and volume in patients affected by a form of mild to severe dementia. These morphological abnormalities correlate to some extent with the severity of the disease as evaluated with neuropsychological tests. Furthermore, these structural measures correlate with electrophysiological parameters of pattern electroretinogram, reflecting integrity of the innermost retinal layers, but not with those of the visual evoked potentials, reflecting activity of the post-chiasmatic visual pathway. The latter evidence suggests that RNFL thickness reduction is related to neuronal degeneration in the ganglion cell layer and not to a retrograde degeneration from the post-chiasmatic visual pathway. These data suggest a possible role of OCT in monitoring the progression of AD and in assessing the effectiveness of purported AD treatments.

Keywords Alzheimer's disease • Optical coherence tomography • Mild cognitive impairment • Electroretinogram • Psychometric testing • Retina

G. Coppola, MD, PhD (✉) • V. Parisi, MD
Department of Neurophysiology of Vision and Neuroophthalmology,
G.B. Bietti Foundation IRCCS, Rome, Italy
e-mail: gianluca.coppola@gmail.com; vmparisi@gmail.com

G. Manni, MD
Department of Clinical Sciences and Translation Medicine, Tor Vergata University of Rome, Rome, Italy
e-mail: gianlucamanni53@gmail.com

F. Pierelli, MD, PhD
Department of Medico-Surgical Sciences and Biotechnologies,
Sapienza University of Rome Polo Pontino, Latina, Italy
e-mail: francesco.pierelli@uniroma1.it

A.A. Sadun, MD, PhD
Doheny Eye Institute, Keck School of Medicine, Pasadena, CA, USA
e-mail: alfredo.sadun@gmail.com

A. Grzybowski, P. Barboni (eds.), *OCT in Central Nervous System Diseases: The Eye as a Window to the Brain*, DOI 10.1007/978-3-319-24085-5_7

Abbreviations

AD	Alzheimer's disease
ADAS-Cog	Alzheimer's Disease Assessment Scale
aMCI	Amnestic type of mild cognitive impairment
APP	Beta-amyloid precursor protein
ERG	Electroretinogram
GCL	Ganglion cell layer
HRT	Heidelberg retina tomograph
OCT	Optical coherence tomography
ON	Optic nerve
PERG	Pattern electroretinogram
PS1	Presenilin 1
RBANS	Repeatable Battery for the Assessment of Neuropsychological Status
RNFL	Retina nerve fiber layer
VEP	Visual evoked potential

7.1 Introduction

Alzheimer's disease (AD) is the most common cause of dementia with an incidence that increases with age exponentially. According to the World Health Organization the worldwide prevalence of Alzheimer' disease (AD) is increasing yearly and receives growing attention not only because it affects quality of life, and also because has a significant economic impact, being a major public-health problem [1]. The recent publication of the Global Burden of Disease survey 2012 shows that among neurological conditions, AD is the third highest cause of disability in the world [2].

AD is a brain degenerative disorder, where inherited susceptibility and environmental factors are probably interrelated [3, 4]. The clinical evolution of AD is a slowly progressive and episodic memory loss as the predominant symptom, with various accompanying signs including aphasia, apraxia, and agnosia, and general cognitive symptomology, such as impaired judgement, decision-making, and orientation [3]. Because of the slowness of the disease's progression, the neurodegenerative processes are likely to start 20–30 years before the clinical manifestation of AD. This transitional phase is recognized as mild cognitive impairment (MCI), which has memory deficit, preservation of general cognitive and functional abilities, and absence of diagnosed dementia as cardinal features [5]. The amnestic type of MCI (aMCI) shows the highest annual incidence conversion rate to AD [6].

Despite great advances in the understanding of AD pathophysiology in the last few years, the exact pathogenesis of AD and its precursor MCI is still not comprehensively understood.

At the histopathologic level, neuronal loss, beta-amyloid plaques, neurofibrillary tangles made of hyperphosphorylated tau and neuritic plaques, and granulovacuolar degeneration characterize the brain of AD [3]. These lesions have been seen in the

hippocampus and other limbic structures, as well as in the visual associative areas [7, 8], the primary visual cortex [9, 10], and in subcortical structures including the lateral geniculate nuclei and the superior colliculi [11–13], and within the retina [14, 15].

AD patients may be affected by various visual disturbances, such as deficit in contrast sensitivity [16–18], motion perception [19, 20], and color discrimination [21–23]. Historically, these visual dysfunctions in AD have been attributed to damage in primary visual cortex and to degenerative processes in primary and associative visual cortical areas, but cortical dysfunction alone cannot explain the pattern of observed defects. Multiple forms of evidence points toward the involvement of retinal ganglion cells and their axons in the optic nerve as a basis of the visual dysfunction in AD [14, 24].

In the last two decades, several studies have searched for the retinal involvement in AD pathophysiology. Sophisticated imaging techniques have been used, such as optical coherence tomography (OCT), scanning laser polarimetry, and pattern electroretinography (PERG), to assess the morphologic and functional changes of the retina in AD.

Optical Coherence Tomography (OCT) permits the objective quantification *in vivo* of the retinal nerve fiber layer (RNFL) that consists of axons that form the optic nerve and contributes partially to the retinal thickness. This method consists of a non-invasive technology allowing cross-sectional imaging of the eye [25, 26]. A relatively recent implementation of OCT, Spectral-Domain OCT, provides advantages in signal-to-noise ratio, permitting faster signal acquisition [27, 28]. Taking in mind that the human eye is an embryological protrusion of the brain, and the nerves and axons of the retinal nerve fiber layer (RNFL) are similar to those in the brain, it is not surprising that OCT has been widely employed in assessing RNFL thickness in several neuro-ophthalmological disorders [29–33].

The intent of this chapter is to provide a comprehensive overview of the results provided by the OCT technique as used to understand morphological retinal changes that occur due to the degenerative processes associated with Alzheimer's disease and other dementing disorders.

7.2 Retina and Alzheimer's Disease

As an integrated part of the nervous system, the retina is physiologically under senescence processes, the majority of them still under intense scrutiny. Therefore, in order to better evaluating AD patients, it is important to quantify the degree of thinning arising with age in the absence of pathological processes. It is also important to determine whether age-related loss is uniformly distributed across the optic disc or has any tendency to be sectorial, and might therefore be a confounding factor for a correct evaluation of disease-related processes.

In the quest for understanding the degenerative changes accompanying AD, researchers performed both histological and *in-vivo* studies on healthy subjects.

Using immunohistochemical techniques, Löffler and colleagues examined the presence and expression of amyloid-related proteins, the same that have been found in specimens of AD patients' brains, in the human retina collected from cadaver

eyes at various ages [15]. They did not find any abnormal deposits or immunoreactivity changes in the outer neural retina. On the other hand, they first proved the presence of tau proteins and amyloid precursor protein in the inner retina layers, including retinal ganglion cells and nerve fiber layer, of the human retina in older persons. Small amounts of beta-amyloid were detected in the sub-retinal pigment epithelium space [15].

The analysis of normal *in-vivo* human retinal nerve fiber layer thickness, as measured by time-domain OCT, has been repeatedly confirmed as an age-related reduction of RNFL thickness in normal subjects [34–37]. This thinning mainly involved the superior and inferior optic disc areas [38–40].

7.2.1 Animal Model of AD

One of the most recognised theories for the genesis of AD, the "amyloid cascade hypothesis", postulates that APP dysmetabolism and beta-amyloid deposition are the primary events that facilitate the disease process of AD [41].

In the past decade, through the use of genetic engineering techniques, transgenic (Tg) animal models over-expressing mutant forms of amyloid precursor protein (APP) and/or presenilin 1 (PS1) have been generated to mimic various aspects of AD pathology, including Aβ deposition, cognitive deficits, inflammation, and synaptic dysfunction, to test newly proposed therapeutic agents [42]. Recent publications have shown the accumulation of Aβ-plaques within the retina [43–46] and its microvasculature [47], retina ganglion cell death [48], and local neuroinflammation [47] in different Tg animal models. Nevertheless, these transgenic models only mimic part of the pathological features of AD.

An interesting and novel Tg AD rat model, TgF344-AD, expressing mutant human amyloid precursor protein (APPsw) and presenilin 1 genes, seems to more faithfully encapsulate all the features of AD. This animal model is characterized by an otherwise healthy long lifespan, but the rats suffer from later age cognitive decline, age-dependent cerebral amyloidosis, taupathy, gliosis, and frank neuronal loss that seems to parallel those in humans [49]. Recently, Tsai and colleagues investigated a group of TgF344-AD rats and age-matched wild type rats [50]. When compared with age-matched controls, the retinas of Tg rats demonstrated the presence of Aβ plaques, hypertrophic retinal pigment epithelial cells, signs of neuroinflammation, and a significant thinning of retinal choroid [50].

7.2.2 Histological Studies in Post-Mortem AD Eyes

In 1986, histological examination in a human post mortem study, revealed depletion of axons in the optic nerves from AD patients [14]. Sadun and colleagues were the first to demonstrate this primary AD-associated optic neuropathy and further, to characterize, by morphometric analysis, that the predominant effect was on the

largest retinal ganglion cells (M-cells) that contribute their large caliber fibers to the optic nerve [24]. Other studies [51, 52] failed to confirm the selective large axon losses. This discrepancy has been attributed, at least in part, to methodological biases such as a different *post-mortem* delays, different techniques in axonal counting and/or difficulties in obtaining well-preserved myelinated axons.

Extensive retinal ganglion cell loss in the central retina in AD was also observed in histological studies [14] or by other methods of evaluating the RNFL *in vitro*. Morphometric analysis of the central retina (fovea/foveola/parafoveal retina) in eyes from 9 AD and 11 age-matched controls revealing an overall decrease of 25 % in total numbers of neurons in the ganglion cell layer (GCL) (fovea/parafoveal retina) in AD as compared with control eyes [53]. Moreover, the most severe decrease was observed in the foveal region (–43 %) over the far temporal region. Similar results were obtained in AD patients with the evaluation of the peripheral retina: the neuronal loss was more pronounced in the superior and inferior quadrants (50–59 %) and a significantly increased ratio of astrocytes to neurons was detected when compared with control eyes [54]. Moreover, histological signs of degeneration in the retinal ganglion cells (RGCs) were described to include a vacuolated, "frothy" appearance of the cytoplasm in the absence of neurofibrillary tangles within the RGCs, or of neuritic plaques or amyloid angiopathy in the retinas or optic nerves in AD [55].

Koronyo-Hamaoui and colleagues recently identified retinal Aβ plaques in *post-mortem* eyes from 8 AD patients and in five suspected early stage cases, but not in five age-matched non-AD individuals [45].

Plaque-like structures were seen in two retinas from two AD patients, with thickening of retinal choroid and no changes in the retinal pigment epithelial cells [50]. Fibrillar tau or Aβ aggregates were seen in *post-mortem* retinas from the same AD patients that had been previously observed by using an *in-vivo* imaging technique [56].

7.2.3 Clinical Studies Based on the Subjective Evaluation of Fundus Photographs

The RNFL includes axons of ganglion cells, which form the origin of the optic nerve.

That retinal ganglion cell degeneration occurs in AD is further evident by means of the use of a boundary-tracking program and RNFL photographs. A higher proportion of AD patients showed signs of optic neuropathy manifesting as optic disc atrophy, pathologic optic disc cupping, and thinning of the neuroretinal rim and of the RNFL [57, 58]. Tsai et al. [57] observed an increased cup-to-disc ratio, cup volume, and decreased optic disc rim area in AD patients by optic nerve analyser.

Analyzing mild to moderate AD patients with RNFL fundus photographs, Lu and colleagues found that all the AD patients had different types of RNFL abnormalities, including diffuse and wedge shape nerve fiber layer drop-out [59]. These abnormalities in AD patients were associated with a higher cup–disc ratio of 39–43 % when compared to that in the control group.

However, it must be mentioned that these studies may have been biased by the subjective evaluation of fundus photographs.

7.3 *In-Vivo* Morphological Analysis in AD and MCI Patients

One confounding factor in analysing MCI and AD -related late-onset progressive changes is that there are anatomical and physiological changes normally found in aging eyes. In animal [60] and human [60, 61] studies a physiological age-dependent progressive loss of optic nerve fibers, with progressive decrease of mean axonal diameter has been demonstrated [62–64].

Optical coherence tomography (OCT) is a technique that can also be used in ophthalmology for the measurement of the macular thickness and volume. OCT can determine RNFL thickness of the peripapillary region reflecting axons and would allow quantification of axonal loss, measurement of macular thickness and volume would reflect retinal neurons, allowing quantification of neuronal loss [25].

Several previous studies using OCT techniques have examined the relationship between age and RNFL measurements. These have consistently shown that optic nerve, RNFL, and macular measurements with OCT all varied with age [36, 65], with the greatest decrease in mean RNFL occurring in the superior [39] and inferior quadrants [37], especially after age 50 years [38], and with the least decrease in the nasal and temporal quadrants [66, 67]. This age-related decline in normal RNFL measurements needs to be considered when considering or monitoring ocular disease.

However, as described below, the reduction in RNFL thickness observed in most studies on AD patients was significantly greater than that observed in the age-matched controls and thus cannot be exclusively ascribed to aging (see some illustrative OCT imaging in Fig. 7.1 and a synopsis of published OCT studies in AD and MCI in Table 7.1).

Parisi and colleagues were the first who used OCT to study a group of 17 AD patients affected from mild severity cognitive impairment and compared them with a group of 14 age-matched controls. In AD patients, OCT results showed thinning of the average peripapillary RNFL and in all quadrants examined, showing the involvement of the neuroretinal tissue in AD [68, 69].

The mean RNFL thickness was corroborated to be reduced in AD patients by several independent groups [59, 72, 77, 78], and even in patients affected with MCI [73]. Individual examination of the quadrants was even more revealing. Most studies observed a significant reduction of RNFL thickness in the superior quadrant [59, 70, 73, 74, 78], but for some also in the inferior quadrant [59, 73]. In contradistinction, the inferior quadrant seems more involved in MCI patients [73].

Some researchers studied optic nerves of AD patients by using confocal scanning laser ophthalmoscopy (cSLO). Ophthalmoscopy in combination with cSLO, revealed an enlargement in the mean vertical cup-to-disc ratio (clinician and instrument derived), rim volume, rim area, and reduced RNFL thickness in patients with AD with respect to controls [81]. Compared with individuals in the lowest quarter of values of cup-to-disc ratios, those with higher values generally had an increased risk of AD [81]. Lu et al. [59] also observed an enlarged cup-to-disc ratio and a thinner RNFL thickness in their 22 mild to moderate AD patients. In contrast, Kergoat

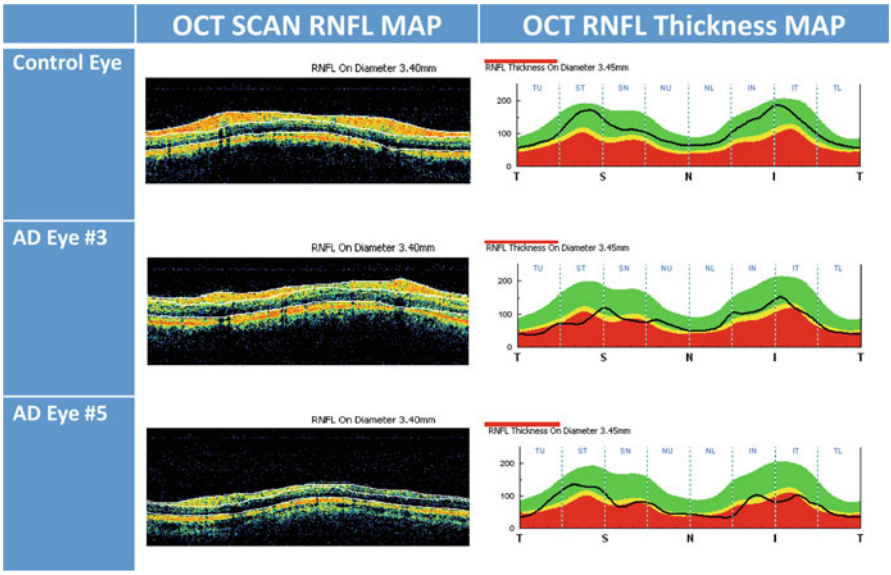

Fig. 7.1 Optical Coherence Tomography (*OCT*) imaging taken in cylindrical section of tissue surrounding the optic disc of a control eye and of 2 AD patients eyes. The images in the *left panel* are raw OCT data, while the maps in the *right panel* are quantitative data curve. In AD patients eyes OCT shows a decrease of RNFL reflection (reduced RNFL thickness) in each examined quadrant, with particular prevalence of the temporal ones

et al. [82] found no differences in the regional distribution of RNFL thickness between patients with mild to moderate AD and healthy controls evaluated with scanning laser polarimetry. The same researchers did not observed optic nerve head structural abnormalities in AD by using real-time topographical images obtained with a Heidelberg retina tomograph (HRT) from individuals in the early stages of AD compared with age-matched controls [83].

Berisha et al. [71] tried to determine whether regional thinning of the RNFL occurred in the nine patients with mild to moderate AD and to determine whether the retinal circulation was abnormal in these patients. AD patients showed a marked narrowing of the retinal venous blood column diameter and a reduction in retinal blood flow rate compared with eight age-matched control subjects. OCT data confirmed a significant thinning of the peripapillary RNFL that was most pronounced in the superior quadrant, which did not correlate with the retinal blood flow [71]. They argued that the mechanisms producing reduced blood flow in the retina are related to those that produce cerebral blood flow abnormalities, which are known to occur in AD, such as increased venous wall thickness due to collagen and β-amyloid deposition [84].

In a cross-sectional study on 150 patients with low-to-moderate dementia and 61 controls, researchers compared the parameters provided by two commercially available spectral domain OCT devices, the Cirrus and the Spectralis OCT instruments

Table 7.1 Demographic data and RNFL thickness measurements in patients and controls as determined by OCT

Reference	No. of subjects and diagnosis	Mean MMSE/ AD stage	Mean age ± SD	OCT machine	Mean RNFL (μm)	Superior quadrant (μm)	Inferior quadrant (μm)	Nasal quadrant (μm)	Temporal quadrant (μm)	Note
Parisi et al. [68, 69]	17 AD 14 controls	/mild	70.37 ± 6.1	Humphrey	59.5 ± 16.70[a] 99.9 ± 8.95	72.1 ± 21.4[a] 104.6 ± 12.1	77.9 ± 26.4[a] 116.2 ± 9.87	50.4 ± 23.2[a] 93.4 ± 13.7	37.9 ± 17.60[a] 85.6 ± 8.21	RNFL overall values correlated with PERG
Iseri et al. [70]	14 AD 15 controls	18.5/mild to moderate 29.4	70.1 ± 9.7 65.1 ± 9.8	Carl Zeiss Meditec, Model 3000	87.4 ± 23.7[a] 113.1 ± 6.7	112.6 ± 35.3[a] 137.1 ± 16.4	103.1 ± 33.6[a] 141.5 ± 19.1	63.5 ± 19.1[a] 96.0 ± 34.4	64.9 ± 17.7 72.3 ± 16.4	Decline in both peripapillary and macular thickness and volume in AD eyes
Berisha et al. [71]	9 AD 8 HV	23.8/mild to moderate 29.5	74.3 ± 3.3 74.3 ± 5.8	Carl Zeiss Meditec, Model 3000		92.2 ± 21.6[a] 113.6 ± 10.8	117.0 ± 15.3 128.1 ± 11.4	67.0 ± 15.0 69.5 ± 11.1	65.7 ± 15.1 64.1 ± 7.3	Narrowing of the retinal microvasculature
Paquet et al. [72]	23 MCI 14 AD 12 AD 15 controls	28.8 22.6/mild 16.6/ severe 28.9	78.7 ± 6.2 78.3 ± 5.1 78.8 ± 4.9 75.5 ± 5.1	Carl Zeiss Stratus OCT 3	89.3 ± 2.7[a] 89.2 ± 2.9[a] 76.6 ± 3.8[a] 102.2 ± 1.8					The involvement of retina is an early event in the course of this disorder
Lu et al. [59]	22 AD 22 controls		73 ± 8 68 ± 9	Carl Zeiss Meditec, Model 3000	90 ± 18[a,b] 98 ± 12	107 ± 30[a,b] 124 ± 16	116 ± 35[a,b] 128 ± 18	66 ± 26 70 ± 17	70 ± 20 71 ± 13	Enlarged optic cup to disc ratio in AD
Kesler et al. [73]	24 MCI 30 AD 24 controls	28.1 23.6	71.0 ± 10.0 73.7 ± 9.9 70.9 ± 9.2	Carl Zeiss Stratus OCT 3	85.8 ± 10.0[a] 84.7 ± 10.6[a] 94.3 ± 11.3	101.3 ± 15.2 99.0 ± 18.0[a] 110.0 ± 16.7	111.9 ± 16.1[a] 110.1 ± 19.1[a] 127.0 ± 15.5	65.9 ± 15.1 66.8 ± 14.5 76.4 ± 21.8	64.2 ± 13.9 61.7 ± 10.9 67.8 ± 15.1	RNFL thickness not correlated with MMSE

Kromer et al. [74, 75]	22 AD 22 controls	22.6/mild to moderate	75.9 ± 6.1 64.0 ± 8.2	Spectralis Heidelberg Engineering	80[b,c]	46[b,c]		47[b,c]		The RNFL of the AD patients did not correlate with pattern VEP latencies.
Moreno-Ramos et al. [76]	10 AD 10 LB 10 PD 10 controls	16.4 14.9 16.4 29.2	73.0 ± 6.5 74.2 ± 5.1 74.3 ± 5.0 70.2 ± 5.5	TOPCON 3D OCT-1000	94.5 ± 2.2[a] 93.3 ± 1.5[a] 94.8 ± 2.0[a] 108.0 ± 2.2					Retinal involvement measured by OCT may also be present in non-AD dementias
Marziani et al. [77]	21 AD 21 controls	19.9/mild to moderate 27.9	79.3 ± 5.7 77.0 ± 4.2	(1) Optovue RTVue-100 & (2) Spectralis Heidelberg Engineering	244.1 ± 17.9[1] 277.5 ± 21.7[2] 252.3 ± 19.2[1] 283.8 ± 27.3[2] Central sector	274.8[1a,d] 304.3[2a,d] 288.9[1d] 319.3[2d]	273.25[1a,d] 301.7[2a,d] 286.25[1d] 314.75[2d]	278.4[1a,d] 309.35[2a,d] 290.85[1d] 323.55[2d]	271.8[1a,d] 291.95[2a,d] 286.25[1d] 304.45[2d]	Reduced RNFL in AD patients using 2 different OCT instruments
Kirbas et al. [78]	40 AD 40 controls	21.5	69.3 ± 4.9 68.9 ± 5.1	Spectral domain OCT	65 ± 6.2[a] 75 ± 3.8	76 ± 6.7[a] 105 ± 4.8	106 ± 11.5 108 ± 8.7	75 ± 2.8 76 ± 2.7	74 ± 6.7 77 ± 7.3	No correlation between MMSE and OCT results
Larrosa et al. [79]	151 AD 61 controls	18.31	75.29 74.87	(1) Carl Zeiss Meditec Cirrus & (2) Spectralis Heidelberg Engineering	97.5 ± 14.1[1] 98.2 ± 17.1[2a] 100.5 ± 13.0[1] 102.7 ± 6.7[2]	113.2 ± 18.7[1a] 117.8 ± 19.0[1a]	120.4 ± 20.1[1a] 127.4 ± 21.0[1]	72.7 ± 17.3[1] 74.5 ± 17.2[1]	64.5 ± 21.7[1a] 67.8 ± 20.0[1]	RNFL measurements were a very useful and precise tool for AD diagnosis.

(continued)

Table 7.1 (continued)

Reference	No. of subjects and diagnosis	Mean MMSE/ AD stage	Mean age ± SD	OCT machine	Mean RNFL (μm)	Superior quadrant (μm)	Inferior quadrant (μm)	Nasal quadrant (μm)	Temporal quadrant (μm)	Note
Ascaso et al. [80]	21 aMCI 18 AD 41 controls	19.3 28.8	72.1 (AD + aMCI) 72.9	Stratus OCT 3	86.0 ± 7.2[a] 64.7 ± 15.2[a,e] 103.6 ± 8.9 (data showed from the right eye only)	96.7 ± 14.6[a] 73.2 ± 22.0[a,e] 126.6 ± 13.8	110.1 ± 17.7[a] 86.2 ± 25.7[a,e] 135.6 ± 17.6	71.0 ± 16.7[a] 43.3 ± 20.4[a,e] 77.8 ± 16.7	66.3 ± 12.1[a] 56.7 ± 14.9[a,e] 75.8 ± 16.6	A significant association between RNFL thickness in superior and nasal quadrants, and MMSE score

AD Alzheimer's disease, *aMCI* amnestic mild cognitive impairment, *LB* dementia with Lewy bodies, *MCI* mild cognitive impairment, *MMSE* mini mental state examination, *RNFL* retinal nerve fiber layer, *PD* dementia associated with Parkinson's disease

[a]Significantly different from controls

[b]Data extrapolated from the bar chart

[c]Statistics do not clearly show

[d]Mean of internal plus external sectors

[e]Significantly different from MCI

[1,2]OCT machine

[79]. With both devices, they confirmed the retinal thinning in AD patients, and they found that the best parameter for distinguishing AD patients from healthy controls using OCT measurements was the Spectralis looking at RNFL [79]. Along these lines, Marziani et al. [77] used both Optovue RTVue-100 and Spectralis instruments to evaluate retinal thickness in 21 patients affected by AD in comparison with 21 healthy controls. Both instruments showed a significant difference in full retinal thickness between patients and controls in all the macular sectors except in the central sector and for the superior external sector [77].

In order to verify whether involvement of the retina is an early event in the course of AD, few studies compared MCI versus AD patients and healthy aged people. Paquet and coworkers [72] enrolled 23 MCI patients, 14 mild AD, 12 moderate to severe AD patients, and 15 healthy subjects. Overall, mean RNFL thickness was reduced in all patient groups in respect to controls. The subgroup analyses revealed no difference between the results observed in MCI and in mild AD patients, whereas RNFL thickness assessed in moderate to severe AD patients was significantly reduced in respect with that assessed in MCI patients [72]. Kesler et al. [73] obtained similar results finding that the mean RNFL was significantly thinner in both AD and MCI patients groups compared to controls, and that the MCI group fell in between the other two groups. This difference was particularly prominent in the inferior quadrant, whereas the AD patients had significantly thinner retinal NFL values also in the superior quadrant [73].

Recently, investigators attempted to identify individuals who might be at a high risk of developing AD, and observed that, despite the reduction in peripapillary RNFL thickness, central 1-mm foveal thickness and macular volume were significantly increased in aMCI patients, but not in AD patients, when compared with age-matched controls. The authors argued that retinal swelling might be the first sign of macular retinal ganglion cell degeneration probably due to inflammation and/or gliosis in the early stages of AD [80].

Finally, it is worth noting that thinning of RNFL is also present in other types of dementia, such as dementia with Lewy bodies, dementia associated with Parkinson's disease [76] and with cerebral autosomal dominant arteriopathy with subcortical infarcts and leuco-encephalopathy (CADASIL) [85] challenging the specificity of OCT findings in AD patients.

7.4 Structural-Functional Correlations

The functional activity of the visual system can be dissected by the use of electrophysiological techniques such as pattern electroretinogram (PERG) and visual evoked potentials (VEPs) that have the capability of assessing, respectively, the bioelectrical activity of retinal ganglion cells and their fibers, and the functional integrity of the entire visual pathways from retina to the visual cortex.

The implicit times were delayed and/or the amplitudes reduced [68, 69, 86–89] in most of the PERG studies performed in AD patients at various stages, reflecting

retinal ganglion cell dysfunction. However, in some studies PERG parameters were within the range of normality [90, 91]. In one study luminance pattern ERGs were delayed and amplitudes reduced, whereas isoluminant chromatic ERGs were always within the normal ranges [89].

The implicit time of patterned VEP was normal in some studies [86, 89, 92, 93] and in others delayed [88, 91, 94, 95], with the amplitudes within the range of normality. A delayed P2 component of the flash VEP is a common finding across studies in AD patients [86, 92, 96, 97], with one exception [94].

Taken as a whole, these electrophysiological results are consistent with the early histological studies showing retinal ganglion cell dysfunction in AD [12, 22] and supports the notion that this damage in AD preferentially affects the larger, faster-conducting retinal ganglion cells and their retinocortical projections.

Parisi and coworkers [68, 69] used OCT and PERG in a group of 17 mild severity AD patients compared with a group of 14 healthy controls. They observed that the general reduction of peripapillary RNFL thickness was accompanied with delayed N35, P50 and N95 implicit times and reduced N35-P50 and P50-N95 amplitudes in their AD patients. More interestingly, in AD eyes, the RNFL overall values were positively correlated to the PERG P50 and N95 implicit times and PERG P50-N95 amplitude. This was not so in controls [68, 69]. However, Iseri et al. [70] did not find significant differences in VEP P100 implicit times and N75-P100 amplitudes recorded at high spatial frequency in a group of 14 mild to moderate AD patients when compared with a group of 15 controls. Moreover, they saw no correlation between any of the abnormally in RNFL and macular OCT thickness and VEP in AD [70]. This negative correlation, between VEPs parameters recorded at both high and low spatial frequency and OCT peripapillary scans, was later corroborated [75].

7.5 Correlations with Psychometric Measures

Along with personal history, physical examination and laboratory tests, questionnaires are often used to help test a range of everyday mental skills of persons with symptoms of dementias. Widely used tests include the mini mental state examination (MMSE), the Alzheimer's disease assessment scale- (ADAS-Cog), and the Repeatable Battery for the Assessment of Neuropsychological Status (RBANS).

The previously mentioned parameters of increased cup-to-disc ratio, cup volume, and decreased optic disc rim area, all found in AD patients by optic nerve analyser, positively correlated with ADAS-Cog scores and disease's duration [57]. Moreover, the reduced total macular volume in patients with AD was positively correlated with the severity of the disease as assessed by the MMSE [70, 76]. However, other studies failed to find the same associations [72–75, 78]. RNFL thickness of AD or MCI patients was non associated with other patient demographic features, such as age [72, 79], gender, and AD stage [74].

In AD patients, but not in aMCI, multiple linear regression models showed a strong association between overall RNFL thickness and MMSE score. The same

association was found between MMSE and RNFL thickness in superior and nasal quadrants. Macular thickness and volume were not associated with MMSE score either in aMCI or in AD patients [80].

A prospective study attempted to determine whether deterioration of patients' cognitive functions, as verified with the RBANS test, correlated to specific OCT findings [98–100]. These investigators followed, for a period of 25 months, two groups of subjects: 82 participants with a normal cognitive status and 22 MCI patients. The participants who completed the observational period were further categorized as 60 participants experiencing a stable cognitive status and 18 participants who experienced a worsening of their cognitive status. The investigators found that in those participants who remained stable, greater attenuation of RNFL in the superior quadrant could predict specific cognitive deteriorations. In contradistinction, in participants who worsened, less attenuation of RNFL in the inferior quadrant could predict greater cognitive deterioration [98–100]. These findings suggest that patients who have less reduction in the thickness of the inferior quadrant of RNFL over time may have a higher risk of developing MCI and dementia, leading the authors to put forward RNFL thickness as a potential biomarker of dementia.

7.6 Conclusions

The diagnosis of AD is often based on psychometric assessments by a multidisciplinary team (neurologists, psychiatrists, and psychologist) and an objective neurological examination. Because of inter- and intra-individual variability, neurophysiological and neuroimaging tests have not yet been considered as criteria on which to base a diagnosis. In fact, neurophysiological as well as other paraclinical tests are recommended only on suspicion of secondary causes of dementia as part of the differential diagnosis of AD. The AD diagnosis is confirmed only with *post mortem* histopathology. Nonetheless, the last few decades have seen the use of structural and functional techniques as potential biomarkers that might also identify factors that may predispose individuals to AD. The optical coherence tomography (OCT) technique for the measurement of the peripapillary RNFL, the macular thickness and volume, has been demonstrated as useful for the demonstration of significant retinal changes in patients that roughly correlate with the severity of the disease (Fig. 7.2).

Particularly intriguing results of recent experiments include:

- In both animal models, expressing mutant forms of amyloid precursors, and histological studies on *post mortem* AD eyes, researchers have observed various retinal pathological changes, such as accumulation of Aβ aggregates within the retina and its microvasculature, retina ganglion cell death and signs of neuroinflammation.
- In evaluations with the optic nerve analyser, a higher proportion of AD patients show signs of optic neuropathy manifesting as optic disc atrophy, pathologic optic disc cupping, and thinning of the neuroretinal rim and of the RNFL.

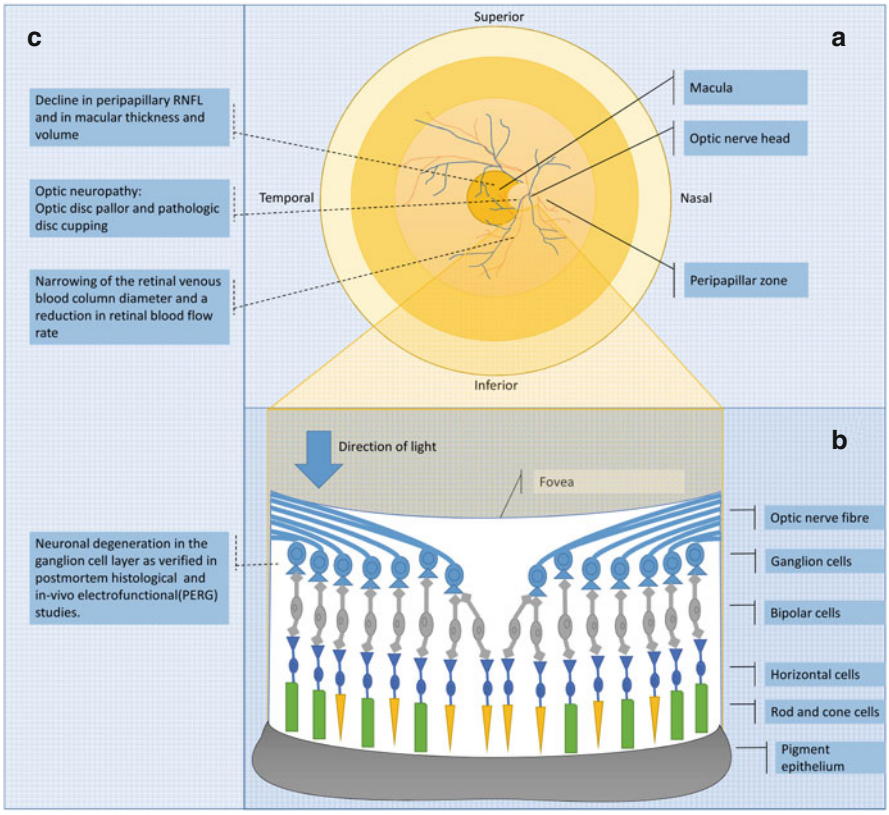

Fig. 7.2 Schematic representation of an entire retina with superimposed anatomic zones (*upper panel* **a**) and a schematic enlargement of a portion of the retina with the main cell classes (*lower panel* **b**). On the *left panel* (**c**) are summarized the findings from the OCT and electrophysiological studies in AD

- In agreement with *post mortem* studies, OCT data studies indicate a significant decline in peripapillary RNFL and also changes in macular thickness and volume that is progressive from MCI to AD eyes.
- Electrophysiological and OCT studies in AD patients show RNFL thickness reduction that is related to neuronal degeneration in the retinal ganglion cell layer that is not a consequence of retrograde degeneration from the post-chiasmatic visual pathway.
- The correlations between morphological and clinical features tend to suggest a potential role for optic nerve head analysis in monitoring the progression of AD and as outcome measures in the assessment of any purported AD treatments.

Overall, these results suggest that degeneration of the retinal ganglion cells should be added to the constellation of neuropathologic changes found in patients with Alzheimer's disease.

Other neurodegenerative disorders, like Parkinson's disease and glaucoma, may enter in the differential diagnosis of RNFL thinning [101]. A particular mention merits the controversial association between primary open angle glaucoma (POAG) and AD. This is based on various indirect evidence of some shared genetic, histopathological and functional features [102, 103]. However, even not considering the prevalent involvement of cognitive areas, especially of the hippocampus, that accompanies AD respect neurodegenerative processes confined to the visual pathway of POAG, the mutual association of the two clinical entities is poorly supported by conflicting epidemiological studies [104, 105].

Future research in this subject area will include a better assessment of the specificity of these OCT findings in AD. We will see RNFL thickness measurements in patients with vascular dementia as an aide to diagnosis and we will see whether the RNFL can be used as a surrogate for magnetic resonance imaging measurements of the brain. These and similar studies will use OCT parameters of retinal changes as criteria against which to measure new molecules purported to help in the treatment of AD.

References

1. Stefanacci R. The costs of Alzheimer's disease and the value of effective therapies. Am J Manag Care. 2011;13:S356–62.
2. Global burden of disease survey [Internet]. [updated 2012; cited Available from: http://www.who.int/entity/healthinfo/global_burden_disease/GHE_DALY_Global_2000_2012.xls?ua=1.
3. Blennow K, Leon MJD, Zetterberg H. Alzheimer's disease. Lancet. 2006;368(9533):387–403.
4. Waring S, Rosenberg R. Genome-wide association studies in Alzheimer disease. Arch Neurol. 2008;65(3):329–34.
5. Morris J, Storandt M, Miller J, McKeel D, Price J, Rubin E, et al. Mild cognitive impairment represents early-stage Alzheimer disease. Arch Neurol. 2001;58(3):397–405.
6. Winblad B, Palmer K, Kivipelto M, Jelic V, Fratiglioni L, Wahlund L, et al. Mild cognitive impairment--beyond controversies, towards a consensus: report of the International Working Group on Mild Cognitive Impairment. J Intern Med. 2004;256(3):240–6.
7. Whitehouse P, Price D, Clark A, Coyle J, DeLong M. Alzheimer disease: evidence for selective loss of cholinergic neurons in the nucleus basalis. Ann Neurol. 1981;10(2):122–6.
8. van de Nes J, Nafe R, Schlote W. Non-tau based neuronal degeneration in Alzheimer's disease -- an immunocytochemical and quantitative study in the supragranular layers of the middle temporal neocortex. Brain Res. 2008;1213:152–65.
9. Leuba G, Kraftsik R. Visual cortex in Alzheimer's disease: occurrence of neuronal death and glial proliferation, and correlation with pathological hallmarks. Neurobiol Aging. 1994;15(1):29–43.
10. Armstrong R. Is there a spatial association between senile plaques and neurofibrillary tangles in Alzheimer's disease? Folia Neuropathol. 2005;43(3):133–8.
11. Leuba G, Saini K. Pathology of subcortical visual centres in relation to cortical degeneration in Alzheimer's disease. Neuropathol Appl Neurobiol. 1995;21(5):410–22.
12. Baloyannis S, Mauroudis I, Manolides S, Manolides L. Synaptic alterations in the medial geniculate bodies and the inferior colliculi in Alzheimer's disease: a Golgi and electron microscope study. Acta Otolaryngol. 2009;129(4):416–8.

13. Dugger B, Tu M, Murray M, Dickson D. Disease specificity and pathologic progression of tau pathology in brainstem nuclei of Alzheimer's disease and progressive supranuclear palsy. Neurosci Lett. 2011;491(2):122–6.
14. Hinton D, Sadun A, Blanks J, Miller C. Optic-nerve degeneration in Alzheimer's disease. N Engl J Med. 1986;315(8):485–7.
15. Löffler K, Edward D, Tso M. Immunoreactivity against tau, amyloid precursor protein, and beta-amyloid in the human retina. Invest Ophthalmol Vis Sci. 1995;36(1):24–31.
16. Hutton J, Morris J, Elias J, Poston J. Contrast sensitivity dysfunction in Alzheimer's disease. Neurology. 1993;43(11):2328–30.
17. Gilmore G, Whitehouse P. Contrast sensitivity in Alzheimer's disease: a 1-year longitudinal analysis. Optom Vis Sci. 1995;72(2):83–91.
18. Crow R, Levin L, LaBree L, Rubin R, Feldon S. Sweep visual evoked potential evaluation of contrast sensitivity in Alzheimer's dementia. Invest Ophthalmol Vis Sci. 2003;44(2):875–8.
19. Gilmore G, Wenk H, Naylor L, Koss E. Motion perception and Alzheimer's disease. J Gerontol. 1994;49(2):P52–7.
20. Rizzo M, Nawrot M. Perception of movement and shape in Alzheimer's disease. Brain. 1998;121:2259–70.
21. Wijk H, Berg S, Sivik L, Steen B. Colour discrimination, colour naming and colour preferences among individuals with Alzheimer's disease. Int J Geriatr Psychiatry. 1999;14(12): 1000–5.
22. Wijk H, Berg S, Bergman B, Hanson A, Sivik L, Steen B, et al. Colour perception among the very elderly related to visual and cognitive function. Scand J Caring Sci. 2002;16(1):91–102.
23. Salamone G, Di L, Mosti S, Lupo F, Cravello L, Palmer K, et al. Color discrimination performance in patients with Alzheimer's disease. Dement Geriatr Cogn Disord. 2009;27(6):501–7.
24. Sadun A, Bassi C. Optic nerve damage in Alzheimer's disease. Ophthalmology. 1990;97(1): 9–17.
25. Huang D, Swanson E, Lin C, Schuman J, Stinson W, Chang W, et al. Optical coherence tomography. Science. 1991;254(5035):1178–81.
26. Puliafito C, Hee M, Lin C, Reichel E, Schuman J, Duker J, et al. Imaging of macular diseases with optical coherence tomography. Ophthalmology. 1995;102(2):217–29.
27. Yaqoob Z, Wu J, Yang C. Spectral domain optical coherence tomography: a better OCT imaging strategy. Biotechniques. 2005;39(6 Suppl):S6–13.
28. Kiernan D, Mieler W, Hariprasad S. Spectral-domain optical coherence tomography: a comparison of modern high-resolution retinal imaging systems. Am J Ophthalmol. 2010;149(1): 18–31.
29. Schuman J, Hee M, Puliafito C, Wong C, Pedut-Kloizman T, Lin C, et al. Quantification of nerve fiber layer thickness in normal and glaucomatous eyes using optical coherence tomography. Arch Ophthalmol. 1995;113(5):586–96.
30. Parisi V, Manni G, Gandolfi SA, Centofanti M, Colacino G, Bucci MG, et al. Visual function correlates with nerve fiber layer thickness in eyes affected by ocular hypertension. Invest Ophthalmol Vis Sci. 1999;40(8):1828–33.
31. Parisi V, Manni G, Spadaro M, Colacino G, Restuccia R, Marchi S, et al. Correlation between morphological and functional retinal impairment in multiple sclerosis patients. Invest Ophthalmol Vis Sci. 1999;40(11):2520–7.
32. Parisi V, Manni G, Centofanti M, Gandolfi SA, Olzi D, Bucci MG, et al. Correlation between optical coherence tomography, pattern electroretinogram, and visual evoked potentials in open-angle glaucoma patients. Ophthalmology. 2001;108(5):905–12.
33. Kardon R. Role of the macular optical coherence tomography scan in neuro-ophthalmology. J Neuroophthalmol. 2011;31(4):353–61.
34. Sung K, Wollstein G, Bilonick R, Townsend K, Ishikawa H, Kagemann L, et al. Effects of age on optical coherence tomography measurements of healthy retinal nerve fiber layer, macula, and optic nerve head. Ophthalmology. 2009;116(6):1119–24.
35. Mwanza J, Durbin M, Budenz D, Girkin C, Leung C, Liebmann J, et al. Profile and predictors of normal ganglion cell-inner plexiform layer thickness measured with frequency-domain optical coherence tomography. Invest Ophthalmol Vis Sci. 2011;52(11):7872–9.

36. Girkin C, McGwin G, Sinai M, Sekhar G, Fingeret M, Wollstein G, et al. Variation in optic nerve and macular structure with age and race with spectral-domain optical coherence tomography. Ophthalmology. 2011;118(12):2403–8.
37. Alasil T, Wang K, Keane P, Lee H, Baniasadi N, de Boer JF, et al. Analysis of normal retinal nerve fiber layer thickness by age, sex, and race using spectral domain optical coherence tomography. J Glaucoma. 2013;22(7):532–41.
38. Parikh R, Parikh S, Sekhar G, Prabakaran S, Babu J, Thomas R, et al. Normal age-related decay of retinal nerve fiber layer thickness. Ophthalmology. 2007;114(5):921–6.
39. Feuer W, Budenz D, Anderson D, Cantor L, Greenfield D, Savell J, et al. Topographic differences in the age-related changes in the retinal nerve fiber layer of normal eyes measured by Stratus optical coherence tomography. J Glaucoma. 2011;20(3):133–8.
40. Lee J, Hwang Y, Lee S, Kim Y. Age and retinal nerve fiber layer thickness measured by spectral domain optical coherence tomography. Korean J Ophthalmol. 2012;26(3):163–8.
41. Hardy J, Allsop D. Amyloid deposition as the central event in the aetiology of Alzheimer's disease. Trends Pharmacol Sci. 1991;12(10):383–8.
42. Braidy N, Muñoz P, Palacios A, Castellano-Gonzalez G, Inestrosa N, Chung R, et al. Recent rodent models for Alzheimer's disease: clinical implications and basic research. J Neural Transm. 2012;119(2):173–95.
43. Ning A, Cui J, To E, Ashe K, Matsubara J. Amyloid-beta deposits lead to retinal degeneration in a mouse model of Alzheimer disease. Invest Ophthalmol Vis Sci. 2008;49(11): 5136–43.
44. Perez S, Lumayag S, Kovacs B, Mufson E, Xu S. Beta-amyloid deposition and functional impairment in the retina of the APPswe/PS1DeltaE9 transgenic mouse model of Alzheimer's disease. Invest Ophthalmol Vis Sci. 2009;50(2):793–800.
45. Koronyo-Hamaoui M, Koronyo Y, Ljubimov A, Miller C, Ko M, Black K, et al. Identification of amyloid plaques in retinas from Alzheimer's patients and noninvasive in vivo optical imaging of retinal plaques in a mouse model. Neuroimage. 2011;1:S204–17.
46. Koronyo Y, Salumbides B, Black K, Koronyo-Hamaoui M. Alzheimer's disease in the retina: imaging retinal aβ plaques for early diagnosis and therapy assessment. Neurodegener Dis. 2012;10(1–4):285–93.
47. Liu B, Rasool S, Yang Z, Glabe C, Schreiber S, Ge J, et al. Amyloid-peptide vaccinations reduce {beta}-amyloid plaques but exacerbate vascular deposition and inflammation in the retina of Alzheimer's transgenic mice. Am J Pathol. 2009;175(5):2099–110.
48. Cordeiro M, Guo L, Coxon K, Duggan J, Nizari S, Normando E, et al. Imaging multiple phases of neurodegeneration: a novel approach to assessing cell death in vivo. Cell Death Dis. 2010;1:10.
49. Cohen R, Rezai-Zadeh K, Weitz T, Rentsendorj A, Gate D, Spivak I, et al. A transgenic Alzheimer rat with plaques, tau pathology, behavioral impairment, oligomeric aβ, and frank neuronal loss. J Neurosci. 2013;33(15):6245–56.
50. Tsai Y, Lu B, Ljubimov A, Girman S, Ross-Cisneros F, Sadun A, et al. Ocular changes in TgF344-AD rat model of Alzheimer's disease. Invest Ophthalmol Vis Sci. 2014;55(1): 523–34.
51. Curcio C, Drucker D. Retinal ganglion cells in Alzheimer's disease and aging. Ann Neurol. 1993;33(3):248–57.
52. Davies D, McCoubrie P, McDonald B, Jobst K. Myelinated axon number in the optic nerve is unaffected by Alzheimer's disease. Br J Ophthalmol. 1995;79(6):596–600.
53. Blanks J, Torigoe Y, Hinton D, Blanks R. Retinal pathology in Alzheimer's disease. I. Ganglion cell loss in foveal/parafoveal retina. Neurobiol Aging. 1996;17(3):377–84.
54. Blanks JC, Schmidt SY, Torigoe Y, Porrello KV, Hinton DR, Blanks RH, et al. Retinal pathology in Alzheimer's disease. II. Regional neuron loss and glial changes in GCL. Neurobiol Aging. 1996;17(3):385–95.
55. Blanks J, Hinton D, Sadun A, Miller C. Retinal ganglion cell degeneration in Alzheimer's disease. Brain Res. 1989;501(2):364–72.
56. Schön C, Hoffmann N, Ochs S, Burgold S, Filser S, Steinbach S, et al. Long-term in vivo imaging of fibrillar tau in the retina of P301S transgenic mice. PLoS One. 2012;7(12):10.

57. Tsai C, Ritch R, Schwartz B, Lee S, Miller N, Chi T, et al. Optic nerve head and nerve fiber layer in Alzheimer's disease. Arch Ophthalmol. 1991;109(2):199–204.
58. Hedges T, Perez G, Speigelman D, Barbas N, Peli E, Yardley C, et al. Retinal nerve fiber layer abnormalities in Alzheimer's disease. Acta Ophthalmol Scand. 1996;74(3):271–5.
59. Lu Y, Li Z, Zhang X, Ming B, Jia J, Wang R, et al. Retinal nerve fiber layer structure abnormalities in early Alzheimer's disease: evidence in optical coherence tomography. Neurosci Lett. 2010;480(1):69–72.
60. Balazsi A, Rootman J, Drance S, Schulzer M, Douglas G. The effect of age on the nerve fiber population of the human optic nerve. Am J Ophthalmol. 1984;97(6):760–6.
61. Fortune B, Reynaud J, Cull G, Burgoyne C, Wang L. The effect of age on optic nerve axon counts, SDOCT scan quality, and peripapillary retinal nerve fiber layer thickness measurements in rhesus monkeys. Transl Vis Sci Technol. 2014;3(3):2.
62. Johnson BM, Miao M, Sadun AA. Age-related decline of human optic nerve axon populations. Age. 1987;10(1):5–9.
63. Repka M, Quigley H. The effect of age on normal human optic nerve fiber number and diameter. Ophthalmology. 1989;96(1):26–32.
64. Sadun A. Discussion of the effect of age on normal human optic nerve fiber number and diameter. Ophthalmology. 1989;96:31–2.
65. Bowd C, Zangwill L, Blumenthal E, Vasile C, Boehm A, Gokhale P, et al. Imaging of the optic disc and retinal nerve fiber layer: the effects of age, optic disc area, refractive error, and gender. J Opt Soc Am A Opt Image Sci Vis. 2002;19(1):197–207.
66. Leung C, Yu M, Weinreb R, Ye C, Liu S, Lai G, et al. Retinal nerve fiber layer imaging with spectral-domain optical coherence tomography: a prospective analysis of age-related loss. Ophthalmology. 2012;119(4):731–7.
67. Celebi A, Mirza G. Age-related change in retinal nerve fiber layer thickness measured with spectral domain optical coherence tomography. Invest Ophthalmol Vis Sci. 2013;54(13):8095–103.
68. Parisi V, Restuccia R, Fattapposta F, Mina C, Bucci M, Pierelli F, et al. Morphological and functional retinal impairment in Alzheimer's disease patients. Clin Neurophysiol. 2001;112(10):1860–7.
69. Parisi V. Correlation between morphological and functional retinal impairment in patients affected by ocular hypertension, glaucoma, demyelinating optic neuritis and Alzheimer's disease. Semin Ophthalmol. 2003;18(2):50–7.
70. Iseri P, Altinaş O, Tokay T, Yüksel N. Relationship between cognitive impairment and retinal morphological and visual functional abnormalities in Alzheimer disease. J Neuroophthalmol. 2006;26(1):18–24.
71. Berisha F, Feke G, Trempe C, McMeel J, Schepens C. Retinal abnormalities in early Alzheimer's disease. Invest Ophthalmol Vis Sci. 2007;48(5):2285–9.
72. Paquet C, Boissonnot M, Roger F, Dighiero P, Gil R, Hugon J, et al. Abnormal retinal thickness in patients with mild cognitive impairment and Alzheimer's disease. Neurosci Lett. 2007;420(2):97–9.
73. Kesler A, Vakhapova V, Korczyn A, Naftaliev E, Neudorfer M. Retinal thickness in patients with mild cognitive impairment and Alzheimer's disease. Clin Neurol Neurosurg. 2011;113(7):523–6.
74. Kromer R, Serbecic N, Hausner L, Froelich L, Aboul-Enein F, Beutelspacher S, et al. Detection of retinal nerve fiber layer defects in Alzheimer's disease using SD-OCT. Front Psychiatry. 2014;5:22.
75. Kromer R, Serbecic N, Hausner L, Froelich L, Beutelspacher S. Comparison of visual evoked potentials and retinal nerve fiber layer thickness in Alzheimer's disease. Front Neurol. 2013;4:203.
76. Moreno-Ramos T, Benito-León J, Villarejo A, Bermejo-Pareja F. Retinal nerve fiber layer thinning in dementia associated with Parkinson's disease, dementia with Lewy bodies, and Alzheimer's disease. J Alzheimers Dis. 2013;34(3):659–64.
77. Marziani E, Pomati S, Ramolfo P, Cigada M, Giani A, Mariani C, et al. Evaluation of retinal nerve fiber layer and ganglion cell layer thickness in Alzheimer's disease using spectral-domain optical coherence tomography. Invest Ophthalmol Vis Sci. 2013;54(9):5953–8.

78. Kirbas S, Turkyilmaz K, Anlar O, Tufekci A, Durmus M. Retinal nerve fiber layer thickness in patients with Alzheimer disease. J Neuroophthalmol. 2013;33(1):58–61.
79. Larrosa J, Garcia-Martin E, Bambo M, Pinilla J, Polo V, Otin S, et al. Potential new diagnostic tool for Alzheimer's disease using a linear discriminant function for Fourier domain optical coherence tomography. Invest Ophthalmol Vis Sci. 2014;55(5):3043–51.
80. Ascaso F, Cruz N, Modrego P, Lopez-Anton R, Santabárbara J, Pascual L, et al. Retinal alterations in mild cognitive impairment and Alzheimer's disease: an optical coherence tomography study. J Neurol. 2014;261(8):1522–30.
81. Danesh-Meyer H, Birch H, Ku J, Carroll S, Gamble G. Reduction of optic nerve fibers in patients with Alzheimer disease identified by laser imaging. Neurology. 2006;67(10):1852–4.
82. Kergoat H, Kergoat M, Justino L, Chertkow H, Robillard A, Bergman H, et al. An evaluation of the retinal nerve fiber layer thickness by scanning laser polarimetry in individuals with dementia of the Alzheimer type. Acta Ophthalmol Scand. 2001;79(2):187–91.
83. Kergoat H, Kergoat M, Justino L, Robillard A, Bergman H, Chertkow H, et al. Normal optic nerve head topography in the early stages of dementia of the Alzheimer type. Dement Geriatr Cogn Disord. 2001;12(6):359–63.
84. Jellinger K. Alzheimer disease and cerebrovascular pathology: an update. J Neural Transm. 2002;109(5–6):813–36.
85. Parisi V, Pierelli F, Coppola G, Restuccia R, Ferrazzoli D, Scassa C, et al. Reduction of optic nerve fiber layer thickness in CADASIL. Eur J Neurol. 2007;14(6):627–31.
86. Katz B, Rimmer S, Iragui V, Katzman R. Abnormal pattern electroretinogram in Alzheimer's disease: evidence for retinal ganglion cell degeneration? Ann Neurol. 1989;26(2):221–5.
87. Trick G, Barris M, Bickler-Bluth M. Abnormal pattern electroretinograms in patients with senile dementia of the Alzheimer type. Ann Neurol. 1989;26(2):226–31.
88. Krasodomska K, Lubiński W, Potemkowski A, Honczarenko K. Pattern electroretinogram (PERG) and pattern visual evoked potential (PVEP) in the early stages of Alzheimer's disease. Doc Ophthalmol. 2010;121(2):111–21.
89. Sartucci F, Borghetti D, Bocci T, Murri L, Orsini P, Porciatti V, et al. Dysfunction of the magnocellular stream in Alzheimer's disease evaluated by pattern electroretinograms and visual evoked potentials. Brain Res Bull. 2010;82(3–4):169–76.
90. Strenn K, Dal-Bianco P, Weghaupt H, Koch G, Vass C, Gottlob I, et al. Pattern electroretinogram and luminance electroretinogram in Alzheimer's disease. J Neural Transm Suppl. 1991;33:73–80.
91. Kergoat H, Kergoat M, Justino L, Chertkow H, Robillard A, Bergman H, et al. Visual retinocortical function in dementia of the Alzheimer type. Gerontology. 2002;48(4):197–203.
92. Philpot M, Amin D, Levy R. Visual evoked potentials in Alzheimer's disease: correlations with age and severity. Electroencephalogr Clin Neurophysiol. 1990;77(5):323–9.
93. Justino L, Kergoat M, Bergman H, Chertkow H, Robillard A, Kergoat H, et al. Neuroretinal function is normal in early dementia of the Alzheimer type. Neurobiol Aging. 2001;22(4):691–5.
94. Pollock V, Schneider L, Chui H, Henderson V, Zemansky M, Sloane R, et al. Visual evoked potentials in dementia: a meta-analysis and empirical study of Alzheimer's disease patients. Biol Psychiatry. 1989;25(8):1003–13.
95. Partanen J, Hartikainen P, Könönen M, Jousmäki V, Soininen H, Riekkinen P, et al. Prolonged latencies of pattern reversal visual evoked early potentials in Alzheimer disease. Alzheimer Dis Assoc Disord. 1994;8(4):250–8.
96. Coburn K, Ashford J, Moreno M. Visual evoked potentials in dementia: selective delay of flash P2 in probable Alzheimer's disease. J Neuropsychiatry Clin Neurosci. 1991;3(4):431–5.
97. Moore N, Tucker K, Jann M, Hostetler R, Coburn K. Flash P2 delay in primary degenerative dementia of the Alzheimer type. Prog Neuropsychopharmacol Biol Psychiatry. 1995;19(3):403–10.
98. Shen Y, Shi Z, Jia R, Zhu Y, Cheng Y, Feng W, et al. The attenuation of retinal nerve fiber layer thickness and cognitive deterioration. Front Cell Neurosci. 2013;7:142.
99. Shen Y, Liu L, Cheng Y, Feng W, Shi Z, Zhu Y, et al. Retinal nerve fiber layer thickness is associated with episodic memory deficit in mild cognitive impairment patients. Curr Alzheimer Res. 2014;11(3):259–66.

100. Shi Z, Wu Y, Wang M, Cao J, Feng W, Cheng Y, et al. Greater attenuation of retinal nerve fiber layer thickness in Alzheimer's disease patients. J Alzheimers Dis. 2014;40(2):277–83.
101. Yu J, Feng Y, Xiang Y, Huang J, Savini G, Parisi V, et al. Retinal nerve fiber layer thickness changes in Parkinson disease: a meta-analysis. PLoS One. 2014;9(1):10.
102. Janssen S, Gorgels T, Ramdas W, Klaver C, van Duijn C, Jansonius N, et al. The vast complexity of primary open angle glaucoma: disease genes, risks, molecular mechanisms and pathobiology. Prog Retin Eye Res. 2013;37:31–67.
103. Ghiso J, Doudevski I, Ritch R, Rostagno A. Alzheimer's disease and glaucoma: mechanistic similarities and differences. J Glaucoma. 2013;5:S36–8.
104. Tamura H, Kawakami H, Kanamoto T, Kato T, Yokoyama T, Sasaki K, et al. High frequency of open-angle glaucoma in Japanese patients with Alzheimer's disease. J Neurol Sci. 2006;246(1–2):79–83.
105. Ou Y, Grossman D, Lee P, Sloan F. Glaucoma, Alzheimer disease and other dementia: a longitudinal analysis. Ophthalmic Epidemiol. 2012;19(5):285–92.

Chapter 8
Friedreich's Ataxia and More: Optical Coherence Tomography Findings in Rare Neurological Syndromes

Chiara La Morgia and Michele Carbonelli

Abstract Optic nerve and retinal involvement are a frequent finding in many neurodegenerative disorders. Optic atrophy can be severe and diffuse or sectorial and can be associated with visual complaints and reduction of visual acuity.

We here report the main optical coherence tomography (OCT) findings in rare neurological syndromes for which OCT data are available.

In Friedreich's ataxia, which is an autosomal recessive disease, there is evidence of subclinical optic neuropathy. OCT studies describe a diffuse reduction of the retinal nerve fiber layer (RNFL) thickness without a specific and preferential involvement of the papillo-macular bundle.

Jansky-Bielschowsky disease is a late infantile neuronal ceroid lipofuscinosis characterized by both retinal and optic nerve atrophy. Only one OCT study is available describing retinal abnormalities of various degrees.

DNA (cytosine-5)-methyltransferase 1 (DNMT1) disease is an autosomal dominant multisystem disorder characterized by the association of narcolepsy, deafness, sensory neuropathy and optic atrophy. The only OCT study available from our group describes the presence of subclinical optic atrophy more evident in the temporal quadrant.

Hereditary spastic paraplegia due to *SPG7* mutation is an autosomal recessive neurodegenerative disorder characterized by spastic paraparesis. RNFL thinning is a frequent and consistent finding in this disease.

Cerebral autosomal dominant arteriopathy with subcortical infarcts and leukoencephalopathy (CADASIL) is an autosomal dominant disorder in which retinal vascular changes and neurodegeneration of the neuroretina are frequent findings.

C. La Morgia, MD, PhD (✉)
IRCCS Institute of Neurological Sciences, Unit of Neurology, Bellaria Hospital, Via Altura, 3, 40139 Bologna, Italy

Department of Biomedical and Neuromotor Sciences, University of Bologna, Via Altura, 3, 40139 Bologna, Italy
e-mail: chiaralamorgia@gmail.com

M. Carbonelli, MD
IRCCS Institute of Neurological Sciences, Unit of Neurology, Bellaria Hospital, Bologna, Italy

A. Grzybowski, P. Barboni (eds.), *OCT in Central Nervous System Diseases: The Eye as a Window to the Brain*, DOI 10.1007/978-3-319-24085-5_8

Wolfram's disease is a disorder characterized by the occurrence of diabetes mellitus and optic atrophy. The only two OCT studies available report a diffuse optic atrophy which leads to a severe reduction of visual acuity.

Autosomal recessive spastic ataxia of Charlevoix-Saguenay (ARSACS) is a hereditary spastic ataxia due to progressive degeneration of the cerebellum and spinal cord, characterized by retinal nerve fiber hypertrophy detected by OCT.

Spinocerebellar ataxias (SCAs) are heterogeneous genetically determined disorders for which OCT studies available show variable findings ranging from isolated thinning of the temporal RNFL to retinal photoreceptor abnormalities.

Keywords Optical coherence tomography • Optic nerve • Retina • Macula • Fundus • Friedreich's ataxia • Jansky-Bielschowsky • Neuronal ceroid lipofuscinosis • DNMT1 • SPG7 • Cadasil • Wolfram syndrome • Autosomal recessive spastic ataxia of Charlevoix-Saguenay • Spinocerebellar ataxias

8.1 Friedreich's Ataxia

Friedreich's ataxia (FA) is an autosomal recessive slowly progressive neurodegenerative disorder starting usually in young adulthood or childhood [1]. FA is characterized by spinocerebellar and sensory ataxia with absence of deep tendon reflexes, dysarthria, hypertrophic cardiomyopathy and scoliosis [2]. FA is due to a GAA triplet expansion in the first intron of the frataxin gene (FXN) on chromosome 9q13-q21.1. A minority of FA patients are compound heterozygotes for the GAA triplet expansion and a point mutation [3].

Frataxin is a mitochondrial protein with a crucial role in the insertion of Fe-S cluster in different enzymes of the mitochondrial respiratory chain and in particular complex I, II and III and aconitase [4, 5]. The abnormal function of FXN leads to dysregulation of cellular iron metabolism with mitochondrial accumulation [6]. Evidence of mitochondrial defective respiration has been demonstrated in the heart and muscle of FA patients [7, 8]. Recent studies demonstrated that mitochondrial dysfunction induced by frataxin is also related to abnormal calcium handling in the mitochondria leading to increased autophagy [9]. Overall, frataxin deficiency leads to abnormal iron homeostasis [10] and increased oxidative stress [11, 12].

Visual system involvement is well characterized in FA [13]. In particular, abnormalities of the visual efferent system such as fixation instability (square wave jerks), saccadic dysmetria, disrupted pursuit, and vestibular abnormalities have been reported [13]. Moreover, optic neuropathy, optic radiation abnormalities and retinitis pigmentosa have been described in FA patients [14–19].

The optic neuropathy described in FA is usually asymptomatic and does not affect central vision [16]. The most severe visual phenotype has been associated with large GAA expansion of the FTX gene and with compound heterozygous mutations [16]. Visual evoked potentials demonstrated delayed latency and reduced

amplitude of the cortical responses [15, 16]. Visual field defects may vary from small paracentral or arcuate to diffuse and generalized defects [16]. Only rarely FA patients present an acute loss of visual acuity, which resembles Leber's hereditary optic neuropathy (LHON) [16].

A few optical coherence tomography (OCT) studies are available for FA. These described a diffuse reduction of the retinal nerve fiber layer (RNFL) thickness without a preferential involvement of the temporal quadrant [16–19], unlike mitochondrial optic neuropathies [20]. The severity of optic atrophy can be variable and usually is not associated with a subjective visual complaint [15, 16]. Specifically, time-domain OCT studies reported a generalized RNFL thinning in FA patients [16–18]. Interestingly, in the largest OCT series (63 FA patients) available to now, the only sector with a significant RNFL thinning was the superior [18] (Table 8.1).

Retinal nerve fiber layer thinning significantly correlated with age at onset and International Cooperative Ataxia Rating Scale (ICARS) in the series (n = 26) by Fortuna and coauthors [16]; with ICARS score, disease duration, visual acuity (VA) and low-contrast letter VA in the series (n = 23) by Noval and coauthors [17] and with VA, GAA repeat length, Friedreich's Ataxia Rating Scale (FARS) and age at onset in the series (n = 63) by Seyer and coauthors [18] (Table 8.1).

Table 8.1 Optical coherence tomography findings in FA

	OCT	N. of pts	Main findings	Correlations
Fortuna et al. [16]	TD-Stratus	26	↓avg RNFL ↓RNFL in all 4 sectors	ICARS, age at onset
Noval et al. [17]	TD-Stratus	17	↓avg RNFL in 75 % Temporal RNFL thickness normal Normal Macular morphology and thickness	ICARS, disease duration, VA, low-contrast VA
Seyer et al. [18]	TD-Stratus	63	↓RNFL (52.7 % of eyes below 5th percentile of controls) Only superior thickness significantly lower	VA, GAA expansion, age at onset, FARS
Seyer et al. [18]	SD-Cirrus	23	Macular thickness below the 1st percentile of controls in 20.7 %	Not significant
Dağ et al. [19]	SD	10	↓avg RNFL ↓RNFL in all 4 quadrants ↓Peripapillary and foveal retinal thickness Choroidal thickness not significant ↓GC thickness in superior and inferior macula	VA, ICARS (RNFL thickness) Disease duration (foveal thickness)

RNFL retinal nerve fiber layer, *avg* average, *ICARS* International Cooperative Ataxia Rating Scale, *FARS* Friedreich's Ataxia Rating Scale, *VA* visual acuity

The only spectral domain (SD) OCT study available to date documented a reduction of the average RNFL thickness and in all four optic disc sectors in 10 FA patients [19]. Moreover, ganglion cell thickness was significantly reduced in superior and inferior macula [19] (Table 8.1).

Macular thickness has been reported as normal in one study [17], significantly reduced [19] and below the 1st percentile of controls in 20.7 % of the FA patients examined in another series [18] (Table 8.1).

Correlation of OCT measurement with VA is not consistent across the studies and the degree of VA loss is reported as variable, but usually not clinically significant [16, 17]. Differently, low contrast visual acuity is significantly reduced in FA patients [17]. Fundus oculi abnormalities are detected only in a small percentage of the FA subjects with loss of retinal nerve fibers documented by OCT [17].

Overall, OCT measurements in FA are able to detect subclinical optic neuropathy in the large majority of FA cases (about 70 %) being a more sensible measure of optic nerve degeneration than other metrics (visual acuity, visual fields and/or fundus examination). It is not clear yet why the papillomacular bundle is not primarily affected in FA, even if a mitochondrial dysfunction is well known in FA.

In line with OCT data, visual evoked potentials (VEPs) documented an increased P100 latency and reduced amplitude of cortical responses [15, 16] in the large majority of patients. These electrophysiological and anatomical data suggest a slowly progressive degeneration of the anterior and posterior optic pathway, as proved also by the increased diffusion in optic radiations demonstrated in FA patients by magnetic resonance imaging studies [16].

An example of time-domain OCT and Humphrey visual fields is provided for a 15 year-old FA patient, who started presenting ataxia and dysarthria since she was 11 years old (Fig. 8.1).

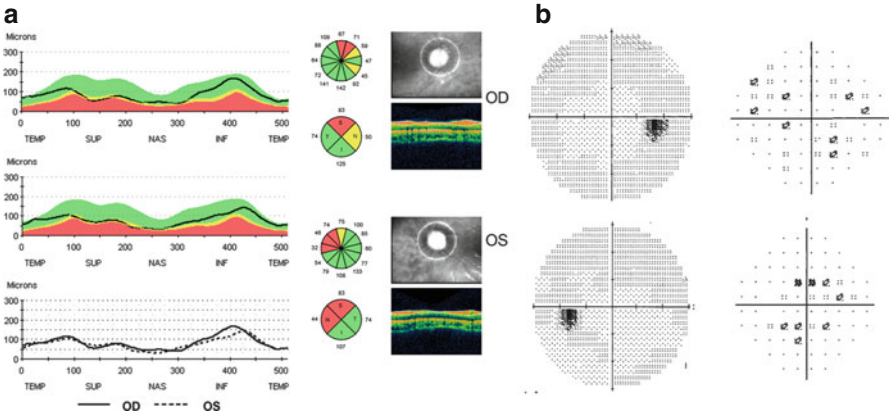

Fig. 8.1 OCT findings in a FA patient. (**a**) Time-domain OCT shows RNFL thinning in the supero-nasal sectors in both eyes. (**b**) Visual fields (total deviation on right) show mild reduction of the sensitivity bilaterally

8.2 Jansky-Bielschowsky Disease (CLN2)

Jansky-Bielschowsky disease (JBD) is a late infantile neuronal ceroid lipofuscinosis (LINCL) disorder due to mutation of the *CLN2* gene (cr 11p15), which encodes for the tripetidylpeptidase 1 protein [21, 22]. Similarly to other Neuronal Ceroid Lipofuscinosis (NCL) JBD is a lysosomal storage disease characterized by the accumulation of autofluorescent material in the cytoplasm of neurons [23]. JBD disease is characterized by mental and motor retardation, psychomotor regression, ataxia, seizures and visual dysfunction [23].

Visual dysfunction is common in NCL and usually manifests early in juvenile forms and later in the LINCL [24]. The typical ocular manifestation of NCL is retinal degeneration of variable severity (from mild pigmentary changes to Bull's eye maculopathy to severe outer retina atrophy) [24]. Retinal changes in LINCL have been documented by fundus oculi examination, histopathology and electrophysiological studies [24–27]. Furthermore, the presence of inner retina and optic nerve degeneration has been demonstrated in different animal models of NCL [28–31]. Besides outer retina degeneration, optic atrophy is a frequent finding in LINCL [25, 32]. The only OCT study available to now in JBD applied a comprehensive ophthalmologic evaluation in 25 LINCL patients with mutations in the *CLN2* gene [33]. The protocol included fundus oculi, spectral domain macula OCT, fluorangiography and indocyanine green angiography (IGA) and was carried out under anesthesia. The results obtained were used to generate a Weill Cornell LINCL Ophthalmologic Severity Scale score. According to the degree of pigmentary changes at fundus oculi examination, Fluorangiography and IGA and the severity of outer retina degeneration documented by OCT the patients were graded as score 0-5 (from normal to severe changes). The average score in this case series was 2.6. This score correlated strongly with the neurological score suggesting that the retinal involvement is parallel to the neurological deterioration. Interestingly, the authors failed to document any abnormality in the anterior segment, at difference with other lysosomal storage diseases. The posterior segment showed variable degrees of optic nerve and retinal atrophy. In particular, retinal degeneration typically starts from the fovea in which the first pigmentary changes are visible expanding to the far periphery [33]. The OCT was able, in this case series, to detect subtle abnormalities not visible at fundus examination or with FA. The OCT changes documented by Orlin and coauthors for the 5 stages were: *Stage 1*: normal; *Stage 2*: Normal retinal layers immediately adjacent at fovea; immediately outside fovea, outer retinal/photoreceptor atrophy; *Stage 3*: Outer retinal atrophy/photoreceptor loss extending to 1.0 disc diameter from fovea; retinal layers appear normal outside fovea; *Stage 4*: Early buildup of outer retinal hyper-reflective material in macula; more extensive outer retinal abnormalities extending 1.0–2.0 disc diameters from fovea; beyond 2.0 disc diameters, outer retina appears normal; *Stage 5*: Severe retinal thinning with generalized loss of photoreceptors and outer retina, involving the entire macula; extensive clumps of outer retinal hyper-reflective material; thickness map shows central thinning with paracentral thickening, with outer ring of further thinning (with bull's eye

appearance); outer retinal changes also found outside the macula [33]. The majority of patients in this case series presented normal or mildly abnormal ocular findings (32 % stage 0, 24 % stage 1, 8 % stage 3, 24 % stage 4 and 12 % stage 5) [33].

8.3 DNMT1 Disease

DNA (cytosine-5)-methyltransferase 1 (DNMT1) disease is a complex neurodegenerative disorder due to autosomal dominant mutations in the *DNMT1* gene (DNA-methyltransferase 1) [34].

Two distinct phenotypes have been described in association with mutations in the *DNMT1* gene: the autosomal dominant cerebellar ataxia, deafness and narcolepsy (ADCA-DN) [35] associated with mutations in exon 21 of the *DNMT1* gene and the hereditary sensory autonomic neuropathy with dementia and hearing loss type IE (HSAN IE), described in association with mutations in exon 20 [34]. Recently, our group demonstrated that the boundaries between these two distinct entities are less pronounced [36]. In fact, both diseases share the presence of narcolepsy as a prominent feature [36]. Moreover, we demonstrated that subclinical optic atrophy is a common finding to both phenotypes [36].

Visual acuity was normal in all five DNMT1 patients included in the study (two with the ADCA-DN and three with the HSAN IE phenotype). Fundus oculi disclosed temporal pallor in one ADCA-DN case, diffuse pallor in the other ADCA-DN and mild temporal pallor of the optic disc in all three HSAN IE subjects. Pattern VEPs were abnormal in both ADCA-DN probands, showing increased latency and decreased amplitude of cortical responses, whereas they were normal in HSAN IE patients [36]. OCT showed reduction of the RNFL thickness more evident in the temporal than in the superior and inferior quadrants with nasal sparing in one ADCA-DN patient, more diffuse in the other ADCA-DN patient with nasal sparing. In the HSAN IE cases OCT disclosed a diffuse reduction of retinal nerve fiber layer thickness in one case, a diffuse reduction with nasal sparing in the second case, and temporal and less evident superior/inferior quadrants thinning in the third case.

Macular ganglion cell layer (GCL) analysis disclosed diffuse atrophy in both ADCA-DN probands and diffuse thinning in all three HSAN IE subjects [36].

An example of spectral-domain OCT (RNFL and macular GCL) and fundus oculi image is reported for a DNMT1 patient carrying the p.Gly605Ala mutation [36] (Fig. 8.2).

Interestingly, optic atrophy was previously reported in the ADCA-DN phenotype [37, 38] but never described in the HSAN IE phenotype. OCT investigation in our DNMT1 case series revealed a subclinical optic nerve involvement in all cases with a prevalent involvement of the temporal sector and relative nasal sparing that resembles the pattern observed in mitochondrial optic neuropathies [20]. The mitochondrial pattern of optic nerve degeneration may be explained by the possible effect of defective methylation of nuclear DNA on nuclear encoded mitochondrial proteins [39] or a direct effect on DNA methylation of the mitochondrial-targeted isoform of DNMT1 [40, 41].

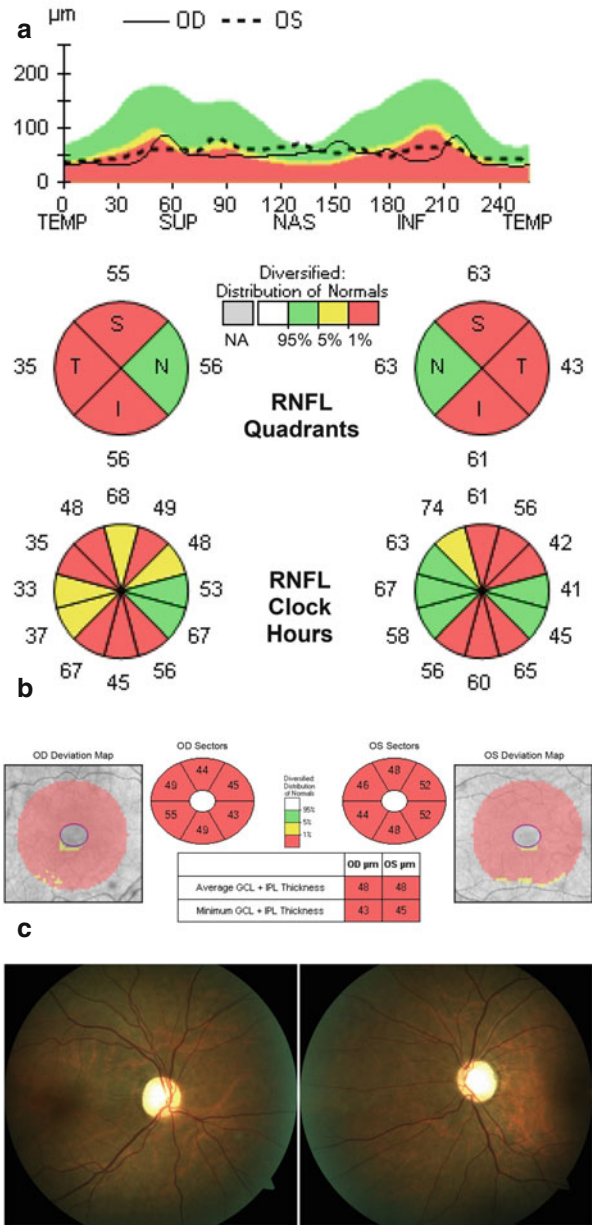

Fig. 8.2 OCT findings of a DNMT1 patient with the ADCA-DN phenotype. (**a**) Spectral-domain OCT shows diffuse thinning of the RNFL thickness in both eyes. (**b**) Macular ganglion cell layer (*GCL*) analysis discloses diffuse atrophy. (**c**) Fundus oculi examination shows diffuse pallor bilaterally

8.4 Hereditary Spastic Paraplegia Due to SPG7 Mutations

Hereditary spastic paraplegias (HSP) are a heterogeneous group of neurodegenerative disorders characterized by a variable phenotypic expression, which includes a pure spastic paraparesis or "uncomplicated" and a "complicated" form. The genetic basis of HSP is heterogeneous including autosomal dominant, autosomal recessive, X-linked, or maternally inherited (mitochondrial) inheritance [42].

To date, more than 56 HSP loci and 41HSP-related genes have been identified [42].

Mutations in the *SPG7* gene are responsible for autosomal recessive SPG7-HSP. The first *SPG7* mutation was identified in 1998 [43, 44]. *SPG7* gene encodes for paraplegin, which is a metalloprotease protein belonging to the AAA (ATPase associated with various cellular activities) proteins. Paraplegin is a mitochondrial protein localized to the inner mitochondrial membrane and it assembles with the paralogous AFG3L2 protein in the mAAA protease complex [45–47]. Mitochondrial dysfunction has been described in SPG7 pedigrees including OXPHOS defects in muscle biopsy [43, 48]. Interestingly, mAAA protease like paraplegin plays also a role in the processing of the OPA1 protein [49]. Given the mitochondrial pathogenesis of SPG7 HSP the presence of optic atrophy is expected, but not systematically investigated. Optic atrophy has been reported in the first identified pedigrees [43, 44, 48]. Recently, Klebe and coauthors extensively described the phenotype of 23 SPG7 families. In a subgroup (n = 10) investigated by OCT, RNFL thinning was detected in 100 % of cases even if it was symptomatic only in one case, associated with reduced visual acuity in 40 % and with optic disc pallor at fundus examination in 50 % of cases. These data suggest that the OCT investigation may detect subtle abnormalities in SPG7 patients and the presence of optic atrophy in the context of an autosomal recessive spastic paraplegia should point to the *SPG7* gene. In this case series one French pedigree positive for the SPG7 mutation presented with an isolated autosomal dominant early onset (1st decade of life) progressive optic atrophy. Electroneurography disclosed in this pedigree also the presence of mixed peripheral polyneuropathy [50].

On the basis of the clinical findings of this cohort the authors proposed that *SPG7* gene should be screened in autosomal recessive or sporadic HSP patients with middle-age onset particularly if spastic paraplegia is associated with cerebellar atrophy/signs and/or optic neuropathy (also if detected only with OCT).

Van Gassen and coauthors, in another large SPG7 Dutch case-series (n = 49), demonstrated the presence of a severe optic atrophy with childhood onset in two siblings carrying a homozygous missense mutation (p.Arg470Gln, exon 10) *SPG7* mutation and in one case with compound heterozygous (p.Arg485_Glu487 and p.Leu706fs) *SPG7* mutation. For one of the p. Arg470Gln mutation carriers, postmortem tissues including the optic nerve were available. In this case a severe optic atrophy was documented. Interestingly, the p. Arg470Gln mutation was located in the ATPase AAA core domain and the authors hypothesized that the severe optic nerve involvement can be explained by a possible deleterious interaction of SPG7 with OPA1. Unfortunately, for these patients OCT data were not available [51].

Moreover, Marcotulli and coauthors have recently described a 43-year-old male SPG7 case presenting with severe congenital optic atrophy. This patient developed spastic paraparesis at 30 years of age. OCT documented reduced RNFL and macular thickness [52].

Overall, these data suggest that optic neuropathy is a common finding in SPG7-related HSP and the use of OCT screening in large cohort of HSP patients might be a useful tool to reveal subclinical optic atrophy and guide the diagnostic process.

Finally, Wiethoff and coauthors conducted an OCT study on 28 HSP patients including "pure" (n = 22) and "complicated" (n = 6) HSP demonstrating a significant reduction of the RNFL only in the "complicated" group. The case series included also 3 SPG7 cases and two of them with a complicated phenotype disclosed global RNFL thickness reduction, especially in the temporal quadrant [53].

8.5 CADASIL

Cerebral autosomal dominant arteriopathy with subcortical infarcts and leukoencephalopathy (CADASIL) is an autosomal dominant disorder characterized by the occurrence of juvenile subcortical ischemic events, migraine, epilepsy, psychiatric disturbances and cognitive impairment in variable combinations [54]. Brain MRI typically shows T2 hyperintensity involving the white matter of the temporal pole and/or the external capsulae, but the severity of white matter involvement can be highly variable evolving in most cases to a diffuse bilateral subcortical leukoencephalopathy [55].

CADASIL is due to mutations of the *NOTCH3* (*Neurogenic locus notch homolog protein 3*) gene, located on chromosome 19 [56]. Notch3 is a protein mainly expressed in vascular smooth cells with a crucial role in the control of vascular tone [57]. Cerebral vasculopathy is the main hallmark of the disease, due to the degeneration of the vascular smooth muscle cells with deposition of granular osmiophilic material, but also retinal vascular changes have been described in CADASIL [58–61]. These changes include retinal arteriolar narrowing, ateriovenous nicking and arteriolar sheating [59, 61]. Moreover, electrophysiological [62], histological [63] and OCT studies [61, 64, 65] documented a specific neurodegeneration of the neuroretina in CADASIL. In particular, Parisi and coauthors demonstrated by time-domain OCT a diffuse reduction of the RNFL thickness involving all the quadrants in 6 CADASIL patients (three asymptomatic mutation carriers) [64]. The authors interpreted these findings as secondary to the chronic vascular changes characterizing the disease. Similarly, Rufa and coauthors demonstrated with time-domain OCT a diffuse RNFL thinning in all optic nerve quadrants except the nasal one in 17 CADASIL patients. In particular, this thinning was more evident in the superior sector [65]. Similarly, fundus oculi examination revealed neuroretinal rim pallor in 41 % and a crowded optic disc in 18 % of the 34 CADASIL patients described by Pretegiani and coauthors. The optic nerve involvement in CADASIL is also confirmed by histological findings in a postmortem study, which demonstrated diffuse demyelination of the optic nerve and chiasm with loss of nerve fibers [63]. The loss

of fibers in the optic nerve is usually not associated with a reduction of the visual acuity and can be associated with variable visual field defects [61].

8.6 Wolfram Syndrome

Wolfram syndrome (WS) was first described in 1938 [66]. It is a rare neurodegenerative disorder characterized by the occurrence of diabetes mellitus and optic atrophy starting in childhood and a variable association of diabetes insipidus, other endocrinopathies, deafness, cerebellar ataxia, neurogenic bladder, cardiomyopathy and psychiatric disturbances [67]. In fact, it is also known as DIDMOAD (Diabetes Insipidus, Diabetes Mellitus, Optic Atrophy) [68, 69]. Usually diabetes is the first sign of the disease. Optic atrophy appears in the first-second decade of life and it is severe in most cases [68, 70]. Wolfram's disease is due to mutations in the wolframin gene (*WFS1*) [71] and in the large majority of cases is inherited in an autosomal recessive fashion, but autosomal dominant inheritance has also been reported [72]. In these latter cases optic atrophy can be milder [72] and can be associated with deafness without diabetes [73]. Autosomal dominant mutations in the *WFS1* gene have been associated also with non-syndromic deafness [74], diabetes [75] and cataract [76]. Neuropathological studies reported atrophy of the optic nerve, chiasm, lateral geniculate nucleus, optic tracts and occipital cortex in WS [77–81].

The only OCT data available for WS are derived from two case reports. In one [82], spectral domain OCT documented a diffuse optic atrophy more evident in the superior and inferior quadrants in a 21 year-old male. Bucca and coauthors reported time-domain findings in a 13 year-old female showing loss of retinal nerve fibers in the temporal quadrant [83]. Interestingly, a recent postmortem study documented a specific pattern of optic atrophy predominantly involving the temporal and inferior quadrants, i.e. the papillomacular bundle of the optic nerve, in a WS case. This pattern resembles that described in mitochondrial optic neuropathies [81].

We here show the OCT findings of three WS patients with a brief summary of their clinical history.

Case 1
The first case is a 25 year-old male who presented diabetes mellitus since he was 3 years old. Optic atrophy was documented at 10 years of age. He also presented hearing loss and psychiatric disturbances since 15 years of age. Genetic analysis showed the presence of compound heterozygous mutations in the *WFS1* gene T461P and A559T.

Visual acuity was 0.16 in OD and 0.1 in OS. Fundus oculi examination revealed diffuse optic atrophy. Brain MRI at 17 years of age was normal. OCT demonstrated diffuse bilateral optic atrophy (Fig. 8.3a, upper panel). Humphrey visual fields (VFs) showed a diffuse defect bilaterally (Fig. 8.3a, lower panel).

Case 2
This 22 year-old female presented growth hormone deficiency at 8 years of age and diabetes mellitus at 10 years. She suffered from migraine since she was 17 years old,

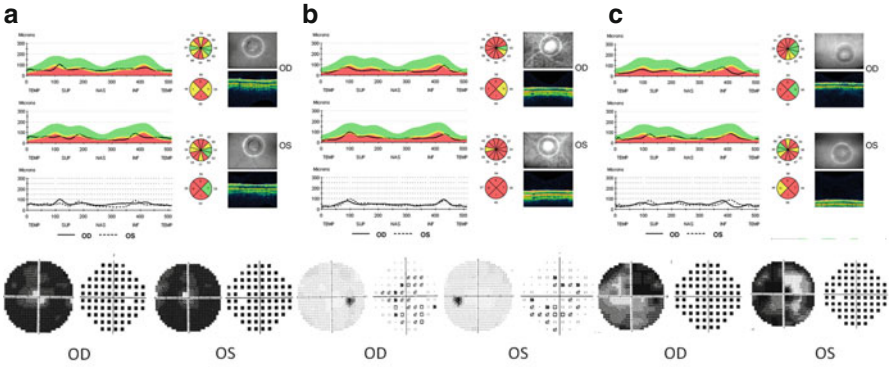

Fig. 8.3 OCT findings in Wolfram disease patients. (**a**) OCT demonstrates in this 25-year-old male a diffuse RNFL thinning in both eyes (*upper*) corresponding to a diffuse reduction of the sensitivity at visual fields (gray scale and total deviation). (**b**) OCT reveals in this 22-year-old female diffuse optic atrophy. Visual fields show a mild diffuse reduction of sensitivity (gray scale and total deviation). (**c**) OCT shows in this 39 year-old male diffuse optic atrophy. Visual fields reveal a diffuse reduction of the sensitivity bilaterally (gray scale and total deviation)

age at which optic atrophy was also discovered. Genetic analysis showed the presence of compound heterozygous mutations c.409_426dup16 and c.2104 G>A in the *WFS1* gene. Brain MRI at 22 years of age was normal. Visual acuity was 0.4 in OD and 0.5 in OS. OCT demonstrated diffuse thinning of the retinal nerve fibers (Fig. 8.3b, upper panel). VFs showed a mild diffuse reduction of sensitivity (Fig. 8.3b, lower panel).

Case 3

This 39-year-old male presented diabetes since he was 13 years old. Since the age of 10 years he complained of progressive visual loss with evidence of optic atrophy at 13 years of age.

Genetic investigation revealed the presence of compound heterozygous mutation in the *WFS1* gene (c.2002C>T;p. Gln668X e c.2126 T>G;p. Val709Gly).

Brain MRI at 39 years old showed cerebellar, pons and mesencephalon atrophy, optic nerve, chiasm and occipital cortex atrophy with gliosis of optic radiations.

Visual acuity was 0.02 in OD and 0.05 in OS. OCT showed bilateral diffuse optic atrophy (Fig. 8.3c, upper panel). VFs disclosed diffuse reduction of sensitivity bilaterally (Fig. 8.3c, lower panel).

8.7 Autosomal Recessive Spastic Ataxia of Charlevoix-Saguenay (ARSACS)

Autosomal recessive spastic ataxia of Charlevoix-Saguenay (ARSACS) is a complex hereditary neurodegenerative disorder characterized by early childhood-onset cerebellar ataxia [84], peripheral neuropathy [85] and pyramidal tract signs [86, 87].

The name of the disease derives from its high prevalence, as a result of a founder effect, in the French-Canadian population of the Charlevoix-Saguenay region in the northeast of Quebec. After these initial reports, ARSACS was also described in other countries and ethnic groups worldwide [88, 89].

ARSACS is due to mutations in the *SACS* gene, which were first identified by Engert and coauthors in 2000. The *SACS* gene is located on chromosome 13q12.12 and encodes the protein sacsin with a chaperone activity [90–92]. Furthermore, a recent study on a sacsin-knockout mouse model described a disruption of mitochondrial fission/fusion dynamics [93].

The majority of ARSACS patients show early ocular signs including: alteration of smooth ocular pursuit and prominent myelinated fibers radiating from the optic disc and embedding the retinal vessels. These myelinated fibers are visible at fundoscopy and were considered the main clinical manifestations of ARSACS. However, the presence of myelinated fibers was rarely described in non-Quebec patients [94–101].

In the original characterization of ARSACS the authors described yellow streaks of hypermyelinated fibers that focally cover the retinal vessels, emanating radially from the edges of the optic disc [88]. In recent years, with the advent of new and more sophisticated quantitative retinal imaging technologies, the nature of the myelinated fibers in ARSACS has been debated.

In 2011, different OCT studies demonstrated that the typical fundoscopic appearance in ARSACS patients is due to the increased hyper-reflectivity and thickness of the peripapillar RNFL and not to the presence of myelinated fibers [102–104].

Monochromatic RNFL images (through a blue filter), showing enhanced visibility of the RNFL and OCT demonstrated an increase in RNFL thickness in ARSACS patients compared with healthy controls.

Vingolo and coauthors [102] showed that the absence of shadowing behind the fibers in the OCT of ARSACS patients differentiates them from subjects with persistent myelinated fibers. In the latter, in fact, OCT clearly revealed a posterior shadowing, due to the hyper-reflectivity of the myelinated areas, which does not allow the OCT infrared laser to cross the retina (Fig. 8.4).

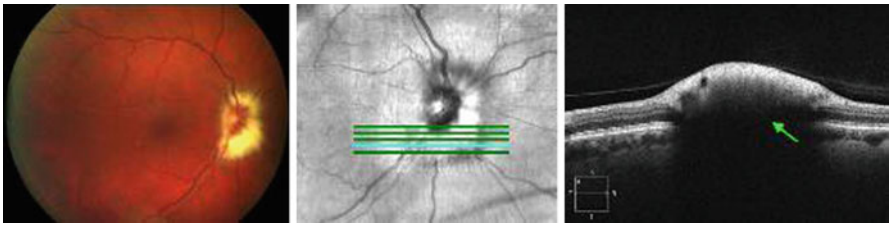

Fig. 8.4 OCT findings in persistent myelinated fibers. In the left panel fundus oculi of persistent myelinated fibers. In the middle and right panels OCT of myelin fibers: thickening of the retinal fibers hiding the deep layers of retina (*green arrow*) (From Desserre et al. [104], with kind permission of Springer Science + Business Media)

The thickening of the retinal fibers in the peripapillar region in ARSACS also includes the macula. Thus, the average macular thickness (mainly in nasal quadrant) and the average foveolar thickness may be increased in ARSACS patients [104] (Fig. 8.5).

Typically, in ARSACS patients visual acuity is normal or slightly reduced, and only mild and peripheral visual defects are reported. These findings overall support the absence of myelin deposition in the retina of these patients, given that the presence of myelin, would have caused more evident visual field defects [105].

Thus, it is preferable to use the term "pseudomyelination" [102] or "retinal nerve fiber hypertrophy" [103] to define the retinal aspect of patients with ARSACS. In

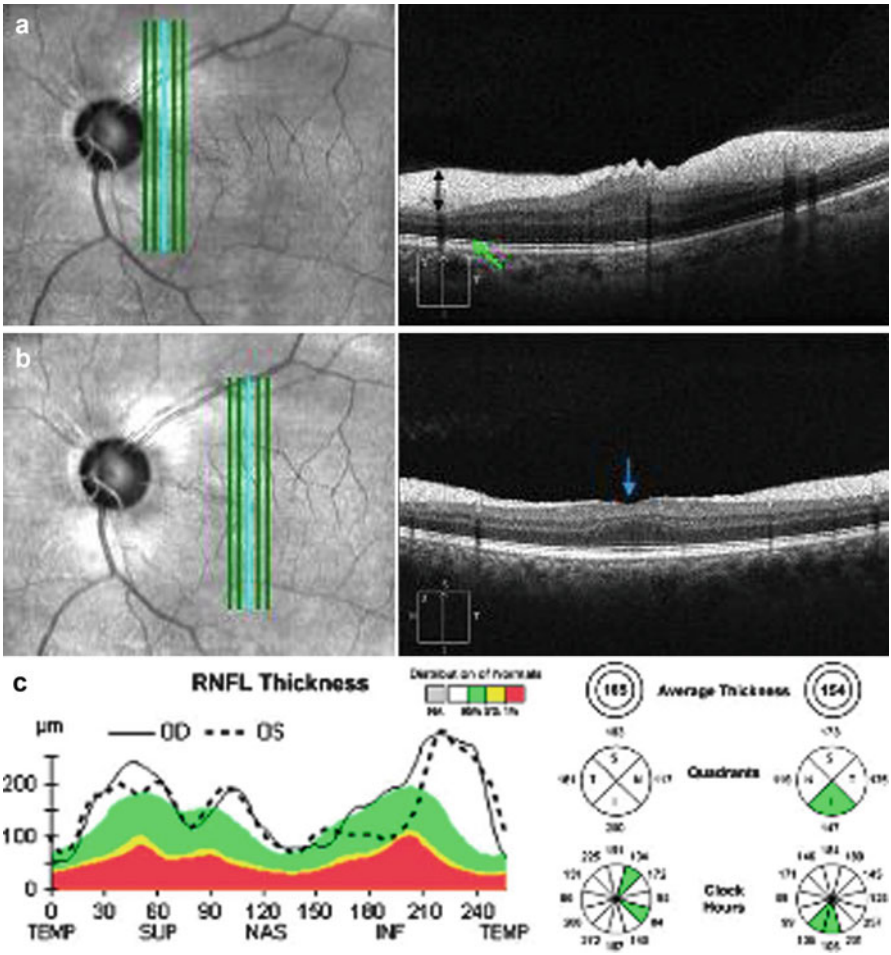

Fig. 8.5 OCT findings in ARSACS patient. (**a**) OCT: hypertrophia of the nerve fiber layer (*black arrow*), absence of attenuation of the deep layers of retina (*green arrow*). (**b**) Filling of the foveolar depression (*blue arrow*). (**c**) Increased thickness of peripapillar RNFL predominant in upper and lower temporal (From Desserre et al. [104]; with kind permission of Springer Science + Business Media)

fact, the recent OCT findings, at least among non-Quebec patients, suggest that retinal hypermyelination has been used inappropriately to describe the striated appearance of a thickened RNFL around the optic discs in ARSACS patients [106]. Yu-Wai-Man and coauthors in 2013 have proposed the speculative hypothesis that the RNFL thickening in ARSACS could be related to the axoplasmic stasis within the long axons of the retinal ganglion cells as they converge to form the optic nerve in the anatomically tight region of the lamina cribrosa [106].

8.8 Spinocerebellar Ataxias (SCAs)

Spinocerebellar ataxias (SCAs) are a genetically heterogeneous group of autosomal dominant neurodegenerative disorders characterized by ataxia, ocular motor abnormalities, and variable other neurological features, such as pyramidal tract, basal ganglia or brainstem dysfunction [107, 108]. The SCAs are classified on the basis of the genotype. SCA1, 2, 3, and 6, the most common ones, are caused by a trinucleotide CAG repeat expansion encoding glutamine in four unrelated proteins. SCA1, 2, and 3 are characterized by cerebellar degeneration and variable degrees of involvement of other central nervous system regions, whereas SCA6 is associated with a nearly pure cerebellar atrophy [107].

Abnormal afferent visual testing and optic atrophy have been described as a feature of SC1, SCA2 and SCA3 [109, 110]. Rarely, SCA2 is also associated with retinitis pigmentosa, most notably in the infantile form with extremely expanded CAG repeats [111], and pigmentary retinopathy has been reported in a patient homozygous for a pathological repeat expansion in the SCA6 gene [112].

Unlike other SCAs, patients with SCA7 exhibit a spectrum of severity of retinal disease from mild to severe dysfunction. Early functional abnormalities occur in both cones and rods, but greater centrally than peripherally [113, 114].

8.8.1 Spinocerebellar Ataxia Type 2-3-6 (SCA2-3-6)

Pula et al. [115] in a spectral-domain OCT study reported in 29 SCA and cerebellar multisystem atrophy patients (SCA1-2-3-6 and MSA-C) a significant reduction of the peripapillar RNFL thickness for SCA2 and SCA3 patients only. This RNFL thinning correlated with the severity of the disease (Scale for the Assessment and Rating of Ataxia, SARA score).

Another study by Alvarez and colleagues [116] demonstrated a significant reduction of the average RNFL thickness in nine SCA3 patients compared to age- and sex-matched controls. There was a reduction in the RNFL thickness in all quadrants except the temporal one, preserved in all eyes. Therefore, papillomacular bundle probably is not primarily involved in SCA-3 and consequently visual acuity is preserved in these patients (mean BCVA 20/25 and normal colour vision in all patients, except for the one

with congenital dyscromatopsia). RNFL thickness was inversely correlated to SARA score. The mean macular thickness was lower compared to the control group only in two eyes (11.11 %). In four patients, (eight eyes) OCT studies were performed with an average follow-up of 14.25 months, and in five eyes (62.50 %) there was a trend towards a RNFL thickness reduction. Thus, the authors concluded that the pattern of the optic nerve involvement in SCA-3 is more similar to that observed in Alzheimer's and Parkinson's disease than to SCA-1 and toxic or mitochondrial optic nerve diseases where there is a preferential involvement of the papillo-macular bundle [116].

8.8.2 Spinocerebellar Ataxia Type 1 (SCA1)

Spinocerebellar ataxia type 1 (SCA1) is an autosomal dominantly inherited, late-onset neurodegenerative disease primarily affecting the cerebellar cortex and brainstem. Affected patients suffer from disturbed motor coordination, slurred speech, dysphagia, spasticity, extrapyramidal movements such as dystonia or chorea, cerebellar oculomotor disturbances, ophthalmoparesis, saccade slowing and cognitive impairment [117].

SCA1 is due to a CAG-repeat expansion of variable length reaching between 39 and 83 repeats encoding for a prolonged polyglutamine chain in the *ATXN1* gene on chromosome 6p23 encoding for the ataxin1 protein [117].

In SCA1 patients, besides the well-described cerebellar oculomotor abnormalities, there is also evidence of ocular pathology. There is evidence of visual acuity reduction, color vision impairment and central scotoma or contraction of visual fields [118, 119]. In some case series there is evidence of worsening of ocular symptoms with disease duration [120, 121]. The reduced visual acuity in SCA1 has been attributed to optic atrophy, which was first described at fundus examination [121]. Optic nerve involvement was also suggested by abnormal VEP findings in SCA1 patients [122, 123]. However, VEPs were normal in 40–50 % of SCA1 patients and retinal or optic nerve pathology was not consistently reported in SCA1 [124].

Stricker et al. [125], in a series of 9 SCA1 subjects compared to age- and sex-matched controls, demonstrated with OCT a pattern of temporal atrophy of the RNFL in most of the patients, suggesting a preferential involvement of the papillo-macular bundle. Segmentation analysis of the retina confirmed temporal RNFL thickness reduction whereas there was no significant difference in the average ganglion cell layer, inner and outer plexiform layer, photoreceptor layer and pigment epithelium. SCA1 patients showed a reduction in visual acuity and average RNFL thickness compared to healthy controls (84.0 μm vs. 97.2 μm) RNFL thinning was predominant and significant in temporal sectors ($p < 0.001$,) and was not found in nasal sectors. OCT findings were correlated with disease duration and disease severity measured by SARA score. The patient with the longest disease duration and highest SARA score showed additional severe macular atrophy, indicating that, at a later disease stage, nerve fiber atrophy could lead to ganglion cell degeneration and consecutively to macular volume reduction. Differently, VEP P100 latencies were not significantly different between SCA1 patients and controls [125].

The authors speculated that the selective temporal RNFL involvement could be explained by a differential vulnerability of the parvocellular axons to mutated ataxin1. In fact, the pattern of temporal RNFL thinning seen in these SCA1 patients could be due to localized oxidative dysfunction, which does not involve the magnocellular ganglion cell axons and the photoreceptors [125].

In 2013, two different groups [118, 119] simultaneously described a case series of six SCA1 patients presenting with progressive maculopathy and retinal dysfunction. The patients exhibited bilateral, progressive painless visual loss with macular drusen and mild pigmentary alterations at fundus examination.

In particular, Vaclavik and coauthors [119] showed two genetically confirmed SCA1 patients with bilateral areas of hypopigmented retinal pigment epithelium within the macula. Autofluorescence imaging revealed a central macular hyperautofluorescence surrounded by a ring of hypoautofluorescence. Spectral-domain OCT disclosed bilateral hyporeflective "foveal cavitation" corresponding to loss of the highly reflective inner segment/outer segment junction, as well as thinning of the outer nuclear layer. Outside the macula, the retina was within normal range. Fluorescein angiography showed small areas of patchy hyperfluorescence in the macula, corresponding to areas of depigmented retinal pigment epithelium without any leakage at later stages. Goldmann kinetic manual perimetry revealed a relative central scotoma bilaterally. The retinal function was tested using full-field ERG which was within normal limits under photopic and scotopic conditions. Multifocal electroretinography (mfERG) was not performed [119].

Two other patients with bilateral foveal cavities had OCT features similar to those reported previously in achromatopsia [126], and cone dystrophy [127], whereas RNFL thickness was not evaluated. Similarly, Lebranchu and coauthors reported a SCA1 family with maculopathy [118]. Four SCA1 patients showed central scotoma in most of the eyes at visual field examination and visual acuities ranged between 20/20 and 20/200. Central retinal thinning with disorganized photoreceptor layers or foveal cavitation were found at OCT. Two patients showed mild temporal optic disc pallor at fundoscopy and thinning of the temporal RNFL at OCT, confirming the involvement of the papillomacular bundle [118]. In one patient, multifocal electro-

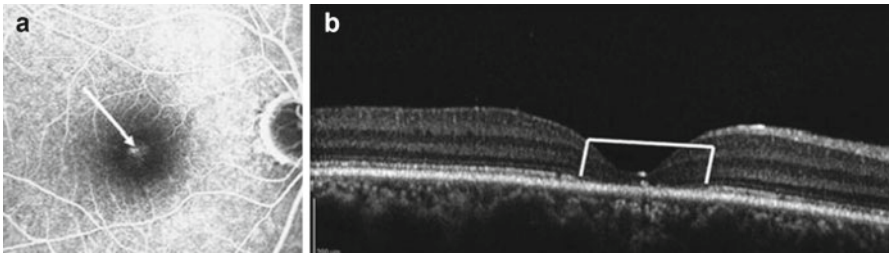

Fig. 8.6 OCT findings in SCA7 maculopathy. (**a**) Fluorescein angiography shows a small central window defect in the macula (**b**) Optical coherence tomography image shows foveal photoreceptor loss between the outer nuclear layer and retinal pigment epithelium in a patient with SCA7 maculopathy (From Kumar and Pulido [131]; with kind permissions of Springer Science + Business Media)

retinography (mfERG) revealed central retinal dysfunction. In these patients, OCT demonstrated alterations of the external layers of the fovea, suggesting a loss of structural integrity of the photoreceptors. The authors suggested that foveolar cavitation associated with the thinning of the whole macular area (including the surrounding perifoveolar retina) could be related to a cone dystrophy, as supported by the fact that a cluster of genes (*GUCA1A, PRPH2*) involved in macular diseases is located in a chromosome region (6p21.1) near the *SCA1* gene [118].

8.8.3 Spinocerebellar Ataxia Type 7 (SCA7)

Spinocerebellar ataxia type 7 (SCA7) is a progressive ataxia that is characterized by a high prevalence of retinal photoreceptor abnormalities. Recent studies suggest that the retinopathy of SCA7 is a cone-rod dystrophy [113, 114]. This degenerative retinopathy initially affects cones, and then progresses to cone–rod dystrophy [113]. Fundus examination demonstrates macular pigmentary changes, sometimes associated with mild temporal optic disc pallor [128]. The gene encodes for a protein (ataxin-7) widely expressed in the human retina [129]. This protein may interact with the function of CRX (cone–rod homeobox), a known transcription factor implicated in human cone–rod dystrophy [130].

An example of high-resolution spectral domain optical coherence tomography (SD-OCT) is provided for one SCA7 patient showing loss of the normal foveal lamination pattern between the outer nuclear layer and the retinal pigment epithelium, thus indicating focal photoreceptor loss [131] (Fig. 8.6).

Manrique et al. [132] have described a case series of seven patients with SCA7 in which the subjects with mild disease showed retinal thinning only at the fovea and subjects with more advanced disease tended to present retinal thinning also in the outer zone of the macula. Mean peripapillary RNFL thickness was decreased in all patients with sparing of the temporal quadrant until the advanced phases of the disease.

Furthermore, another study by Ahn et al. [133], using OCT and mfERG, revealed that retinal thinning extended outside the visible atrophic lesions and that the areas of functional deficits were greater than those of anatomic deficits.

Additionally, at a later stage of disease the maculopathy can evolve into a “bull’s eye” pattern [132]. The sparing of the temporal sector has been discussed as a possible result of the relative sparing of the inner macula around the central fovea associated with normal ganglion cell layer thickness at an earlier disease stage [134].

8.9 Conclusions

In summary, OCT is a useful tool for investigating optic nerve and retinal involvement in many rare neurological disorders. Up to now, only a limited number of diseases have been extensively studied, as reported in this chapter. Single case

reports with OCT findings are available for other rare neurological disorders such as Charcot-Marie-Tooth type 2A [135], and the X-linked adrenoleukodystrophy [136]. Thus, the application of this technique to larger case series will allow a better characterization of the ocular phenotype in these and other neurological diseases.

References

1. Collins A. Clinical neurogenetics: friedreich ataxia. Neurol Clin. 2013;31:1095–120.
2. Parkinson MH, Boesch S, Nachbauer W, Mariotti C, Giunti P. Clinical features of Friedreich's ataxia: classical and atypical phenotypes. J Neurochem. 2013;126 Suppl 1:103–17.
3. Campuzano V, Montermini L, Moltò MD, Pianese L, Cossée M, Cavalcanti F, et al. Friedreich's ataxia: autosomal recessive disease caused by an intronic GAA triplet repeat expansion. Science. 1996;271:1423–7.
4. Tan G, Napoli E, Taroni F, Cortopassi G. Decreased expression of genes involved in sulfur amino acid metabolism in frataxin-deficient cells. Hum Mol Genet. 2003;12:1699–711.
5. Shan Y, Napoli E, Cortopassi G. Mitochondrial frataxin interacts with ISD11 of the NFS1/ISCU complex and multiple mitochondrial chaperones. Hum Mol Genet. 2007;16:929–41.
6. Martelli A, Puccio H. Dysregulation of cellular iron metabolism in Friedreich ataxia: from primary iron-sulfur cluster deficit to mitochondrial iron accumulation. Front Pharmacol. 2014;5:130.
7. Rötig A, de Lonlay P, Chretien D, Foury F, Koenig M, Sidi D, et al. Aconitase and mitochondrial iron-sulphur protein deficiency in Friedreich ataxia. Nat Genet. 1997;17:215–7.
8. Lodi R, Cooper JM, Bradley JL, Manners D, Styles P, Taylor DJ, et al. Deficit of in vivo mitochondrial ATP production in patients with Friedreich ataxia. Proc Natl Acad Sci U S A. 1999;96:11492–5.
9. Bolinches-Amorós A, Mollá B, Pla-Martín D, Palau F, González-Cabo P. Mitochondrial dysfunction induced by frataxin deficiency is associated with cellular senescence and abnormal calcium metabolism. Front Cell Neurosci. 2014;8:124.
10. Babcock M, de Silva D, Oaks R, Davis-Kaplan S, Jiralerspong S, Montermini L, et al. Regulation of mitochondrial iron accumulation by Yfh1p, a putative homolog of frataxin. Science. 1997;276:1709–12.
11. Wong A, Yang J, Cavadini P, Gellera C, Lonnerdal B, Taroni F, et al. The Friedreich's ataxia mutation confers cellular sensitivity to oxidant stress which is rescued by chelators of iron and calcium and inhibitors of apoptosis. Hum Mol Genet. 1999;8:425–30.
12. Gomes CM, Santos R. Neurodegeneration in Friedreich's ataxia: from defective frataxin to oxidative stress. Oxid Med Cell Longev. 2013;2013:487534.
13. Kersten HM, Roxburgh RH, Danesh-Meyer HV. Ophthalmic manifestations of inherited neurodegenerative disorders. Nat Rev Neurol. 2014;10:349–62.
14. Andermann E, Remillard GM, Goyer C, Blitzer L, Andermann F, Barbeau A. Genetic and family studies in Friedreich's ataxia. Can J Neurol Sci. 1976;3:287–301.
15. Carroll WM, Kriss A, Baraitser M, Barrett G, Halliday AM. The incidence and nature of visual pathway involvement in Friedreich's ataxia. A clinical and visual evoked potential study of 22 patients. Brain. 1980;103:413–34.
16. Fortuna F, Barboni P, Liguori R, Valentino ML, Savini G, Gellera C, et al. Visual system involvement in patients with Friedreich's ataxia. Brain. 2009;132:116–23.
17. Noval S, Contreras I, Sanz-Gallego I, Manrique RK, Arpa J. Ophthalmic features of Friedreich ataxia. Eye (Lond). 2012;26:315–20.
18. Seyer LA, Galetta K, Wilson J, Sakai R, Perlman S, Mathews K, et al. Analysis of the visual system in Friedreich ataxia. J Neurol. 2013;260:2362–9.
19. Dağ E, Örnek N, Örnek K, Erbahçeci-Timur IE. Optical coherence tomography and visual field findings in patients with Friedreich ataxia. J Neuroophthalmol. 2014;34:118–21.

20. Barboni P, Carbonelli M, Savini G, Ramos Cdo V, Carta A, Berezovsky A, et al. Natural history of Leber's hereditary optic neuropathy:longitudinal analysis of the retinal nerve fiber layer by optical coherence tomography. Ophthalmology. 2010;117:623–7.
21. Cotman SL, Karaa A, Staropoli JF, Sims KB. Neuronal ceroid lipofuscinosis: impact of recent genetic advances and expansion of the clinicopathologic spectrum. Curr Neurol Neurosci Rep. 2013;13:366.
22. Wheeler RB, Schlie M, Kominami E, Gerhard L, Goebel HH. Neuronal ceroid lipofuscinosis: late infantile or Jansky Bielschowsky type–re-revisited. Acta Neuropathol. 2001;102:485–8.
23. Bennett MJ, Rakheja D. The neuronal ceroid-lipofuscinoses. Dev Disabil Res Rev. 2013;17:254–9.
24. Hainsworth DP, Liu GT, Hamm CW, Katz ML. Funduscopic and angiographic appearance in the neuronal ceroid lipofuscinoses. Retina. 2009;29:657–68.
25. Worgall S, Kekatpure MV, Heier L, Ballon D, Dyke JP, Shungu D, et al. Neurological deterioration in late infantile neuronal ceroid lipofuscinosis. Neurology. 2007;69:521–35.
26. Goebel HH, Zeman W, Damaske E. An ultrastructural study of the retina in the Jansky-Bielschowsky type of neuronal ceroid-lipofuscinosis. Am J Ophthalmol. 1977;83:70–9.
27. Weleber RG. The dystrophic retina in multisystem disorders: the electroretinogram in neuronal ceroid lipofuscinoses. Eye (Lond). 1998;12:580–90.
28. Sappington RM, Pearce DA, Calkins DJ. Optic nerve degeneration in a murine model of juvenile ceroid lipofuscinosis. Invest Ophthalmol Vis Sci. 2003;44:3725–31.
29. Weimer JM, Custer AW, Benedict JW, Alexander NA, Kingsley E, Federoff HJ, et al. Visual deficits in a mouse model of Batten disease are the result of optic nerve degeneration and loss of dorsal lateral geniculate thalamic neurons. Neurobiol Dis. 2006;22:284–93.
30. Mahmood F, Fu S, Cooke J, Wilson SW, Cooper JD, Russell C. A zebrafish model of CLN2 disease is deficient in tripeptidyl peptidase 1 and displays progressive neurodegeneration accompanied by a reduction in proliferation. Brain. 2013;136:1488–507.
31. Groh J, Stadler D, Buttmann M, Martini R. Non-invasive assessment of retinal alterations in mouse models of infantile and juvenile neuronal ceroid lipofuscinosis by spectral domain optical coherence tomography. Acta Neuropathol Commun. 2014;2:54.
32. Nardocci N, Verga ML, Binelli S, Zorzi G, Angelini L, Bugiani O. Neuronal ceroid-lipofuscinosis: a clinical and morphological study of 19 patients. Am J Med Genet. 1995;57:137–41.
33. Orlin A, Sondhi D, Witmer MT, Wessel MM, Mezey JG, Kaminsky SM, et al. Spectrum of ocular manifestations in CLN2-associated batten (Jansky-Bielschowsky) disease correlate with advancing age and deteriorating neurological function. PLoS One. 2013;8:e73128.
34. Klein CJ, Botuyan MV, Wu Y, Ward CJ, Nicholson GA, Hammans S, et al. Mutations in DNMT1 cause hereditary sensory neuropathy with dementia and hearing loss. Nat Genet. 2011;43:595–600.
35. Winkelmann J, Lin L, Schormair B, Kornum BR, Faraco J, Plazzi G, et al. Mutations in DNMT1 cause autosomal dominant cerebellar ataxia, deafness and narcolepsy. Hum Mol Genet. 2012;21:2205–10.
36. Moghadam KK, Pizza F, La Morgia C, Franceschini C, Tonon C, Lodi R, et al. Narcolepsy is a common phenotype in HSAN IE and ADCA-DN. Brain. 2014;137:1643–55.
37. Melberg A, Hetta J, Dahl N, Nennesmo I, Bengtsson M, Wibom R, et al. Autosomal dominant cerebellar ataxia deafness and narcolepsy. J Neurol Sci. 1995;134:119–29.
38. Lundberg PO, Wranne I, Brun A. Family with optic atrophy and neurological symptoms. Acta Neurol Scand. 1967;43:87–105.
39. Takasugi M, Yagi S, Hirabayashi K, Shiota K. DNA methylation status of nuclear-encoded mitochondrial genes underlies the tissue-dependent mitochondrial functions. BMC Genomics. 2010;11:481.
40. Shock LS, Thakkar PV, Peterson EJ, Moran RG, Taylor SM. DNA methyltransferase 1, cytosine methylation, and cytosine hydroxymethylation in mammalian mitochondria. Proc Natl Acad Sci U S A. 2011;108:3630–5.
41. Bellizzi D, D'Aquila P, Scafone T, Giordano M, Riso V, Riccio A, et al. The control region of mitochondrial DNA shows an unusual CpG and non-CpG methylation pattern. DNA Res. 2013;20:537–47.

42. Lo Giudice T, Lombardi F, Santorelli FM, Kawarai T, Orlacchio A. Hereditary spastic paraplegia: clinical-genetic characteristics and evolving molecular mechanisms. Exp Neurol. 2014;261C:518–39.
43. Casari G, De Fusco M, Ciarmatori S, Zeviani M, Mora M, Fernandez P, et al. Spastic paraplegia and OXPHOS impairment caused by mutations in paraplegin, a nuclear-encoded mitochondrial metalloprotease. Cell. 1998;93:973–83.
44. De Michele G, De Fusco M, Cavalcanti F, Filla A, Marconi R, Volpe G, et al. A new locus for autosomal recessive hereditary spastic paraplegia maps to chromosome 16q24.3. Am J Hum Genet. 1998;63:135–9.
45. Rugarli EI, Langer T. Translating m-AAA protease function in mitochondria to hereditary spastic paraplegia. Trends Mol Med. 2006;12:262–9.
46. Nolden M, Ehses S, Koppen M, Bernacchia A, Rugarli EI, Langer T. The m-AAA protease defective in hereditary spastic paraplegia controls ribosome assembly in mitochondria. Cell. 2005;123:277–89.
47. Atorino L, Silvestri L, Koppen M, Cassina L, Ballabio A, Marconi R, et al. Loss of m-AAA protease in mitochondria causes complex I deficiency and increased sensitivity to oxidative stress in hereditary spastic paraplegia. J Cell Biol. 2003;163:777–87.
48. McDermott CJ, Dayaratne RK, Tomkins J, Lusher ME, Lindsey JC, Johnson MA, et al. Paraplegin gene analysis in hereditary spastic paraparesis (HSP) pedigrees in northeast England. Neurology. 2001;56:467–71.
49. Ehses S, Raschke I, Mancuso G, Bernacchia A, Geimer S, Tondera D, et al. Regulation of OPA1 processing and mitochondrial fusion by m-AAA protease isoenzymes and OMA1. J Cell Biol. 2009;187:1023–36.
50. Klebe S, Depienne C, Gerber S, Challe G, Anheim M, Charles P, et al. Spastic paraplegia gene 7 in patients with spasticity and/or optic neuropathy. Brain. 2012;135:2980–93.
51. van Gassen KL, van der Heijden CD, de Bot ST, den Dunnen WF, van den Berg LH, Verschuuren-Bemelmans CC, et al. Genotype-phenotype correlations in spastic paraplegia type 7: a study in a large Dutch cohort. Brain. 2012;135:2994–3004.
52. Marcotulli C, Leonardi L, Tessa A, De Negris AM, Cornia R, Pierallini A, et al. Early-onset optic neuropathy as initial clinical presentation in SPG7. J Neurol. 2014;261:1820–1.
53. Wiethoff S, Zhour A, Schöls L, Fischer MD. Retinal nerve fibre layer loss in hereditary spastic paraplegias is restricted to complex phenotypes. BMC Neurol. 2012;12:143.
54. Chabriat H, Joutel A, Dichgans M, Tournier-Lasserve E, Bousser MG. Cadasil. Lancet Neurol. 2009;8:643–53.
55. O'Sullivan M, Jarosz JM, Martin RJ, Deasy N, Powell JF, Markus HS. MRI hyperintensities of the temporal lobe and external capsule in patients with CADASIL. Neurology. 2001;56:628–34.
56. Joutel A, Corpechot C, Ducros A, Vahedi K, Chabriat H, Mouton P, et al. Notch3 mutations in cerebral autosomal dominant arteriopathy with subcortical infarcts and leukoencephalopathy (CADASIL), a mendelian condition causing stroke and vascular dementia. Ann N Y Acad Sci. 1997;826:213–7.
57. Belin de Chantemèle EJ, Retailleau K, Pinaud F, Vessières E, Bocquet A, Guihot AL, et al. Notch3 is a major regulator of vascular tone in cerebral and tail resistance arteries. Arterioscler Thromb Vasc Biol. 2008;28:2216–24.
58. Robinson W, Galetta SL, McCluskey L, Forman MS, Balcer LJ. Retinal findings in cerebral autosomal dominant arteriopathy with subcortical infarcts and leukoencephalopathy (cadasil). Surv Ophthalmol. 2001;45:445–8.
59. Roine S, Harju M, Kivelä TT, Pöyhönen M, Nikoskelainen E, Tuisku S, et al. Ophthalmologic findings in cerebral autosomal dominant arteriopathy with subcortical infarcts and leukoencephalopathy: a cross-sectional study. Ophthalmology. 2006;113:1411–7.
60. Haritoglou C, Rudolph G, Hoops JP, Opherk C, Kampik A, Dichgans M. Retinal vascular abnormalities in CADASIL. Neurology. 2004;62:1202–5.
61. Pretegiani E, Rosini F, Dotti MT, Bianchi S, Federico A, Rufa A. Visual system involvement in CADASIL. J Stroke Cerebrovasc Dis. 2013;22:1377–84.

62. Parisi V, Pierelli F, Fattapposta F, Bianco F, Parisi L, Restuccia R, et al. Early visual function impairment in CADASIL. Neurology. 2003;60:2008–10.
63. Rufa A, Malandrini A, Dotti MT, Berti G, Salvadori C, Federico A. Typical pathological changes of CADASIL in the optic nerve. Neurol Sci. 2005;26:271–4.
64. Parisi V, Pierelli F, Coppola G, Restuccia R, Ferrazzoli D, Scassa C, et al. Reduction of optic nerve fiber layer thickness in CADASIL. Eur J Neurol. 2007;14:627–31.
65. Rufa A, Pretegiani E, Frezzotti P, De Stefano N, Cevenini G, Dotti MT, et al. Retinal nerve fiber layer thinning in CADASIL: an optical coherence tomography and MRI study. Cerebrovasc Dis. 2011;31:77–82.
66. Wolfram D, Wagener HP. Diabetes mellitus and simple optic atrophy among siblings: report of four cases. Proc Staff Meet Mayo Clin. 1938;13:715–8.
67. Rigoli L, Di Bella C. Wolfram syndrome 1 and Wolfram syndrome 2. Curr Opin Pediatr. 2012;24:512–7.
68. Barrett TG, Poulton K, Bundey S. DIDMOAD syndrome; further studies and muscle biochemistry. J Inherit Metab Dis. 1995;18:218–20.
69. Barrett TG, Bundey SE. Wolfram (DIDMOAD) syndrome. J Med Genet. 1997;34:838–41.
70. Barrett TG, Bundey SE, Fielder AR, Good PA. Optic atrophy in Wolfram (DIDMOAD) syndrome. Eye (Lond). 1997;11:882–8.
71. Inoue H, Tanizawa Y, Wasson J, Behn P, Kalidas K, Bernal-Mizrachi E, et al. A gene encoding a transmembrane protein is mutated in patients with diabetes mellitus and optic atrophy (Wolfram syndrome). Nat Genet. 1998;20:143–8.
72. Eiberg H, Hansen L, Kjer B, Hansen T, Pedersen O, Bille M, et al. Autosomal dominant optic atrophy associated with hearing impairment and impaired glucose regulation caused by a missense mutation in the WFS1 gene. J Med Genet. 2006;43:435–40.
73. Rendtorff ND, Lodahl M, Boulahbel H, Johansen IR, Pandya A, Welch KO, et al. Identification of p.A684V missense mutation in the WFS1 gene as a frequent cause of autosomal dominant optic atrophy and hearing impairment. Am J Med Genet A. 2011;155A:1298–313.
74. Bai X, Lv H, Zhang F, Liu J, Fan Z, Xu L, et al. Identification of a novel missense mutation in the WFS1 gene as a cause of autosomal dominant nonsyndromic sensorineural hearing loss in all-frequencies. Am J Med Genet A. 2014;164:3052–60.
75. Bonnycastle LL, Chines PS, Hara T, Huyghe JR, Swift AJ, Heikinheimo P, et al. Autosomal dominant diabetes arising from a Wolfram syndrome 1 mutation. Diabetes. 2013;62:3943–50.
76. Berry V, Gregory-Evans C, Emmett W, Waseem N, Raby J, Prescott D, et al. Wolfram gene (WFS1) mutation causes autosomal dominant congenital nuclear cataract in humans. Eur J Hum Genet. 2013;21:1356–60.
77. Carson MJ, Slager UT, Steinberg RM. Simultaneous occurrence of diabetes mellitus, diabetes insipidus, and optic atrophy in a brother and sister. Am J Dis Child. 1977;131:1382–5.
78. Jackson MJ, Bindoff LA, Weber K, Wilson JN, Ince P, Alberti KG, et al. Biochemical and molecular studies of mitochondrial function in diabetes insipidus, diabetes mellitus, optic atrophy, and deafness. Diabetes Care. 1994;17:728–33.
79. Shannon P, Becker L, Deck J. Evidence of widespread axonal pathology in Wolfram syndrome. Acta Neuropathol. 1999;98:304–8.
80. Hilson JB, Merchant SN, Adams JC, Joseph JT. Wolfram syndrome: a clinicopathologic correlation. Acta Neuropathol. 2009;118:415–28.
81. Ross-Cisneros FN, Pan BX, Silva RA, Miller NR, Albini TA, Tranebjaerg L, et al. Optic nerve histopathology in a case of Wolfram Syndrome: a mitochondrial pattern of axonal loss. Mitochondrion. 2013;13:841–5.
82. Bababeygy SR, Wang MY, Khaderi KR, Sadun AA. Visual improvement with the use of idebenone in the treatment of Wolfram syndrome. J Neuroophthalmol. 2012;32:386–9.
83. Bucca BC, Klingensmith G, Bennett JL. Wolfram Syndrome: a rare optic neuropathy in youth with type 1 diabetes. Optom Vis Sci. 2011;88:E1383–90.
84. Bouhlal Y, Amouri R, El Euch-Fayeche G, Hentati F. Autosomal recessive spastic ataxia of Charlevoix-Saguenay: an overview. Parkinsonism Relat Disord. 2011;17:418–22.

85. Berciano J, García A, Infante J. Peripheral nerve involvement in hereditary cerebellar and multisystem degenerative disorders. Handb Clin Neurol. 2013;115:907–32.
86. Duquette A, Brais B, Bouchard JP, Mathieu J. Clinical presentation and early evolution of spastic ataxia of Charlevoix-Saguenay. Mov Disord. 2013;28:2011–4.
87. Baets J, Deconinck T, Smets K, Goossens D, Van den Bergh P, Dahan K, et al. Mutations in SACS cause atypical and late-onset forms of ARSACS. Neurology. 2010;75:1181–8.
88. Bouchard JP, Barbeau A, Bouchard R, Bouchard RW. Autosomal recessive spastic ataxia of Charlevoix-Saguenay. Can J Neurol Sci. 1978;5:61e9.
89. De Braekeleer M, Giasson F, Mathieu J, Roy M, Bouchard JP, Morgan K. Genetic epidemiology of autosomal recessive spastic ataxia of CharlevoixeSaguenay in northeastern Quebec. Genet Epidemiol. 1993;10:17e25.
90. Engert JC, Bérubé P, Mercier J, Doré C, Lepage P, Ge B, Bouchard JP, Mathieu J, et al. ARSACS, a spastic ataxia common in northeastern Québec, is caused by mutations in a new gene encoding an 11.5-kb ORF. Nat Genet. 2000;24:120e5.
91. Cheetham ME, Caplan AJ. Structure, function and evolution of DnaJ: conservation and adaptation of chaperone function. Cell Stress Chaperones. 1998;3:28e36.
92. Parfitt DA, Michael GJ, Vermeulen EG, Prodromou NV, Webb TR, Gallo JM, et al. The ataxia protein sacsin is a functional co-chaperone that protects against polyglutamine-expanded ataxin-1. Hum Mol Genet. 2009;18:1556e65.
93. Girard M, Larivière R, Parfitt DA, Deane EC, Gaudet R, Nossova N, et al. Mitochondrial dysfunction and Purkinje cell loss in autosomal recessive spastic ataxia of Charlevoix-Saguenay (ARSACS). Proc Natl Acad Sci U S A. 2012;109:1661–6.
94. El Euch-Fayache G, Lalani I, Amouri R, Turki I, Ouahchi K, Hung WY, et al. Phenotypic features and genetic findings in sacsin-related autosomal recessive ataxia in Tunisia. Arch Neurol. 2003;60:982e8.
95. Grieco GS, Malandrini A, Comanducci G, Leuzzi V, Valoppi M, Tessa A, et al. Novel SACS mutations in autosomal recessive spastic ataxia of Charlevoixe-Saguenay type. Neurology. 2004;62:103e6.
96. Criscuolo C, Banfi S, Orio M, Gasparini P, Monticelli A, Scarano V, et al. A novel mutation in SACS gene in a family from southern Italy. Neurology. 2004;62:100e2.
97. Takiyama Y. Autosomal recessive spastic ataxia of CharlevoixeSaguenay. Neuropathology. 2006;26:368e75.
98. Bouhlal Y, Zouari M, Kefi M, Ben Hamida C, Hentati F, Amouri R. Autosomal recessive ataxia caused by three distinct gene defects in a single consanguineous family. J Neurogenet. 2008;22:139e48.
99. Vermeer S, Meijer RP, Pijl BJ, Timmermans J, Cruysberg JR, Bos MM, et al. ARSACS in the Dutch population: a frequent cause of early-onset cerebellar ataxia. Neurogenetics. 2008;10:87.
100. Bouhlal Y, El Euch-Fayeche G, Hentati F, Amouri R. A novel SACS gene mutation in a Tunisian family. J Mol Neurosci. 2009;39:333e6.
101. Takiyama Y. Sacsinopathies: sacsin-related ataxia. Cerebellum. 2007;6:353–9.
102. Vingolo EM, Di Fabio R, Salvatore S, Greco G, Bertini E, Lezzi V, et al. Myelinated retinal fibers in autosomal recessive spastic ataxia of Charlevoix-Saguenay. Eur J Neurol. 2011;18:1187–90.
103. Pablo LE, Garcia-Martin E, Gazulla J, Larrosa JM, Ferreras A, Santorelli FM, et al. Retinal nerve fiber hypertrophy in ataxia of Charlevoix-Saguenay patients. Mol Vis. 2011;17:1871–6.
104. Desserre J, Devos D, Sautière BG, Debruyne P, Santorelli FM, Vuillaume I, et al. Thickening of peripapillar retinal fibers for the diagnosis of autosomal recessive spastic ataxia of Charlevoix-Saguenay. Cerebellum. 2011;10:758–62.
105. Gazulla J, Benavente I, Vela AC, Marín MA, Pablo LE, Tessa A, Barrena MR, et al. New findings in the ataxia of Charlevoix-Saguenay. J Neurol. 2012;259:869–78.
106. Yu-Wai-Man P, Pyle A, Griffin H, Santibanez-Korev M, Chinnery PF. Abnormal retinal thickening is a common feature among patients with ARSACS-related phenotypes. Br J Ophthalmol. 2014;98:711–3.

107. Koeppen AH. The pathogenesis of spinocerebellar ataxia. Cerebellum. 2005;4:62–73.
108. Durr A. Autosomal dominant cerebellar ataxias: polyglutamine expansions and beyond. Lancet Neurol. 2010;9:885–94.
109. Pula JH, Gomez CM, Kattah JC. Ophthalmologic features of the common spinocerebellar ataxias. Curr Opin Ophthalmol. 2010;21:447–53.
110. Newman NJ, Biousse V. Hereditary optic neuropathies. Eye (Lond). 2004;18(11):1144–60.
111. Rufa A, Dotti MT, Galli L, Orrico A, Sicurelli F, Federico A. Spinocerebellar ataxia type 2 (SCA2) associated with retinal pigmentary degeneration. Eur Neurol. 2002;47:128–9.
112. Fukutake T, Kamitsukasa I, Arai K, Hattori T, Nakajima T. A patient homozygous for the SCA6 gene with retinitis pigmentosa. Clin Genet. 2002;61:375–9.
113. Aleman TS, Cideciyan AV, Volpe NJ, Stevanin G, Brice A, Jacobson SG. Spinocerebellar ataxia type 7 (SCA7) shows a cone-rod dystrophy phenotype. Exp Eye Res. 2002;74:737–45.
114. Abe T, Tsuda T, Yoshida M, Wada Y, Kano T, Itoyama Y, et al. Macular degeneration associated with aberrant expansion of trinucleotide repeat of the SCA7 gene in 2 Japanese families. Arch Ophthalmol. 2000;118:1415–21.
115. Pula JH, Towle VL, Staszak VM, Cao D, Bernard JT, Gomez CM. Retinal nerve fibre layer and macular thinning in spinocerebellar ataxia and cerebellar multisystem atrophy. Neuroophthalmology. 2011;35(3):108–14.
116. Alvarez G, Rey A, Sanchez-Dalmau FB, Muñoz E, Ríos J, Adán A. Optical coherence tomography findings in spinocerebellar ataxia-3. Eye (Lond). 2013;27:1376–81.
117. Schöls L, Bauer P, Schmidt T, Schulte T, Riess O. Autosomal dominant cerebellar ataxias: clinical features, genetics, and pathogenesis. Lancet Neurol. 2004;3:291–304.
118. Lebranchu P, Le Meur G, Magot A, David A, Verny C, Weber M, et al. Maculopathy and spinocerebellar ataxia type 1: a new association? J Neuroophthalmol. 2013;33:225–31.
119. Vaclavik V, Borruat FX, Ambresin A, Munier FL. Novel maculopathy in patients with spinocerebellar ataxia type 1 autofluorescence findings and functional characteristics. JAMA Ophthalmol. 2013;131:536–8.
120. Abe T, Abe K, Tsuda T, Itoyama Y, Tamai M. Ophthalmological findings in patients with spinocerebellar ataxia type 1 are not correlated with neurological anticipation. Graefes Arch Clin Exp Ophthalmol. 2001;239:722–8.
121. Abe T, Abe K, Aoki M, Itoyama Y, Tamai M. Ocular changes in patients with spinocerebellar degeneration and repeated trinucleotide expansion of spinocerebellar ataxia type 1 gene. Arch Ophthalmol. 1997;115:231–6.
122. Abele M, Bürk K, Andres F, Topka H, Laccone F, Bösch S, et al. Autosomal dominant cerebellar ataxia type I. Nerve conduction and evoked potential studies in families with SCA1, SCA2 and SCA3. Brain. 1997;120:2141–8.
123. Perretti A, Santoro L, Lanzillo B, Filla A, De Michele G, Barbieri F, et al. Autosomal dominant cerebellar ataxia type I: multimodal electrophysiological study and comparison between SCA1 and SCA2 patients. J Neurol Sci. 1996;142:45–53.
124. Robitaille Y, Schut L, Kish SJ. Structural and immunocytochemical features of olivopontocerebellar atrophy caused by the spinocerebellar ataxia type 1 (SCA-1) mutation define a unique phenotype. Acta Neuropathol. 1995;90:572–81.
125. Stricker S, Oberwahrenbrock T, Zimmermann H, Schroeter J, Endres M, Brandt AU, et al. Temporal retinal nerve fiber loss in patients with spinocerebellar ataxia type 1. PLoS One. 2011;6:e23024.
126. Varsányi B, Somfai GM, Lesch B, Vámos R, Farkas A, et al. Optical coherence tomography of the macula in congenital achromatopsia. Invest Ophthalmol Vis Sci. 2007;48:2249–53.
127. Birch DG, Wen Y, Locke K, Hood DC. Rod sensitivity, cone sensitivity, and photoreceptor layer thickness in retinal degenerative diseases. Invest Ophthalmol Vis Sci. 2011;52:7141–7.
128. Gouw LG, Digre KB, Harris CP, Haines JH, Ptacek LJ. Autosomal dominant cerebellar ataxia with retinal degeneration: clinical, neuropathologic, and genetic analysis of a large kindred. Neurology. 1994;44:1441–7.

129. Cancel G, Duyckaerts C, Holmberg M, Zander C, Yvert G, Lebre AS, et al. Distribution of ataxin-7 in normal human brain and retina. Brain. 2000;123:2519–30.
130. La Spada AR, Fu Y, Sopher BL, Libby RT, Wang X, Li LY, et al. Polyglutamine-expanded ataxin-7 antagonizes CRX function and induces cone-rod dystrophy in a mouse model of SCA7. Neuron. 2001;31:913–27.
131. Kumar N, Pulido JS. High-definition spectral domain optical coherence tomography in the evaluation of ataxia with visual impairment. Br J Ophthalmol. 2011;95:591–8.
132. Manrique RK, Noval S, Aguilar-Amat MJ, Arpa J, Rosa I, Contreras I. Ophthalmic features of spinocerebellar ataxia type 7. J Neuroophthalmol. 2009;29:174–9.
133. Ahn JK, Seo JM, Chung H, Yu HG. Anatomical and functional characteristics in atrophic maculopathy associated with spinocerebellar ataxia type 7. Am J Ophthalmol. 2005;139:923–5.
134. McLaughlin ME, Dryja TP. Ocular findings in spinocerebellar ataxia 7. Arch Ophthalmol. 2002;120:655–9.
135. Gowrisankaran S, Anastasakis A, Fishman GA, Alexander KR. Structural and functional measures of inner retinal integrity following visual acuity improvement in a patient with hereditary motor and sensory neuropathy type VI. Ophthalmic Genet. 2011;32:188–92.
136. Grainger BT, Papchenko TL, Danesh-Meyer HV. Optic nerve atrophy in adrenoleukodystrophy detectable by optic coherence tomography. J Clin Neurosci. 2010;17:122–4.

Chapter 9
Other Neurological Disorders: Migraine, Neurosarcoidosis, Schizophrenia, Obstructive Sleep Apnea-Hypopnea Syndrome (OSAHS)

Andrzej Grzybowski, Francisco J. Ascaso, Javier Mateo, Laura Cabezón, and Paula Casas

Abstract Optical coherence tomography (OCT) is a relatively recent, reproducible, noninvasive, noncontact in vivo imaging technique similar to ultrasonography except that it uses infrared wavelengths and has a sensitivity of 8–10 μm. Numerous studies have demonstrated a thinning in retinal nerve fiber layer (RNFL) measurements in neurodegenerative disorders including multiple sclerosis, Alzheimer's disease, and Parkinson's disease. In this chapter we present an update on the use of OCT in other neurological disorders, such as migraine, neurosarcoidosis, schizophrenia and obstructive sleep apnea-hypopnea syndrome (OSAHS).

Keywords Optical coherence tomography • Retinal nerve fiber layer • Migraine • Neurosarcoidosis • Schizophrenia • Obstructive sleep apnea-hypopnea syndrome

9.1 Introduction

Optical coherence tomography (OCT) is a relatively recent, reproducible, noninvasive, noncontact in vivo imaging technique similar to ultrasonography except that it uses infrared wavelengths and has a sensitivity of 8–10 μm. It has been used as an

A. Grzybowski, MD, PhD, MBA (✉)
Professor of Ophthalmology, Head of Ophthalmology Department, Poznan City Hospital, Poznan, Poland

Chair of Department of Ophthalmology, University of Warmia and Mazury, Olsztyn, Poland
e-mail: ae.grzybowski@gmail.com

F.J. Ascaso
Department of Ophthalmology, Hospital Clínico Universitario "Lozano Blesa", Zaragoza, Spain

School of Medicine, University of Zaragoza, Zaragoza, Spain

Instituto de Investigación Sanitaria (IIS) de Aragón, Zaragoza, Spain

J. Mateo • L. Cabezón • P. Casas
Department of Ophthalmology, Hospital Clínico Universitario "Lozano Blesa", Zaragoza, Spain

A. Grzybowski, P. Barboni (eds.), *OCT in Central Nervous System Diseases: The Eye as a Window to the Brain*, DOI 10.1007/978-3-319-24085-5_9

imaging technique for evaluating the retinal nerve fiber layer (RNFL), ganglion cell layer (GCL), and choroid in various neuro-ophthalmological disorders [1, 2]. Moreover, the new-generation spectral domain OCT (SD-OCT) devices use special software techniques, such as enhanced depth imaging (EDI) program, to acquire high-resolution OCT images and effectively evaluate the choroidal thickness [3, 4]. Numerous studies have demonstrated different retinal and choroid changes detectable with OCT in neurodegenerative disorders such as multiple sclerosis, Alzheimer's disease, and Parkinson's disease [5–8]. In this chapter we present an update on the use of OCT in other neurological disorders, such as migraine, neurosarcoidosis, schizophrenia and obstructive sleep apnea-hypopnea syndrome (OSAHS).

9.2 Optical Coherence Tomography in Migraine Patients

Migraine, one of the most common debilitating disorders in the world [9], is a chronic and episodic neurological disease presenting with recurrent attacks of typically unilateral, moderate-to severe headaches capable of causing significant dysfunction [10, 11]. The prevalence of chronic migraine ranges between 1 and 3 % of the population [12]. The pain is generally aggravated by physical activity and is often in association with a number of autonomic nervous system symptoms, such as nausea and vomiting [13]. There are two types of migraine: migraine with aura, namely classic migraine, and migraine without aura or common migraine [14]. The migraine aura is a combination of focal neurological disturbances which are seen prior to an attack, during an attack, and rarely following an attack [15]. It usually lasts for less than one hour. In up to one-third of migraneurs the headache is preceded by transient neurological and sensory symptoms, most frequently visual [16]. Accompanying ocular symptoms may include periorbital pain, photophobia, or other visual complaints. Because of this, ophthalmologists are often the first doctors to evaluate migraine patients. Moreover, migraine is a well-known risk factor for developing glaucoma [17].

Although its pathophysiology is still unclear [18, 19], migraine is a multifactorial syndrome precipitated by intrinsic or extrinsic factors in individuals with a genetic predisposition [20]. Several mechanisms have been proposed, including the vasogenic, neurogenic, hormonal and genetic hypotheses [20, 21]. A prolonged vasospasm in the occipital hemisphere followed by vasodilation, detected by transcranial Doppler ultrasound in migraine patients, is the most accepted theory in the explanation of migraine attacks with visual aura [9, 16, 22]. In certain patients, the reduction in brain blood flow secondary to cerebral vasospasm has been shown to start from other parts of the brain or even in tissues located outside the brain, especially in the retina [23–25]. Ocular blood flow can be estimated by color duplex imaging, Doppler flowmetry and laser speckle contrast imaging. Improvements in OCT software, like the "enhanced depth imaging OCT" (EDI-OCT), or the more recent "swept source OCT" (SS-OCT), have provided the method to explore the choroidal structure [13]. Besides an increased risk for ischemic stroke [26, 27], local infarctions caused by retinal artery occlusions

have been reported in migraine patients with aura [23, 24]. Furthermore, in chronic migraine, the altered perfusion in retinal microcirculation would cause ganglion cell death, leading to permanent structural abnormalities of the retina [18].

A few studies have investigated the RNFL thickness in patients who have migraine with and without aura by using scanning laser polarimetry [19] or optical coherence tomography [14, 15, 18, 28–31]. According to these authors, the RNFL thinning would be secondary to the neurodegenerative changes in the central nervous system (CNS) after ischemia in the migraine patients with aura (Table 9.1).

The choroid is the vascular compartment of the eye and is directly influenced by intraocular and perfusion pressures [13]. It supplies oxygen and nutrients to the outer retina [15]. In fact, the major blood supply to the retina is the choroid, especially in darkness, where 90 % of the oxygen comes from choroidal circulation [30]. In term of accuracy of measuring choroidal thickness, SD-OCT is even better than histology, as this cannot estimate the thickness of the living choroid [32]. Nevertheless, although it is not clear the relationship between choroidal thickness and choroidal blood flow, changes in choroidal thickness were recently described as a consequence of the vasodilatory effect on choroidal circulation of certain drugs, including sildenafil and cigarette smoking [33, 34]. Likewise, choroidal thickness has been reported to be reduced in high myopia, retinal dystrophy and age-related choroidal atrophy, whereas increased choroidal thickness was reported in Vogt-Koyanagi-Harada disease and central serous chorioretinopathy [34–39]. According to the above-mentioned articles,

Table 9.1 RNFL thickness in patients with migraine

Author, year, (Ref.)	Imaging technique	Findings
Tan et al. 2005 [19]	SLP	No differences in RNFL thickness between patients with migraine & healthy controls
Martínez et al. 2008 [18]	TD-OCT	Mean RNFL thickness in migraineurs was similar to that of controls, but RNFL thickness in temporal quadrant was thinner in patients compared to normal people
Martínez et al. 2009 [28]	TD-OCT	A significant difference between the migraine patients with aura and those without aura
Gipponi et al. 2013 [29]	SD-OCT	No significant differences in foveal thickness and total macular volume in female migraine patients compared to healthy women, but demonstrated a significant thinning in the RNFL thickness in the superior quadrant in the female migraine patients
Sorkhabi et al. 2013 [14]	SD-OCT	Nasal quadrant RNFL thickness was significantly thinner in migraine patients compared with that of age-matched healthy individuals
Ekincy et al. 2014 [15]	SD-OCT	A thinning of the RNFL and GCL only in patients who had migraine with aura
Simsek et al. 2015 [30]	SD-OCT	Migraine disease with or without aura does not have any effect on the thickness of the RNFL

Abbreviations: *SLP* scanning laser polarimetry, *TD-OCT* time-domain optical coherence tomography, *SD-OCT* spectral-domain optical coherence tomography, *RNFL* retinal nerve fiber layer, *GCL* ganglion cell layer

migraine seems to be a neurovascular disorder in which there is a reduction in the central retinal artery and posterior ciliary artery blood flow; the choroidal thinning would be an expected clinical outcome in patients with migraine. Likewise, a thinning of the choroidal layer is observed in migraine patients both with aura and without aura [15]. Dadaci et al. were the first authors to estimate the changes in the choroidal thickness during the attack episode in migraine patients using EDI-OCT [11]. They observed a significant increase in the choroidal thickness during the migraine attack. Ekinci et al. reported a significant thinning of the RNLF, GCL and choroid in migraine patients with aura, but no significant differences in RNFL and GCL measurements between migraine patients without aura and healthy individuals [15]. Zengin et al. [13] evaluated choroidal thickness by using SD-OCT in patients who had migraine and compared the results with healthy subjects. To avoid the possible effects of systemic drugs, only recently diagnosed migraine patients who were not using any medication and were non-smokers were included. The difference in choroidal thickness between migraineurs (276.8 ± 37.8 μm) and controls (300.4 ± 24.9 μm) was significant ($p = 0.001$). Although it is not easy to obtain OCT images during a painful episode, an acute decrease in choroidal thickness of approximately 45 μm was reported during the attack period when compared to basal levels in a small group of five patients [13]. Nevertheless, there was no correlation between severity and type of migraine with choroidal thickness ($p > 0.05$). This decrease in mean choroidal thickness may be related to the vasogenic etiology of migraine. Autonomic nervous system dysfunctions are often reported in migraine patients and related to trigeminovascular pain pathway activation. They are commonly ipsilateral to the headache and provide another explanation for the increased choroidal thickness during the migraine attack [40–42]. The reproducibility of this technique is high, although the relatively long duration of manual measuring of choroidal thickness (5 min per scan), may lead to observer fatigue and increase the possibility of false measurements [43].

In conclusion, peripapillary RNFL thickness and choroidal thickness measurement by using SD-OCT could be a new interesting method to evaluate the migraine patients, identifying localized neuronal loss.

9.3 Optical Coherence Tomography in Neurosarcoidosis

Sarcoidosis is a granulomatous disease of unknown origin that can affect most of the organs of the body, although the lungs, skin, lymph nodes (mainly thoracic), liver and the eyes, are most commonly affected. The non-caseating granulomas are formed by macrophages, epithelioid cells and lymphocytes, and can be found in different organs after an abnormal immune response of the body [44, 45]. Its incidence is low in people from countries such as Japan or Spain (0.2–2 out of 100,000), but is very high in Scandinavian and African origin patients (5–82 out of 100,000). It usually appears before 50 years of age; however, the incidence is higher between 20 and 39 years [44–47].

Sarcoidosis is diagnosed after radiologic, clinical and histologic findings. Differential diagnosis includes other granulomatous diseases, lymphoma, adverse reactions to certain drugs or infections such as tuberculosis or fungal infections [46].

Although often asymptomatic, sarcoidosis can show various clinical signs, depending on the organs that are affected. Common symptoms including fatigue, weakness, asthenia, dry cough, dyspnea, weight loss, fever, erythema nodosum, joint pain, presence of lymph nodes and night sweating [45, 46].

Sarcoidosis can affect the CNS in 5 % of cases, thus being called neurosarcoidosis [44, 48, 49]. Basal leptomeninges are usually affected, causing cranial polyneuropathies, aseptic meningitis, hydrocephalus and polyradiculopathy. Cranial neuropathies are also frequently present, mainly showing facial palsy, but also alteration of the cranial nerve VIII and, less commonly, nerves V, VI, IX and X. Other possible neurologic symptoms are seizures, fever, headaches or dysfunction of the hypothalamic-pituitary axis [48–50].

The most frequent ophthalmologic finding in sarcoidosis is anterior granulomatous uveitis with mutton-fat endothelial precipitates. Less common ocular manifestations include conjunctival nodules, dry eye, iris nodules, vitritis, intermediate uveitis with aggregates of inflammatory cells in the vitreous (snowballs), posterior segment uveitis with associated macular edema, choroiditis and perivascular sheathing [44, 46, 51].

Nevertheless, in neurosarcoidosis, even though anterior uveitis is still the most common alteration, other important signs that can be found include optic neuropathy, followed by cranial nerve involvement (mainly diplopia caused by common ocular motor nerve palsy) [52–55].

Some studies have analysed choroidal and retinal granulomas in sarcoidosis [56–58]. They were described as hyporeflective choroidal thickening with thinning of the overlying choriocapillaris [56]. The study was made with SD-OCT in the case of retinal granulomas and with EDI-OCT in choroidal granulomas [56]. After treatment with corticosteroids, the granulomas decreased their size or even disappeared [56].

A few case reports of cystoids macular edema (CME) in patients with posterior uveitis or panuveitis and sarcoidosis can also be found. In these cases OCT helped to make the diagnosis of sarcoidosis and to make a detailed study of the macular edema and its favorable evolution following treatment [59–61]. On the other hand, a thinning of the choroid has been described when the posterior uveitis is not active in patients with sarcoidosis [62].

As in other neurologic diseases, OCT can show alteration of the optic nerve in sarcoidosis [61]. Peripapillary RNFL abnormalities could be detected and, even when the patients showed no ophthalmologic clinical signs, the RNFL was thinner when compared with healthy controls, likely being a consequence of previous optic neuropathy [61]. Macular thickness had decreased in numerous patients, probably as a result of neuropathy and/or repeated CME in uveitis [61]. Increased RNFL thickness was found in some patients, probably as a manifestation of optic neuritis [62].

9.4 Optical Coherence Tomography in Schizophrenic Patients

Schizophrenia is a devastating mental condition which involves one of the most important psychiatric disorders from the viewpoint of public health [63]. The course of the disease is often chronic and highly variable, causing a great loss of quality of life of patients and their families, as well as a high social cost. Only in the USA over 2 million people are affected by this disorder [64].

Schizophrenia is a clinical syndrome with a variable psychopathology that affects cognition, emotion, perception, and other behavioural aspects. The expression of these manifestations is different in each patient and varies with time [65, 66]. However, schizophrenia lacks a clearly defined or diagnostic neuropathological signature and its etiology remains poorly understood. The diagnosis of schizophrenia is still based on clinical history and symptoms observed and reported by the patient [67, 68].

The best validated neuropathological abnormalities include possible reductions of neuronal density in the thalamus, reductions in the number of some interneurons and in the number and function of oligodendrocytes [69]. Neuroimaging techniques, such as structural magnetic resonance imaging (sMRI) and functional magnetic resonance imaging (fMRI), have been extensively studied in recent years aiming at developing new diagnostic biomarkers for schizophrenia. These studies have been very important to try to understand the biological substrate of the disease. The most striking abnormal findings include white and gray matter abnormalities [70–72]. Nevertheless, it is difficult to establish solid conclusions regarding the precise neuropathological changes that underlie these neuroimaging findings [73, 74].

One of the difficulties in measuring brain volumes in schizophrenic patients with MRI is that the volumetric loss is less than 4 % per year, which may be near the limit of detection by MRI, known the precision of the volumetric methods [75]. In the search for new biomarkers in schizophrenia, which may be obtained quickly, non-invasively and with less cost than MRI, lie the observable changes in the retina, as this through the optic nerve is not more than a projection of CNS. Jindahra et al. [76] reviewed the utility of OCT in clinical practice of neurological diseases such as multiple sclerosis, neuromyelitis, Alzheimer's disease and Parkinson's disease. The decrease of RGCs observed in these disorders can reflect degenerative changes in the brain. Therefore, they proposed RNFL thickness as a biological marker in these disorders. Similarly, it was thought that measurement of macular thickness and volume by OCT could reflect neuronal cell bodies and allow to quantify the neuronal loss [77].

In 2010, a preliminary study relating the schizophrenic disease with RNFL thickness changes measured by OCT was published [78]. This study showed that patients with schizophrenia have a decreased peripapillary RNFL thickness. This reduction was statistically significant, both in terms of value average (in all four quadrants) RNFL thickness as in relation to nasal quadrant (Fig. 9.1).

A similar research has been carried out by Chu et al. in patients with schizophrenia [79]. In this study, which included 38 patients with schizophrenia and 11 patients with schizo-affective disorder, no statistically significant differences were found in

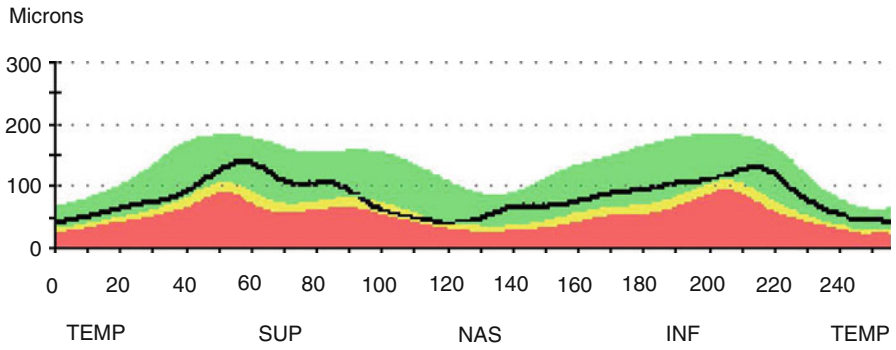

Fig. 9.1 OCT showing decreased peripapillary RNFL thickness specifically in nasal quadrant in a patient with schizophrenia

the RNFL thickness globally and individually in each of its quadrants between healthy controls and patients. However, it was observed that patients with schizo-affective disorder had RNFL nasal quadrant thickness of the right eye statistically decreased than those patients with schizophrenia. This difference from the previous study may be due to these authors recruited patients with first episode of psychosis and included in their sample not only patients with schizophrenia, but also patients with schizo-affective disorder. Moreover, an inverse and significant association was found between the values of macular volume in patients with schizophrenia and schizo-affective disorder and the severity of positive symptomatology. Also, if the analysis took into account only the patients with schizophrenia this association between macular volume and severity of positive symptoms was stronger [79].

Recently, Lee et al. reported that schizophrenic patients showed a statistically significant reduction in overall peripapillary RNFL thickness, macular thickness, as well as macular volume. Furthermore, the degree of thinning and reduction was more significant in the chronic phase of the disease and correlated with the duration of illness [80].

There is still the controversy in schizophrenia in relation to neurodegenerative model, that begins at about the time of symptom onset and manifests as progressive volumetric loss thereafter, and neurodevelopmental model that results in abnormal brain volume beginning at an early age [81], so that only longitudinal studies using OCT may help to clarify the underlying neurobiological processes in both models [82, 83].

9.5 Optical Coherence Tomography in Obstructive Sleep Apnea: Hypopnea Patients

Obstructive sleep apnea–hypopnea syndrome (OSAHS) is part of a broad group of disorders known as *"sleep-related breathing disorders"*. OSAHS is characterized by brief episodes of complete or partial upper airway collapse during sleep,

causing an increased thoraco-abdominal effort and decreased arterial oxygen saturation, leading to an arousal response which takes the form of apneas and periodic hypopneas during sleep [84]. This fact produces an excessive daytime sleepiness. Local and systemic inflammation play an important role in the pathogenesis of OSAHS, contributing to anatomic narrowing of the upper airway, increased collapsibility of the airway tissues, and abnormalities in reflexes that affect upper respiratory tract caliber and pharyngeal inspiratory muscle function [85]. In OSAHS, balance between vasodilators, such as nitric oxide, and vasoconstrictors such as endothelin, is disturbed [86]. As well as hypoxia-reoxygenation pattern contributes to the activation of sympathetic system [87]. Moreover, there is some evidence that OSAHS is a risk factor for neurovascular and cardiovascular diseases. Arterial hypertension, cardiac arrhythmia and/or ischemia, congestive heart failure, and cerebrovascular disease are events more likely in the presence of the obstructive sleep disturbance [88, 89].

Clinical features of OSAHS have inspired studies about brain structural abnormalities in this disease. MRI studies have reported a loss of gray and white matter in certain brain areas, suggesting a premature CNS degeneration in patients suffering from OSAHS [90, 91].

In the last few years, multiple investigators have studied the relationship between the apneic syndrome and some ophthalmological disorders such as floppy eyelid syndrome [92–95], retinal vein occlusion [96], central serous chorioretinopathy [97, 98], and certain optic nerve dysfunctions. Thus, papilledema and increased intracranial pressure have been reported in OSAHS patients [99, 100], improving after continuous positive airway pressure (CPAP) treatment [101, 102]. It was postulated that non-arteritic anterior ischemic optic neuropathy has a higher incidence in patients with the apneic dysfunction [103]. Likewise, an increased frequency of normal and high tension glaucoma in patients with OSAHS was shown [104–109].

9.5.1 Peripapillar Rnfl Findings in Apneic Disorder

However, the latest research reveals a diffuse loss of ganglion cells in the optic nerve of patients with apnea, without the characteristics of glaucomatous neuropathy, including generalized/focal enlargement of the cup, usually at superior and inferior poles, accompanied of visual field defects as nasal step, paracentral or arcuate scotomas, or arcuate blind spot enlargement [110]. Kargi et al. [111] published a diffuse loss of RNFL thickness measured with GDx polarimetry in patients with OSAHS. Sagiv et al. [112] and Lin et al. [113] in the same group of patients detected a decresased RNFL thickness in the superior, inferior and temporal quadrants compared with a control group. Reduction in the peripapillary RNFL thickness was also confirmed by Moghimi et al. [114] (with laser polarimetry GDX®), Lin [115], Xin [116] and Gutiérrez-Díaz [117]. Nevertheless, they did not exclude patients with glaucoma, what could have influenced their results. All these studies suggest a diffuse loss in the RNFL without any preferential location. On the other hand, Casas

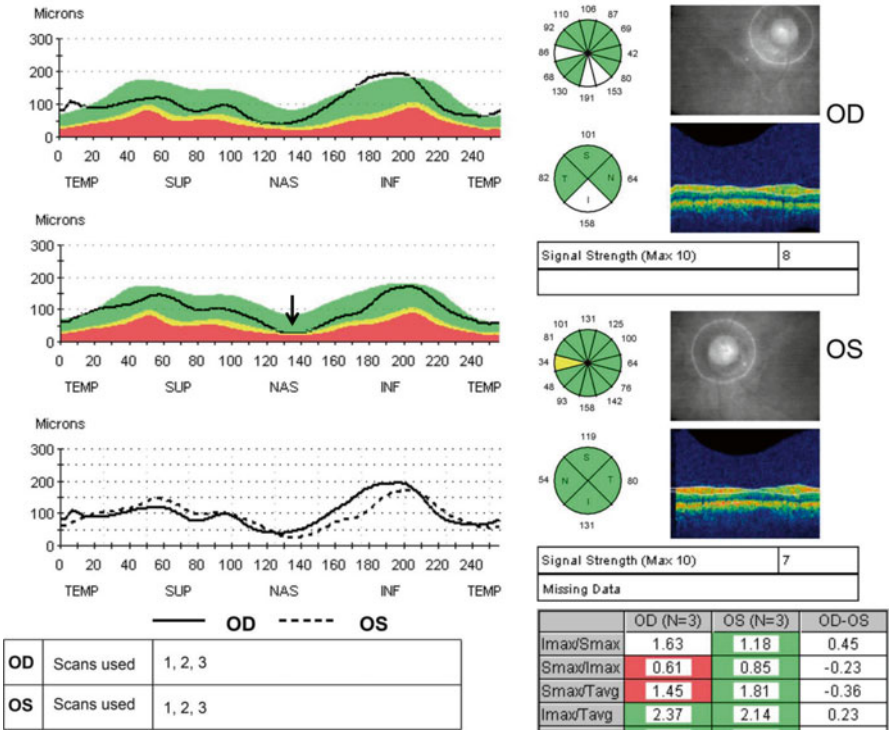

Fig. 9.2 Reduction of the peripapillary RNFL thickness in the nasal quadrant of the left eye in an OSAHS patient (*arrow*)

et al. [118] found a localized RNFL reduction in nasal sector of optic nerve in OSAHS patients (Fig. 9.2).

Zengin et al. [119] described in OSAHS patients a progressive thinning of RNFL thickness, over 1 year-follow up, in spite using CPAP device. In addition, severe OSAHS patients showed a greater decrease of RNFL thickness compared with mild-moderate OSAHS and controls [113, 120]. Furthermore, certain studies have found a significant negative correlation between the RNFL thickness and apnea-hypopnea index (AHI) [111, 119–121].

Despite these promising impressions, opposing results have also been published. Nowak et al. [122] and Adam et al. [123] found no significant differences between OSAHS and controls regarding the average RNFL thickness. Salzgeber et al. [124] found no differences in RNFL and optic nerve morphological parameters in their study with laser polarimetry GDX® and confocal laser scanning HRT II ®. Thus, there is no consensus whether the severity of OSAHS reflects the RNFL thickness.

Although several theories have been proposed, the pathogenesis of optic nerve damage in OSAHS is complex and remains still unknown. Thus, recurrent episodes of nocturnal hypoxia during apnea may result in direct anoxic damage, or in an

indirect effect on optic nerve head blood flow, vascular dysregulation of the optic nerve by OSAHS could result from hypoxia-induced imbalance between nitric oxide and endothelin [125]. Another presumption is the recurrent papilledema, which would be secondary to a hypoxemic cerebral vasodilation phenomenon. The perpetuation of RNFL swelling could lead to a cellular loss, with the consequent thinning of RNFL as the disease progresses [118]. Based on this idea, Huseyinoglu et al. [120] do not approve OCT to demonstrate neurodegeneration in OSAHS patients, considering that different confusing data such as normal or increased RNFL thickness as a result of optic nerve subtle edema, could mask possible peripapillary axonal loss.

9.5.2 Macular and Choroidal Findings in Apneic Disorder

On the other hand, Casas et al. [118] reported that temporal inner macular thickness was significantly higher in mild–moderate OSAHS compared to severe patients and controls. Xin et al. [126] found that macular and foveal thickness in nasal area of healthy individuals were significantly thinner than those in OSAHS patients with severe disorder, whereas subfoveal and nasal choroid were thinner in severe OSAHS comparing to controls. They suggested that a sympathetic nervous regulation disorder exists in OSAHS patients because of chronic intermittent hypoxia, which is followed by changes in the structure of the normal retina and choroid. However, the authors did not exclude the subjects having systemic diseases, such as arterial hypertension, what could be a possible error source. Nevertheless, Bahyan et al. [127] confirm the difference in choroidal thickness between severe OSAHS versus moderate-controls in a group of patients without systemic pathologies.

The proposed hypothesis for these findings is in relation with the double retinal blood supply from the central retinal artery and the choroid. The inner retina is provided by retinal blood vessels and is sensitive to tissue oxygen partial pressure changes. Thus, anoxia may result in an increased blood flow to the retina [128]. On the other hand, outer retina and choroid is supplied by choroidal system. The adaptation of choroidal resistance is achieved through the sympathetic nervous system [129]. The hypoxia-reoxygenation pattern and sleep fragmentation associated with OSHAS contribute to the activation of sympathetic system. Thus, expecting choroidal structural changes is reasonable.

There are also studies presenting no macular and choroidal disturbances in apneic patients [113, 130–132], Zengin et al. [130] and Karaca et al. [131] compared choroidal thickness in patients recently diagnosed with OSAHS and healthy controls and found that the difference in mean choroidal thickness was not statistically significant. Furthermore, choroidal thickness did not significantly differ among mild, moderate, and severe OSAHS groups and no correlation between AHI and choroidal thickness was found [130, 131]. Khayi et al. [132] did not found any differences in choroidal vascular responses to posture and exercise between healthy control subjects and healthy OSAHS patients.

Similar results were reported by Lin et al. [113] regarding to macular thickness in OSAHS patients and controls.

Tonini et al. [133] studied vascular choroidal reactivity during hyperoxia and hypercapnia with choroidal laser Doppler flowmetry. Patients with OSAHS, without comorbidities, and control subjects exhibited similar choroidal reactivity during hyperoxia and hypercapnia. The author suggested that other microvascular comorbidities as atherosclerosis or arterial hypertension had an important role in the choroidal vascular regulation and healthy individuals with OSAHS have long-term adaptive mechanisms active in ocular microcirculation.

9.6 Conclusions

The presented analysis shows that different retinal and choroidal changes were detected by OCT in diseases such as migraine, neurosarcoidosis, schizophrenia and OSAHS. Nevertheless, they were based on different OCT generations (what could have influenced the precision and repeatability of the results), different patients populations (with or without concomitant disorders, different stage of the diseases, etc.), and different methodology. They also provided different, and sometimes opposite, results. Most of them, however, confirm the usefulness of OCT studies in different neurodegenerative conditions. Moreover, it is clear that non-invasive character and increasing precision, reliability, as well as the increasing number of ocular structures to be studied make OCT a promising technique for future studies.

References

1. Syc SB, Saidha S, Newsome SD, Ratchford JN, Levy M, Ford E, Crainiceanu CM, Durbin MK, Oakley JD, Meyer SA, Frohman EM, Calabresi PA. Optical coherence tomography segmentation reveals ganglion cell layer pathology after optic neuritis. Brain. 2012;135:521–33.
2. Kardon R. The role of the macula OCT scan in neuro-ophthalmology. J Neuroophthalmol. 2011;31:353–61.
3. Branchini L, Regatieri CV, Flores-Moreno I, Baumann B, Fujimoto JG, Duker JS. Reproducibility of choroidal thickness measurements across three spectral domain optical coherence tomography systems. Ophthalmology. 2012;119:119–23.
4. Manjunath V, Taha M, Fujimoto JG, Duker JS. Choroidal thickness in normal eyes measured using Cirrus-HD optical coherence tomography. Am J Ophthalmol. 2010;150:325–9.
5. Frohman E, Costello F, Zivadinov R, Stuve O, Conger A, Winslow H, Trip A, Frohman T, Balcer L. Optical coherence tomography in multiple sclerosis. Lancet Neurol. 2006;5:853–63.
6. Galetta KM, Calabresi PA, Frohman EM, Balcer LJ. Optical coherence tomography (OCT): imaging the visual pathway as a model for neurodegeneration. Neurotherapeutics. 2011;8:117–32.
7. Ascaso FJ, Cruz N, Modrego PJ, López-Antón R, Santabárbara J, Pascual LF, Lobo A, Cristóbal JA. Retinal alterations in mild cognitive impairment and Alzheimer's disease: an optical coherence tomography study. J Neurol. 2014;261:1522–30.
8. Jiménez B, Ascaso FJ, Cristóbal JA, López del Val J. Development of a prediction formula of Parkinson disease severity by optical coherence tomography. Mov Disord. 2014;29:68–74.

9. Friberg L, Olesen J, Lassen NA, Olsen TS, Karle A. Cerebral oxygen extraction, oxygen consumption, and regional cerebral blood flow during the aura phase of migraine. Stroke. 1994;25:974–9.
10. Kirbas S, Tufekci A, Turkyilmaz K, Kirbas A, Oner V, Durmus M. Evaluation of the retinal changes in patients with chronic migraine. Acta Neurol Belg. 2013;113:167–72.
11. Dadaci Z, Doganay F, Acir NO, Aydin HD, Borazan M. Enhanced depth imaging optical coherence tomography of the choroid in migraine patients: implications for the association of migraine and glaucoma. Br J Ophthalmol. 2014;98:972–5.
12. Carod-Artal FJ, Irimia P, Ezpeleta D. Chronic migraine: definition, epidemiology, risk factors and treatment. Rev Neurol. 2012;54:629–37.
13. Zengin MO, Elmas Z, Cinar E, Kucukerdonmez C. Choroidal thickness changes in patients with migraine. Acta Neurol Belg. 2015;115(1):33–7.
14. Sorkhabi R, Mostafaei S, Ahoor M, Talebi M. Evaluation of retinal nerve fiber layer thickness in migraine. Iran J Neurol. 2013;12:51–5.
15. Ekinci M, Ceylan E, Çağatay HH, Keleş S, Hüseyinoğlu N, Tanyildiz B, Çakici O, Kartal B. Retinal nerve fibre layer, ganglion cell layer and choroid thinning in migraine with aura. BMC Ophthalmol. 2014;14:75. doi:10.1186/1471-2415-14-75.
16. Lipton R, Bigal M, Diamond M, Freitag F, Reed M, Stewart W. Migraine prevalence, disease burden and the need for preventive therapy. Neurology. 2007;68:343–9.
17. Worley A, Grimmer-Somers K. Risk factors for glaucoma: what do they really mean? Aust J Prim Health. 2011;17:233–9.
18. Martínez A, Proupim N, Sánchez M. Retinal nerve fiber layer thickness measurements using optical coherence tomography in migraine patients. Br J Ophthalmol. 2008;92:1069–75.
19. Tan FU, Akarsu C, Güllü R. Retinal nerve fiber layer thickness is unaffected in migraine patients. Acta Neurol Scand. 2005;112:19–23.
20. Bolay H, Moskowitz MA. The neurobiology of migraine and transformation of headache therapy. In: Waxman S, editor. From neuroscience to neurology: neuroscience, molecular medicine, and the therapeutic transformation of neurology. San Diego: Elsevier; 2004. p. 107–23.
21. Panconesi A, Bartolozzi ML, Guidi L. Migraine pain: reflections against vasodilatation. J Headache Pain. 2009;10:317–25.
22. Thie A, Spitzer K, Lachenmayer L, Kunze K. Prolonged vasospasm in migraine detected by noninvasive transcranial Doppler ultrasound. Headache. 1988;28:183–6.
23. Killer HE, Forrer A, Flammer J. Retinal vasospasm during an attack of migraine. Retina. 2003;23:253–4.
24. Beversdof D, Stommel E, Allen C, Stevens R, Lessel S. Recurrent branch retinal infarcts in association with migraine. Headache. 1997;37:396–9.
25. Abdul-Rahman AM, Gilhotra JS, Selva D. Dynamic focal retinal arteriolar vasospasm in migraine. Indian J Ophthalmol. 2011;59:51–3.
26. Kurth T, Slomke MA, Kase CS, Cook NR, Lee IM, Gaziano JM, Diener HC, Buring JE. Migraine, headache, and the risk of stroke in women: a prospective study. Neurology. 2005;64:1020–6.
27. Sacco S, Ricci S, Carolei A. Migraine and vascular diseases: a review of the evidence and potential implications for management. Cephalalgia. 2012;32:785–95.
28. Martínez A, Proupim N, Sánchez M. Scanning laser polarimetry with variable corneal compensation in migraine patients. Acta Ophthalmol. 2009;87:746–53.
29. Gipponi S, Scaroni N, Venturelli E, Forbice E, Rao R, Liberini P, Padovani A, Semeraro F. Reduction in retinal nerve fiber layer thickness in migraine patients. Neurol Sci. 2013;34:841–5.
30. Simsek IB, Aygun D, Yildiz S. Retinal nerve fibre layer thickness in migraine patients with or without aura. Neuroophthalmology. 2015;39:17–21.
31. Linsenmeier RA, Braun RD. Oxygen distribution and consumption in the cat retina during normoxia and hypoxia. J Gen Physiol. 1992;99:177–97.
32. Maul EA, Friedman DS, Chang DS, Boland MV, Ramulu PY, Jampel HD, Quigley HA. Choroidal thickness measured by spectral domain optical coherence tomography: factors affecting thickness in glaucoma patients. Ophthalmology. 2011;118:1571–9.

33. Sizmaz S, Küçükerdönmez C, Pinarci EY, Karalezli A, Canan H, Yilmaz G. The effect of smoking on choroidal thickness measured by optical coherence tomography. Br J Ophthalmol. 2013;97:601–4.
34. Fujiwara T, Imamura Y, Margolis R, Slakter JS, Spaide RF. Enhanced depth imaging optical coherence tomography of the choroid in highly myopic eyes. Am J Ophthalmol. 2009; 148:445–50.
35. Ikuno Y, Tano Y. Retinal and choroidal biometry in highly myopic eyes with spectral-domain optical coherence tomography. Invest Ophthalmol Vis Sci. 2009;50:3876–80.
36. Yeoh J, Rahman W, Chen F, Hooper C, Patel P, Tufail A, Webster AR, Moore AT, Dacruz L. Choroidal imaging in inherited retinal disease using the technique of enhanced depth imaging optical coherence tomography. Graefes Arch Clin Exp Ophthalmol. 2010;248:1719–28.
37. Spaide RF. Age-related choroidal atrophy. Am J Ophthalmol. 2009;147:801–10.
38. Imamura Y, Fujiwara T, Margolis R, Spaide RF. Enhanced depth imaging optical coherence tomography of the choroid in central serous chorioretinopathy. Retina. 2009;29:1469–73.
39. Maruko I, Iida T, Sugano Y, et al. Subfoveal choroidal thickness after treatment of Vogt-Koyanagi-Harada disease. Retina. 2011;31:510–7.
40. Peroutka SJ. Migraine: a chronic sympathetic nervous system disorder. Headache. 2004;44:53–64.
41. Drummond PD. The effect of sympathetic blockade on facial sweating and cutaneous vascular responses to painful stimulation of the eye. Brain. 1993;116:233–41.
42. Gupta R, Bhatia MS. A report of cranial autonomic symptoms in migraineurs. Cephalalgia. 2007;27:22–8.
43. Karaca EE, Ozdek S, Yalçin NG, Ekici F. Reproducibility of choroidal thickness measurements in healthy Turkish subjects. Eur J Ophthalmol. 2014;24:202–8.
44. Whitcup SM. Sarcoidosis. In: Nussenblatt RB, Whitcup SM, editors. Uveitis. Fundamentals and clinical practice. 3rd ed. Philadelphia: Mosby; 2004. p. 301–10.
45. Ianuzzi MC, Rybicki BA, Teirstein AS. Sarcoidosis. N Engl J Med. 2007;357:2153–65.
46. Nunes H, Bouvry D, Valeyre D. Sarcoidosis. Orphanet J Rare Dis. 2007;2:46.
47. Reich JM. A critical analysis of sarcoidosis incidence assessment. Multidiscip Respir Med. 2013;8:57.
48. Hoyle JC, Jablonski C, Newton HB. Neurosarcoidosis: clinical review of a disorder with challenging inpatient presentations and diagnostic considerations. Neurohospitalist. 2014;4:94–101.
49. Nowak DA, Widenka DC. Neurosarcoidosis: a review of its intracranial manifestation. J Neurol. 2001;248:363–72.
50. Titlic M, Bradic-Hammoud M, Miric L, Punda A. Clinical manifestations of neurosarcoidosis. Bratisl Lek Listy. 2009;110:576–9.
51. Bezo C, Majzoub S, Nochez Y, Leruez S, Charlin JF, Milea D, Pisella PJ. Sarcoïdose oculaire et neuro-ophtalmologique: étude retrospective sur 30 cas. J Fr Ophtalmol. 2013;36:473–80.
52. Koczman JJ, Rouleau J, Gaunt M, Kardon RH, Wall M, Lee AG. Neuro-ophthalmic sarcoidosis: the University of Iowa experience. Semin Ophthalmol. 2008;23:157–68.
53. Menezo V, Lobo A, Yeo TK, du Bois RM, Lightman S. Ocular features in neurosarcoidosis. Ocul Immunol Inflamm. 2009;17:170–8.
54. Frohman LP, Guirgis M, Turbin RE, Bielory L. Sarcoidosis of the anterior visual pathway: 24 new cases. J Neuroophthalmol. 2003;23:190–7.
55. Beardsley TL, Brown SV, Sydnor CF, Grimson BS, Klintworth GK. Eleven cases of sarcoidosis of the optic nerve. Am J Ophthalmol. 1984;97:62–77.
56. Modi YS, Epstein A, Bhaleeya S, Harbour JW, Albini T. Multimodal imaging of sarcoid choroidal granulomas. J Ophthalmic Inflamm Infect. 2013;3:58.
57. Wong M, Javowicz M, Tessler HH, Goldstein DA. Hight-resolution optical coherence tomography of presumed sarcoid retinal granulomas. Retina. 2009;29:1545–6.
58. Rostaqui O, Querques G, Haymann P, Fardeau C, Coscas G, Souied EH. Visualization of sarcoid choroidal granuloma by enhanced depth imaging optical coherence tomography. Ocul Immunol Inflamm. 2014;22:239–41.
59. Cabrillo-Estévez L, de Juan-Marcos L, Kyriakou D, Hernández-Galilea E. Cistoid macular edema as first manifestation of sarcoidosis. Int Ophthalmol. 2014;34:961–5.

60. Simmons-Rear A, Yeh S, Chan-Kai BT, Lauer AK, Flaxel CJ, Smith JR, Rosenbaum JT, Suhler EB. Characterization of serous retinal detachments in uveitis patients with optical coherence tomography. J Ophthalmic Inflamm Infect. 2012;2:191–7.
61. Eckstein C, Saidha S, Sotirchos ES, Byraiah G, Seigo M, Stankiewicz A, Syc SB, Ford E, Sharma S, Calabresi PA, Pardo CA. Detection of clinical and subclinical retinal abnormalities in neurosarcoidosis with optical coherence tomography. J Neurol. 2012;259:1390–8.
62. Güngör SG, Akkoyun I, Reyhan HN, Yesilirmak N, Yilmaz G. Choroidal thickness in ocular sarcoidosis during quiescent phase using enhanced depth imaging optical coherence tomography. Ocul Immunol Inflamm. 2014;22:287–93.
63. Mueser KT, McGurk SR. Schizophrenia. Lancet. 2004;363:2063–72.
64. Wu EQ, Birnbaum HG, Shi L, et al. The economic burden of schizophrenia in the United States in 2002. J Clin Psychiatry. 2005;66:1122–9.
65. Sadock B, Sadock V. Sinopsis de Psiquiatría. In: Kaplan & Sadock. 10th ed. Madrid: Wolters Kluwer; 2008.
66. Svensson AC, Lichtenstein P, Sandin S, Öberg S, Sullivan PF, Hultman CM. Familial aggregation of schizophrenia: the moderating effect of age at onset, parental immigration, paternal age and season of birth. Scand J Public Health. 2012;40:43–50.
67. Steen RG, Mull C, McClure R, Hamer RM, Lieberman JA. Systematic review and meta-analyisis of magnetic resonance imaging studies. Br J Psychiatry. 2006;188:510–8.
68. Siever LJ, Davis KL. The pathophysiology of schizophrenia disorders: perspectives from the spectrum. Am J Psychiatry. 2004;161:398–413.
69. Harrison PJ, Weinberger DR. Schizophrenia genes, gene expression, and neuropathology: on the matter of their convergence. Mol Psychiatry. 2005;10:40–68.
70. Bracht T, Horn H, Strik W, Federspiel A, Razavi N, Stegmayer K, Wiest R, Dierks T, Müller TJ, Walther S. White matter pathway organization of the reward system is related to positive and negative symptoms in schizophrenia. Schizophr Res. 2014;153:136–42.
71. Takayanagi M, Wentz J, Takayanagi Y, Schretlen DJ, Ceyhan E, Wang L, Suzuki M, Sawa A, Barta PE, Ratnanather JT, Cascella NG. Reduced anterior cingulate gray matter volume and thickness in subjects with deficit schizophrenia. Schizophr Res. 2013;150:484–90.
72. Glahn DC, Laird AR, Ellison-Wright I, Thelen SM, Robinson JL, Lancaster JL, Bullmore E, Fox PT. Meta-analysis of gray matter anomalies in schizophrenia: application of anatomic likelihood estimation and network analysis. Biol Psychiatry. 2008;64:774–81.
73. Arnone D, Cavanagh J, Gerber D, Lawrie SM, Ebmeier KP, Mcintosh AM. Magnetic resonance imaging studies in bipolar and schizophrenia: meta-analysis. Br J Psychiatry. 2009;195:194–201.
74. Fornito A, Yücel M, Dean B, Wood SJ, Pantelis C. Anatomical abnormalities of the anterior cingulate cortex in schizophrenia: bridging the gap between neuroimaging and neuropathology. Schizophr Bull. 2009;35:973–93.
75. Howard MA, Roberts N, García-Fiñana M, Cowell PE. Volume estimation of prefrontal cortical subfields using MRI and stereology. Brain Res Brain Res Protoc. 2003;10:125–38.
76. Jindahra P, Hedges TR, Mendoza-Santiesteban CE, Plant GT. Optical coherence tomography of the retina: applications in neurology. Curr Opin Neurol. 2010;23:16–23.
77. Lamirel C, Newman N, Biousse V. The use of optical coherence tomography in neurology. Rev Neurol Dis. 2009;6:E105–20.
78. Ascaso FJ, Cabezón L, Quintanilla MA, Gutiérrez-Galve L, López-Antón R, Cristóbal JA, Lobo A. Retinal nerve fiber layer thickness measured by optical coherence tomography in patients with schizophrenia: a short report. Eur J Psychiat. 2010;24:227–35.
79. Chu EM, Kolappan M, Barnes TR, Joyce EM, Ron MA. A window into the brain: an in vivo study of the retina in schizophrenia using optical coherence tomography. Psychiatry Res. 2012;203:89–94.
80. Lee WW, Tajunisah I, Sharmilla K, Peyman M, Subrayan V. Retinal nerve fiber layer structure abnormalities in schizophrenia and its relationship to disease state: evidence from optical coherence tomography. Invest Ophthalmol Vis Sci. 2013;54:7785–92.
81. Maynard TM, Sikich L, Lieberman JA, LaMantia AS. Neural development, cell-cell signaling, and the 'two-hit' hypothesis of schizophrenia. Schizophr Bull. 2001;27:457–76.

82. Kochunov P, Hong LE. Neurodevelopmental and neurodegenerative models of schizophrenia: white matter at the center stage. Schizophr Bull. 2014;40:721–8.
83. Pantelis C, Yücel M, Wood SJ, Velakoulis D, Sun D, Berger G, Stuart GW, Yung A, Phillips L, McGorry PD. Structural brain imaging evidence for multiple pathological processes at different stages of brain development in schizophrenia. Schizophr Bull. 2005;31:672–96.
84. Guilleminault C. Clinical features and evaluation of obstructive sleep apnea syndrome. In: Kryger MH, Roth T, Dement WC, editors. Principles and practice of sleep medicine. Philadelphia: WB Saunders; 1994. p. 667–77.
85. Hatipoğlu U, Rubinstein I. Inflammation and obstructive sleep apnea syndrome pathogenesis: a working hypothesis. Respiration. 2003;70:665–71.
86. Lavie L, Hefetz A, Luboshitzky R, Lavie P. Plasma levels of nitric oxide and L-arginine in sleep apnea patients: effects of nCPAP treatment. J Mol Neurosci. 2003;21:57–63.
87. Grover DP. Obstructive sleep apnea and ocular disorders. Curr Opin Ophthalmol. 2010;21: 454–8.
88. Shahar E, Whitney CW, Redline S, Lee ET, Newman AB, Javier Nieto F, O'Connor GT, Boland LL, Schwartz JE, Samet JM. Sleep-disordered breathing and cardiovascular disease: cross sectional results of the Sleep Heart Health Study. Am J Respir Crit Care Med. 2001;163:19–25.
89. Rudnicka A, Pływaczewski R, Jończak L, Górecka D, Sliwiński P. Prevalence of stroke in patients with obstructive sleep apnoea. Pneumonol Alergol Pol. 2010;78:121–5.
90. Macey PM, Henderson LA, Macey KE, Alger JR, Frysinger RC, Woo MA, Harper RK, Yan-Go FL, Harper RM. Brain morphology associated with obstructive sleep apnea. Am J Respir Crit Care Med. 2002;166:1382–7.
91. Kumar R, Birrer BV, Macey PM, Woo MA, Gupta RK, Yan-Go FL, Harper RM. Reduced mammillary body volume in patients with obstructive sleep apnea. Neurosci Lett. 2008;438:330–4.
92. McNab AA. Floppy eyelid syndrome and obstructive sleep apnea. Ophthal Plast Reconstr Surg. 1997;13:98–114.
93. Woog JJ. Obstructive sleep apnea and the floppy eyelid syndrome. Am J Ophthalmol. 1990;110:314–5.
94. Karger RA, White WA, Park WC, et al. Prevalence of floppy eyelid syndrome in obstructive sleep apnea-hypopnea syndrome. Ophthalmology. 2006;113:1669–74.
95. Muniesa M, Sánchez-de-la-Torre M, Huerva V, Lumbierres M, Barbé F. Floppy eyelid syndrome as an indicator of the presence of glaucoma in patients with obstructive sleep apnea. J Glaucoma. 2014;23:81–5.
96. Leroux les Jardins G, Glacet-Bernard A, Lasry S, Housset B, Coscas G, Soubrane G. Retinal vein occlusion and obstructive sleep apnea syndrome. J Fr Ophtalmol. 2009;32:420–4.
97. Kloos P, Laube I, Thoelen A. Obstructive sleep apnea in patients with central serous chorioretinopathy. Graefes Arch Clin Exp Ophthalmol. 2008;246:1225–8.
98. Jain AK, Kaines A, Schwartz S. Bilateral central serous chorioretinopathy resolving rapidly with treatment for obstructive sleep apnea. Graefes Arch Clin Exp Ophthalmol. 2010;248:1037–9.
99. Purvin VA, Kawasaki A, Yee RD. Papilledema and obstructive sleep apnea syndrome. Arch Ophthalmol. 2000;118:1626–30.
100. Franklin KA. Cerebral haemodynamics in obstructive sleep apnoea and Cheyne Stokes respiration. Sleep Med Rev. 2002;6:429–41.
101. Lee AG, Golnik K, Kardon R, Wall M, Eggenberger E, Yedavally S. Sleep apnea and intracranial hypertension in men. Ophthalmology. 2002;109:482–5.
102. O'Donoghue FJ, Briellmann RS, Rochford PD, Abbott DF, Pell GS, Chan CH, Tarquinio N, Jackson GD, Pierce RJ. Cerebral structural changes in severe obstructive sleep apnea. Am J Respir Crit Care Med. 2005;171:1185–90.
103. Hayreh SS, Zimmerman MB, Podhajsky P, Alward WL. Nocturnal arterial hypotension and its role in optic nerve head and ocular ischemic disorders. Am J Ophthalmol. 1994;17:603–24.
104. Mojon DS, Hess CW, Goldblum D, Fleischhauer J, Koerner F, Bassetti C, Mathis J. High prevalence of glaucoma in patients with sleep apnea syndrome. Ophthalmology. 1999;106:1009–12.

105. Mojon DS, Hess CW, Goldblum D, Böhnke M, Körner F, Mathis J. Primary open-angle glaucoma is associated with sleep apnea syndrome. Ophthalmologica. 2000;214:115–8.
106. Bendel RE, Kaplan J, Heckman M, Fredrickson PA, Lin SC. Prevalence of glaucoma in patients with obstructive sleep apnea—a cross-sectional case-series. Eye (Lond). 2008;22: 1105–9.
107. Faridi O, Park SC, Liebmann JM, Ritch R. Glaucoma and obstructive sleep apnea syndrome. Clin Exp Ophthalmol. 2012;40:408–19.
108. Sergi M, Salerno DE, Rizzi M, Blini M, Andreoli A, Messenio D, Pecis M, Bertoni G. Prevalence of normal tension glaucoma in obstructive sleep apnea syndrome patients. J Glaucoma. 2007;16:42–6.
109. Bilgin G. Normal-tension glaucoma and obstructive sleep apnea syndrome: a prospective study. BMC Ophthalmol. 2014;14:27.
110. Examen del paciente. Campo visual. In: European glaucoma society, editor. Terminología y pautas para el glaucoma. 3rd ed. Savona: Dogma; 2009. p. 61–89.
111. Kargi SH, Altin R, Koksal M, Kart L, Cinar F, Ugurbas SH, Ayoglu F. Retinal nerve fibre layer measurements are reduced in patients with obstructive sleep apnoea syndrome. Eye (Lond). 2005;19:575–9.
112. Sagiv O, Fishelson-Arev T, Buckman G, Mathalone N, Wolfson J, Segev E, Peled R, Lavi I, Geyer O. Retinal nerve fiber layer thickness measurements by optical coherence tomography in patients with sleep apnea syndrome. Clin Experiment Ophthalmol. 2014;42:132–8.
113. Lin PW, Friedman M, Lin HC, Chang HW, Pulver TM, Chin CH. Decreased retinal nerve fiber layer thickness in patients with obstructive sleep apnea/hypopnea syndrome. Graefes Arch Clin Exp Ophthalmol. 2011;249:585–93.
114. Moghimi S, Ahmadraji A, Sotoodeh H, Sadeghniat K, Maghsoudipour M, Fakhraie G, Latifi G, Nassiri N, Giaconi JA. Retinal nerve fiber thickness is reduced in sleep apnea syndrome. Sleep Med. 2013;14:53–7.
115. Lin PW, Friedman M, Lin HC, Chang HW, Wilson M, Lin MC. Normal tension glaucoma in patients with obstructive sleep apnea/hypopnea syndrome. J Glaucoma. 2011;20:553–8.
116. Xin C, Zhang W, Wang L, Yang D, Wang J. Changes of visual field and optic nerve fiber layer in patients with OSAS. Sleep Breath. 2015;19(1):129–34.
117. Gutiérrez-Díaz E, Pérez-Rico C, de Atauri MJ, Mencía-Gutiérrez E, Blanco R. Evaluation of the visual function in obstructive sleep apnea syndrome patients and normal-tension glaucoma by means of the multifocal visual evoked potentials. Graefes Arch Clin Exp Ophthalmol. 2012;250:1681–8.
118. Casas P, Ascaso FJ, Vicente E, Tejero-Garcés G, Adiego MI, Cristóbal JA. Retinal and optic nerve evaluation by optical coherence tomography in adults with obstructive sleep apnea-hypopnea syndrome (OSAHS). Graefes Arch Clin Exp Ophthalmol. 2013;251:1625–34.
119. Zengin MO, Tuncer I, Karahan E. Retinal nerve fiber layer thickness changes in obstructive sleep apnea syndrome: one year follow-up results. Int J Ophthalmol. 2014;7:704–8.
120. Huseyinoglu N, Ekinci M, Ozben S, Buyukuysal C, Kale MY, Sanivar HS. Optic disc and retinal nerve fiber layer parameters as indicators of neurodegenerative brain changes in patients with obstructive sleep apnea syndrome. Sleep Breath. 2014;18:95–102.
121. Shiba T, Takahashi M, Sato Y, Onoda Y, Hori Y, Sugiyama T, Bujo H, Maeno T. Relationship between severity of obstructive sleep apnea syndrome and retinal nerve fiber layer thickness. Am J Ophthalmol. 2014;157:1202–8.
122. Nowak MS, Jurowski P, Gos R, Prost ME, Smigielski J. Pulsatile ocular blood flow in subjects with sleep apnoea syndrome. Arch Med Sci. 2011;7:332–6.
123. Adam M, Okka M, Yosunkaya S, Bozkurt B, Kerimoğlu H, Turan M. The evaluation of retinal nerve fiber layer thickness in patients with obstructive sleep apnea syndrome. J Ophthalmol. 2013;2013:292158.
124. Salzgeber R, Iliev ME, Mathis J. Do optic nerve head and visual field parameters in patients with obstructive sleep apnea syndrome differ from those in control individuals? Klin Monbl Augenheilkd. 2014;231:340–3.

125. Kato M, Roberts-Thomson P, Phillips BG, Haynes WG, Winnicki M, Accurso V, Somers VK. Impairment of endotheliumdependent vasodilation of resistance vessels in patients withobstructive sleep apnea. Circulation. 2000;102:2607–10.
126. Xin C, Wang J, Zhang W, Wang L, Peng X. Retinal and choroidal thickness evaluation by SD-OCT in adults with obstructive sleep apnea-hypopnea syndrome (OSAS). Eye (Lond). 2014;28:415–21.
127. Bayhan HA, Bayhan SA, Intepe YS, Muhafız E, Gurdal C. Evaluation of the macular choroidal thickness using spectral optical coherence tomography in patients with obstructive sleep apnea syndrome. Clin Experiment Ophthalmol. 2014 (in press). doi.
128. Frayser R, Gray GW, Houston CS. Control of the retinal circulation at altitude. J Appl Physiol. 1974;37:302–4.
129. Delaey C, Van De Voorde J. Regulatory mechanisms in the retinal and choroidal circulation. Ophthalmic Res. 2000;32:249–56.
130. Zengin MÖ, Oz T, Baysak A, Cinar E, Küçükerdönmez C. Changes in choroidal thickness in patients with obstructive sleep apnea syndrome. Ophthalmic Surg Lasers Imaging Retina. 2014;45:298–304.
131. Karaca EE, Ekici F, Yalçin NG, Ciftçi TU, Ozdek S. Macular choroidal thickness measurements in patients with obstructive sleep apnea syndrome. Sleep Breath. 2015;19(1):335–41.
132. Khayi H, Pepin JL, Geiser MH, Tonini M, Tamisier R, Renard E, Baguet JP, Levy P, Romanet JP, Chiquet C. Choroidal blood flow regulation after posture change or isometric exercise in men with obstructive sleep apnea syndrome. Invest Ophthalmol Vis Sci. 2011;52:9489–96.
133. Tonini M, Khayi H, Pepin JL, Renard E, Baguet JP, Lévy P, Romanet JP, Geiser MH, Chiquet C. Choroidal blood-flow responses to hyperoxia and hypercapnia in men with obstructive sleep apnea. Sleep. 2010;33:811–8.

Chapter 10
Hereditary Optic Neuropathies

Piero Barboni, Giacomo Savini, and Alfredo A. Sadun

Abstract Optical coherence tomography (OCT) has improved our understanding of hereditary optic neuropathies like Leber's hereditary optic neuropathy (LHON) and dominant optic atrophy (DOA). These diseases differentially involve different zones of retinal nerve fibers that progress around the ONH as a wave.

LHON carriers show a thickening of the peripapillary retinal nerve fiber layer (RNFL) in the temporal quadrant, due to a preferential involvement of the papillomacular bundle. Once visual loss occurs, the RNFL reveals an early swelling of the temporal fibers, whose thickness start decreasing soon because of atrophy. A simultaneous thickening takes place in the inferior RNFL sectors for the first 3 months, after which the fibers begin to thin. The superior and nasal sector are involved later. Once the optic nerve is atrophic, all RNFL quadrants are thinner. Analysis of the optic nerve head (ONH) reveals that larger optic discs are associated with a better prognosis.

In DOA, the RNFL reveals diffuse atrophy in all quadrants. The RNFL thinning is more pronounced in the temporal and inferior quadrants and less evident in the superior and nasal ones. Analysis of the macular ganglion cells suggests an earlier involvement of the macular area.

Keywords LHON • DOA • Mitochondria • OCT • mtDNA • RNFL • Retinal Ganglion Cell • RGC • Macular Microcyst • Optic Disk

Hereditary optic neuropathies are diseases affecting the optic nerve. They may presented as isolated optic neuropathies or in association with systemic diseases. The minimum point prevalence of hereditary optic neuropathies is 1 per 10,000 subjects [1]. The most common isolated optic neuropathies are: Leber's Hereditary Optic

P. Barboni, MD
Scientific Institute San Raffaele, Milan, Italy

G. Savini, MD (✉)
Fondazione GB Bietti IRCCS, Rome, Italy
e-mail: giacomo.savini@alice.it

A.A. Sadun, MD, PhD
Doheny Eye Institute, UCLA, Los Angeles, CA, USA

A. Grzybowski, P. Barboni (eds.), *OCT in Central Nervous System Diseases: The Eye as a Window to the Brain*, DOI 10.1007/978-3-319-24085-5_10

Neuropathy (LHON) and Dominant Optic Atrophy (DOA). They both share a mitochondrial pathogenesis that leads to the selective loss of retinal ganglion cells and axons, in particular of the papillo-macular bundle. Over the last decade optical coherence tomography (OCT) has been extensively used to investigate the changes occurring in and optic nerve and macular areas in these diseases.

10.1 Leber's Hereditary Optic Neuropathy

Leber's hereditary optic neuropathy is a maternally inherited genetic disorder usually leading to large bilateral centrocecal scotomas in otherwise healthy young adults [2, 3]. It predominantly affects men and is related to retinal ganglion cell (RGC) degeneration and axonal loss in the optic nerve [4, 5]. The smaller-caliber fibers of the papillomacular bundle are selectively lost at a very early stage of the pathologic process, which eventually extends to the rest of the nerve, leading to optic atrophy [6, 7].

Leber's hereditary optic neuropathy has been associated with mitochondrial DNA (mtDNA) mutations. The three most frequent worldwide and well-established pathogenic mutations affect nucleotide positions 11778, 3460, and 14484, respectively, in ND4, ND1, and ND6 subunit genes of complex I [2, 3]. The mtDNA mutation is necessary but not sufficient to induce the disease. Other, still poorly defined, genetic or environmental factors may be implicated [8]. Thus, penetrance in LHON is not complete and may vary even in different sub-branches of the same family harboring a homoplasmic mtDNA mutation [9].

Clinically, most patients with LHON go through pre-symptomatic ophthalmoscopic changes before the acute phase, characterized by visual loss, developes. Ophthalmoscopic features, already present at the presymptomatic stage, include peripapillary microangiopathy, small vessel tortuosity, swelling of the retinal nerve fiber layer (RNFL) and lack of vessel leakage at fluorescein angiography [10, 11]. These characteristics may wax and wane throughout life in many carrier subjects. Once the disease becomes symptomatic and the patient experiences loss of central vision, the vascular changes increase with swelling of the superior and inferior fiber arcades and rapid loss of the papillomacular bundle [11, 12]. As the pathologic process progresses, temporal pallor may become evident. Then nerve fiber swelling decreases concomitantly with the extension of optic disc pallor toward complete atrophy; vascular changes follow a similar pattern. By 6 months after onset, optic atrophy is usually evident, and visual loss stabilizes, having reached the nadir [13, 14]. The chronic phase is universally reached by 1 year after onset. Rare reports described a stepwise worsening of visual acuity, whereas some individuals may recover different degrees of visual acuity, more frequently those harboring the 14484 mutation [2, 3, 14].

10.1.1 Retinal Nerve Fiber Layer Analysis

Optical coherence tomography has been used to investigate the RNFL of LHON unaffected carriers [15], as well as LHON affected patients in the early and atrophic stage of the diseases [16].

As regards LHON unaffected carriers, a significant thickness increase has been observed in the temporal RNFL quadrant and, in males, it also in the inferior quadrant (Fig. 10.1) [15]. This finding confirms that in subclinical LHON the papillomacular bundle is selectively affected. The preferential involvement of the papillomacular bundle has been linked to the disadvantageous energetic conditions of small axons from macular parvocellular retinal ganglion cells. These small fibers have a high firing rate, and are thought to be very energy dependent [6]. A mathematical model of these fibers and their susceptibility to mitochondrial dysfunction, predicts the pattern of fiber involvement in LHON as shown by histology and morphology [7, 17, 18]. Retinal nerve fiber layer thickening seems mostly related to axonal swelling, which has been proposed to be a sign of impaired axonal transport, with redistribution of mitochondria within the dysfunctional retinal ganglion cells, particularly affecting the prelaminar, unmyelinated portion of the axons at the optic nerve head [6, 18]. Moreover, the peripapillary RNFL in LHON carriers showed higher thickness variability compared to controls, when measured at different time points [19]. The explanation of the RNFL variability could be either a compensatory mechanism (due to increased mitochondrial biogenesis) or an axonal stasis preceding the RGCs loss [6]. Another subclinical factor which may cause RNFL variability, is LHON microangiopathy [19].

In the acute phase, and more precisely within 6 months after onset of the visual defect, RNFL analysis of LHON patients shows thickening in the superior and inferior quadrants, whereas the temporal quadrant shows no significant differences compared to the controls (Fig. 10.2a, b) [16]. Finally, once the optic nerve is atrophic, all quadrants of the peripapillary RNFL show a thinning of the fibers. The lack of any thickening of the papillomacular bundle in the acute phase has been interpreted as early atrophy of the fibers in this sector following the pseudo-edematous stage.

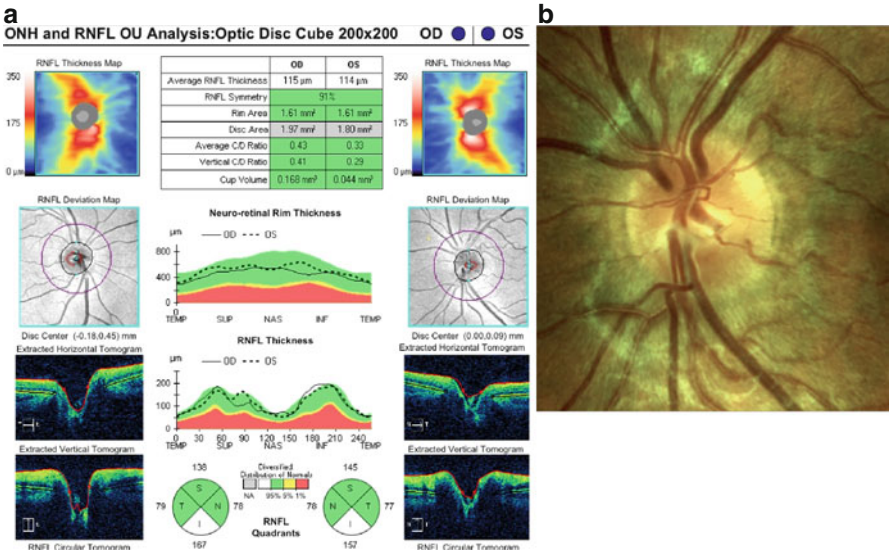

Fig. 10.1 (**a**) Peripapillary RNFL thickening more evident in the inferior quadrant of an unaffected LHON-carrier. (**b**) The left eye optic disc of the same patient

In the atrophic stage of the disease, patients with visual recovery maintain a thicker RNFL than the subgroup without visual recovery in all quadrants but the temporal one [16].

Optical coherence tomography has also been used to investigate the temporal sequence of RNFL changes during the acute phase of LHON [20, 21]. The papillomacular fibers show marked swelling at the time of visual loss, but their thickness starts decreasing soon due to early atrophy. A simultaneous thickening takes place in the inferior RNFL sectors for the first 3 months, after which the fibers begin to thin [20]. These findings are in good agreement with the larger temporal and inferior thickening observed in LHON carriers [15]. The superior and nasal sector are involved in a subsequent stage and show thickening after 3 months, when the other sectors are already in the atrophic phase [20]. The acute phase of LHON has proven to be a more dynamic and progressive phase than was previously envisaged, being characterized by a series of events lasting at least 3 months (Fig. 10.3a, b) [20].

A recent study on RNFL pattern of swelling and subsequent atrophy, hypothesized a different natural course between patients carrying 11778 vs 14484 mutations

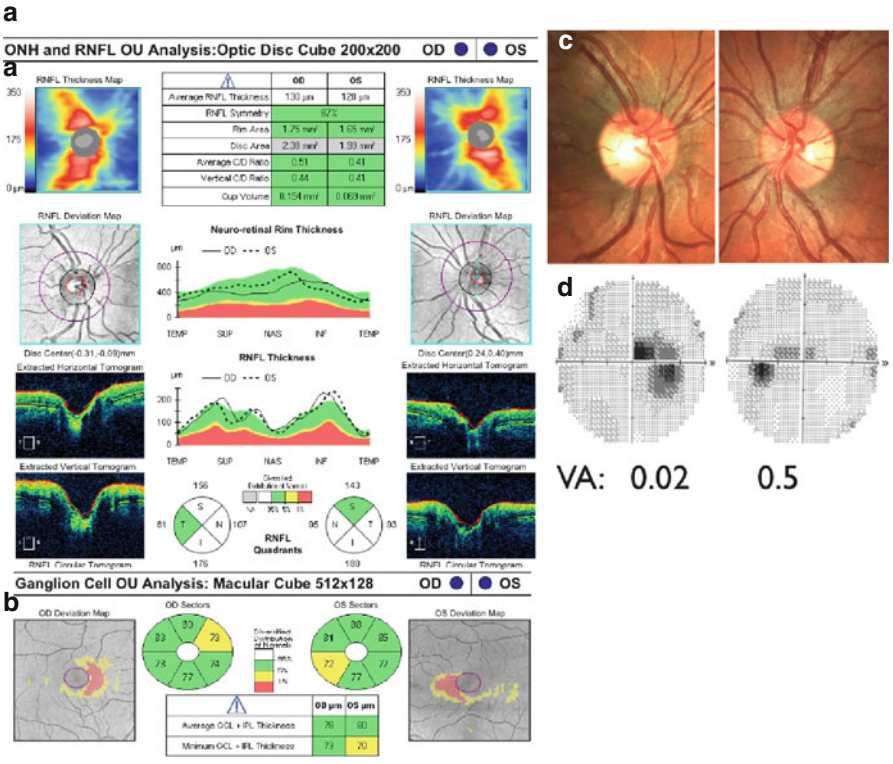

Fig. 10.2 (**a**) Acute phase of LHON with (*A*) peripapillary RNFL thickening, (*B*) early ganglion cell atrophy, (*C*) temporal pallor of the optic disc and (*D*), central scotoma in the visual field. (**a**) RNFL thickness and deviation maps (*top*) RNFL progression analysis (*bottom*), (**b**) Progressive RNFL thinning in LHON from the acute (*top*) to the atrophic (*bottom*) stage, (**c**) RNFL thickness profile

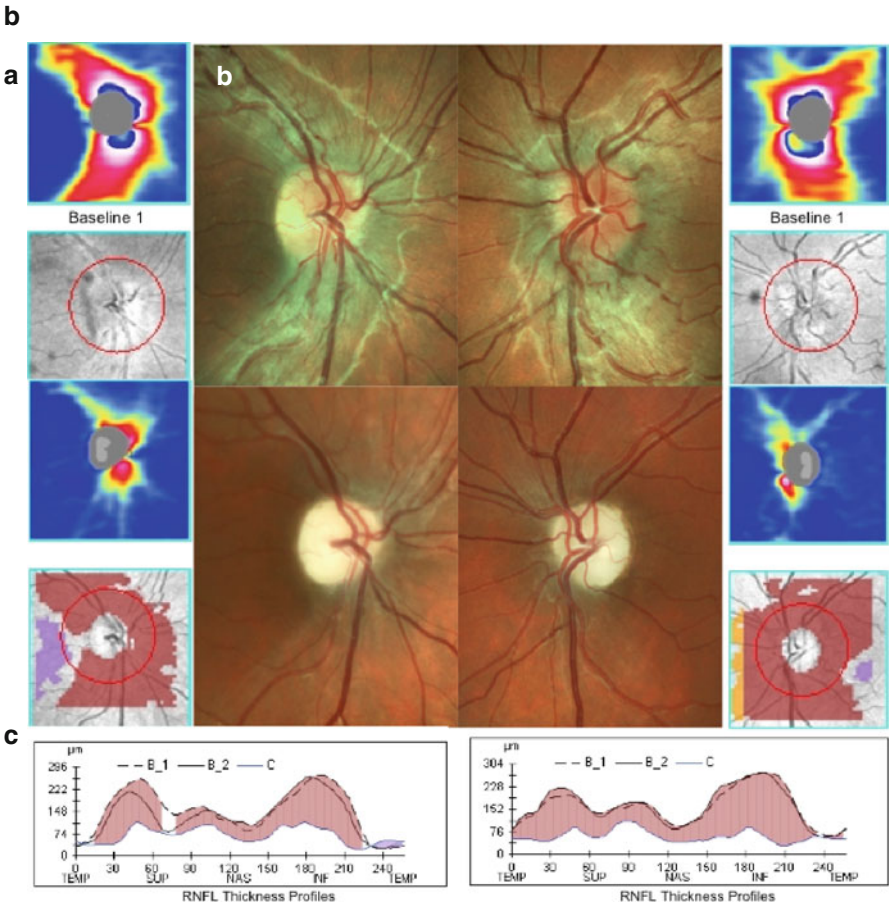

Fig. 10.2 (continued)

[22]. The RNFL thickening in early stage (<6 month from onset) and thinning in the late stage of the disease (>6 months) was significant greater in 11778 patients than in 14484 [22]. These results could explained the different visual prognosis between mutations and establishes a correlation between the initial swelling of RNFL and the visual prognosis [22].

OCT analysis of the RNFL in childhood LHON shows that in acute forms there is diffuse fiber atrophy affecting all quadrants (Fig. 10.4a, b) [23]. This finding holds for all acutely affected eyes, in both bilateral and unilateral forms. In this sense, the childhood forms do not differ from adult-onset ones. Slowly progressive forms show a significant fiber reduction in the temporal quadrant, which extends, albeit mildly, to the inferior quadrant, with relative preservation of fibers in the other sector [23]. Finally, in eyes with a subclinical course of disease, the situation in terms of fiber loss is comparable to that of slowly progressive forms, with preferential involvement of the temporal quadrant and, to a lesser extent, of the inferior one.

In these two atypical forms, slowly progressive and subclinical, the ophthalmoscopic picture and pattern of fiber loss, though clinically reminiscent of DOA, are more typical of LHON, since the damage remains limited to the papillomacular bundle without extending to other fibers, as occurs in DOA [23].

The three primary mtDNA mutations have different visual prognosis: worst for 3460/ND1, intermediate for 11778/ND4, and better for 14484/ND6 [13]. OCT studies did not show any difference in RNFL thickness between chronic patients without visual recovery carrying 11778 and 3460 mutations [16]. Patients experiencing recovery of vision showed a thicker RNFL in all quadrants but the temporal compared with patients without visual recovery [16].

A recent study in a large cohort of Korean LHON patients demonstrated a similar pattern of RNFL thinning in patients carrying primary and secondary mtDNA mutations, despite the better visual prognosis in patients with secondary mutation [24].

There is evidence, also involving rare LHON mtDNA mutations of a variable pattern of RNFL thinning. For example, the 3890/ND1 mutation is associated with a bad visual prognosis and a severe thinning of the peripapillary RNFL [25].

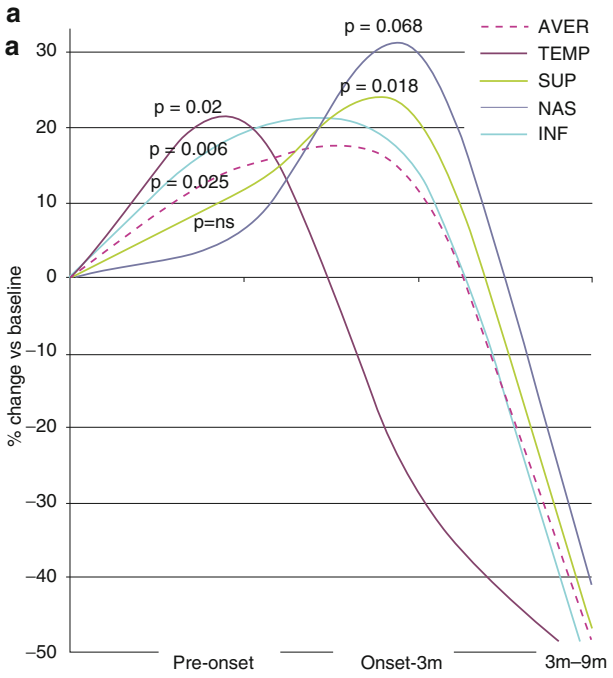

Fig. 10.3 (**a**) Progressive RNFL changes from the onset to the atrophic stage of LHON. The temporal quadrant reveals early thickening, whereas the remaining quadrants undergo later thickening up to 3 months. *AVER* average, *INF* inferior, *NAS* nasal, *SUP* superior, *TEMP* temporal (Reproduced with permission from: Barboni et al. [20]). (**b**) Example of progressive RNFL thinning in a patient with atrophic LHON

b

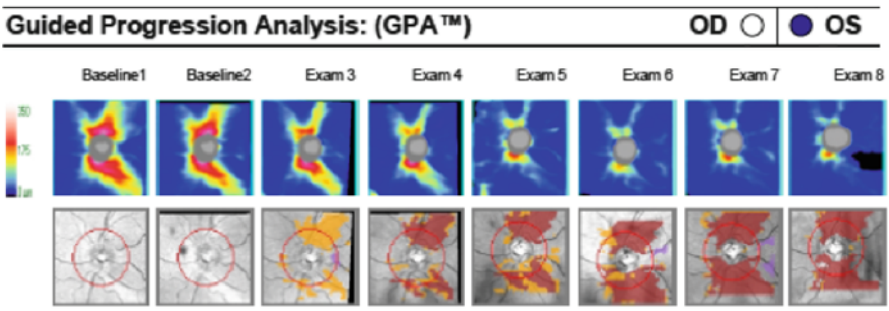

RNFL and ONH Summary Parameters

		Exam Date/Time	Serial Number	Registration Method	SS	Avg RNFL Thickness (µm)	Inf Quadrant RNFL (µm)	Sup Quadrant RNFL (µm)	Rim Area (mm^2)	Average Cup-to-Disc Ratio	Vertical Cup-to-Disc Ratio	Cup Volume (mm^3)
Baseline1:	1	12/16/2010 1:16:30 PM	4000-2487		9/10	105	144	130	1.76	0.46	0.37	0.136
Baseline2:	2	1/20/2011 12:40:56 PM	4000-2487	R2	7/10	96	136	125	1.86	0.46	0.37	0.142
	3	6/27/2011 1:38:32 PM	4000-2487	R2	8/10	80	116	91	1.54	0.54	0.45	0.193
	4	9/29/2011 1:31:33 PM	4000-2487	R2	7/10	70	99	79	1.36	0.60	0.50	0.231
	5	3/16/2012 3:06:54 PM	4000-2487	R1	7/10	61	76	66	1.23	0.67	0.56	0.273
	6	11/26/2012 1:31:48 PM	4000-2487	R1	7/10	59	69	64	1.18	0.69	0.60	0.304
	7	4/16/2013 1:18:51 PM	4000-2487	R1	8/10	58	68	57	1.08	0.69	0.60	0.287
Current:	8	11/25/2013 1:09:17 PM	4000-2487	R1	6/10	55	66	58	1.31	0.72	0.63	0.350

Fig. 10.3 (continued)

10.1.2 Optic Nerve Head Analysis

Optical coherence tomography also enables to investigate the size of the optic nerve head (ONH). LHON carriers show a larger ONH than symptomatic patients and even healthy controls (Fig. 10.5) [26]. Therefore, it has been suggested that a larger ONH size, probably associated with less crowding of RGC axons, may represents a favorable prognostic factor and be a protective factor preserving LHON carriers from developing the acute phase of the disease. Moreover, since the LHON-affected subgroup of patients with visual recovery also had a significantly larger ONH, this anatomic feature may also improve the visual prognosis and influence the final visual outcome in those individuals who develop the optic neuropathy. After stratifying LHON affected and carrier patients by mtDNA mutations, 11778, 3460 and 3733 carriers had larger optic nerve discs than affected [26]. 14484 affected and carrier patients had the same disc size that was larger than the other mutations [26].

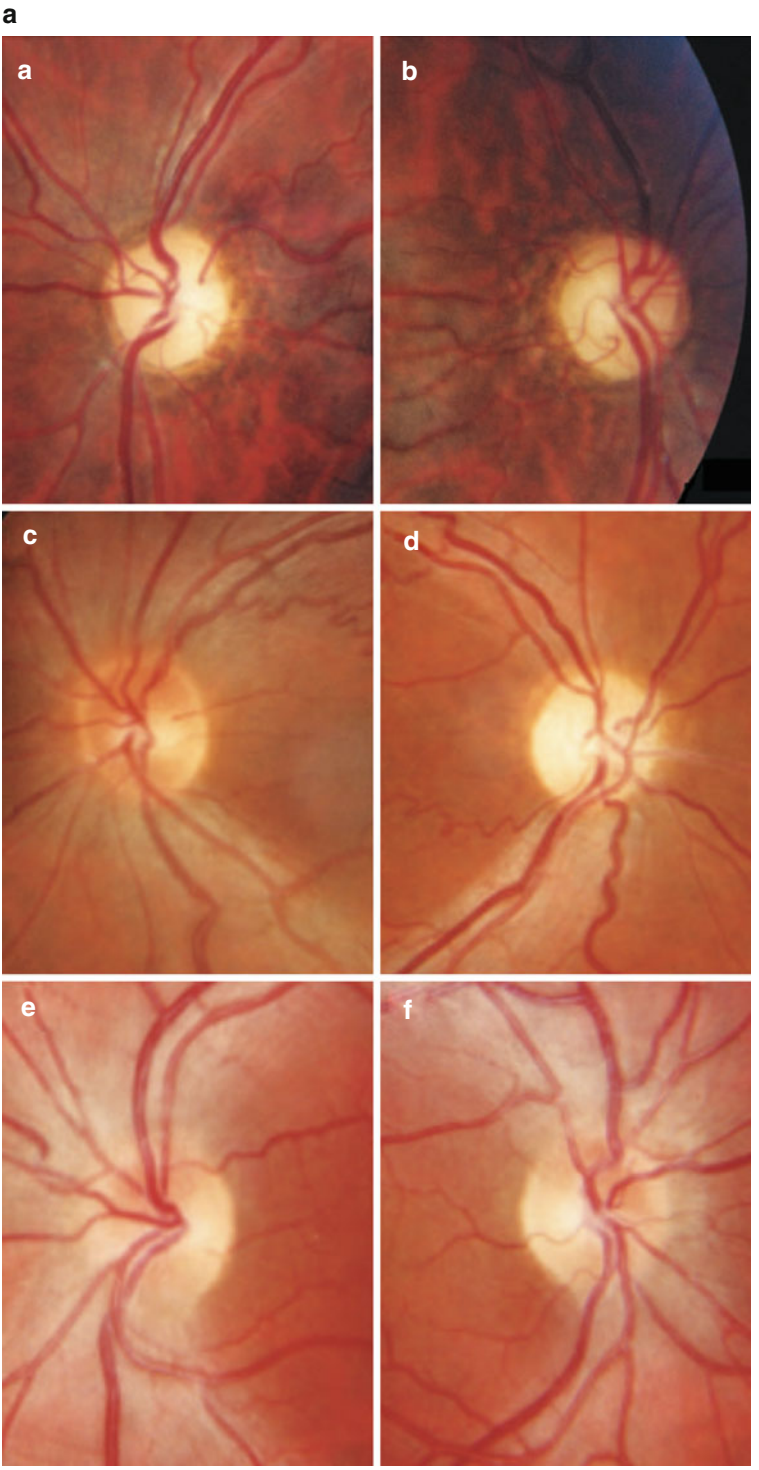
a
a
b
c
d
e
f

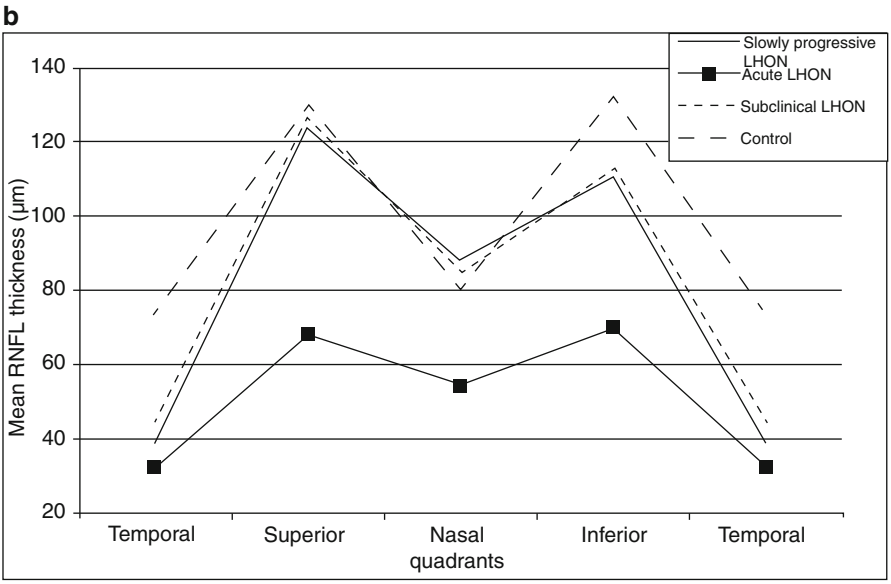

Fig. 10.4 (continued)

Moreover, ONH analysis in acute childhood LHON patients showed smaller optic disc areas compared with patients with slowly progressive and subclinical courses of the disease and controls (Fig. 10.4a) [23].

The role of the ONH size is likely to be related to the mechanical compression of the papillo-macular bundle fibers, which are the first and most severely affected in the subclinical and early stages. The subsequent swelling of the RNFL along the superior and inferior arcades, typical of the acute stage, may induce a mechanical compression of the temporal fibers and thus trigger dysfunction and axonal death in the papillo-macular bundle. The greater space for nerve fibers may reduce the risk

Fig. 10.4 (**a**) Color fundus pictures of the right and left eyes. Acute bilateral LHON: Diffuse atrophy of the optic discs is evident without microangiopathy (*A*, *B*). Acute unilateral LHON: The affected eye (*C*) shows optic disc atrophy, more evident in the temporal quadrant, whereas the fellow eye (*D*), classified as subclinical, reveals temporal atrophy of the optic disc, a mild degree of microangiopathy, and nerve fiber layer swelling as the most prominent signs. LHON with a slowly progressive course: Temporal optic atrophy with mild nerve fiber layer swelling of the other quadrant is detected in both eyes (*E*, *F*) (Reproduced with permission from: Barboni et al. [23]). (**b**) RNFL thickness in each quadrant of slowly progressive, acute, and subclinical Leber's hereditary optic neuropathy (*LHON*), compared to that in the control group. Compared with the control group, the eyes with acute LHON showed a significantly thinner RNFL in all quadrants. Patients with slowly progressive LHON presented a significant reduction of the temporal quadrant and a not statistically significant reduction of the inferior quadrant. Eyes with a subclinical course showed a reduction (although not statistically significant) of the temporal quadrant and, to a lesser extent, of the inferior quadrant (Reproduced with permission from: Barboni et al. [23])

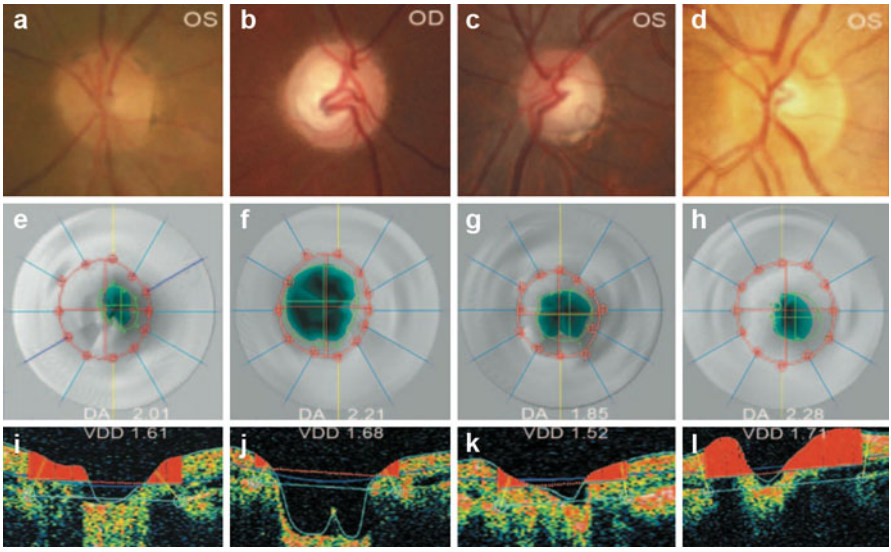

Fig. 10.5 Representative optic nerve head color pictures and OCT analysis (*DA* optic disc area, *VDD* vertical disc diameter) of a control subject (*A*, *E*, *I*), an LHON-affected patient with visual recovery (*B*, *F*, *J*), an LHON-affected patient without visual recovery (*C*, *G*, *K*), and an LHON carrier (*D*, *H*, *L*) (*OD*) right eye, (*OS*) left eye. (Reproduced with permission from: Ramos Cdo et al. [26])

of focal compression of swelling axons and, in cases where the damage occurs, improve the chance of visual recovery.

10.1.3 Retinal Ganglion Cell Analysis

The macular RGC layer is diffusely thinner in LHON affected patients [27, 28]. The early and preferential involvement of RGCs has been demonstrated in the acute stage of the disease [27, 28]. Ganglion cell analysis can detect early damage of the macular RGCs, which precedes axonal loss and RNFL thinning. Topographical analysis of the macular region demonstrated an early involvement of the inner ring, occurring at a higher extent than in the outer ring (Fig. 10.6) [29]. Moreover, analyzing total macular thickness, the temporal quadrant of the outer ring became thinner earlier (within 3–6 months) than the superior and inferior quadrants (within 6–9 months) [30]. These results confirm the ability of OCT to study macular structure and the early involvement of nasal sectors corresponding to the papillo-macular bundle in LHON.

Retinal segmentation of the macular region shows, in addition, that a minority (about 6 %) of LHON and DOA patients have microcystic changes in the inner nuclear layer (Fig. 10.7) [31]. Microcystic macular degeneration is present in the absence of any leakage at the fluorescein angiography and has been related to focal

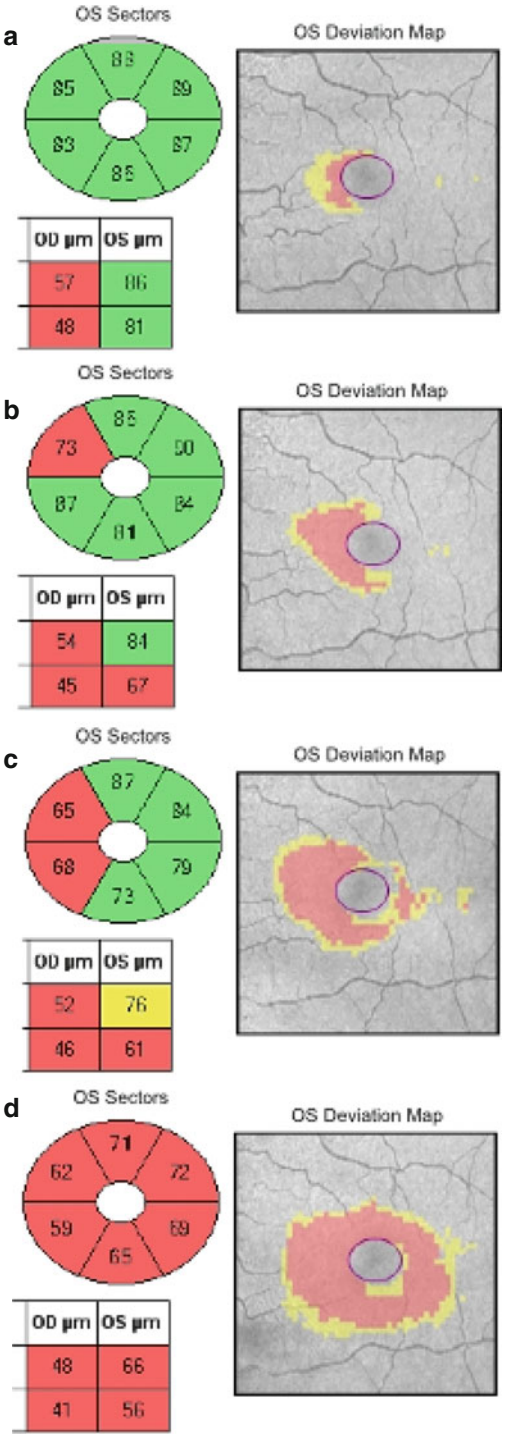

Fig. 10.6 Progressive retinal ganglion cells atrophy in a patient with acute LHON. GC-IPL sectors and deviation map in pre-sypmtomatic stage (**a**), at 1 month (**b**), 2 month (**c**) and 5 month (**d**) from disease onset

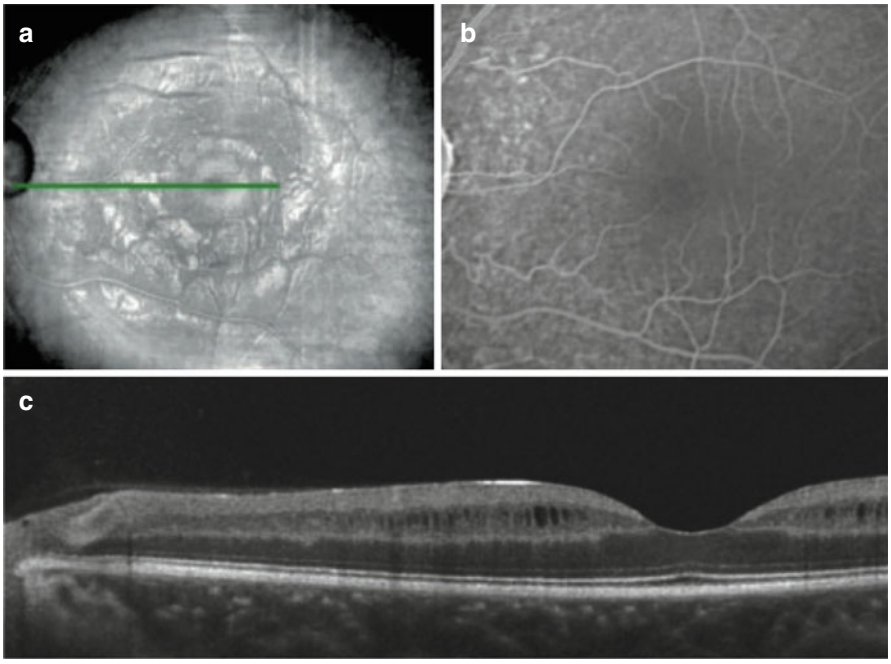

Fig. 10.7 Microcystic macular degeneration in a patient with LHON. (**a**) red free fundus picture, (**b**) fluorescein angiography and (**c**) corresponding HD-OCT line of the macula

retinal schisis induced by vitreous traction in association with RNFL atrophy [31]. Macular microcysts has been originally described in inflammatory optic neuritis in MS and NMO, possibly correlating with the severity of the inflammatory process [32–35]. However, macular microcysts have also been described in compressive optic neuropathy [36], in optic neuritis not due to MS [37, 38], and in glaucoma [39].

10.2 Dominant Optic Atrophy (DOA)

DOA is a similar hereditary degenerative optic neuropathy to LHON. However, DOA is due to a mutation in the nuclear genome. Most cases of DOA have been associated with mutations in the OPA1 gene on the long arm of chromosome 3q28–q29, which encodes a dynamin-related GTPase targeted to mitochondria [40]. Seventy-five percent of DOA patients have a mutation in OPA1 gene; two loci, OPA4 and OPA5, are associated to pure DOA, one X-linked, OPA2, and two recessive, OPA6 and OPA7, and two syndromic recessive or dominant, OPA3 and OPA8 [41–43]. DOA patients can be also defined by the mutation type: OPA1 mutation causing haploinsufficiency and OPA1 missense mutation [44].

DOA has a clinical picture more insidious than that of LHON, as it is characterized by very slowly progressive bilateral visual loss starting in childhood and ultimately leading to moderate or severe optic atrophy [45–48]. The disease has incomplete penetrance and variable expression between and within families; it ranges from subclinical manifestations to legal blindness. Twenty percent of DOA patients with OPA1 mutations have a more severe disease with neuromuscular features (DOA plus) [49, 50].

10.2.1 Retinal Nerve Fiber Layer Analysis

OCT analysis of the RNFL in DOA reveals fiber atrophy affecting all quadrants [51–53]. The retinal thinning involves the RNFL and RGC layers, whereas the photoreceptor layers are morphologically unaffected (Fig. 10.8).

The RNFL thinning is more pronounced in the temporal and inferior quadrants and less evident in the superior and nasal ones [51–53]. This pattern of RNFL atrophy is generally comparable to the pattern observed in LHON, confirming the vulnerability of the small fibers of the papillomacular bundle as a pathognomonic sign

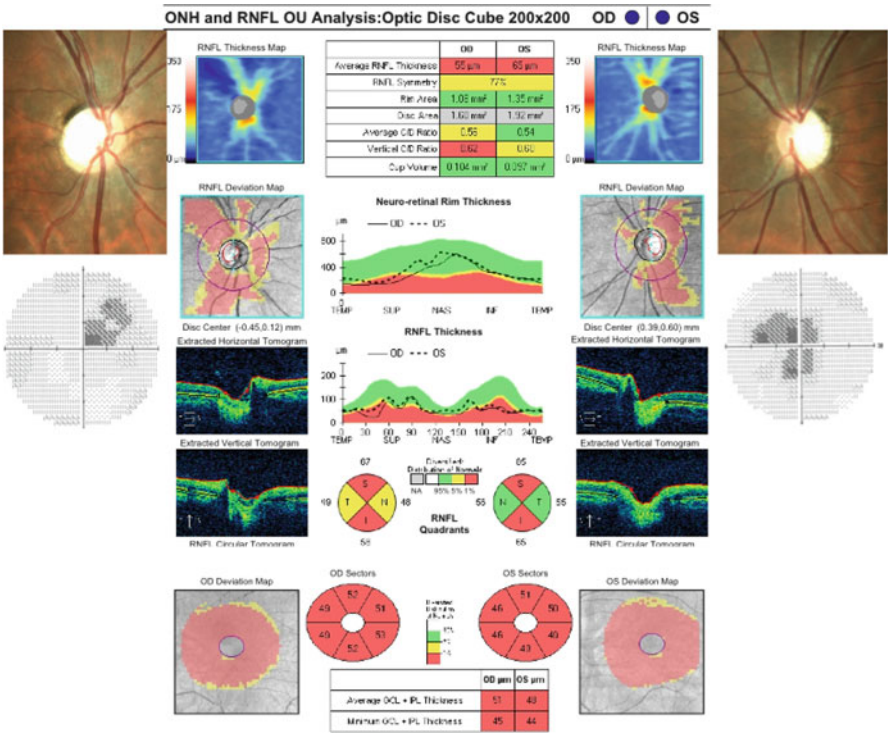

Fig. 10.8 Peripapillary RNFL and macular ganglion cell analysis in a patient with DOA

of mitochondrial optic neuropathies. Patients with DOA plus disease show a more severe thinning of RNFL in all quadrants compared with simple DOA patients [53].

The progressive fiber loss in affected patients (0.19–0.20 μm/year for the 360° average measurement) is similar to that occurring with age in healthy subjects, where the loss ranges between 0.16 and 0.25 μm/year [54–56]. This observation, in combination to the smaller ONH of DOA patients (see the next paragraph), suggests that visual loss in DOA patients is related to progressive fiber loss in eyes with already lower congenital or neonatal fiber counts.

The pattern of fiber loss, studied by OCT, in OPA8 patients did not differ from that found in OPA1 patients [57].

10.2.2 Retinal Ganglion Cell Analysis

Spectral domain OCT of patients with DOA shows an earlier involvement of the macular RGCs, whose thickness is more reduced compared to that of the RNFL in patients with highest visual acuity [58, 29]. All macular sectors are involved and the thinner sectors were the nasal and inferior zones [29, 59]. As the disease progresses and visual acuity worsens, the macular RGCs measurements correlated with visual acuity losses better than measures of RNFL thinning (Fig. 10.8) [29, 59]. A genotype/phenotype correlation, stratifying OCT measurement by OPA1 mutation type, shows that missense mutations had the most severe reductions in both RNFL and macular RGCs thickness [29].

Microcystic changes of the macular inner nuclear layer have been identified in about 6 % of patients affected with DOA [31].

10.2.3 Optic Nerve Head Analysis

Patients affected with DOA and carrying OPA1 gene mutations reveal a smaller ONH than controls (Fig. 10.9) [61]. Both the optic disc area and ONH diameters are significantly smaller [61]. By stratifying these results according to OPA1 mutation, it is possible to identify different degrees of optic disc size, where the mutations range from those associated with a normal optic disc size to those associated with much smaller sizes and more severe clinical features of DOA. The proposed hypothesis is that OPA1 expression regulates apoptosis, thereby playing an important role in the embryonic development of the eye and contributing to the determination of optic disc size and conformation. As stated in the previous paragraph, a constitutive low content of fibers in the optic nerve and the age-related RNFL loss may explain the progressive visual loss in DOA. DOA patients with the lowest visual acuity have a smaller disc area, measured by OCT, compared to controls [60].

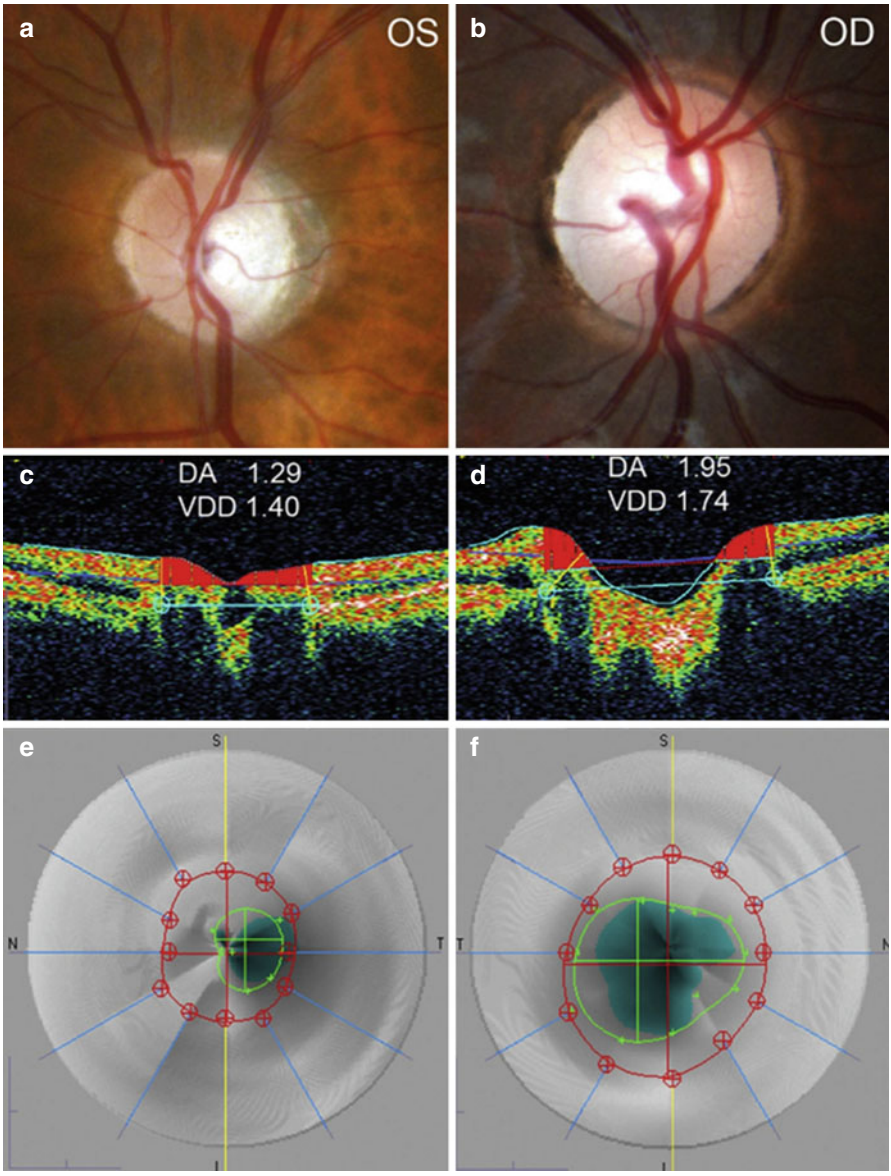

Fig. 10.9 Representative optic nerve head color pictures and OCT analysis of a DOA patient with a small optic disc (*A*, *C*, *E*), and a DOA patient with normal optic disc size (*B*, *D*, *F*). *DA* optic disc area, *VDD* vertical disc diameter (Reproduced with permission from: Barboni et al. [60])

OCT analysis showed that DOA patients who do not recover vision on Idebenone therapy, have thinner RNFL and smaller ONH than patients with visual

recovery [61]. This result add further evidence for the prognostic value of OCT in therapeutic protocols.

10.3 Conclusions

Over the last decade, OCT enabled us to better understand the diagnosis and follow-up of optic neuropathies. Moreover, the additional information achieved by OCT about the pathophysiology of this disease has improved our knowledge on the disease conversion and progression. In the next step, OCT will be able to indicate the timing and the prognosis of future therapeutic approaches.

References

1. Yu-Wai-Man P, Griffiths PG, Chinnery PF. Mitochondrial optic neuropathies disease mechanisms and therapeutic strategies. Prog Retin Eye Res. 2011;30:81–114.
2. Newman NJ. Hereditary optic neuropathies. In: Miller NR, Newman NJ, editors. Walsh and Hoyt's clinical neuro-ophthalmology. 5th ed. Baltimore: Williams & Wilkins; 1998. p. 742–53.
3. Carelli V. Leber's hereditary optic neuropathy. In: Schapira AHV, DiMauro S, editors. Mitochondrial disorders in neurology. Blue books of practical neurology, vol. 26. 2nd ed. Boston: Butterworth-Heinemann; 2002. p. 115–42.
4. Sadun AA, Kashima Y, Wurdeman AE, et al. Morphological findings in the visual system in a case of Leber's hereditary optic neuropathy. Clin Neurosci. 1994;2:165–72.
5. Kerrison JB, Howell N, Miller NR, Hirst L, Green WR. Leber hereditary optic neuropathy. Electron microscopy and molecular genetic analysis of a case. Ophthalmology. 1995;102:1509–16.
6. Sadun AA, Win PH, Ross-Cisneros FN, Walker SO, Carelli V. Leber's hereditary optic neuropathy differentially affects smaller axons in the optic nerve. Trans Am Ophthalmol Soc. 2000;98:223–32; discussion 232–5.
7. Pan BX, Ross-Cisneros FN, Carelli V, Rue KS, Salomao SR, Moraes-Filho MN, et al. Mathematically modeling the involvement of axons in Leber's hereditary optic neuropathy. Invest Ophthalmol Vis Sci. 2012;53:7608–17.
8. Carelli V, Giordano C, d'Amati G. Pathogenic expression of homoplasmic mtDNA mutations needs a complex nuclear- mitochondrial interaction. Trends Genet. 2003;19:257–62.
9. Howell N, Mackey DA. Low-penetrance branches in matrilinear pedigrees with Leber hereditary optic neuropathy. Am J Hum Genet. 1998;63:1220–4.
10. Nikoskelainen E, Hoyt WF, Nummelin K. Ophthalmoscopic findings in Leber's hereditary optic neuropathy. I. Fundus findings in asymptomatic family members. Arch Ophthalmol. 1982;100:1597–602.
11. Nikoskelainen E, Hoyt WF, Nummelin K. Ophthalmoscopic findings in Leber's hereditary optic neuropathy. II. The fundus findings in affected family members. Arch Ophthalmol. 1983;101:1059–68.
12. Smith JL, Hoyt WF, Susac JO. Ocular fundus in acute Leber optic neuropathy. Arch Ophthalmol. 1973;90:349–54.
13. Riordan-Eva P, Sanders D, Govan GG, Sweeney MG, Da Costa J, Harding AE. The clinical features of Leber's hereditary optic neuropathy defined by the presence of a pathogenic mitochondrial DNA mutation. Brain. 1995;118:319–37.

14. Nikoskelainen EK, Huoponen K, Juvonen V, Lamminen T, Nummelin K, Savontaus ML. Ophthalmologic findings in Leber hereditary optic neuropathy, with special reference to mtDNA mutations. Ophthalmology. 1996;103:504–14.
15. Savini G, Barboni P, Valentino ML, Montagna P, Cortelli P, De Negri AM, et al. Retinal nerve fiber layer evaluation by optical coherence tomography in unaffected carriers with Leber's hereditary optic neuropathy mutations. Ophthalmology. 2005;112:127–31.
16. Barboni P, Savini G, Valentino ML, Montagna P, Cortelli P, De Negri AM, et al. Retinal nerve fiber layer evaluation by optical coherence tomography in Leber's hereditary optic neuropathy. Ophthalmology. 2005;112:120–6.
17. Sadun AA, La Morgia C, Carelli V. Mitochondrial optic neuropathies: our travels from bench to bedside and back again. Clin Experiment Ophthalmol. 2013;41:702–12.
18. Carelli V, Ross-Cisneros FN, Sadun AA. Mitochondrial dysfunction as a cause of optic neuropathies. Prog Retin Eye Res. 2004;23:53–89.
19. Barboni P, Savini G, Feuer WJ, Budenz DL, Carbonelli M, Chicani F, et al. Retinal nerve fiber layer thickness variability in Leber hereditary optic neuropathy carriers. Eur J Ophthalmol. 2012;4(22):985–91.
20. Barboni P, Carbonelli M, Savini G, Ramos Cdo V, Carta A, Berezovsky A, et al. Natural history of Leber's hereditary optic neuropathy: longitudinal analysis of the retinal nerve fiber layer by optical coherence tomography. Ophthalmology. 2010;117:623–7.
21. Zhang Y, Huang H, Wei S, Qiu H, Gong Y, Li H, et al. Characterization of retinal nerve fiber layer thickness changes associated with Leber's hereditary optic neuropathy by optical coherence tomography. Exp Ther Med. 2014;7:483–7.
22. Seo JH, Hwang JM, Park SS. Comparison of retinal nerve fibre layers between 11778 and 14484 mutations in Leber's hereditary optic neuropathy. Eye (Lond). 2010;24:107–11.
23. Barboni P, Savini G, Valentino ML, La Morgia C, Bellusci C, De Negri AM, et al. Leber's hereditary optic neuropathy with childhood onset. Invest Ophthalmol Vis Sci. 2006;47:5303–9.
24. Yum HR, Chae H, Shin SY, Kim Y, Kim M, Park SH. Pathogenic mitochondrial DNA mutations and associated clinical features in Korean patients with Leber's hereditary optic neuropathy. Invest Ophthalmol Vis Sci. 2014;55:8095–101.
25. Caporali L, Ghelli AM, Iommarini L, Maresca A, Valentino ML, La Morgia C, et al. Cybrid studies establish the causal link between the mtDNA m.3890G>A/MT-ND1 mutation and optic atrophy with bilateral brainstem lesions. Biochim Biophys Acta. 2013;1832:445–52.
26. Ramos C do V, Bellusci C, Savini G, Carbonelli M, Berezovsky A, Tamaki C, et al. Association of optic disc size with development and prognosis of Leber's hereditary optic neuropathy. Invest Ophthalmol Vis Sci. 2009;50:1666–74.
27. Akiyama H, Kashima T, Li D, Shimoda Y, Mukai R, Kishi S. Retinal ganglion cell analysis in Leber's hereditary optic neuropathy. Ophthalmology. 2013;120:1943–5.
28. Mizoguchi A, Hashimoto Y, Shinmei Y, Nozaki M, Ishijima K, Tagawa Y, et al. Macular thickness changes in a patient with Leber's hereditary optic neuropathy. BMC Ophthalmol. 2015;15:27.
29. Barboni P, Savini G, Cascavilla M, Caporali L, Milesi J, Borrelli E, et al. Early macular retinal ganglion cell loss in dominant optic atrophy: genotype-phenotype correlation. Am J Ophthalmol. 2014;158:628–36.
30. Zhang Y, Huang H, Wei S, Gong Y, Li H, Dai Y, et al. Characterization of macular thickness changes in Leber's hereditary optic neuropathy by optical coherence tomography. BMC Ophthalmol. 2014;14:105.
31. Barboni P, Carelli V, Savini G, Carbonelli M, La Morgia C, Sadun AA. Microcystic macular degeneration from optic neuropathy: not inflammatory, not trans-synaptic degeneration. Brain. 2013;136(Pt 7):e239.
32. Gelfand JM, Nolan R, Schwartz DM, Graves J, Green AJ. Microcystic macular oedema in multiple sclerosis is associated with disease severity. Brain. 2012;135:1786–93.
33. Gelfand JM, Cree BA, Nolan R, Arnow S, Green AJ. Microcystic inner nuclear layer abnormalities and neuromyelitis optica. JAMA Neurol. 2013;70:629–33.

34. Saidha S, Sotirchos ES, Ibrahim MA, Crainiceanu CM, Gelfand JM, Sepah YJ, et al. Microcystic macular oedema, thickness of the inner nuclear layer of the retina, and disease characteristics in multiple sclerosis: a retrospective study. Lancet Neurol. 2012;11:963–72. Erratum in: Lancet Neurol. 2012;11:1021.
35. Schneider E, Zimmermann H, Oberwahrenbrock T, Kaufhold F, Kadas EM, Petzold A, et al. Optical coherence tomography reveals distinct patterns of retinal damage in neuromyelitis optica and multiple sclerosis. PLoS One. 2013;8:e66151.
36. Abegg M, Zinkernagel M, Wolf S. Microcystic macular degeneration from optic neuropathy. Brain. 2012;135:e225.
37. Balk L, Killestein J, Polman C, Uitdehaag BM, Petzold A. Microcystic macular oedema confirmed, but not specific for MS. Brain. 2012;135:e226; author reply e227.
38. Kaufhold F, Zimmermann H, Schneider E, Ruprecht K, Paul F, Oberwahrenbrock T, et al. Optic neuritis is associated with inner nuclear layer thickening and microcystic macular edema independently of multiple sclerosis. PLoS One. 2013;8:e71145.
39. Wolff B, Basdekidou C, Vasseur V, Mauget-Faÿsse M, Sahel JA, Vignal C. Retinal inner nuclear layer microcystic changes in optic nerve atrophy: a novel spectral-domain OCT finding. Retina. 2013;33:2133–8.
40. Alexander C, Votruba M, Pesch UE, Thiselton DL, Mayer S, Moore A, et al. OPA1, encoding a dynamin-related GTPase, is mutated in autosomal dominant optic atrophy linked to chromosome 3q28. Nat Genet. 2000;26:211–5.
41. Ferre M, Amati-Bonneau P, Tourmen Y, Malthièry Y, Reynier P. eOPA1: an online database for OPA1 mutations. Hum Mutat. 2005;25:423–8 [PubMed: 15832306].
42. Ferre M, Bonneau D, Milea D, Chevrollier A, Verny C, Dollfus H, et al. Molecular screening of 980 cases of suspected hereditary optic neuropathy with a report on 77 novel OPA1 mutations. Hum Mutat. 2009;30:E692–705.
43. Yu-Wai-Man P, Shankar SP, Biousse V, Miller NR, Bean LJ, Coffee B, et al. Genetic screening for OPA1 and OPA3 mutations in patients with suspected inherited optic neuropathies. Ophthalmology. 2010;118:558–63.
44. Amati-Bonneau P, Valentino ML, Reynier P, Gallardo ME, Bornstein B, Boissière A, et al. OPA1 mutations induce mitochondrial DNA instability and optic atrophy 'plus' phenotypes. Brain. 2008;131:338–51.
45. Kjer P. Infantile optic atrophy with dominant mode of inheritance: a clinical and genetic study of 19 Danish families. Acta Ophthalmol Suppl. 1959;164(suppl):1–147.
46. Newman NJ. Hereditary optic neuropathies. In: Miller NR, Newman NJ, Biousse V, Kerrison JB, Assoc, editors. Walsh and Hoyt's clinical neuro-ophthalmology. 6th ed, vol. 1. Philadelphia: Lippincott Williams & Wilkins; 2005. p. 465–501.
47. Cohn AC, Toomes C, Hewitt AW, Kearns LS, Inglehearn CF, Craig JE, et al. The natural history of OPA1-related autosomal dominant optic atrophy. Br J Ophthalmol. 2008;92:1333–6.
48. Yu-Wai-Man P, Griffiths PG, Burke A, Sellar PW, Clarke MP, Gnanaraj L, et al. The prevalence and natural history of dominant optic atrophy due to OPA1 mutations. Ophthalmology. 2010;117:1538–46.
49. Amati-Bonneau P, Guichet A, Olichon A, Chevrollier A, Viala F, Miot S, Ayuso C, et al. OPA1 R445H mutation in optic atrophy associated with sensorineural deafness. Ann Neurol. 2005;58:958–63.
50. Hudson G, Amati-Bonneau P, Blakely EL, Stewart JD, He L, Schaefer AM, et al. Mutation of OPA1 causes dominant optic atrophy with external ophthalmoplegia, ataxia, deafness and multiple mitochondrial DNA deletions: a novel disorder of mtDNA maintenance. Brain. 2008;131:329–37.
51. Milea D, Sander B, Wegener M, Jensen H, Kjer B, Jørgensen TM, et al. Axonal loss occurs early in dominant optic atrophy. Acta Ophthalmol. 2010;88:342–6.
52. Barboni P, Savini G, Parisi V, Carbonelli M, La Morgia C, Maresca A, et al. Retinal nerve fiber layer thickness in dominant optic atrophy measurements by optical coherence tomography and correlation with age. Ophthalmology. 2011;118:2076–80.

53. Yu-Wai-Man P, Bailie M, Atawan A, Chinnery PF, Griffiths PG. Pattern of retinal ganglion cell loss in dominant optic atrophy due to OPA1 mutations. Eye (Lond). 2011;25:596–602.
54. Parikh RS, Parikh SR, Sekhar GC, Prabakaran S, Babu JG, Thomas R. Normal age-related decay of retinal nerve fiber layer thickness. Ophthalmology. 2007;114:921–6.
55. Sung KR, Wollstein G, Bilonick RA, Townsend KA, Ishikawa H, Kagemann L, et al. Effects of age on optical coherence tomography measurements of healthy retinal nerve fiber layer, macula and optic nerve head. Ophthalmology. 2009;116:1119–24.
56. Budenz DL, Anderson DR, Varma R, Schuman J, Cantor L, Savell J, et al. Determinants of normal retinal nerve fiber layer thickness measured by Stratus OCT. Ophthalmology. 2007;114:1046–52.
57. Carelli V, Schimpf S, Fuhrmann N, Valentino ML, Zanna C, Iommarini L, et al. A clinically complex form of dominant optic atrophy (OPA8) maps on chromosome 16. Hum Mol Genet. 2011;20:1893–905.
58. Ito Y, Nakamura M, Yamakoshi T, Lin J, Yatsuya H, Terasaki H. Reduction of inner retinal thickness in patients with autosomal dominant optic atrophy associated with OPA1 mutations. Invest Ophthalmol Vis Sci. 2007;48:4079–86.
59. Rönnbäck C, Milea D, Larsen M. Imaging of the macula indicates early completion of structural deficit in autosomal-dominant optic atrophy. Ophthalmology. 2013;120:2672–7.
60. Barboni P, Carbonelli M, Savini G, Foscarini B, Parisi V, Valentino ML, et al. OPA1 mutations associated with dominant optic atrophy influence optic nerve head size. Ophthalmology. 2010;117:1547–53.
61. Barboni P, Valentino ML, La Morgia C, Carbonelli M, Savini G, De Negri A, et al. Idebenone treatment in patients with OPA1-mutant dominant optic atrophy. Brain. 2013;136(Pt2):e231.

Chapter 11
Trans Neuronal Retrograde Degeneration to OCT in Central Nervous System Diseases

Bernardo F. Sanchez-Dalmau, Ruben Torres-Torres, Johannes Keller, Elena H. Martínez-Lapiscina, and Pablo Villoslada

Abstract The anterior visual pathway is composed of the axons from retinal ganglion cells, which form the optic nerve, optic chiasm, and optic tract, and synapse in the lateral geniculate nucleus (LGN). The posterior visual pathway is composed of axons from the LGN that form the optic radiations (OR) and project into the visual cortex. Anterior visual pathway can be affected by transneuronal retrograde degeneration secondary to posterior visual pathway lesins.

Keywords Trans neuronal Retrograde Degeneration • Congenital • Homonymous hemianopia • Acquired Homonymous hemianopia • Epilepsy surgery • Multiple sclerosis • Alzheimer disease • OCT and retrograde degeneration • Retinal nerve fiber layer • Ganglion cells complex layer • Posterior visual pathway

B.F. Sanchez-Dalmau, MD (✉)
Neuroophthalmology Unit, Ophthalmology Department, Hospital Clínic, Barcelona, Sabino d'Arana 1, Barcelona 08028, Spain

Visual Pathway Lab, Neuroimmunology Group, Institute of Biomedical Research August Pi Sunyer (IDIBAPS), Hospital Clinic of Barcelona, Barcelona 08023, Spain
e-mail: bsanchezdalmau@gmail.com

Ophthalmology Department, Hospital Clinic seu Maternitat, C/Sabino d'Arana s/n, 08027 Barcelona, Spain

R. Torres-Torres, MD • J. Keller, MD
Neuroophthalmology Unit, Ophthalmology Department, Hospital Clínic, Barcelona, Sabino d'Arana 1, Barcelona 08028, Spain

Visual Pathway Lab, Neuroimmunology Group, Institute of Biomedical Research August Pi Sunyer (IDIBAPS), Hospital Clinic of Barcelona, Barcelona 08023, Spain
e-mail: rotorres@clinic.cat; johannes_keller@hotmail.com

E.H. Martínez-Lapiscina, PhD • P. Villoslada, PhD
Visual Pathway Lab, Neuroimmunology Group, Institute of Biomedical Research August Pi Sunyer (IDIBAPS), Hospital Clinic of Barcelona, Barcelona 08023, Spain
e-mail: hernandez@clinic.ub.es; pvilloslada@clinic.ub.es

A. Grzybowski, P. Barboni (eds.), *OCT in Central Nervous System Diseases: The Eye as a Window to the Brain*, DOI 10.1007/978-3-319-24085-5_11

11.1 Introduction

The anterior visual pathway is composed of the axons from retinal ganglion cells, which form the optic nerve, optic chiasm, and optic tract, and synapse in the lateral geniculate nucleus (LGN). The posterior visual pathway is composed of axons from the LGN that form the optic radiations (OR) and project into the visual cortex.

About 90 % of the retinal axons synapse in the LGN, and travel with the optic radiations to the occipital cortex. The remain 10 % project into the pretectal region of the midbrain.

Damage from the posterior to anterior visual pathway requires its transmission through the synapses in the LGN by a process called retrograde trans-synaptic degeneration or trans-neuronal degeneration (Fig. 11.1).

Retrograde trans-synaptic degeneration in humans is well known and has been demonstrated from the early twentieth century [1], but clinical evidence of trans-synaptic retrograde degeneration was controversial for many years. The reasons for this controversy were mainly three:

(a) The presence of retinal degeneration no related with the brain injury
(b) The possibility of direct damage to the optic tracts in patients with occipitotemporal lesions and
(c) The lack of good retinal neurohistology in humans.

The indirect analysis with different techniques like pattern electroretinogram [2–5], fundus photography and ophthalmic examination [6] were used but the results were contradictory.

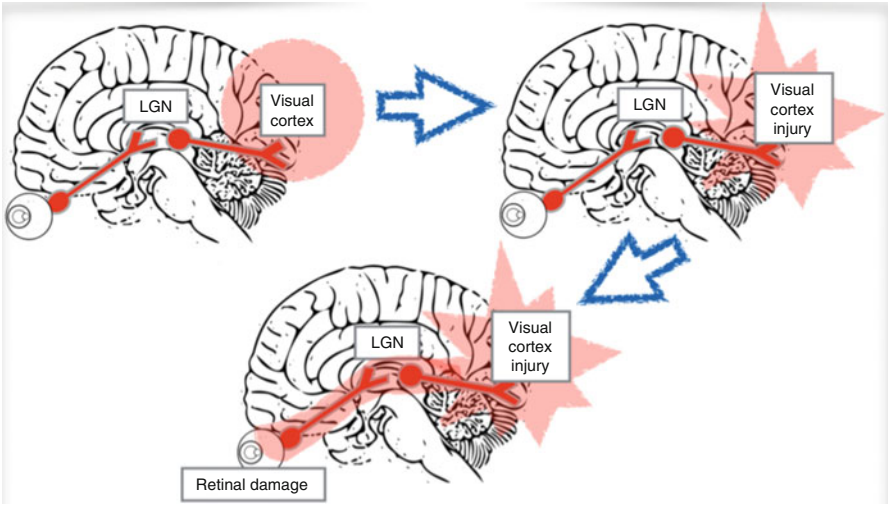

Fig. 11.1 The visual pathway as a model to study trans-synaptic neuronal degeneration. *LGN* Lateral Geniculate Body

In this condition, the advent of the Optical Coherence Tomography (OCT) and their subsequent use in neuro-ophthalmology allowed the first reliable and reproducible analysis of the retinal anatomy in humans. Since that moment it was possible to understand the trans-synaptic retrograde degeneration following damage of the central nervous system (CNS) pathways.

Levin suggested in 2005 that retrograde trans-synaptic degeneration of neurons of retinal ganglion cells and their axons in the optic nerve and the optic tract occurred only following prenatal (not post-natal) acquired damage to the posterior visual pathway [7].

More recent studies demonstrated thinning of the retinal nerve fiber layer (RNFL) using OCT [8] or thinning of the optic tract using MRI [9] in acquired damage.

The use of OCT to evaluate trans-synaptic retrograde degeneration has been described on different clinical settings such as congenital/long standing homonymous hemianopia, acquired homonymous hemianopia and neurodegenerative diseases like multiple sclerosis or Alzheimer's disease.

11.2 Trans-Synaptic Retrograde Degeneration in Congenital/ Long-Standing Homonymous Hemianopia

The first description of using OCT for trans-synaptic retrograde degenerating retinal nerve fiber layer thinning was reported by Cowey [10]. One year later another group, published a report with two female patients with no visual symptoms and homonymous hemianopia secondary to an old occipital infarction showing a RNFL thinning in nasal and temporal regions compatible with the visual field deficit [11].

These results were subsequently confirmed by the same group with a higher number of patients (seven cases) [8]. In both studies there was a strong correlation between the size of brain lesion, visual fields and thinning of the retinal nerve fiber layer, but it was not possible to determine an appropriate temporal sequence between the occipital damage and thinning of the RNFL due to the lack of the exact timing of occipital damage and no follow-up of patients in this series.

11.3 Trans-Synaptic Retrograde Degeneration by OCT in Acquired Homonymous Hemianopia

Jindahra et al. described by first time retinal nerve fiber layer thinning in a series of 19 cases with acquired homonymous hemianopia in 2009 [8]. The observed thinning had the same characteristics and magnitude as previously described in patients with congenital defects.

In 2012, 15 patients with homonymous hemianopia or smaller homonymous visual field defects with occipital cerebral infarction were studied by OCT after the onset of stroke and follow-up in the next years. All patients with homonymous

hemianopia showed a retinal nerve fiber layer thinning with a decreasing trend during the period of measurement [12], maximal in the first years after the occipital injury, followed by a much slower rate the following years.

Similar results were observed in another study comparing 46 patients with occipital infarction and 46 healthy controls [13]. The RNFL thickness was reduced significantly as early as 3.6 months in the superior, inferior, and nasal quadrants in the contralateral eyes and in the superior, inferior, and temporal quadrants in the ipsilateral eyes.

The change from the time-domain optical coherence tomography (TD-OCT) to the spectral-domain OCT (SD-OCT) and the development of better segmentation software allowed the measurement of all the retinal lays. Evaluating ganglion cell layer appeared more effective and reliable than the nerve fiber layer of the retina in the quantification of trans-synaptic degeneration. We can quantify only each of the inner layer (RNFL, ganglion cells or inner plexiform), although there is a tendency to group them into two forms, GCcomplex (GCC) including the three layers described, or including only the ganglion cell (GCL) and inner plexiform (IPL) layers, forming the GCIP.

Yamashita et al. used this technology in three patients with unilateral posterior cerebral artery (PCA) infarction, all of these patients showed a GCC thinning in the hemiretinae corresponding to the affected hemifields without fundoscopic evidence of optic atrophy [14].

A study of Keller et al. [15] showed macular GCL atrophy in patients that have suffered a retrogeniculate lesion with at least 1-year evolution. Therefore, the finding of sector macular GCL atrophy proves retrograde trans-synaptic degeneration of neurons in the visual pathway in cases without other ophthalmic or neurological disease. The functional correlation between sector thinning of the GCL and the sensitivity loss of the visual field in the corresponding field indicates that this may occur in lesions regardless their size as shown by Jindahra el al. in quadrantanopic cases [12]. However, we found a significantly stronger correlation between the VF defect and the thickness of GCL rather than that of the peripapillar RNFL. This is probably due to the fact that at the macula, the bodies of the neurons are more numerous and topographically organised to correspond to the VF. In contrast, the anatomical distribution of fibres in the peripapillar RNFL is more complex, making a correlation with the visual field more difficult to establish (Fig. 11.2).

Another important element is the absence of blood vessels or other structures that may interfere with the OCT image acquisition. The higher resolution of spectral-domain OCT also allows studying the segmentation of the retina in layers in more detail [16]. It is noteworthy that cases with macular sparing hemi- and quadrantanopia also showed macular GCL atrophy away from the fovea, perhaps explained due to the representation of 15–20° of visual field in the area scanned by the OCT instrument used and the absence of ganglion cells on the fovea.

Similar findings can be observed in patients with homonymous visual field defects after epilepsy surgery (Fig. 11.3).

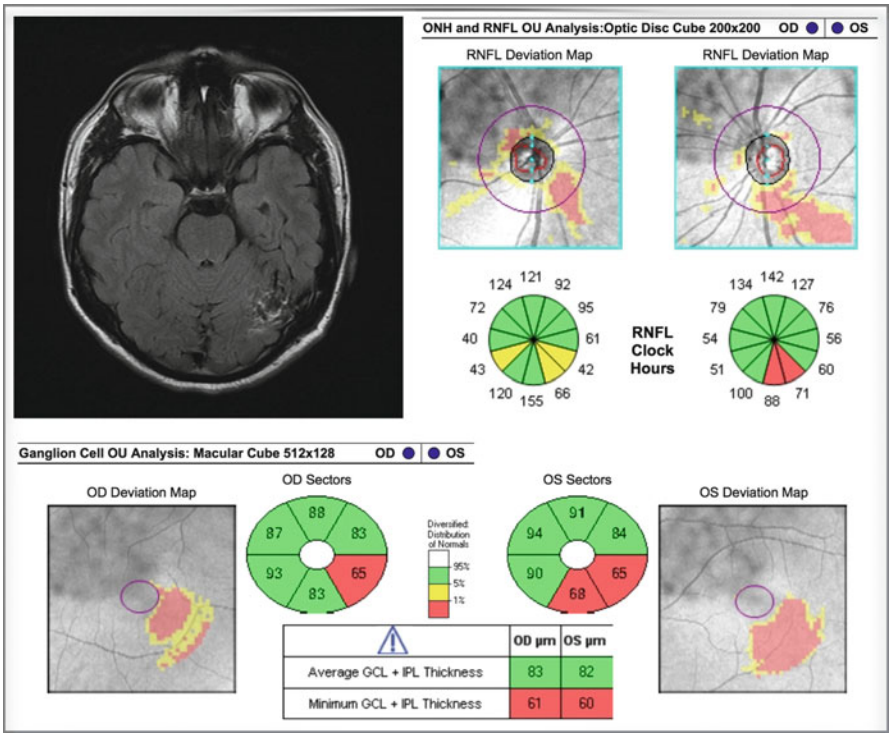

Fig. 11.2 Sectorial RNFL and CGL thinning in patient with occipital arteriovenous malformation

11.4 Trans-Synaptic Axonal Degeneration by OCT in Multiple Sclerosis

There is evidence of postmortem atrophy of retinal layers after long-standing disease [16], but due the multiple CNS lesions that may be developed in patients with multiple sclerosis establish the presence of trans-synaptic degeneration is difficult.

Because patients with multiple sclerosis lesions can have both the anterior visual pathway and the posterior visual pathway can exist anterograde trans-synaptic degeneration in patients with a history of optic neuritis, and moreover, trans-synaptic retrograde degeneration in patients with lesions of the posterior visual pathway [17].

This is important, because to specifically assess retrograde trans-synaptic degeneration patients who have had previous optic neuritis should be differentiated and excluded from the analysis because trans-synaptic RGC degeneration could be masked by the pronounced loss caused by damage to the anterior visual pathways in multiple sclerosis optic neuritis (MSON). Previous optic neuritis may generate residual impairment of RNFL and CGL distorting the quantification of trans-synaptic degeneration on the anterior visual pathway [17, 18].

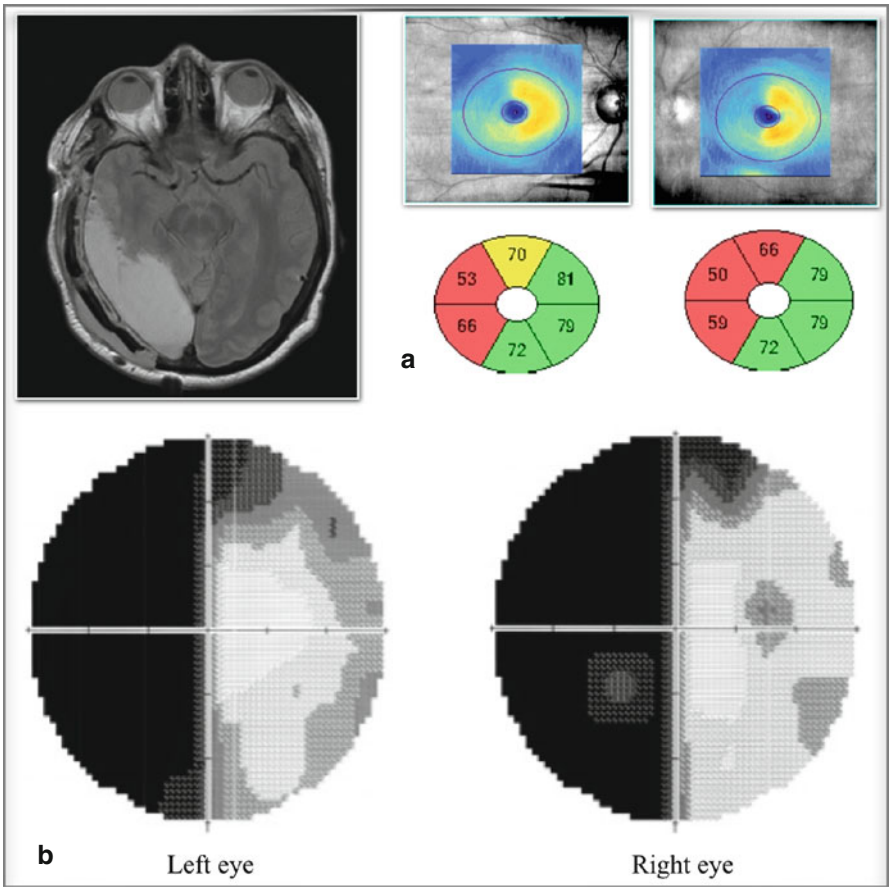

Fig. 11.3 Sectorial ganglion cells layer thinning secondary to an epilepsy surgery, 6 months after surgery (**a**) Visual field shows a complete left homonymous hemianopia (**b**)

The measurement of damage to the anterior visual pathway by OCT [19] and his association with other variables have improved the understanding of neurodegenerative processes in MS.

Gabilondo et al. [20], using a cohort of 100 patients with multiple sclerosis, evaluated the influence of the damage to the posterior visual pathway on retinal atrophy by linear regression analysis. Retinal atrophy was used as the dependent variable, and measures of posterior visual pathway damage and other relevant clinical measures (sex, age at study inclusion, and EDSS score) were used as independent variables. Their regression model indicated that a decrease of 1 cm^3 in visual cortex volume predicts a reduction of 0.6 um in retinal nerve fiber layer thickness independent of other variables.

Balk et al. [17] analyzed OCT from 230 patients with MS with and without Optic Neuritis (ON) and its relation with occipital volume. They showed that there was a

significant amount of atrophy of the inner, but not the outer layers of retina, specifically in the macular RNFL and GCC. The inner nuclear layer and the outer retinal layers of the macular area showed the largest relative thickness in MS with ON, compared with MS without ON or healthy eyes.

Based on these results the authors suggested that in the inner nuclear layer (INL) existed a neural plasticity due to the interaction between bipolar, amacrinal and horizontal cells that blocked the posterior trans-synaptic degeneration, allowing the affectation of ganglion cells only.

Klistorner et al. [21] reported the effects of posterior visual pathway pathology on the retina in MS patients, finding an association between MRI measures of optic radiation integrity and retinal integrity measured by temporal quadrant RNFL thickness using OCT. This finding also supports the occurrence of trans-synaptic degeneration in MS, in this case in a retrograde direction. The authors evaluated the posterior pathways with two methods—lesion analysis and diffusion tensor imaging—with each yielding similar results, increasing confidence in the results and exposing both lesional and non lesional pathology.

In this cohort, with optic neuritis–affected eyes specifically excluded, posterior visual pathway pathology accounted for as much as 35–40 % of the atrophy of the RNFL. There was also an association between posterior visual pathway integrity and low-contrast letter acuity [21].

Future treatment trials need to anticipate that predefined analyses for patients without multiple sclerosis optic neuritis (MSON) are likely to be of stronger statistical power than for patients with previous neuritis, and that alternative measures of disability that better reflect generalized neurological function, including cognition, might need to be used for indirect assessment of diffuse axonal loss in the CNS [22].

11.5 Trans-Synaptic Axonal Degeneration by OCT in Alzheimer's Disease

Visual impairment is often one of the earliest complaints in patients with Alzheimer's Disease (AD) [23]. Several researchers attribute this impairment to damage in primary the visual cortex with degeneration of cortical areas and secondarily, retrograde loss of nerve fibers in the retina and optic nerve. However, it has been reported the presence of beta-amyloid and tau deposits in the retina [24], its presence in the retinal ganglion cells and internal plexiform layer induce neuroinflammation that could cause retinal degeneration [25]. Accordingly the visual damage is determined by direct toxicity of beta-amyloid and its derivatives in the retina and the retrograde degeneration of retinal nerve fibers.

Thinning of the retinal nerve fiber layer and ganglion cells layer has been described in patients with AD and mild cognitive impairment [26–29] and has good correlation with the Mini Mental State Examination (MMSE) and the disease stage.

It has been postulated that the retinal nerve fiber layer thinning may be the earliest sign of AD even before the hippocampal region damage that affects memory [30].

Larrosa et al. [31] proposed a linear discriminant function (LDF) based on OCT and designed for AD diagnosis. According to their results the most reliable tool for diagnosing Alzheimer's disease was the Spectralis® LDF with an area under the ROC curves of 0.967, sensitivity of 94.3 and specificity of 88.3 %.

Despite these promising preliminary studies, it remains to be determined whether the Alzheimer disease affects the retina directly, secondarily by trans-synaptic degeneration, or both.

11.6 Summary

The visual pathway is made up of 4-neuron chain that transfer visual information from the retina to the primary visual cortex. Acute or chronic damage on the posterior visual pathway induce a trans-neuronal retrograde degeneration.

Measuring the degeneration of the anterior visual pathway was difficult before the OCT imaging technology. With this technology the trans-neuronal retrograde degeneration has been well described in several CNS diseases like multiple sclerosis, stroke, homonimous hemianopia and Alzheimer's disease.

The OCT allows to measure reliably and noninvasively the macular RNFL and GCC, and these measurements have a high correlation with the CNS lesions and the function of the visual system [32].

OCT helps in evaluation of the magnitude and timing of damage, supporting our understanding the pathophysiology of the diseases and can be used as a reliable biomarker of axonal loss in neurological diseases.

References

1. Campbell AW. Histological studies on the localization of cerebral function. Cambridge: Cambridge University Press; 1905. p. 52–64.
2. Stoerig P, Zrenner E. A pattern ERG study of transneuronal retrograde degeneration in the human retina after a post-geniculate lesion. In: Kulikowski JJ, Dickinson CL, Murray JJ, editors. Seeing contour and colour. Oxford: Pergamon Press; 1993. p. 553–6.
3. Porrello G, Falsini B. Retinal ganglion cell dysfunction in humans following post-geniculate lesions: specific spatio–temporal losses revealed by pattern ERG. Vision Res. 1999;39:1739–48.
4. Azzopardi P, King SM, Cowey A. Pattern electroretinograms after cerebral hemispherectomy. Brain. 2001;124:1228–40.
5. Skrandies W, Leipert KP. Visual field defects are not accompanied by electrophysiological evidence of transsynaptic retrograde degeneration. Clin Vis Sci. 1988;3:45–57.
6. Hoyt WF, Kommerell G. Der fundus oculi bei homonymer hemianopie. Klin Monbl Augenheilkd. 1973;162:456.
7. Levin LA. Topical diagnosis of chiasmal and retrochiasmal disorders. In: Miller NR, Newman NJ, editors. Walsh and Hoyt's clinical neuro-ophthalmology. 6th ed. Baltimore/Philadelphia: Lippincott, Williams & Wilkins; 2005. p. 517.
8. Jindahra P, Petrie A, Plant GT. Retrograde trans-synaptic retinal ganglion cell loss identified by optical coherence tomography. Brain. 2009;132:628–34.

9. Bridge H, Jindahra P, Barbur J, Plant GT. Imaging reveals optic tract degeneration in hemianopia. Invest Ophthalmol Vis Sci. 2011;52:382–8.
10. Cowey A. Fact and artefact and myth about blindsight. Q J Exp Psychol. 2004;57A:577–609.
11. Mehta JS, Plant GT. Optical coherence tomography (OCT) findings in congenital/long-standing homonymous hemianopia. Am J Ophthalmol. 2005;140:727–9.
12. Jindahra P, Petrie A, Plant GT. The time course of retrograde trans-synaptic degeneration following occipital lobe damage in humans. Brain. 2012;135:534–41.
13. Park HYL, Park YG, Cho AH, Park CK. Transneuronal retrograde degeneration of the retinal ganglion cells in patients with cerebral infarction. Ophthalmology. 2013;120:1292–9.
14. Yamashita T, Miki A, Iguchi Y, Kimura K, Maeda F, Kiryu J. Reduced retinal ganglion cell complex thickness in patients with posterior cerebral artery infarction detected using spectral-domain optical coherence tomography. Jpn J Ophthalmol. 2012;56:502–10.
15. Keller J, Sánchez-Dalmau BF, Villoslada P. Lesions in the posterior visual pathway promote trans-synaptic degeneration of retinal ganglion cells. PLoS One. 2014;9:e97444.
16. Green AJ, McQuaid S, Hauser SL, et al. Ocular pathology in multiple sclerosis: retinal atrophy and inflammation irrespective of disease duration. Brain. 2010;133:1591–601.
17. Balk LJ, Twisk JWR, Steenwijk MD, Daams M, Tewarie P, Killestein J, et al. A dam for retrograde axonal degeneration in multiple sclerosis? J Neurol Neurosurg Psychiatry. 2014;85:782–9.
18. Balk LJ, Steenwijk MD, Tewarie P, Daams M, Killestein J, Wattjes MP, Vrenken H, Barkhof F, Polman CH, Petzold A. Bidirectional trans-synaptic axonal degeneration in the visual pathway in multiple sclerosis. J Neurol Neurosurg Psychiatry. 2015;86(4):419–24.
19. Galetta KM, Calabresi PA, Frohman EM, Balcer LJ. Optical coherence tomography (OCT): imaging the visual pathway as a model for neurodegeneration. Neurotherapeutics. 2011;8:117–32.
20. Gabilondo I, Martínez-Lapiscina EH, Martínez-Heras E, Fraga-Pumar E, Llufriu S, Ortiz S, et al. Trans-synaptic axonal degeneration in the visual pathway in multiple sclerosis. Ann Neurol. 2014;75:98–107.
21. Klistorner A, Sriram P, Vootakuru N, Wang C, Barnett MH, et al. Axonal loss of retinal neurons in multiple sclerosis associated with optic radiation lesions. Neurology. 2014;82:2165–72.
22. Sriram P, Wang C, Yiannikas C, Garrick R, Barnett M, Parratt J, Graham SL, Arvind H, Klistorner A. Relationship between optical coherence tomography and electrophysiology of the visual pathway in non-optic neuritis eyes of multiple sclerosis patients. PLoS One. 2014;9:e102546.
23. Berisha F, Feke GT, Trempe CL, McMeel JW, Schepens CL. Retinal abnormalities in early Alzheimer's disease. Invest Ophthalmol Vis Sci. 2007;48:2285–9.
24. Koronyo Y, Salumbides BC, Black KL, Koronyo-Hamaoui M. Alzheimer's disease in the retina: imaging retinal Aß plaques for early diagnosis and therapy assessment. Neurodegener Dis. 2012;10(1–4):285–93.
25. Garcia-Martin ES, Rojas B, Ramirez AI, de Hoz R, Salazar JJ, Yubero R, Gil P, Triviño A, Ramirez JM. Macular thickness as a potential biomarker of mild Alzheimer's disease. Ophthalmology. 2014;121:1149–51.
26. Iseri PK, Altinaş O, Tokay T, Yüksel N. Relationship between cognitive impairment and retinal morphological and visual functional abnormalities in Alzheimer disease. J Neuroophthalmol. 2006;26:18–24.
27. Kesler A, Vakhapova V, Korczyn AD, Naftaliev E, Neudorfer M. Retinal thickness in patients with mild cognitive impairment and Alzheimer's disease. Clin Neurol Neurosurg. 2011;113:523–6.
28. Kirbas S, Turkyilmaz K, Anlar O, Tufekci A, Durmus M. Retinal nerve fiber layer thickness in patients with Alzheimer disease. J Neuroophthalmol. 2013;33:58–61.
29. Marziani E, Pomati S, Ramolfo P, Cigada M, Giani A, Mariani C, et al. Evaluation of retinal nerve fiber layer and ganglion cell layer thickness in Alzheimer's disease using spectral-domain optical coherence tomography. Invest Ophthalmol Vis Sci. 2013;54:5953–8.

30. He X-F, Liu Y-T, Peng C, Zhang F, Zhuang S, Zhang J-S. Optical coherence tomography assessed retinal nerve fiber layer thickness in patients with Alzheimer's disease: a meta-analysis. Int J Ophthalmol. 2012;5:401–5.
31. Larrosa JM, Garcia-Martin E, Bambo MP, Pinilla J, Polo V, Otin S, et al. Potential new diagnostic tool for Alzheimer's disease using a linear discriminant function for Fourier domain optical coherence tomography. Invest Ophthalmol Vis Sci. 2014;55:3043–51.
32. Moon H, Yoon JY, Lim HT, Sung KR. Ganglion cell and inner plexiform layer thickness determined by spectral domain optical coherence tomography in patients with brain lesions. Br J Ophthalmol. 2015;99(3):329–35.

Chapter 12
OCT in Toxic and Nutritional Optic Neuropathies

Carl Arndt, Sourabh Sharma, Dan Milea, Tony Garcia, and Andrzej Grzybowski

Abstract Despite the recent developments of OCT in neuro-ophthalmology, its use for diagnosing and monitoring nutritional and toxic optic neuropathies is still limited, due to the lack of powered, longitudinal studies. Small series have suggested that OCT may be useful in various toxic optic neuropathies in the acute stage, disclosing subtle retinal nerve fibre layer thickening, ophthalmoscopically undetectable. At later stages, retinal nerve fibre layer thinning affects the papillomacular bundle, and then, all quadrants, but only rarely before visual loss. Macular volume OCT studies have suggested that in toxic optic neuropathies, the primary site of injury may involve the retinal ganglion cells layers. Retinal nerve fibre layer thinning in the nasal quadrant in patients treated with vigabatrin appears to be predictive of visual field constriction.

Keywords Toxic optic neuropathy • Ethambutol • Methanol • Amiodarone • Nutritional optic neuropathy • Mitochondria • Malabsorption • Vitamin B deficiency • Baric surgery • Vigabatrin

C. Arndt (✉) • T. Garcia
Ophthalmology, CHU Reims, Reims, France
e-mail: prarndt@gmail.com

S. Sharma
Singapore Eye Research Institute, Singapore, Singapore

D. Milea
Singapore Eye Research Institute, Singapore, Singapore

Singapore National Eye Centre, Singapore, Singapore

CHU Angers, Angers, France

Duke-NUS, Singapore, Singapore
e-mail: dmilea@free.fr

A. Grzybowski, MD, PhD, MBA
Professor of Ophthalmology, Head of Ophthalmology Department, Poznan City Hospital, Poznan, Poland

Chair of Department of Ophthalmology, University of Warmia and Mazury, Olsztyn, Poland

A. Grzybowski, P. Barboni (eds.), *OCT in Central Nervous System Diseases: The Eye as a Window to the Brain*, DOI 10.1007/978-3-319-24085-5_12

12.1 OCT and Toxic Optic Neuropathies

The anterior visual pathways are susceptible to damage from numerous toxic agents [1]. Toxic optic neuropathies can classically be caused by ingestion of numerous substances, including alcohol (methanol, ethylene glycol), antitubercular drugs (ethambutol, isoniazid), antibiotics (linezolid, sulphonamides, chloramphenicol), antimalarials (chloroquine, quinine), anti-cancer drugs (vincristine, methotrexate), antiarrhythmic (digitalis, amiodarone). Although this list of potentially toxic agents for the optic nerves is constantly increasing, due to the current exponential development of new therapies, only few drugs exhibit a firm evidence of causal relationship.

Toxic optic neuropathies, which are clinically often undistinguishable from nutritional optic neuropathies, typically present as painless, progressive, symmetric and bilateral visual impairment due to central or centrocecal scotoma, dyschromatopsia often being the initial symptom. The site of the primary injury can be very variable, including the retina, retinal ganglion cells, intraocular nerve fibre axons, or chiasm. The majority of clinical findings are caused by selective damage to the papillomacular bundle, which fibres are most susceptible due to their long unmyelinated part in the retina and their relatively small calibre. Preferential involvement of the papillomacular bundle is a common feature to many acquired and genetic optic neuropathies. On the cellular level they also share the similar pathophysiology mechanism based on disruption of oxidative phosphorylation in mitochondria, esp. in retinal ganglion cells, and this is the reason to name them mitochondrial optic neuropathies. Drugs shown to cause mitochondrial optic neuropathy by blocking oxidative phosphorylation include ethambutol, chloramphenicol, linezolid, erythromycin, streptomycin, and antiretroviral drugs [2].

Other drugs provoking optic neuropathy, less strongly related to mitochondrial dysfunction include amiodarone, infliximab, quinine, dapsone, pheniprazine, suramin, and isoniazid [2].

It was suggested that since axonal transport is highly energy dependent and mitochondria need to be transported from the neuron body to the distal synaptic terminals, retinal ganglion cells (RGC) with their long axons are particularly vulnerable [2]. In early drug toxicity mitochondria accumulate within RGC axons, and this is detectable as axonal swelling by OCT [3]. In subacute and chronic stages of mitochondrial optic neuropathies OCT demonstrates RNFL thinning of the papillomacular bundle, esp. in the inferotemporal sector. In the later stages, OCT reveals thinning of RNFL in all layers [2]. Early diagnosis is crucial for intervention, i.e. discontinuation of the drug, which may allow clinical recovery. However, early clinical diagnosis may be difficult, due to the normal ophthalmoscopic appearance of the optic disc pallor. Only at later stages is optic disc palor or atrophy is clinically visible. For this reason, optical coherence tomography (OCT), has been initially considered as a potential method for early diagnosis and possibly monitoring drug toxicity affecting the retina, the retinal ganglion cells complex or the retinal nerve fiber layer (RNFL). Indeed, beyond its extensive use in glaucoma [4], OCT

is now commonly used for the evaluation of various optic neuropathies including optic neuritis, ischemic optic neuropathies, papilledema, traumatic optic neuropathy [5–7]. However, interestingly, the number of OCT studies dedicated to toxic optic neuropathies remains relatively small and no OCT guidelines exist to monitor optic nerve drug toxicities.

12.1.1 Ethambutol

Ethambutol hydrochloride is a bacteriostatic antitubercular agent and probably the most common therapy implicated in toxic optic neuropathy. Ethambutol and its metabolite ethylenediaminodibutyric acid chelates several metal-containing enzyme systems like copper and zinc in the nucleic acid structures of mycobacteria leading to decreased levels of metalloproteins [8, 9]. Similar disruption is seen within the cytochromes of the human mitochondria, leading to apoptosis of retinal ganglion cells [8, 9] and subsequent optic neuropathy [10]. Early animal experiments have also demonstrated ethambutol toxicity affecting the retinal ganglion cells, the optic nerve, chiasm and optic tracts [11, 12].

Ethambutol induced optic neuropathy, which may become clinically patent at any time from 2 to 12 months after the initial treatment, is often reversible, if the condition is early recognized, However, permanent damage may occur at toxic or even standard doses (15–25 mg/kg/day), especially in debilitated patients, i.e. with associated renal failure. The ethambutol induced optic neuropathy has a predilection for the papillo-macular bundle of the retinal nerve fibre layer. Therefore, ophthalmoscopic changes of the optic nerve head are often subtle at the early stages, making OCT a good candidate for early ethambutol optic nerve toxicity detection.

The most common OCT finding in advanced optic nerve ethambutol toxicity is thinning of the retinal nerve fibre layer, especially in the infero-temporal quadrant, corresponding to the papillo-macular bundle [9, 12, 13]. Patients with thinner temporal quadrants display lower visual acuity and significantly reduced colour vision. These OCT findings may also correspond well with the visual field defects on Humphrey visual field analysis. Limited case series have suggested that at early stages, the ethambutol induced optic neuropathy might be associated with increased RNFL thickness [14]. In addition, after cessation of ethambutol, reversible RNFL changes, detectable by OCT may occur [14]. Apart from RNFL, significant decreases in retinal thickness have been observed at various levels including ganglion cell layer and inner plexiform layer [15, 16].

In summary, OCT is a potentially interesting tool to assess the degree of optic nerve damage in the ethambutol induced optic neuropathy, especially in the early stages of the condition, when the optic disc has a normal ophthalmoscopic appearance. However, large studies are missing to confirm these preliminary findings, especially regarding early localized temporal RNFL thickening, as an early sign of the disease. Therefore, OCT is not recommended as the sole method for monitoring potential ethambutol optic nerve toxicity.

12.1.2 Methanol

Methanol is a common cause of toxic optic neuropathy especially in the developing world. It is also the most dreaded cause, due to its systemic consequences, potentially leading to metabolic acidosis, visual loss, coma and death. These adverse effects are due to indirect toxicity related to formic acid, catabolised from methyl alcohol via formaldehyde by the enzyme alcohol dehydrogenase in the liver and red blood cells.

The changes in the optic nerves are mostly due to cytotoxic oedema within the retina and the optic nerve, occurring during the first 48 h after methanol ingestion. The retinal ganglion cells and the retrolaminar myelin sheath are also affected due to degeneration of optic nerve axons. Several animal studies also supported these findings by identifying demyelination of optic nerve sheath [17]. The treatment of methanol intoxication is based on ethanol, B-group vitamins, and systemic steroids; however, the prognosis is usually poor and the final visual acuity is counting fingers or worse [18]. It was shown that fomepizole is safe and effective in the treatment of methanol poisoning [19], but high costs limits its availability. The visual improvement after treatment of 2 patients with a combination of intravenous erythropoietin, systemic corticosteroids, vitamins, and folic acid was reported [20]. OCT has been used for exploring macula and peripapillary retina in methanol-induced retinal toxicity, showing peripapillary nerve fibre swelling and accumulation of intraretinal fluid in the acute phase, with subsequent thinning in the chronic phase (Fig. 12.1). Therefore, OCT could be a useful tool in this setting, for evaluation of the severity of retinal edema and the temporal changes in the retinal profile [21].

12.1.3 Tobacco

The toxic optic neuropathy caused by tobacco seems to be mysterious entity since all confirmed cases were reported many years ago, in the era before OCT and genetic studies. It was shown that at least part of this disorder in fact was Leber's Hereditary Optic Neuropathy (LHON) [22–24]. It was proposed that smoking, especially in genetically susceptible individuals might affect sulphur metabolism, leading to chronic cyanide intoxication [25, 26]. The disorder was characterized by slowly progressive papillomacular bundle damage, centrocecal scotoma and visual loss. The appearance of the optic nerve is usually normal at the initial stages, with occasional peripapillary dilated vessels and haemorrhages, while pallor ensues only in the later stages [26]. Since the clinical picture of TON is similar to other optic neuropathies, the diagnosis of TON is by exclusion only of other toxic, nutritional and hereditary optic neuropathies. A few new articles [27–29] claimed that they presented patients with tobacco optic neuropathy, but they were undermined as they did not convincingly proofed the diagnosis [30–34].

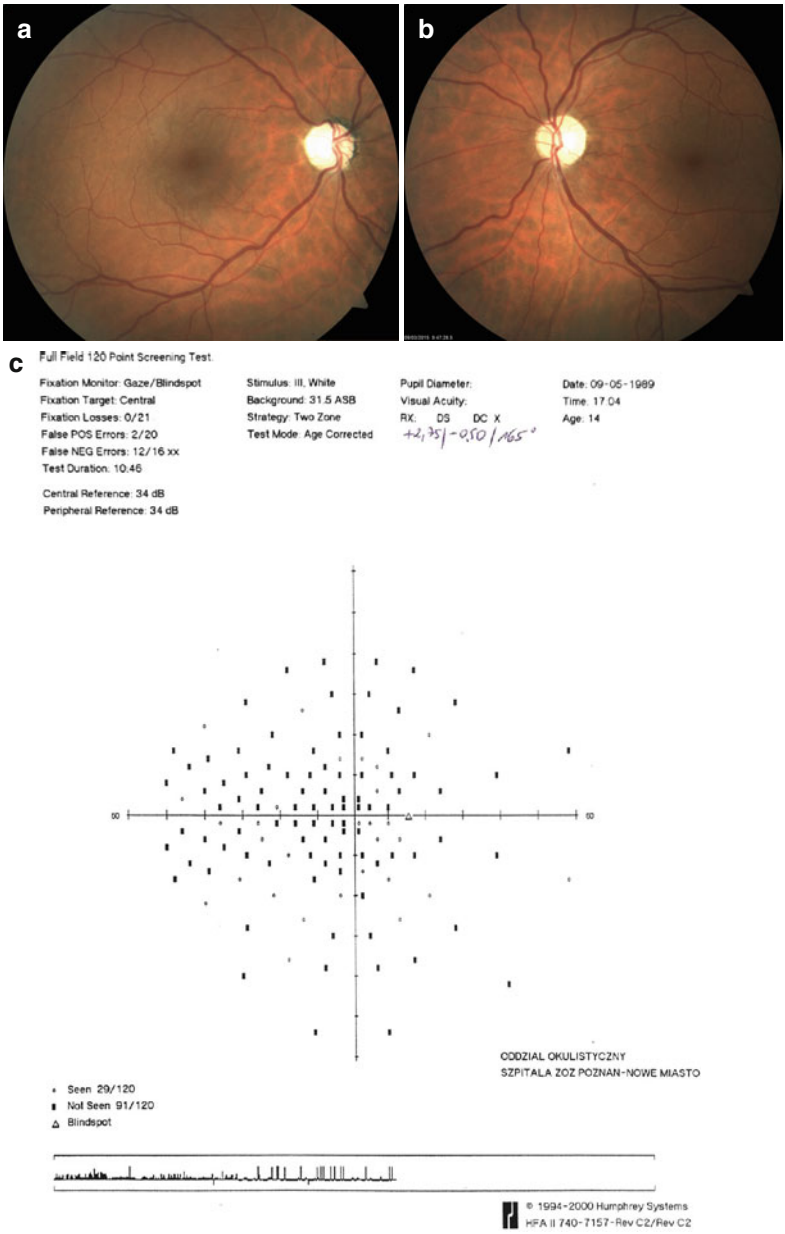

Fig. 12.1 Case report of Methanol Optic Neuropathy. A 40 year old patient with no light perception in both eyes and dilated non-responsive pupils transferred from Toxicology Department after accidental methanol intoxication. After one-month follow up patient presented improvement of VA in both eyes (counting fingers in right eye and 0.16 in left eye) and kept stable. After 3 months optic nerve atrophy was clearly recognized with pale optic discs in fundoscopy (**a**, **b**), centrocecal scotoma in both eyes (**c**, **d**), decrease in RNFL thickness in both eyes (**e**), and decreased volume of ganglion cells in both eyes (**f**, **g**)

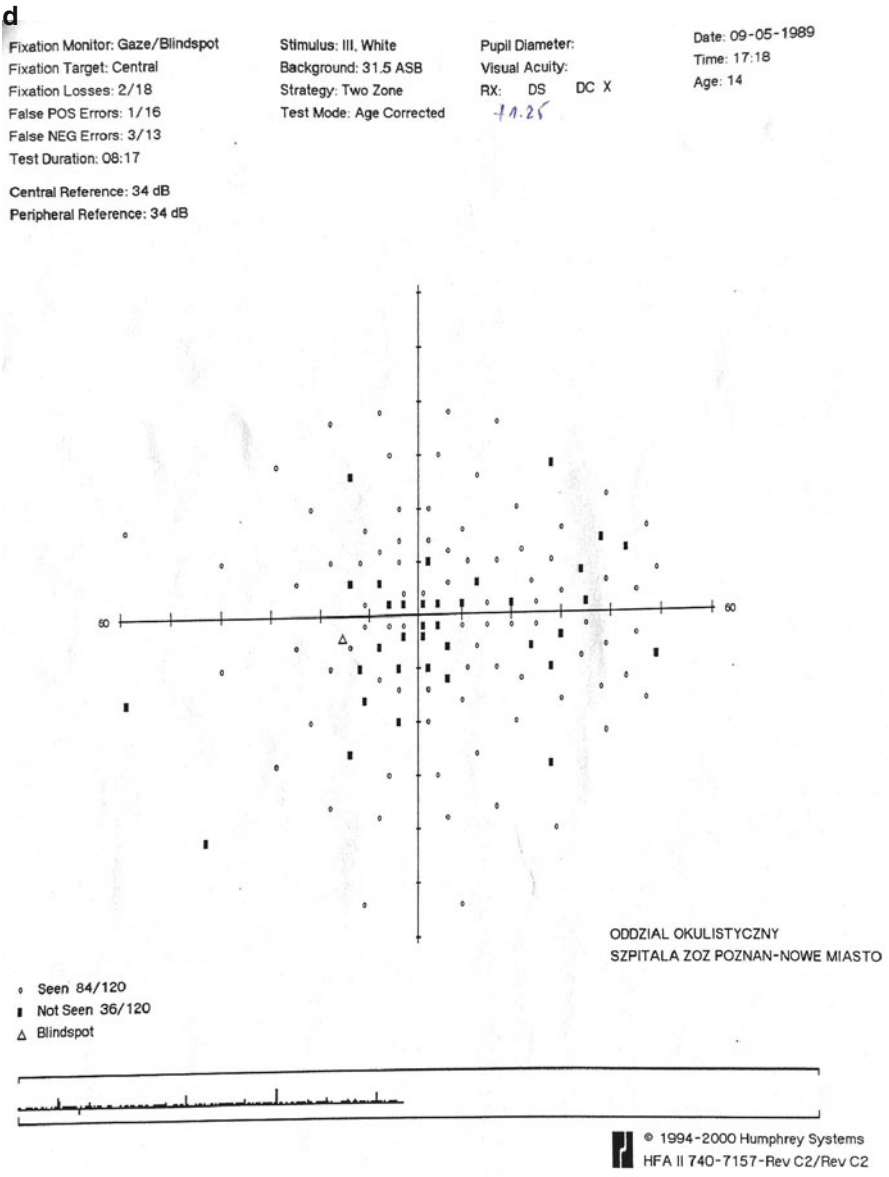

Fig. 12.1 (continued)

e

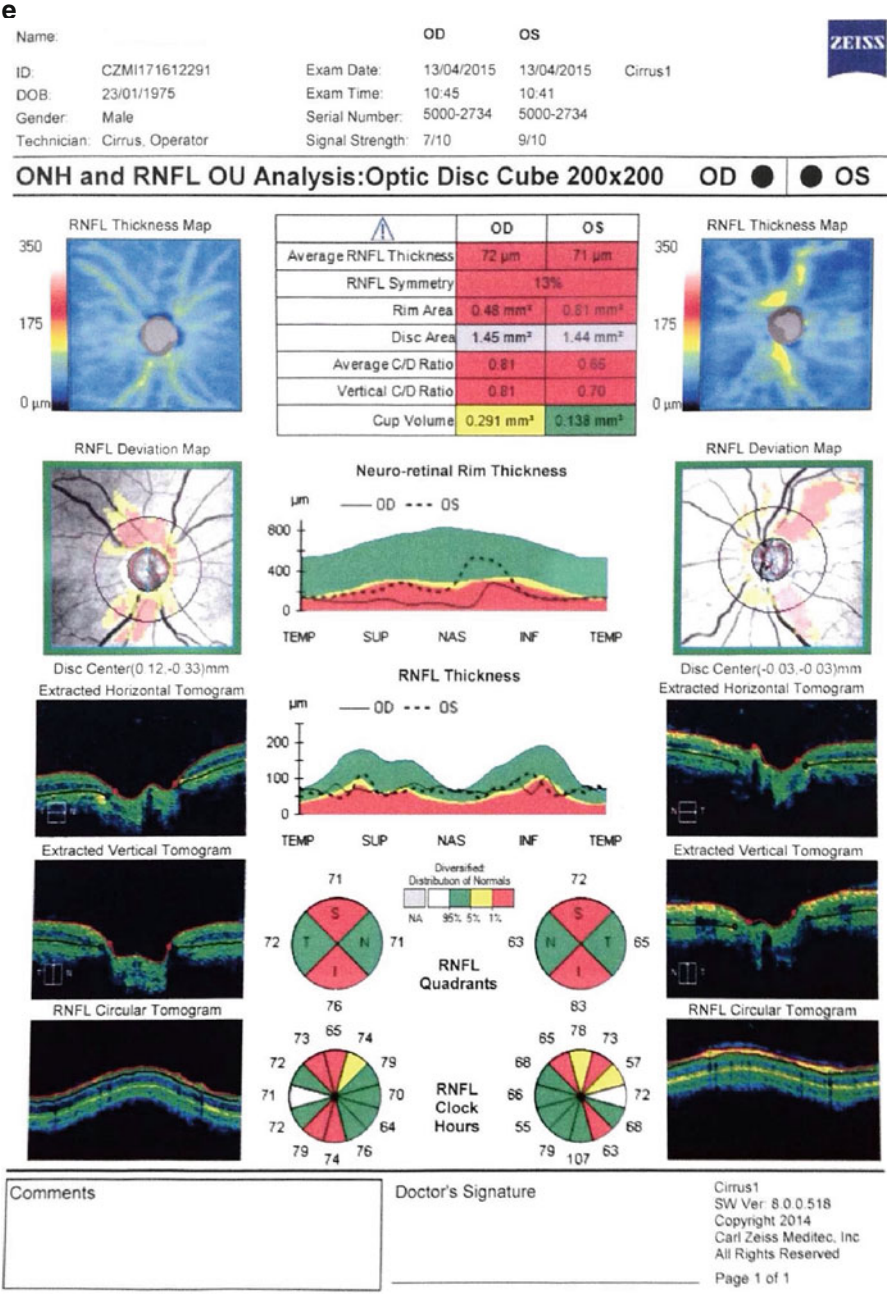

Fig. 12.1 (continued)

f

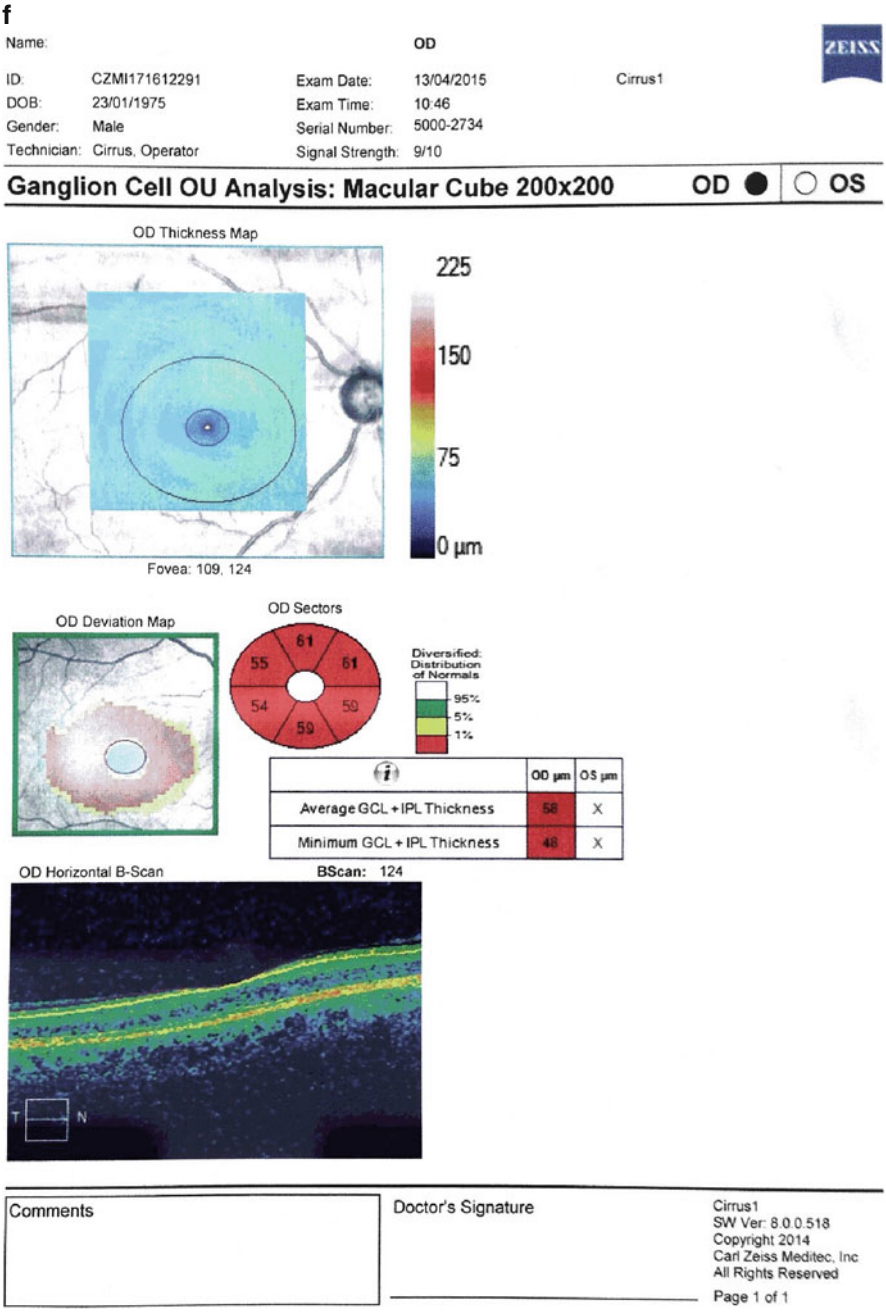

Fig. 12.1 (continued)

g

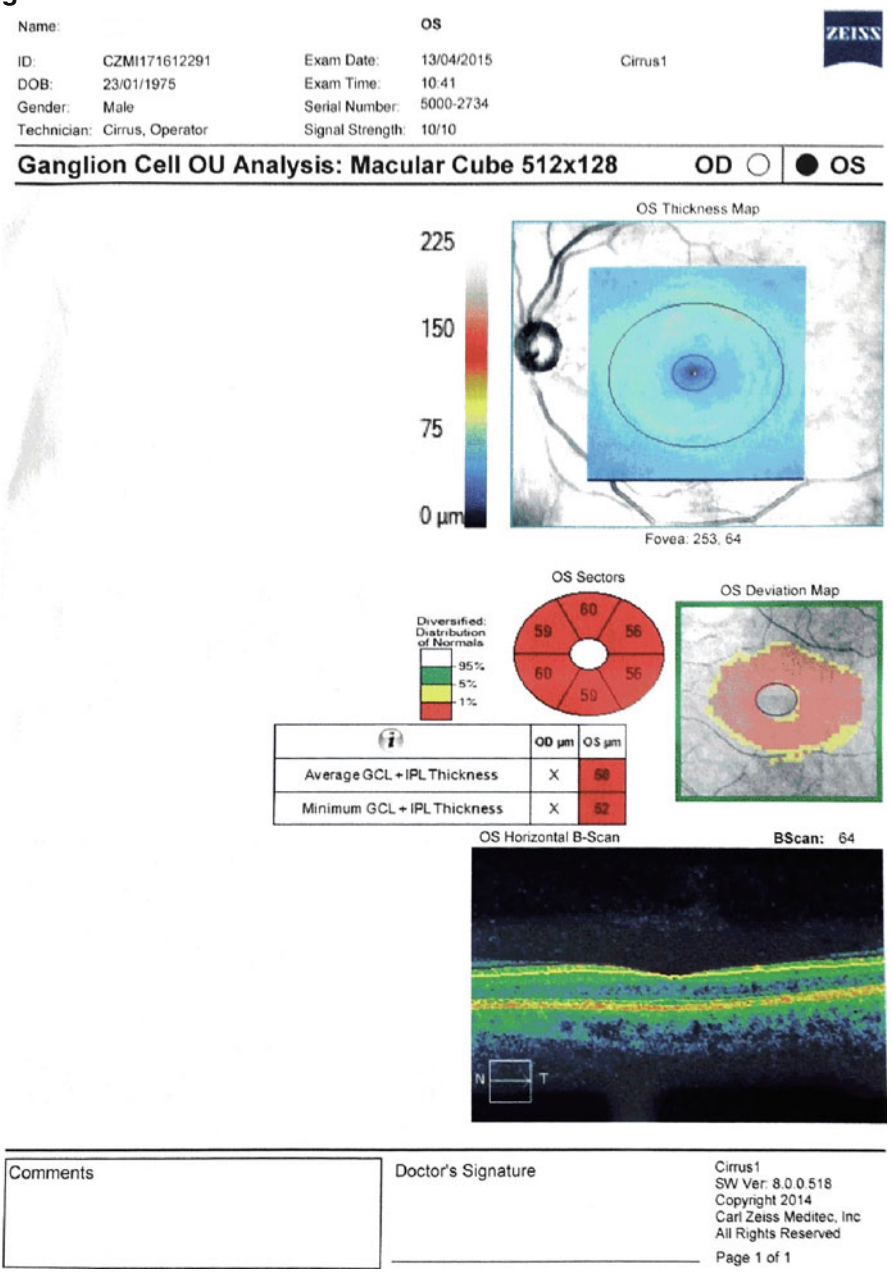

Fig. 12.1 (continued)

12.1.4 Amiodarone

Amiodarone is a very efficient antiarrhythmic agent primarily used to treat atrial or ventricular tachyarrhythmias and fibrillation. The clinical presentation of amiodarone induced optic neuropathy may be sometimes indistinguishable from that of non-arteritic anterior ischaemic optic neuropathy (NAION) [35]. Amiodarone induced optic neuropathy has typically an insidious onset with a milder degree of visual loss, a longer duration of disc edema, and is more commonly bilateral than typical NAION, though there can be a considerable overlapping between these two conditions. Furthermore, disc edema and optic neuropathy may continue to progress even after cessation of the drug [35]. The mechanism of amiodarone-induced optic neuropathy is possibly due to the accumulation of cytoplasmic lamellar inclusions in the lysosomes due to binding of amiodarone with phospholipids. These complexes are not degraded by phospholipase enzymes leading to deposition of amiodarone deposits in the optic nerve as well as in other ocular tissues, including cornea and lens.

OCT has shown that in amiodarone-related optic neuropathy, there is transient RNFL thickening, during the initial months of therapy, followed by subsequent axonal loss and optic nerve atrophy [36]. OCT has been proposed as follow-up method for documenting edema or RNFL thinning in this setting.

12.2 OCT and Nutritional Optic Neuropathies

Nutritional optic neuropathy is more common among alcohol abusers and those who are undernourished [37]. Isolated nutritional optic neuropathies are rare, they are more frequent in regions of famine, where they may be epidemic. Nutritional optic neuropathies may be associated with various causes, including unbalanced diet, bariatric surgery, hunger strike, anorexia nervosa, absorption deficiency of vitamin B [38].

As in toxic neuropathies, the anterior visual pathways are susceptible to nutritional deficiency associating papillomacular bundle damage, central or cecocentral scotoma and reduction of color vision. The primary lesion is not necessarily localized into the optic nerve itself; it may be located at various levels, such as the retinal ganglion cells, nerve fiber layers, chiasm, or the optic tracts [39].

The exact mechanism by which nutritional deficits damage the optic nerve remains largely unknown. Specific deficiencies of vitamin B-12 (cyanocobalamin), thiamine (vitamin B-1) [40], other vitamins (riboflavin, niacin, and pyridoxine), folic acid, copper [41, 42] and other proteins with sulfur-containing amino acids have been associated with optic neuropathies [43]. It has been postulated that these deficiencies affect mitochondrial oxidative phosphorylation, and therefore nutritional optic neuropathies may be part of the acquired mitochondrial optic neuropathies spectrum [44]. The visual prognosis depends on multiple factors, including the cause

and the duration of symptoms. At advanced stages of the condition, associated with optic atrophy, recovery is less likely to occur than at early stages [41]. Nutritional optic neuropathies are very rare in children.

Nutritional and toxic optic neuropathies have similar clinical presentations, i.e. bilateral, painless visual loss associated with colour vision disturbances and central scotoma. When an optic neuropathy is suspected, a thorough history should cover diet, drug/toxin exposure, social history (including alcohol consumption) and the professional environment. Treatment of any chronic disease such as pernicious anemia should be elucidated. Sensory symptoms and gait disturbance may be associated, due to either peripheral neuropathy or cerebellar dysfunction. A family history should be taken, to identify environmental factors or predisposition for hereditary optic neuropathies.

Clinically, patients with nutritional optic neuropathies complain of gradual blurring of vision, at far and near. Often, the slow progression of the symptoms delays diagnosis and treatment. Rarely, the visual symptoms may be asymmetric, but almost never strictly unilateral. Dyschromatopsia can be the initial symptom in nutritional optic neuropathies. In case of orbital pain, pain on ocular movement, unilateral vision loss, other diagnoses should be considered.

In nutritional optic neuropathies, visual acuity may vary from minimal reduction of vision to no light perception (NLP). However, most patients have 20/200 vision or better. Both pupils are sluggish to light, and there is no relative afferent pupillary defect due to the bilateral involvement. The optic disc may be normal or slightly hyperemic (Fig. 12.2) in the early stages, with small peripapillary hemorrhages. After several weeks to months, a papillomacular bundle dropout and temporal disc pallor may occur, followed by optic atrophy (Fig. 12.2). Isolated, purely nutritional optic neuropathies have been rarely explored with OCT, which might be able to closely monitor subtle RNFL changes, i.e. thickening at initial stages, followed at later stages by RNFL thinning, predominantly encountered in the temporal sector [42] (Figs 12.3 and 12.4).

12.3 OCT and Antiepileptic Drug Toxic Maculopathy

Vigabatrin (Sabril) is a second-line anti-epileptic drug prescribed in partial epilepsy, with or without secondary generalization (mainly after failure of other drugs). As a first-line/monotherapy, Vigabatrin is licensed only for the treatment of infantile spasms (West's syndrome). Vigabatrin acts as a selective irreversible inhibitor of GABA-transaminase. Treatment therefore causes an increase in the concentration of GABA (gamma aminobutyric acid), the major inhibitory neurotransmitter in the brain but also in the retina. Maximal efficacy in adults is usually seen in the 2–3 g/day range. The recommended maintenance dose in children is 50–100 mg/kg/day.

During its clinical development, vigabatrin has rarely been associated with symptomatic visual field constriction and retinal disorders. In 1997, 3 cases of

severe, symptomatic, persistent visual field constriction attributed to vigabatrin (VAVFC) were described by Eke [45].

Vigabatrin toxicity is typically associated with bilateral, concentric, predominantly nasal constriction of visual fields. However, patients with perimetric loss due to vigabatrin exhibit normal visual acuity and are unaware of the visual field constriction unless it extends into the central field [46]. The prevalence of VAVFC varies widely between studies, but is generally estimated to be 30–40 % [47, 48]. The precise site of toxicity is controversial, but retina is involved in this condition.

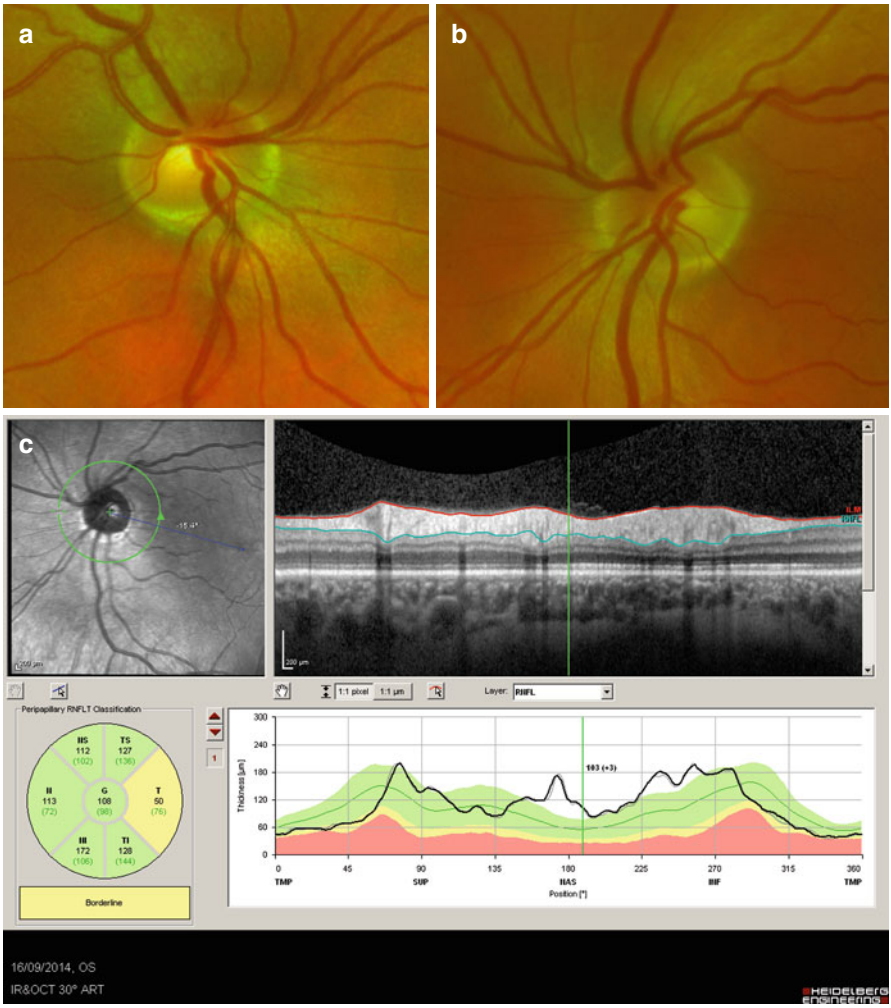

Fig. 12.2 Nutritional optic neuropathy, associated with reduced serum thiamine (Vitamin B1), in a 30-year-old female patient presenting with blurred vision, painful dysesthesia in both legs and gait instability. Visual acuity was 20/200 in both eyes. Bilateral temporal pallor of the optic discs (**a**, **b**) and moderate reduction of the temporal retinal nerve fibre layer, visible on OCT (**c**, **d**). Vision recovered after intramuscular vitamin B1 administration

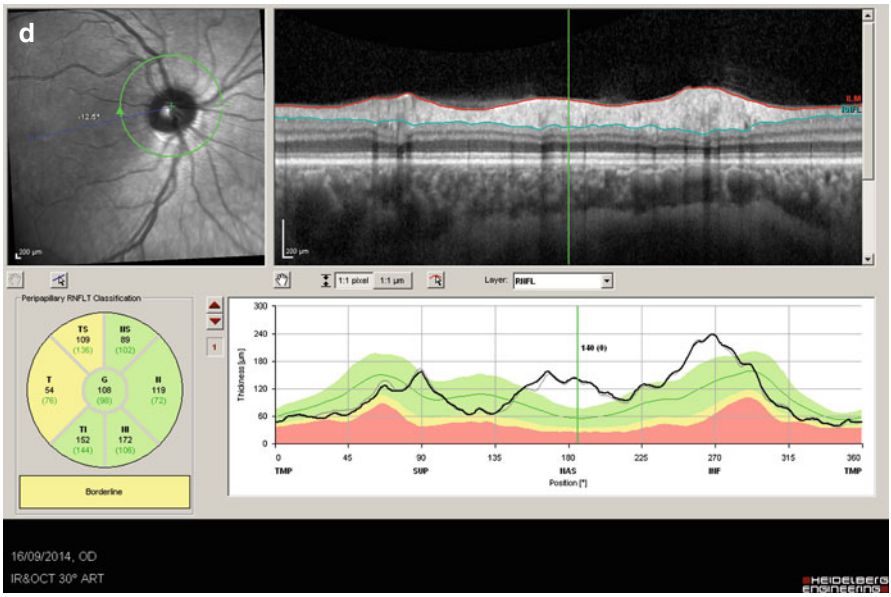

Fig. 12.2 (continued)

Previous studies have shown correlations between the severity of the ERG changes and duration of therapy, as well as with severity of VAVFC. The amplitude of the cone flicker response has the best predictive value for VAVFC, with a sensitivity of 100 % and a specificity of 75 % [48]. Therefore, ERG screening is currently used for toxicity detection in patients unable to perform perimetry.

Although visual field (VF) loss may occur in this setting despite any clinically detectable retinal changes, patients on Vigabatrin may exhibit optic nerve head pallor and RNFL thinning (Fig. 12.5) [49]. RNFL loss displayed on time domain OCT has previously shown a significant correlation between VAVFC and cumulative vigabatrin doses [50]. Patients with VAVFC displayed a reduced mean RNFL thickness compared with those under Vigabatrin but without field loss. Since none of the patients with VAVFC had normal RNFL thickness, the OCT sensitivity for detecting VF changes was 100 % and specificity 70 % [49].

Thickness of the nasal quadrant of RNFL appears to be particularly interesting in predicting vigabatrin associated visual filed constriction, with comparable results in terms of sensitivity (67–100 %) and specificity (66–73 %) [50, 51]. On the opposite, the temporal RNFL sector was not significantly different from control patients with epilepsy (not treated with gabaergic medications) and healthy volunteers [50, 51].

Thus, time domain and spectral domain optical coherence tomography seem to be reliable, in terms of sensitivity, for detecting RNFL thinning associated with vigabatrin-related visual field loss. It appears that both time domain and spectral domain OCT (Table 12.1) screening for vigabatrin treated patients may accurately

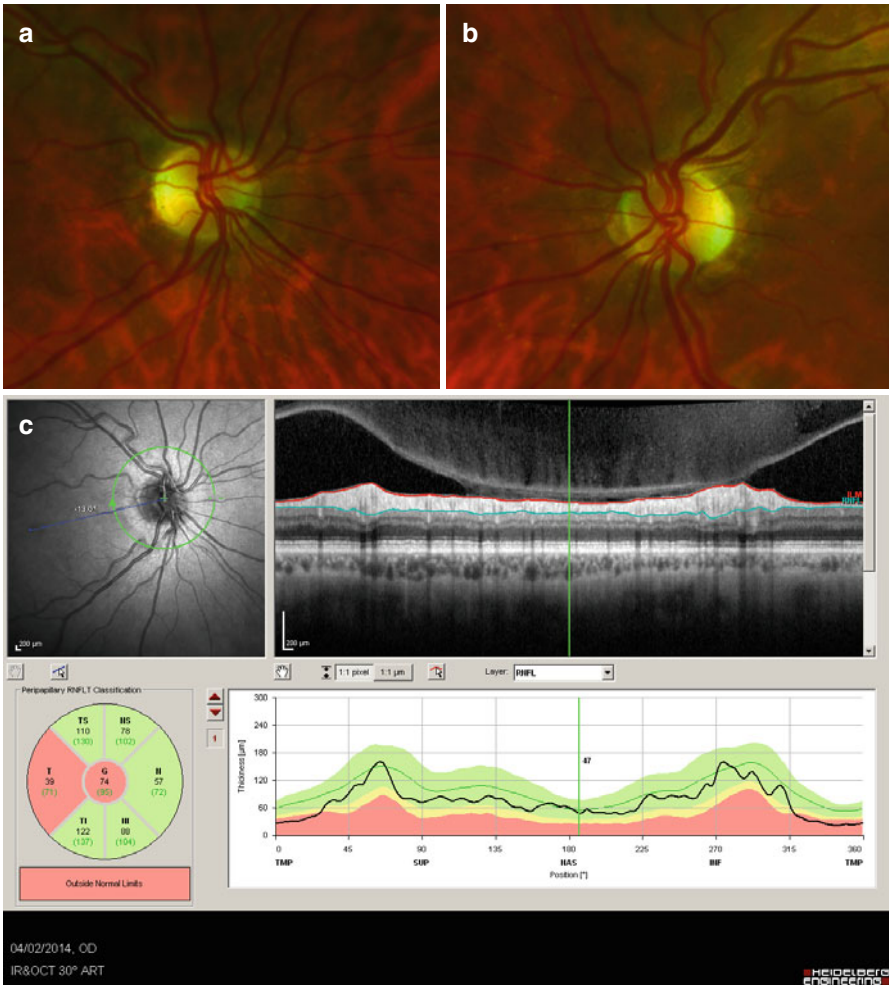

Fig. 12.3 A 60-year-old patient presented with bilateral visual loss ongoing for 6 months, (visual acuity was 20/200 in the right eye and 20/400 in the left eye), temporal disc pallor (**a**, **b**) and severe weight loss. There was no history of smoking or alcohol abuse. Decreased RNFL thickness was selectively located in the temporal area (**c**, **d**). Bilateral centrocaecal scotomas were encountered on Goldmann perimetry in both eyes (**e**, **f**). A megaloblastic anemia and folate deficiency was found on the blood test. Eventually a glucagonoma was discovered on abdominal MRI. Malabsorption responsible for malnutrition and particularly for folate deficiency was the suspected mechanism. After successful surgery and folate supplementation, visual acuity improved to 20/30 in the right eye and 20/80 in the left eye

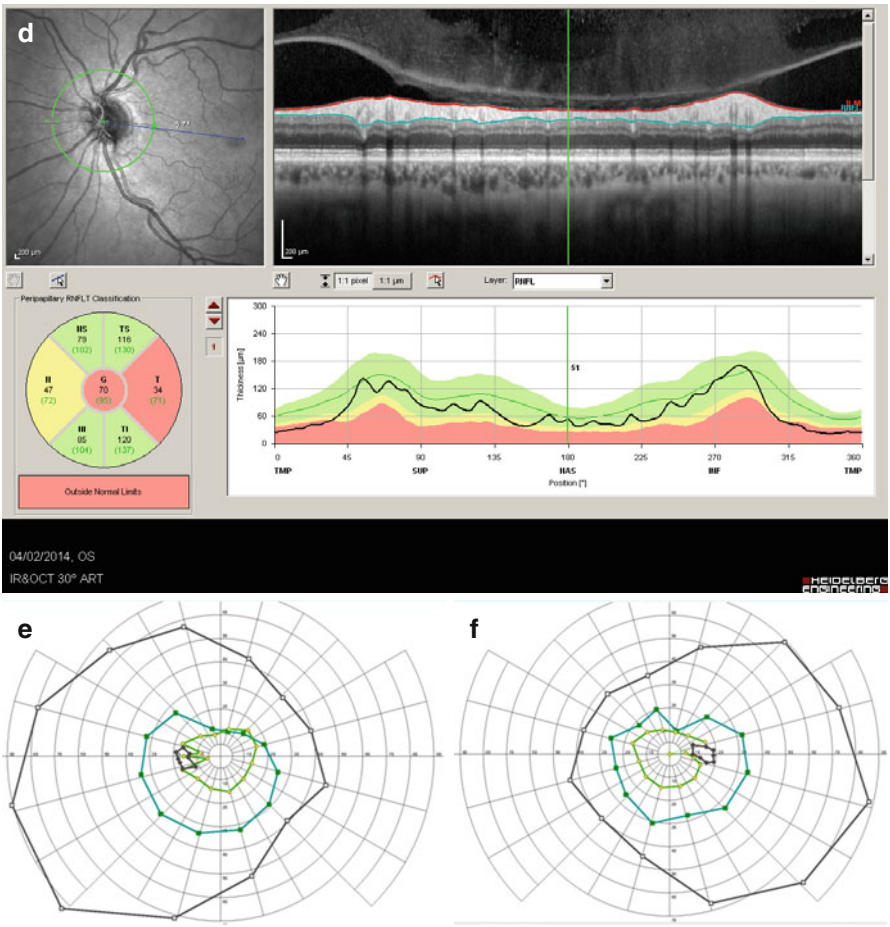

Fig. 12.3 (continued)

monitor those at risk for VAVFC, especially when they are unable to perform perimetry.

In conclusion, OCT may be useful for quantifying the RNFL and retinal ganglion cells complex parameters in toxic and nutritional optic neuropathies. Several studies have suggested that at early stages, localized, subtle RNFL thickening may be detected with OCT, prior to ophthalmoscopically visible changes. In the long term, localized, followed by diffuse RNFL thinning may occur, witnessing global axonal death.

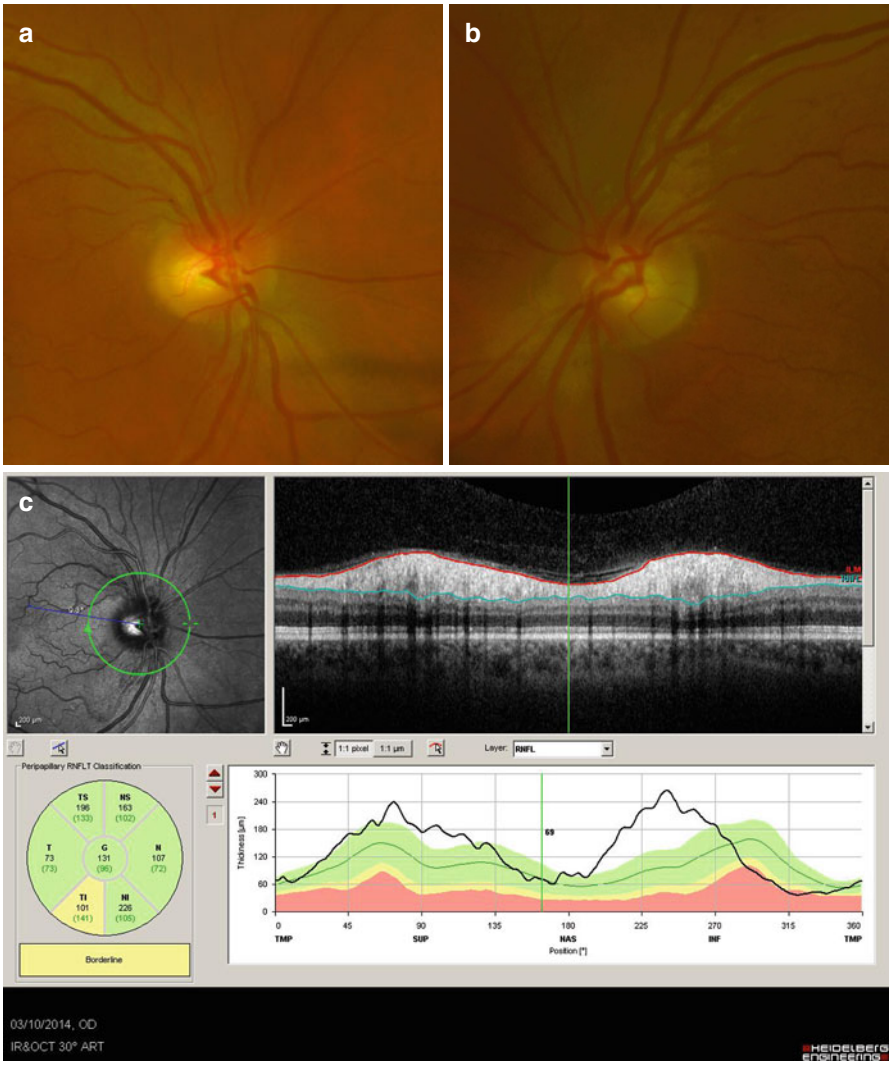

Fig. 12.4 A 40-year-old female patient presented with isolated severe visual loss and a history of mental anorexia in her teens. She stated being well aware of her irregular and unbalanced food intake. Visual acuity was 20/200 in both eyes. The optic disc are slightly hyperaemic with telangiectasia in the peripapillar retina (**a**, **b**). RNFL thickness was at higher normal limit in both eyes (**c**, **d**). The ganglion cell layer was normal in both eyes (**e**, **f**). Leber's hereditary optic neuropathy was ruled out, and the work-up disclosed low vitamin pp and carnitine levels. Six months after supplementation, visual acuity dramatically improved to 20/30 in the right eye and 20/40 in the left eye, although bilateral optic disc pallor had developed and temporal RNFL loss (**g**, **h**) and central ganglion cell loss in both eyes had occurred (**i**, **j**)

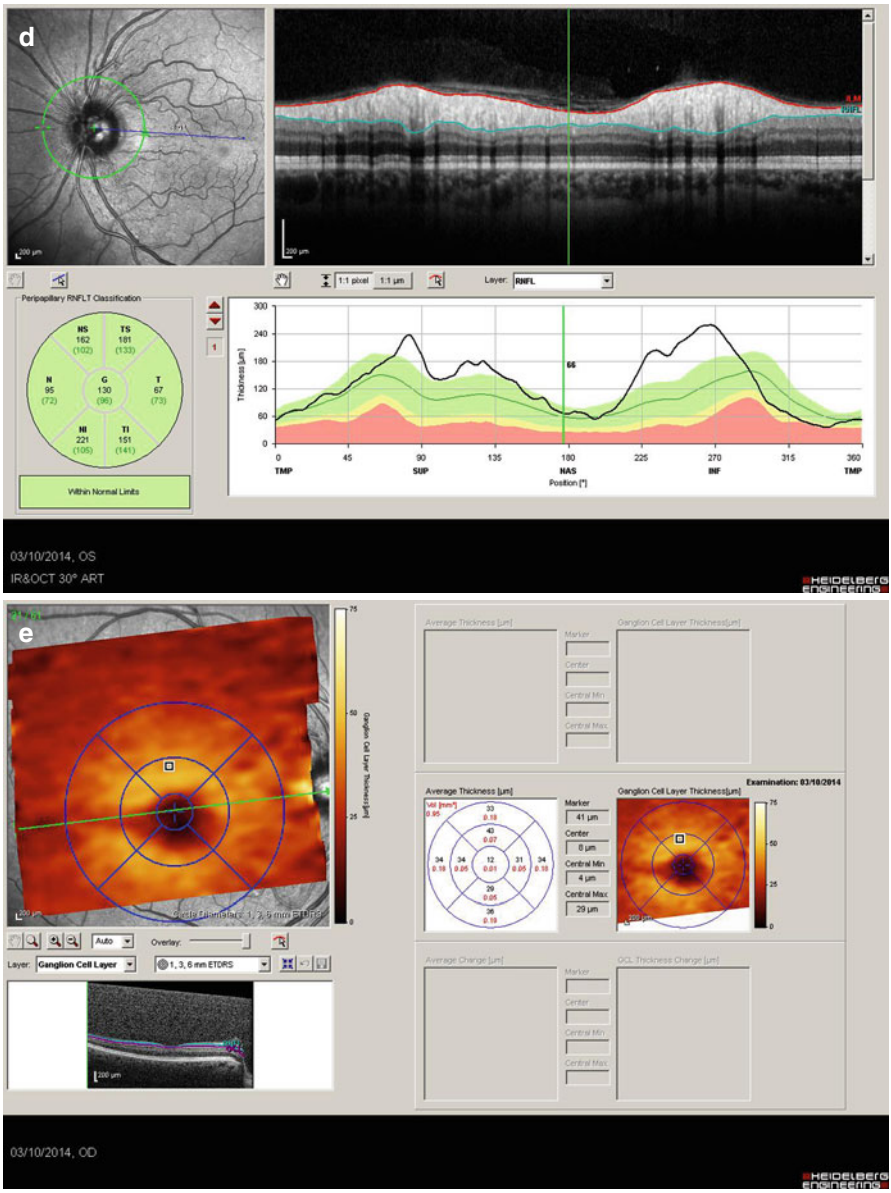

Fig. 12.4 (continued)

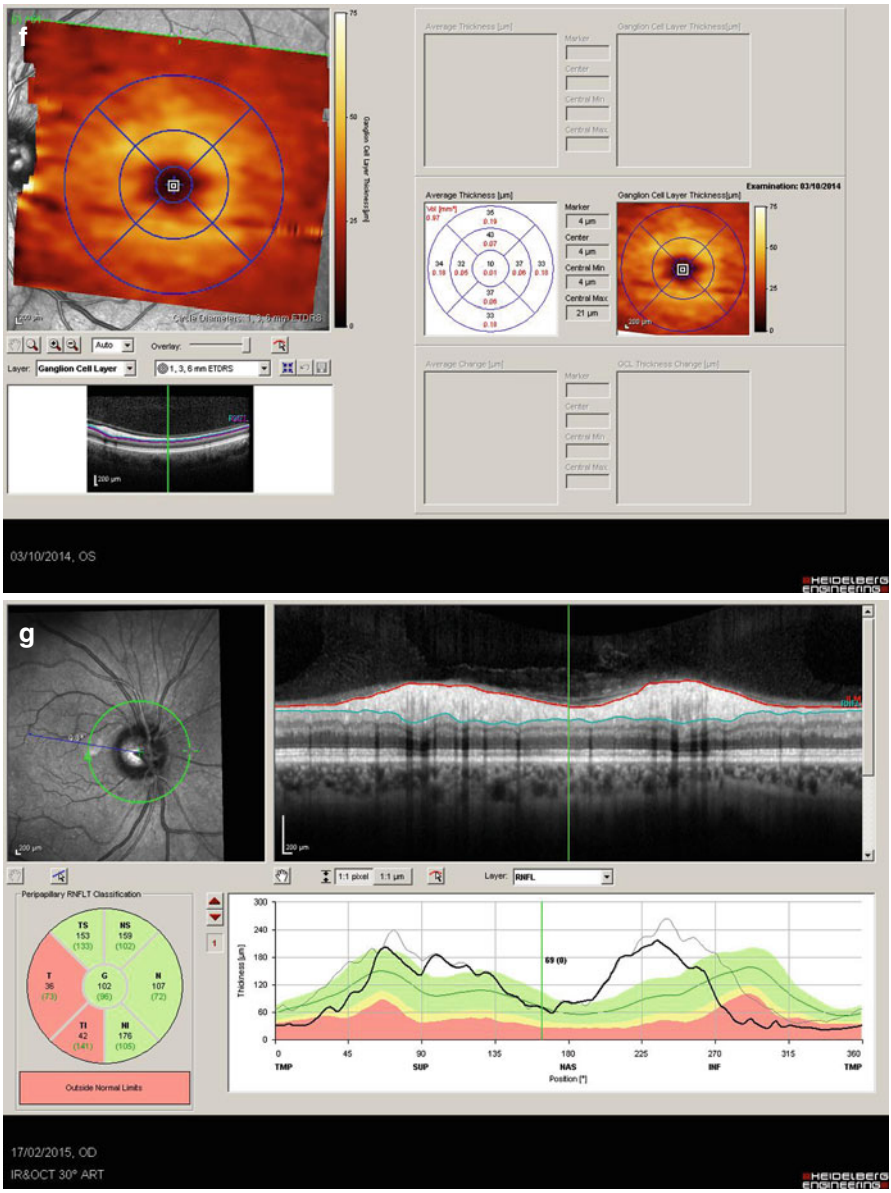

Fig. 12.4 (continued)

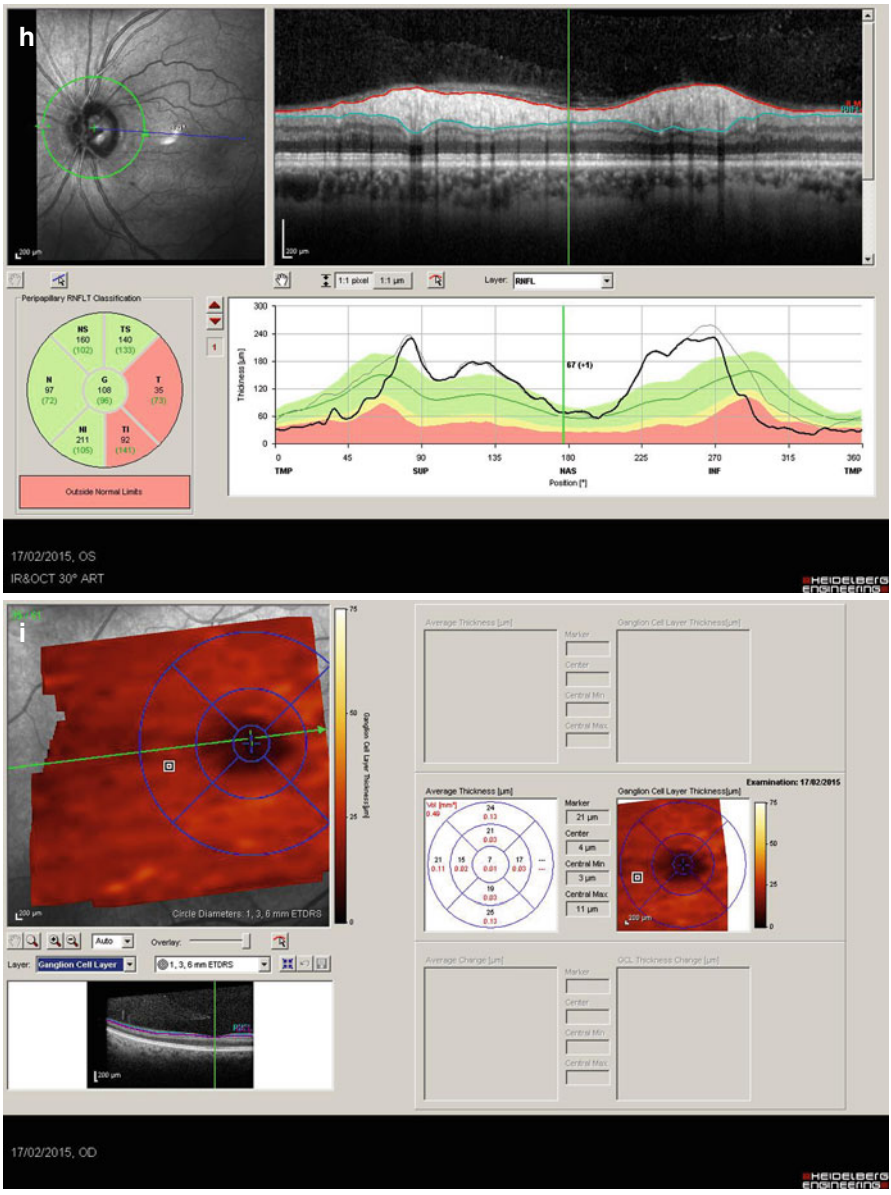

Fig. 12.4 (continued)

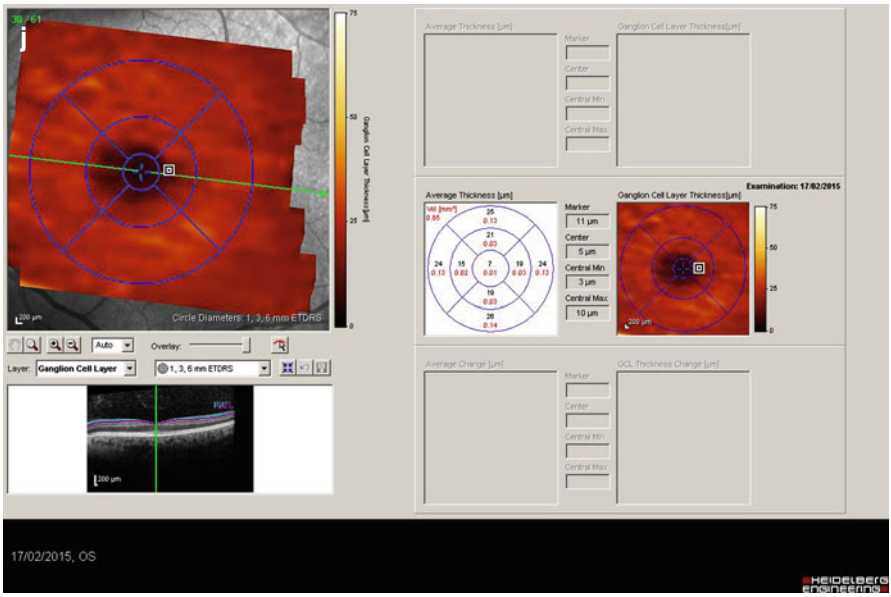

Fig. 12.4 (continued)

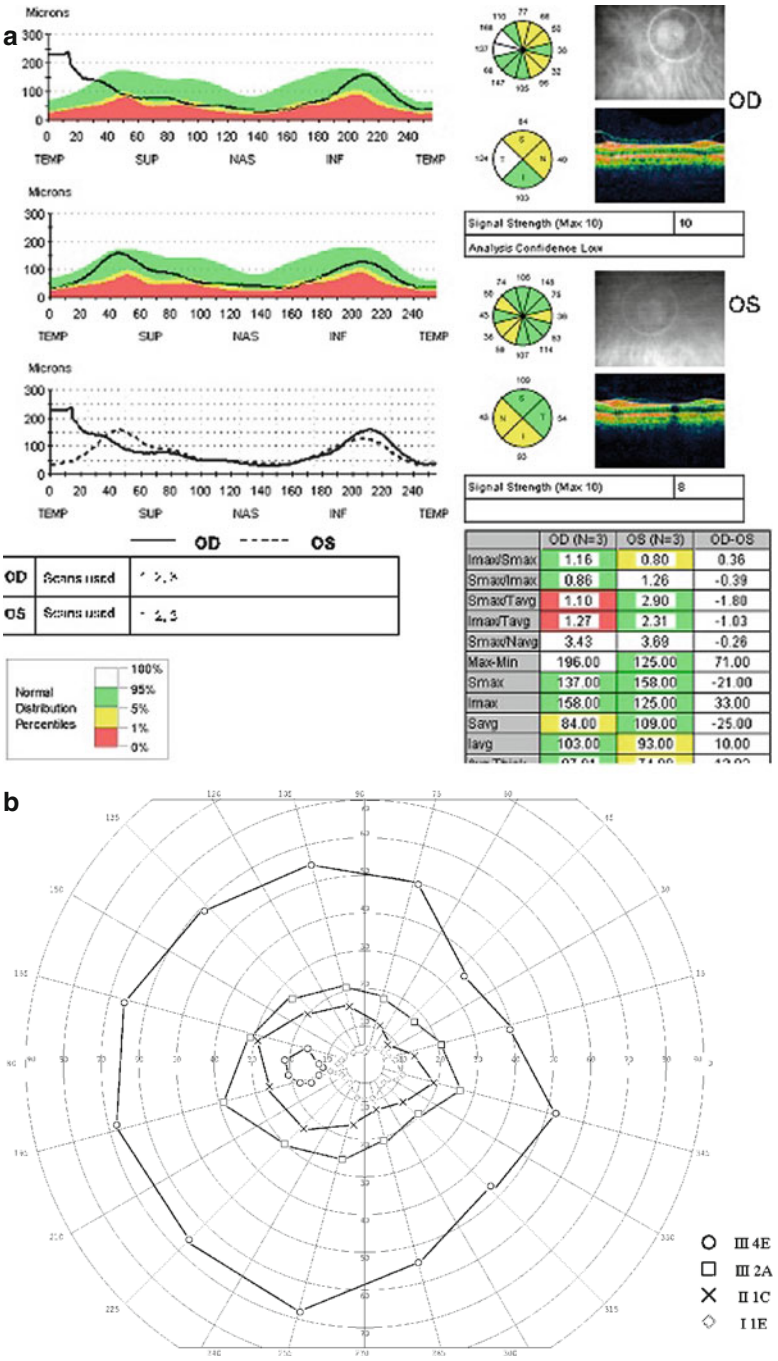

	OD (N=3)	OS (N=3)	OD-OS
Imax/Smax	1.16	0.80	0.36
Smax/Imax	0.86	1.26	-0.39
Smax/Tavg	1.10	2.90	-1.80
Imax/Tavg	1.27	2.31	-1.03
Smax/Navg	3.43	3.69	-0.26
Max-Min	196.00	125.00	71.00
Smax	137.00	158.00	-21.00
Imax	158.00	125.00	33.00
Savg	84.00	109.00	-25.00
Iavg	103.00	93.00	10.00

OD	Scans used	[illegible]
OS	Scans used	[illegible]

Fig. 12.5 Reduced nasal thickness on time domain OCT (**a**) in a patient treated with vigabatrin and presenting with vigabatrin associated visual field constriction in the nasal hemifield of the left eye (**b**)

Table 12.1 Overview of different studies evaluating sensitivity and specificity of OCT findings versus VF defects in vigabatrin (VGN) treated patients

Author	Year	n VGB treated	OCT	RNFL defect	Sensitivity versus VF	Sensitivity vs VF
Wild [52]	2006	21	Time domain	Global	100 %	70 %
Lawthom [53]	2009	27	Time domain	Nasal	100 %	73 %
Moseng [54]	2011	18	Time domain	Nasal, superior, inferior	67 %	n.a.
Kjellström [55]	2014	12	Spectral domain	Nasal, superior, inferior	90 %	66 %

References

1. Grzybowski A, Zulsdorff M, Wilhelm H, Tonagel F. Toxic optic neuropathies: an updated review. Acta Ophthalmol. 2015;93:402–10. doi:10.1111/aos.12515.
2. Wang MY, Sadun AA. Drug-related mitochondrial optic neuropathies. J Neuroophthalmol. 2013;33:172–8.
3. Zoumalan CI, Agarwal M, Sadun AA. Optical coherence tomography can measure axonal loss in patients with ethambutol-induced optic neuropathy. Graefes Arch Clin Exp Ophthalmol. 2005;243:410–6.
4. Sihota R, Sony P, Gupta V, et al. Diagnostic capability of optical coherence tomography in evaluating the degree of glaucomatous retinal nerve fiber damage. Invest Ophthalmol Vis Sci. 2006;47:2006–10.
5. Rebolleda G, Noval S, Contreras I, et al. Optic disc cupping after optic neuritis evaluated with optic coherence tomography. Eye (Lond). 2008;23:890–4.
6. Medeiros FA, Moura FC, Vessani RM, Susanna R. Axonal loss after traumatic optic neuropathy documented by optical coherence tomography. Am J Ophthalmol. 2003;135:406–8.
7. Fisher JB, Jacobs DA, Markowitz CE, et al. Relation of visual function to retinal nerve fiber layer thickness in multiple sclerosis. Ophthalmology. 2006;113:324–32.
8. Kozak SF, Inderlied CB, Hsu HY, et al. The role of copper on ethambutol's antimicrobial action and implications for ethambutol-induced optic neuropathy. Mycobacteriology. 1998;30:83–7.
9. Masvidal D, Parrish II RK, Lam BL. Structural-functional dissociation in presumed ethambutol optic neuropathy. J Neuroophthalmol. 2010;30:305–10.
10. Sadun AA, Wang MY. Ethambutol optic neuropathy: how we can prevent 100,000 new cases of blindness each year. J Neuroophthalmol. 2008;28:265–8.
11. Sivakumaran P, Harrisson AC, Marschner J. Ocular toxicity from ethambutol: a review of four cases and recommended precautions. N Z Med J. 1998;13:428–30.
12. Kinoshita J, Iwata N, Maejima T, Kimotsuki T, Yasuda M. Retinal function and morphology in monkeys with ethambutol-induced optic neuropathy. Invest Ophthalmol Vis Sci. 2012;53:7052–62.
13. Chai SJ, Foroozan R. Decreased retinal nerve fibre layer thickness detected by optical coherence tomography in patients with ethambutol-induced optic neuropathy. Br J Ophthalmol. 2007;91:895–7.
14. Kim U, Hwang JM. Early stage ethambutol optic neuropathy: retinal nerve fiber layer and optical coherence tomography. Eur J Ophthalmol. 2009;19:466–9.
15. Han J, Byun MK, Lee J, Han SY, Lee JB, Han SH. Longitudinal analysis of retinal nerve fiber layer and ganglion cell-inner plexiform layer thickness in ethambutol-induced optic neuropathy. Graefes Arch Clin Exp Ophthalmol. 2015.
16. Vieira LM, Silva NF, et al. Retinal ganglion cell layer analysis by optical coherence tomography in toxic and nutritional optic neuropathy. J Neuroophthalmol. 2015;35(3):242–5.

17. Fanta H, Mayer-Oberditsch l. Ein Beitrag zur Pathologie im Sehnerven bei Methylalkoholvergiftung (Tierversuche). Klin Monatsbl Augenheilkd. 1953;122:288–394.
18. Sanaei-zadeh H, Zamani N, Shadnia SH. Outcomes of visual disturbances after methanol poisoning. Clin Toxicol (Phila). 2011;49:102–7.
19. Brent J, McMartin K, Phillips S, Aaron C, Kulig K. Fomepizole for the treatment of methanol poisoning. N Engl J Med. 2001;344:424–9.
20. Pakravan M, Sanjari N. Erythropoietin treatment for methanol optic neuropathy. J Neuroophthalmol. 2012;32:325–8.
21. Fujihara M, Kikuchi M, Kurimoto Y. Methanol-induced retinal toxicity patient examined by optical coherence tomography. Jpn J Ophthalmol. 2006;50:239–41.
22. Cullom ME, Heher KL, Miller NR, Savino PJ, Johns DR. Leber's hereditary optic neuropathy masquerading as tobacco-alcohol amblyopia. Arch Ophthalmol. 1993;111:1482–5.
23. Mackey D, Howell N. Tobacco amblyopia. Am J Ophthalmol. 1994;117:817–9.
24. Johns DR, Heher KL, Miller NR, Smith KH. Leber's hereditary optic neuropathy. Clinical manifestations of the 14484 mutation. Arch Ophthalmol. 1993;111:495–8.
25. Freeman AG. Optic neuropathy and chronic cyanide intoxication: a review. J R Soc Med. 1988;81:103–6.
26. Grzybowski A, Holder GE. Tobacco optic neuropathy (TON) - the historical and present concept of the disease. Acta Ophthalmol. 2011;89:495–9.
27. Behbehani R, Sergott RC, Savino PJ. Tobacco-alcohol amblyopia: a maculopathy? Br J Ophthalmol. 2005;89:1543–4.
28. Kee C, Hwang J-M. Optical coherence tomography in a patient with tobacco-alcohol amblyopia. Eye (Lond). 2008;22:469–70.
29. Moura FC, Monteiro ML. Evaluation of retinal nerve fiber layer thickness measurements using optical coherence tomography in patients with tobacco-alcohol-induced toxic optic neuropathy. Indian J Ophthalmol. 2010;58:143–6.
30. Grzybowski A. Tobacco amblyopia: does it really exist? Eye (Lond). 2007;21:1448–9.
31. Grzybowski A, Pieniazek M. Tobacco-alcohol amblyopia: nonexistent entity. Ind Psychiatry J. 2012;21:79.
32. Grzybowski A, Pieniążek M. Tobacco-alcohol amblyopia does not exist. Acta Ophthalmol. 2014;92:e77–8.
33. Grzybowski A. Mitochondrial optic neuropathies: additional facts and concepts. Clin Experiment Ophthalmol. 2013. doi:10.1111/ceo.
34. Grzybowski A, Pieniążek M. Tobacco-alcohol amblyopia–nonexistent entity cannot be diagnosed. J Neurol Sci. 2013;332:156.
35. Macaluso DC, Shults WT, Fraunfelder FT. Features of amiodarone-induced optic neuropathy. Am J Ophthalmol. 1999;127:610–2.
36. Martínez-LóPez-Portillo A, Martínez-Gamero BO, Mohamed-Noriega J, Cavazos-Adame H, Mohamed-Hamsho J. Behaviour of disc oedema during and after amiodarone optic neuropathy: case report. J Clin Diagn Res. 2014;8:VD04–5.
37. Orssaud C, Roche O, Dufier JL. Nutritional optic neuropathies. J Neurol Sci. 2007;262:158–64.
38. Sawicka-Pierko A, Obuchowska I, Hady RH, Mariak Z, Dadan J. Nutritional optic neuropathy following bariatric surgery. Wideochir Inne Tech Maloinwazyjne. 2014;9(4):662–6.
39. Becker M, Masterson K, Delavelle J, Viallon M, Vargas MI, Becker CD. Imaging of the optic nerve. Eur J Radiol. 2010;74:299–313.
40. Gratton SM, Lam BL. Visual loss and optic nerve head swelling in thiamine deficiency without prolonged dietary deficiency. Clin Ophthalmol. 2014;8:1021–4.
41. Pineles SL. Combined optic neuropathy and myelopathy secondary to copper deficiency. Surv Ophthalmol. 2010;55:386–92.
42. Naismith RT, Shepherd JB, Weihl CC, Tutlam NT, Cross AH. Acute and bilateral blindness due to optic neuropathy associated with copper deficiency. Arch Neurol. 2009;66:1025–7.
43. Spinazzi M, De Lazzari F, Tavolato B, Angelini C, Manara R, Armani M. Myelo-optico-neuropathy in copper deficiency occurring after partial gastrectomy: do small bowel bacterial

overgrowth syndrome and occult zinc ingestion tip the balance? J Neurol. 2007;254:1012–7.
44. Woon C, Tang RA, Pardo G. Nutrition and optic nerve disease. Semin Ophthalmol. 1995;10:195–202.
45. Eke T, Talbot JF, Lawden MC. Severe persistent visual field constriction associated with vigabatrin. BMJ. 1997;314:180–1.
46. Daneshvar H, Racette L, Coupland SG, Kertes PJ, Guberman A, Zackon D. Symptomatic and asymptomatic visual loss in patients taking vigabatrin. Ophthalmology. 1999;106:1792–8.
47. Lawden MC, Eke T, Degg C, Harding GF, Wild JM. Visual field defects associated with vigabatrin therapy. J Neurol Neurosurg Psychiatry. 1999;67:716–22.
48. Miller NR, Johnson MA, Paul SR, Girkin CA, Perry JD, Endres M, et al. Visual dysfunction in patients receiving vigabatrin: clinical and electrophysiologic findings. Neurology. 1999;53:2082–7.
49. Wild JM, Ahn HS, Baulac M, Bursztyn J, Chiron C, Gandolfo E, et al. Vigabatrin and epilepsy: lessons learned. Epilepsia. 2007;48:1318–27.
50. Versino M, Veggiotti P. Reversibility of vigabratin-induced visual-field defect. Lancet. 1999;354:486.
51. Frisen L, Malmgren K. Characterization of vigabatrin-associated optic atrophy. Acta Ophthalmol Scand. 2003;81:466–73.
52. Wild JM, Robson CR, Jones AL, Cunliffe IA, Smith PE. Detecting vigabatrin toxicity by imaging of the retinal nerve fiber layer. Invest Ophthalmol Vis Sci. 2006;47:917–24.
53. Lawthom C, Smith PE, Wild JM. Nasal retinal nerve fiber layer attenuation: a biomarker for vigabatrin toxicity. Ophthalmology. 2009;116:565–71.0.
54. Moseng L, Sæter M, Mørch-Johnsen GH, Hoff JM, Gajda A, Brodtkorb E, Midelfart A. Retinal nerve fibre layer attenuation: clinical indicator for vigabatrin toxicity. Acta Ophthalmol. 2011;89:452–8.
55. Kjellström U, Andréasson S, Ponjavic V. Attenuation of the retinal nerve fibre layer and reduced retinal function assessed by optical coherence tomography and full-field electroretinography in patients exposed to vigabatrin medication. Acta Ophthalmol. 2014;92:149–57.

Chapter 13
Animal Models in Neuro Ophthalmology

Eduardo M. Normando, James T. Brodie, and M. Francesca Cordeiro

Abstract Neuro-ophthalmology is the branch of ophthalmology dedicated to the study of neurological conditions which affect the visual system. An adequate understanding of the aetiology and pathophysiology of neuro-ophthalmic conditions is fundamental for establishing successful therapeutic strategies. Animal models are therefore considered crucial for understanding and investigating pathological events. Several animal models have been developed for studying neuro-ophthalmic disorders. However, their validity is closely related to the level of similarity with the human pathology. Rodent models are extensively used due to their accessibility and cost efficiency. In particular, mouse models are recognised as among the best genetic models due to the ability to easily alter their genome. Rats are easy to breed and mostly used for toxic/pharmacological and surgical models. Nevertheless, rodent models are still suboptimal for human neuro-ophthalmic conditions because of anatomical differences between species. Primate models have the obvious advantage of sharing vast anatomical and genomic similarities with humans. However, monkeys are expensive, difficult to breed and can only be handled by qualified personnel, all of which limits their suitability. Hence, there is no perfect species for studying neuro-ophthalmic conditions.

This chapter will focus on the most common animal models of neuro-ophthalmic conditions.

Keywords Neuro-ophthalmology • Multiple Sclerosis • Ischemic Optic Neuropathy • Leber Hereditary Optic Neuropathy • Alzheimer 's disease • Parkinson's disease

E.M. Normando, MD, PhD, FEBO • M.F. Cordeiro, PhD, MRCP, FRCOphth (✉)
Imperial College Ophthalmology Research Group (ICORG),
Western Eye Hospital, Imperial College Healthcare Trust, London, UK

Glaucoma and Retinal Neurodegeneration Research, Visual Neuroscience,
UCL Institute of Ophthalmology, London, UK
e-mail: eduardomaria.normando@imperial.nhs.uk; e.normando@ucl.ac.uk;
m.cordeiro@ucl.ac.uk

J.T. Brodie, MBBS
Glaucoma and Retinal Neurodegeneration Research, Visual Neuroscience,
UCL Institute of Ophthalmology, London, UK
e-mail: jtbrodie@doctors.org.uk

A. Grzybowski, P. Barboni (eds.), *OCT in Central Nervous System Diseases: The Eye as a Window to the Brain*, DOI 10.1007/978-3-319-24085-5_13

13.1 Animal Models of Demyelinating Conditions

Demyelinating conditions such as multiple sclerosis (MS) are a major cause of disability and appropriate neuroprotective strategies have not been successfully developed yet [1]. MS can affect the visual system and therefore the eye can be used as a surrogate in assessing both the natural history of the disease and possible neuroprotective treatments. Although MS is a human specific condition, animal models of similar diseases have been developed such as Experimental autoimmune encephalomyelitis (EAE), viral induced models (mainly mediated by Theiler's Murine Encephalomyelitis Virus), and toxicity-induced models such as the cuprizone model and lysolecithin-induced focal demyelination [2] (Table 13.1).

13.1.1 Experimental Autoimmune Encephalomyelitis (EAE)

EAE is an animal model of neuro-inflammation and is the most commonly used model of MS [22]. It is based on both antigen-antibody and cell-mediated response. It can be induced in several animal species (rat, mouse, rabbit, guinea pig and monkey) by spinal cord homogenate inoculation or by injection of different emulsified proteins or peptides in the animal CNS [3]. The proteins/peptides commonly used to induce EAE are myelin constituent peptides such as myelin basic protein (MBP), myelin proteolipid protein (PLP), and myelin oligodendrocyte glycoprotein (MOG) [23]. EAE is primarily mediated by specific T cells (CD4+), which migrate to the CNS and cause the autoimmune inflammatory response. The natural history of EAE can be variable, in a similar fashion as in human MS, and it is both species and agent dependent [24]. Hallmark signs include weight loss, ataxia, spastic/flaccid paralysis, and incontinence. The lesions in the EAE model are characterized mainly by spinal inflammation and demyelination, while in human MS, lesions are more commonly seen in the brain [25]. Literature reviews have shown that in recent decades several possible MS therapeutic strategies were successfully tested in animal models of EAE and that it was possible to control the disease in these immune-induced models [4, 5]. However, these successes in animal studies did not translate into a success when it came to human clinical trials [26].

The infection of the central nervous system with the Theiler's virus induces an immune-mediated demyelinating disease and provides an important model for the study of MS [27]. The demyelinating disease induced by Theiler's Murine Encephalomyelitis Virus (TMEV) is similar to chronic-progressive MS and is characterized by demyelination of the CNS mediated by a Th1 response with manifestation of spastic paralysis of the lower limbs. In particular, in the mouse model of TMEV, the damage to myelin is closely dependent on the CD8 mediated antiviral action, demonstrating how brain inflammation could result in demyelination and axonal damage [28–30].

Table 13.1 Animal models in neuro ophthalmology

Disease	Animal model	Method	Benefits	Limitations	References
MS	EAE (rat, mouse, monkey)	Induced	Similar variation in natural history	Limited brain involvement	[2–9]
	Cuprizone, lysolecithin (mouse)		Simplicity; rapid	Reversible	
AD	PS-1 and/or PS-2 APP transgenic Mutation mouse	Genetic	Progressive development of senile plaques	Difficult connection between injuries and increased deposition of Aß oligomers	[10–15]
	P301L tau mutation mouse		Robust model of NFT pathology	1st generation model	
	5xFAD mouse		Rapid deposition of large amounts of Aß	No NFT formation	
	3xTg-AD mouse		Follows natural history of AD		
ION	Rat, primate	Rose Bengal injection	Resembles human AION pathology	Does not reflect pathogenesis of-ION	[16]
LHON	CBA/J mice	Rotenone-induced	Quick and simple, reproduce the pathophysiologic phenotype–reduced RGC layer thickness, increased apoptosis, decrease dretinal metabolic capacity, increased superoxide.	The causal role of toxins in human LHON has not been demonstrated	[17–19]
	Mice, Rats	Mitochondrial ND4 mutation	Reproduction of LHON phenotype	The mutation can be fatal	
	Mice	Mitochondrial ND6 mutation	Clinical, biochemical and anatomical hallmarks of human LHON when induced in animal at 14 and 24 months	(ND4 mutation), technically demanding	

(continued)

Table 13.1 (continued)

Disease	Animal model	Method	Benefits	Limitations	References
NOM	EAE 'passive transfer' mouse	Passive transfer of IgG	Very similar pathology to human NMO	No injury to myelin	[20]
	Mice	Injection of IgG	Similar pathology with myelin involvement also	Dependent on co-injection of human complement	
	"2D2" EAE mouse	Genetic	Similar clinical picture to human NMO	No histological changes in keeping with NMO	[21]

13.1.2 Toxic Models of Demyelinating Conditions

Toxic models of demyelination have also been developed. Cuprizone, a copper chelating agent is able to induce rapid oligodendrocyte apoptosis with subsequent demyelination. The most important advantage of the cuprizone model is its simplicity. Mice, orally exposed to cuprizone express a rapid onset of MS like symptoms including ataxia and spastic paralysis. Histological features of this model are oligodendrocyte apoptosis, microglial infiltration, disruption of myelin sheets and macrophage activation which are in keeping with Human MS. However this is a reversible model; when cuprizone is eliminated from the mouse diet, remyelinization occurs followed by complete restitutio-ad-integrum [6, 7].

Lysolecithin, an activator of phospholipase A2, is also able to induce demyelination when injected into the spinal cord of experimental animals. It generates rapid demyelination due to activation of lymphocytes B and T followed by macrophage infiltration with subsequent disruption of myelin sheets. Like the cuprizone model, after Lysolecithin injection, remyelinization occurs in 6–8 weeks. Hence, this model is also not entirely representative of human MS [8, 9].

In conclusion, none of the currently available animal models of MS can replicate in-toto the human disease and further research is needed in the field.

13.1.3 Animal Models of Neuromyelitis Optica

Neuromyelitis Optica (NMO) is a neuroinflammatory disorder that preferentially targets the optic nerves and spinal cord, causing recurrent and simultaneous inflammation and demyelination of these structures, leading to blindness and paralysis. Once thought to be a subtype of MS, the discovery that NMO is associated with the

NMO-IgG biomarker, an antibody which targets the aquaporin-4 (AQP4) water channel on the endfeet of astrocytes, has seen it recognised as a spectrum of disorders distinct from MS [31]. Classical presentation is with an episode of optic neuritis causing a loss of vision, or visual field defects and dyschomatopsia occurring in isolation; accompanied by acute spinal cord dysfunction such as paraparesis or quadriparesis with sensory signs, or loss of bladder control.

There is circumstantial evidence from studies which suggests that NMO-IgG is pathogenic in humans, with the presence of the antibodies in patients with transverse myelitis or optic neuritis conferring a strong likelihood that these patients with develop NMO in the future compared to patients who test negative for the antibodies [20]. One animal model of NMO involves passive transfer of NMO-IgG via intraperitoneal injection into the EAE rat model. The IgG appears to exacerbate inflammation and modulate the immune response in the context of this model resulting in complement activation, immunoglobulin deposition, and granulocyte influx in perivascular areas of the spinal cord [32]. These changes represent very similar pathology to that seen in human NMO lesions, however the major limitation in this model is the lack of injury to the myelin. Another model of NMO involves direct injection of NMO-IgG into the brain of mice. Lesion development was dependent on the co-injection of human complement, resulting in similar pathological changes to those seen in human NMO lesions, and in contrast to the rat NMO models also demonstrated damage to the myelin [33]. A genetic animal model of NMO which does not involve IgG has also been developed. The "2D2" EAE model was developed in which mice born with T cells directed against myelin oligodendrocyte glycoprotein (MOG35–55) were crossed with mice that have a transgenic B cell receptor to MOG. The resultant progeny spontaneously developed a clinical picture involving optic neuritis and severe inflammatory spinal cord lesions, with sparing of the brain, as seen in human NMO patients [21]. In this model the drawback was that histological changes such as complement deposition and granulocyte recruitment were not seen. As yet no single animal model has recreated all of the clinical and pathological features of NMO, but a combination of active immunization, passive transfer, and genetic models is helping to elucidate individual pathological events in NMO.

13.2 Animal Models of Ischemic Optic Neuropathy

Ischemic optic neuropathy (ION) is caused by an ischaemia of the optic nerve head and is the most frequent cause of sudden visual loss in patients older than 50 years. ION is characterized by a severe reduction in visual acuity associated with visual field defect, oedema of the optic nerve head and disc haemorrhages. Ischemic optic neuropathy is differentiated into two different clinical forms: non-arteritic (NAION), which is caused by an infarct of the short posterior ciliary arteries associated with anatomical risk factors such as small optic disc; and the arteritic form (AION), which is part of a generalized disease (e.g. giant cells arteritis),

caused by an inflammatory reaction. The ischaemic outcome of either event will result in nerve fibre atrophy and often gives rise to a pale optic disc on clinical examination [34, 35].

The major problem regarding animal models of ION lies in the anatomical differences between the optic nerve head (ONH) in human and small animals. The ONH in rodents lacks a lamina cribrosa, and the connective tissue surrounding the axon bundles has different collagen components and hysteresis compared to what is found in humans [36]. The vascular structure of the rodent ONH is also different. While rats have a vascular ring around the ONH which is somewhat similar to primates, mice often lack this anatomical feature [37]. Therefore, this intrinsic inter-species variability translates into completely different manifestations of an ischaemic event. Furthermore, the number of axons which constitute the optic nerve is different between species. Human and non-human primates have 1–1.2 million axons, rats 100,000 and mice 50,000 [38–40]. Again, this crucial anatomical difference results in contrasting manifestations of ONH ischaemia.

The most diffuse model of ION is found in an induced model where a dye (Rose Bengal – RB) is injected intravenously and then locally activated by a focal laser beam (532 nμ) projected onto the ONH of the animal [16]. The activation of the RB provokes reactive oxygen species formation which subsequently triggers platelet activation and capillary endothelial disruption [41]. Repeatability, which was the major problem of this model, has been overcome recently by the introduction of custom made rodent contact lenses which enables constant and reproducible insults [42]. The generated damage has similar features to human ION, however the ischaemia resolves rapidly and the disc oedema disappears after a maximum of 5 days post insult. However, Retinal Ganglion Cell (RGCs) apoptosis occurs and reduction in retinal fibres is clearly visible 1 month after laser exposure using both direct visualization and computerised techniques. The hallmark of the disease, RGC apoptosis is also clearly assessable histologically, alongside structural changes to vessels, ONH oligodendrocytes apoptosis and ONH fibrosis [43].

The same method generates similar results when applied to mice and non-human primates, making this technique a very easy model of ION [44, 45] (Table 13.1).

13.3 Animal Models of Leber Hereditary Optic Neuropathy

Leber's hereditary optic neuropathy (LHON) is a rare disorder caused by mitochondrial DNA point mutations in genes coding for specific protein subunits of the respiratory chain complex I (G3460A, T14484C, G11778A) [46]; it is characterized by severe, painless acute unilateral visual loss which becomes bilateral within days or weeks. LHON predominantly affects young men (20 years) and, less frequently, women. However, a small number of paediatric and elderly cases have been reported [47]. The classic manifestation of LHON consists of rapid, painless loss of central

vision in one eye, accompanied by dyschromatopsia, followed by the involvement of the fellow eye within days or weeks. The evolution of the visual field defect is generally represented by progressive enlargement of the blind spot with rapid progress towards the central vision. Diagnosis of LHON should be always considered in young male patients with bilateral optic neuritis, regardless of their age [47].

Genetic studies of LHON began over two decades ago, however the pathogenic mechanisms that produce the specific RGCs degeneration are still not fully understood and aetiological therapeutic strategies are still under development. This is due largely to the lack of a good animal models of LHON. The first animal model was generated by intravitreal administration of rotenone, a mitochondrial complex I inhibitor, directly into the mouse eye where histological analysis showed a significant decrease of RGC layer thickness 1 day after injection of rotenone [48]. Another experimental mouse model consists of an intravitreal injection of a genetically-engineered ribozyme. This procedure is responsible for a specific degradation of nuclear mRNA which results in the onset of an optic neuropathy with reduced superoxide dismutase activity and similar histological features observed in patients with LHON [17]. Another model of rodent LHON can be generated by injecting rotenone microspheres directly into the rat's superior colliculus [18]. These animal models showed most common signs of LHON: visual loss within 2 weeks of injection, absence of early RGCs loss with subsequent apoptosis. Intravitreal injections of yeast NADH dehydrogenase (Ndi1) in these models produces restoration of normal vision, which has opened a window of opportunity for novel therapeutic strategies [18]. Genetic models of LHON are also available. A mouse with a G14600A mutation has been developed which results in mouse optic atrophy with synaptosomes and increased ROS production [19].

13.4 Animal Models of Alzheimer's Disease

Alzheimer's disease (AD), the most common cause of dementia, is characterized by the insidious onset of a progressive decline in cognitive function due to the loss of neurons in the brain [49]. The pathology underlying the degeneration of neurons in AD brain is the formation of extracellular senile plaques via amyloid-beta (Aß) deposition and intracellular neurofibrillary tangles (NFTs) via hyperphosphorylation of tau protein [50]. Although much progress has been made in our understanding of AD, early and more accurate diagnosis is currently unavailable, and a definitive diagnosis of AD can still only be made by neuropathology after the patient has died [51]. This prevents effective treatment in the early stages of the disease. Perhaps the main problem in the early diagnosis of AD is the inability to directly visualize changes in the brain.

However, increasing evidence has shown that the retina is also affected in AD, along with the changes in the brain [52]. More significantly, the hallmarks of Alzheimer's in the brain have also been identified in the retina in both animal

models and human subjects. Histological studies in transgenic AD mouse models have demonstrated the present of Aß in the retina. Using a single transgenic Tg2576 mouse model which contains the APP double Swedish mutation, Liu et al. have shown increased Aß immunoreaction occurring predominantly in the retinal ganglion cell layer and the outer retina [53]. Retinal Aß deposition along with increased APP has also been found in double transgenic mouse models expressing APP and presenilin (PS) mutations; a finding which increased with age [54–56]. Using a triple transgenic AD mouse model that harbours three mutations of APP, tau and PS, a recent study has also demonstrated increased Aß deposition and tau hyperphosphorylation in the RGC layer compared to age-matched controls. A particularly exciting finding is that retinal Aß plaques in AD mice can be stained with curcumin and imaged *in-vivo*; and more significantly, that the retinal plaques occurred prior to the development of plaques in the brain [57]. This is hugely relevant as it suggests that retinal changes could potentially be used to make an early diagnosis of AD. Similar to the findings in mice, APP immunoreaction has also been demonstrated in human retina, being prominent in RGCs and the RNFL, and again found in increased abundance with age [58]. In AD patients, Aß specific plaques have been identified in the retina and increased with the severity of the disease by histological analysis of post-mortem eyes [57].

The clinical endpoint for AD pathology is neuronal loss and tissue atrophy in the brain, in which both apoptosis and necrosis play a crucial role [59].

13.4.1 PS-1 and/or PS-2 APP Transgenic Mutation

Copies of human APP and PS1-2, which are implicated in familial AD have been used to create models of transgenic AD mice [10]. Transgenic models generated APP mutation with deposition of amyloid peptide, which is similar but not identical to the one found in human senile plaques, and commonly associated with amyloid angiopathy. Deposit of amyloid peptide are observed with associated dystrophic alterations in axons and dendrites. These models have often been used to understand the natural history of senile plaques [60], to study the plaque removing action of microglia [61], and to study protein interactions [62]. The double APP+ PS1 mutant transgenic models, show a progressive and rapid development of senile plaques at 3 months of age with maximum expression at 12 months [63].

Since the development of this model, several questions have been raised regarding the mechanism of neuronal loss, the accumulation of Aß in the cell body, inflammation, and gliosis. This model has also been used to determine the involvement of oxidative stress in AD [64, 65]. The biggest drawback of this model is the difficulty to draw a connection between symptoms, injuries and increased deposition of Aß oligomers [66]. Another problem of this mouse model is that neurofibrillary tangles (NFTs) are present only in mouse lines that overexpress mutated tau protein [66, 67].

13.4.2 Transgenic Tauopathies

Tauopathies are a group of degenerative diseases characterized histologically by the presence of filamentous inclusions in neurons (neurofibrillary pathology) and occasionally in the glial cells. These filaments are composed of hyperphosphorylated forms of tau protein which together generates NFT. The discovery of the tau gene mutation on chromosome 17 in frontotemporal dementia has facilitated the development of tau-transgenic mice [11–13].

There has been significant progress in the development of models of this group of diseases. In particular mice expressing P301L tau mutation demonstrated that it is possible to generate robust animal models of neurofibrillary pathology [68] which can be assessed in vivo. However, this transgenic model only represents a first generation of mice which are affected by human tauopathies [69].

13.5 Mutations Model

This model, developed by Oakley et al. is based on five mutations that occur in APP and presenilins (PS-1 and PS-2) which lead to an increased production of Aß-42. This model is known as 5xFAD, which represent the five mutations that occur in familial AD. In this model there is a rapid production of Aß-42 that leads to the formation of senile plaques similar to those found in patients with AD [14]. Aß deposits begin at 2 months of age in the neuronal soma and dendrites especially in deep cortical layers, well before the formation of senile plaques.

In this model synaptic dysfunction occurs with aging, showing a marked decrease in synaptophysin, syntaxin and PDS95 and loss of pyramidal cortical neurons [14] with marked memory loss [14, 70]. Moreover it has been reported that this transgenic mouse has behavioural and motor deficiencies [71].

This may be a useful model for studying the processes related to the formation of senile plaques, synaptic loss and cognitive decline. This model has the advantage that it produces a large amount of Aß deposition in a short period of time. However, this model does not produce the same NFTs that are characteristic of AD in humans.

13.5.1 Triple – Transgenic Model

In 2003 a triple-transgenic model was described for the first time in which both senile plaques and NFT called 3xTg-AD were present [15].

This mouse expresses extracellular Aß deposits prior to the formation of NFT. This phenotype is in keeping with the natural history of the AD in humans where there is progressive loss of synaptic plasticity followed by extracellular deposits of Aß and the deposition of NFTs, associated with Aß immunoreactivity

[72, 73]. Therefore, it is considered that this particular type of transgenic mouse is useful for studying the impact of Aß and tau protein accumulation on synaptic plasticity. Moreover, this model presents with behavioural and cognitive deficits that increase with aging. These characteristics are similar to what happens in humans with AD [74]. Since the creation of the 3xTg-AD mouse, a variety of research projects have been initiated which seek to elucidate our understanding of AD.

It has been demonstrated that the accumulation of Aß which triggers tau deposition occurs before it is undergoes hyperphosphorylation [75, 76]. In 2005, a study showing that chronic nicotine administration exacerbates tauopathy in this model was published [77, 78]. The relationship between Aß, tau and synaptic dysfunction was also assessed [15]. Likewise the ratio of Aß deposition and cognitive deficits was also demonstrated [79]. The 3xTg-AD model has been correlated with glial activation and Aß deposition [80], and has also been used to study the inflammation in specific areas of the CNS in order to evaluate potential inflammatory markers of AD [80]. In a paper published in 2005, primary cultures of 3xTgAD were used to study calcium release induced by caffeine [81]. The triple-transgenic mouse has proven to be a useful model for studying the development of AD, its neurobiochemical, neuropathological and neuropharmacological characteristics. Studies with this model outnumber those made with other types of models. However, there will always be controversy about the extent to which animal models are representative of the disease in humans.

Although an age-dependent increase of the level of RGC apoptosis has been documented histologically in the double AD (APP/PS1) mouse [56, 82], this has not yet been confirmed in real time. Using the triple transgenic mouse model of AD (3xTgAD), it has been attempted to assess both apoptosis and necrosis simultaneously *in-vivo*. Both RGC apoptosis and necrosis are present in the retina of AD mice, and quantitative analysis revealed that the majority of apoptotic RGCs are in their early phase of apoptosis rather than in the late phase or necrosis, compared with age matched controls. This would suggest that early phase apoptosis of RGCs may be characteristic in 3xTgAD mice, and they could be reversed or rescued in this early stage of degeneration.

Increased evidence shows that oxidative stress is heavily implicated in AD pathology, along with increased Aß accumulation and deposition in the brain [83]. As Aß accumulation in the retina has been demonstrated in this AD model [84, 85].

Thus, the novel approach of *in-vivo* retinal imaging not only provides a means to detect RGC death which could reflect the changes in the brain, but also enables differentiation of apoptosing and necrosing processes simultaneously in the same living eye over time.

13.6 Animal Models of Parkinson's Disease

Although the use of L-DOPA has revolutionized the treatment of PD, this is only a symptomatic treatment, which cannot arrest or delay the degeneration of dopaminergic neurons. The most significant obstacle to the development of new neuroprotective drugs is the lack of knowledge of the specific molecular events that lead to neurodegeneration in PD [86].

The development of animal models represents a valuable tool for testing therapeutic strategies. To date, the agents used to induce degeneration of cells producing dopamine include MPTP (1-Methyl-4–phenyl-1,2,3,6-tetrahydropyridine) [87], and pesticides such as rotenone [88].

The treatment of animals with neurotoxins such as rotenone, paraquat, 6-OHDA, MPTP and -synuclein, provide important models for the study of the causes and the molecular mechanisms involved in the death of dopaminergic neurons in PD. Although these toxins induce CNS neurodegeneration, each one produces different clinical and neuropathological effects. Each neurotoxic model of PD has its own advantages and disadvantages and currently no one model is capable of representing all aspects of PD. For this reason, the choice of toxins used to induce a PD model is related to the type of study to be undertaken [89]. A summary of models is presented in the table below (Table 13.2).

13.6.1 Paraquat (1,1'-Dimethyl-4,4'-Bipyridinium Dichloride)

When administered systemically in rodents, paraquat can induce reduced motor activity, a dose dependant loss of dopaminergic neurons in the SN, and a reduction of dopaminergic fibres in the striatum [90]. Rats treated with paraquat are reported to also express pathological levels of α-syn in the SN [91]. However, a limitation of this model is that paraquat also induces severe lung, liver, and kidney toxicity causing a high mortality rate in treated animals [92].

13.6.2 6-OHDA (6-Hydroxyl Dopamine or 2, 4, 5-Trihydroxy Phenethylamine)

6-OHDA does not easily cross the Blood Brain Barrier (BBB) and therefore cannot reach toxic concentrations in the CNS following a systemic administration. However, systemic administration of 6-OHDA causes damage to the peripheral nervous system [114]. Due to its inability to cross the BBB, direct administration of 6-OHDA in different brain area has been achieved using stereotactic methods to better model PD [89]. Used firstly on rats, the direct administration of 6-OHDA has subsequently been characterised in mice and monkeys [93–97]. The most common method to induce a lesion in the nigrostriatal pathway is the unilateral administration of 6-OHDA in the forebrain bundle (which includes the nigrostriatal tract) or in the striatum [115], however, a bilateral lesion with 6-OHDA is fatal. After direct administration of 6-OHDA, apoptosis of dopaminergic neurons is reported to occur within 24 h [116]. The maximum reduction in the levels of striatal DA occurs between 3 and 4 days after lesion onset, when the residual striatal DA neuron population is reduced to less than 20 % of age matched controls [117]. Therefore, this is a rapid model but very invasive. The presence of Lewy's Bodies (LB) has not yet been documented in this model.

Table 13.2 Comparing the common animal models of PD

Model	Administration route	Type of damage	Histological findings	Symptoms	Disadvantages	References
Paraquat	Systemic	Loss of striatal dopaminergic fibres	α-syn inclusions	Reduced motor activity	Active on other neurotensmitter	[90–92]
6-OHDA	Local, stereotaxic	Loss of striatal dopaminergic neurons	Absence of α-syn inclusions	Rotational behaviours	Intracranial injections are fatal	[93–97]
MPTP	Systemic, subcutaneous, intravenous, intraperitoneal or intramuscular	Selective loss of Da neurons, reduced DA fibers	Absence of α-syn inclusions	Reduced motor activity	Acute model, does not progress	[98–101]
α-synuclein	Viral vectors, transgenic model	Selective degeneration of dopaminergic neurons	Overexpression of α-syn	Heavily reduced motor activity	Scarce evidence of neuronal death	[102–105]
Rotenone	Systemic, subcutaneous, intravenous, intraperitoneal or intramuscular	Loss of striatal dopaminergic neurons	α-syn inclusions, reduced tyrosine hydroxylase levels, nigrostriatal microglial activation	Reduced motor activity, altered posture, sleep and gastrointestinal alteration	Time consuming, high rate of mortality	[106–110]
LRRK-2	Transgenic	Minor loss of striatal dopaminergic neurons	Presence of Lewy bodies	Reduced motor activity	Absence of α-syn inclusions, poorly reproducible	[111–113]

13.6.3 MPTP (1-Methyl-4-Phenyl-1,2,3,6-Tetrahydropyridine)

Neuropathological data, derived mainly from experiments on non-human primates, has demonstrated that administration of MPTP causes damage to the nigrostriatal dopaminergic pathway similar to that found in PD [98]. The most reliable and reproducible disease model is induced through systemic administration of MPTP via intranasal [118], subcutaneous [119], intravenous [120], intra-peritoneal [121] or intramuscular [122] injection. As in human PD, a large loss of dopaminergic neurons in the CNS and ventral tegmental area is reported in this model [99, 100]. However, MPTP induced models of PD do not present with LBs [101].

13.6.4 α-Synuclein

Chronologically, the most recent model of PD, this model is based on the genetic link between Parkinson's disease and neuropathological effect of α-synuclein (α-syn) [102]. There are two types of α-syn animal models, either transgenic or non-transgenic. Transgenic model organisms in Drosophila and mice have been developed which over-express both the human wild-type α-syn and the mutated (A3OP and A53T) forms [123]. In models of Drosophila a significant loss of DA neurons is reported, while murine models do not demonstrate significant anomalies in dopaminergic neurons [103]. Non-transgenic models are based instead on the insertion of α-syn encoding genes into the SNPC using viral vectors [104, 105]. The mutation of α-syn in this way is reported to cause the selective degeneration of dopaminergic neurons in the rat SNPC, with the formation of cytoplasmic structures containing a-syn which are very similar to LBs [124].

13.6.5 Rotenone ((2R, 6aS, 12aS) -1, 2, 6, 6a, 12, 12a-Hexahydro- 2-Isopropenyl- 8, 9- Dimethoxy Chromeno [3, 4- b] Furo (2, 3- h) Chromen- 6- One)

Among the various models of PD, the rotenone model has recently drawn particular attention because it reproduces most of the motor defect symptoms and the histopathological features of PD [125, 126].

This insecticide found in the roots of leguminous plants, interacts specifically with the mitochondrial respiratory chain complex [127]. Rotenone acts by blocking the mitochondrial electron transport form complex I to CoenzymeQ10 leading to energy starvation and cellular death.

Rotenone may have initially been used by Indians as a poison when hunting for fish [128]. Today it is commonly used as a pesticide due to its high biodegradability, degrading within days. It is highly lipophilic so it quickly passes through the cell

membrane, the blood brain barrier and accumulates in subcellular organelles such as mitochondria.[129] Both pulsatile [130] and chronic [106] administration of rotenone *in-vivo* and *in-vitro* models induces degeneration of nigrostriatal neurons, with formation of cytoplasmic inclusions similar to Lewy bodies, oxidative damage and parkinsonian bradykinesia and rigidity.

The mechanism by which complex I dysfunction induces neurotoxicity is still not known. The most common pathway seems to involve increased levels of oxidative stress [131], resulting in reduced levels of glutathione and oxidative modification of DNA, lipids, proteins and antioxidants such as α-tocopherol [132, 133]. Inhibition of Complex I was also demonstrated to increase levels of H_2O_2 and inhibition of Reactive Oxygen Species (ROS) [134]. It is believed that increased levels of ROS are mediated by microglia, which are also activated by the rotenone [135]. This massive oxidative stress produces alterations in mitochondrial function and activation of the apoptosing cascade [134]. The resulting decrease in intracellular levels of ATP causes the opening of Na^+K^+-ATP channels [136]. It has been shown that the hyperpolarization induced by the application of rotenone on dopamine cells of the CNS is mediated by the opening of these channels. In addition, the dopaminergic cells that contain the SUR-1 subunit of the Na^+ K^+-ATP channels are more sensitive to metabolic changes induced by the toxin [137].

The selectivity of rotenone on the dopaminergic system has been explained on the basis of the cytotoxic effect mediated by the same endogenous mechanism [138]. It has been shown that rotenone induced blockade of mitochondrial complex I occurs in all cells indiscriminately [139], but this inhibition does not induce cell death in non-dopaminergic cells. The association between ROS – dopamine in dopaminergic cells could be the basis of the initial apoptotic process [140].

Biehlmaier et al. have demonstrated that rotenone-treated rats show a depletion of DA in the striatum and substantia nigra (SN), in association to a significant reduction in retinal dopaminergic amacrine cells, similar to that found in PD patients [90, 141].

In 2000, it was first reported that chronic systemic rotenone exposure in rats produced phenotypical features of PD [142]. Rotenone is reported to exert highly selective toxicity on DA neurons both *in-vitro* [143, 144] and *in-vivo* [106, 145, 146].

The mechanisms of action of rotenone are various [147]; rotenone is reported to inhibit mitochondrial complex 1, impeding the oxidation of NADH to NAD^+ so causing a reduction in cellular respiration [147]. The consequence of complex 1 inhibition is a cascade of events which leads to elevated oxidative stress [148] and ultimately apoptosis [149].

In-vivo models have been obtained through different routes of rotenone administration; Oral administration (via food), is reported to cause only mild neurotoxicity [107]. Stereotactic administration of rotenone in the medial forebrain bundle is reported to cause depletion of striatal DA neurons [150]. Systemic administration, including intravenous (i.v.), subcutaneous (s.c.), or intraperitoneal (I.P.), has been found to induce the formation of α-syn cytoplasmatic particles, in the substantia

nigra of treated rats in a similar manner to the typical LBs found in PD [106, 151]. Systemic administration of rotenone is also reported to promote the production of pro inflammatory factors and microglial activation triggering further oxidative insult to DA neurons [152, 153].

Rotenone administration also causes symptomatic changes in rodents including motor rigidity, behavioural alterations, catalepsy, sleep and gastrointestinal alterations. L-DOPA therapy is able to reverse temporarily the motor deficits reported in these models [154, 155]. Furthermore, systemic rotenone administration, frequently causes neurotoxicity and mortality in a dose-dependent manner.

Systemic rotenone administration has been reported ,through its ability to penetrate all cells, to act also on non-dopaminergic neurons such as Retinal Ganglion Cells (RGCs) [156]. Additional supporting evidence for the use of rotenone as a PD model can be found in epidemiological studies which demonstrated a correlation between PD and rotenone exposure in humans [157, 158].

13.6.6 LRRK2 Model (Table 13.3)

Leucine Rich Repeat Kinase (LRRK2) is a gene responsible for coding an enzyme called dardarin which has kinase activities and is responsible for signal transmission, protein-protein interaction, and amino acid phosphorylation [159]. Mutation of the *lrrk2* gene has been implicated in the pathogenesis of familial PD [111]. *lrrk2* was associated with the locus Park8 (Parkinson family of type 8) for the first time in 2002, in a large Japanese family that presented parkinsonian symptoms with autosomal dominant inheritance, but without the appearance of Lewy bodies [112]. Since 2004, mutations in *lrrk2*-linked to PD have been found in many families, which also included cases with the presence of LBs [111]. The relationship between

Table 13.3 Mutation involved in genetic PD

	Locus	Gene	Transmission	Number of family	Reference
PARK 1	4q21-23	α-synuclein	AD	18	[167]
PARK 2	6q25-27	Parkin	AR	Many	[168]
PARK 3	2p13	–	AD	6	[169]
PARK 4	4q21-23	α-synuclein	AD	Many	[170]
PARK 5	4p14	Ubiquitin	AD	1	[171]
PARK 6	1p35-36	Pink-1	AR	Sporadic cases	[172]
PARK 7	1p36	DJ-1	AR	2	[173]
PARK 8	12p11-q13	Dardarin (LRKK2)	AD	Many + sporadic cases	[174] [175]
PARK 9	1p36	–	AR	Kulford-Rakeb Syndrome	[176]

PD and *lrrk2* was later confirmed by gene sequencing which has revealed numerous pathogenic amino acid substitutions [160]. The *lrrk2* mutation Gly2019Ser is the most frequent replacement in the Caucasian population, which is statistically present in 0.5–2 % of cases of sporadic and 5 % of MP in familial Parkinsonism [161]. The probability that a heterozygote manifests symptoms below the age of 50 is less than 20 %, but this increases with age to more than 80 % after 75 years [113]. Biopsies of the substantia nigra of patients with PD caused by expression of mutated LRRK2 show the presence of Lewy bodies [162, 163]. La Morgia and colleagues have shown also retinal modifications in patients affected by the mutation of *lrrk2* [164] and reported the same RNFL thinning that occurs in patients with sporadic PD [165]. Retinal modifications have also been shown in a LRRK2 transgenic drosophila melanogaster model [166]. Using this model, Hindle et al. demonstrated a loss of visual response and concomitant photoreceptor degeneration.

13.7 Conclusion

Accessibility and cost efficiency combined with the great accessibility of the eye make animal models a precious tool for studying the natural history of neuro-ophthalmological diseases suggesting these models could provide a source of novel biomarkers for the early diagnosis and follow up of neurodegenerative diseases. Nevertheless, due to anatomical and physiological differences, the validity of animal models is closely related to the level of similarity with the human pathology. Therefore prudence should be always applied in choosing the appropriate model for each individual neuro-ophthalmolgocial condition (Fig. 13.1).

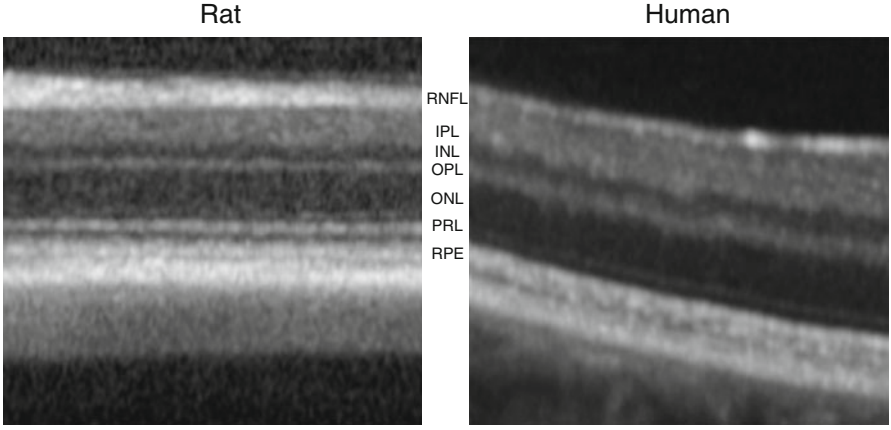

Fig. 13.1 OCT differences between Rat retina and Human Retina. *RNFL* retinal nerve fibre layer. *IPL* inner plexiform layer, *INL* inner nuclear layer, *OPL* outer plexiform layer, *ONL* outer nuclear layer, *PRL* photoreceptor layer, *RPE* retinal pigmented epithelium

References

1. Sormani MP, Bruzzi P. Can we measure long-term treatment effects in multiple sclerosis? Nature reviews Neurology. 2015;11(3):176–82.
2. Gold R, Hartung HP, Toyka KV. Animal models for autoimmune demyelinating disorders of the nervous system. Mol Med Today. 2000;6(2):88–91.
3. Klaren RE, Motl RW, Woods JA, Miller SD. Effects of exercise in experimental autoimmune encephalomyelitis (an animal model of multiple sclerosis). J Neuroimmunol. 2014;274(1–2):14–9.
4. Vesterinen HM, Sena ES, ffrench-Constant C, Williams A, Chandran S, Macleod MR. Improving the translational hit of experimental treatments in multiple sclerosis. Mult Scler. 2010;16(9):1044–55.
5. Pryce G, O'Neill JK, Croxford JL, Amor S, Hankey DJ, East E, et al. Autoimmune tolerance eliminates relapses but fails to halt progression in a model of multiple sclerosis. J Neuroimmunol. 2005;165(1–2):41–52.
6. Praet J, Guglielmetti C, Berneman Z, Van der Linden A, Ponsaerts P. Cellular and molecular neuropathology of the cuprizone mouse model: clinical relevance for multiple sclerosis. Neurosci Biobehav Rev. 2014;47C:485–505.
7. Sachs HH, Bercury KK, Popescu DC, Narayanan SP, Macklin WB. A new model of cuprizone-mediated demyelination/remyelination. ASN Neuro. 2014;6(5):1–16.
8. van der Star BJ, Vogel DY, Kipp M, Puentes F, Baker D, Amor S. In vitro and in vivo models of multiple sclerosis. CNS Neurol Disord Drug Targets. 2012;11(5):570–88.
9. Nastasijevic B, Wright BR, Smestad J, Warrington AE, Rodriguez M, Maher 3rd LJ. Remyelination induced by a DNA aptamer in a mouse model of multiple sclerosis. PLoS One. 2012;7(6):e39595.
10. Duff K, Eckman C, Zehr C, Yu X, Prada CM, Perez-tur J, et al. Increased amyloid-beta42(43) in brains of mice expressing mutant presenilin 1. Nature. 1996;383(6602):710–3.
11. Gotz J, Chen F, van Dorpe J, Nitsch RM. Formation of neurofibrillary tangles in P301l tau transgenic mice induced by Abeta 42 fibrils. Science. 2001;293(5534):1491–5.
12. Higuchi M, Ishihara T, Zhang B, Hong M, Andreadis A, Trojanowski J, et al. Transgenic mouse model of tauopathies with glial pathology and nervous system degeneration. Neuron. 2002;35(3):433–46.
13. Lewis J, McGowan E, Rockwood J, Melrose H, Nacharaju P, Van Slegtenhorst M, et al. Neurofibrillary tangles, amyotrophy and progressive motor disturbance in mice expressing mutant (P301L) tau protein. Nat Genet. 2000;25(4):402–5.
14. Oakley H, Cole SL, Logan S, Maus E, Shao P, Craft J, et al. Intraneuronal beta-amyloid aggregates, neurodegeneration, and neuron loss in transgenic mice with five familial Alzheimer's disease mutations: potential factors in amyloid plaque formation. J Neurosci Off J Soc Neurosci. 2006;26(40):10129–40.
15. LaFerla FM, Oddo S. Alzheimer's disease: Abeta, tau and synaptic dysfunction. Trends Mol Med. 2005;11(4):170–6.
16. Zhao BQ, Suzuki Y, Kondo K, Kawano K, Ikeda Y, Umemura K. A novel MCA occlusion model of photothrombotic ischemia with cyclic flow reductions: development of cerebral hemorrhage induced by heparin. Brain Res Brain Res Protoc. 2002;9(2):85–92.
17. Qi X, Lewin AS, Hauswirth WW, Guy J. Suppression of complex I gene expression induces optic neuropathy. Ann Neurol. 2003;53(2):198–205.
18. Marella M, Seo BB, Thomas BB, Matsuno-Yagi A, Yagi T. Successful amelioration of mitochondrial optic neuropathy using the yeast NDI1 gene in a rat animal model. PLoS One. 2010;5(7), e11472.
19. Lin CS, Sharpley MS, Fan W, Waymire KG, Sadun AA, Carelli V, et al. Mouse mtDNA mutant model of Leber hereditary optic neuropathy. Proc Natl Acad Sci U S A. 2012;109(49):20065–70.

20. Frohman EM, Kerr D. Is neuromyelitis optica distinct from multiple sclerosis?: something for "lumpers" and "splitters". Arch Neurol. 2007;64(6):903–5.
21. Bettelli E, Baeten D, Jager A, Sobel RA, Kuchroo VK. Myelin oligodendrocyte glycoprotein-specific T and B cells cooperate to induce a Devic-like disease in mice. J Clin Invest. 2006;116(9):2393–402.
22. Hoglund RA, Maghazachi AA. Multiple sclerosis and the role of immune cells. World J Exp Med. 2014;4(3):27–37.
23. Robinson AP, Harp CT, Noronha A, Miller SD. The experimental autoimmune encephalomyelitis (EAE) model of MS: utility for understanding disease pathophysiology and treatment. Handb Clin Neurol. 2014;122:173–89.
24. Kuerten S, Lehmann PV. The immune pathogenesis of experimental autoimmune encephalomyelitis: lessons learned for multiple sclerosis? J Interferon Cytokine Res Off J Int Soc Interferon and Cytokine Res. 2011;31(12):907–16.
25. Handel AE, Lincoln MR, Ramagopalan SV. Of mice and men: experimental autoimmune encephalitis and multiple sclerosis. Eur J Clin Invest. 2011;41(11):1254–8.
26. Friese MA, Montalban X, Willcox N, Bell JI, Martin R, Fugger L. The value of animal models for drug development in multiple sclerosis. Brain J Neurol. 2006;129(Pt 8):1940–52.
27. Takizawa S, Kaneyama T, Tsugane S, Takeichi N, Yanagisawa S, Ichikawa M, et al. Role of the Programmed Death-1 (PD-1) pathway in regulation of Theiler's murine encephalomyelitis virus-induced demyelinating disease. J Neuroimmunol. 2014;274(1–2):78–85.
28. Martinez NE, Karlsson F, Sato F, Kawai E, Omura S, Minagar A, et al. Protective and detrimental roles for regulatory T cells in a viral model for multiple sclerosis. Brain Pathol. 2014;24(5):436–51.
29. Zhang J, Lipton HL, Perelson AS, Dahari H. Modeling the acute and chronic phases of Theiler murine encephalomyelitis virus infection. J Virol. 2013;87(7):4052–9.
30. Mecha M, Carrillo-Salinas FJ, Mestre L, Feliu A, Guaza C. Viral models of multiple sclerosis: neurodegeneration and demyelination in mice infected with Theiler's virus. Prog Neurobiol. 2013;101–102:46–64.
31. Jones MV, Collongues N, de Seze J, Kinoshita M, Nakatsuji Y, Levy M. Review of animal models of neuromyelitis optica. Mult Scler Relat Disord. 2012;1(4):174–9.
32. Kinoshita M, Nakatsuji Y, Kimura T, Moriya M, Takata K, Okuno T, et al. Neuromyelitis optica: passive transfer to rats by human immunoglobulin. Biochem Biophys Res Commun. 2009;386(4):623–7.
33. Saadoun S, Waters P, Bell BA, Vincent A, Verkman AS, Papadopoulos MC. Intra-cerebral injection of neuromyelitis optica immunoglobulin G and human complement produces neuromyelitis optica lesions in mice. Brain J Neurol. 2010;133(Pt 2):349–61.
34. Arnold AC, Hepler RS. Natural history of nonarteritic anterior ischemic optic neuropathy. J Neuroophthalmol Off J North Am Neuroophthalmol Soc. 1994;14(2):66–9.
35. Arnold AC. Pathogenesis of nonarteritic anterior ischemic optic neuropathy. J Neuroophthalmol Off J North Am Neuroophthalmol Soc. 2003;23(2):157–63.
36. Albrecht MC. Comparative anatomy of the optic nerve head and inner retina in non-primate animal models used for glaucoma research. Open Ophthalmol J. 2008;2:94–101.
37. Bernstein SL, Guo Y, Kelman SE, Flower RW, Johnson MA. Functional and cellular responses in a novel rodent model of anterior ischemic optic neuropathy. Invest Ophthalmol Vis Sci. 2003;44(10):4153–62.
38. Williams RW, Strom RC, Rice DS, Goldowitz D. Genetic and environmental control of variation in retinal ganglion cell number in mice. J Neurosci Off J Soc Neurosci. 1996;16(22):7193–205.
39. Perry VH, Henderson Z, Linden R. Postnatal changes in retinal ganglion cell and optic axon populations in the pigmented rat. J Comp Neurol. 1983;219(3):356–68.
40. Morrison JC, Cork LC, Dunkelberger GR, Brown A, Quigley HA. Aging changes of the rhesus monkey optic nerve. Invest Ophthalmol Vis Sci. 1990;31(8):1623–7.
41. Mosinger JL, Olney JW. Photothrombosis-induced ischemic neuronal degeneration in the rat retina. Exp Neurol. 1989;105(1):110–3.

42. Bernstein SL, Johnson MA, Miller NR. Nonarteritic anterior ischemic optic neuropathy (NAION) and its experimental models. Prog Retin Eye Res. 2011;30(3):167–87.
43. Goldenberg-Cohen N, Guo Y, Margolis F, Cohen Y, Miller NR, Bernstein SL. Oligodendrocyte dysfunction after induction of experimental anterior optic nerve ischemia. Invest Ophthalmol Vis Sci. 2005;46(8):2716–25.
44. Feng G, Mellor RH, Bernstein M, Keller-Peck C, Nguyen QT, Wallace M, et al. Imaging neuronal subsets in transgenic mice expressing multiple spectral variants of GFP. Neuron. 2000;28(1):41–51.
45. Chen CS, Johnson MA, Flower RA, Slater BJ, Miller NR, Bernstein SL. A primate model of nonarteritic anterior ischemic optic neuropathy. Invest Ophthalmol Vis Sci. 2008;49(7): 2985–92.
46. Ziccardi L, Sadun F, De Negri AM, Barboni P, Savini G, Borrelli E, et al. Retinal function and neural conduction along the visual pathways in affected and unaffected carriers with Leber's hereditary optic neuropathy. Invest Ophthalmol Vis Sci. 2013;54(10):6893–901.
47. La Morgia C, Carbonelli M, Barboni P, Sadun AA, Carelli V. Medical management of hereditary optic neuropathies. Front Neurol. 2014;5:141.
48. Zhang X, Jones D, Gonzalez-Lima F. Mouse model of optic neuropathy caused by mitochondrial complex I dysfunction. Neurosci Lett. 2002;326(2):97–100.
49. Musardo S, Saraceno C, Pelucchi S, Marcello E. Trafficking in neurons: searching for new targets for Alzheimer's disease future therapies. Eur J Pharmacol. 2013;719(1–3):84–106.
50. Nogueras-Ortiz CJ, De Jesus-Cortes HJ, Vaquer-Alicea J, Vega IE. Novel autoimmune response in a tauopathy mouse model. Front Neurosci. 2014;7:277.
51. Ni R, Gillberg PG, Bergfors A, Marutle A, Nordberg A. Amyloid tracers detect multiple binding sites in Alzheimer's disease brain tissue. Brain J Neurol. 2013;136(Pt 7):2217–27.
52. Krantic S, Torriglia A. Retina: source of the earliest biomarkers for Alzheimer's disease? J Alzheimers Dis JAD. 2014;40(2):237–43.
53. Liu B, Rasool S, Yang Z, Glabe CG, Schreiber SS, Ge J, et al. Amyloid-peptide vaccinations reduce {beta}-amyloid plaques but exacerbate vascular deposition and inflammation in the retina of Alzheimer's transgenic mice. Am J Pathol. 2009;175(5):2099–110.
54. Dutescu RM, Li QX, Crowston J, Masters CL, Baird PN, Culvenor JG. Amyloid precursor protein processing and retinal pathology in mouse models of Alzheimer's disease. Graefes Arch Clin Exp Ophthalmol. 2009;247(9):1213–21.
55. Perez SE, Lumayag S, Kovacs B, Mufson EJ, Xu S. Beta-amyloid deposition and functional impairment in the retina of the APPswe/PS1DeltaE9 transgenic mouse model of Alzheimer's disease. Invest Ophthalmol Vis Sci. 2009;50(2):793–800.
56. Ning A, Cui J, To E, Ashe KH, Matsubara J. Amyloid-beta deposits lead to retinal degeneration in a mouse model of Alzheimer disease. Invest Ophthalmol Vis Sci. 2008;49(11):5136–43.
57. Koronyo-Hamaoui M, Koronyo Y, Ljubimov AV, Miller CA, Ko MK, Black KL, et al. Identification of amyloid plaques in retinas from Alzheimer's patients and noninvasive in vivo optical imaging of retinal plaques in a mouse model. Neuroimage. 2011;54 Suppl 1: S204–17.
58. Loffler KU, Edward DP, Tso MO. Immunoreactivity against tau, amyloid precursor protein, and beta-amyloid in the human retina. Invest Ophthalmol Vis Sci. 1995;36(1):24–31.
59. de Lemos ML, de la Torre AV, Petrov D, Brox S, Folch J, Pallas M, et al. Evaluation of hypoxia inducible factor expression in inflammatory and neurodegenerative brain models. Int J Biochem Cell Biol. 2013;45(7):1377–88.
60. Park JH, Widi GA, Gimbel DA, Harel NY, Lee DH, Strittmatter SM. Subcutaneous Nogo receptor removes brain amyloid-beta and improves spatial memory in Alzheimer's transgenic mice. J Neurosci Off J Soc Neurosci. 2006;26(51):13279–86.
61. Simard AR, Soulet D, Gowing G, Julien JP, Rivest S. Bone marrow-derived microglia play a critical role in restricting senile plaque formation in Alzheimer's disease. Neuron. 2006;49(4):489–502.
62. Yao J, Taylor M, Davey F, Ren Y, Aiton J, Coote P, et al. Interaction of amyloid binding alcohol dehydrogenase/Abeta mediates up-regulation of peroxiredoxin II in the brains of Alzheimer's

disease patients and a transgenic Alzheimer's disease mouse model. Mol Cell Neurosci. 2007;35(2):377–82.
63. Holcomb L, Gordon MN, McGowan E, Yu X, Benkovic S, Jantzen P, et al. Accelerated Alzheimer-type phenotype in transgenic mice carrying both mutant amyloid precursor protein and presenilin 1 transgenes. Nat Med. 1998;4(1):97–100.
64. Schuessel K, Schafer S, Bayer TA, Czech C, Pradier L, Muller-Spahn F, et al. Impaired Cu/Zn-SOD activity contributes to increased oxidative damage in APP transgenic mice. Neurobiol Dis. 2005;18(1):89–99.
65. Esposito L, Raber J, Kekonius L, Yan F, Yu GQ, Bien-Ly N, et al. Reduction in mitochondrial superoxide dismutase modulates Alzheimer's disease-like pathology and accelerates the onset of behavioral changes in human amyloid precursor protein transgenic mice. J Neurosci Off J Soc Neurosci. 2006;26(19):5167–79.
66. Duyckaerts C, Potier MC, Delatour B. Alzheimer disease models and human neuropathology: similarities and differences. Acta Neuropathol. 2008;115(1):5–38.
67. Hutton M, Lewis J, Dickson D, Yen SH, McGowan E. Analysis of tauopathies with transgenic mice. Trends Mol Med. 2001;7(10):467–70.
68. Terwel D, Lasrado R, Snauwaert J, Vandeweert E, Van Haesendonck C, Borghgraef P, et al. Changed conformation of mutant Tau-P301L underlies the moribund tauopathy, absent in progressive, nonlethal axonopathy of Tau-4R/2N transgenic mice. J Biol Chem. 2005;280(5):3963–73.
69. Gotz J, Deters N, Doldissen A, Bokhari L, Ke Y, Wiesner A, et al. A decade of tau transgenic animal models and beyond. Brain Pathol. 2007;17(1):91–103.
70. Ohno M, Cole SL, Yasvoina M, Zhao J, Citron M, Berry R, et al. BACE1 gene deletion prevents neuron loss and memory deficits in 5XFAD APP/PS1 transgenic mice. Neurobiol Dis. 2007;26(1):134–45.
71. Jawhar S, Trawicka A, Jenneckens C, Bayer TA, Wirths O. Motor deficits, neuron loss, and reduced anxiety coinciding with axonal degeneration and intraneuronal Abeta aggregation in the 5XFAD mouse model of Alzheimer's disease. Neurobiol Aging. 2012;33(1):196 e29–40.
72. Oddo S, Caccamo A, Shepherd JD, Murphy MP, Golde TE, Kayed R, et al. Triple-transgenic model of Alzheimer's disease with plaques and tangles: intracellular Abeta and synaptic dysfunction. Neuron. 2003;39(3):409–21.
73. Oddo S, Caccamo A, Kitazawa M, Tseng BP, LaFerla FM. Amyloid deposition precedes tangle formation in a triple transgenic model of Alzheimer's disease. Neurobiol Aging. 2003;24(8):1063–70.
74. Gimenez-Llort L, Blazquez G, Canete T, Johansson B, Oddo S, Tobena A, et al. Modeling behavioral and neuronal symptoms of Alzheimer's disease in mice: a role for intraneuronal amyloid. Neurosci Biobehav Rev. 2007;31(1):125–47.
75. Rissman RA, Poon WW, Blurton-Jones M, Oddo S, Torp R, Vitek MP, et al. Caspase-cleavage of tau is an early event in Alzheimer disease tangle pathology. J Clin Invest. 2004;114(1):121–30.
76. Oddo S, Billings L, Kesslak JP, Cribbs DH, LaFerla FM. Abeta immunotherapy leads to clearance of early, but not late, hyperphosphorylated tau aggregates via the proteasome. Neuron. 2004;43(3):321–32.
77. Oddo S, Caccamo A, Green KN, Liang K, Tran L, Chen Y, et al. Chronic nicotine administration exacerbates tau pathology in a transgenic model of Alzheimer's disease. Proc Natl Acad Sci U S A. 2005;102(8):3046–51.
78. Smith IF, Green KN, LaFerla FM. Calcium dysregulation in Alzheimer's disease: recent advances gained from genetically modified animals. Cell Calcium. 2005;38(3–4):427–37.
79. Billings LM, Oddo S, Green KN, McGaugh JL, LaFerla FM. Intraneuronal Abeta causes the onset of early Alzheimer's disease-related cognitive deficits in transgenic mice. Neuron. 2005;45(5):675–88.
80. Janelsins MC, Mastrangelo MA, Oddo S, LaFerla FM, Federoff HJ, Bowers WJ. Early correlation of microglial activation with enhanced tumor necrosis factor-alpha and monocyte che-

moattractant protein-1 expression specifically within the entorhinal cortex of triple transgenic Alzheimer's disease mice. J Neuroinflammation. 2005;2:23.
81. Smith IF, Hitt B, Green KN, Oddo S, LaFerla FM. Enhanced caffeine-induced Ca2+ release in the 3xTg-AD mouse model of Alzheimer's disease. J Neurochem. 2005;94(6):1711–8.
82. Shimazawa M, Inokuchi Y, Okuno T, Nakajima Y, Sakaguchi G, Kato A, et al. Reduced retinal function in amyloid precursor protein-over-expressing transgenic mice via attenuating glutamate-N-methyl-d-aspartate receptor signaling. J Neurochem. 2008;107(1):279–90.
83. Lee CW, Shih YH, Kuo YM. Cerebrovascular pathology and amyloid plaque formation in Alzheimer's disease. Curr Alzheimer Res. 2014;11(1):4–10.
84. Alexandrov PN, Pogue A, Bhattacharjee S, Lukiw WJ. Retinal amyloid peptides and complement factor H in transgenic models of Alzheimer's disease. Neuroreport. 2011;22(12): 623–7.
85. Savini G, Barboni P, Carbonelli M, Hoffer KJ. Comparison of methods to measure corneal power for intraocular lens power calculation using a rotating Scheimpflug camera. J Cataract Refract Surg. 2013;39(4):598–604.
86. Worth PF. How to treat Parkinson's disease in 2013. Clin Med. 2013;13(1):93–6.
87. Nicklas WJ, Vyas I, Heikkila RE. Inhibition of NADH-linked oxidation in brain mitochondria by 1-methyl-4-phenyl-pyridine, a metabolite of the neurotoxin, 1-methyl-4-phenyl-1,2,5,6-tetrahydropyridine. Life Sci. 1985;36(26):2503–8.
88. McNaught KS, Perl DP, Brownell AL, Olanow CW. Systemic exposure to proteasome inhibitors causes a progressive model of Parkinson's disease. Ann Neurol. 2004;56(1):149–62.
89. Bove J, Prou D, Perier C, Przedborski S. Toxin-induced models of Parkinson's disease. NeuroRx J Am Soc Exp Neurother. 2005;2(3):484–94.
90. Blesa J, Phani S, Jackson-Lewis V, Przedborski S. Classic and new animal models of Parkinson's disease. J Biomed Biotechnol. 2012;2012:845618.
91. Manning-Bog AB, McCormack AL, Li J, Uversky VN, Fink AL, Di Monte DA. The herbicide paraquat causes up-regulation and aggregation of alpha-synuclein in mice: paraquat and alpha-synuclein. J Biol Chem. 2002;277(3):1641–4.
92. Freire C, Koifman S. Pesticide exposure and Parkinson's disease: epidemiological evidence of association. Neurotoxicology. 2012;33(5):947–71.
93. Annett LE, Torres EM, Clarke DJ, Ishida Y, Barker RA, Ridley RM, et al. Survival of nigral grafts within the striatum of marmosets with 6-OHDA lesions depends critically on donor embryo age. Cell Transplant. 1997;6(6):557–69.
94. Crofts HS, Dalley JW, Collins P, Van Denderen JC, Everitt BJ, Robbins TW, et al. Differential effects of 6-OHDA lesions of the frontal cortex and caudate nucleus on the ability to acquire an attentional set. Cereb Cortex. 2001;11(11):1015–26.
95. He Y, Appel S, Le W. Minocycline inhibits microglial activation and protects nigral cells after 6-hydroxydopamine injection into mouse striatum. Brain Res. 2001;909(1–2):187–93.
96. Ma KH, Huang WS, Chen CH, Lin SZ, Wey SP, Ting G, et al. Dual SPECT of dopamine system using [99mTc]TRODAT-1 and [123I]IBZM in normal and 6-OHDA-lesioned formosan rock monkeys. Nucl Med Biol. 2002;29(5):561–7.
97. Lundblad M, Picconi B, Lindgren H, Cenci MA. A model of L-DOPA-induced dyskinesia in 6-hydroxydopamine lesioned mice: relation to motor and cellular parameters of nigrostriatal function. Neurobiol Dis. 2004;16(1):110–23.
98. Allen JM, Cross AJ, Crow TJ, Javoy-Agid F, Agid Y, Bloom SR. Dissociation of neuropeptide Y and somatostatin in Parkinson's disease. Brain Res. 1985;337(1):197–200.
99. Seniuk NA, Tatton WG, Greenwood CE. Dose-dependent destruction of the coeruleus-cortical and nigral-striatal projections by MPTP. Brain Res. 1990;527(1):7–20.
100. Sirinathsinghji DJ, Kupsch A, Mayer E, Zivin M, Pufal D, Oertel WH. Cellular localization of tyrosine hydroxylase mRNA and cholecystokinin mRNA-containing cells in the ventral mesencephalon of the common marmoset: effects of 1-methyl-4-phenyl-1,2,3,6-tetrahydropyridine. Brain Res Mol Brain Res. 1992;12(1–3):267–74.
101. Ovadia A, Zhang Z, Gash DM. Increased susceptibility to MPTP toxicity in middle-aged rhesus monkeys. Neurobiol Aging. 1995;16(6):931–7.

102. Blandini F, Armentero MT. Animal models of Parkinson's disease. FEBS J. 2012;279(7): 1156–66.
103. Corti O, Lesage S, Brice A. What genetics tells us about the causes and mechanisms of Parkinson's disease. Physiol Rev. 2011;91(4):1161–218.
104. Lindgren HS, Lelos MJ, Dunnett SB. Do alpha-synuclein vector injections provide a better model of Parkinson's disease than the classic 6-hydroxydopamine model? Exp Neurol. 2012;237(1):36–42.
105. Recchia A, Debetto P, Negro A, Guidolin D, Skaper SD, Giusti P. Alpha-synuclein and Parkinson's disease. FASEB J Off Publ Fed Am Soc Exp Biol. 2004;18(6):617–26.
106. Betarbet R, Sherer TB, MacKenzie G, Garcia-Osuna M, Panov AV, Greenamyre JT. Chronic systemic pesticide exposure reproduces features of Parkinson's disease. Nat Neurosci. 2000;3(12):1301–6.
107. Marking LL. Oral toxicity of rotenone to mammals. Investigations in fish control. La Crosse, WI: U.S. Fish and Wildlife Service; 1988.
108. Mastroberardino PG, Hoffman EK, Horowitz MP, Betarbet R, Taylor G, Cheng D, et al. A novel transferrin/TfR2-mediated mitochondrial iron transport system is disrupted in Parkinson's disease. Neurobiol Dis. 2009;34(3):417–31.
109. Lapointe N, St-Hilaire M, Martinoli MG, Blanchet J, Gould P, Rouillard C, et al. Rotenone induces non-specific central nervous system and systemic toxicity. FASEB J Off Publ Fed Am Soc Exp Biol. 2004;18(6):717–9.
110. Drolet RE, Cannon JR, Montero L, Greenamyre JT. Chronic rotenone exposure reproduces Parkinson's disease gastrointestinal neuropathology. Neurobiol Dis. 2009;36(1):96–102.
111. Houlden H, Singleton AB. The genetics and neuropathology of Parkinson's disease. Acta Neuropathol. 2012;124(3):325–38.
112. Gasser T. Molecular genetic findings in LRRK2 American, Canadian and German families. J Neural Transm Suppl. 2006;70:231–4.
113. Farrer MJ. Genetics of Parkinson disease: paradigm shifts and future prospects. Nat Rev Genet. 2006;7(4):306–18.
114. Zheng LF, Wang ZY, Li XF, Song J, Hong F, Lian H, et al. Reduced expression of choline acetyltransferase in vagal motoneurons and gastric motor dysfunction in a 6-OHDA rat model of Parkinson's disease. Brain Res. 2011;1420:59–67.
115. Javoy F, Sotelo C, Herbet A, Agid Y. Specificity of dopaminergic neuronal degeneration induced by intracerebral injection of 6-hydroxydopamine in the nigrostriatal dopamine system. Brain Res. 1976;102(2):201–15.
116. Jeon BS, Jackson-Lewis V, Burke RE. 6-Hydroxydopamine lesion of the rat substantia nigra: time course and morphology of cell death. Neurodegeneration J Neurodegenerative Disord Neuroprotection Neuroregeneration. 1995;4(2):131–7.
117. Faull RL, Laverty R. Changes in dopamine levels in the corpus striatum following lesions in the substantia nigra. Exp Neurol. 1969;23(3):332–40.
118. Lao CL, Kuo YH, Hsieh YT, Chen JC. Intranasal and subcutaneous administration of dopamine D3 receptor agonists functionally restores nigrostriatal dopamine in MPTP-treated mice. Neurotox Res. 2013;24(4):523–31.
119. Kim JI, Yang EJ, Lee MS, Kim YS, Huh Y, Cho IH, et al. Bee venom reduces neuroinflammation in the MPTP-induced model of Parkinson's disease. Int J Neurosci. 2011;121(4):209–17.
120. Liu K, Shi N, Sun Y, Zhang T, Sun X. Therapeutic effects of rapamycin on MPTP-induced Parkinsonism in mice. Neurochem Res. 2013;38(1):201–7.
121. Yabuki Y, Ohizumi Y, Yokosuka A, Mimaki Y, Fukunaga K. Nobiletin treatment improves motor and cognitive deficits seen in MPTP-induced Parkinson model mice. Neuroscience. 2013;259C:126–41.
122. Masilamoni GJ, Bogenpohl JW, Alagille D, Delevich K, Tamagnan G, Votaw JR, et al. Metabotropic glutamate receptor 5 antagonist protects dopaminergic and noradrenergic neurons from degeneration in MPTP-treated monkeys. Brain J Neurol. 2011;134(Pt 7):2057–73.
123. Xun Z, Sowell RA, Kaufman TC, Clemmer DE. Quantitative proteomics of a presymptomatic A53T alpha-synuclein Drosophila model of Parkinson disease. Mol Cell Proteomics MCP. 2008;7(7):1191–203.

124. Recchia A, Rota D, Debetto P, Peroni D, Guidolin D, Negro A, et al. Generation of a alpha-synuclein-based rat model of Parkinson's disease. Neurobiol Dis. 2008;30(1):8–18.
125. Betarbet R, Sherer TB, Greenamyre JT. Animal models of Parkinson's disease. BioEssays News Rev Mol Cell Dev Biol. 2002;24(4):308–18.
126. Schober A. Classic toxin-induced animal models of Parkinson's disease: 6-OHDA and MPTP. Cell Tissue Res. 2004;318(1):215–24.
127. Schuler F, Casida JE. Functional coupling of PSST and ND1 subunits in NADH:ubiquinone oxidoreductase established by photoaffinity labeling. Biochim Biophys Acta. 2001;1506(1): 79–87.
128. Prance G. The poisons and narcotics of the Amazonian Indians. J R Coll Physicians Lond. 1999;33(4):368–76.
129. Talpade DJ, Greene JG, Higgins Jr DS, Greenamyre JT. In vivo labeling of mitochondrial complex I (NADH:ubiquinone oxidoreductase) in rat brain using [(3)H]dihydrorotenone. J Neurochem. 2000;75(6):2611–21.
130. Alam M, Schmidt WJ. Rotenone destroys dopaminergic neurons and induces parkinsonian symptoms in rats. Behav Brain Res. 2002;136(1):317–24.
131. Sherer TB, Betarbet R, Testa CM, Seo BB, Richardson JR, Kim JH, et al. Mechanism of toxicity in rotenone models of Parkinson's disease. J Neurosci Off J Soc Neurosci. 2003;23(34):10756–64.
132. Alam ZI, Jenner A, Daniel SE, Lees AJ, Cairns N, Marsden CD, et al. Oxidative DNA damage in the parkinsonian brain: an apparent selective increase in 8-hydroxyguanine levels in substantia nigra. J Neurochem. 1997;69(3):1196–203.
133. Floor E, Wetzel MG. Increased protein oxidation in human substantia nigra pars compacta in comparison with basal ganglia and prefrontal cortex measured with an improved dinitrophenylhydrazine assay. J Neurochem. 1998;70(1):268–75.
134. Tada-Oikawa S, Hiraku Y, Kawanishi M, Kawanishi S. Mechanism for generation of hydrogen peroxide and change of mitochondrial membrane potential during rotenone-induced apoptosis. Life Sci. 2003;73(25):3277–88.
135. Beal MF. Mitochondria, oxidative damage, and inflammation in Parkinson's disease. Ann N Y Acad Sci. 2003;991:120–31.
136. Aguilar-Bryan L, Clement JP, Gonzalez G, Kunjilwar K, Babenko A, Bryan J. Toward understanding the assembly and structure of KATP channels. Physiol Rev. 1998;78(1):227–45.
137. Liss B, Bruns R, Roeper J. Alternative sulfonylurea receptor expression defines metabolic sensitivity of K-ATP channels in dopaminergic midbrain neurons. EMBO J. 1999;18(4):833–46.
138. Stokes AH, Hastings TG, Vrana KE. Cytotoxic and genotoxic potential of dopamine. J Neurosci Res. 1999;55(6):659–65.
139. Spector S, Sjoerdsma A, Udenfriend S. Blockade of endogenous norepinephrine synthesis by alpha-methyl-tyrosine, an inhibitor of tyrosine hydroxylase. J Pharmacol Exp Ther. 1965;147:86–95.
140. Sakka N, Sawada H, Izumi Y, Kume T, Katsuki H, Kaneko S, et al. Dopamine is involved in selectivity of dopaminergic neuronal death by rotenone. Neuroreport. 2003;14(18):2425–8.
141. Biehlmaier O, Alam M, Schmidt WJ. A rat model of Parkinsonism shows depletion of dopamine in the retina. Neurochem Int. 2007;50(1):189–95.
142. Betarbet R, Sherer TB, MacKenzie G, Garcia-Osuna M, Panov AV, Greenamyre JT. Chronic systemic pesticide exposure reproduces features of Parkinson's disease. Nat Neurosci. 2000;3(12):1301–6.
143. Marey-Semper I, Gelman M, Levi-Strauss M. A selective toxicity toward cultured mesencephalic dopaminergic neurons is induced by the synergistic effects of energetic metabolism impairment and NMDA receptor activation. J Neurosci Off J Soc Neurosci. 1995; 15(9):5912–8.
144. Huang J, Liu H, Gu W, Yan Z, Xu Z, Yang Y, et al. A delivery strategy for rotenone microspheres in an animal model of Parkinson's disease. Biomaterials. 2006;27(6):937–46.
145. Feng Y, Liang ZH, Wang T, Qiao X, Liu HJ, Sun SG. alpha-Synuclein redistributed and aggregated in rotenone-induced Parkinson's disease rats. Neurosci Bull. 2006;22(5): 288–93.

146. Xiong N, Huang J, Zhang Z, Zhang Z, Xiong J, Liu X, et al. Stereotaxical infusion of rotenone: a reliable rodent model for Parkinson's disease. PLoS One. 2009;4(11):e7878.
147. Xiong N, Long X, Xiong J, Jia M, Chen C, Huang J, et al. Mitochondrial complex I inhibitor rotenone-induced toxicity and its potential mechanisms in Parkinson's disease models. Crit Rev Toxicol. 2012;42(7):613–32.
148. Testa CM, Sherer TB, Greenamyre JT. Rotenone induces oxidative stress and dopaminergic neuron damage in organotypic substantia nigra cultures. Brain Res Mol Brain Res. 2005;134(1):109–18.
149. Isenberg JS, Klaunig JE. Role of the mitochondrial membrane permeability transition (MPT) in rotenone-induced apoptosis in liver cells. Toxicol Sci Off J Soc Toxicol. 2000;53(2): 340–51.
150. Heikkila RE, Nicklas WJ, Vyas I, Duvoisin RC. Dopaminergic toxicity of rotenone and the 1-methyl-4-phenylpyridinium ion after their stereotaxic administration to rats: implication for the mechanism of 1-methyl-4-phenyl-1,2,3,6-tetrahydropyridine toxicity. Neurosci Lett. 1985;62(3):389–94.
151. Schmidt WJ, Alam M. Controversies on new animal models of Parkinson's disease pro and con: the rotenone model of Parkinson's disease (PD). J Neural Transm Suppl. 2006;70:273–6.
152. Hu LF, Lu M, Tiong CX, Dawe GS, Hu G, Bian JS. Neuroprotective effects of hydrogen sulfide on Parkinson's disease rat models. Aging Cell. 2010;9(2):135–46.
153. Pan-Montojo F, Anichtchik O, Dening Y, Knels L, Pursche S, Jung R, et al. Progression of Parkinson's disease pathology is reproduced by intragastric administration of rotenone in mice. PLoS One. 2010;5(1):e8762.
154. Alam M, Schmidt WJ. L-DOPA reverses the hypokinetic behaviour and rigidity in rotenone-treated rats. Behav Brain Res. 2004;153(2):439–46.
155. Alam M, Mayerhofer A, Schmidt WJ. The neurobehavioral changes induced by bilateral rotenone lesion in medial forebrain bundle of rats are reversed by L-DOPA. Behav Brain Res. 2004;151(1–2):117–24.
156. Kamalden TA, Ji D, Osborne NN. Rotenone-induced death of RGC-5 cells is caspase independent, involves the JNK and p38 pathways and is attenuated by specific green tea flavonoids. Neurochem Res. 2012;37(5):1091–101.
157. Hancock DB, Martin ER, Mayhew GM, Stajich JM, Jewett R, Stacy MA, et al. Pesticide exposure and risk of Parkinson's disease: a family-based case-control study. BMC Neurol. 2008;8:6.
158. Dhillon AS, Tarbutton GL, Levin JL, Plotkin GM, Lowry LK, Nalbone JT, et al. Pesticide/environmental exposures and Parkinson's disease in East Texas. J Agromedicine. 2008;13(1):37–48.
159. Chan SL, Angeles DC, Tan EK. Targeting leucine-rich repeat kinase 2 in Parkinson's disease. Expert Opin Ther Targets. 2013;17(12):1471–82.
160. Lesage S, Brice A. Parkinson's disease: from monogenic forms to genetic susceptibility factors. Hum Mol Genet. 2009;18(R1):R48–59.
161. Peeraully T, Tan EK. Genetic variants in sporadic Parkinson's disease: East vs West. Parkinsonism Relat Disord. 2012;18 Suppl 1:S63–5.
162. Mamais A, Raja M, Manzoni C, Dihanich S, Lees A, Moore D, et al. Divergent alpha-synuclein solubility and aggregation properties in G2019S LRRK2 Parkinson's disease brains with Lewy Body pathology compared to idiopathic cases. Neurobiol Dis. 2013;58:183–90.
163. Healy DG, Falchi M, O'Sullivan SS, Bonifati V, Durr A, Bressman S, et al. Phenotype, genotype, and worldwide genetic penetrance of LRRK2-associated Parkinson's disease: a case-control study. Lancet Neurol. 2008;7(7):583–90.
164. La Morgia C, Barboni P, Rizzo G, Carbonelli M, Savini G, Scaglione C, et al. Loss of temporal retinal nerve fibers in Parkinson disease: a mitochondrial pattern? Eur J Neurol Off J Eur Fed Neurol Soc. 2013;20(1):198–201.

165. Satue M, Garcia-Martin E, Fuertes I, Otin S, Alarcia R, Herrero R, et al. Use of Fourier-domain OCT to detect retinal nerve fiber layer degeneration in Parkinson's disease patients. Eye (Lond). 2013;27(4):507–14.
166. Hindle SJ, Elliott CJ. Spread of neuronal degeneration in a dopaminergic, Lrrk-G2019S model of Parkinson disease. Autophagy. 2013;9(6):936–8.
167. Polymeroulos MH, Lavedan C, Leroy E, et al. Mutation in the Alpha-synuclein gene identified in families with Parkinson's disease. Science. 1997;276:2045–47.
168. Kitada T, Asakawa S, Hattori N, Matsumine H, Yamamura Y, Minoshima S, et al. Mutations in the parkin gene cause autosomal recessive juvenile parkinsonism. Nature. 1998;392(6676): 605–8.
169. Gasser T, Muller-Myhsok B, Wszolek ZK, Oehlmann R, Calne DB, Bonifati V, Bereznai B, et al. A susceptibility locus for Parkinson's disease maps to chromosome 2p13. Nature Genet. 1998;18(3):262–5.
170. Singleton AB, Farrer M, Johnson J, Singleton A, Hague S, Kachergus J, et al. Alpha-Synuclein locus triplication causes Parkinson's disease. Science. 2003;302(5646):841.
171. Leroy E, Boyer R, Auburger G, Leube B, Ulm G, Mezey E, Harta G, Brownstein MJ, Jonnalagada S, Chernova T, Dehejia A, Lavedan C, Gasser T, Steinbach PJ, Wilkinson KD, Polymeropoulos MH. The ubiquitin pathway in Parkinson's disease. (Letter) Nature. 1998;395:451–2.
172. Valente EM, Bentivoglio AR, Dixon PH, Ferraris A, Ialongo T, Frontali M, et al. Localization of a novel locus for autosomal recessive early-onset parkinsonism, PARK6, on human chromosome 1p35-p36. Am J Hum Genet. 2001;68(4):895–900.
173. Bonifati V, Rizzu P, Squitieri F, Krieger E, Vanacore N, van Swieten JC, et al. DJ-1(PARK7), a novel gene for autosomal recessive, early onset parkinsonism. Neurol Sci. 2003;24(3): 159–60.
174. Funayama M, Hasegawa K, Kowa H, Saito M, Tsuji S, Obata F. A new locus for Parkinson's disease (PARK8) maps to chromosome 12p11.2-q13.1. Ann Neurol. 2002;51(3):296–301.
175. Bonifati V. Genetics of Parkinson's disease. Minerva Med. 2005;96(3):175–86.
176. Hampshire DJ, Roberts E, Crow Y, Bond J, Mubaidin A, Wriekat AL, et al. Kufor-Rakeb syndrome, pallido-pyramidal degeneration with supranuclear upgaze paresis and dementia, maps to 1p36. J Med Genet. 2001;38(10):680–2.

Chapter 14
Optical Coherence Tomography (OCT) in Glaucoma

Kaweh Mansouri and Robert N. Weinreb

Abstract Imaging with optical coherence tomography (OCT) has become a mainstay of glaucoma diagnosis and management. In recent years, evidence has accumulated to show that OCT-derived rates of change are associated with progression of glaucoma and reduction of quality of life. OCT technology improves rapidly. Recent innovations such as swept source OCTs enable visualization of the lamina cribrosa. While noninvasive OCT angiography may shed some light into perfusion of the optic nerve head in glaucoma.

Keywords Glaucoma • Optical coherence tomography • Swept-source • Lamina cribrosa

14.1 Introduction

Glaucoma is the leading cause of irreversible blindness worldwide [1]. It is an optic neuropathy characterized by progressive structural loss of retinal ganglion cells and optic nerve damage that results in characteristic visual field loss. Early identification of the disease is of utmost importance because appropriate treatment can prevent or slow disease progression and preserve vision. Detection of visual field loss by means of standard functional testing has been one of the mainstays in the diagnosis of glaucoma. However, the subjective nature of perimetry creates large variation in

Supported in part by Core grant NEI P30EY022589 an unrestricted grant from Research to Prevent Blindness (New York, NY)

K. Mansouri, MD, MPH (✉)
Department of Ophthalmology, Geneva University Hospitals, Geneva, Switzerland
e-mail: kawehm@yahoo.com

R.N. Weinreb, MD
Hamilton Glaucoma Center and Shiley Eye Institute, La Jolla, CA, USA

Department of Ophthalmology, University of California, San Diego, La Jolla, CA, USA

A. Grzybowski, P. Barboni (eds.), *OCT in Central Nervous System Diseases: The Eye as a Window to the Brain*, DOI 10.1007/978-3-319-24085-5_14

results, which make it difficult to reliably assess disease state and progression. Structural changes in the optic nerve head (ONH) and retinal nerve fibre layer (RNFL) often are visible before the appearance of detectable loss by perimetry [2, 3]. The ability to detect structural loss at the level of the ONH and peripapillary RNFL is, therefore, fundamental in the diagnosis and management of glaucoma. While this can be done subjectively by clinical examination and fundus photography, the introduction of ocular imaging modalities into clinical management has allowed for quantifiable and reproducible assessment of glaucomatous structural changes. Imaging technologies such as confocal scanning laser ophthalmoscopy (CSLO) and scanning laser polarimetry (SLP) were introduced in the late 1980s and were initially used for this purpose.

Optical coherence tomography (OCT) was introduced in 1991 and is a non-invasive optical technique that allows for in vivo cross-sectional imaging of the ONH and retina. Briefly, OCT technology measures echo time delay and the magnitude of reflected light using low-coherence interferometry [4]. Cross-sectional images are obtained by measuring the backscattered light. The first generation of OCTs were time-domain (TD)-based instruments and were limited by a low scan speed (100–400 A scans/s) and an axial resolution of ca. 8–10 μm. Yet, the technology rapidly evolved and become widely adopted for the detection of glaucomatous damage and progression. The current second generation OCT instruments, spectral-domain OCT (SD-OCT), have an approximately 50 times faster scan speed (between 26,000 and 53,000 A-scans/s) than TD-OCTs and an axial resolution of approximately of 5 μm. These improvements lead to lower susceptibility to motion artifacts due to eye movement and improved reproducibility, both essential factors for the detection of glaucomatous changes. As a consequence, SD-OCT has been shown to have improved ability to monitor for glaucoma progression [5]. SD-OCT devices can also provide 3D datasets, which enable enhanced image registration in consecutive testing and further improve glaucoma diagnosis and detection of progression. There are currently several commercially available SD-OCT instruments with varying parameters and unique features.

OCT technology is rapidly evolving with faster scanning speeds, deeper signal penetration, and improved segmentation algorithms. This chapter will focus on SD-OCT and discuss the recent introduction of the next iteration of OCT instruments, swept-source OCT.

14.2 Diagnosis of Glaucoma

The basic requirement to diagnose glaucoma using imaging instruments is the ability to define what constitutes normality. This is achieved by normative databases that include corresponding age- and ethnicity-matched measures to the patient under investigation. The ability of these instruments to discriminate healthy from glaucoma, and to detect glaucomatous progression over time is, therefore, significantly limited by the quality of reference databases associated with the available commercial devices [6]. For instance, the normative database for the Stratus TD-OCT (Carl Zeiss Meditec, Dublin, CA, USA) includes 350 subjects (63 % Caucasian, 24 % Hispanic, 8 % African-American, and 3 % Asian) with a mean age of 47 years [7].

Even though they are not common, a limitation of all normative databases is the absence of individuals with refractive errors beyond −12.00 D and +8.00 D.

The performances of the commercially available SDOCT instruments in detecting eyes with glaucoma, specifically measures of diagnostic accuracy such as sensitivity, specificity, and receiver operating characteristic (ROC) curves have been extensively evaluated [8, 9]. Leung et al. [8] compared SD-OCT (Cirrus HD-OCT; Carl Zeiss Meditec, Inc., Dublin, CA) to TD-OCT (Stratus OCT; Carl Zeiss Meditec, Inc.). They reported an intra-visit repeatability of SD-OCT ranging between 5.12 and 15.02 μm, and an inter-visit reproducibility between 4.31 and 22.01 μm. The inter-visit variabilities of sectoral and average RNFL thicknesses were lower in Cirrus HD-OCT compared with Stratus OCT. There were proportional biases of RNFL measurements between the two OCT devices, which are related to the different inherent characteristics of the two OCT systems. The diagnostic sensitivity and specificity was examined with the area under the receiver operating characteristic curve (AUC). The average RNFL thickness (AUC, 0.962 for SD-OCT and 0.956 TD-OCT) were similar in both instruments. Although the diagnostic accuracies were comparable between the two instruments, SD-OCT demonstrated lower measurement variability. These results further suggest that measurements between different devices are not interchangeable. Several other investigators have studied the diagnostic accuracy of SD-OCT [10–13].

The clinical utility of OCT in glaucoma has primarily focused on the assessment of the peripapillary RNFL because it enables a comprehensive evaluation of all the RGC axons as they approach the ONH (Figs. 14.1 and 14.2). It has been shown that diagnostic accuracy of OCT-derived parameters is superior to CSLO and SLP [5]. Some investigators have suggested that macular RNFL measurements are equal to and potentially superior to peripapillary RNFL measurements for the diagnosis of early glaucoma. (Figs. 14.3 and 14.4) Jeoung et al. [14], found one measurement parameter (minimum macular ganglion cell-inner plexiform layer, GCIPL) to be superior to RNFL and ONH measurements. They concluded that GICPL showed better glaucoma diagnostic performance than the other parameters at comparable specificities. However, other GCIPL parameters showed performances comparable to those of the RNFL parameters. However, there is a paucity of data in favor of macular measurements for detection of glaucoma. Mwanza et al. [13] compared the diagnostic performances of macular ganglion cell-inner plexiform layer (GCIPL) to RNFL and ONH measurements to discriminate normal eyes and eyes with early glaucoma. They found high (AUC >0.9) and similar diagnostic accuracies for all parameters. Their results were confirmed by other investigators [12, 15]. A large study, however, could not confirm these findings and found that macular measurements using SD-OCT had a lower accuracy for detecting preperimetric glaucoma [16].

However, the accuracy measures reported by these studies have not taken into account the possible effects of important covariates on test results, such as disease severity. Diagnostic tests tend to be more sensitive in advanced stages of the disease, and measures of diagnostic accuracy obtained in studies that include only patients with moderate or severe disease may not be applicable to patients with early disease or those with suspected disease. For example, it is possible that a particular parameter is more sensitive at early stages of the disease, whereas another may be more sensitive at moderate or advanced stages. A study comparing the diagnostic accuracy of the Cirrus SD-OCT in different stages of glaucoma, as defined by the visual

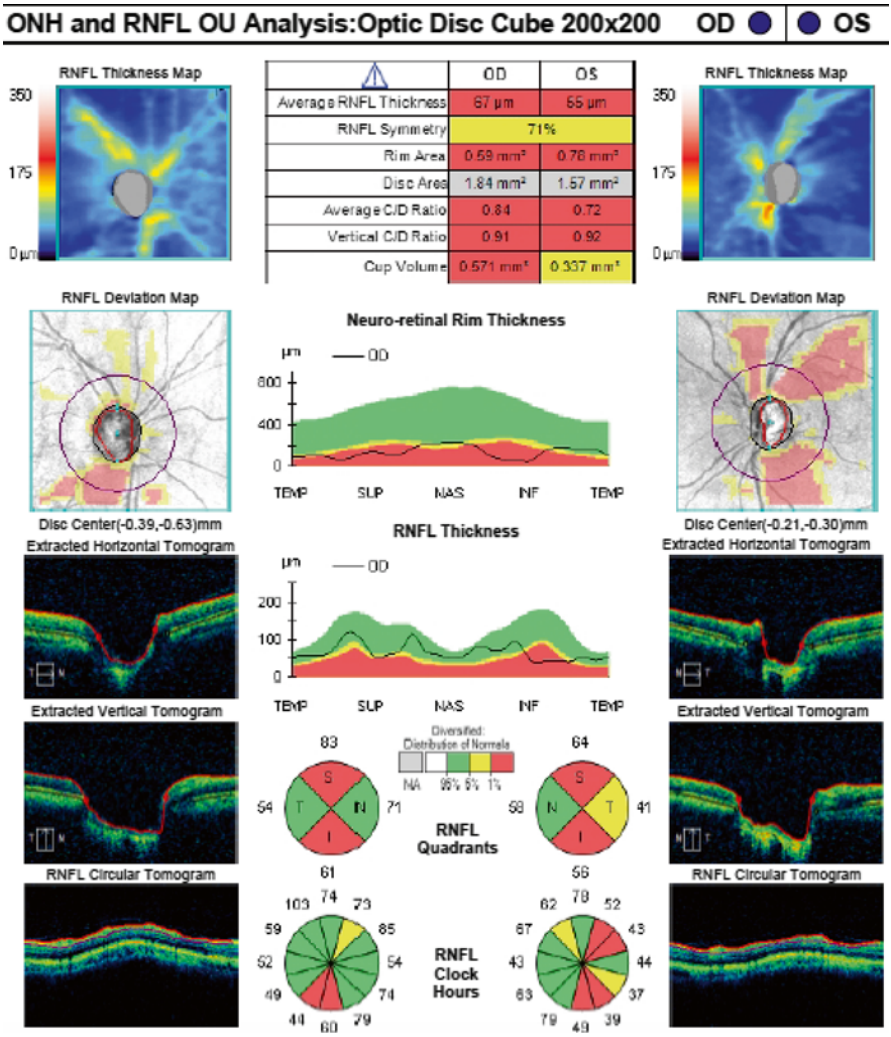

Fig. 14.1 Characteristic early to moderate glaucomatous damage of the retinal nerve fiber layer (RNFL)

field index (VFI), found that the disease severity had a significant influence on the detection of glaucoma [17]. For the average RNFL thickness parameter, AUCs were 0.962, 0.932, 0.886, and 0.822 for VFIs of 70 %, 80 %, 90 %, and 100 %, respectively. Therefore, it is important to characterize the relationship between the performance of the diagnostic test and the severity of disease and to evaluate how this relationship affects the comparison between different tests.

Recently, a new generation of OCT instruments has been introduced. Swept-source OCT (SS-OCT) uses a short cavity swept laser with a tunable wavelength of operation instead of the superluminescent diode laser used in SD-OCT [18]. SS-OCT provides reduced sensitivity roll-off versus depth compared to SD-OCT. Currently, two

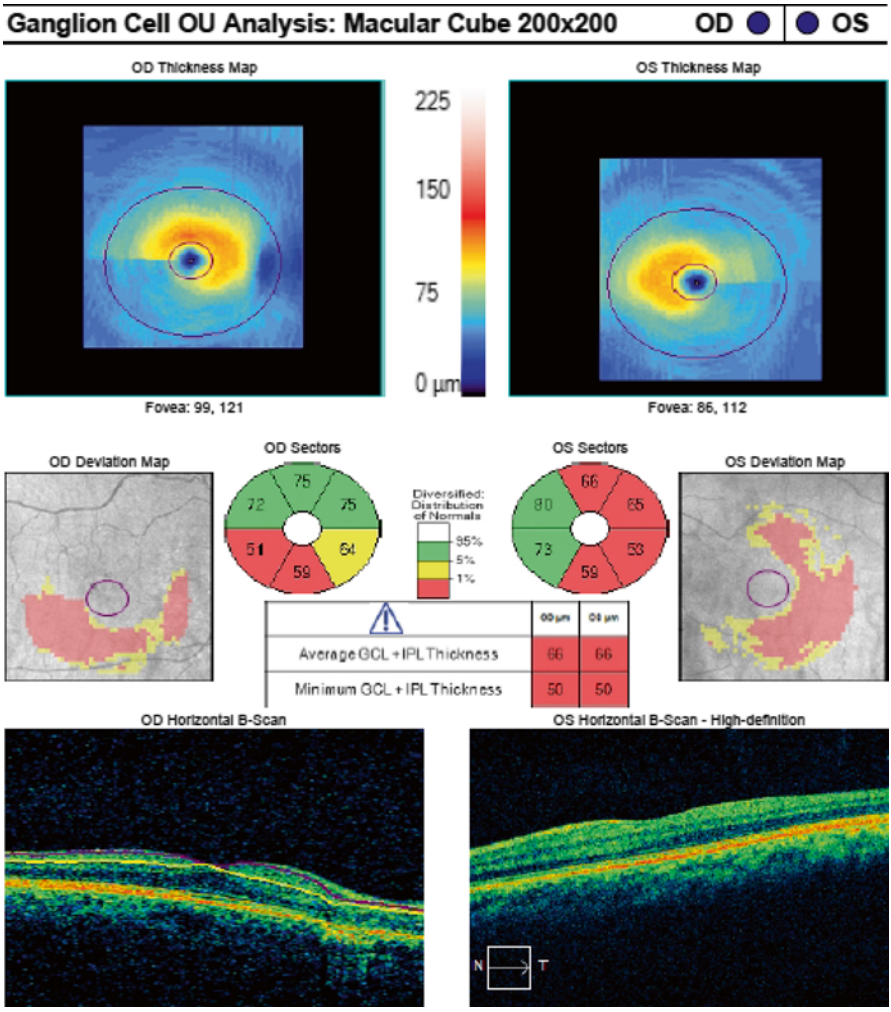

Fig. 14.2 Characteristic advanced glaucomatous damage of the RNFL. Visual field MD is −15.60 dB

instruments from two different manufacturers are commercially available. The Casia SS-1000 SS-OCT (Tomey Corp., Tokyo, Japan) is an anterior segment OCT instrument and will be discussed later (see: Sect. 14.5). The DRI-Atlantis SS-OCT (Topcon Inc., Tokyo, Japan) has a center wavelength of 1050 nm and a sweeping range of approximately 100 nm, compared to the fixed 850 nm wavelength typical of SD-OCT [18]. Its scan rate is 100,000 Hz (compared to 40,000 Hz commonly used in spectral-domain OCT) achieved by the use of two parallel photodetectors, yielding approximately 8 mm axial resolution in tissue. Beside the reduction of eye motion artifacts, high speed scanning enables averaging over several B-scans without the use of an eye tracker. These features allow deep penetration of deep ocular structures and higher image quality. (see: Sect. 14.4) The longer wavelength also provides an improved image quality in patients

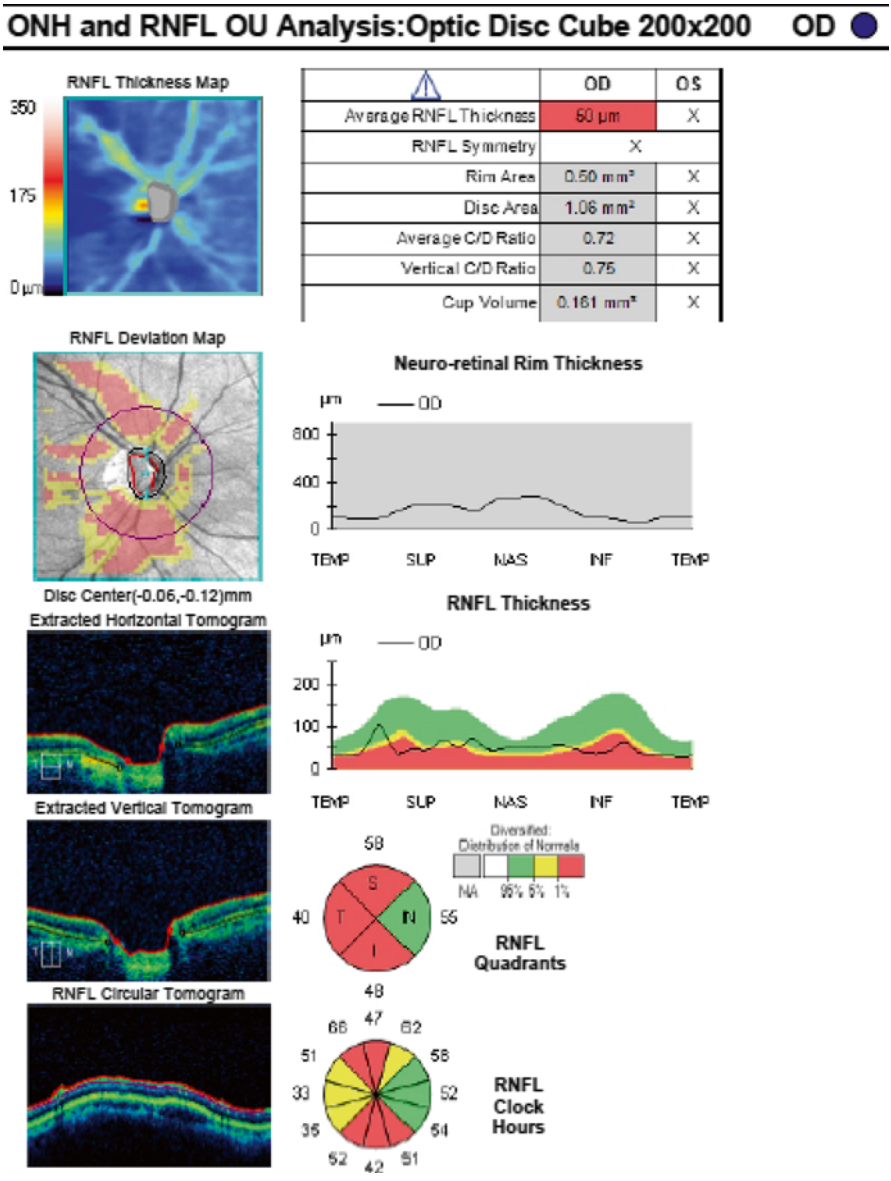

Fig. 14.3 Glaucomatous damage using macular analysis (same patient as in Fig. 14.1)

with cataract but has some drawbacks compared with the 840 nm one. These include lower axial resolution, since the spectral bandwidth that can be used at this wavelength region is limited by the "absorption window" of water, as well as lower transverse resolution, which is directly proportional to the wavelength. Good repeatability of retinal and choroidal measurements with SS-OCT has been shown [19]. Yang et al. [20] compared the diagnostic accuracies of SS-OCT wide-angle and RNFL measurement and compared these to standard SD-OCT measurements. In all, 144 glaucomatous and

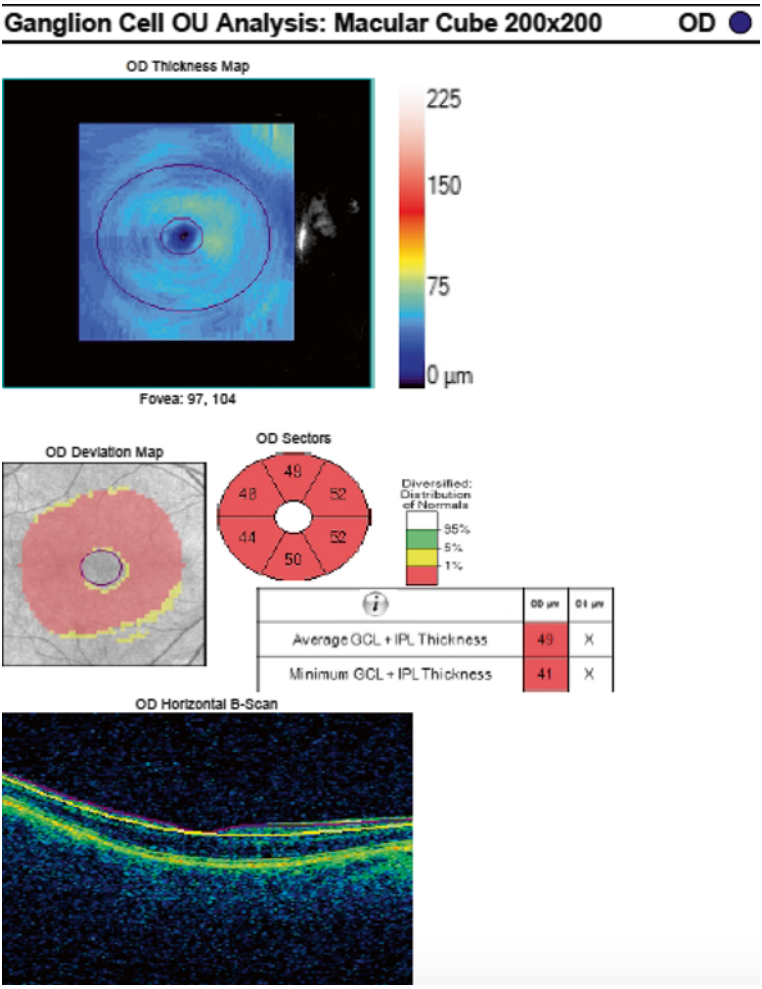

Fig. 14.4 Glaucomatous damage using macular analysis (same patient as in Fig. 14.2)

66 healthy control eyes from the longitudinal Diagnostic Innovations in Glaucoma Study were enrolled. They reported AUCs of 0.88 and 0.89 for of swept-source OCT wide-angle and peripapillary RNFL thickness, respectively. Swept-source OCT performed similar to average peripapillary RNFL thickness obtained by spectral-domain OCT (area under the ROC curve of 0.90).

14.3 Detection of Glaucoma Progression

Glaucoma is characterized by progressive structural changes that may lead to loss of visual function and decreased vision-related quality of life. The fundamental goal of glaucoma management is to prevent patients during their lifetime from developing

visual impairment that is sufficient to produce disability in their daily activities and reduce their quality of life. The clinician is confronted with the difficulty in discriminating glaucomatous structural changes, which are typically slowly progressive, from natural age-related structural loss. Leung et al. [21], reported an age-related loss in average RNFL thickness of −0.52 μm per year. Different studies have shown inter-visit 95 % tolerance limits for average RNFL thicknesses of approximately 4 μm, when image acquisition was performed by well-trained personnel. Despite excellent repeatability of RNFL thickness measurements with SDOCT, device-related measurement variability remains another factor to consider when assessing structural changes over time.

The initial reports of the ability of TD-OCT to detect glaucoma were published a decade ago. Wollstein et al. [22] showed the potential use of OCT in detecting glaucomatous progression with an event-based approach. They concluded that the OCT has a greater likelihood to detect glaucoma progression than standard visual fields. In their study, 22 % of eyes had a significant change measured by the OCT without corresponding deterioration of the visual fields. Medeiros et al. [23], evaluated the ability of different parameters such as RNFL thickness, optic nerve head and macular thickness measurements to detect glaucomatous progression. They reported the RNFL thickness parameters as having better ability than optic nerve head and macular thickness parameters to detect progression. For average RNFL thickness, a rate of change of −0.72 μm (approximately 1 %) per year for the progressors compared to 0.14 μm per year in nonprogressors was reported, with a wide variation of rates of change. Similar results were found by Leung et al. [24] who evaluated the guided progression analysis (GPA) software of Stratus OCT. Variation of rates of change are based on individual characteristics, such as stage of disease and response to treatment. However, the quality of image acquisition (e.g., signal strength, image centering etc.) and the presence of image artifacts can affect the ability to detect change [25, 26].

Several studies have evaluated the ability of SD-OCT to detect glaucoma progression (Figs. 14.4, 14.5, and 14.6). Leung et al. [27] have demonstrated that SD-OCT is more sensitive than TD-OCT in detecting reduction of RNFL thickness in progressing eyes. Na et al. [28] compared the rate of change of RNFL thickness and optic nerve head (ONH) parameters assessed using SD-OCT between eyes of 162 glaucoma patients with progressing and non-progressing disease. Sixty-three eyes (22.6 %) from 52 subjects were identified as progressors. They found that glaucoma progressors have significantly higher rates of RNFL thickness loss than non-progressors (−1.26 μm vs −0.94 μm/year). Wessel et al. [29] compared the structural loss of RNFL in healthy individuals and glaucoma patients. They included 62 eyes, comprising 38 glaucomatous eyes with open angle glaucoma and 24 healthy controls from a longitudinal study (Erlangen Glaucoma Registry). They found a significant difference in the rate of change between glaucoma progressors and non-progressors (−2.12 μm/year vs. −1.18 μm/year).

Several SD-OCT instruments have the ability to analyze changes in the macular region, such as the ganglion cell complex (GCC) parameter, which selectively measures the inner retina in the macular region. The GCC has shown similar diagnostic accuracy for detecting glaucoma as the RNFL thickness and may be useful for monitoring the disease [30]. Na et al. [31], evaluated the clinical use of segmented macular

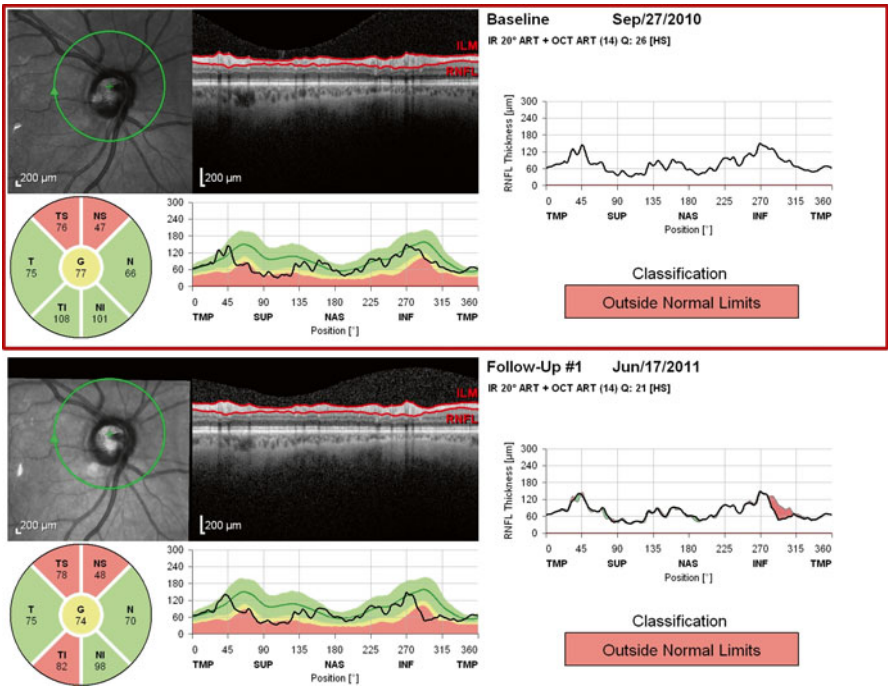

Fig. 14.5 Glaucoma progression documented by RNFL analysis

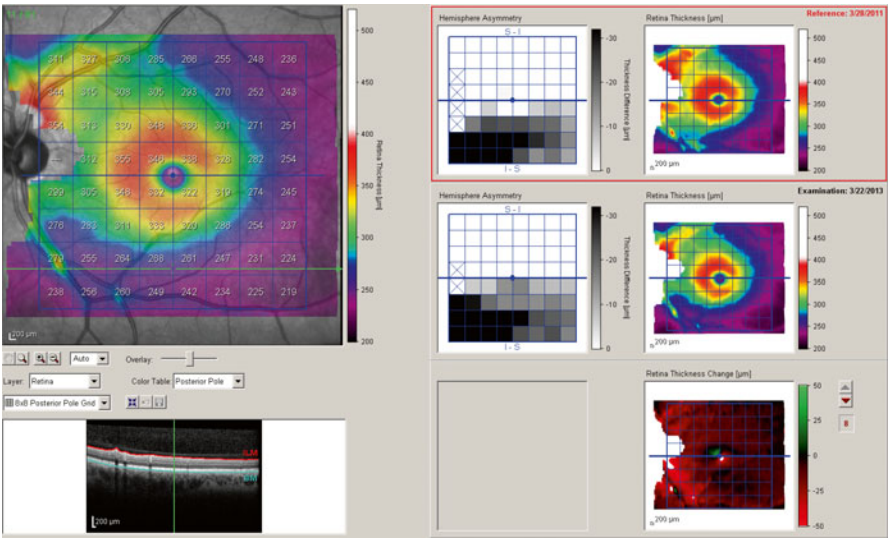

Fig. 14.6 Glaucoma progression documented by macular analysis

layer thickness measurement in terms of glaucoma diagnosis and the ability to detect progression and compare these to circumpapillary RNFL measurements. They showed that the ganglion cell and inner plexiform layer (GCA) parameter was superior to other macular segmentation parameters in terms of diagnostic accuracy. The sensitivity for detecting progression was similar between GCA and RNFL measurements (8 % vs 5 %). Naghizadeh et al. [32], investigated the ability of different parameters of the RTVue-100 SD-OCT to detect early glaucomatous progression in 51 glaucoma patients during a 1.5–3 year period. Glaucoma eyes had non-significant rates of structural loss in RNFL (−0.33 μm/year), cup area (0.03 mm^2/year), and rim area (−0.03 mm^2/year), while the change in the global and focal ganglion cell complex (GCC) parameters (−3.8 and −1.5 %/year) was statistically significant. They concluded that early structural progression of glaucoma may be better detected with macular parameters than with the ONH, RNFL thickness parameters of the same instrument.

The demonstrated ability of SD-OCT to detect progression of glaucoma has the potential to address the absence of a suitable surrogate endpoint in glaucoma clinical trials for neuroprotective agents. Currently, structural endpoints for glaucoma trials have not been acceptable to regulatory agencies. Although IOP has traditionally been used as a surrogate end point, it is an imperfect surrogate for the clinically relevant outcomes of the disease, as many patients can progress despite low IOP levels [33]. The other commonly used endpoint is visual field status, which is potentially limited by the need for large samples, variability of results, both due to a learning curve, and long-term follow-up. Structural endpoints may be more consistent than functional endpoints. Therefore, efforts are ongoing to evaluate the suitability of structural measurements as replacement for visual function. At present, the FDA requirement for adoption of structural endpoint in glaucoma is a strong correlation ($R^2 \approx 0.9$) to visual function [34]. The follow-up duration of above studies evaluating the ability of SD-OCT to detect glaucoma progression is relatively short. Longer duration of follow-up is required to account for the typically slowly progressive nature of glaucoma. Medeiros et al. [35] have demonstrated R^2 values of up to 81 % for confocal scanning laser ophthalmoscopy to detect the development of visual field progression in glaucoma over a period of 6.6 years. In the future, innovations in OCT hardware and software are expected to improve the predictive value of structural endpoints. Efforts to combine results of structural and functional measurements may further enhance the agreement between structural tests and visual function results. In fact, a proposed combined structure-function index was shown to have better diagnostic ability to detect glaucoma (AUC = 0.94) than structural (AUC = 0.92) or functional (AUC = 0.89) measurements alone [36].

14.4 Imaging Deep Ocular Structures

14.4.1 Choroid

In 2008, Spaide and co-workers [37–39] described the new technique of enhanced depth imaging (EDI) to provide improved imaging of the posterior ocular structures, such as the choroid. With EDI, the SD-OCT device is placed at a distance from the eye

so that an inverted image of the fundus is created, which increases the image clarity of the deeper structural layers. The coherence gate is placed at the deeper retinal layers instead of in the vitreous humor. The deep choroid and inner sclera are placed closer to the zero delay, which give them a smaller frequency and lower shift [40]. EDI-OCT, therefore, improves the imaging sensitivity of the posterior ocular layers.

EDI-OCT was initially used to study choroidal features in retinal diseases, such as choroidal thickness, volume, calcification, and cavitation [41–44]. A study using EDI-OCT to visualize the choroidal boundaries in the undilated healthy eyes reported a mean choroidal thickness at the macula of 318 μm in right eyes and 335 μm in left eyes [40]. These measurements of choroidal thickness had good inter-observer repeatability ($r=0.93$ OD, $r=0.97$ OS; $p<0.001$). Branchini et al. [45] studied the reproducibility of choroidal thickness measurements, in 28 subjects by three different SD-OCT devices: Cirrus HD-OCT, the EDI-OCT option of the Heidelberg Spectralis, and the chorioretinal imaging mode of Optovue RTVue. The choroidal thickness measurements at the fovea were determined to be 347.5 μm (Cirrus), 347.4 μm (Spectralis), and 337.6 μm (RTVue), with no significant difference between the apparatuses. They found that the three instruments provided good reproducibility. Rahman et al. [46] examined the repeatability of choroidal thickness measurements obtained by manual calipers, in 50 healthy volunteers. Using coefficient of repeatability (CR), they reported the difference between two measurements on the same eye's choroidal thickness to be less than the CR for 95 % of pairs of observations. Although these studies provide initial data on the accuracy and precision of EDI-OCT, information on the quality of visualization of the choroidal boundaries is lacking.

Visualization of the deeper ocular structures may be enhanced by the introduction of swept-source (SS-)OCT instruments. The longer wavelength of the SS-OCT probe limits the light scatter and absorption at the photoreceptors and retinal pigment epithelium, which enables clearer imaging of the deeper choroid and sclera [47–50]. SS-OCT, therefore, has the potential to provide more accurate and detailed characterization of the choroid (and lamina cribrosa, see below) in the research and clinical setting (Fig. 14.7). Initial versions of SS-OCT have been used to evaluate the choroid in the setting of various retinal diseases. Ikuno et al. [51, 52] used SS-OCT to measure choroidal thickness at various regions in healthy subjects. They calculated the mean thicknesses to be 354 μm at the fovea, 345 μm inferiorly, 364 μm superiorly, 227 μm nasally, and 337 μm temporally. The investigators found that SS-OCT has improved sensitivity for the structures posterior to the retinal pigment epithelium, including the chorio-scleral interface, when compared to SD/EDI-OCT. They also compared the choroidal thickness measurements determined by SS-OCT to those obtained by EDI-OCT [53]. Intersystem, interexaminer, and intervisit reproducibility were high using SS-OCT (respectively, $ICC=0.921$ for choroidal thickness and 0.661 for retinal thickness; $ICC=0.921$ for choroidal thickness and 0.630 for retinal thickness; $ICC=0.893$ for choroidal thickness and 0.504 for retinal thickness).

SS-OCT has also been used to determine choroidal thickness in glaucoma patients. Matsuo et al. [54] compared measurements of subfoveal choroidal thickness obtained by two SD-OCT instruments (Spectralis SD-OCT and Topcon SD-OCT) and one SS-OCT apparatus (DRI-SS-OCT): measurements were comparable among the two

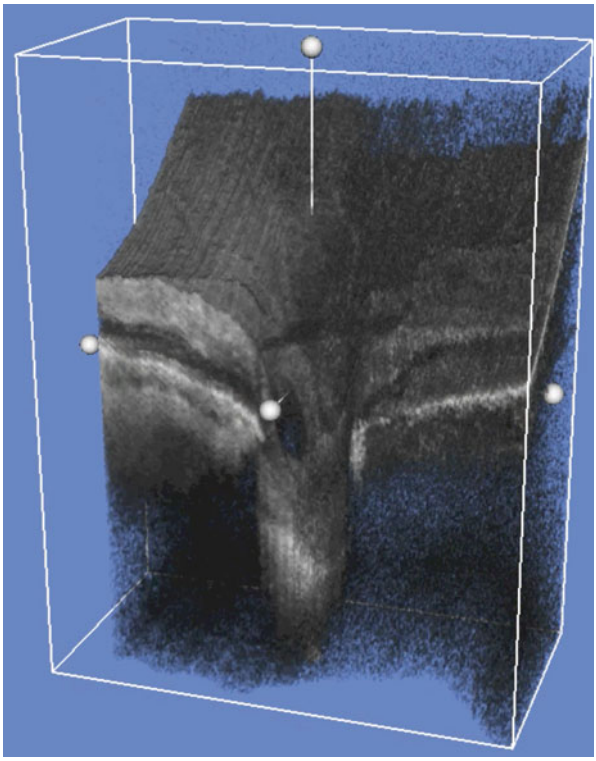

Fig. 14.7 Three-dimensional scans of the optic nerve head, lamina cribrosa and choroid obtained by swept-source OCT

SD-OCT instruments, but the SS-OCT measured choroidal thickness was greater than that measured by both SD-OCT devices. This may indicate that SS-OCT can visualize and thus measure more of the choroid, leading to a greater measurement of thickness. Usui et al. [55] determined choroidal thickness in eyes with highly myopic eyes with normal tension glaucoma (NTG). They found that the choroid in these cases was substantially thinner than in non-glaucomatous myopic subjects, at the superior ($p<0.05$), superotemporal ($p<0.01$), temporal ($p<0.01$), and inferotemporal ($p<0.05$) regions around the optic disc and at the fovea ($p<0.001$). The authors theorized that choroidal thinning may lead to progressive vessel loss and impede choroidal circulation, thereby playing a role in disease progression. SS-OCT, with its ability to provide high resolution and signal penetrance to the deeper choroidal and scleral layers, may contribute significantly to visual evaluation of glaucomatous progression.

Mansouri et al. [18] investigated changes in choroidal thickness and volume after the water drinking test (WDT) in healthy subjects. For this purpose, software was developed to obtain automated segmentation of the choroid. Using that software, a statistically significant increase in thickness and volume of the choroid after the WDT was shown. Automated segmentation of the choroid is a significant improvement to the manual measurements used in the previous studies, particularly in light of the wide anatomic variations of the choroid. The authors showed that the

automated segmentation method provided excellent reproducibility of retinal and choroidal measurements [19]. The WDT is a provocative test in which 1 l of water is ingested in 5 min. The amount of subsequent rise in IOP has been postulated to be predictive of peak circadian IOPs.

14.4.2 Lamina Cribrosa

The lamina cribrosa (LC) is a multi-layered sieve-like structure in the sclera where retinal ganglion cell axons exit from the eye. The LC has been known to play a critical role in the pathogenesis of glaucoma [2]. Blockage of axonal transport within the LC has been proposed as a salient pathogenic mechanism for glaucoma. However, the exact process of the pathogenic cascade within the LC is yet to be determined. It is assumed that the LC provides mechanical support to the nerve fibers traversing the deeper ocular structures [4]. Thinning of the LC has been associated with glaucomatous progression, through deformation and compression of the structure presumably from elevated IOP [5] Changes in pore shape and size in the LC also have been correlated with glaucoma [6, 7]. These deformations in the LC structure likely hinders axoplasmic flow and thus disrupts transport of trophic factors critical to retinal ganglion cells [8, 9], thereby causing neuronal death that is characteristic of glaucoma. Furthermore, the LC represents a biomechanical discontinuity in the spherical casing of the eye, so that the globe is more vulnerable to stress loading that may play a role in glaucoma [10]. Understanding such forces that affect the structure of the LC, through both focal and general morphologic changes, would clarify the mechanisms of glaucoma. A detailed study of the LC, however, requires accurate and clear visualization of this structure. In clinical practice, assessment of glaucoma damage is performed by examining the ONH and its surroundings for signs of structural loss, such as neuroretinal rim loss or enlarged cupping. Clinical examination of the LC structures cannot be performed routinely with current diagnostic methods.

The main challenge in imaging the LC with SD-OCT is the attenuation of light by tissue. The presence of RNFL tissue impedes therefore, the clear delineation of the anterior and posterior boundaries of the LC. Decreased resolution with signal loss and light scattering, and decreased maximal dynamic range all limit image clarity at the deeper ocular layers [40]. Recently, EDI-OCT has also been used to evaluate the ONH. Park et al. [56] evaluated the utility of EDI-OCT for imaging the ONH in eyes with glaucoma. They analyzed the following parameters: LC, accompanying vascular structures, peripapillary choroid and sclera, and the subarachnoid space surrounding the optic nerve. They found that the anterior surface of the LC could be at least partially distinguished from the surrounding areas – even posterior to the neuroretinal rim, vascular structures, and scleral rim – in 65 % of the studied eyes. In 76 % of the eyes, the size and direction of the pores in the LC were also defined. In addition, EDI-OCT was used to determine the course of various vessels, such as the short posterior ciliary artery (in 86 % of eyes), and the space of the subarachnoid

(in 18 % of eyes). The technique, however, could not adequately and consistently visualize the posterior laminar boundary. Also, the periphery of the structure could not be as well visualized as the central area, due to increased scleral and neural tissue thickness, greater pigmentation of the retinal and choroidal layers, and the presence of vascular structures around the margins of the LC. However, the authors reported difficulty imaging the periphery of the LC, given that the relatively thick neuroretinal and scleral rims and the presence of vasculature at the edge of the LC (compared to the center) interfered significantly with light penetration.

Focal structural irregularities of the LC, and their corresponding functional deficiencies, have also been rigorously studied using EDI-OCT, as SD-OCT is sufficiently detailed only to describe general morphologic changes such as thinning and outward migration of the posterior boundary. In a cross-sectional study, Kiumehr et al. [57], characterized specific deformities of the LC in 92 healthy eyes (46 patients) and 45 glaucomatous eyes (31 patients). They defined a focal defect as an anterior laminar surface irregularity of specific size and direction that breaks the smooth curvilinear U- or W-shaped contour. These irregularities were categorized based on the shape and location within the structure. The authors determined that the observed focal defects using EDI-OCT correlated well with level of visual field loss ($\rho = -0.498$; $p = 0.003$). Similarly to previous studies, the major limitation with the study entailed poor visualization of the deeper posterior layers and of the peripheral borders.

Contrary to SD-OCT, SS-OCT does not require averaging of multiple B-scans to visualize deep ocular structures and provides 3D scans with high sampling density. With SD-OCTs, the need for averaging B-scans translates into lower density scans or wider distances between B-scans to keep acquisition times reasonable. SS-OCT has been shown to improve imaging clarity of the LC. (Fig. 14.7) [58] Comparing results of EDI-OCT and SS-OCT in obtaining images from 32 myopic glaucoma subjects, Park et al. [59] found that SS-OCT was superior to EDI in visualizing the posterior structures, but did not offer an advantage in imaging the LC; both modalities had difficulties visualizing the LC especially beneath the neuroretinal rim. Despite these difficulties, 3D reconstructions of LC images with SS-OCT have been used to uncover details regarding glaucomatous changes in the micro-structural parameters of the LC, such as pore count, pore diameter, and beam thickness [60]. Previous studies had been limited to evaluating the LC macro-structure, such as focal surface defects and gross thickness, but with SS-OCT, further detail can be delineated and described. These results have been demonstrated to be repeatable with automated segmentation analysis [61].

SS-OCT has also been used to study structural changes to the LC after introduction of glaucoma therapy. Using EDI-OCT to visualize the LC in glaucomatous eyes, Lee et al. [62] showed increased LC thickness and reversal of LC posterior displacement at 6 months post successful trabeculectomy. The same authors demonstrated similar findings at 3–6 months of IOP lowering topical treatment [62]. A shortcoming of their results was the poor visualization of the posterior LC boundary. Yoshikawa et al. [63] using SS-OCT, found decreased LC depth and increased prelaminar neural tissue after glaucoma surgery; these changes also correlated significantly with IOP change ($p = 0.008$) and visual field mean deviation ($p = 0.035$).

14.5 Imaging of the Anterior Segment

In angle-closure glaucoma, closure of the anterior chamber angle occurs due to obstruction of the trabecular meshwork by the iris, resulting in impaired aqueous outflow and increased IOP. Advances in imaging techniques such as ultrasound biomicroscopy (UBM) and anterior segment OCT (AS-OCT) have aided in identifying the mechanisms behind angle closure and response to laser treatment. AS-OCT instruments generally use longer wavelength light (1310 nm) than posterior segment OCTs. The longer wavelength enables increased penetration of non-transparent tissues such as the sclera. There are currently several AS-OCT devices commercially available: (1) the Visante TD-OCT (Carl Zeiss Meditec Inc., Dublin, CA, USA) is a stand-alone AS-OCT instrument, compared to (2) the slit-lamp OCT (Heidelberg Engineering GmbH, Heidelberg, Germany) which has to be attached to a slit lamp. The Visante TD-OCT has a scanning speed of 2000 A-scans/s, a scan depth of 6 mm and an axial resolution of 18–25 μm [64]. Both devices have been demonstrated to detect more closed angles than gonioscopy [65]. Several posterior segment OCT instruments (RTVue OCT, Optovue Inc., Fremont, CA, USA and Cirrus HD-OCT, Carl Zeiss Meditec Inc., Dublin, CA, USA) are capable to visualize the anterior segment using optical adapters [66].

The latest addition to AS-OCT instruments has been the introduction of swept-source technology. The Casia SS-1000 SS-OCT (Tomey Corp., Tokyo, Japan) is commercially available AS-OCT instrument with a wavelength of 1310 nm, a scan speed of 30,000 Hz, and an axial resolution of <10 μm [67–70]. It provides a 360° evaluation and 3D datasets of the anterior chamber angle. Studies have shown improved imaging of angle structures, such as the scleral spur and Schlemm's canal with this technology compared to Visante AS-OCT [69] (Figs. 14.8 and 14.9).

The main application of AS-OCT in glaucoma is the evaluation and documentation of eyes with narrow or closed angles. The advantage of these devices to gonioscopy lies in their non-contact nature and ease of use. A further advantage is the fact of not using visible light and preventing pupil constriction, which yield fewer false negative results. In addition, they allow the collection of quantitative and qualitative data on angle parameters. Established risk factors for angle closure include a shallow central anterior chamber depth (ACD), short axial length (AL), and a thicker and more anteriorly positioned lens [71]. Among these, a shallow ACD is considered the major risk factor for angle closure [71]. However, population-based studies show that only a minority of individuals with shallow ACD ultimately develop PACG. Recently, novel anatomical landmarks have been identified using AS-OCT, some of which, such as smaller anterior chamber width (ACW), area, and volume, and increased lens vault (LV) have been shown to be risk factors for angle closure [72–74]. A small ACW implies a smaller anterior chamber volume that may cause angle crowding. LV corresponds to the amount of lens that is located anterior to the plane of the scleral spurs. It has been found to better quantify the relationship between the lens and the anterior chamber angles. A greater LV was observed to be strongly associated with an increased risk of angle closure. This parameter seems to be only slightly influenced by laser peripheral iridotomy.

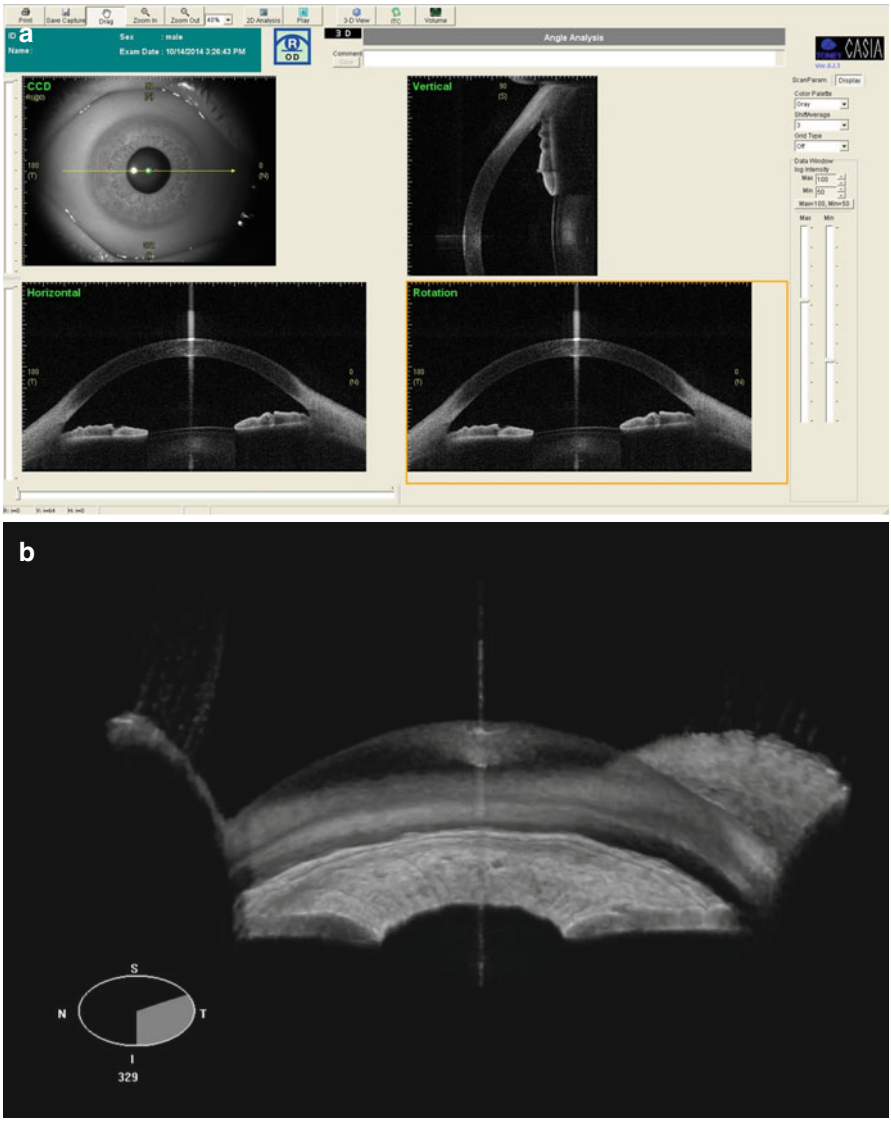

Fig. 14.8 (**a**) High-density scans obtained with the Casia SS-1000 AS-OCT, revealing open angles (Image courtesy of Christopher K. S. Leung, MD, Department of Ophthalmology and Visual Sciences, The Chinese University of Hong Kong, Hong Kong, PRC). (**b**) Three-dimensional display of the same eye showing angle structures

AS-OCT may also play an increasingly important role for evaluating anatomical features after glaucoma surgery. After filtering surgery, bleb morphology is often subjectively assessed as cystic, encapsulated, or flat. Leung et al. [75] described the use of AS-OCT for imaging bleb morphology after trabeculectomy. They qualified blebs based on AS-OCT features as diffuse filtering, cystic,

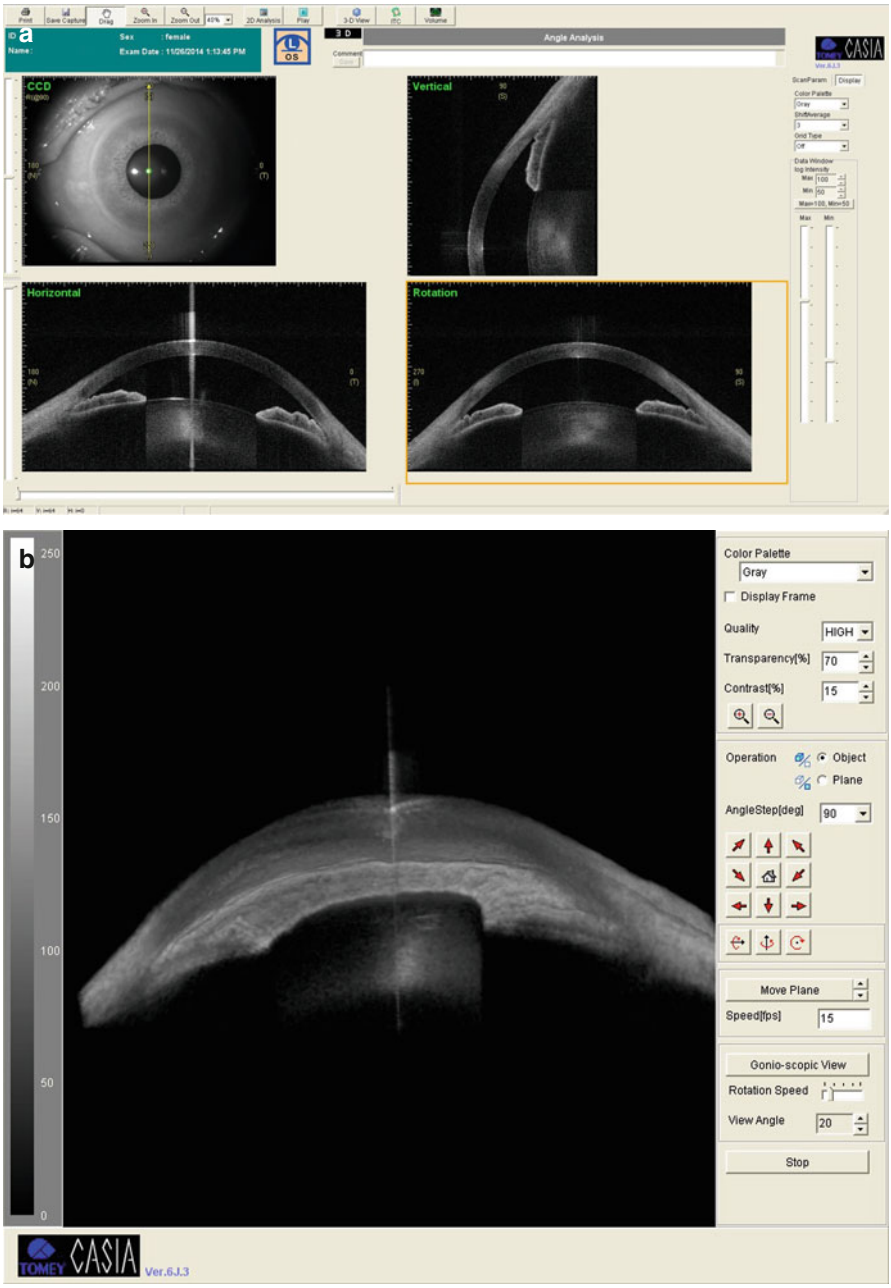

Fig. 14.9 (**a**) High-density scans obtained with the Casia SS-1000 AS-OCT, showing closed open angles. (**b**) Three-dimensional display of the same eye showing angle structures (Images courtesy of Christopher K. S. Leung, MD, Department of Ophthalmology and Visual Sciences, The Chinese University of Hong Kong, Hong Kong, PRC)

encapsulated, and flattened. Diffuse blebs were noted to have subconjunctival fluid collections. AS-OCT can also be used to visualize the position and patency of glaucoma drainage devices [76, 77]. With the advent of newer surgical options in glaucoma, which focus on the Schlemm's canal or suprachoroidal drainage, the place of AS-OCT for high-definition imaging of these structures is expected to gain in importance.

14.6 Future Directions

OCTs have revolutionized ocular imaging and diagnostics and the place of imaging in glaucoma is rapidly expanding. Current OCT technologies are intensity-based and cannot directly differentiate between different tissues and instead have to rely on signal intensity. Future developments in OCT technology have the potential to further advance macro- and microscopic imaging:

1. Polarization sensitive OCT (PS-OCT) is an extension of the standard OCT technique. It measures the polarization state of light and is based on the fact that some tissues can change the polarization state of the probing light beam. PS-OCT has the ability to measure intrinsic tissue specific properties such as phase retardation due to birefringence and visualize these in conjunction with anatomy [78–82]. Thus, PS-OCT combines the polarization sensitivity of scanning laser polarimetry with the depth information of OCT in a single instrument, potentially improving glaucoma diagnosis.
2. Adaptive optics (AO)-OCT corrects high-order optical aberrations and astigmatism, enabling enhanced transverse resolution of up to 5 μm (instead of the usual 20 μm) [83–85]. By incorporating automated wavefront sensing and correction into OCT platforms, it is possible to acquire images of the retina with cellular-level resolution. The drawback of this technology is the small field of view (e.g., 4°×4° vs. 30–50° with standard OCT platforms) Takayama et al. [86] have demonstrated that it is possible to identify individual RNFL bundles in great detail using AO technology. In future, newer technologies capable of *molecular imaging* will be able to capture early cellular and biochemical processes [87].
3. Optical coherence tomography angiography (OCTA) is based on the high-speed, sequential acquisition of images at the same retinal locus with assessment of differences in scans that occur as a result of blood flow. Two technologies are currently being investigated: (1) Doppler-OCT measures the phase shift between sequential A-scans that enable contrast generation [88]; (2) Phase-contrast-OCT measures differences in sequential B-scans that enable the detection of motion (e.g., blood flow) [89]. Jia et al. [90], using OCTA recently suggested that normal optic discs had a denser microvascular network than glaucomatous discs. They also found that there appeared to be attenuated flow in the deeper LC region of glaucomatous eyes compared to healthy eyes.

14.7 Conclusion

In the last decade, advances in ophthalmic imaging instrumentation have enabled visualization of the retina and the optic nerve head at an unprecedented resolution. These developments have contributed toward early detection of the glaucoma, monitoring of disease progression, and potentially assessment of response to therapy [62, 91]. These powerful technologies are being further harnessed to formulate new disease biomarkers in evaluation of glaucoma progression. With the rapid proliferation of these techniques, the formulation of standardized nomenclature and methods for clinical validation have only recently been proposed and need to be introduced into clinical and research practice [92].

References

1. Resnikoff S, Pascolini D, Etya'ale D, Kocur I, Pararajasegaram R, Pokharel GP, et al. Global data on visual impairment in the year 2002. Bull World Health Organ. 2004;82(11):844–51.
2. Quigley HA, Addicks EM. Quantitative studies of retinal nerve fiber layer defects. Arch Ophthalmol. 1982;100(5):807–14.
3. Harwerth RS, Carter-Dawson L, Smith 3rd EL, Barnes G, Holt WF, Crawford ML. Neural losses correlated with visual losses in clinical perimetry. Invest Ophthalmol Vis Sci. 2004;45(9):3152–60.
4. Huang D, Swanson EA, Lin CP, Schuman JS, Stinson WG, Chang W, et al. Optical coherence tomography. Science. 1991;254(5035):1178–81.
5. Mansouri K, Leite MT, Medeiros FA, Leung CK, Weinreb RN. Assessment of rates of structural change in glaucoma using imaging technologies. Eye (Lond). 2011;25(3):269–77.
6. Realini T, Zangwill LM, Flanagan JG, Garway-Heath D, Patella VM, Johnson CA, et al. Normative databases for imaging instrumentation. J Glaucoma. 2015;24(6):480–3.
7. Budenz DL. Symmetry between the right and left eyes of the normal retinal nerve fiber layer measured with optical coherence tomography (an AOS thesis). Trans Am Ophthalmol Soc. 2008;106:252–75.
8. Leung CK, Cheung CY, Weinreb RN, Qiu Q, Liu S, Li H, et al. Retinal nerve fiber layer imaging with spectral-domain optical coherence tomography: a variability and diagnostic performance study. Ophthalmology. 2009;116(7):1257–63, 63 e1–2.
9. Sung KR, Kim DY, Park SB, Kook MS. Comparison of retinal nerve fiber layer thickness measured by Cirrus HD and Stratus optical coherence tomography. Ophthalmology. 2009;116(7):1264–70, 70 e1.
10. Mwanza JC, Oakley JD, Budenz DL, Anderson DR, Cirrus Optical Coherence Tomography Normative Database Study Group. Ability of cirrus HD-OCT optic nerve head parameters to discriminate normal from glaucomatous eyes. Ophthalmology. 2011;118(2):241–8. e1.
11. Sung KR, Na JH, Lee Y. Glaucoma diagnostic capabilities of optic nerve head parameters as determined by Cirrus HD optical coherence tomography. J Glaucoma. 2012;21(7):498–504.
12. Kotowski J, Folio LS, Wollstein G, Ishikawa H, Ling Y, Bilonick RA, et al. Glaucoma discrimination of segmented cirrus spectral domain optical coherence tomography (SD-OCT) macular scans. Br J Ophthalmol. 2012;96(11):1420–5.
13. Mwanza JC, Durbin MK, Budenz DL, Sayyad FE, Chang RT, Neelakantan A, et al. Glaucoma diagnostic accuracy of ganglion cell-inner plexiform layer thickness: comparison with nerve fiber layer and optic nerve head. Ophthalmology. 2012;119(6):1151–8.

14. Jeoung JW, Choi YJ, Park KH, Kim DM. Macular ganglion cell imaging study: glaucoma diagnostic accuracy of spectral-domain optical coherence tomography. Invest Ophthalmol Vis Sci. 2013;54(7):4422–9.
15. Takayama K, Hangai M, Durbin M, Nakano N, Morooka S, Akagi T, et al. A novel method to detect local ganglion cell loss in early glaucoma using spectral-domain optical coherence tomography. Invest Ophthalmol Vis Sci. 2012;53(11):6904–13.
16. Lisboa R, Paranhos Jr A, Weinreb RN, Zangwill LM, Leite MT, Medeiros FA. Comparison of different spectral domain OCT scanning protocols for diagnosing preperimetric glaucoma. Invest Ophthalmol Vis Sci. 2013;54(5):3417–25.
17. Leite MT, Zangwill LM, Weinreb RN, Rao HL, Alencar LM, Sample PA, et al. Effect of disease severity on the performance of Cirrus spectral-domain OCT for glaucoma diagnosis. Invest Ophthalmol Vis Sci. 2010;51(8):4104–9.
18. Mansouri K, Medeiros FA, Marchase N, Tatham AJ, Auerbach D, Weinreb RN. Assessment of choroidal thickness and volume during the water drinking test by swept-source optical coherence tomography. Ophthalmology. 2013;120(12):2508–16.
19. Mansouri K, Medeiros FA, Tatham AJ, Marchase N, Weinreb RN. Evaluation of retinal and choroidal thickness by swept-source optical coherence tomography: repeatability and assessment of artifacts. Am J Ophthalmol. 2014;157(5):1022–32.
20. Yang Z, Tatham AJ, Zangwill LM, Weinreb RN, Zhang C, Medeiros FA. Diagnostic ability of retinal nerve fiber layer imaging by swept-source optical coherence tomography in glaucoma. Am J Ophthalmol. 2015;159(1):193–201.
21. Leung CK, Yu M, Weinreb RN, Ye C, Liu S, Lai G, et al. Retinal nerve fiber layer imaging with spectral-domain optical coherence tomography: a prospective analysis of age-related loss. Ophthalmology. 2012;119(4):731–7.
22. Wollstein G, Ishikawa H, Wang J, Beaton SA, Schuman JS. Comparison of three optical coherence tomography scanning areas for detection of glaucomatous damage. Am J Ophthalmol. 2005;139(1):39–43.
23. Medeiros FA, Zangwill LM, Alencar LM, Bowd C, Sample PA, Susanna Jr R, et al. Detection of glaucoma progression with stratus OCT retinal nerve fiber layer, optic nerve head, and macular thickness measurements. Invest Ophthalmol Vis Sci. 2009;50(12):5741–8.
24. Leung CK, Cheung CY, Weinreb RN, Qiu K, Liu S, Li H, et al. Evaluation of retinal nerve fiber layer progression in glaucoma: a study on optical coherence tomography guided progression analysis. Invest Ophthalmol Vis Sci. 2010;51(1):217–22.
25. Vizzeri G, Bowd C, Medeiros FA, Weinreb RN, Zangwill LM. Effect of improper scan alignment on retinal nerve fiber layer thickness measurements using Stratus optical coherence tomograph. J Glaucoma. 2008;17(5):341–9.
26. Cheung CY, Leung CK, Lin D, Pang CP, Lam DS. Relationship between retinal nerve fiber layer measurement and signal strength in optical coherence tomography. Ophthalmology. 2008;115(8):1347–51, 51 e1–2.
27. Leung CK, Liu S, Weinreb RN, Lai G, Ye C, Cheung CY, et al. Evaluation of retinal nerve fiber layer progression in glaucoma a prospective analysis with neuroretinal rim and visual field progression. Ophthalmology. 2011;118(8):1551–7.
28. Na JH, Sung KR, Lee JR, Lee KS, Baek S, Kim HK, et al. Detection of glaucomatous progression by spectral-domain optical coherence tomography. Ophthalmology. 2013;120(7):1388–95.
29. Wessel JM, Horn FK, Tornow RP, Schmid M, Mardin CY, Kruse FE, et al. Longitudinal analysis of progression in glaucoma using spectral-domain optical coherence tomography. Invest Ophthalmol Vis Sci. 2013;54(5):3613–20.
30. Rao HL, Zangwill LM, Weinreb RN, Sample PA, Alencar LM, Medeiros FA. Comparison of different spectral domain optical coherence tomography scanning areas for glaucoma diagnosis. Ophthalmology. 2010;117(9):1692–9.
31. Na JH, Sung KR, Baek S, Kim YJ, Durbin MK, Lee HJ, et al. Detection of glaucoma progression by assessment of segmented macular thickness data obtained using spectral domain optical coherence tomography. Invest Ophthalmol Vis Sci. 2012;53(7):3817–26.
32. Naghizadeh F, Garas A, Vargha P, Hollo G. Detection of early glaucomatous progression with different parameters of the RTVue optical coherence tomograph. J Glaucoma. 2014;23(4):195–8.

33. Kass MA, Heuer DK, Higginbotham EJ, Johnson CA, Keltner JL, Miller JP, et al. The Ocular Hypertension Treatment Study: a randomized trial determines that topical ocular hypotensive medication delays or prevents the onset of primary open-angle glaucoma. Arch Ophthalmol. 2002;120(6):701–13; discussion 829–30.
34. Weinreb RN, Kaufman PL. Glaucoma research community and FDA look to the future, II: NEI/FDA Glaucoma Clinical Trial Design and Endpoints Symposium: measures of structural change and visual function. Invest Ophthalmol Vis Sci. 2011;52(11):7842–51.
35. Medeiros FA, Lisboa R, Zangwill LM, Liebmann JM, Girkin CA, Bowd C, et al. Evaluation of progressive neuroretinal rim loss as a surrogate end point for development of visual field loss in glaucoma. Ophthalmology. 2014;121(1):100–9.
36. Medeiros FA, Lisboa R, Weinreb RN, Girkin CA, Liebmann JM, Zangwill LM. A combined index of structure and function for staging glaucomatous damage. Arch Ophthalmol. 2012;130(9):1107–16.
37. Yeoh J, Rahman W, Chen F, Hooper C, Patel P, Tufail A, et al. Choroidal imaging in inherited retinal disease using the technique of enhanced depth imaging optical coherence tomography. Graefes Arch Clin Exp Ophthalmol Albrecht Von Graefes Arch Klin Exp Ophthalmol. 2010;248:1719–28.
38. Dell'Omo R, Costagliola C, Di Salvatore F, Cifariello F, Dell'Omo E. Enhanced depth imaging spectral-domain optical coherence tomography. Retina (Philadelphia, Pa). 2010;30:378–9.
39. Margolis R, Spaide RF. A pilot study of enhanced depth imaging optical coherence tomography of the choroid in normal eyes. Am J Ophthalmol. 2009;147:811–5.
40. Spaide RF, Koizumi H, Pozzoni MC, Pozonni MC. Enhanced depth imaging spectral-domain optical coherence tomography. Am J Ophthalmol. 2008;146:496–500.
41. Rao RC, Choudhry N, Gragoudas ES. Enhanced depth imaging spectral-domain optical coherence tomography findings in sclerochoroidal calcification. Retina (Philadelphia, Pa). 2012;32:1226–7.
42. Goldenberg D, Moisseiev E, Goldstein M, Loewenstein A, Barak A. Enhanced depth imaging optical coherence tomography: choroidal thickness and correlations with age, refractive error, and axial length. Ophthalmic Surg Lasers Imaging Off J Int Soc Imaging Eye. 2012;43:296–301.
43. Chhablani J, Barteselli G, Wang H, El-Emam S, Kozak I, Doede AL, et al. Repeatability and reproducibility of manual choroidal volume measurements using enhanced depth imaging optical coherence tomography. Invest Ophthalmol Vis Sci. 2012;53:2274–80.
44. Spaide RF, Akiba M, Ohno-Matsui K. Evaluation of peripapillary intrachoroidal cavitation with swept source and enhanced depth imaging optical coherence tomography. Retina (Philadelphia, Pa). 2012;32:1037–44.
45. Branchini L, Regatieri CV, Flores-Moreno I, Baumann B, Fujimoto JG, Duker JS. Reproducibility of choroidal thickness measurements across three spectral domain optical coherence tomography systems. Ophthalmology. 2012;119:119–23.
46. Rahman W, Chen FK, Yeoh J, Patel P, Tufail A, Da Cruz L. Repeatability of manual subfoveal choroidal thickness measurements in healthy subjects using the technique of enhanced depth imaging optical coherence tomography. Invest Ophthalmol Vis Sci. 2011;52:2267–71.
47. Unterhuber A, Povazay B, Hermann B, Sattmann H, Chavez-Pirson A, Drexler W. In vivo retinal optical coherence tomography at 1040 nm – enhanced penetration into the choroid. Opt Express. 2005;13:3252–8.
48. Yasuno Y, Hong Y, Makita S, Yamanari M, Akiba M, Miura M, et al. In vivo high-contrast imaging of deep posterior eye by 1-microm swept source optical coherence tomography and scattering optical coherence angiography. Opt Express. 2007;15:6121–39.
49. Srinivasan VJ, Adler DC, Chen Y, Gorczynska I, Huber R, Duker JS, et al. Ultrahigh-speed optical coherence tomography for three-dimensional and en face imaging of the retina and optic nerve head. Invest Ophthalmol Vis Sci. 2008;49:5103–10.
50. Chen Y, Burnes DL, de Bruin M, Mujat M, de Boer JF. Three-dimensional pointwise comparison of human retinal optical property at 845 and 1060 nm using optical frequency domain imaging. J Biomed Opt. 2009;14:024016.

51. Ikuno Y, Kawaguchi K, Nouchi T, Yasuno Y. Choroidal thickness in healthy Japanese subjects. Invest Ophthalmol Vis Sci. 2010;51:2173–6.
52. Agawa T, Miura M, Ikuno Y, Makita S, Fabritius T, Iwasaki T, et al. Choroidal thickness measurement in healthy Japanese subjects by three-dimensional high-penetration optical coherence tomography. Graefes Arch Clin Exp Ophthalmol Albrecht Von Graefes Arch Klin Ophthalmol. 2011;249:1485–92.
53. Ikuno Y, Maruko I, Yasuno Y, Miura M, Sekiryu T, Nishida K, et al. Reproducibility of retinal and choroidal thickness measurements in enhanced depth imaging and high-penetration optical coherence tomography. Invest Ophthalmol Vis Sci. 2011;52:5536–40.
54. Matsuo Y, Sakamoto T, Yamashita T, Tomita M, Shirasawa M, Terasaki H. Comparisons of choroidal thickness of normal eyes obtained by two different spectral-domain OCT instruments and one swept-source OCT instrument. Invest Ophthalmol Vis Sci. 2013;54(12):7630–6.
55. Usui S, Ikuno Y, Miki A, Matsushita K, Yasuno Y, Nishida K. Evaluation of the choroidal thickness using high-penetration optical coherence tomography with long wavelength in highly myopic normal-tension glaucoma. Am J Ophthalmol. 2012;153:10–6.e1.
56. Park SC, De Moraes CGV, Teng CC, Tello C, Liebmann JM, Ritch R. Enhanced depth imaging optical coherence tomography of deep optic nerve complex structures in glaucoma. Ophthalmology. 2012;119:3–9.
57. Kiumehr S, Park SC, Syril D, Teng CC, Tello C, Liebmann JM, et al. In vivo evaluation of focal lamina cribrosa defects in glaucoma. Arch Ophthalmol. 2012;130:552–9.
58. Mansouri K, Nuyen B. R NW. Improved visualization of deep ocular structures in glaucoma using high penetration optical coherence tomography. Expert Rev Med Devices. 2013;10(5):621–8.
59. Park HY, Shin HY, Park CK. Imaging the posterior segment of the eye using swept-source optical coherence tomography in myopic glaucoma eyes: comparison with enhanced-depth imaging. Am J Ophthalmol. 2014;157(3):550–7.
60. Wang B, Nevins JE, Nadler Z, Wollstein G, Ishikawa H, Bilonick RA, et al. In vivo lamina cribrosa micro-architecture in healthy and glaucomatous eyes as assessed by optical coherence tomography. Invest Ophthalmol Vis Sci. 2013;54(13):8270–4.
61. Wang B, Nevins JE, Nadler Z, Wollstein G, Ishikawa H, Bilonick RA, et al. Reproducibility of in-vivo OCT measured three-dimensional human lamina cribrosa microarchitecture. PLoS One. 2014;9(4):e95526.
62. Lee EJ, Kim T-W, Weinreb RN. Reversal of lamina cribrosa displacement and thickness after trabeculectomy in glaucoma. Ophthalmology. 2012;119(7):1359–66.
63. Yoshikawa M, Akagi T, Hangai M, Ohashi-Ikeda H, Takayama K, Morooka S, et al. Alterations in the neural and connective tissue components of glaucomatous cupping after glaucoma surgery using swept-source optical coherence tomography. Invest Ophthalmol Vis Sci. 2014;55(1):477–84.
64. Mansouri K, Sommerhalder J, Shaarawy T. Prospective comparison of ultrasound biomicroscopy and anterior segment optical coherence tomography for evaluation of anterior chamber dimensions in European eyes with primary angle closure. Eye (Lond). 2010;24(2):233–9.
65. Sakata LM, Wong TT, Wong HT, Kumar RS, Htoon HM, Aung HT, et al. Comparison of Visante and slit-lamp anterior segment optical coherence tomography in imaging the anterior chamber angle. Eye (Lond). 2010;24(4):578–87.
66. Wong HT, Lim MC, Sakata LM, Aung HT, Amerasinghe N, Friedman DS, et al. High-definition optical coherence tomography imaging of the iridocorneal angle of the eye. Arch Ophthalmol. 2009;127(3):256–60.
67. Jhanji V, Yang B, Yu M, Ye C, Leung CK. Corneal thickness and elevation measurements using swept-source optical coherence tomography and slit scanning topography in normal and keratoconic eyes. Clin Experiment Ophthalmol. 2013;41(8):735–45.
68. Lai I, Mak H, Lai G, Yu M, Lam DS, Leung CK. Anterior chamber angle imaging with swept-source optical coherence tomography: measuring peripheral anterior synechia in glaucoma. Ophthalmology. 2013;120(6):1144–9.

69. McKee H, Ye C, Yu M, Liu S, Lam DS, Leung CK. Anterior chamber angle imaging with swept-source optical coherence tomography: detecting the scleral spur, Schwalbe's Line, and Schlemm's Canal. J Glaucoma. 2013;22(6):468–72.
70. Liu S, Yu M, Ye C, Lam DS, Leung CK. Anterior chamber angle imaging with swept-source optical coherence tomography: an investigation on variability of angle measurement. Invest Ophthalmol Vis Sci. 2011;52(12):8598–603.
71. Nongpiur ME, Ku JY, Aung T. Angle closure glaucoma: a mechanistic review. Curr Opin Ophthalmol. 2011;22(2):96–101.
72. Nongpiur ME, Sakata LM, Friedman DS, He M, Chan YH, Lavanya R, et al. Novel association of smaller anterior chamber width with angle closure in Singaporeans. Ophthalmology. 2010;117(10):1967–73.
73. Wu RY, Nongpiur ME, He MG, Sakata LM, Friedman DS, Chan YH, et al. Association of narrow angles with anterior chamber area and volume measured with anterior-segment optical coherence tomography. Arch Ophthalmol. 2011;129(5):569–74.
74. Cornes BK, Khor CC, Nongpiur ME, Xu L, Tay WT, Zheng Y, et al. Identification of four novel variants that influence central corneal thickness in multi-ethnic Asian populations. Hum Mol Genet. 2012;21(2):437–45.
75. Leung CK, Yick DW, Kwong YY, Li FC, Leung DY, Mohamed S, et al. Analysis of bleb morphology after trabeculectomy with Visante anterior segment optical coherence tomography. Br J Ophthalmol. 2007;91(3):340–4.
76. Mendrinos E, Dosso A, Sommerhalder J, Shaarawy T. Coupling of HRT II and AS-OCT to evaluate corneal endothelial cell loss and in vivo visualization of the Ahmed glaucoma valve implant. Eye (Lond). 2009;23(9):1836–44.
77. Sarodia U, Sharkawi E, Hau S, Barton K. Visualization of aqueous shunt position and patency using anterior segment optical coherence tomography. Am J Ophthalmol. 2007;143(6):1054–6.
78. Gotzinger E, Pircher M, Baumann B, Schmoll T, Sattmann H, Leitgeb RA, et al. Speckle noise reduction in high speed polarization sensitive spectral domain optical coherence tomography. Opt Express. 2011;19(15):14568–85.
79. Pircher M, Hitzenberger CK, Schmidt-Erfurth U. Polarization sensitive optical coherence tomography in the human eye. Prog Retin Eye Res. 2011;30(6):431–51.
80. Schlanitz FG, Baumann B, Spalek T, Schutze C, Ahlers C, Pircher M, et al. Performance of automated drusen detection by polarization-sensitive optical coherence tomography. Invest Ophthalmol Vis Sci. 2011;52(7):4571–9.
81. Yamanari M, Lim Y, Makita S, Yasuno Y. Visualization of phase retardation of deep posterior eye by polarization-sensitive swept-source optical coherence tomography with 1-microm probe. Opt Express. 2009;17(15):12385–96.
82. Yamanari M, Miura M, Makita S, Yatagai T, Yasuno Y. Phase retardation measurement of retinal nerve fiber layer by polarization-sensitive spectral-domain optical coherence tomography and scanning laser polarimetry. J Biomed Opt. 2008;13(1):014013.
83. Fernandez EJ, Vabre L, Hermann B, Unterhuber A, Povazay B, Drexler W. Adaptive optics with a magnetic deformable mirror: applications in the human eye. Opt Express. 2006;14(20):8900–17.
84. Fernandez EJ, Povazay B, Hermann B, Unterhuber A, Sattmann H, Prieto PM, et al. Three-dimensional adaptive optics ultrahigh-resolution optical coherence tomography using a liquid crystal spatial light modulator. Vision Res. 2005;45(28):3432–44.
85. Hermann B, Fernandez EJ, Unterhuber A, Sattmann H, Fercher AF, Drexler W, et al. Adaptive-optics ultrahigh-resolution optical coherence tomography. Opt Lett. 2004;29(18):2142–4.
86. Takayama K, Ooto S, Hangai M, Arakawa N, Oshima S, Shibata N, et al. High-resolution imaging of the retinal nerve fiber layer in normal eyes using adaptive optics scanning laser ophthalmoscopy. PLoS One. 2012;7(3):e33158.
87. Capozzi ME, Gordon AY, Penn JS, Jayagopal A. Molecular imaging of retinal disease. J Ocul Pharmacol Ther Off J Assoc Ocul Pharmacol Ther. 2013;29(2):275–86.

88. Kurokawa K, Sasaki K, Makita S, Hong YJ, Yasuno Y. Three-dimensional retinal and choroidal capillary imaging by power Doppler optical coherence angiography with adaptive optics. Opt Express. 2012;20(20):22796–812.
89. Kim DY, Fingler J, Zawadzki RJ, Park SS, Morse LS, Schwartz DM, et al. Optical imaging of the chorioretinal vasculature in the living human eye. Proc Natl Acad Sci U S A. 2013;110(35):14354–9.
90. Jia Y, Wei E, Wang X, Zhang X, Morrison JC, Parikh M, et al. Optical coherence tomography angiography of optic disc perfusion in glaucoma. Ophthalmology. 2014;121(7):1322–32.
91. Lee EJ, Kim TW, Weinreb RN. Variation of lamina cribrosa depth following trabeculectomy. Invest Ophthalmol Vis Sci. 2013;54(8):5392–9.
92. Staurenghi G, Sadda S, Chakravarthy U, Spaide RF, International Nomenclature for Optical Coherence Tomography Panel. Proposed lexicon for anatomic landmarks in normal posterior segment spectral-domain optical coherence tomography: the IN*OCT consensus. Ophthalmology. 2014;121(8):1572–8.

Chapter 15
OCT in Amblyopia

Paolo Nucci, Andrea Lembo, Greta Castellucci, and Francesco Pichi

Abstract The purpose of the study is to analyze the advantages of optical coherence tomography (OCT) to detect retinal nerve fiber layer (RNFL) thickness abnormalities and changes in the macula in amblyopic patients. Studies were selected through an electronic search on PUBMED, EMBASE and GOOGLE SCHOLAR using the following terms: "Optical coherence tomography in amblyopia", "OCT and amblyopia", "Optical coherence tomography and anisometropic amblyopia", "Optical coherence tomography and strabismic amblyopia".

We found that optical coherence tomography is a rapid, non-invasive imaging technique allowing objective quantification of retinal structures with high resolution; it can be successfully applied to young children, even those who are neurologically disabled or less cooperative. New generations devices, such as spectral domain OCT, have led to a dramatic increase in sensitivity that enables high-speed imaging. OCT technology could be also an useful biomarker for evaluating progressive thinning of RNFL over time and changes in the macula in amblyopia. Evidence for direct retinal changes in eyes with amblyopia has been controversial, so that further studies with large sample are required.

Keywords Optical coherence tomography • Retinal nerve fiber thickness • Macular thickness • Amblyopia

15.1 Introduction

Amblyopia can be defined as a disorder characterized by a dysfunction of the processing of visual information [1]. It results from degradation of the retinal image during the period of visual development, which historically has been thought to be

P. Nucci, MD (✉) • A. Lembo, MD • G. Castellucci, BMedSci • F. Pichi, MD
University Eye Clinic, San Giuseppe Hospital, University of Milan, IRCCS MultiMedica, Via San Vittore 12, Milan 20123, Italy
e-mail: Paolo.nucci@unimi.it; andrealembo1984@hotmail.com; greta.castellucci@gmail.com; ilmiticopicchio@gmail.com

A. Grzybowski, P. Barboni (eds.), *OCT in Central Nervous System Diseases: The Eye as a Window to the Brain*, DOI 10.1007/978-3-319-24085-5_15

the first 6 years of life [2]. Therefore, amblyopia never occurs in isolation; the disease is not the cause, but the effect of another pathological process. Amblyopia can be seen as a result of either disuse, due to the absence of a clear image on the retina (anisometropia or deprivation), or misuse, due to abnormal binocular interaction (strabismus) [3]. In particular, the degradation of the image, and subsequent central suppression that leads to amblyopia results from one of the three causal processes. In 2003, the American Association for Pediatric Ophthalmology and Strabismus (AAPOS) published a list of risk factors for amblyopia [4]; Arnold [5] attempted to estimate cut-off found by the AAPOS in a meta- analysis. The results obtained were: approximate prevalence of anisometropia of 1.2 %, hyperopia of 6 %, astigmatism of 15 %, myopia of 0.6 %, strabismus of 2.5 %, and a visual acuity less than 20/40 of 6 %. The mean combined prevalence found was 21 % ± 2 % compared to a prevalence of amblyopia 20/40 and worse of 2.5 %. The estimated prevalence of amblyopia in adults is 2–9 %, [6] and it still seems to be the leading cause of monocular vision loss in people aged between 20 and 70 years [7].

Given the numbers, it is easy to imagine how the diagnosis of amblyopia can be important. The diagnosis of unilateral amblyopia is made when reduced visual acuity is recorded in the presence of an amblyogenic factor, and not explained by another ocular abnormality. Residual visual deficits after correction of any amblyogenic factor (for example by spectacles prescription) are assumed to be due to amblyopia [3]. A widely accepted definition of amblyopia based on visual acuity is two or more Snellen or logMAR lines difference between eyes in best-corrected visual acuity. A one-line difference is usually a normal result, based on test-retest variability [8]. One important feature of visual acuity testing to diagnose amblyopia is that there is a distribution or range of typical visual acuity in any population. This range changes with age because of neural maturational processes [3].

15.2 OCT Studies in Animesotropic Amblyopia

Although clinical ocular examination is most often normal in amblyopia, microscopic anatomical and structural abnormalities have been found, starting from Hubel and Wiesel's pioneering work [9] in the retina, lateral geniculate bodies, and visual cortex [10–12]. With the advent of OCT in ophthalmology, there have been numerous attempts to investigate the structural differences in macular and peripapillary retinal nerve fiber layer (RNFL) in amblyopic patients [13–15]. Despite the use of more and more advanced techniques, conflicting results have often been found. Khan [16] compared the anterior and posterior ocular architecture of amblyopic and normal fellow eyes in 14 patients with hyperopic anisometropic amblyopia. Subjects were children between 5 and 10 years of age, with hyperopia >1.5 D and unilateral amblyopia with an interocular difference in spherical equivalent of at least 1D. Patients were examined using two tools: corneal topography to measure anterior and posterior corneal curvature, corneal thickness and volume, anterior chamber volume and depth, and OCT for RNFL, central macular thickness and macular volume measurements. In these children, corneal topography and OCT revealed no differences ($P > 0.05$) in the anterior and posterior architecture between the

amblyopic and the fellow eye. Wu et al. [17] examined a larger sample, including 72 children (range 5–16 years) to compare the RNFL and macular thickness in amblyopic eyes with that in fellow eyes. All enrolled children had unilateral hyperopic anisometropic amblyopia and normal vision in the contralateral eye. After a full ophthalmological assessment, OCT scans were performed using a spectral domain OCT (3D-OCT 1000). The foveolar thickness, central macular thickness and four quadrants of the inner and outer macular thickness were measured for each subject. Peripapillary RNFL thickness was measured using the "fast RNFL thickness (3.4 mm diameter)" scan protocol, which consisted of six radial line scans. OCT measurements found thicker foveolas and peripapillary RNFL in eyes with hyperopic anisometropic amblyopia compared to the contralateral eyes, but no changes in 1-mm central macular thickness (Fig. 15.1). This difference between foveolar thickness and 1-mm central macular thickness needs further histopathologic

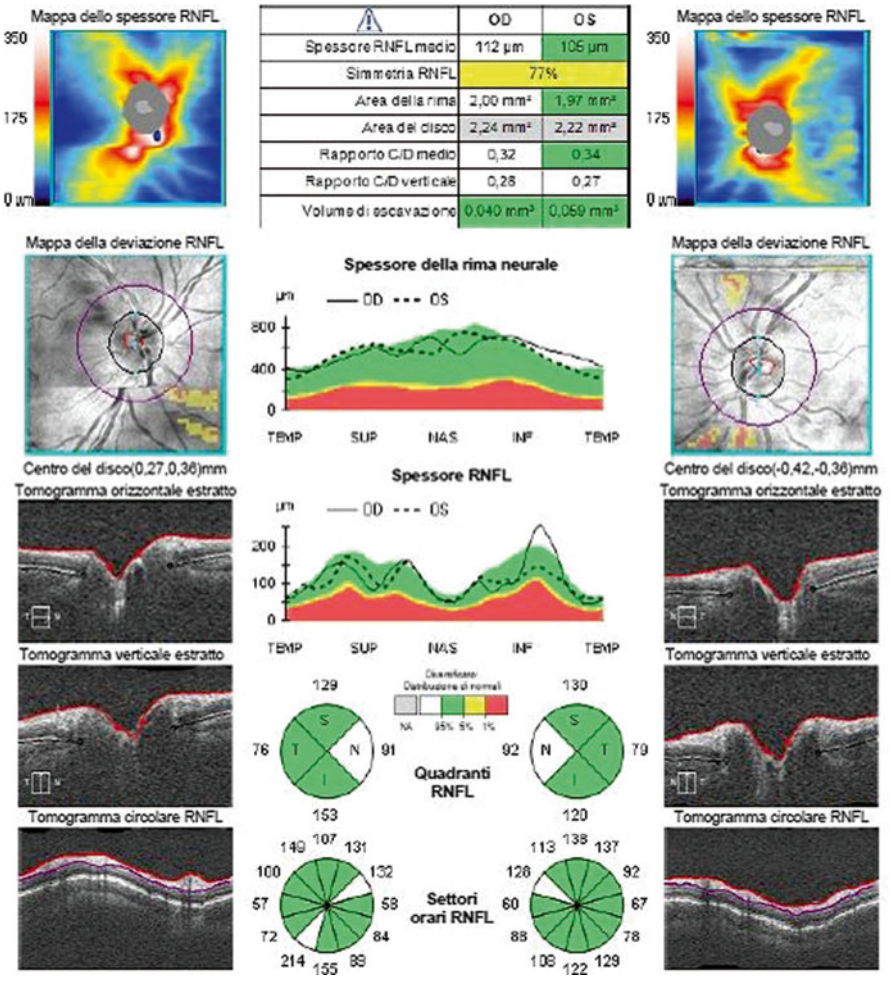

Fig. 15.1 An hyperopic amblyopic patient (OD sf+4.50, OS sf+5.50) with thickened nasal RNFL

investigation. No correlation was found between severity of anisometropia and differences of peripapillary RNFL thickness, or between central macular thickness and foveal thickness in the contralateral eyes, suggesting far more complex pathophysiologic mechanisms for anisometropic amblyopia than we currently know. An interesting biological theory regarding differences in RNFL thickness in eyes with and without amblyopia proposes that in humans the total population of cells in the ganglion cell layer is at its highest approximately between 18 and 30 weeks of gestation and declines rapidly thereafter [18]. The number of axons in the human optic nerve decreases too during gestation [19]. Absence of normal visual stimulation may contribute to the reduced apoptosis of retinal ganglion cells in amblyopic eyes, eventually leading to thicker RNFL compared to non-amblyopic eye. Yen et al. [20] mentioned that the physiological postnatal ganglion cell reduction could be inhibited in amblyopia, while Kok et al. [21] concluded that an hypothetical arrest of the normal ganglion cell reduction is expected to lead to an abnormally thick retinal thickness, especially the pericentral retinal thickness. A second hypothesis seems to regard the macula, which becomes thicker rather than thinner in the perifoveal retina in 6-month embryos, manifesting a slight protrusion. Wu et al. [17] found that the foveola was significantly thicker in amblyopic eyes than in the fellow eyes (181.4 ± 14.2 μm *vs* 175.2 ± 13.3 μm, $P < 0.01$), possibly because blurred vision led to insufficient stimulation in the amblyopic eye, affecting the normal maturation of the macula, including movement of Henle's fibers away from the fovea and a decrease in foveal cone diameter, which would result in increased foveolar thickness.

Regarding myopic amblyopia, Pang et al. [22] conducted a study on 31 children with a mean age of 9.56 years and mean spherical equivalent in amblyopic eyes of -10.79 ± 3.40 diopters. Patients were scanned with TD OCT using the fast macular thickness protocol. The following ten parameters were measured for each subject: foveal minimum thickness, average foveal thickness, inner nasal, superior, temporal, and inferior macular thickness, outer nasal, superior, temporal, and inferior macular thickness. Pang et al. [22] found that amblyopic children with unilateral high myopia tend to have a thicker fovea and thinner inner and outer layers in the amblyopic eye compared to the normal fellow eye. These results indicate that anatomic changes may be present in the retinas of amblyopic children with unilateral high myopia. Anisometropia as the most frequent cause of amblyopia has been evaluated in numerous studies [13, 20, 21]. However, anisometropia associated with high myopia has often been excluded from these studies [20, 21]. The few studies investigating anisometropic amblyopia caused by unilateral high myopia have concluded that this type of amblyopia had poorer treatment outcomes [23]. Underlying structural abnormalities and macular hypoplasia have been proposed as causes for the poor treatment outcomes in myopic anisometropia [24, 25]. Knowledge of the macular structure and associated factors in amblyopia associated with unilateral high myopia will help the understanding of this disease and may assist clinicians in predicting treatment outcomes. Studies that have focused on comparison between strabismic and anisometropic amblyopia, have found differences between the two defects. Dickmann et al. [26] conducted a study to determine whether RNFL thick-

ness, macular thickness, and foveal volume in patients with unilateral amblyopia differed between the amblyopic and the fellow eye. Stratus OCT was performed on 80 eyes of 40 patients (mean age, 15.2 years; range, 5–56 years) with unilateral amblyopia divided into 20 strabismic and 20 anisometropic. OCT found that the difference in RNFL thickness between the amblyopic and fellow eyes was no statistically significant ($p > 0.05$) in both groups. Conversely, macular thickness and foveal volume in strabismic amblyopia were 5 % lower in the fellow eye than in the amblyopic one. On the other hand, in the anisometropic group there was no significant difference between eyes in either macular thickness or foveal volume. Dickmann et al. [27] found similar results on 15 patients with strabismic anysometropia and 15 patients with anisometric amblyopia. In both groups, mean foveal volume and RNFL thickness did not differ significantly between eyes. Only macular thickness in the strabismic group differed significantly between the amblyopic and fellow eyes. This statistically significant difference, also established in other studies [15, 26], was not present in the refractive amblyopia group: amblyopia of different etiologies could therefore be associated with different changes of the retinal tissues. Thickening of the amblyopic fovea could be related to a developmental arrest, with incomplete formation of the foveal depression, even if it's difficult to determine whether this may be caused by a direct effect of abnormal sensory output or the consequence of primary alteration of visual cortex and the lateral geniculate nucleus (Fig. 15.2). There was also a significant correlation between RNFL thickness and macular sensitivity measured with microperimetry (strabismic group, $r = 0.84$, $P = 0.002$; anisometropic group, $r = 0.66$, $P = 0.02$). Although visual fields generally appear normal, amblyopia can be associated with small central and paracentral scotoma in an amblyopic eyes but do not need further evaluations, especially if the patient is asymptomatic. If a deep focal deficit is found, causes of organic pathologies (for example optic neuropathy) should be investigated. Data from Dickmann et al. [27] study suggest that the anatomical differences of RNFL thickness between

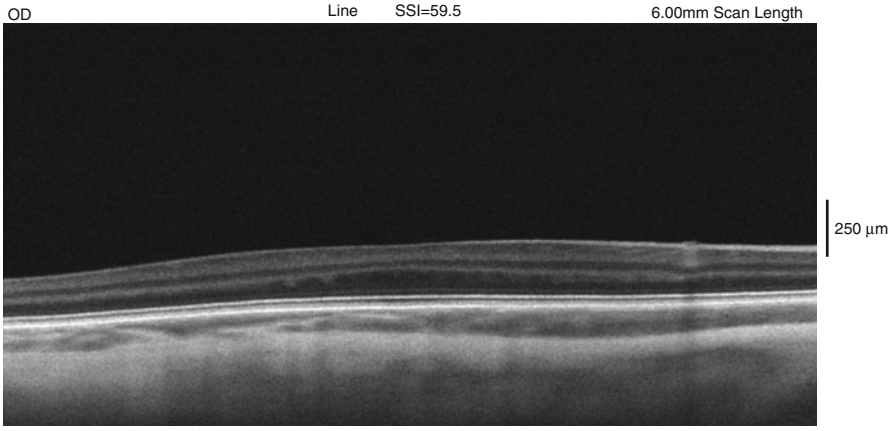

Fig. 15.2 Absence of foveal depression in a patient with nystagmus and foveal hypoplasia

the amblyopic and the fellow eye could determine the difference in macular sensitivity between the two eyes. Additional studies with larger, more diverse cohorts are needed to reveal whether these findings can be confirmed. Szigeti et al. [28] used OCT imaging and image segmentation methodology on 38 patients (range 6–67 years) with different types of amblyopia (strabismus without anisometropia, anisometropia without strabismus, strabismus with anisometropia). They detected structural changes in the outer nuclear layer of the fovea, suggesting the possible involvement of photoreceptor. There is early evidence showing that photoreceptors may be affected in amblyopia. For example, Enoch [29], using the Stiles-Crawford function, suggested that photoreceptor orientation is abnormal in amblyopic eyes, while other authors did not found indication of retinal dysfunction at the level of the cones in amblyopic eyes [30]. Given the results, further studies are warranted to support this hypothesis.

15.3 Oct Studies in Deprivation Amblyopia

As far as deprivation amblyopia in congenital cataract patients is concerned, the first study [31] investigating the structural difference of macular and peripapillary RNFL using OCT in this pathology has been conducted on a small sample: 14 unilateral pseudophakic children with deprivational amblyopia, and 14 age-matched normal children (mean age, 7.45 ± 2.57 years) were scanned with Cirrus HD-OCT. Macular, RNFL, and ganglion cell-inner plexiform layer thicknesses were measured, and compared between the eyes after correction for axial length-related magnification errors. OCT demonstrated significant increase in nasal RNFL thickness compared to fellow non-amblyopic eyes and age-matched normal eyes. The macular and macular ganglion cell-inner plexiform layer thickness did not show any significant difference. Several older studies reported a decrease in nasal visual fields in children treated for unilateral congenital cataract [32]. Kanamori et al. [33] demonstrated the relationship between visual field sensitivity at each tested location in standard automated perimetry and peripapillary RNFL thickness measured with Stratus OCT; the nasal sectoral RNFL corresponded well with nasal visual field area. Taken together, decreased nasal visual field in previous reports may have been due to increased nasal sectoral peripapillary RNFL thickness, as shown in Kim et al. study [31].

15.4 Conclusions

We can therefore conclude that OCT is certainly a rapid, non-invasive, office-based imaging technique allowing objective quantification of retinal structures with high resolution, including determination of peripapillary RNFL thickness and macular thickness, so that it can be successfully applied also in young children. Neverthless, evidence for direct retinal changes in eyes with amblyopia has been controversial:

the results of these studies are equivocal with regard to whether macular and peripapillary RNFL thicknesses differ in amblyopic eyes. Moreover, the majority of the studies have been limited to strabismic or anisometropic amblyopia, and analyzed the fellow non amblyopic eye as control [31]. Further studies with larger sample are required, especially as regards myopic anisometropic amblyopia.

References

1. McKee SP, Levi DM, Movshon JA. The pattern of visual deficits in amblyopia. J Vis. 2003;3(5):380–405.
2. Crawford ML, Harwerth RS, Smith EL, von Noorden GK. Keeping an eye on the brain: the role of visual experience in monkeys and children. J Gen Psychol. 1993;120(1):7–19.
3. Holmes JM, Clarke MP. Amblyopia. Lancet. 2006;367(9519):1343–51.
4. Donahue SP, Arnold RW, Ruben JB. Preschool vision screening: what should we be detecting and how should we report it? Uniform guidelines for reporting results of preschool vision screening studies. J AAPOS. 2003;7(5):314–6.
5. Arnold RW. Amblyopia risk factor prevalence. J Pediatr Ophthalmol Strabismus. 2013; 50(4):213–7.
6. Attebo K, Mitchell P, Cumming R, Smith W, Jolly N, Sparkes R. Prevalence and causes of amblyopia in an adult population. Ophthalmology. 1998;105(1):154–9.
7. Ederer F, Krueger DE. Report on the National Eye Institute's Visual Acuity Impairment Survey Pilot Study. Washington, DC: Office of Biometry and Epidemiology/National Eye Institute/ National Institutes of Health/Public Health Service/Department of Health and Human Services; 1984. p. 81–4.
8. Holmes JM, Beck RW, Repka MX, Leske DA, Kraker RT, Blair RC, et al. The amblyopia treatment study visual acuity testing protocol. Arch Ophthalmol. 2001;119(9):1345–53.
9. Wiesel TN, Hubel DH. Single- cell responses in striate cortex of kittens deprived of vision in one eye. J Neurophysiol. 1963;26:1003–17.
10. Williams C, Papakostopoulos D. Electro-oculographic abnormalities in amblyopia. Br J Ophthalmol. 1995;79(3):218–24.
11. Von Noorden GK, Crawford ML. The lateral geniculate nucleus in human strabismic amblyopia. Invest Ophthalmol Vis Sci. 1992;33(9):2729–32.
12. Horton JC, Hocking DR. Timing of the critical period for plasticity of ocular dominance columns in macaque striate cortex. J Neurosci. 1997;17(10):3684–709.
13. Dickmann A, Petroni S, Perrotta V, Parrilla R, Aliberti S, Salerni A, et al. Measurement of retinal nerve fiber layer thickness, macular thickness, and foveal volume in amblyopic eyes using spectral-domain optical coherence tomography. J AAPOS. 2012;16(1):86–8.
14. Repka MX, Kraker RT, Tamkins SM, Suh DW, Sala NA, Beck RW. Retinal nerve fiber layer thickness in amblyopic eyes. Am J Ophthalmol. 2009;148(1):143–7.
15. Huynh SC, Samarawickrama C, Wang XY, Rochtchina E, Wong TY, Gole GA, et al. Macular and nerve fiber layer thickness in amblyopia: the Sydney Childhood Eye Study. Ophthalmology. 2009;116(9):1604–9.
16. Khan AO. A comparison between the amblyopic eye and normal fellow eye ocular architecture in children with hyperopic anisometropic amblyopia. J AAPOS. 2013;17(1):115–6.
17. Wu SQ, Zhu LW, Xu QB, Xu JL, Zhang Y. Macular and peripapillary retinal nerve fiber layer thickness in children with hyperopic anisometropic amblyopia. Int J Ophthalmol. 2013;6(1):85–9.
18. Provis JM, van Driel D, Billson FA, Russell P. Development of the human retina: patterns of cell distribution and redistribution in the ganglion cell layer. J Comp Neurol. 1985;233(4): 429–51.

19. Provis JM, van Driel D, Billson FA, Russell P. Human fetal optic nerve: overproduction and elimination of retinal axons during development. J Comp Neurol. 1985;238(1):92–100.
20. Yen MY, Cheng CY, Wang AG. Retinal nerve fiber layer thickness in unilateral amblyopia. Invest Ophthalmol Vis Sci. 2004;45(7):2224–30.
21. Kok PH, de Kinkelder R, Braaksma-Besselink YC, Kalkman J, Prick LJ, Sminia ML, et al. Anomalous relation between axial length and retinal thickness in amblyopic children. J AAPOS. 2013;17(6):598–602.
22. Pang Y, Goodfellow GW, Allison C, Block S, Frantz KA. A prospective study of macular thickness in amblyopic children with unilateral high myopia. Invest Ophthalmol Vis Sci. 2011;52(5):2444–9.
23. Kutschke PJ, Scott WE, Keech RV. Anisometropic amblyopia. Ophthalmology. 1991;98(2):258–63.
24. Nucci P, Drack AV. Refractive surgery for unilateral high myopia in children. J AAPOS. 2001;5(6):348–51.
25. Saw SM, Gazzard G, Shih-Yen EC, Chua WH. Myopia and associated pathological complications. Ophthalmic Physiol Opt. 2005;25(5):381–91.
26. Dickmann A, Petroni S, Salerni A, Dell'Omo R, Balestrazzi E. Unilateral amblyopia: an optical coherence tomography study. J AAPOS. 2009;13(2):148–50.
27. Dickmann A, Petroni S, Perrotta V, Salerni A, Parrilla R, Aliberti S, et al. A morpho functional study of amblyopic eyes with the use of optical coherence tomography and microperimetry. J AAPOS. 2011;15(4):338–41.
28. Szigeti A, Tátrai E, Szamosi A, Vargha P, Nagy ZZ, Németh J, et al. A morphological study of retinal changes in unilateral amblyopia using optical coherence tomography image segmentation. PLoS One. 2014;9(2), e88363.
29. Enoch JM. Receptor amblyopia. Am J Ophthalmol. 1959;48(3), Part 2:262–74.
30. Delint PJ, Weissenbruch C, Berendschot TT, Norren DV. Photoreceptor function in unilateral amblyopia. Vision Res. 1998;38(4):613–7.
31. Kim YW, Kim SJ, Yu YS. Spectral-domain optical coherence tomography analysis in deprivational amblyopia: a pilot study with unilateral pediatric cataract patients. Graefes Arch Clin Exp Ophthalmol. 2013;251(12):2811–9.
32. Bowering ER, Maurer D, Lewis TL, Brent HP. Sensitivity in the nasal and temporal hemifields in children treated for cataract. Invest Ophthalmol Vis Sci. 1993;34(13):3501–9.
33. Kanamori A, Naka M, Nagai-Kusuhara A, Yamada Y, Nakamura M, Negi A. Regional relationship between retinal nerve fiber layer thickness and corresponding visual field sensitivity in glaucomatous eyes. Arch Ophthalmol. 2008;126(11):1500–6.

Chapter 16
Conclusion: The Exciting Future of OCT Imaging of Retina

Piero Barboni and Andrzej Grzybowski

Abstract Optical coherence tomography (OCT) has been a major step forward in ophthalmology, enabling us to obtain in vivo images of the retina and optic disc with higher and higher resolution. Since its introduction twenty years ago, OCT in fact underwent continuous technological advances and further improvements are expected over the next few years. These improvements will help us to investigate the retinal and optic nerve function, in addition to their structure, and will be useful to collect new information not only for eye, but also for brain diseases.

Keywords OCT • Eye • Brain • Neurodegeneration • Optic Nerve

The book aims to improve our knowledge of the wide spectrum of neurological diseases that can be investigated by OCT. We focused our attention on different pathologies that in the past were of exclusive interest to neurologists, like stroke or neurodegenerative diseases. From a clinical point of view, the information obtained by this technology will improve the neurological diagnosis and will provide useful parameters for therapeutic trials. Moreover, the development of handheld or mobile and cost-effective OCT instruments could improve systematic screenings for neurological diseases also in patients affected by neurological disability [1, 2].

P. Barboni (✉)
Scientific Institute San Raffaele, Milan, Italy

Studio oculistico d'Azeglio, Bologna, Italy
e-mail: p.barboni@studiodazeglio.it

A. Grzybowski, MD, PhD, MBA
Professor of Ophthalmology, Head of Ophthalmology Department, Poznan City Hospital, Poznan, Poland

Chair of Department of Ophthalmology, University of Warmia and Mazury, Olsztyn, Poland

A. Grzybowski, P. Barboni (eds.), *OCT in Central Nervous System Diseases: The Eye as a Window to the Brain*, DOI 10.1007/978-3-319-24085-5_16

Thanks to the OCT accuracy and diffusion, we are accumulating more and more information about ocular tissues, regarding both anatomy and pathology. In the future we are going to better understand which information will be useful or not.

OCT technology is going to look for the best definition and resolution in order to be more similar to histology and to improve the reliability and the definition of pathological images. Today, many companies are moving toward Swept Source technology and new emerging techniques are in progress such as hyperspectral imaging, photoacoustic ophthalmoscopy and molecular imaging [3–5]. Moreover, physicians often ask to the machine a diagnostic role. This could be achieved if the normative database of each instrument is improved by increasing the control group and stratifying it according to any confounding factor, or if a protocol analysis unaffected by anatomical variability is developed.

In the future, OCT will hopefully be able to obtain data about ocular function too. OCT angiography, for example, is a new technology that can visualize retinal vessels. If promises are maintained, we could get information about vascular density and blood flow. Data about vascular supply could be very useful when studying neurological pathologies and may be related to retinal anatomy (for example ganglion cells and retinal nerve fiber layers thickness) [6, 7].

So, a combination of structural and functional technologies is desirable. At this moment, at least three new techniques are being developed in this area. Flavoprotein fluorescence methodology (Ocusciences, Inc, Ann Arbor, MI) is a kind of autofluorescence, which uses a very specific wavelength to excite natural fluorophores of the retina. This technology can potentially detects mitochondrial damage by measuring oxidized flavoproteins in the retina [8, 9]. In this way, retinal fibers swelling and ganglion cell atrophy due to mitochondrial structural damage can be potentially combined to functional information.

Another high-resolution optical imaging approach was developed to detect beta-amyloid plaques in the retina. The system is based on a specific marker (fluorescent curcumin) as an imaging agent to detect Alzheimer's disease-related plaques in the retinas. The technique, developed at Cedars-Sinai Medical Centers, is a tool for early Alzheimer's disease diagnosis as well as assessment of therapy [10].

DARC (detection of apoptosing retinal cells) technology uses confocal laser-scanning ophthalmoscopy to visualize single neural cell apoptosis in vivo. This fluorescent technique is effective in the identification of the protein annexin 5 that represents an early feature in the apoptotic process. This method is able to image changes occurring in nerve cell apoptosis over time and could provide the opportunity for detailed investigation of fundamental neurodegenerative disease mechanisms and the evaluation of interventions with potential clinical applications [11, 12].

From an experimental point of view OCT could give us important information that we could share with genetist, biochemist and clinicians in order to better define phenotype/genotype correlation and to study animal model.

In conclusion OCT gives us the opportunity to study brain diseases throught the eye window in an objective and not invasive method.

References

1. Jung W, Kim J, Jeon M, et al. Handheld optical coherence tomography scanner for primary care diagnostics. IEEE Trans Biomed Eng. 2011;58:741–4.
2. Chen DL, Kraus M, Potsaid B. Handheld ultrahigh speed swept source optical coherence tomography instrument using a MEMS scanning mirror. Biomed Opt Express. 2014;5:293–311.
3. Mordant DJ, Al-Abboud I, Muyo G, et al. Spectral imaging of the retina. Eye (Lond). 2011;25:309–20.
4. Zhang HF, Puliafito CA, Jiao S. Photoacoustic ophthalmoscopy for in vivo retinal imaging: current status and prospects. Ophthalmic Surg Lasers Imaging. 2011;42:S106–15.
5. Jiao S, Jiang M, Hu J, et al. Photoacoustic ophthalmoscopy for in vivo retinal imaging. Opt Express. 2010;18:3967–72.
6. Makita S, Hong Y, Yamanari M, Yatagai T, Yasuno Y. Optical coherence angiography. Opt Express. 2006;14:7821–40.
7. Huang Y, Zhang Q, Thorell MR, An L, Durbin MK, Laron M, et al. Swept-source OCT angiography of the retinal vasculature using intensity differentiation-based optical microangiography algorithms. Ophthalmic Surg Lasers Imaging Retina. 2014;45:382–9.
8. Field MG, Elner VM, Puro DG, Feuerman JM, Musch DC, Pop-Busui R, et al. Rapid, noninvasive detection of diabetes-induced retinal metabolic stress. Arch Ophthalmol. 2008;126:934–8.
9. Field MG, Yang D, Bian ZM, Petty HR, Elner VM. Retinal flavoprotein fluorescence correlates with mitochondrial stress, apoptosis, and chemokine expression. Exp Eye Res. 2011;93:548–55.
10. Koronyo-Hamaoui M, Koronyo Y, Ljubimov AV, Miller CA, Ko MK, Black KL, et al. Identification of amyloid plaques in retinas from Alzheimer's patients and noninvasive in vivo optical imaging of retinal plaques in a mouse model. Neuroimage. 2011;54 Suppl 1:S204–17.
11. Guo L, Cordeiro MF. Assessment of neuroprotection in the retina with DARC. Prog Brain Res. 2008;173:437–50.
12. Normando EM, Dehabadi MH, Guo L, Turner LA, Pollorsi G, Cordeiro MF. Real-time imaging of retinal cell apoptosis by confocal scanning laser ophthalmoscopy. Methods Mol Biol. 2015;1254:227–37.

Contributors

Francisco J. Ascaso

Chairman of Medical & Surgical Retina Unit, Department of Ophthalmology, Hospital Clínico Universitario "Lozano Blesa", Zaragoza, Spain

Associate Professor of Ophthalmology, Department of Surgery, School of Medicine, University of Zaragoza, Zaragoza, Spain

Researcher at Instituto de Investigación Sanitaria de Aragón (IIS Aragón), Zaragoza, Spain

A. Grzybowski, P. Barboni (eds.), *OCT in Central Nervous System Diseases: The Eye as a Window to the Brain*, DOI 10.1007/978-3-319-24085-5

Dr. Piero Barboni

Dr. Piero Barboni, received his undergraduate degree from University of Bologna in 1986 and his medical and surgical training from University of Bologna, Italy in 1990. Since then he has been working in private practice. Appointed professor at the Department of Neurological Science of Bologna University from 2007 to 2011. Currently, he is consultant neuro-ophthalmologist at Scientific Institute San Raffaele, University of Milan since 2012. He is also devoted to the study of hereditary optic neuropathies, for which he collaborates with several university-based centers (Bologna, London, Los Angeles, Tubingen, Sao Paulo). This project includes the international research project on Leber's Hereditary Optic Neuropathy in Brazil. Sub investigator in many clinical trials. He has authored more than 80 papers on international peer-reviewed journals and several books.

Ivan Bodis-Wollner

I have an interest in vision and neurology. My supervisor at the Physiological Laboratory of Cambridge in 1968 was John Robson and I learned about vision and contrast sensitivity. Later, in 1971 when I was a neurology resident at Mt. Sinai Hospital NY, I established that contrast sensitivity is a measure apart from visual acuity, which reflects neuronal damage (Science 1972, Nature 1976). Then I noticed in the Clinical Research Unit of Mt. Sinai Hospital that some PD patients were affected in their vision as were those who received reserpine. From then on, I explored the vision in PD using psychophysical and electrophysiological techniques. I published the results in several articles in Brain, Annals of Neurology and the EEG Journal. I received a Fulbright Scholarship and spent two half periods in the Laboratory (CNR) of Lamberto Maffei in Pisa and worked on the dopaminergic retina of the turtle with Marco Piccolino. Those studies gave me the insight into the retinal circuitry with opposing D1 and D2 receptor actions to shape the receptive field of central ganglion cells in the parkinsonian and Parkinson model retina. Studying the pattern ERG established by Lamberto Maffeiin Pisa gave me the opportunity to pin down, in my laboratory in the Mt. Sinai Hospital in New York with my postdocs MF Ghilardi, M. Marx, A. Glover and M. Onofrj, some of the visual spatial contrast deficits in the parkinsonian retina and in the parkinsonian monkey model. It was my former postdoc, Carmen Harnois, who did the seminal work, by then at Laval University, in the postmortem human PD retina which showed dopamine deficiency.

By the mid nineties we studied in vitro the human retina with an imaging technique, known as GDX, developed for quantifying nerve fiber layer losses in glaucoma eyes. Some 9 years ago the new imaging technique, Optical Coherence Tomography was just beginning to be applied in various ocular disorders. Our OCT

studies were the first one, which showed that the central macular area, the fovea is affected in PD and that in particular the inner layers of the retina. Finally we observed that the inner fovea is affected in a zone which overlaps and extends the so called foveal avascular zone. These results and studies from Anita Hendrickson ‘s and Janis Provis’s lab led me to think of the role of genes and capillaries in retinal remodeling in PD. Our study on the pathgnomic marker of PD, alpha-synuclein, shows its localization in the inner layers of the parkinsonian retina.

We believe that the retinal research may be a rewarding way to go to solve many open and challenging questions in Parkinson Disease.

Laura Cabezón

Department of Ophthalmology, Hospital Clínico Universitario “Lozano Blesa”, Zaragoza, Spain

Michele Carbonelli, MD

Michele Carbonelli earned M.D. degree in 2001 at the University of Bologna, Italy, where he completed his residency in Ophthalmology in 2005.

Since 2005 he has been working in private practice. His research interests include anterior and posterior segment surgery, retinal diseases and neuro-ophthalmology.

He has participated to many national meetings about optic neuropathy, cataract surgery and retinal pathology with particular focus on choroidal neovascolarization and its treatment.

He is involved since 2006 in different research projects about mitochondrial optic neuropathies.

Since 2015 he has been working as consultant at the neurophthalmology clinic, Bellaria Hospital, UOC Clinica Neurologica, IRCCS Istituto delle Scienze Neurologiche di Bologna.

He was also part of the staff in the double-blind placebo controlled clinical trial on l-acetyl-carnitine in LHON, sponsored by Sigma-tau spa.

He authored more than 45 articles in peer-reviewed journals.

Address:

IRCCS Istituto delle Scienze Neurologiche di Bologna, UOC Clinica Neurologica, Bellaria Hospital, Bologna, Italy

e-mail: dmcarbonelli@gmail.com

tel.: +39-051-6493203

fax: +39-051-2918667

Paula Casas

Department of Ophthalmology, Hospital Clínico Universitario “Lozano Blesa”, Zaragoza, Spain

Gianluca Coppola MD, PhD

Gianluca Coppola is clinical neurologist and scientific fellow at the G.B. Bietti Foundation-IRCCS. He is certified associated Professor of Neurology. His major research interests are neurophthalmology, neurophysiology of headaches, behavioural phenomena of habituation/sensitization, brain plasticity and pain. He personally carried out several experiments using evoked potentials (somatosensory, visual, auditory), transcranial magnetic stimulation, and neuroimaging. He is member of the International Headache Society (IHS), the Italian Society of the Study of Headache (SISC), the Italian Society of Clinical Neurophysiology (SINC), and the Italian Society of Neurology (SIN). He is Author or co-Author of about 90 peer-reviewed journal articles and book chapters (Total Impact Factor: 300; H-index: 18). He is an editorial board member of Journal of Headache and Pain and ad-hoc reviewer for about 20 journals.

Steven Galetta MD

Steven Galetta, **MD** is currently the Philip K. Moskowitz, MD, Professor of Neurology, and Chair of the Department of Neurology at the NYU Langone Medical Center. Formerly, he was the Associate Dean of Admissions for the University of Pennsylvania School of Medicine. He also served as the Director of Neurological Training and Neuro-ophthalmology at Penn for over two decades. Dr. Galetta received his MD from Cornell University Medical College. He then completed his neurology residency at the Hospital of the University of Pennsylvania and his neuro-ophthalmology fellowship at the Bascom Palmer Eye Institute, University of Miami.

Dr. Galetta currently serves on the editorial board for the journals Neurology, and the Journal of Neuro-ophthalmology. He is co-author of the textbook, Neuro-ophthalmology: Diagnosis and Management. In 2004, he was named the American Neurological Association's distinguished teacher of the year. He was also named the Robert J. Glaser Alpha Omega Alpha distinguished teacher of the year by the Association of American Medical Colleges in 2004. In 2008, he received the Parker Palmer award from the ACGME for his contributions to graduate medical education. Dr. Galetta has been involved in various capacities in a large number of clinical trials and has over 250 original publications concerning clinical, radiologic and research aspects of multiple sclerosis, sports related concussion and neuro-ophthalmology.

Sofya Glazman

I have the background, expertise and executive qualities to serve as a coordinator of OCT research.

With the use of optical coherence tomography (OCT) in vivo evidence of retinal thinning and foveal remodeling in PD was demonstrated. We have developed new OCT analytical tools, including a mathematical equation for quantitative description of the fovea. We aim to validate our methods for widespread use in PD clinical diagnosis, follow-up and for research.

Andrzej Grzybowski, MD, PhD, MBA

Present positions:

Professor of Ophthalmology and Chair of Department of Ophthalmology, University of Warmia and Mazury, Olsztyn, Poland

Head of Department of Ophthalmology at Poznań City Hospital, Poland

Major awards

Poznań University Rector Individual Scientific Award (2008); I Zakon Prize (American Society for the History of Dermatology, 2009, 2010), Eye Advances/ Focus Award (Bombay Ophthalmologists Association, 2014), **The Knight's Cross of The Order of Polonia Restituta** (President of Poland, 2014)

Present international scientific societies' activities:

EVER European Association for Vision and Eye Research

Cogan Society

American Society of Cataract and Refractive Surgery

International Fellow of the American Academy of Ophthalmology,

Euretina,

European University Professors of Ophthalmology,

European Academy of Ophthalmology (Chair LIV),

International Society of Bilateral Cataract Surgeons,

Programme Coordinator for World Congress of Ophthalmology (2011–2016) (International Council of Ophthalmology)

Expertise: cataract surgery, presbyopia treatment, clear–lens exchange; neuro-ophthalmology; vitreo-retinal surgery, glaucoma pathogenesis, history of ophthalmology.

Editorial boards: **Acta Ophthalmologica**, Clinics in Dermatology, Neuro-Ophthalmology, Archive of the History and Philosophy of Medicine (editor in chief), Saudi Journal of Ophthalmology, Historia Ophthalmologica Internationalis (editor-in-chief).

Author of 300 peer-reviewed international publications (total **IF of 508**), and r**eviewer for more than 20 journals**, including Ophthalmology, Retina, BJO, and Brain.

Delivered **invited lectures** at SOE, SASCRS, Euretina, EVER, WCO, 12th SOI International Congress 2014 (Italy), EyeAdvance 2014 (Mumbai), XIV International Congress of the Italiana Society Stem Cells and Ocular Surface –SICSSO (2015), and ISOPT (2015).

His professional expertise includes cataract surgery, presbyopia treatment, clear–lens exchange; neuro-ophthalmology; vitreo-retinal surgery, glaucoma pathogenesis, myopia pathogenesis, and history of ophthalmology. He is active in **international scientific societies including Euretina**, AAO (recipient of International Scholar Award 2015), **European Academy of Ophthalmology**, ISBCS, ICO (programme coordinator for WCO in 2011–2016), Cogan Society, EVER ASCRS, and representative of Poland at ISRS (International Society of Refractive Surgery) International Council (2015).

He has been active editor, editor in chief and **author of more than 300** peer-reviewed international publications (total **IF higher than 515**), and **reviewer for more than 20 journals**.

Thomas R. Hedges III, MD

Dr. Hedges is Director of Neuro-ophthalmology at The New England Eye Center, and has been on the staff of the Tufts-New England Medical Center since 1981. He is Professor of Ophthalmology and Neurology at Tufts University where he served as acting Chairman of Ophthalmology, 1990–91 and now serves on the Alumni Council. Dr. Hedges graduated from Moorestown Friends School, Duke University, Rutgers University and from Tufts University School of Medicine in 1975. He completed his ophthalmology residency at Massachusetts Eye and Ear Infirmary, where he became the first Chief Resident in 1979 and completed a fellowship in Ophthalmic Pathology. He was a Heed Fellow in neuro-ophthalmology with William F. Hoyt at the University of California, San Francisco.

Dr. Hedges served as a North American Neuro-ophthalmology Society representative for the Executive Council of the American Academy of Ophthalmology, has taught many courses (some with his father, also a neuro-ophthalmologist) at the annual meetings and served as chair of the Neuro-ophthalmology section of the Basic Clinical Science Course from 1994 to 95. He received a Senior Honor Award from the American Academy of Ophthalmology in 2000. He is on the Editorial Board of the International Neuro-ophthalmology Society journal *Neuro-ophthalmology*. He has reviewed articles for a number of journals including *The*

Archives of Ophthalmology, *The Journal of Neuro-ophthalmology* and *The New England Journal of Medicine*. Dr. Hedges has authored or co-authored over one hundred peer-reviewed manuscripts, book chapters and review articles. He wrote Consultation in Ophthalmology, which was published in 1987.

Dr. Hedges' research interests include the use of optical coherence tomography and electrophysiology, including multifocal testing, in neuro-ophthalmology. He has participated in several multi-center trials and National Institutes of Health review committees. During his tenure at Tufts, Dr. Hedges has trained many medical students, residents and fellows. Most of his fellows have assumed academic positions around the country and in other parts of the world. He has been a visiting professor at many institutions in the United States and has participated actively in international meetings and seminars, especially throughout Latin America.

Principal Investigator/Program Director (Last, First, Middle):

Biographical sketch

Provide the following information for the key personnel and other significant contributors in the order listed on Form Page 2.

Follow this format for each person. **DO NOT EXCEED FOUR PAGES**.

NAME	POSITION TITLE
Thomas R. Hedges III, M.D.	Director of Neuro-ophthalmology, New England Eye Center, Professor of Ophthalmology and Neurology, Tufts University
eRA COMMONS USER NAME	

EDUCATION/TRAINING (*Begin with baccalaureate or other initial professional education, such as nursing, and include postdoctoral training.*)

INSTITUTION AND LOCATION	DEGREE (*if applicable*)	YEAR(s)	FIELD OF STUDY
Duke University	B.A.	1967–71	Chemistry
Rutgers CMDNJ	M.S.	1971–73	Physiology
Tufts University	M.D.	1973–75	Medicine

A. Personal Statement

I have been actively engaged in a variety of research projects in neuro-ophthalmology, particularly optic neuropathy. My clinical research activities have concentrated on evaluation of the retinal nerve fiber layer based on fundus photography, in a variety of neuro-ophthalmic disorders, including Alzheimer's disease. Since the technique of optical coherence tomography was developed for clinical use here at the Tufts, New England Eye Center, I have been engaged in applying this to various optic nerve diseases including papilledema, anterior ischemic optic neuropathy, and cuban epidemic optic neuropathy which in many ways resembles FD optic neuropathy, which I helped Dr. Carlos Mendoza describe in detail for the first time. Dr. Mendoza and I have worked together over the last several years and plan to continue evaluating patients with familial dysautonomia from a variety of perspectives, including the use of OCT to follow the optic neuropathy of FD over time, and to use electrophysiology to further define the nature of the optic neuropathy and to probe the possibility that the retina itself may be affected. I have been engaged in

ophthalmic pathologic studies since I was a fellow in Neuro-ophthalmic pathology at the Massachusetts Eye and Ear Infirmary and Massachusetts General Hospital when I was particularly interested in the pathology of herpes zoster and temporal arteritis. Recently we have had the opportunity to evaluate the histopathology of eyes from patients with familial dysautonomia with Dr. Nora Laver, our ophthalmic pathologist at Tufts. Dr. Mendoza, Dr. Laver and I will continue to evaluate human eyes from FD patients as they become available, and we will be applying this experience to the pathologic study of FD mouse eyes both to characterize the retinal phenotype and to evaluate the efficacy of kinetin.

B. Positions and Honors.

1975–76	Intern, Mt. Auburn Hospital, Cambridge, MA
1976	Harvard Course in Ophthalmology, Harvard Medical School
1977–79	Resident in Ophthalmology, Massachusetts Eye and Ear Infirmary, Harvard Medical School
1979–80	Fellow in Ophthalmic Pathology, Massachusetts Eye and Ear Infirmary
1980–81	Fellow in Neuro-ophthalmology, Neurosurgery, University of California, San Francisco
1981–87	Assistant Professor of Ophthalmology, Tufts University
1982–88	Assistant Professor of Neurology, Tufts University
1987–98	Associate Professor of Ophthalmology, Tufts University
1988–98	Associate Professor of Neurology, Tufts University
1990–91	Acting Chairman, Department of Ophthalmology, Tufts University
1998–	Professor of Ophthalmology, Tufts University
1998–	Professor of Neurology, Tufts University

Other

1980–81	Fellowship Award, The Heed Ophthalmic Foundation
1988	Honor Award, American Academy of Ophthalmology
1989	Alpha Omega Alpha, Tufts University School of Medicine
1989	Senior Honor Award, American Academy of Ophthalmology
1991	Special review committee SRC-4, Optic nerve applications, National Eye Institute
1992	Special review committee, SRC-02, Clinical trial applications, National Eye Institute
1996	Special review committee, SRC-04, Clinical trial applications, National Eye Institute 2000 Senior Honor Award, American Academy of Ophthalmology
2007	Alice Stokes Paul 1901 Moorestown Friends School Alumni Assoc. Merit Award
2010	Outstanding Tufts University School of Medicine Lecturer for 2009–2010

C. Selected Peer-Reviewed Publications

Most Relevant to Current Application

1. Hedges TR III, Albert DM. The progression of the ocular abnormalities of herpes zoster. Ophthalmology. 1982;89:165–77.
2. Hedges TR III, Gieger GL, Albert DM. The clinical value of negative temporal artery biopsy specimens. Arch Ophthalmol. 1982;101:1251–54.
3. Johns DR, Neufeld MJ, Hedges TR III. Mitochondrial DNA mutations in Cuban optic and peripheral neuropathy. J Neuroophthalmol. 1994;14:135–40.
4. Hedges TR III, Galves RP, Speigelman D, Barbas NR, Peli E, Yardley CJ. Retinal nerve fiber layer abnormalities in Alzheimer's disease. Acta Ophthalmol Scand. 1996;74:271–5.
5. Yoon MK, Chen RW, Hedges TR, Srinivasan VJ, Gorczynska I, Fujimoto JG, Wojtkowski M, Schuman JS, Duker JS. High-spead ultrahigh resolution optical coherence tomography of the retina in Hunter syndrome. Ophthalmic Surg Lasers Imaging. 2007;38:423–8.
6. Mendoza-Santiesteban C, Hedges TR, Norcliffe-Kaufmann L,, Warren F, Reddy S, Axelrod F, Kaufmann H. Clinical neuro-ophthalmic findings in familial dysautonomia. J Clinical Neuroophthalmol. 2012;32(1):23–6.

Additional Publications

7. Peli E, Hedges TR, Schwartz B. Computerized enhancement of the retinal nerve fiber layer. Acta Ophthalmol (Copenh). 1986;64:113–22.
8. Sokol S, Hedges TR III, and Moskowitz A. Pattern VEP's and preferential looking acuity in infantile traumatic blindness. Clin Vis Sci. 1987;2:59–61.
9. Hedges, TR III, Legge RH, Peli E, Yardley CJ. Retinal nerve fiber layer changes and visual field loss in idiopathic intracranial hypertension. Ophthalmology. 1995;102:1242–7.
10. Hedges TR III, Hirano M, Tucker K, Carballero B. Epidemic optic and peripheral neuropathy in Cuba: a unique geopolitical public health problem. Survey Ophthalmol. 1997;41:71–83.
11. Mojon DS, Hedges TR, Ehrenberg B, Karam EZ, Goldblum D, Abu-Chebl A, Gugger M, Mathis J. Association between sleep apnea syndrome and nonarteritic ischemic optic neuropathy. Arch Ophthalmol. 2002;120:601–5.
12. Hoye VJ, Berrocal AM, Hedges TR, Amaro-Quireza ML. Optical coherence tomography demonstrates subretinal macular edema from papilledema. Arch Ophthalmol. 2001;119:1287–90.
13. Massicotte,EC, Semela L, Hedges TR. Multifocal visual evoked potential in nonorganic visual field loss. Arch Ophthalmol. 2005;123:364–7.
14. Semela L, Yang E, Hedges TR, Vuong L, Odel JG, and Hood DC. Multifocal visual-evoked potential in unilateral compressive optic neuropathy. Br J Ophthalmol. 2007;91:445–8. Also Online First: 31 October 2006. doi:10.1136/bjo.2006.097980.
15. Rodriguez-Padilla JA, Hedges TR, Monson B, Srinivasan V, Wojtkowski M, Reichel E, Duker JS, Schuman JS, Fujimoto JG. High-speed ultra–high-

resolution optical coherence tomography findings in hydroxychloroquine retinopathy. Arch Ophthalmol. 2007;125:775–80.
16. Hedges TR, Vuong, LN, Gonzalez-Garcia AO, Mendoza-Santiesteban CE, Amaro-Quiereza AL. Subretinal fluid from anterior ischemic optic neuropathy demonstrated by optical coherence tomography. Arch Ophthalmol. 2008;126:812–5.

D. Research Support

Ongoing

XCiDaBLE Study evaluating Xeomin® (incobotulinumtoxinA) for cervical dystonia or blepharospasm in the United States in outpatient settings. Merz Pharmaceuticals, LLC, a North Carolina.

Neuroretinal dysfunction in familial dysautonomia. Dysautonomia Foundation. Co-investigator with Carlos Mendoza. 2012–1013.

Completed

"Computer Processing of Retinal Nerve Fiber Layer Defects" National Institute of Health Grant 1R01EY05450-01 Co-investigator, 7/1/84 – 6/30/87

"Clinical Analysis of Optic Nerve Integrity in Alzheimer's Disease" Alzheimer's Disease and Related Disorders Association, Principle investigator, 11/87 – 10/88

"Clinical Analysis of Optic Nerve Function in Alzheimer's Disease" Massachusetts Lions Eye Research Club, Principle Investigator, 6/1/89 – 10/1/89

A Randomized, Double Blind, Placebo Controlled Study of AVONEX (Interferon Beta 1a) in the Treatment of Subjects at High Risk for Development of Multiple Sclerosis Following the First Onset of an Isolated Demyelinating Event, Biogen C95-812, Principle Site Investigator 1995–98

A Randomized, Multicenter, Double Blind, Parallel Clinical Trial to Compare the Safety and Efficacy of BOTOX Purified Neurotoxin Complex Manufactured from Campbell Complex Lot 1 to Complex Lot 79–1 in Blepharospasm, Allergan 191622–003, Principle Site Investigator, 1997

Prospective, Double-Blind, Placebo-Controlled, Randomized, Multicenter Trial with an Open-label Extension Period to Investigate the Efficacy and Safety of NT-201 in the Treatment of Blepharospasm, MERZ Pharmaceuticals GmbH, MRZ 60201–0433, Principle Site Investigator, 2007–2008

Dr. Hedges is an expert in the diagnosis and management of diseases affecting the optic nerve and intracranial visual pathways, as well as disorders of ocular motility. His clinical practice involves patients with suspected or diagnosed case of neurological disease with ocular involvement. As co-director of the Electrophysiology Laboratory at the New England Eye Center, where Dr. Hedges studies patients with occult macular disease as well as visual pathway disorders. Dr. Hedges also provides botulinum toxin injections for patients with blepharospasm and hemifacial spasm. His major research interests are multifocal electrophysiology, and the evaluation of retinal nerve fiber layer changes due to optic neuropathy and papilledema.

Johannes Keller

Vitreo-Retinal Surgery Fellow at Bristol Eye Hospital

Johannes is an ophthalmologist trained in Venezuela, Spain and the UK. He has worked for the Visual Pathway Laboratory at the University of Barcelona where he worked on the assessment of neuro-ophthalmological conditions through advanced retinal imaging. Currently Johannes works as a retinal surgeon in the UK.

Kendra A. Klein, MD

Dr. Klein graduated summa cum laude from Hobart and William Smith Colleges and became a registered nurse after studying at Stony Brook University. She completed her post-baccalaureate studies at Bryn Mawr College and earned her medical degree at the University of Rochester. Dr. Klein is currently a resident in Ophthalmology at the New England Eye center of Tufts Medical Center and her research interests include the use of optical coherence tomography to understand retinal and optic nerve diseases.

Chiara La Morgia, MD, PhD

Dr. Chiara La Morgia, born December 3rd 1977, received her MD degree at the University of Bologna in 2002 and completed her residency in Neurology in 2008 at the University of Bologna.

She finished her PhD in Sleep Medicine in 2012 at the University of Bologna. Since 2012 she had a research contract at the University of Bologna. From October 5th 2015 she got a research position at the University of Bologna with a project on hereditary optic neuropathies and melanopsin retinal ganglion cells. Since 2008 she had research collaboration with the Doheny Eye Institute, formerly University of Southern California (USC), now affiliated with University California Los Angeles (UCLA), Los Angeles (USA) for the study of circadian photoreception in neurodegenerative disorders.

From March 2014 to October 2014 she had a clinical fellowship in neurophthalmology at Doheny Eye Institute, UCLA, under the supervision of Prof. Alfredo A. Sadun.

She currently runs the neurophthalmology clinic at Bellaria Hospital, UOC Clinica Neurologica, IRCCS Istituto delle Scienze Neurologiche di Bologna.

She is involved since 2004 in many research projects on mitochondrial optic neuropathies and she is responsible for the clinical management of patients with

hereditary optic neuropathies at the Bellaria Hospital. A focus of her research is the melanopsin retinal ganglion cell system in relation to circadian photoreception in different neurodegenerative disorders including mitochondrial optic neuropathies.

She is currently the PI of an Italian Ministry of Health-funded project entitled "Melanopsin retinal ganglion cells and circadian rhythms: function and dysfunction in Alzheimer's disease and aging". Finally, she has been involved in clinical trials on Leber's hereditary optic neuropathy.

Dr. La Morgia authored 50 papers in peer-reviewed journals.

Address:

Chiara La Morgia, MD, PhD

IRCCS Istituto delle Scienze Neurologiche di Bologna, UOC Clinica Neurologica, Bellaria Hospital, Bologna, Italy

Department of Biomedical and Neuromotor Sciences, University of Bologna

Email address: chiaralamorgia@gmail.com

Gianluca Manni, MD

1986, researcher (Ricercatore), Ophthalmic Clinic, University “Tor vergata”, Rome, Italy. 1990, Researcher (renewal), Scientific area of faculty MED/30 ophthalmic diseases, University “Tor Vergata”, Rome, Italy. 2001, Associate Professor, Scientific area of faculty MED/30 ophthalmic diseases. 2002, Associate Professor, Scientific area of faculty MED/30 ophthalmic diseases, University “Tor Vergata”, Rome, Italy. 2005, Associate Professor (renewal), Scientific area of faculty MED/30 ophthalmic diseases, University “Tor Vergata”, Rome, Italy. From 2012 is the reviser for the Ministry of the University of the scientific papers in the ophthalmology field. 2014 Qualified as Full Professor.

Kaweh Mansouri, MD, MPH

Affiliation: (1) Consultant, Glaucoma Sector, Geneva University Hospitals, Geneva, Switzerland. (2) Adjoint Associate Professor, Department of Ophthalmology, University of Colorado School of Medicine, Denver

Areas of Interest: continuous 24-h IOP monitoring; innovations in glaucoma surgery; epidemiology of glaucoma.

Leadership Positions: Associate advisory board member, World Glaucoma Association (WGA); Country Representative and Committee Member, European Society of Ophthalmology Young Ophthalmologists Program (SOE-YO); Founding member and associate advisory board member, International Society for Glaucoma Surgery (ICGS); Associate Editor (Journal of Current Glaucoma Practice); Associate Medical Officer (World Health Organization, Prevention of Blindness and Deafness).

Dr. Elena H. Martínez-Lapiscina

Neurologist at Institut d'Investigacions Biomèdiques August Pi i Sunyer (IDIBAPS), Hospital Clínic de Barcelona.

Elena H. Martínez-Lapiscina earned a medical degree at University of Navarra School of Medicine in Pamplona, Spain in 2006, completed an internal neurology residency in 2012 at Complejo Hospitalario de Navarra, Pamplona Spain. In 2013, Elena H Martínez-Lapiscina received her PhD in Cognition and Neuroscience. In 2012, she incorporated to the Visual Pathway Lab section of the Villoslada's pathogenesis and new therapies lab at IDIBAPS.

She treats adults with Multiple Sclerosis and other immune-mediated disorders of the Central Nervous System.

Her research revolves around neuroimaging modalities of the afferent visual pathway and their potential roles to elucidate relationships between inflammation, demyelination and neurodegeneration in Multiple Sclerosis and Acute Optic Neuritis (pathogenesis) and to track and predict the course of the disease (biomarkers).

Javier Mateo

Medical and Surgical Retina Unit, Department of Ophthalmology, Hospital Clínico Universitario “Lozano Blesa”, Zaragoza, Spain

Shahnaz Miri

I graduated from Tehran University of Medical Sciences in 2013 and working as a Post-Doctoral Research Fellow since then, at SUNY Downstate Medical Center, Brooklyn. Under supervision of Professor Ivan Bodis-Wollner, my research focus is study of the retina in Parkinson's disease. In was involved in evaluating retinal electrophysiology, neural and capillary structure in PD patients. Soon I will pursue a residency in Neurology.

Mário Luiz Ribeiro Monteiro

Mário L. R. Monteiro, MD is a Professor of Ophthalmology, Director of the Neuro-ophthalmology and the Orbital Diseases Services, and Coordinator of the post-doctoral program in Ophthalmology at the University of São Paulo Medical School, São Paulo, Brazil. He received his medical degree and completed a residency in ophthalmology at University of São Paulo and a neuro-ophthalmology fellowship at the University of California, San Francisco where he trained with Prof. William F. Hoyt. Since 1984 he teaches at University of São Paulo Medical school and has trained hundreds of residents, fellows and post doctoral students. He has published 190 papers on peer-reviewed journals, edited 5 books and written more than 100 book chapters. His main research interests include inflammatory and compressive disorders of the optic nerve and chiasm and Graves' orbitopathy, particularly ithe evaluationn of structural and functional abnormalities iusing optical coherence tomography, visual fields and electrophysiologic tests.

Dr Eduardo M. Normando MD, PhD, FEBO

Dr Eduardo M. Normando MD, PhD, FEBO is a fully qualified clinician scientist Ophthalmologist. He is the senior research fellow of ICORG (Imperial College Ophthalmology Research Group) at the Western Eye Hospital in London where he is co-investigator in numerous clinical trial in glaucoma and medical retina. Dr Normando earned his PhD in Visual Neuroscience with a particular emphasis in retinal imaging from the UCL Institute of Ophthalmology in London working in Prof Francesca Cordeiro group. He completed his Specialty Accreditation in Ophthalmology (70/70 cum Laude) at Campus Bio-Medico University of Rome, Italy spending the last year of his training between the UCL Institute of Ophthalmology and the Glaucoma team at the Western Eye Hospital. Further scientific and clinical experience has been achieved by attending the Retinal Degeneration Research Centre, & Ophthalmic Genetics Service at University of Tennessee and the Ocular Microsurgical division and Glaucoma division at San Carlo Hospital in Rome. His research is focused mainly on innovative non-invasive retinal imaging techniques and their applications in assessing novel therapeutic strategies for ophthalmic and neurodegenerative diseases. Dr Normando is co-author of 18 article and has extensive experience in presenting at national and international meetings. He has also wide experience in teaching at undergraduate and postgraduate level.

Vincenzo Parisi, MD

Head of the Department of Neurophysiology of Vision and Neurophthalmology of Fondazione GB Bietti-IRCCS, Certified Associate Professor of Ophthalmology.

Born in Vibo Valentia (Italy) on 08/21/1962. Since 1989, he carried out research on the role of Nerve Growth Factor on the visual system and on the identification of retinal and visual pathways morpho-functional impairment in diabetes, glaucoma, multiple sclerosis, Alzheimer's disease, CADASIL, Leber's optic neuropathy and migraine. He is author of 94 publications on scientific journals (Total Impact Factor: 242; Personal H-index: 27). "Expert reviewer" of several journals from which IOVS, Brain, Ophthalmology, Archive's of Ophthalmology, British Journal of Ophthalmology, Vision Research, Clinical Neurophysiology.

Francesco Pierelli MD, PhD

Francesco Pierelli is Full Professor of Neurology and Chairman of the Neurorehabilitation unit at the Sapienza University, Polo Pontino, Latina, Italy.

He is Director of Postgraduate School in Neurology, President of the graduate course in Physioterapy of the Sapienza University of Rome, Director of the I level Master "Ostheopathy and integrative individual therapy", Honorary President of the "Italian Movement Medicine Society" (SIMM). He is Director of the "Superior Interdisciplinary School of Headaches" of the Italian Society for the Study of Headaches (SISC). He has published more than 190 indexed papers.

Alfredo A. Sadun, MD, PhD

Professor and Thornton Endowed Chair, Doheny Eye Institute. Vice-Chair of Ophthalmology, Dept. Ophthalmology, UCLA. Dr. Sadun graduated from MIT (1972) and after obtaining his Ph.D. and M.D., completed his residency in Ophthalmology at Harvard Medical School followed by a fellowship in Neuro-Ophthalmology. He joined the full-time faculty at Harvard, Department of Ophthalmology in 1983. He was recruited to USC/Doheny where he remained for 30 years. He helped lead Doheny in its transition to UCLA in 2014.

His research has centered on the clinical, psychophysical and laboratory studies of diseases of the optic nerve. In the 1980s Dr. Sadun was one of the first to apply a new tract-tracing technique in order to establish nine anatomical pathways between the eye and the brain. He was the first to describe a human retinal projection to the hypothalamus that subserves the visual entrainment of the circadian rhythm. Dr. Sadun was the first to identify an optic neuropathy associated with Alzheimer's disease. In 1993, he was selected and sponsored by the United Nations to lead an investigative team to determine the cause of an epidemic of optic neuropathy in Cuba. He is author of about 300 peer-reviewed publications (H-index: 47).

Bernardo F. Sánchez Dalmau

Bernardo F. Sánchez Dalmau is a Consultant in neuro-ophthalmology at the Hospital Clínic, Barcelona, Spain and Assistant Professor of Ophthalmology at the Faculty of Medicine, University of Barcelona (UB).

Dr. Sánchez Dalmau graduated in Medicine from the University Autonoma of Barcelona (UAB) in 1987, then undertook an ophthalmology residency at the Hospital de Sant Pau, Barcelona, and completed his formation in Neuro-ophthalmology at Wills Eye Hospital Philadelphia and Wilmer Eye Institute. Prior to his current role, Dr. Sánchez Dalmau was a consultant in neuro-ophthalmology and paediatric ophthalmology at the Hospital Mútua de Terrassa, Barcelona, and Assistant Professor in Ocular Pathology at the College of Optics and Optometry at the Polytechnic University of Catalonia, Spain.

Dr. Sánchez Dalmau's research centres around the Visual Pathway Lab at the August Pi i Sunyer Biomedical Research Institute (IDIBAPS) in Spain. He has authored over 8 books or book chapters and over 35 articles.

Ruben Torres-Torres, MD

Opthalmologist

Clínic Institute of Ophtalmology (ICOF)

Hospital Clinic, Barcelona, Spain

Ruben Torres-Torres received his MD at the Pontifical Catholic University of Chile in 2010.

During his ophthalmology residency has participated actively in the Visual Pathway Lab section with Dr Sanchez-Dalmau and Dr. Villoslada studying the pathogenesis, biomarkers and new therapies of demyelinating diseases.

Pablo Villoslada, MD

Adjunct Professor. Dept Neurology. UCSF
Senior Scientist. IDIBAPS, Spain
Bionure Inc

Pablo Villoslada received his MD at the University of Santiago de Compostela (Spain) in 1990. He completed his speciality in Neurology in 1995 at the Hospital Vall d'Hebron (Spain) and his PhD in Neuroimmunology in 1996 at the Autonomous University of Barcelona (Spain). He moved to the University of California, San Fracisco (USA) as a postdoctoral fellow returning to Barcelona in 1998 and he worked as Assistant and Asociate Professor of the University of Navarra from 2001 to 2008.

He is currently Adjunct Professor at the University of California, San Francisco and Group leader of the Neuroimmunology group of the Institute of Biomedical Research August Pi Sunyer (IDIBAPS), Spain.

Pablo Villoslada has been active in neurosciences and translational research for more than 15 years contributing to the application of systems biology to neurological diseases. He has published more than 120 papers in top journals in the field of neurology and 9 patents in biomarkers and new therapies for brain diseases.

Index

A. Grzybowski, P. Barboni (eds.), *OCT in Central Nervous System Diseases: The Eye as a Window to the Brain*, DOI 10.1007/978-3-319-24085-5